

Analysis of Sonic Hedgehog signalling pathway gene expression in Basal Cell Carcinoma and in GLII induced systems

Ikram, Mohammed. S.

The copyright of this thesis rests with the author and no quotation from it or information derived from it may be published without the prior written consent of the author

For additional information about this publication click this link.

<http://qmro.qmul.ac.uk/jspui/handle/123456789/1527>

Information about this research object was correct at the time of download; we occasionally make corrections to records, please therefore check the published record when citing. For more information contact scholarlycommunications@qmul.ac.uk

**Analysis of Sonic Hedgehog signalling pathway gene
expression in Basal Cell Carcinoma and in GLI1
induced systems.**

A thesis submitted in accordance with regulations for the degree
of Doctor of Philosophy.

May 2007

Mohammed. S. Ikram

Centre for Cutaneous Research

St Bartholomew's and The Royal London School

Of Medicine and Dentistry

Queen Mary's College

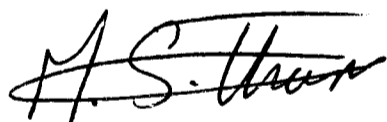
University of London

DECLARATION

I hereby declare that all the work contained in this thesis is the result of my own independent investigations unless otherwise stated.

This work has not already been accepted for any degree, and is not being concurrently submitted for any other degree.

Mohammed S Ikram

A handwritten signature in black ink, appearing to read 'M.S. Ikram', written in a cursive style. The signature is positioned above a horizontal dotted line.

ABSTRACT

Embryonic development is regulated by a number of signalling pathways, which are critical for normal growth. Many of these genes then continue to play an important role in the regulation of cell growth and differentiation in adult. One such pathway is the sonic hedgehog (SHH) pathway; SHH protein is secreted which binds to its receptor patched (PTCH), leading to the activation and repression of target genes via zinc-finger GLI family transcription factors. Deregulation of this pathway, leads to a number of human birth defects and diseases such as Basal Cell Carcinoma (BCC) of the skin. In transgenic mouse model systems activation of GLI1 by SHH-signalling is a key step in initiating BCC formation. However, there is limited understanding of the molecular mechanisms involved in response to hedgehog signalling and GLI activity in human BCC formation and how this pathway interacts with other pathways. The aim of this thesis was to establish *in vitro* and *in vivo* model systems to investigate the molecular events leading to BCC formation. I have shown that *GLI1*, *GLI2*, *GLI3*, *PTCH*, *SMO* and *KIF4* were induced and *α-TUB* was repressed in BCC relative to normal skin. Using an *in vitro* model I further showed that *GLI1*, *GLI2*, *GLI3*, *PTCH*, *SMO* and *α-TUB* were induced and *KIF4* was repressed in GLI1 expressing keratinocytes. Collaborative work with Dr Fritz Aberger's laboratory in Salzburg showed that *GLI1* and *FOXE1* are direct targets of GLI2 and I showed that *GLI2* and *FOXE1* were expressed in the interfollicular epidermis and the outer root sheath of hair follicles in normal skin as well as in BCC tumour islands suggesting a possible link between hair follicle and BCC. I further showed that epidermal growth factor (EGF) signalling reduces transcription activity of GLI1 by shuttling GLI1 out of nucleus and altering the expression of *PTCH*, *SMO*, *GLI2* and *GLI3* SHH genes. In addition, I demonstrated that whilst EGF induced Vimentin and Snail2 expression and GLI1 repressed their expression suggesting that GLI is able to counter epithelial-mesenchymal transition associated with EGF and this may in part explain why BCC very rarely metastasise. Furthermore, GLI1 appears to upregulate stem cell like signature and EGF downregulates this signature. Finally, we were able to generate a *KRT14*- Floxed-*GFP-GLI1* transgenic mouse but were unable to activate the target gene (*KRT14-GFP-GLI1*). In conclusion, I have identified possible targets of GLI activity and shown interactions between EGF signalling and GLI that will help us to understand the potential molecular actions of SHH signalling with the goal of developing better therapeutic strategies.

ACKNOWLEDGEMENTS

I would like to thank my supervisor, Professor Mike Philpott, for his time, advice, generous support, encouragement and patience throughout the course of my study. I would also like to express my sincere thanks to my second supervisor, Professor Irene Leigh, for here support.

I would also like to thank the patients and the Dermatology Department at The Royal London Hospital for providing me with BCC tissue and Dr Nigel Carver who provided me with redundant normal skin tissue.

I would like to thank Dr Graham Neill at the Centre for Cutaneous Research, who provided me with the GLI1 primary keratinocytes and many thanks in particular for his support and advice on experimental techniques and scientific discussions. I would also like to thank Dr Fritz Aberger at the University of Salzburg Austria for their collaborative work and assistance as described in chapters 4 and 5, which enabled me to make progress with my work. Finally thank you to everyone at the Centre for Cutaneous Research.

A big thank you to my wife Shamina my sons Adeel, Hamzah and Haroon and to my parents for their moral support and encouragement.

I dedicate this thesis to my late Grandparents Haji Mohammed Shuker and Mrs Zanib Bibi who sadly passed away during my studies.

CONTENTS

DECLARATION	3
ABSTRACT	4
ACKNOWLEDGEMENTS.....	5
CONTENTS.....	6
ABBREVIATIONS.....	14
LIST OF FIGURES.....	16
LIST OF TABLES.....	22
PRESENTATIONS AND PUBLICATIONS.....	25
PRESENTATIONS AND PUBLICATIONS.....	25
CHAPTER 1	26
Introduction	26
1.1.0 Structure of skin.....	27
1.1.1 The epidermis.	29
1.1.2 Keratins.....	32
1.1.3 The dermis.	34
1.1.4 The basement membrane zone dermal epidermal junction.	35
1.1.5 Extracellular matrix.....	37
1.1.6 Epithelial mesenchymal interactions.....	38
1.1.7 Structure and function of the hair follicle.....	39
1.1.8 Hair follicle bulb.	40
1.1.9 The dermal papilla.....	40
1.1.10 Connective tissue sheath.....	40
1.1.11 Sebaceous gland.....	41
1.1.12 Hair follicle morphogenesis and hair growth cycle.	43
1.1.13 Signalling pathways in hair follicle development and cycling.	47
1.1.14 Epidermal stem cell characteristics and their niche.	50
1.1.15 Epidermal stem cell markers.....	52
1.1.16 Epidermal, homeostasis and regulation.....	53
1.2.0 Basal cell carcinoma (BCC).	54
1.2.1 Histology of basal cell carcinoma.....	58
1.2.2 Factors that lead to basal cell carcinoma formation.....	60
1.2.3 Treatment for basal cell carcinoma.	61
1.3.0 Sonic Hedgehog pathway.....	62

1.3.1 Patched and smoothed.	63
1.3.2 GLI1.	65
1.3.3 GLI2.	66
1.3.4 GLI3.	67
1.3.5 GLI protein processing and their overlapping roles.....	68
1.3.6 Suppressor-Fused.	72
1.3.7 Chicken Ovalbumin Upstream Promoter Transcription Factor II (COUP-TFII).	73
1.3.8 TFIID.....	74
1.4.0 Retroviral gene expression.....	75
1.4.1 Retroviral Structure and Genomic Organisation.	75
1.4.2 Retroviral replication.....	77
1.4.3 Retroviral vector as gene delivery tool.	77
1.4.4 Self Inactivating retroviral vectors.....	78
Aim of this study.....	81
CHAPTER 2	82
Materials and Methods.....	82
2.1.0 Cell Culture.....	83
2.1.1 Mouse 3T3 fibroblast cell line (feeder layer).	83
2.1.2 Isolation of primary keratinocytes from human skin.	85
2.1.3 Passaging keratinocyte cultures.	86
2.1.4 Removal of fibroblast contamination in keratinocyte cultures.....	87
2.1.5 HaCat, A375 and N-TERT-keratinocyte cells.....	88
2.1.6 Freezing and recovery of cells.	88
2.2.0 Retroviral transduction.	89
2.2.1 Generating SIN-EGFP/GLI1 fusion protein retroviral construct.	89
2.2.2 Generating SIN-GLI-EGFP bicistronic retroviral constructs.....	90
2.2.3 Generating a SIN-GLI1-mutated Nuclear Localization Signal (mNLS) construct.	90
2.2.4 Generating retroviral particles in packaging cell line.	96
2.2.5 Transducing primary and N/TERT keratinocytes.....	97
2.3.0 GLI1 polyclonal baby rat kidney cells.....	98
2.3.0 Normal human skin and basal cell carcinoma (BCC).	98
2.5.0 RNA extraction.	98
2.5.1 Total RNA extraction from cultured cells.	98
2.5.2 Total RNA extraction from frozen tissue.	99
2.5.3 Messenger RNA isolation from total RNA.	100
2.5.4 Determining the concentration of purified RNA.	101
2.5.5 Checking the integrity of purified RNA.....	101
2.5.6 Agarose gel electrophoresis.....	102
2.6.0 Analysis of mRNA by northern blot hybridisation.....	102
2.6.1 Electrophoresis of mRNA on formaldehyde agarose gel.....	103
2.6.2 RNA transfer to Hybond-XL membrane.....	104

2.6.3 Probe generation for northern blot analysis.....	106
2.6.4 Probe labelling.	106
2.6.5 Probe purification.....	106
2.6.6 Membrane pre-hybridisation.	107
2.6.7 Membrane hybridisation.....	108
2.7.0 Reverse Transcriptase Polymerase Chain Reaction (RT-PCR).....	109
2.7.1 Primer designing.	109
2.7.2 Removing contaminating DNA from total RNA preps.....	109
2.7.3 First strand cDNA synthesis with Reverse Transcriptase.	110
2.7.4 PCR reaction.....	110
2.7.5 Purification of PCR product form agarose gel.	111
2.8.0 Real-time RT-PCR reaction.	120
2.9.0 Cloning	123
2.9.1 Cloning Smoothend and Suppressor-Fused PCR products.	123
2.9.2 Preparing plasmid miniprep.....	123
2.9.3 Sequencing the cloned inserts.....	126
2.9.4 Cloning a 296 bp <i>GLI2</i> fragment from h <i>GLI2</i> -1.6 kb-pCII-TOPO.	126
2.9.5 Cloning a 1.2 kb keratin <i>KRT14</i> insert from PGEM in to pCII-TOPO vector.	127
2.10.0 In-situ hybridisation.....	129
2.10.1 Linearising h <i>GLI2</i> -1.5 kb-pCII TOPO and h <i>GLI2</i> -296 bp-pCII TOPO plasmids for in-situ probes.	129
2.10.2 Linearising <i>KRT14</i> -1.2 kb-PGEM and <i>KRT14</i> -1.2 kb-pCII TOPO plasmids for in-situ probes.....	130
2.10.3 Linearising <i>FOXE1</i> -(UTR-332bp)-pBluescript-II-KS plasmid for in-situ probes.	130
2.10.4 Purifying linearised plasmids by ethanol precipitation.	131
2.10.5 Transcribing <i>GLI2</i> , Keratin <i>KRT14</i> and <i>FOXE1</i> probes for in-situ hybridisation.	131
2.10.6 Purifying transcribed probe by ethanol, precipitation.....	136
2.10.7 Fragmenting 1.5 kb <i>GLI2</i> and 1.2 kb <i>KRT14</i> transcribed probes.	136
2.10.8 Purifying the fragmented probe by ethanol precipitation.....	136
2.10.9 Quantifying DIG-labelled <i>KRT14</i> , <i>GLI2</i> and <i>FOXE1</i> probe by dot blotting.	136
2.10.10 Cutting paraffin wax embedded and frozen normal skin and BCC tissue sections.....	137
2.10.11. Pre-treatment of tissue sections.....	138
2.10.12. Pre-hybridisation.	138
2.10.13. Hybridisation.....	139
2.10.14. Immunological detection of Digoxigenin-labelled probes.	139
2.11.0 Affymetrix analysis	140
2.11.1 First stand cDNA synthesis.	140
2.11.2 Second strand cDNA synthesis.....	141
2.11.3 Clean-up of double stranded cDNA.....	141
2.11.4 Synthesis and labelling of cRNA.	142
2.11.5 Purification of labelled cRNA and quantification.....	143
2.11.6 cRNA fragmentation.	144
2.11.7 Hybridisation cocktail for human (HG-U133 A) gene chip.	144

2.12.0 Laser-capture micro-dissection of normal skin for gene expression analysis.	146
2.12.1 Tissue freezing and embedding.	146
2.12.2 Staining and dehydration.	146
2.12.3 RNA extraction using picopure RNA extraction kit (Cat No RIT0202 Arcturus USA).	147
2.12.4 DNaseI treatment of pico pure RNA column.	148
2.13.0 Generating a GLI2 monoclonal antibody.	149
2.13.1 Conjugation of C-and-N-terminal peptides of GLI2 to mcKLH.	149
2.13.2 Conjugated peptide purification.	149
2.14.0 SDS Polyacrylamide Gel Electrophoresis and Western blot analysis.	150
2.14.1 Stripping western blot membrane for re-probing.	152
CHAPTER 3	153
Analysis of SHH-Pathway Genes in Normal Skin, BCC and GLI1-transduced Human Primary Keratinocytes	153
3.1.0 Introduction	154
3.2.0 Results	156
3.2.1 Northern blot analysis of SHH-signalling pathway.	156
3.2.2. <i>GLI1</i> expression in normal skin, BCC, <i>GLI1-E1A</i> transformed baby rat kidney and <i>GLI1</i> transduced primary keratinocytes.	156
3.2.3 <i>GLI2</i> expression in <i>GLI1-E1A</i> transformed baby rat kidney cell line, <i>GLI1</i> -primary-keratinocytes, HaCat and A375 cells.	157
3.2.4 <i>PTCH</i> expression in <i>GLI1-E1A</i> transformed baby rat kidney, <i>GLI1</i> primary keratinocytes, HaCat and A375 cells.	157
3.2.5 Summary of northern blot analysis.	161
3.3.0 RT-PCR analysis of SHH signalling pathway.	162
3.3.1 PCR amplification of genomic DNA to check if the RT-PCR primers span the intron/exon boundaries.	162
3.3.2. <i>GLI1</i> expression in BCC, normal skin, HaCat, primary keratinocytes, A375, <i>GLI1</i> -transduced primary keratinocytes and <i>GLI1</i> -transformed 10T1/2 cells.	164
3.3.3 <i>GLI3</i> , <i>SUP-FU</i> , <i>SMO</i> , <i>TFIID</i> , <i>G6PDA</i> , <i>PTCH</i> , α - <i>TUB</i> and <i>KIF4</i> expression in BCC, normal skin, HaCat, primary keratinocytes, A375, GLI1 expressing cells.	164
3.3.4 <i>COUP-TFII</i> expression in BCC, normal skin, HaCat, primary keratinocytes, A375, <i>GLI1</i> -primary keratinocytes and <i>GLI1</i> -10T1/2 cells.	165
3.3.5 <i>GLI2</i> expression in BCC, normal skin, primary keratinocytes, HaCat, A375 and GLI1 expressing cell lines.	168
3.3.6 Real-time RT-PCR analysis.	171
3.3.7 <i>GLI1</i> is only induced in BCC and <i>GLI1</i> -primary keratinocytes and not in HaCat and A375 cells.	172
3.3.8 <i>GLI2</i> expression is induced in BCC, HaCat, A375 and <i>GLI1</i> -primary keratinocytes.	172
3.3.9 <i>GLI3</i> expression is induced in BCC, HaCat, A375 and <i>GLI1</i> -primary keratinocytes.	173

3.3.10 <i>PTCH</i> is induced in BCC, HaCat and <i>GLI1</i> -primary keratinocytes and there is no change in A375 cells.....	173
3.3.11 <i>SMO</i> is induced in BCC, HaCat, A375 and <i>GLI1</i> -primary keratinocytes.....	173
3.3.12 <i>KIF4</i> is induced in BCC, HaCat, A375 and repressed in <i>GLI1</i> -primary keratinocytes.....	174
3.3.13 α - <i>TUB</i> expression is induced in A375 <i>GLI1</i> -primary keratinocytes and repressed in BCC.....	174
3.4.0 Laser Capture Micro-dissection (LCM) of dermal papilla, hair follicle root sheath and epidermis from normal skin and gene expression analysis.	177
3.5 0 Discussion	180
3.5.1 <i>PTCH</i> expression is induced in BCC, HaCat and <i>GLI1</i> expressing cell lines.	180
3.5.2. <i>GLI1</i> expression is up-regulated in BCC and <i>GLI1</i> expressing cells.	181
3.5.3 <i>GLI2</i> is induced in BCC and <i>GLI1</i> expressing cell lines.	182
3.5.4 Induction of <i>GLI3</i> and <i>SMO</i> in HaCat and A375 cells is independent of <i>GLI1</i> and in <i>GLI1</i> -primary keratinocytes and possibly in BCC it is dependent on <i>GLI1</i> expression.....	185
3.5.5 <i>KIF4</i> is induced in BCC, HaCat and A375 cells and <i>GLI1</i> represses it in primary keratinocytes.....	186
3.5.6 <i>COUP-TFII</i> and <i>TFIID</i> are expressed in BCC, normal skin and <i>GLI1</i> - primary keratinocytes.....	188
3.5.7 <i>SUP-FU</i> is expressed in BCC, normal skin and in <i>GLI1</i> expressing and non expressing cells.....	189
3.5.8 α - <i>TUB</i> is repressed in BCC and induced in <i>GLI1</i> primary keratinocytes.....	190
3.5.9 <i>GLI1</i> is not expressed in epidermis of normal skin, whereas <i>GLI2</i> , <i>GLI3</i> and <i>PTCH</i> are. <i>GLI1</i> , <i>GLI2</i> , <i>GLI3</i> and <i>PTCH</i> are expressed in dermal papilla and outer root sheath.	190
3.6.0 Summary	192
3.7.0 Future study	192
CHAPTER 4	194
Localisation of <i>GLI2</i> in Normal Human Skin and BCC and its regulation of <i>GLI1</i>	194
4.1.0 Introduction	195
4.1.1 NHIS- <i>GLI2</i> binds <i>GLI</i> consensus sequence in the <i>GLI</i> promoter and induces <i>GLI1</i> expression in keratinocytes.....	195
4.2.0 Results	198
4.2.1 <i>GLI1</i> expression in NHIS-<i>GLI2</i> human primary keratinocytes.	198
4.2.2 In-situ hybridisation of <i>GLI2</i> expression in normal skin and BCC.	199
4.2.3 Development of the In-situ hybridisation technique.....	199
4.2.4 Localisation of <i>GLI2</i> and <i>KRT14</i> in BCC and normal skin wax sections with citrate method.	199
4.2.5 Localisation of <i>GLI2</i> and <i>KRT14</i> in BCC and normal skin wax sections with proteinase-K method.....	200

4.2.6 Localisation of <i>GLI2</i> and <i>KRT14</i> in BCC and normal skin frozen section with proteinase K and citrate method.....	200
4.2.7 Generation of monoclonal antibody to N-and-C-terminal of GLI2.....	209
4.3.0 Discussion	210
4.3.1 Localisation of <i>GLI2</i> in BCC and normal skin.....	210
4.3.2 A role for human <i>GLI2</i> in regulating epidermal proliferation and skin tumorigenesis.....	213
4.4.0 Summary	214
4.5.0 Future study	215
CHAPTER 5	216
FOXE1 Expression in Normal Skin and BCC.....	216
5.1.0 Introduction	217
5.1.1 Induction of <i>GLI2</i> in human keratinocytes increases <i>FOXE1</i> mRNA expression.....	217
5.1.2 <i>FOXE1</i> is an early target of <i>GLI2</i> in human keratinocytes.....	218
5.1.3 Activation of the <i>FOXE1</i> promoter by NHIS- <i>GLI2</i> -(332) by binding <i>GLI</i> consensus sequence in the <i>FOXE1</i> promoter.....	219
5.2.0 Results	220
5.2.1 Localization of <i>FOXE1</i> in BCC and normal skin.....	220
5.3.0 Discussion	224
5.4.0 Summary	226
5.5.0 Future study	226
CHAPTER 6	227
Effects of EGF on Pattern of Gene Expression in <i>GLI1</i> expressing Keratinocytes	227
6.1.0 Introduction	228
6.2.0 Materials and Methods.....	230
6.3.0 Results	231
6.3.1 Cell morphology of <i>GLI1</i> -primary keratinocytes changes in presence of EGF.....	231
6.3.2 Determining the expression of hedgehog, keratinocyte differentiation, mesenchymal, and stem cell markers in <i>GLI1</i> -primary keratinocytes cultured with EGF.....	235
6.3.3 EGF reduces <i>PTCH</i> , <i>GLI2</i> and <i>SMO</i> expression and restores <i>GLI3</i> expression to control levels whereas <i>GLI1</i> represses <i>GLI3</i> expression.....	238
6.3.4. <i>GLI1</i> induces expression of <i>KRT17</i> , <i>KRT14</i> , <i>KRT19</i> and repress the expression of <i>KIF4</i> , whereas EGF reduces this induction and repression.....	240

6.3.5. GLI1 represses and EGF induces expression of Vimentin and Snail2 transcripts.	242
6.3.6 Determining expression of Vimentin, E-Cadherine, EGFR and keratin K14 proteins in GLI1 primary keratinocytes cultured with and without EGF.	242
6.3.7 Identification of differentially expressed genes in GLI1-primary keratinocytes cultured with and without EGF.	246
6.3.8 Comparing real-time RT-PCR and Affymetrix data for <i>GLI1</i> , <i>GLI2</i> , <i>GLI3</i> , <i>PTC</i> , Vimentin, Snail2, <i>KRT19</i> , <i>KRT17</i> , <i>KRT14</i> and <i>SMO</i> in GLI1-primary keratinocytes cultured with EGF.	248
6.3.9 <i>VAV2</i> , <i>VAV3</i> and <i>VAV3.1</i> are expressed in GLI1- primary keratinocytes cultured with and without EGF.	251
6.3.10 There is no change in <i>VAV2</i> and <i>VAV3.1</i> expression in GLI1-primary keratinocytes cultured with EGF.	252
6.3.11 GLI1-N-TERT keratinocytes express <i>VAV3.1</i> and not <i>VAV3</i> and its expression is lost when cultured with EGF.	255
6.3.12 GLI1 induces <i>VAV3.1</i> and <i>VAV2</i> expression in N/TERT keratinocytes and EGF represses this induction.	255
6.3.13 <i>VAV3.1</i> is expressed in BCC and normal skin.	258
6.4.0 Discussion	259
6.4.1 Localisation of GLI1 in the nucleus is required to cause a change in cell morphology with EGF.	259
6.4.2 EGF alters the transcriptional activity of GLI1.	259
6.4.3 EGFR expression is reduced in GLI1 expressing keratinocytes cultured with EGF.	261
6.4.4 GLI1 induces expression of <i>KRT14</i> , <i>KRT17</i> and <i>KRT19</i> and EGF represses' this induction.	261
6.4.5 GLI1 may be a negative regulator of Epithelial/Mesenchymal transformation (EMT).	262
6.4.6 GLI1 and EGF reduce <i>KIF4</i> mRNA expression in primary keratinocytes.	263
6.4.7 <i>VAV 3.1</i> expressed in BCC is induced by GLI1 and repressed by EGF.	263
6.5.0 Summary	264
6.6.0 Future work	265
CHAPTER 7	266
Generating a Zp3-Cre-GLI1 Transgenic Mouse Model System	266
7.1.0 Introduction	267
7.1.1 Zp3-Cre <i>GLI1</i> transgenic mouse model system.	267
7.2.0 Materials and Methods.	269
7.2.1 Extracting DNA from transgenic mouse tail.	269
7.2.2 Screening transgenic mouse DNA using PCR analysis.	270
7.3.0 Results	272
7.3.1 <i>In vitro</i> Cre mediated recombination of <i>KRT14-Floxed-GFP-GLI1</i> to <i>KRT14-GFP-GLI1</i> in 293 cells.....	272
7.3.2 Generating a K14-Floxed-GFP-GLI1 mouse model under control of Zp3-Cre activation.	272

7.4.0 Discussion	274
7.5.0 Summary	274
CHAPTER 8	275
Conclusion.....	275
APPENDIX I.....	284
Affymetrix analysis of genes differentially expressed in GLI1-primary keratinocytes cultured with and without EGF.	284
APPENDIX II.	288
Standard Buffers and Solutions	288
Cell culture.....	288
Northern blot	293
In-Situ Hybridisation.....	295
Affymetrix.....	298
Western blotting	299
REFERENCE	301

ABBREVIATIONS

General abbreviation

Abs.....	Absorbance
AMV-RT.....	Avian Myeloblastosis Virus Reverse
.....	Transcriptase
α -TUB.....	Alpha- Tubulin
BCC.....	Basal Cell Carcinoma
CBP.....	CREB-Binding Protein
cDNA.....	Complimentary DNA
<i>Ci</i>	<i>Cubitus interruptus</i>
CNS.....	Central Nervous System
Cos-2.....	Costal-2
COUP-TFII.....	Chicken Ovalbumin Upstream Promoter
.....	Transcription Factor II
CR/UK.....	Cancer Research UK
DEPC.....	Diethyl Pyrocarbonate
DIG.....	Digoxigenin
DMEM.....	Dulbecco-Vogt Modified Egale's Medium
DMSO.....	Dimethylsulphoxide
dNTP.....	deoxyNucliotide Triphospate
EB.....	Elution buffer
EDTA.....	Ethylene Diamine Tetra-Acetic acid
EtBr.....	Ethidium Bromide
FCS.....	Foetal calf serum
FISH.....	Fluorescence In Situ Hybridisation
Fu.....	Fused
GCPS.....	Greig Cephalopolsyndactyl Syndrome
GFP.....	Green Fluorescent Protein
GI.....	Gastrointestinal
G6PDA.....	Glucose-6-Phosphate Dehydrogenase A
HH.....	Hedgehog
<i>HNF-3β</i>	Hepatocyte Nuclear Factor 3, beta
IRES.....	Internal Ribosomal Entry Site

KCM.....	Keratinocyte culture medium
<i>KRT</i>	keratin
LB.....	Liquid broth
LCM.....	Laser capture microdissection
MOPS.....	3-[N-morpholino] propane-sulphonic acid
mRNA.....	messenger RNA
NBCCS.....	Naevoid Basal Cell Carcinoma Syndrome
NCBI.....	National Centre of Biotechnology
NEB.....	New England Biolabs
NS.....	Normal skin
NSS.....	Normal sheep serum
PAPA.....	Postaxial Polydactyl type A
PBS.....	Phosphate buffer solution
PHS.....	Pallister-Hall syndrome
PTCH.....	Patched
RM.....	Ready Mix
rRNA.....	Ribosomal RNA
RT-PCR.....	Reverse transcriptase polymerase Chain reaction
RTS.....	Rubinstein-Taybi syndrome
SCC.....	Squamous Cell Carcinomas
SCS.....	Saether-Chozen Syndrome
SHH.....	Sonic Hedgehog
SLOS.....	Smith-Lemli-Opitz Syndrome
SMO.....	Smoothened
SSC.....	Standard Saline Citrate
STDNA.....	Salmon Testes DNA
SUP-FU.....	Suppressor-Fused
TBE.....	Tris-borate EDTA
TFIID.....	Transcription Factor II D
T_m	Melting temperature
tRNA.....	Transfer RNA
TRRM.....	Terminator ready reaction mix
UV.....	Ultraviolet
VIM.....	Vimentin

LIST OF FIGURES

CHAPTER 1: Introduction

Figure 1.1: Diagrammatic representation of the structure of human skin and its appendages.	28
Figure 1.2: Haematoxylin Eosin (H & E) staining of thin skin indicating different compartments of skin and hair follicle.	31
Figure 1.3: Summary of the major consensus patterns of keratin expression in normal epidermis and epidermal appendages (Lane and McLean, 2004).....	33
Figure 1.4: The different layers of the basement membrane zone at the dermal-epidermal junction.	36
Figure 1.5: Diagrammatic representation of hair follicle.	42
Figure 1.6: Different stages of hair follicle morphogenesis.....	45
Figure 1.7: Hair follicle cycle.	46
Figure 1.8: Schematic representation of the Wnt signaling pathway in follicle development.	49
Figure 1.9: Nodular basal cell carcinoma.	56
Figure 1.10: Nodular basal cell carcinoma presenting as a waxy translucent papule with central depression and a few small erosions.	56
Figure 1.11: Superficial basal cell carcinoma.	56
Figure 1.12: Larger superficial basal cell carcinoma.	57
Figure 1.13: Morpheaform infiltrating basal cell carcinoma.	57
Figure 1.14: Histology of nodular basal cell carcinoma, nodular aggregates (indicated by black arrows) of basalioma cells are present in the dermis (Ramsey, 2004).	58
Figure 1.15: Histology of superficial basal cell carcinoma.	59
Figure 1.16: Histology of morpheaform basal cell carcinoma.....	59
Figure 1.17: Overview of the SHH-PTCH-GLI signal transduction pathway.....	64
Figure 1.18: The genomic structure of the retrovirus and the changes that take place during integration into the host genome.	76
Figure 1.19: An overview of retroviral replication.	79
Figure 1.20: Basic principles of retroviral transduction.	80

CHAPTER 2: Materials and Methods

- Figure 2.1:** Diagram showing the plasmids used and the cloning sites of EGFP-GLI1 fusion protein construct into the SIN-IP-GFP retroviral vector to generate SIN-EGFP-GLI1 retroviral vector..... 92
- Figure 2.2:** Vectors used and the cloning sites to generate SIN-GLI1-EGFP retroviral vector. 93
- Figure 2. 3:** Diagram showing GLI1 constructs used to transform baby rat kidney cell line and GLI1 construct used to transduce human primary keratinocytes and also expected mRNA transcripts from these cell lines. 94
- Figure 2. 4:** SIN-EGFP-GLI1-mNLS (mutated-Nuclear-Localisation-Signal) construct. 95
- Figure 2.5:** Different components of northern blot apparatus and how it was assembled. 105
- Figure 2.6:** Features of pCRII-TOPO vector map in which *SMO*, *SUP-FU*, and *GLI2* were cloned, and sequence surrounding the TOPO cloning site..... 125
- Figure 2.7:** A diagrammatic representation of the *GLI2* (1.5 kb and 296 bp) anti-sense and sense probes generated from h*GLI2*-1.5 kb-pCRII-TOPO..... 133
- Figure 2.8:** A diagrammatic representation of the *KRT14* 1.2 kb anti-sense and sense probes generated from *KRT14*-1.2 kb-PGEM..... 134
- Figure 2.9:** A diagrammatic representation of the *FOXE1* 332-bp anti-sense and sense probes generated from *FOXE1* (UTR-332 bp)-PGEM plasmid..... 135

CHAPTER 3: Analysis of SHh Pathway Genes in Normal Skin, BCC and GLI1 transduced Human Primary Keratinocytes

- Figure 3.1:** Northern blot analysis of *GLI1* and β -*ACT* mRNA expression in polyclonal (pc) *GFP-GLI1-E1A* transformed baby rat kidney cell line, BCC, normal skin (NS) and HaCat. 159
- Figure 3.2:** Northern blot analysis of *GLI1*, *GLI2*, *PTCH* and β -*ACT* mRNA. In polyclonal (pc) *GFP/GLI1-E1A* transformed baby rat kidney, EGFP infected normal skin (N/S) primary keratinocytes, *GLI1/EGFP* infected N/S primary keratinocytes. HaCat, A375, NS primary keratinocytes cell lines..... 160
- Figure 3.3:** RT-PCR agarose gel showing *GLI1*, *GLI3*, *SUP-FU*, *SMO*, *COUP-TFII*, *TFIID*, *PTCH*, α -*TUB* (Alpha-Tubulin) and *KIF4* expression. In total RNA samples

from basal cell carcinoma, normal skin, spontaneously immortalised keratinocytes (HaCat), A375 melanoma, <i>GLII</i> -transduced primary keratinocytes (<i>GLII</i> -primary keratinocytes) and <i>GLII</i> -transduced 10T1/2 mouse fibroblast (<i>GLII</i> -10T1/2) and EGFP-transduced primary keratinocytes (Primary keratinocytes) cells.....	166
Figure 3.4: Showing different <i>GLI2</i> isoforms.....	169
Figure 3.5: RT-PCR of α/β <i>GLI2</i> transcript from basal cell carcinoma, normal skin, spontaneously immortalised keratinocyte (HaCat) cell line, primary keratinocytes, A375 melanoma cells, <i>GLII</i> -transduced primary keratinocytes (<i>GLII</i> -primary keratinocytes), <i>GLII</i> -transformed mouse fibroblast cells (<i>GLII</i> -10T1/2).	170
Figure 3.6: Real-time-RT-PCR analysis showing induction or repression of <i>GLII</i> , <i>GLI2</i> , <i>GLI3</i> , <i>PTCH</i> , <i>SMO</i> , <i>KIF4</i> and α - <i>TUB</i> genes expressed in basal cell carcinoma (BCC) relative to normal skin (control). Genes expressed in spontaneously immortalised keratinocytes (HaCat), A375 melanoma and <i>GLII</i> -transduced primary-keratinocytes (<i>GLII</i> -primary keratinocytes) relative to control EGFP-transduced primary keratinocytes (EGFP-primary keratinocytes).....	175
Figure 3.7: (A) Dermal papilla, outer root sheath and epidermis before Laser capture micro-dissection (LCM), after LCM and LCM caps with captured cells. (B) RT-PCR showing <i>GLII</i> expression in dermal papilla and outer root sheath in normal skin and there is no <i>GLII</i> expression in cells captured from epidermis. <i>GLI2</i> , <i>GLI3</i> , <i>PTCH</i> , α -Tubulin (α - <i>TUB</i>) and β -Actin (β - <i>ACT</i>) are all expressed in dermal papilla, outer root sheath and the epidermis. The negative control –RT sample (dermal papilla with no reverse transcriptase) was negative for all the genes analysed.	179

CHAPTER 4: Localisation of *GLI2* in Normal Human Skin and BCC and its regulation of *GLI1*

Figure 4.1: <i>GLII</i> mRNA and protein expression in NHIS- <i>GLI2</i> human primary keratinocytes.....	198
Figure 4.2: In-situ hybridisation analysis of <i>KRT14</i> expression in BCC and normal skin (wax sections using citrate buffer method).	202
Figure 4.3: In-situ hybridisation analysis of <i>GLI2</i> expression in BCC (wax section using citrate buffer method).	202
Figure 4.4: In-situ hybridisation analysis of <i>GLI2</i> expression in normal skin (wax sections using citrate buffer method).....	203
Figure 4.5: In-situ hybridisation analysis of <i>GLI2</i> expression in BCC (wax sections with proteinase K method).....	203

Figure 4.6: In-situ hybridisation analysis of <i>KRT14</i> expression in BCC (wax sections with proteinase K method).....	204
Figure 4.7: In-situ hybridisation of <i>GLI2</i> and <i>KRT14</i> expression in normal skin (frozen sections using citrate buffer method).....	205
Figure 4.8: In-situ hybridisation analysis of <i>GLI2</i> and <i>KRT14</i> expression in BCC (frozen section using citrate buffer method).....	206
Figure 4.9: In-situ hybridisation analysis of <i>GLI2</i> expression in BCC and normal skin frozen section (using citrate method).	208

CHAPTER 5: FOXE1 Expression in Normal Skin and BCC

Figure 5.1: <i>FOXE1</i> mRNA localisation in BCC frozen sections (using Citrate method).	221
Figure 5.2: <i>FOXE1</i> mRNA localisation in normal skin frozen sections (using citrate method).	222

CHAPTER 6: Effects of EGF on Pattern of Gene Expression in GLI1 over expressing Keratinocytes

Figure 6.1: Change in EGFP-GLI1-primary keratinocyte cell morphology when cultured with growth supplement.	232
Figure 6.2: Expression of EGFP/GLI1 in primary keratinocytes cultured with EGF and the change in cell morphology of these cells.	233
Figure 6.3: Expression of EGFP/GLI1 that has mutated Nuclear Localisation Signal (EGFP/GLI1mNLS) in primary keratinocytes cultured with EGF.	234
Figure 6.4: Real-time RT-PCR analysis showing induction or repression of <i>GLI1</i> , <i>GLI2</i> , <i>GLI3</i> , Patched (<i>PTCH</i>) and Smoothend (<i>SMO</i>) in GLI1, EGFP transduced primary keratinocytes cultured without growth supplement (-GS) and with epidermal growth factor. (+EGF) relative to control cells (EGFP primary keratinocytes cultured without growth supplement [EGFP-GS]).	239
Figure 6.5: Real-time RT-PCR analysis showing induction or repression of keratins <i>KRT14</i> , <i>KRT17</i> , <i>KRT19</i> and kinesin superfamily protein 4 (<i>KIF4</i>) in GLI1, EGFP transduced primary keratinocytes cultured without growth supplement (-GS) and with epidermal growth factor (+EGF).	241

Figure 6.6: Real-time RT-PCR analysis showing induction or repression vimentin (*VIM*) and Snail2 (*SNAI2*) in GLI1, EGFP transduced primary keratinocytes cultured without growth supplement (-GS) and with epidermal growth factor (+EGF)..... 243

Figure 6.7: Western blot showing expression of Vimentin, E-Cadherin. Epidermal growth factor receptor (EGFR), Keratin 14 (K14), GLI1 and EGFP in EGFP/GLI1 transduced primary keratinocytes cultured with out growth supplement with EGF.... 245

Figure 6.8: Expression profile of scatter plot of EGFP/GLI1-primary keratinocytes cultured without growth supplement and with EGF..... 247

Figure 6.9: Affymetrix expression analysis of *GLI1*, *GLI2*, *PTCH*, vimentin (*VIM*), snail2 (*SNAI2*), keratins *KRT19*, *KRT17*, *KRT14*, smoothend (*SMO*) and *GLI3* in GLI1, EGFP transduced primarykeratinocytes cultured without growth supplement (-GS) and with EGF (+EGF). 250

Figure 6.10: RT-PCR analysis showing *VAV2*, *VAV3*, *VAV3.1* and β -Actin expression in GLI1-primary keratinocytes cultured without growth supplement (GLI1-GS) and with EGF (GLI1+EGF)..... 253

Figure 6.11: Real-time-RT-PCR analysis indicating no change in *VAV2* and *VAV3.1* expression in GLI1- and EGFP-transduced primary keratinocytes culture without growth supplement (GLI1-GS, EGFP-GS) and with EGF (GLI1+EGF, EGFP+EGF) compared to control cells (EGFP-primary keratinocytes culture without growth supplement [EGFP-GS]). 254

Figure 6.12: RT-PCR analysis showing expression of *VAV2*, *VAV3*, *VAV3.1* and β -Actin expression in GLI1 and GLI1–mutant Nuclear Localisation Sequence (mNLS) transduced N/TERT-keratinocytes without growth supplement (GLI1-GS, GLI1mNLS-GS control) and with EGF (GLI1+EGF, GLI1-mNLS +EGF). 256

Figure 6.13: Real-time-RT-PCR analysis showing relative fold repression of *VAV2* and *VAV3.1* in GLI1- and GLI1–mutant Nuclear Localisation Sequence (mNLS) transduced N/TERT keratinocytes without growth supplement (GLI1-GS, GLI1mNLS-GS control) and with EGF (GLI1+EGF, GLI1-mNLS +EGF). 257

Figure 6.14: RT-PCR analysis showing expression of *VAV3.1* and *G6PDH* (control) in basal cell carcinoma (BCC) and normal skin (NS). 258

CHAPTER 7: Generating a Zp3-Cre-GLI1 Transgenic Mouse Model System

Figure 7.1: Diagrammatic representation of the mating scheme to generate *KRT14-Floxed-GFP-GLI1 Cre* female germ line transgenic mice. 268

Figure 7.2: Diagram of *KRT14-Floxed-GFP-GLI1* construct indicating the (F) Forward and (R) reverse primers and LoxP position. A 638 bp *Floxed* PCR product was expected from unrecombined *KRT14-Floxed-GFP-GLI1* allele and a 278 bp PCR product was expected from recombined *KRT14-GFP-GLI1* allele..... 271

Figure 7.3: RT-PCR of *KRT14-Floxed-GFP-GLI1* and *KRT14-Floxed-GFP-GLI1* cotransfected pPGK-*Cre* 293 cell line..... 273

CHAPTER 8: Conclusion

Figure 8. 1 A possible regulatory mechanism of GLI activity largely based on results from studies of *Drosophila* HH-signalling and a model of tumourgenesis resulting from constitutive HH/GLI signalling in human cancer..... 282

LIST OF TABLES

CHAPTER 2: Materials and Methods

Table 2.1: Amino acid residues of GLI1 nuclear localisation signals (NLS1, 2 and 3) and nuclear export signal (NES) and the positions of the residues mutated.....	95
Table 2.2: PCR primer sequence designed for RT-PCR from the NCBI data base (http://www.ncbi.nlm.nih.gov/) and the size of PCR product expected from these primers.	113
Table 2.3: List of total RNA samples extracted from different tissue and cultured cell used in RT-PCR and real-time-RT-PCR gene expression analysis.....	116
Table 2.4: Total RNA samples from transduced primary keratinocytes for real-time-RT-PCR gene expression analysis.....	117
Table 2.5: List of primers with optimum annealing temperature used in the RT-PCR and expected amplicon size for each set of primers.	118
Table 2.6: Primers used with DyNAmo™ SYBR® Green qPCR kit and the optimum annealing temperature and fluorescence data collection temperatures used for each set of primers.	122
Table 2.7: Components of the first strand cDNA synthesis reactions set up for Affymetrix analysis.	140
Table 2.8: Components of the reaction set up for the synthesis and labeling of cRNA using a BioArray High Yield RNA Transcript Labeling Kit (Cat No 900182, ENZO, Affymetrix)	142
Table 2.9: Hybridisation master mix for the arrays HG-U133A gene chip.....	145

CHAPTER 3: Analysis of SHH Pathway Genes in Normal Skin, BCC and GLI1 transduced Human Primary Keratinocytes

Table 3.1: Summary of results for PCR amplification from normal skin genomic DNA (samples M5, N37) using primers designed for RT-PCR.....	163
Table 3.2: Summary of the data from RT-PCR 1% agarose gel from Figure 3.4. Showing number of total RNA samples from Basal Cell Carcinoma (BCC), normal skin, spontaneously immortalised keratinocytes (HaCat), primary keratinocytes, A375 melanoma, <i>GLI1</i> -transduced primary keratinocytes (<i>GLI1</i> -primary keratinocytes) and <i>GLI1</i> -transduced 10T1/2 mouse fibroblast (<i>GLI1</i> -10T1/2) cell lines that were positive	

for *GLI1*, *GLI3*, *SUP-FU*, *SMO*, *COUP-TFII*, *TFIID*, *PTCH*, *α-TUB* and *KIF4* expression..... 167

Table 3.3: Size of PCR products expected from different isoforms of human *GLI2* using Moh-a,bb and Moh-c, dd, *GLI2* α/β and *GLI2* γ/δ primers. 169

Table 3.4: Relative fold induction or repression of *GLI1*, *GLI2*, *GLI3*, *PTCH*, *SMO*, *KIF4* and *α-TUB* in basal cell carcinoma (BCC) relative to normal skin, and in spontaneously immortalised keratinocytes (HaCat), A375 melanoma and *GLI1* transduced primary keratinocytes (*GLI1*-primary keratinocytes) relative to control *EGFP*-transduced primary keratinocytes (*EGFP*-primary keratinocytes) and the average fold induction or repression from all the samples. 176

CHAPTER 4: Localisation of *GLI2* in Normal Human Skin and BCC and its regulation of *GLI1*

Table 4.1: *GLI2* and *KRT14* expression in normal skin and basal cell carcinoma..... 207

CHAPTER 5: FOXE1 Expression in Normal Skin and BCC

Table 5.1: In-situ hybridisation of *FOXE1* mRNA expression in basal cell carcinoma and normal skin 223

CHAPTER 6: Effects of EGF on Pattern of Gene Expression in *GLI1* over expressing Keratinocytes

Table 6.1: PCR products amplified from cDNA from *GLI1* and *EGFP* (control) transduced primary keratinocyte cultured without growth supplement and with EGF.237

Table 6.2: Real-time-RT-PCR analysis showing relative fold induction or repression of *GLI1*, *GLI2*, *GLI3*, patched (*PTCH*), vimentin (*VIM*), Snail2 (*SNAI2*), keratins *KRT19*, *KRT17*, *KRT14*, smoothend (*SMO*) and Kinesin superfamily protein 4 (*KIF4*) in *GLI1*-primary keratinocytes cultured without growth supplement (-GS) and *GLI1*, *EGFP* primary keratinocytes cultured with EGF (+EGF) relative to control (*EGFP* primary keratinocytes cultured without growth supplement). 244

Table 6.3: Relative fold induction or repression of *VAV2*, *VAV3* and *VAV3.1* in *GLI1* and *EGFP* transduced primary keratinocytes cultured without growth supplement (-GS) and with EGF (+EGF). Also in *GLI1*-mutated Nuclear Localisation Signal (*GLI1*-

mNLS) transduced N-TERT keratinocytes cultured without growth supplement and with EGF..... 258

CHAPTER 7: Generating a Zp3-Cre-GLI1 Transgenic Mouse Model System

Table 7.1: Genes carried by transgenic litter one and two from the second (female) founder line. None of the litters were positive for recombined *KRT14-GFP-GLI1* gene.
..... 273

PRESENTATIONS AND PUBLICATIONS

I have presented the work described in this thesis at the following scientific conferences:

19th Gene & Cancer Meeting University of Warwick, UK, December 2002. GLI2 is expressed in normal human epidermis and BCC and induces GLI1 expression by binding to its promoter (poster presentation).

International Investigation of Dermatology Meeting Fontainebleau Hilton Miami Beach, Florida USA, April 30th-4th May 2003. GLI2 is expressed in normal human epidermis and BCC and induces GLI1 expression by binding to its promoter (poster presentation)

Work presented in this thesis has also been published or submitted for publication:

Mohammed S Ikram, Graham W Neill, Gerhard Regl, Thomas Eichberger, Anna-Maria Frischauf, Fritz Aberger, Anthony Quinn and Mike Philpott. GLI2 Is Expressed in Normal Human Epidermis and BCC and Induces GLI1 Expression by Binding to its Promoter. *Journal of Investigative Dermatology* (2004) **122**, 1503–1509.

Thomas Eichberger, Gerhard Regl, **Mohammed S Ikram**, Graham W Neill, Michael P Philpott, Fritz Aberger and Anna-Maria Frischauf. FOXE1, A New Transcriptional Target of GLI2 Is Expressed in Human Epidermis and Basal Cell Carcinoma. *Journal of Investigative Dermatology* (2004) **122**, 1180–1187

Graham W Neill^{1*}, Wesley J Harrison¹, **Mohammed S Ikram**¹, Tomos D Williams¹, Judith L Green^{1,3}, Lucy Ghali^{1,4}, Anne-Marie Frischauf², Edel O'Toole¹, Fritz Aberger², Michael P Philpott¹. Attenuation of EGFR-ERK signalling by GLI1 highlights a mechanism to promote the epithelial phenotype and may account for the poor metastatic potential of basal cell carcinoma (submitted JBC).

CHAPTER 1

Introduction

1.1.0 Structure of skin

The integumentary system consists of skin together with its appendages; hair follicles, apocrine sebaceous and sweat glands and nails. A diagrammatical representation of the structure of skin is given in **Figure 1.1**. The skin covers the entire body and is the largest organ of the body making up in total about 16% of normal body weight. Its function is to act as a barrier to physical, biological and chemical agents, as well as to ultraviolet (UV) radiation. The barrier function also prevents dehydration by controlling loss and gain of fluid. Other functions include sensory and thermoregulatory roles, vitamin D synthesis, immune surveillance, excretion of wastes through sweat glands, sociosexual communication and reproduction, by virtue of its appearance and smell (e.g. hormones and pheromones). The skin consists of two layers epidermis and dermis during embryogenesis epidermis is derived from the ectoderm and the dermis from the mesoderm and these two layers are firmly attached to each other. Skin is also classified according to thickness of the epidermis, thick or thin. Thick skin covers palms and soles and has sweat glands, erector pili muscles, and sebaceous glands, but lacks hair follicles. Thin skin covers most of the body contains hair follicles, erector pili muscles, sweat glands, and sebaceous glands.

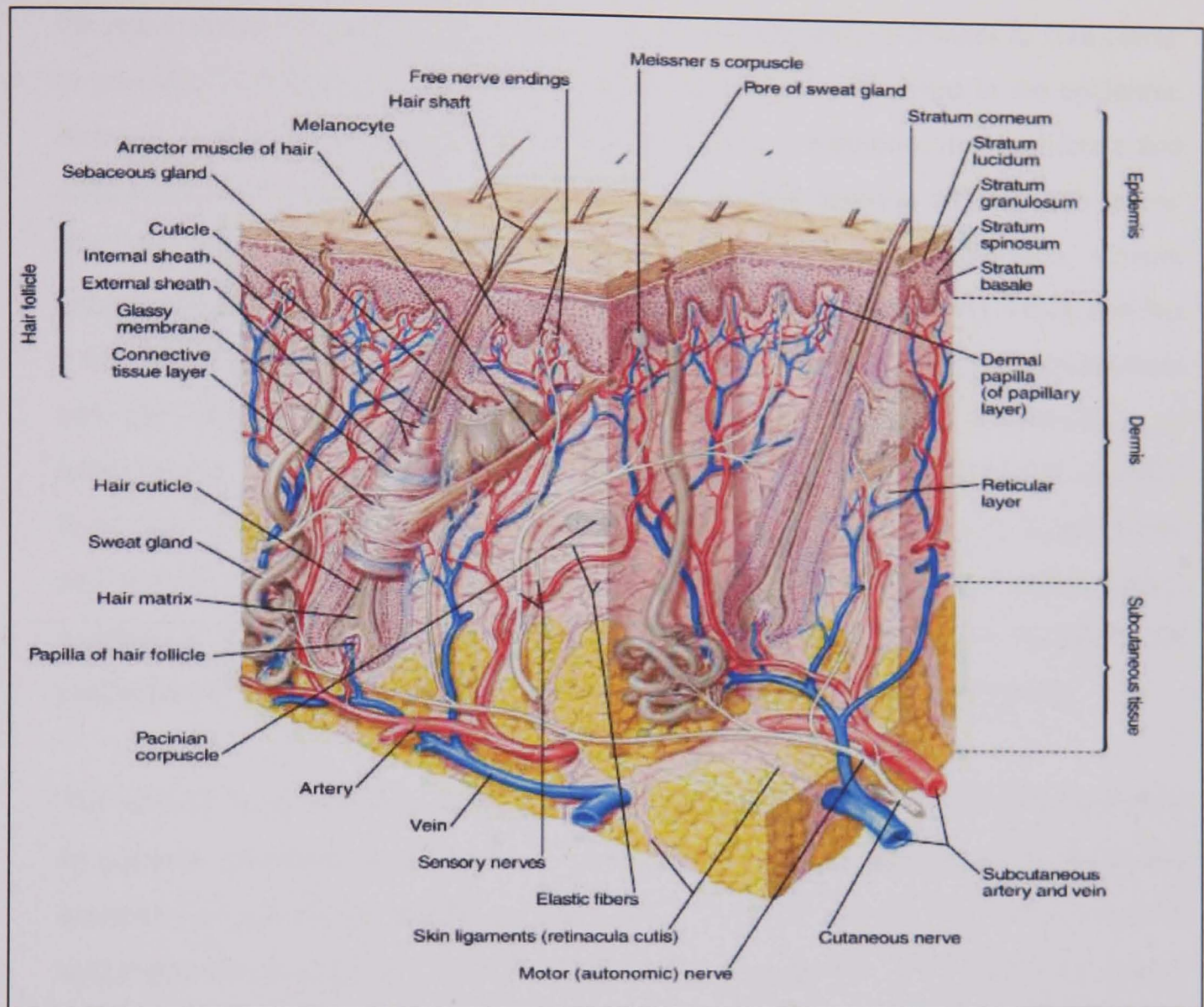


Figure 1.1: Diagrammatic representation of the structure of human skin and its appendages, image was obtained from http://www.healthandage.com/html/art_popup/skin1.htm.

1.1.1 The epidermis.

The epidermis is the major protective layer 80% of which consists of keratinocytes and the rest consists of; Melanocytes which produce melanin and contributes to skin colour to provide UV protection, Dendritic (Langerhans) cells are involved in the epidermal immune system, Merkel cells have a sensory function. Keratinocytes proliferate and differentiate from the basal layer and rise to the surface forming different sub layers. The four main layers of epidermis are stratum basal, stratum spinosum, stratum granulosum and stratum corneum (**Figure 1.2**) reviewed in (Watt, 1989). Thick skin has a fifth layer called the stratum lucidum which is found between the stratum granulosum and the stratum corneum. These layers reflect the sequential differentiation of keratinocytes. As keratinocytes migrate from the basal layer to the outermost cornified layer, they are committed to terminal differentiation and lose the ability to proliferate and are shed from the surface as dead cells. The process of terminal differentiation involves a series of biochemical and morphological changes, which result in the production of anucleated cornified keratinocytes that form the stratum corneum.

The stratum basal layer has a single layer of cells attached to the basement membrane by adheren junctions these consist of hemidesmosomes that containing integrins and desmosomes containing cadherins. The majority of cells in this layer are mitotically active and are involved in continual renewal of the epidermis. These mitotically active cells derive from a population of putative stem cells that are thought to reside in the deep ridges of the skin and at the tips of the dermal papillae in interfollicular epidermis (Jensen et al., 1999) or in the bulge region of the outer root sheath (ORS) of adult human hair follicles in hairy skin (Cotsarelis et al., 1990; Lyle et al., 1998b). Basal cells contain cytokeratins organised in bundles around the periphery of the nucleus and attached to desmosomes.

The stratum spinosum layer consists of several layers of irregularly shaped cells that display spiky projections. As cells from the basal layer loose contact with the basement membrane and are subsequently pushed up to form the stratum spinosum layer, some cells remain mitotically active and become progressively flattened. As they move up wards they start to acquire lamellar granules which contain epidermal lipids responsible for the barrier properties of the stratified corneum and more desmosomes for stronger cell to cell adhesion.

CHAPTER 1: Introduction

The stratum granulosum layer comprises of three to five layers of flattened cells which have lamellar granules containing lipids and keratohyalin granules within the cytoplasm. Keratohyalin granules contain pro-filaggrin, a precursor of filaggrin that bundles the keratin filaments together.

The stratum lucidum layer has several layers of flattened cells without nuclei and organelles, and these cells have keratin rich cytoplasm.

The stratum corneum layer consists of dead keratinised cells called squames or corneocytes. Keratin filaments polymerise by forming strong disulphide bonds. Filaggrin, a protein component of the keratohyalin granule is involved in this process. The cornified envelope forms due to the catalytic activity of the enzyme transglutaminase which crosslinks proteins such as involucrin (an insoluble cysteine rich protein) in the plasma membrane. Other proteins found as components of the cornified cell envelope include keratolinin, loricrin, small proline-rich proteins, the serine proteinase inhibitor elafin, filaggrin linker-segment peptide, and envoplakin. Lipids discharged by lamellar granules fill the intercellular spaces which contribute to the barrier properties of the epidermis. The lack of desmosomes in the cells that are closest to the outermost layer results in shedding of corneocytes from the skin (Latkowski, 1999).

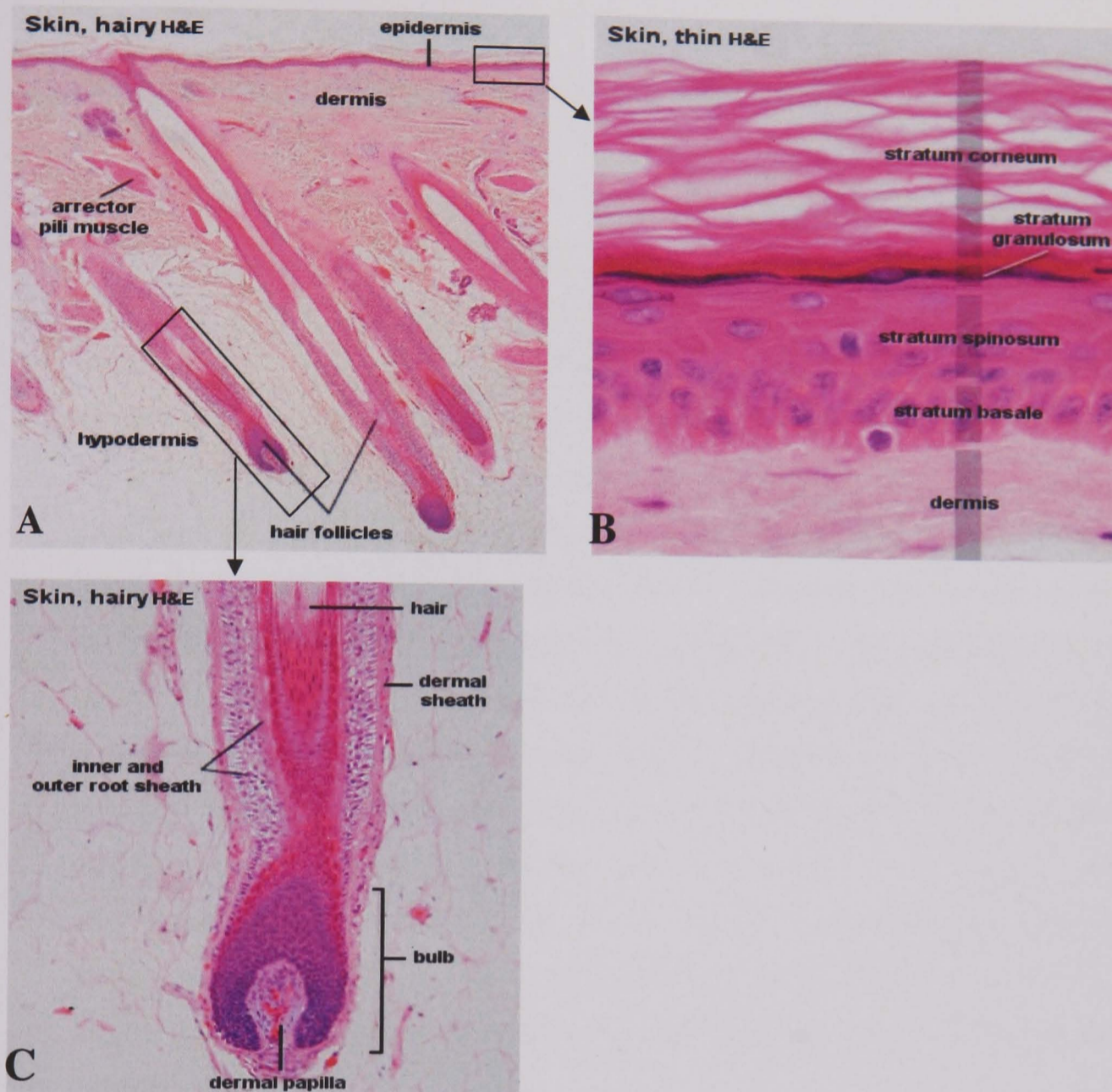


Figure 1.2: Haematoxylin Eosin (H & E) staining of thin skin indicating different compartments of skin and hair follicle. (A) Showing the epidermis, dermis, hypodermis, erector pili muscle and hair follicles. (B) Different layers of the epidermis; stratum basale, stratum spinosum, stratum granulosum and stratum corneum. (C) Different regions of hair follicle; dermal papilla, bulb, inner & outer root sheath, dermal sheath and hair (Slomianka, 2002 <http://www.lab.anhb.uwa.edu.au/mb140/CorePages/Integumentary/Integum.htm>).

1.1.2 Keratins.

The cytoskeleton of all epithelial cells is formed from three groups of filaments, actin (microfilaments), tubulin (microtubules) and intermediate filaments. Keratins belong to the intermediate filament group of proteins. Recent genomic analysis has determined that there are total of 54 functional keratin genes of which 28 are type I keratins (acidic) and 26 type II keratins. Example of type I keratins are keratin K9 (K9) to K20, and type II keratins are K1 to K8 (Hesse et al., 2001; Hesse et al., 2004; Moll et al., 1982; Rogers et al., 2005; Rogers et al., 2004; Smack et al., 1994). In most cases type I and type II keratin subunits pair up and form heterodimers which are expressed according to epithelial type and in a differentiation-specific manner. For example, in simple epithelia, K8 and K18 are expressed and in basal layer of stratified epithelia K5 and K14 are expressed. The differentiating suprabasal layers are characterised by expression of keratin K1 and keratin K10 pair, whereas, keratin K6 and keratin K16 are not expressed in normal epidermis except in the outer root sheath (ORS) of hair follicle and junctional region of sublayers (Wilson et al., 1994). K6 and K16 pair is also constitutively expressed in certain stratified squamous mucosal epithelia and in the skin of palm and sole (Morgan et al., 1987). Expression of K6 and K16 is induced in wound healing epidermis, hyperproliferative epidermis such as psoriasis, squamous cell carcinomas and hypertrophic scarring (Machesney et al., 1998). Therefore, keratin expression has been used as specific epithelial cell marker to assess epithelial proliferation and differentiation (see figure **Figure 1.3** for expression profile of different keratins in normal skin).

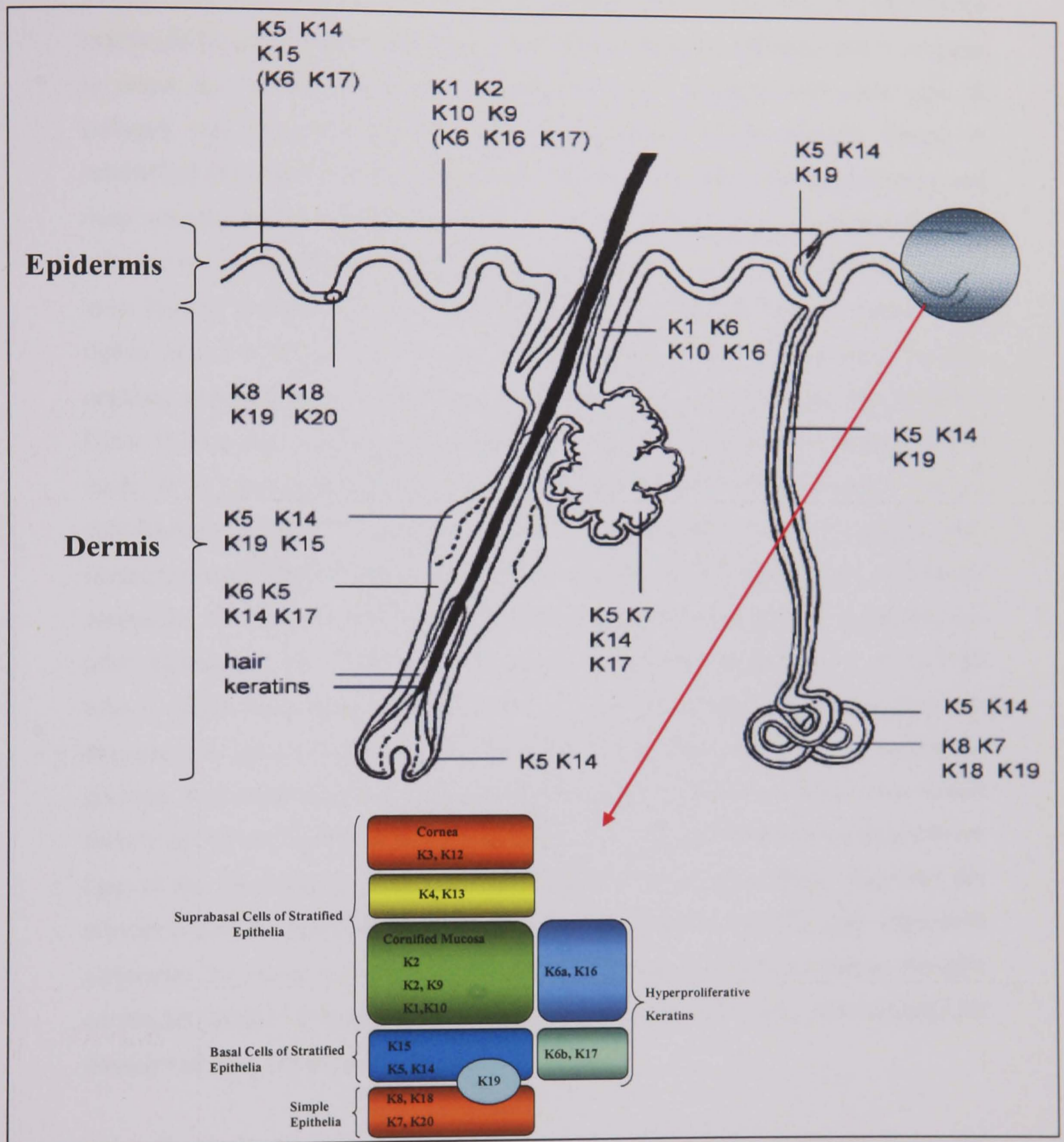


Figure 1.3: Summary of the major consensus patterns of keratin expression in normal epidermis and epidermal appendages (Lane and McLean, 2004)

1.1.3 The dermis.

Dermis consists mostly of fibroelastic connective tissue composed of extracellular matrix (ECM, see **section 1.1.5**) and is much thicker than the epidermis and is irregular in shape. It is mostly composed of interwoven type I collagen with some type III collagen which provides the skin with its mechanical, tensile strength. Dermis is subdivided into superficial papillary dermis, which is in contact with the epidermis, and deep reticular dermis. Superficial papillary dermis is loosely woven and interdigitates with the epidermal ridges along the dermo-epidermal junction and contains thinner and more loosely arranged collagen and elastin fibres. The reticular dermis contains more tightly bound collagen fibres. At the arbitrary plane of this division there are sub-papillary plexus of blood vessels which supplies the avascular epidermis with nutrients. Other ECM material making up the dermis consists of an amorphous substance that is made up of glycosaminoglycans (GAGs) namely, hyaluronic acid, dermatan sulphate, chondroitin-6-sulphate, chondroitin-4-sulphate, and heparin sulphate. Dermis also contains; Sweat Gland, Sebaceous Gland (see **section 1.1.11**), Hair Follicle, Meissner's corpuscles, Pacinian corpuscles and free nerve endings that pass through the dermis and often extend into the underlying subcutaneous fat. Sweat Glands consist of a single tube, a coiled body and a superficial duct. They are involved in thermoregulation, as they cool the skin by producing sweat. Hair follicles generate from the epidermal tissue growing downward into the dermis and produce hair. Different structural areas of hair follicle can be seen in **Figure 1.1 and Figure 1.5**). Erector pili muscle is attached to the base of the hair follicle (**Figure 1.1 and Figure 1.2**). Cold or fright stimulates the muscle to contract and pulls the hair follicle up, causing it to stand up right. Meissner's corpuscles are receptors that detect light touch and soft, fleeting movements. Pacinian corpuscles function as receptors for deep pressure and vibration. Free nerve endings are sensitive to pain, temperature changes and itchiness.

The subcutaneous layer is below the dermis, it consists of loose connective tissue and fat (**Figure 1.1 and 1.2**). It acts as a protective cushion and helps to insulate the body by monitoring heat gain and heat loss. Not all authors consider this layer a part of the skin, but it definitely has a strong impact on the way the skin looks.

The cell types found in the dermis include fibroblasts, macrophages and mast cells (reviewed in (Haake, 1999)). The predominant cell type of the dermis is the fibroblast.

These cells synthesise and degrade connective tissue matrix proteins and a number of proteins that provide structural ECM and basement membrane framework involved in dermal modelling (Sorrell and Caplan, 2004; Wang et al., 2004). Fibroblasts migrate on and between the surfaces of collagen fibre bundles and promote the interaction between epidermis and dermis by synthesising growth factors/cytokines include the keratinocyte growth factor (KGF) 1 and 2, transforming growth factor- β 1 (TGF- β 1), platelet derived growth factor-A (PDGF-A), vascular endothelial growth factor (VEGF) and granulocyte/macrophage colony-stimulating factor (GM-CSF) (Maas-Szabowski and Fusenig, 1996; Smola et al., 1993) that are important in the regulation of normal skin physiology as well as in wound healing. This suggests that fibroblasts engage in paracrine and autocrine interactions in skin. Fibroblasts also exist as a highly diverse population (Sempowski et al., 1995). For example, the papillary dermis and reticular dermis have distinct fibroblast subpopulations with different characteristics (Sorrell et al., 2004).

1.1.4 The basement membrane zone dermal epidermal junction.

The basement membrane zone is at the interface between the epidermis and the dermis and its function is to strongly attach these two layers together and supports the avascular epidermis. Four layers have been identified within the basement membrane zone, these layers are; 1) The plasma membrane of the basal keratinocyte, which is penetrated by hemidesmosomes, 2) The lamina lucida that contains laminin, bullous pemphigoid glycoprotein, anchoring filaments and sub-basal dense plates, 3) The lamina densa that contains collagen type IV and proteoglycans. 4) The collagen type VII rich-lamina fibroreticularis that contains anchoring fibrils (**Figure 1.4**). Fibroblasts and or keratinocytes are capable of synthesising many of the components of the basement membrane zone (McKay et al., 1994). However, the combination of both cell types leads to the correct assembly of the basement membrane zone (Bohnert et al., 1986).

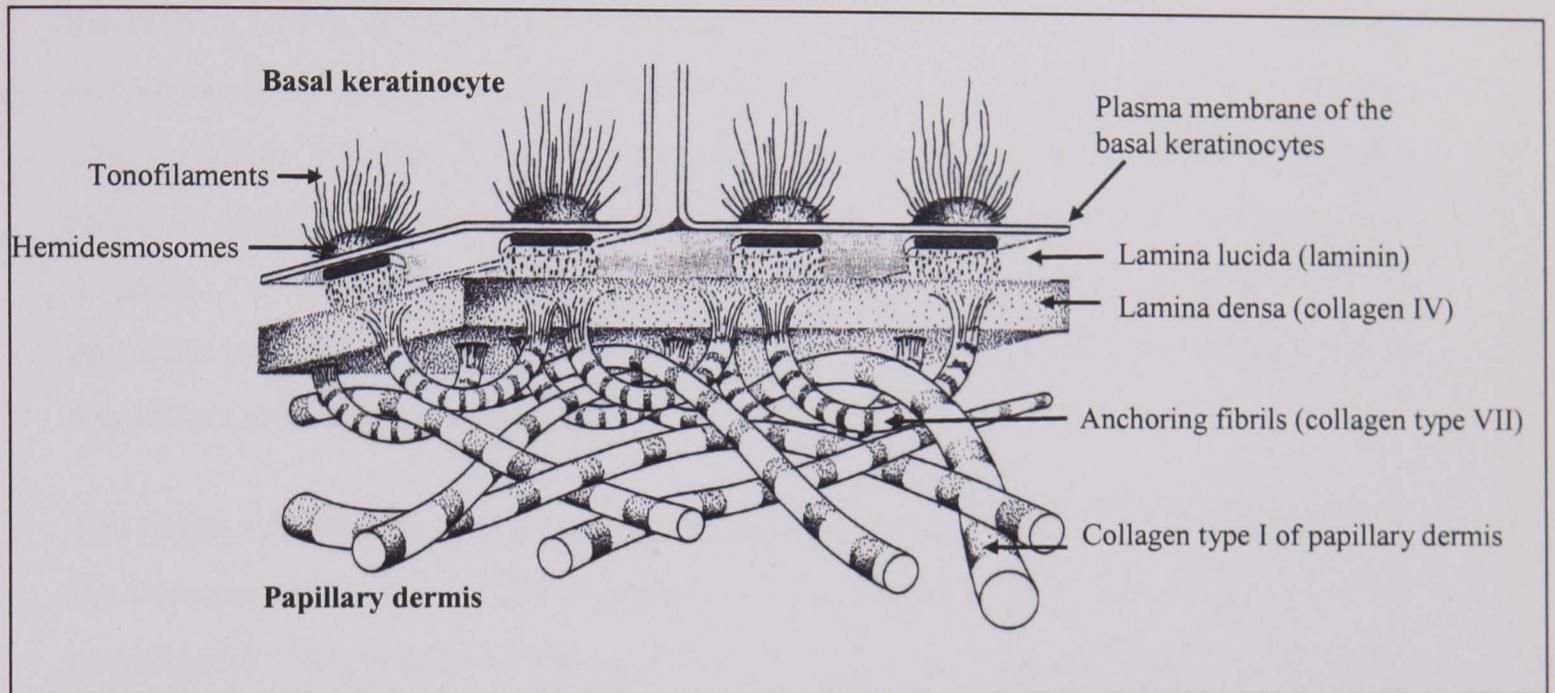


Figure 1.4: The different layers of the basement membrane zone at the dermal-epidermal junction (IBC Ltd, USA "Bioengineering of Skin Substitutes" handbook September 1997).

1.1.5 Extracellular matrix.

The extracellular matrix (ECM) is also known as the connective tissue or mesenchyme. ECM is composed of a mixture of proteins and polysaccharides in which cells are embedded. The two main classes of extracellular macromolecules are structural and adhesive proteins and proteoglycans. Within the structural proteins it is collagen that is the most abundant ECM component that provides tensile strength and helps to organise the matrix. In the dermis matrix macromolecules are secreted and oriented largely by fibroblasts. ECM degradation and remodeling appears to be tightly controlled (Alberts, 2002). Elastin, another structural protein, functions to give resilience to the matrix. The adhesive proteins link components of the ECM both to one another and to the surfaces of cells. For example, laminin, an adhesive protein, promotes the attachment of epithelial cells to the basement membrane and; fibronectin promotes the attachment of fibroblasts and other cells to the ECM in the dermis (Alberts, 2002).

The major cell surface receptors responsible for the attachment of cells to the ECM are the transmembrane glycoproteins, integrins. The extracellular portion of integrins binds to collagens, laminins and fibronectin whereas; the intracellular portion binds to the actin filaments of the cytoskeleton. This cytoskeleton-ECM linkage is responsible for providing the stability of cell-matrix junctions (Alberts, 2002).

The proteoglycans are polymorphic macromolecules consisting predominantly of molecules with a core protein and glycosaminoglycan (GAG) side chain extensions consisting of repeating disaccharide units. They are divided into intracellular, membrane-bound and extracellular groups. The extracellular molecules are relatively inflexible, take up a spiral shape and have following properties; negative charge, hygroscopic and hydrostatic. Proteoglycans regulate the function of several cellular processes cell proliferation, differentiation and exert control over the behavior of the tissue as a whole under normal physiological conditions, during morphogenesis and tissue repair processes. Proteoglycans, GAGs and the basal lamina associate to form large complexes of ECM, they can also bind potentially active ligand polypeptides and modulate their bioactivity to influence cell adhesion and or transmembrane signaling (Alberts, 2002). The ECM function is to provide structural support, substrates for cell adhesion, cell migration and to regulate cell behavior. This enables the cell to influence development, migration, proliferation, shape and function.

1.1.6 Epithelial mesenchymal interactions.

Mesenchyme (Dermis) plays a crucial role in epidermal homeostasis. Epidermis (Epithelia) influence the dermis with regards to structural remodelling, re-innervations and vascularisation (Kangesu et al., 1998; McKay and Leigh, 1991). Epithelial-mesenchymal interactions are orchestrated by a complex body of networks involving communications between cell to cell and cell matrix, cytokines and growth factors (Harris et al., 2001), (Fusenig, 1994).

The size and position of the developing hair follicles is determined by direct mesenchymal signals (Oliver and Jahoda, 1988). During hair follicle morphogenesis epithelial-mesenchymal interactions take place, this is initiated first by the dermal signal which results in the formation of a fully developed hair follicle (Hardy, 1992). Signalling between dermal papilla (DP) and hair follicle epithelium is crucial for hair follicle development and function (reviewed in (Jahoda and Reynolds, 1996). The importance of DP has been demonstrated in a variety of studies some of which are summarised in **section 1.1.9**.

The mesenchyme determines the fate of the epithelium. For example, the formation of epidermis and hair follicles is induced when cultured rabbit corneal epithelium is combined with embryonic hair-forming mouse dermis (Ferraris et al., 1994; Ferraris et al., 2000).

An understanding of the epithelial-mesenchymal interactions that takes place in skin has been brought about by wound healing studies. Initially, Rheinwald and Green (1975) showed that keratinocytes grown on an irradiated mouse fibroblast feeder layer have improved growth rates (Rheinwald and Green, 1975b). Since then, the importance of a dermal component for the improved clinical uptake of cultured epithelium has been well documented (Cuono et al., 1986; Navsaria et al., 1994).

In vitro skin models have been used to study the importance of epithelial mesenchymal interactions. These organotypic cultures are composed of keratinocytes and mesenchymal cells grown *in vitro* via an ECM at an air-liquid interface that induces differentiation. They also share similarities with wound healing, hyperproliferative and psoriatic skin (Asselineau et al., 1986; Leigh et al., 1995). These models have been

useful for elucidating the importance of epithelial-mesenchymal interactions on a number of processes including epidermal homeostasis, production and deposition of basement membrane and ECM components and secretion of diffusible factors (Ghosh et al., 1997; Krejci et al., 1991; Maas-Szabowski et al., 2001; Ralston et al., 1999; Saintigny et al., 1993; Smola et al., 1998).

1.1.7 Structure and function of the hair follicle.

Adult humans have an estimated 5 million hair follicles in the skin of which 1×10^5 hair follicles are found on the scalp. The growth of human scalp hairs is approximately 0.35 mm per day (Myers and Hamilton, 1951). In humans, hair functions in social and sexual interactions, it also acts as a sensory organ for skin, provides protection from the environment (e.g. eyelashes, eyebrows, nostril hairs and external ear hairs) and has insulating properties (Lavker, 1999).

The hair follicle is a dynamic and complex skin appendage that comprises both epithelial portions; outer root sheath, inner root sheath and matrix and dermal portions; dermal sheath and dermal papilla. The basic adult human late anagen hair follicle structure is shown in **Figure 1.1** and **Figure 1.5**. The hair follicle is arranged into several concentric cellular compartments. The innermost hair fibre or shaft consists of three layers; the cuticle, the cortex that forms the bulk of the hair fibre, and the medulla. Surrounding the hair fibre is the inner root sheath (IRS) composed of three layers: Henle's layer, Huxle's layer and the IRS cuticle. On the periphery of the IRS is the outer root sheath (ORS) compartment which is continuous with the epidermis. Cells in the distal ORS are similar in structure with the epidermis. The sebaceous gland arises from an outgrowth of ORS. The epithelial compartments of the hair follicle are bounded by a basement membrane and connective tissue sheath (dermal sheath).

1.1.8 Hair follicle bulb.

At the base of the hair follicle is located the follicle bulb consisting of the germinative and hair matrix epithelium, dermal sheath cells, melanocytes and endothelial cells and dermal papilla (DP) which is richly vascularised and contains abundant nerve endings. (Spearman, 1977). The germinative epithelium are highly proliferative cells (Weinstein and Mooney, 1980) which give rise to hair matrix cells that undergo lineage restricted differentiation to form the IRS and hair fibre. This differentiation process results in the expression of hair-specific keratins (reviewed in (Yu et al., 1993).

1.1.9 The dermal papilla.

The dermal papilla (DP) is an almond-shaped structure surrounded by the follicle bulb epithelium. The DP contains mesoderm-derived fibroblasts and receives a rich neurovascular supply. DP size is closely related with hair follicle size (Elliott et al., 1999). DP plays a pivotal role in the induction of hair follicle formation and growth (Jahoda et al., 1984; Sengel, 1976). DP implanted into vibrissal follicles in which the lower bulbs were excised has been shown to induce new bulb formation and hair growth (Oliver, 1967). Follicle formation is also induced when cultured sole epithelium is combined with DP and sole dermis in a recombinant study (Xing and Kobayashi, 2001). Whisker growth stops following amputation of DP (Oliver, 1966b) but commences when DP is re introduced (Jahoda et al., 1984). DP or cultured DP cells implanted into skin adjacent to the epidermis induce hair follicle formation (Jahoda, 1992; Reynolds and Jahoda, 1992).

1.1.10 Connective tissue sheath.

The connective tissue sheath (CTS), also known as the dermal sheath, is specialised mesenchyme that surrounds the epithelial components of the hair follicle (**Figure 1.1 and Figure 1.5**). It provides the follicle with structural support. The CTS is composed of a collagen rich ECM embedded with fibroblasts and endothelial cells, the latter of which forms perifollicular blood vessels. Epithelial-mesenchymal interactions occur between the CTS and ORS, which are important in hair follicle function. The CTS is adjacent to DP in the follicle bulb and migration may take place between both

compartments. CTS cells can form new DP and follicle bulb thus restoring hair function when the base of the follicle is amputated (Jahoda et al., 1992; Oliver, 1966a; Oliver, 1966b). In addition, the transplantation of male derived CTS onto female skin wounds leads to the production of new follicles and fibres in a human model without any apparent sign of rejection (Reynolds et al., 1999). In the context of wound healing, it has been hypothesised that CTS may provide a progenitor population for wound healing fibroblasts (Jahoda and Reynolds, 2001). Indeed, they express α -smooth muscle actin, similar to wound healing fibroblasts (Jahoda et al., 1991) and behave in a manner similar to dermal fibroblasts in an *in vivo* wound healing model in rats (Gharzi et al., 2003). In addition, both CTS and DP cells have been shown to display haematopoietic activity both *in vivo* and *in vitro* (Lako et al., 2002) as well as adipogenic and osteogenic differentiation *in vitro* (Jahoda et al., 2003).

1.1.11 Sebaceous gland.

The hair follicle is often associated with the sebaceous gland and together, is termed the pilosebaceous unit. The sebaceous gland develops from an outgrowth of the hair follicle ORS and is attached at the base of the infundibulum by a duct. The sebaceous gland is a holocrine gland that secretes sebum, a lipid rich substance required for processing the hair fibre and protecting the surface of the epidermis. Sebaceous glands are found all over the body, but they are more numerous in the scalp area and around the forehead, chin, cheeks and nose (Deplewski and Rosenfield, 2000).

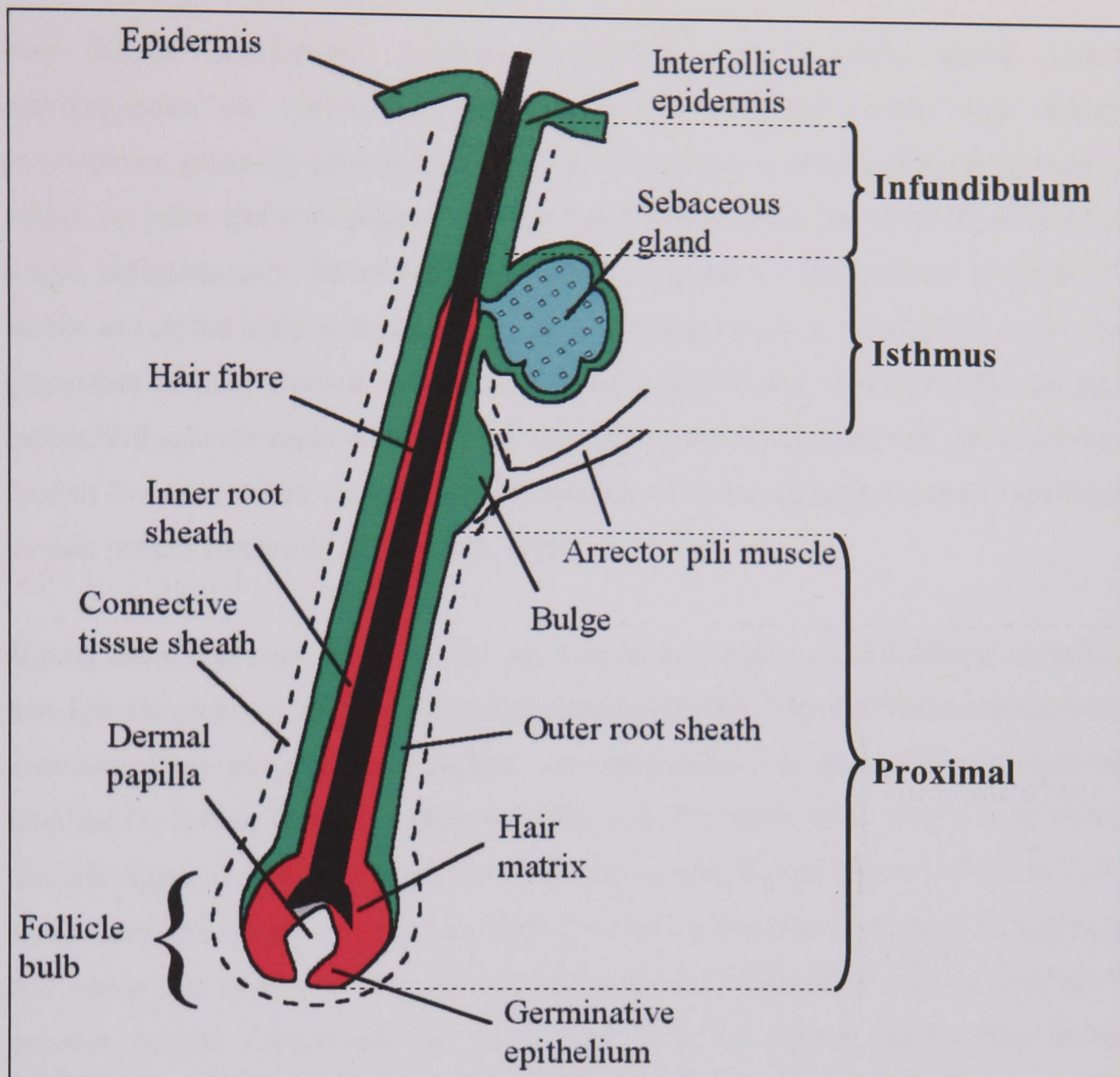


Figure 1.5: Diagrammatic representation of hair follicle. Longitudinally, the hair follicle is arranged into three distinct anatomical regions. 1) The infundibulum, distal upper end of hair follicle which extends from the interfollicular epidermis down to the opening of the sebaceous duct. 2) The isthmus, distal upper end of hair follicle which comprises the area of the sebaceous gland down to the bulge region, near the site of insertion of the arrector pili muscle. The bulge region is thought to be the reservoir for follicle epithelial stem cells. 3) The proximal, lower portion of the hair follicle which comprises the area just below the bulge arrector pili muscle complex right down to the base of the follicle including the bulb region. Diagram reproduced by kind permission of Centre for Cutaneous Research, Queen Mary University of London.

1.1.12 Hair follicle morphogenesis and hair growth cycle.

Hair follicle development commences around 8 to 9 weeks during human embryogenesis on eyebrows, eyelids, upper lip, chin and scalp. Hair follicle development generally expands in a symmetrical fashion to other regions of the embryo except on palm and sole regions. Not all hair follicles reach the same developmental stages simultaneously, for example, hair starts to appear on the eyebrow at around 17 weeks and on the scalp at around 18-21 weeks. Lanugo hairs is a term given to the first generation of hairs formed, which are fine and unpigmented. Most of these are shed before birth and are replaced by coarser hairs during the prenatal period. After birth hair growth is synchronised for the first few months, but soon changes to an asynchronous mosaic pattern (reviewed in (Philpott, 1998)).

During embryogenesis, hair follicles are formed as a result of coordinated signalling between the embryonic epithelial and mesenchymal cells. This epithelial-mesenchymal communication governs the induction, morphogenesis and differentiation processes required for follicle formation (Hardy, 1992). The first signal from dermis to epidermis 'dermal signal', induces the formation of the epidermal placode (Hardy, 1992). Next the signal from epidermis to dermis 'epithelial signal', causes the mesoderm to aggregate just below the epidermal placode to form a dermal condensate. This is destined to become the hair follicle and DP. As a result of a 'sec dermal signal', from dermal condensate to epidermal placode, the cells of the epidermal placode undergo proliferation and invade the dermis causing a downward growth into the dermis, eventually enclosing the DP. Further proliferation and differentiation of the follicular epithelial cells take place, resulting in the formation of a fully developed hair follicle (Hardy, 1992). A summary diagrammatic representation of different stages of human hair follicle morphogenesis is shown in **Figure 1.6**. (Philpott, 1998). **Stage 0**, Uniform ectoderm appears. **Stage 1**, Epidermal placode formation and mesenchymal aggregate. **Stage 2**, Hair germ elongates as cords of epithelial cells (called 'hair peg') with a convex proximal end into the dermis at a slight angle. dermal condensate remains adjacent to the convex proximal end of the hair peg. **Stage 3**, Hair peg grows into the dermis with a concave proximal end, still in contact with the dermal fibroblast condensate. **Stage 4**, Bulb region starts to develop at the proximal end of the hair peg and encloses the DP cells. Hair peg cells start to differentiate into the hair matrix and give rise to IRS. **Stage 5**, Hair peg and IRS elongates and DP cells are further enclosed

CHAPTER 1: Introduction

by the follicle epithelium. Buds develop towards the distal end of the growing hair peg which become the bulge region, sebaceous gland and in some hair follicle, the apocrine sweat gland. **Stage 6**, Hair follicle continues to elongate, the hair fibre shaft is formed by hair matrix cell differentiation and grows up into the developing hair canal. Further development of the bulge region, sebaceous gland and apocrine gland takes place. The apocrine gland only develops in axillary and pubic body regions. In other body regions, it atrophies. **Stage 7**, Hair follicle continues to elongate and the hair fibre elongates further up towards the developing distal hair canal. The sebaceous gland also continues further development. **Stage 8**, Maximum length of the hair follicle is reached and the hair fibre emerges from the surface of the epidermis. Morphogenesis is completed resulting in the appearance of a mature late anagen hair follicle.

Hair growth and cycle (**Figure 1.7**) in adult mammals has three distinct phases: Anagen phase, which is an active hair growth phase during which the hair fibre is produced; Catagen Phase, in which regression, shortening and partial degeneration of the follicle takes place and Telogen phase, is a resting phase where no cell proliferation takes place and the hair follicle awaits signals to re-enter anagen (Dry, 1926). During hair follicle cycling, only the upper part of the hair follicle is permanent but undergoes remodelling (Lindner et al., 2000).

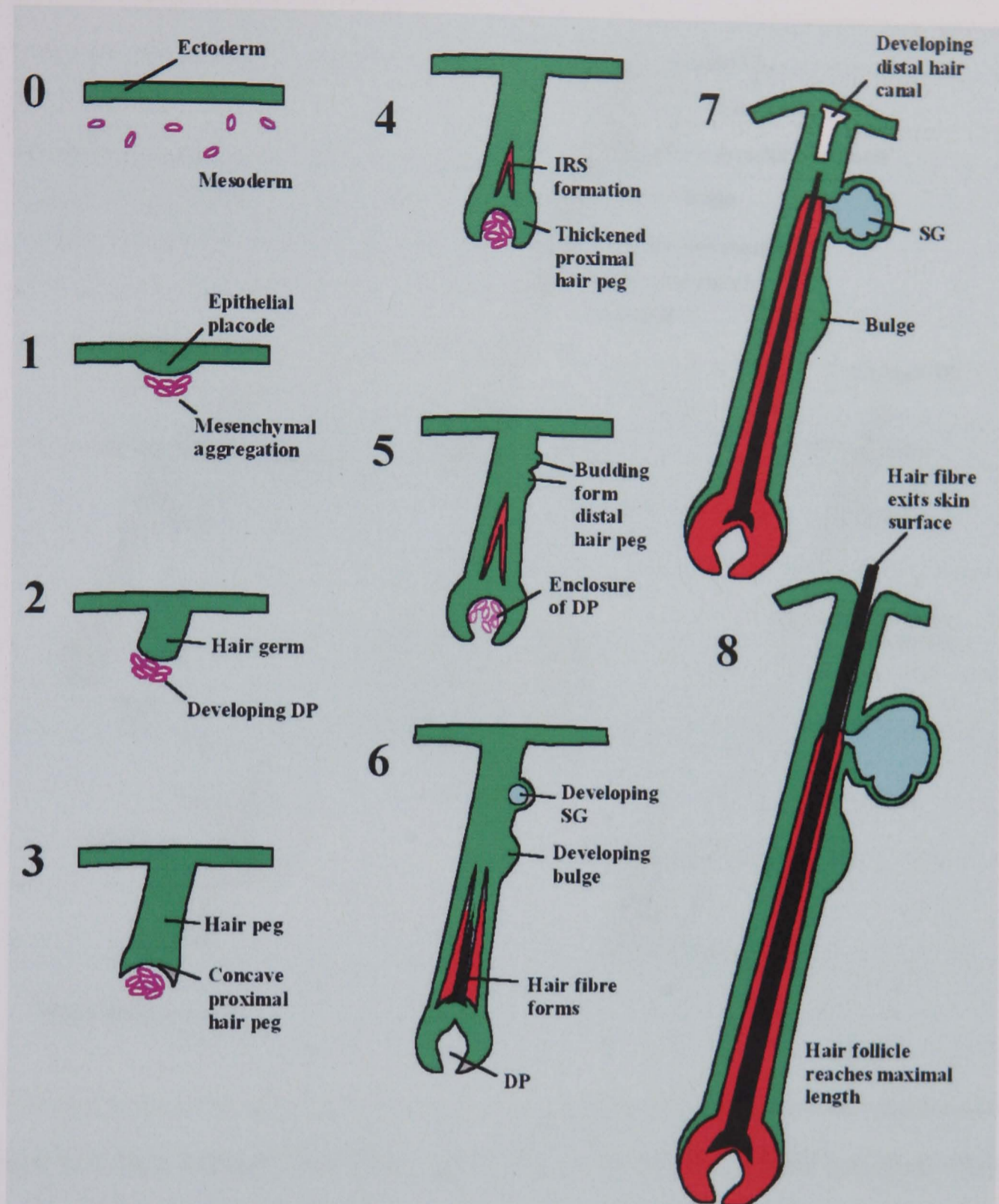


Figure 1.6: Different stages of hair follicle morphogenesis. Induction phase (stage 0-1) coordinated signalling between ectoderm and underlying mesenchymal cells induce placode formation. Morphogenesis phase (stages 2-4) appendage elongates into hair peg. Elongation phase (stages 5-8) further proliferation and differentiation into distinct compartments to form developed hair follicle. Abbreviations: DP, dermal papilla; IRS, inner root sheath; SG, sebaceous gland. (Centre for Cutaneous Research, Queen Mary College University of London).

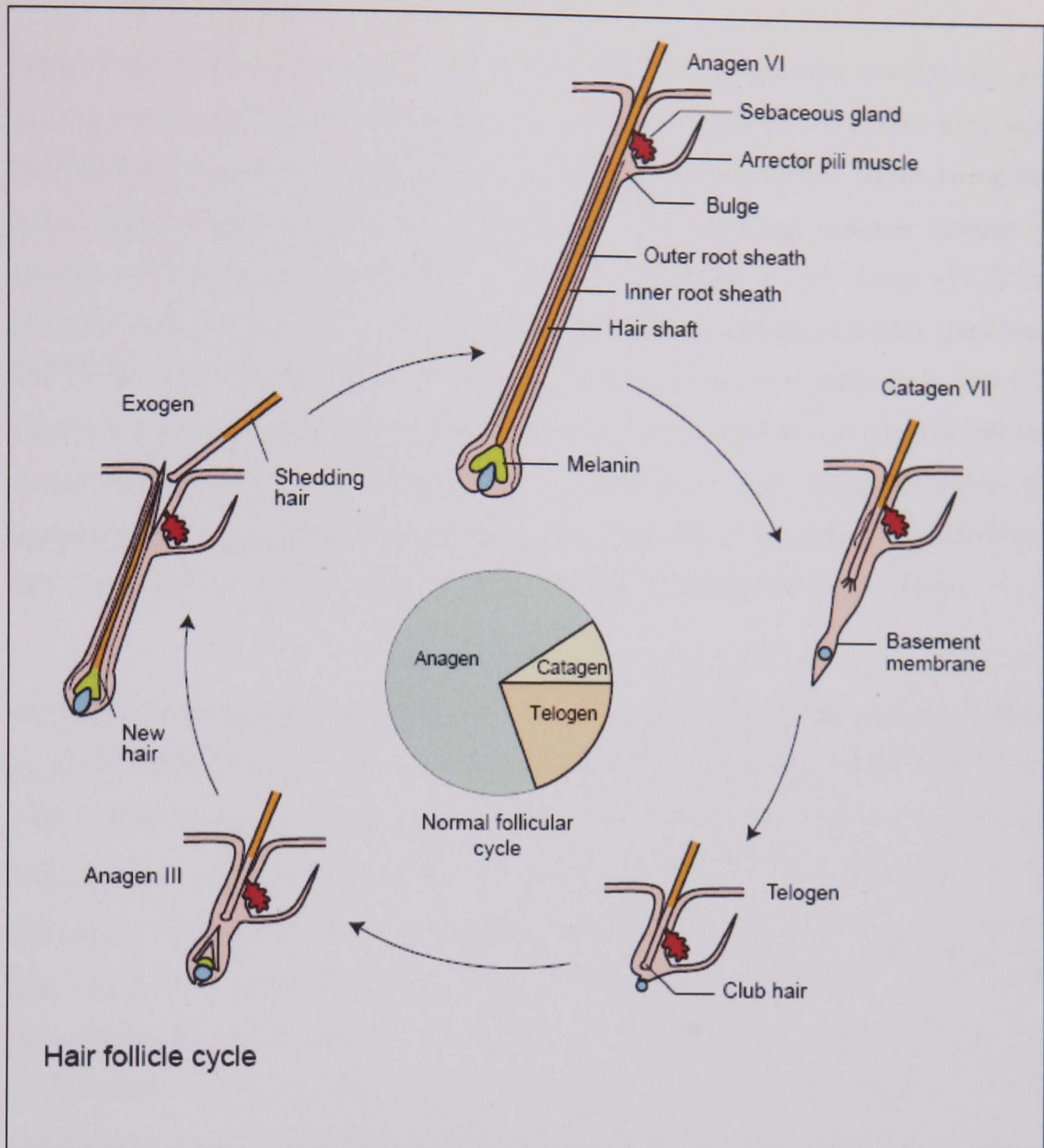


Figure 1.7: Hair follicle cycle. The normal hair cycle can be divided into four relatively distinct, successive periods: active growth phase (Anagen), a short transition phase with regression (Catagen), a resting phase (Telogen) and a shedding stage (Exogen). In the anagen phase, the follicle regenerates from the active epithelial stem cells, which reside in, or close to, the permanent ‘bulge’ region of the follicle. Although the size and length of the hair shaft are related to the size of the hair follicle and the duration of anagen, these attributes are remarkably diverse with body site and can change as a result of disease (Stenn and Paus, 2001)

1.1.13 Signalling pathways in hair follicle development and cycling.

Many of the processes that occur during hair follicle morphogenesis, development and cycling require epithelial-mesenchymal interactions. Several key regulators have been identified and implicated in these processes, although the first dermal signal during hair follicle development has yet to be determined. Wnt signalling pathway through β -catenin, Lymphoid enhancer binding factor 1 (Lef1) and T cell factor (TCF) are involved in the early stages of hair follicle morphogenesis and development (DasGupta and Fuchs, 1999; Millar, 2002). A simplified version of the Wnt pathway is shown in **Figure 1.8**. Wnts proteins are a family of secreted glycoproteins that control cell fate during development and differentiation. A number of Wnt family members are expressed at different stages of the developing hair follicle some of these include Wnt 3, Wnt 3A, Wnt 4, Wnt 5A, Wnt 7A, Wnt 10A and Wnt 10B (Reddy et al., 2001).

Wnts bind to frizzled (Fz) receptors as well as co-receptors lipoprotein receptor-related proteins 5 and 6 (LRP5/6), this activates Dishevelled (Dsd) proteins which then interact with a multi-protein complex consisting of glycogen synthase kinase-3 β (GSK-3 β), adenomatous polyposis coli (APC) and Axin that controls β -catenin levels in the cytoplasm. Phosphorylation of β -catenin by GSK-3 β is inhibited (reviewed in (Nelson and Nusse, 2004). This causes the stabilisation and accumulation of β -catenin which then translocates to the nucleus where it forms a transcription complex with the Lef-1/TCF family of DNA-binding proteins and switches on specific target genes including c-myc and cyclin D1, which then influence various developmental processes (Barker et al., 2000). Hair follicle placodes fail to develop in mice with a mutation in the β -catenin gene (Huelsenken et al., 2001). A new hair follicle in neo-natal mice was induced when a truncated and stabilised form of β -catenin was ectopically expressed in murine epidermis (Gat et al., 1998). In the absence of Wnt signalling, excess cytoplasmic β -catenin are phosphorylated and targeted for ubiquitination and degradation in the proteasome except for the pools of β -catenin that form the structural component of the adherens junctions that link cadherins through α -catenin to the actin cytoskeleton (reviewed in (Nelson and Nusse, 2004).

During embryonic development transcripts of sonic hedgehog (*SHH*) (see section 1.3.0) and secreted protein are expressed in epithelial cells of the proliferating hair follicles. SHH also influences proliferating hair follicle cells and adjacent aggregating dermal cells as indicated by their expression of SHH target genes *Ptch1* and *Glil* (see section 1.3.1 and section 1.3.2) (Bitgood and McMahon, 1995; Oro et al., 1997). SHH null mice form dermal condensate but fail to develop a mature hair follicle (Chiang et al., 1999a; Karlsson et al., 1999b). β -catenin null mice lack SHH expression which indicates that SHH is down stream of Wnt signalling in hair follicle development (Huelsken et al., 2001).

Bone morphogenic proteins (BMP) are a large family of secreted signalling molecules of the transforming growth factor- β (TGF- β) superfamily. BMP signalling has been shown to promote hair follicle cell differentiation. Inhibition of this pathway leads to impaired hair shaft differentiation (Kulesa et al., 2000). Noggin inhibits BMP signalling and is required for new hair growth (Botchkarev et al., 1999). Noggin also acts in conjunction with the Wnt pathway to activate Lef-1 for placode formation in first stage of hair follicle morphogenesis (Jamora et al., 2003). Lef-1 induces placode formation by simultaneously downregulating and upregulating E-Cadherin and P-Cadherin of the adherens junction, respectively. The cellular interactions that govern placode formation are thus represented by integrating different signalling pathways.

Other key mediators of hair follicle development include fibroblast growth factors, transforming growth factor- α and transforming growth factor- β , Delta 1, epidermal growth factor and hepatocyte growth factor (reviewed in (Millar, 2002) and recently, GATA-3 (Kaufman et al., 2003). Many of these growth factors and receptors are also important in hair cycling. For a detailed review of key mediators involved in hair cycling see (Stenn and Paus, 2001). The hair follicle plays a key role in epidermal homeostasis, wound repair and has been implicated in skin tumourigenesis (Miller et al., 1993; Morris et al., 2000).

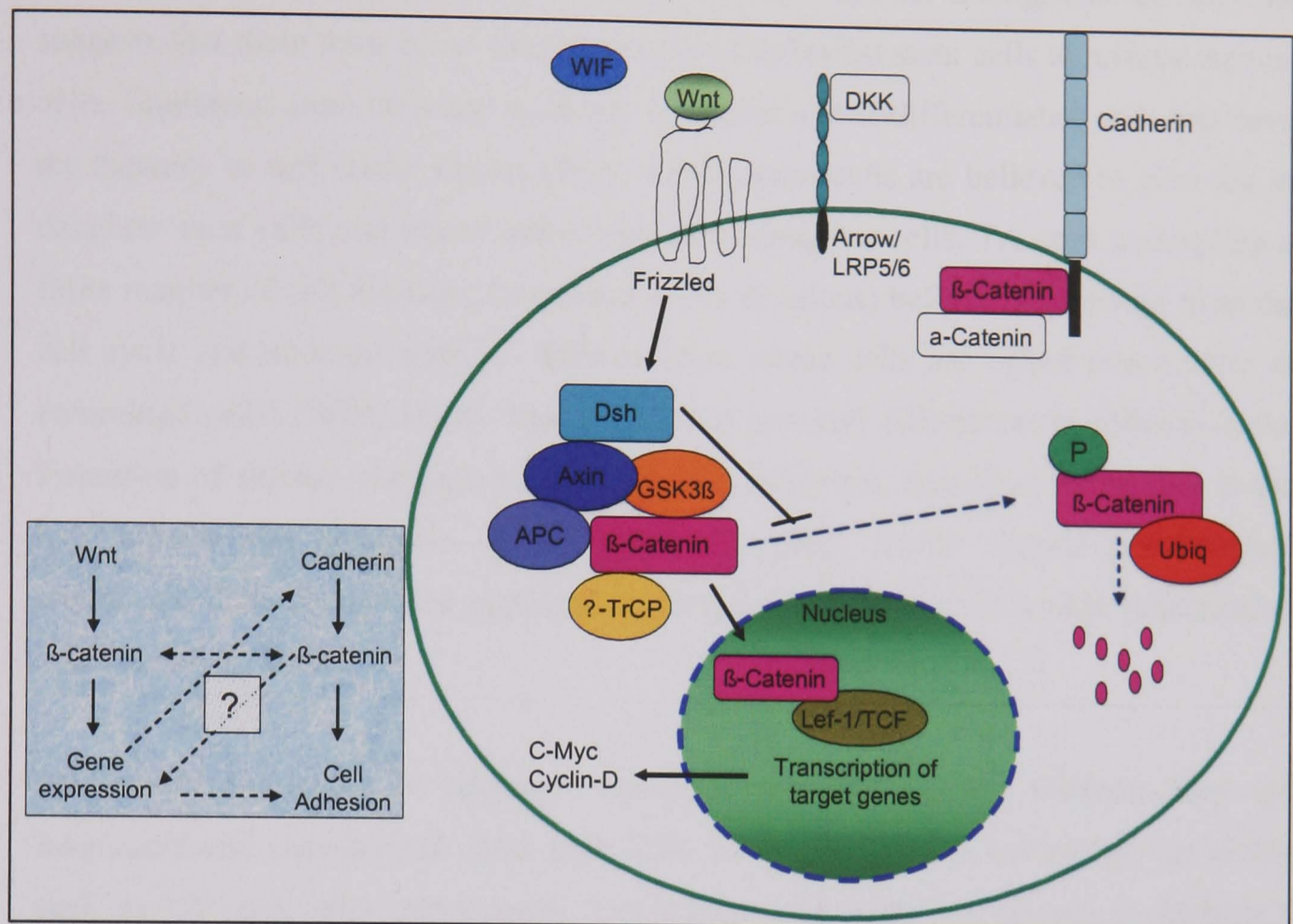


Figure 1.8: Schematic representation of the Wnt signalling pathway in follicle development. Wnts bind to frizzled (Fz) receptors as well as co-receptors lipoprotein receptor related proteins 5 and 6 (LRP5/6), this activates Dishevelled (Dsd) proteins which then interact with a multi-protein complex consisting of glycogen synthase kinase-3 β (GSK-3 β), adenomatous polyposis coli (APC), Axin and β -catenin (β -Catenin also exists in a cadherin bound form that regulates adhesion) and phosphorylation of β -catenin by GSK-3 β is inhibited. This causes the stabilisation and accumulation of β -catenin which then translocates to the nucleus where it forms a transcription complex with Lef-1/TCF family of DNA-binding proteins and switches on specific target genes including c-myc and cyclin D, which then influence various developmental processes. The Wnt pathway is also subject to regulation and feedback control by extracellular factors that bind Wnt [Wnt inhibitory factor (WIF) and Frizzled-related protein (FRP)] or the coreceptor LRP (Dickkopf). The box displays possible levels of interactions between Wnt signalling and cadherin-mediated adhesion indicated by dotted lines (Nelson and Nusse, 2004).

1.1.14 Epidermal stem cell characteristics and their niche.

The epidermis and its appendage undergo constant renewal throughout life and this suggests that there must be an existing source of epithelial stem cells to replace the lost cells. Epidermal stem cells are relatively quiescent and undifferentiated cells that have the capacity to self renew tissues (Watt, 1998). Stem cells are believed to give rise to daughter stem cells and transit amplifying (TA) daughter cells. TA cells undergoing a finite number of cell divisions (estimated at 3-5 divisions) before withdrawing from the cell cycle and undergo terminal differentiation (these cells are called post-mitotic or committed cells) (Watt, 1998). The endpoint of terminal differentiation pathway is the formation of stratum corneum in interfollicular epidermis, hair fibre production in the hair follicle and sebocytes in the sebaceous gland. Under normal physiological conditions, distinct stem cell populations maintain each epidermal lineage (Ghazizadeh and Taichman, 2001).

Stem cells are found in protected microenvironments (called 'niches'), they are innervated and vascularised. Here stem cells are protected from environmental insults such as UV and other carcinogens. The human hair follicle is known to harbour a population of stem cells, mostly located at fraction lower down from the bulge region (Rochat et al., 1994). Other studies contradictory to this study demonstrated that the hair follicle stem cell population is situated in the bulge region (Cotsarelis et al., 1990; Lyle et al., 1998b), and these cells are more proliferative than those of the interfollicular epidermis (Yang et al., 1993). The bulge region of the hair follicle is maintained throughout the hair cycle whereas the area below this undergoes remodelling. It also remains after hair plucking and its position below the epidermis allows the region to be spared if the overlying epidermis is damaged. As a result, it can contribute to the regeneration of the overlying epithelium. This has been shown in partial-thickness wounds where epidermal regeneration from the skin appendages is a well recognised event in humans (Irvin, 1981) and in mice (Argyris, 1976). In a wound repair mouse model and chimeric vibrissal follicle-transplantation study cells from the ORS of the upper follicle gave rise to the regenerated epidermis (Oshima et al., 2001; Taylor et al., 2000b). Thus, bulge cells act as a reserve of stem cells for both interfollicular and follicular epithelium in hairy skin. Its advantageous, protected and well vascularised position makes the bulge a very suitable niche for the presence of stem cells.

CHAPTER 1: Introduction

Ultrastructural studies propose that stem cells and their progeny are organised in an epidermal proliferative unit (EPU) in mouse epidermis (Christophers, 1971; Mackenzie et al., 1981; Potten, 1981). The slow cycling stem cells appear to make up 10% of the total basal cells and are found at the centre of the EPU. The more proliferative, transit amplifying cells are found at the periphery of the EPU (Christophers, 1971; Mackenzie et al., 1981; Potten, 1981).

In several studies using a cell surface $\beta 1$ integrin as primary keratinocytes stem cell marker (Gandarillas and Watt, 1997; Jones et al., 1995; Jones and Watt, 1993; Zhu and Watt, 1999) have shown that in human interfollicular epidermis, clusters of stem cells reside in the tips of the dermal papilla, they are also found in the bottom of the deep ridges of the interfollicular epidermis (Jensen et al., 1999; Jones et al., 1995). Actively dividing TA cells displayed a more scattered distribution away from the stem cell clusters in the basal layers and moved upwards to the suprabasal layers (Watt, 1998).

TA cells are also found to be more motile *in vitro* compared to stem cells (Jensen et al., 1999). Stem cells are normally slow cycling *in vivo* (Tomakidi et al., 1997), this is biologically significant as this conserves their proliferative potential and minimises DNA errors that could occur during replication thereby protecting the tissue from neoplastic transformation. Slow cycling cells are detected by administering mice with tritiated thymidine ($^3\text{H-TdR}$), a radioactively labelled DNA precursor (Bickenbach, 1981) or 5-bromodeoxy-uridine (BrdU), a thymidine analogue (Tomakidi et al., 1997). These labels get incorporated into the DNA of cells during S-phase of the cell cycle. During the chase period when no label is administered, the normal cycling cells continue to divide and the label gets diluted. However, cells that divide less frequently retain the label for longer periods and are known as 'label retaining cells' (LRCs). Based on this technique, label retaining studies have confirmed the model of the EPU in mouse epidermis (Morris et al., 1985). This technique has located LRCs to the bulge region of the hair follicle ORS in mice (Cotsarelis et al., 1990; Lavker et al., 1993; Morris and Potten, 1999). Human scalp skin grafted onto athymic mice shows label retaining cells in the bulge region (Lyle et al., 1998b). Where the chase period of more than 1 year shows the bulge region contains the slowest cycling cells of the entire cutaneous epithelium (reviewed in (Cotsarelis et al., 1999) thus, the bulge cells of the hair follicle may be the main repository of stem cells for the entire epidermis.

CHAPTER 1: Introduction

Keratinocytes in culture have a heterogeneous population with regards to their clonogenicity, based on the morphology criteria. Three types of colonies are produced from keratinocytes isolated from skin, these are holoclones, paraclones and meroclones (Barrandon and Green, 1987). Holoclones are large and circular colonies containing small regular shaped cells that have the greatest proliferative potential. These colonies have the ability to self renew and generate terminally differentiated cells that give rise to both meroclones and paraclones. Paraclones form small irregular shaped colonies and are believed to be post mitotic committed cells. These cells only possess a short replicative life span. Meroclones form an intermediary population group containing a mixture of cells of varying growth potential, giving rise to both paraclones and meroclones and are believed to be TA cells and keratinocyte size is inversely proportional to clonogenic potential in first passage (Barrandon and Green, 1985).

Further confirmation of the presence of stem cells in *in-vitro* culture comes from the use of sheets of cultured epithelial auto grafts, derived from non-hairy skin, used in the treatment of burn patients. These produce a normal epidermis that persists for several years (Compton et al., 1998). These observations confirm the survival of stem cells *in vitro* and that stem cells from the hair follicles are not mandatory for the long term upkeep of interfollicular epidermis. The identification of some stem cell markers is now leading to the elucidation of molecules and signalling pathways involved in the process of epidermal cell fate and regulation.

1.1.15 Epidermal stem cell markers.

Lack of molecular markers for epidermal stem cells causes a major problem in terms of precise stem cell identification and hence, their exact location *in vivo*. As yet *in vivo* label retaining cell experiments and *in vitro* colony forming assays are still the best methods of choice for the selection of stem cells. However, other molecules have been put forward as putative epidermal stem cell markers. These include $\beta 1$ integrin (Jones and Watt, 1993), $\alpha 6$ -integrin positive and transferrin receptor dull ($\alpha 6^{\text{bri}}\text{CD71}^{\text{dim}}$) (Tani et al., 2000a), p63 (Pellegrini et al., 2001), keratin 15 (Lyle et al., 1998b) and keratin 19 (Commo et al., 2000; Michel et al., 1996a). Adhesion molecules present on the keratinocyte may be used as additional markers. These include the Notch ligand, Delta 1

(Lowell et al., 2000), β -catenin (Zhu and Watt, 1999), E-Cadherin and plakoglobin (γ -catenin) (reviewed in (O'Shaughnessy and Christiano, 2001)).

1.1.16 Epidermal, homeostasis and regulation.

Epidermal homeostasis is achieved by controlled regulation of cell proliferation, differentiation and apoptosis. Any imbalance in these processes may give rise to varying epidermal thickness, example a very thick epidermis may be caused by hyperproliferative disorders of the skin such as psoriasis and carcinomas, whereas a very thin epidermis may be due to aging or Discoid Lupus Erythematosus. In response to tissue damage homeostasis is still maintained because the proliferation rates of stem cells and TA cells increases leading to the regeneration of the epidermis. However, many questions remain unanswered such as what are the exact processes that are required for keratinocyte stem cells to renew proliferate or differentiate and when does a keratinocyte stem cell transit to a TA cell? What are the specific cues that direct lineage commitment? The mechanisms underlying all these processes are not properly understood but it appears that the fate of stem cells is dependant upon cellular interaction with its microenvironment rather than being pre-programmed. This is indicated by a study that shows some differentiated keratinocytes in the suprabasal layers of regenerating epidermis in leg ulcers reverted back to an undifferentiated stem cell phenotype (de-differentiation) in the presence of growth factors, as assessed by β 1 integrin and K19 expression (Fu et al., 2001). The control of epidermal homeostasis regulation is influenced by microenvironment factors these includes cell-to-cell interaction, basement membrane, ECM, growth factors, cytokines, signalling pathways (Watt, 1998).

The epidermis is almost unique in that it continues to proliferate and differentiate. from formation of cornified squames and the continual cycling of hair follicles throughout life. There are human diseases that affect any or all of this processes, from the earliest point of differentiation of the ectoderm, through to terminal differentiation of the epidermis and hair follicle cycling. The discovery of the genetic basis of these diseases is the primary source of insight into the molecular mechanisms of epidermal development and differentiation.

Skin is the most environmentally exposed organ of the human body. Thus, somatic mutations accumulate in the epidermis far more than any other region of the body. It has been known for many years that mutations of genes involved in DNA repair can lead to skin cancer predisposition, the classical example being xeroderma pigmentosum (Cleaver et al., 1999) and Gorlin syndrome [Naevoid Basal Cell Carcinoma Syndrome (NBCCS)] a disorder that predisposes to the formation of basal cell carcinomas (see **section 1.2.0**) (Gorlin, 1987; Gorlin, 1995). Basal cell carcinoma arises from the basal layer of the epidermis which is the subject of this study.

1.2.0 Basal cell carcinoma (BCC).

Nonmelanoma skin cancers (NMSCs) constitute more than one-third of all cancers in the United States with an estimated incidence of over 600,000 cases per year. NMSCs are the most common malignancies occurring in the Caucasian population each year. Of these 600,000 cases approximately 500,000 are Basal cell carcinoma (BCC) (Miller and Weinstock, 1994), BCC was first described by Jacob in 1827 (Jacob, 1827). In 1994 it was estimated that lifetime risks to a child born in 1994 getting BCC was 22-33%. BCC represents 75% of NMSC (Miller and Weinstock, 1994) and is, therefore, the most common malignant disease throughout the western world. Worldwide incidence of BCC is increasing by about 10% per annum, so the prevalence of BCC will soon equal that of all other cancers combined (Karagas MR, 1995). There is a geographical variation in incidence of BCC, in the UK the age-standardised annual incidence was estimated as 114.2 per 100,000 population, while in Australia the figure is much higher at 726 per 100,000 (Holme et al., 2000; Marks et al., 1993).

There are several clinical and histological subtypes of BCC (see **section 1.2.1**), which exhibit different patterns of behaviour. Clinically BCC are divided into five major types; nodular, superficial, morpheaform, pigmented, solid cystic (Crowson, 2006; Ramsey, 2004). Nodular BCC (**Figure 1.9 and 1.10**) is the most common variety of BCC it often occurs on the head, neck, and upper back and has some of the following features: Waxy papule(s) with central depression and crusted erosion. Superficial BCC presents as scaly patches or papules that are pink to red brown in colour, often with central clearing (**Figure 1.11 and 1.12**). A threadlike border is common. Superficial BCC is common on the trunk and has little tendency to become invasive. Morpheaform (**Figure 1.13**) an infiltrating BCC are aggressive subtypes with sclerotic (scar like)

CHAPTER 1: Introduction

plaques or papules. The border usually is not well defined and often extends well beyond clinical margins. Clinically, ulceration, bleeding, and crusting are uncommon in this subtype of tumour and they are often mistaken for scar tissue (Ramsey, 2004)



Figure 1.9 Nodular basal cell carcinoma. This translucent pink papule has dilated superficial blood vessels and crusted erosion, characteristic of nodular basal cell carcinoma (Ramsey ML, 2002).



Figure 1.10 Nodular basal cell carcinoma presenting as a waxy translucent papule with central depression and a few small erosions (Ramsey ML, 2002).



Figure 1.11 Superficial basal cell. Scale, erythema (an abnormal redness of the skin), and a threadlike raised border are present in this superficial basal cell carcinoma on the trunk (Ramsey ML, 2002).



Figure 1.12 Larger superficial basal cell carcinoma (Ramsey ML, 2002).



Figure 1.13 Morpheaform infiltrating basal cell cancer has ill defined borders and telangiectases (Ramsey ML, 2002).

1.2.1 Histology of Basal Cell carcinoma

Tumour cells of nodular BCC, sometimes called basalioma cells, typically have large, hyperchromatic, oval nuclei and little cytoplasm. Cells appear rather uniform, and, if present, mitotic figures are usually few in numbers. Nodular tumour aggregates may be of varying sizes, but tumour cells tend to align more densely has islands (**Figure 1.14**). Superficial BCC appears as buds of basaloid cells attached to the under surface of the epidermis. Nests of various sizes often are seen in the upper dermis (**Figure 1.15**). Morpheaform BCC has thin strands of tumour cells extending deeper into the dermis and the tumour as a whole is poorly defined histologically, as it is clinically (**Figure 1.16**) (Ramsey, 2004).

BCC is believed to arise from the epidermis and occasionally from the outer root sheath of a hair follicle, specifically from hair follicle stem cells residing just below the sebaceous gland duct in an area called the bulge (**Figure 1.5**) (Kruger et al., 1999).

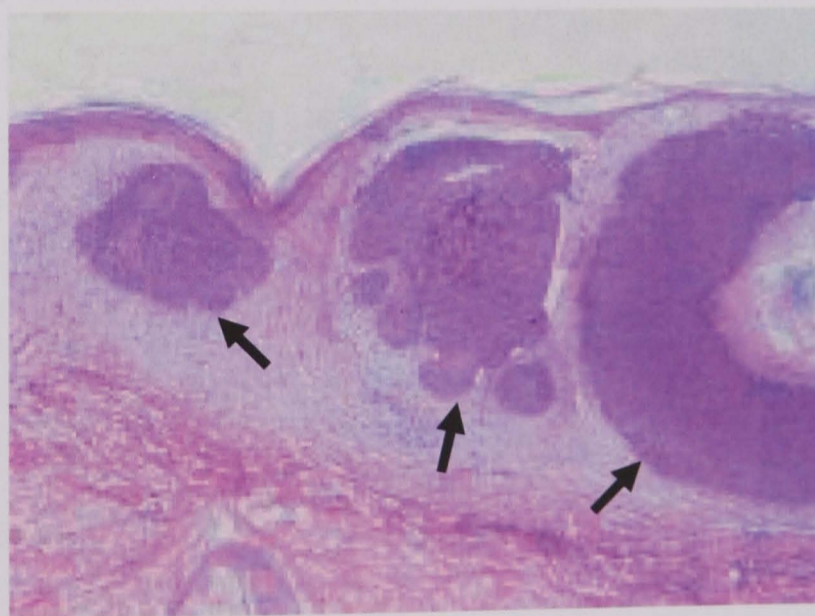


Figure 1.14 Histology of nodular basal cell carcinoma, nodular aggregates (indicated by black arrows) of basalioma cells are present in the dermis (Ramsey ML, 2002).

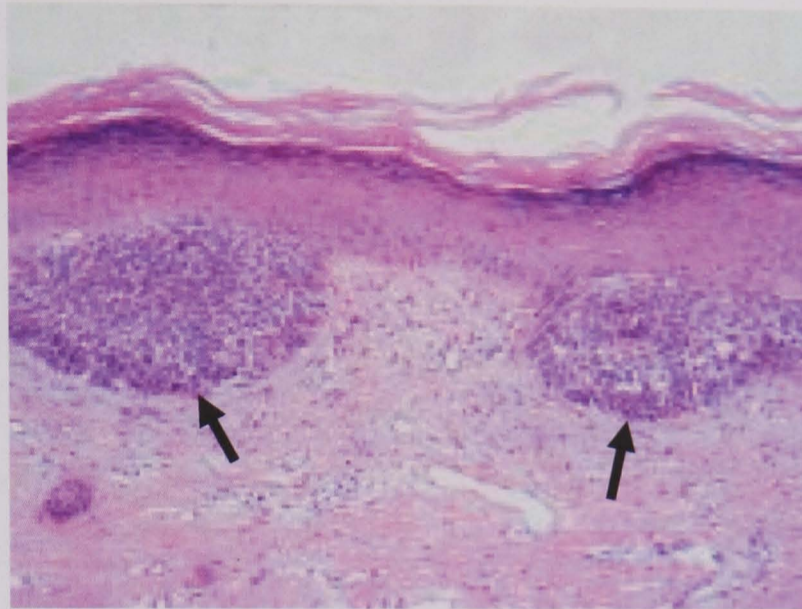


Figure 1.15 Histology of superficial basal cell carcinoma. Nests of basaloid cells (indicated by black arrows) are seen budding from the undersurface of the epidermis (Ramsey ML, 2002).

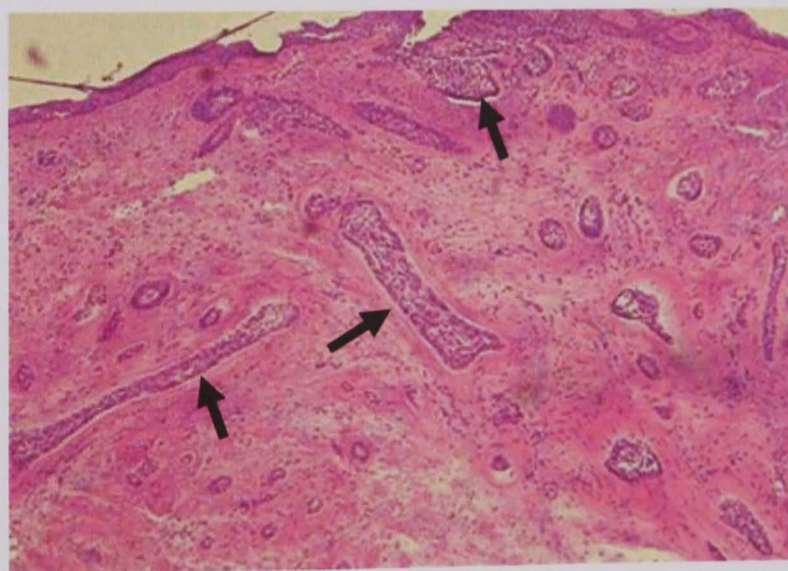


Figure 1.16 Histology of morpheaform basal cell carcinoma, thin strands of tumour cells (indicated by black arrows) extending deeper into the dermis (www.drmelton.com).

1.2.2 Factors that lead to basal cell carcinoma formation.

There is an increased risk of non melanoma skin cancers (NMSC) in the white population, especially those who have blue eyes, a fair complexion, sunburn easily, suntan poorly, freckle with sun exposure, have red blonde or light brown hair (Wong et al., 2003). BCC is uncommon in Black, Asian, and Hispanic populations. There is a higher incidence of BCC in the Albino black population than in normally pigmented black population. Compared with the white population, the black population have a decreased risk of BCC on sun-exposed areas, but have same incidence of BCC on non sun-exposed skin. BCC develops on hair-bearing skin, most frequently on sun exposed areas, approximately 85% of BCC are found on the head, neck and most commonly on the nose (Ramsey, 2004; Wong et al., 2003).

The reported increases in the incidence of BCC have partially been attributed to a larger amount of UV-B exposure, such as outdoor workers, or those with more frequent outdoor activities are at greater risk of developing BCC (Brooke, 2005; Ramsey, 2004; Wong et al., 2003). The risk of developing a BCC also increasing with age, the incidence of BCC in individuals over 75 years old is approximately 5 times higher compared to individuals between 50 and 55 years old (Holme et al., 2000). Exposure to short wavelength UV-B radiation (280-320nm) is believed to play a greater role in BCC formation than is longer wavelength UV-A radiation (320-400 nm) used in tanning saloons. A long latency period of 20-50 years is typical between the time of UV damage and clinical onset of BCC (Brooke, 2005; Ramsey, 2004).

Individuals who never tan and always get sun burnt have red or blond hair and blue or green eyes have been shown to have increased risk of BCC development. Family history of BCC, exposure to ionising radiation, low vitamin intake, high intake of fats, various chemical and particularly arsenic from 'tonics' and dust exposures predispose to BCC development (Wong et al., 2003). Renal transplant patients who have immunosuppressive therapy have a tenfold greater risk of developing skin cancers (Hartevelt et al., 1990). There is a modest increased risk of BCC formation in patient treated with Psoralen and UVA (PUVA) for psoriasis (Brooke, 2005). Several groups of diseases which are due to genetically determined disorders are associated with the development of BCC, these including albinism is a defect of melanin production, xeroderma pigmentosa is an inherited inability of the skin to repair DNA damage from

ultraviolet light, predisposes to rapid ageing of sun exposed skin, starting with pigmentary changes and progressing to skin tumours (Ramsey, 2004). Naevoid basal cell carcinoma syndrome (NBCC) also called Gorlin's syndrome is an autosomal dominant disorder in which multiple BCCs develop with associated palmer and plantar pits, jaw cysts, spine and rib abnormalities, calcification of the falx cerebri and cataracts (Bale et al., 1994; Gorlin, 1995; Howell and Caro, 1959; Howell and Mehregan, 1970; Ramsey, 2004). NBCC patients also present developmental abnormalities, these include bossing of the forehead, coarse facial features, bifid ribs and wedge shaped vertebrae. cardiac and ovarian fibromas also occur in some individuals (Goldstein et al., 1993; Gorlin, 1995; Howell and Mehregan, 1970; Kimonis et al., 1997; Smith et al., 2002). Some children with NBCCS develop medulloblastoma with a peak incidence of two years of age (Amlashi et al., 2003).

Genetic studies of Gorlin syndrome identified a germline mutation which inactivates Hedgehog (HH) (See section 1.3.0) developmental pathway receptor protein Patched (PTCH) (see section 1.3.1) to be the primary event in the formation of BCC which was mapped to chromosome 9q22-31 and the same region is deleted in high percentages of BCCs and other tumours related to this disorder (Gailani et al., 1996; Hahn et al., 1996b; Johnson et al., 1996). Further evidence supporting the role of activated HH-signalling in BCC comes from studies of genetic mouse models and skin grafting experiments: upon UV irradiation heterozygous *Ptc*^{+/-} mice develop BCC like tumours, although sporadic BCC formation does not normally occur in these mice (Aszterbaum et al., 1999) and human keratinocytes expressing Sonic hedgehog (SHH) (see section 1.3.0) grafted onto the back of nude mice form BCC like structures (Fan et al., 1997).

1.2.3 Treatment for basal cell carcinoma.

A variety of treatment options are available for BCC and these dependent on histological confirmation, type, number, site and size of lesion(s). There may also be implications for the patient, such as age and previous clinical history, which influences treatment strategies employed. The main treatments currently available for BCC's are as follows, excision surgery and Moh's surgery; destructive surgical techniques, e.g. cryosurgery, curette and cautery; topical chemotherapy; non-invasive techniques, e.g. photodynamic therapy (PDT) and radiotherapy (Telfer et al., 1999). Early detection and treatment has a high success rate in treating BCC. However, the high occurrence

increases the cost of treatment. Understanding the molecular events leading to BCC will allow us to develop better strategies for treatment and preventative measures that are cost effective.

1.3.0 Sonic Hedgehog pathway.

Hedgehog (HH) proteins are a highly conserved family of extracellular signalling molecules with fundamental roles in embryonic development both in vertebrates and in invertebrates (Hammerschmidt et al., 1997; Ingham, 1998; Weed et al., 1997). The most extensively characterised mammalian homolog is Sonic Hedgehog (SHH), an overview of this pathway is given in **Figure 1.17**. SHH belongs to a vertebrate evolutionarily conserved family of genes including Desert hedgehog (DHH) and Indian hedgehog (IHH), which are related to the *Drosophila* segment polarity Hh gene (Echelard et al., 1993; Goodrich et al., 1996; Marigo et al., 1995). During the development of the human embryo, SHH is expressed in the brain, developing limbs and the gut (Odent et al., 1999). The tissue specific expression of SHH-pathway genes has not yet been determined in human embryogenesis. However, in mouse and chick development SHH has been shown to play a key role in the central nervous system (CNS), limb, lung, gut, teeth development and in controlling growth and morphogenesis of the hair follicle (Bellusci et al., 1997; Goodrich et al., 1996; Hardcastle et al., 1998; Litingtung et al., 1998; Marigo and Tabin, 1996; Riddle et al., 1993; St-Jacques et al., 1998). SHH is expressed in numerous tissues known to have polarizing activities during development, its expression is initially detected in the node, and later in the notochord, floor plate of the neural tube, and in the zone of polarizing activity in the limb buds (Echelard et al., 1993; Krauss et al., 1993; Riddle et al., 1993; Roelink et al., 1994). DHH is involved in germline spermatogenesis and IHH in skeletal development (Bitgood et al., 1996; Vortkamp et al., 1996). *In vitro* studies suggest that SHH, DHH and IHH can act through the same signal transduction pathway (Echelard et al., 1993; Marigo et al., 1996b; Stone et al., 1996).

In humans, sporadic and inherited mutations in the *SHH* gene have been shown to cause Holoprosencephaly (HPE) which is the most common developmental defect of the forebrain and the face (Belloni et al., 1996; Nanni et al., 1999; Roessler et al., 1996; Roessler et al., 1997). SHH protein is cleaved to an active N-terminal form, which is then modified by the addition of a cholesterol moiety (Pepinsky et al., 1998; Williams et

al., 1999) a defects in addition of a cholesterol moiety can lead to the autosomal recessive Smith-Lemli-Opitz syndrome (SLOS). This is a genetic disorder that affects the development of children before and after birth with poor growth, developmental delay and a common pattern of congenital heart defects including cleft palate, genital malformations, and extra fingers and toes (Donnai et al., 1987; Kelley et al., 1996; Tint et al., 1994).

1.3.1 Patched and smoothened.

An overview of the SHH pathway is shown in **Figure 1.17**. SHH functions by binding a 12-span transmembrane receptor protein Patched1 (PTCH1) and Patched2 (PTCH2) in target cells (Smyth et al., 1999; Stone et al., 1996). PTCH1 normally inhibits downstream signalling through a physical interaction with a 7-span transmembrane protein Smoothened (SMO). PTCH2 can also interact with Hedgehog proteins, but its functional role in HH-pathway is currently unclear (Motoyama et al., 1998b; Smyth et al., 1999). SHH binding to PTCH1 releases the inhibition of SMO by PTCH1 which leads to increased expression of down stream HH target genes *GLI1* (See section 1.3.2) and PTCH1 itself (Goodrich and Scott, 1998; Hahn et al., 1999; Ingham, 1998; Murone et al., 1999; Toftgard, 2000; Villavicencio et al., 2000).

Mutations in human PTCH1, PTCH2 and SMO have all been detected in BCC and in a childhood brain tumour (medulloblastomas), which result in deregulated SHh-PTCH signalling (Johnson et al., 1996; Stone et al., 1996; Xie et al., 1998). Sporadic inactivating PTCH-1 mutations have also been reported in trichoepitheliomas, which are multiple small benign nodules that occur mostly on the face, derived from basal cells of hair follicles enclosing small keratin cysts (Vorechovsky et al., 1997) and in oesophageal squamous cell carcinomas (SCC) (Maesawa et al., 1998).

The molecular mechanism of HH signalling pathway has been worked out in greatest detail in *Drosophila* development (Hammerschmidt et al., 1997), down stream of the pathway is the zinc-finger containing transcription factor Cubitus interruptus (*Ci*), which appears to be required for all aspects of Hh signalling in *Drosophila* (Methot and Basler, 1999).

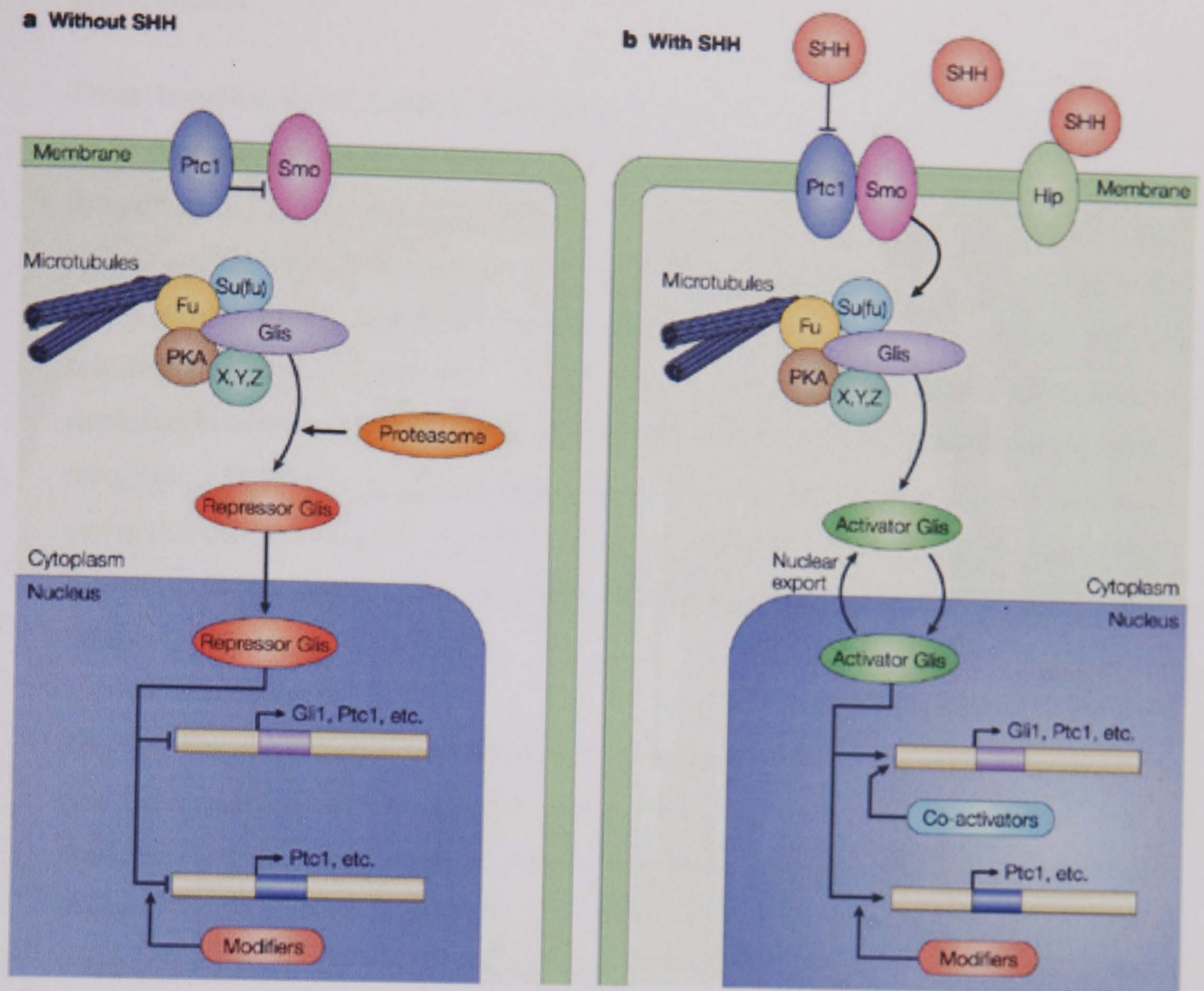


Figure 1.17 Overview of the SHH-PTCH-GLI signal transduction pathway. (a) In the absence of sonic hedgehog (SHH), Patched 1 (Ptc1) inhibits Smoothed (Smo), thereby inhibits the downstream cascade. The Gli proteins are phosphorylated by protein kinase A (PKA) and this leads to their cleavage by the proteasome and the formation of carboxyl-terminus truncated repressor Glis. Which move to the nucleus and repress the Gli dependent transcription of target genes Ptc1, etc (Rowitch et al.). On SHH binding to Ptc1 (Smo receptor), a macromolecular complex that is associated with the cytoskeleton, and this includes Su (fu) (Suppressor of fused), Fu (Fused), PKA, Gli proteins and other possible components (represented as X, Y, Z), acts to produce labile Gli activators. These are imported into the nucleus and transactivate target genes. The regulation of Gli activity takes place at many levels, including nuclear export and the presence of positive or negative cofactors. The inhibitory Hedgehog-interacting protein (Hip) also regulates Gli activity through inhibition of SHH. In addition, SHH activates transcription of Ptc1, which, when overexpressed, attenuates the SHH response by preventing SHH from binding Ptc1 molecules within the receptor complex (Ruiz et al., 2002).

1.3.2 GLI1.

Three homologues of *Cubitus interruptus* (*Ci*), GLI1, GLI2 (see section 1.3.3) and GLI3 (see section 1.3.4) have been identified in human and mouse (Hui et al., 1994; Ruppert et al., 1990). All three GLI proteins share high homology to *Ci* in their five zinc-finger domains, but limited homology outside of this region (Matise and Joyner, 1999). GLI1, GLI2, and GLI3 encode transcription factors that share five highly conserved tandem C2-H2 zinc fingers and a consensus histidine-cysteine linker sequence between zinc fingers (Ruppert et al., 1988). The GLI1 and GLI3 proteins recognize a conserved GACCACCCA nucleotide sequence in the promoters of target genes (Kinzler and Vogelstein, 1990a; Pavletich and Pabo, 1993; Ruppert et al., 1990; Vortkamp et al., 1995). GLI2 recognizes a GAACCACCCA motif (Tanimura et al., 1998).

The first human GLI gene to be discovered was GLI1 (also known as GLI), which was amplified in a glioblastoma (Kinzler et al., 1987). GLI1 has also been detected as an amplified gene in some malignant bone tumour (osteosarcomas), and B cell lymphomas (Roberts et al., 1989; Werner et al., 1997). GLI1 is also overexpressed in BCC compared with normal human skin (Dahmane et al., 1997; Ghali et al., 1999), and the degree of GLI1 overexpression correlates with tumour grade in adult bone and soft-tissue sarcomas (Stein et al., 1999). GLI1 is classified as an oncogene because it can transform cells when co-transfected with adenovirus E1A (Ruppert et al., 1991). Overexpression of human GLI1 in transgenic mice results in a range of developmental defects, including failure to thrive, early death and Hirschsprung-like dilatation of the gastrointestinal tract (Yang et al., 1997). Overexpression of human GLI1 in basal keratinocytes of transgenic mice results in the development of several types of skin tumours some of which show BCC like features (Nilsson et al., 2000). Further evidence for a critical role of GLI1 in tumorigenesis comes from overexpression studies in frogs, where *Gli1* can also induce structures resembling epidermal tumours (Dahmane et al., 1997; Hynes et al., 1997).

Mouse Twist protein can activate human GLI1 at the transcriptional level by interacting with E-boxes in first intron of GLI1. TWIST is a developmental regulatory gene and potential oncogene (Bourgeois et al., 1998; Gitelman, 1997; Maestro et al., 1999). Nonsense, miss-sense, deletion, and insertion mutations in several regions of the human

TWIST gene have been shown to cause Saethre-Chotzen syndrome (SCS), an autosomal dominant disease characterised by the following traits: fusion of the cranial structures which sometimes produces an asymmetric head and face. Low set hairline droopy eyelids (ptosis) and/or widely spaced eyes, beaked nose and possible deviated septum. Abnormalities of the fingers and/or toes, which are often short (brachydactyly) and intelligence is usually not impaired (El Ghouzzi et al., 2000; Howard et al., 1997).

Some patients with SCS have a mutation in the TWIST gene that appears to disrupt either the stability of protein or its ability to correctly localise to the nucleus (El Ghouzzi et al., 2000). The clinical phenotype of SCS partially overlaps with those of other SHh pathway related human diseases, indicating that deregulation of GLI family transcription factors by either SHh signalling defects or TWIST mutations may lead to similar downstream effects. It is not yet known if SHh signalling regulates TWIST. However, it does appear to be linked to SHh signal transduction.

1.3.3 GLI2.

There are four isoforms of human GLI2, alpha, beta, gamma, and delta and these isoforms encode 133, 131, 88, and 86-kDa proteins, respectively (Tanimura et al., 1998). *Gli2*-null mice display a lack of hair follicle development with a reduction in cell proliferation and a loss of SHH/GLI mediated signalling but epidermal differentiation remains unchanged. However, restoration of a constitutively active form of GLI2 increases cell proliferation and restores SHH/GLI function (Mill et al., 2003a). This indicates that GLI2 plays a key role in mediating SHH responses in skin and a major role in epithelial homeostasis, in particular to hair follicle development, by stimulating proliferation. Most studies of GLI2 have focused on embryonic development, where it plays a crucial role in neural, lung, and skeletal development (Ding et al., 1998; Hardcastle et al., 1998; Matisse et al., 1998; Motoyama et al., 1998a; Park et al., 2000; Ruiz i Altaba, 1998). Overexpression of mouse GLI2 in the basal epidermal layer of transgenic mice induces the formation of BCC like tumours and skeletal defects (Grachtchouk et al., 2000; Park et al., 2000; Sasaki et al., 1999). GLI2 mutants with a deletion of the exons encoding zinc finger domains 3-5 have numerous skeletal defects and abnormal lungs (Mo et al., 1997b; Motoyama et al., 1998a). Overexpression of SHH, GLI1 and GLI2 and an oncogenic form of Smoothened (SMO) in epidermal cells of transgenic mice leads to induction of BCC like tumours (Fan et al., 1997;

Grachtchouk et al., 2000; Nilsson et al., 2000; Oro et al., 1997; Xie et al., 1998). We have shown GLI2 expression to be up regulated in BCC compared to normal skin, and there is a positive feedback mechanism between GLI1 and GLI2 in human keratinocytes (Regl et al., 2002). Expression of the key antiapoptotic factor BCL2 is predominantly activated by GLI2 compared with GLI1, and GLI2 and BCL2 are co-expressed in the outer root sheath of hair follicles and BCC and in plasma cells that infiltrated BCC tumour islands (Regl et al., 2004). This suggests that GLI2 activates prosurvival factor BCL2 and this may represent an important mechanism in development or maintenance of cancers associated with HH signalling.

1.3.4 GLI3.

The only reported association of mutation in the GLI gene with tumour formation and development defects is with GLI3. A translocations, deletions, and point mutations throughout the GLI3 gene causes Greig cephalo polysyndactyly syndrome (GCPS). GCPS is characterised by joined fingers (syndactyly), predominantly thumb duplication (preaxial polydactyly), and facial anomalies in which eyes are too far apart grossly deforming the appearance (hypertelorism) (Jones, 1997; Kalff-Suske et al., 1999; Vortkamp et al., 1991; Wild et al., 1997). Frame shift and nonsense mutations in GLI3 lead to Pallister-Hall syndrome (PHS) which is an autosomal dominant disease, involving hypothalamic hamartoma (benign brain tumour located near the hypothalamus), central or postaxial polydactyly, syndactyly, imperforate anus and other facial abnormalities (Jones, 1997; Kang et al., 1997).

Human GLI3 protein has been shown to bind and be co-activated by mouse Creb-binding protein (CBP), which is a common transcriptional co-activator (Akimaru et al., 1997; Dai et al., 1999). Human mutation in CBP lead to insufficiency of CBP and this causes Rubinstein-Taybi syndrome RTS (Blough et al., 2000; Petrij et al., 1995). RTS is a developmental disorder with symptoms that include broad thumbs and first toes, short stature, delayed osseous maturation, vertebrate anomalies, mental retardation, and an increased risk of neural and developmental tumours (Jones, 1997; Miller and Rubinstein, 1995; Rubinstein, 1990). The similarity between the RTS and diseases caused by GLI3 mutations suggests that the biochemical interaction between CBP and GLI3 may significantly influence SHH signalling. CBP interacts with GLI2 and GLI3 but not GLI1 (Dai et al., 1999; Hammerschmidt et al., 1997).

1.3.5 GLI protein processing and their overlapping roles.

The three GLI proteins that participate in the mediation, interpretation of or response to the SHH signal, act in a combinatorial fashion, GLI1 and GLI2 have activating effects, whereas GLI3 (and at times GLI2) antagonises the function of SHH-GLI1 (Lee et al., 1997; Litington and Chiang, 2000; Ruiz, 1999).

A GLI homologue in *Drosophila*, Ci-155 a full-length form is detected primarily in the cytoplasm which is cleaved via protein kinase-A (PKA) mediated phosphorylation to C-terminal truncated nuclear form Ci-75 (Chen et al., 1999; Jiang and Struhl, 1995; Li et al., 1995; Price and Kalderon, 1999). Ci-75 appears to repress Hh and full-length Ci-155 activates *ptc* (Aza-Blanc et al., 1997; Methot and Basler, 1999). An important feature of post-translational regulation of Ci by Hh is that Ci can either activate or repress Hh targets depending on the concentration of Hh.

In vertebrate C-terminally truncated forms of both GLI2 and GLI3 proteins have been shown to repress reporter genes expressed in cell lines or SHH target genes *in vivo* (Dai et al., 1999; Ruiz i Altaba, 1999b; Shin et al., 1999). Full-length GLI2 and to a lesser extent GLI3 can also activate reporter gene expression in cell lines (Sasaki et al., 1999; Shin et al., 1999), a full-length GLI2 can also induce motoneuron differentiation in frog embryos (Ruiz i Altaba, 1998). GLI1 does not appear to possess an N-terminal repressor domain instead it functions only as an activator of transcription in its full length form (Sasaki et al., 1999; Shin et al., 1999). This demonstrates that GLI2 and GLI3 to have activator and repressor activities, while GLI1 may only function as an activator. Deletion of N-terminal sequences proximal to the zinc-finger domains in both GLI2 and GLI3 produces proteins with a constitutive strong activation function both *in vitro* and *in vivo* (Sasaki et al., 1999). This indicates that both GLI2 and GLI3 may have additional regulatory domains in the N-terminal.

There is no evidence as yet whether any of the human GLI proteins are cleaved *in vivo*. However, human GLI3 transfected into 10T1/2 mouse embryonic fibroblast cell line produces a single full-length GLI3 band, whereas the same construct transfected into monkey COS cell line has shown a full-length band 170-kD, as well as a 100-kD band (Ruiz i Altaba, 1999b). In mouse cells, human GLI3 is detected as a full-length form at all times, but additional processed forms are observed in absence of SHH (Dai et al.,

CHAPTER 1: Introduction

1999). Phosphorylation of full-length GLI3 and PKA dependent cleavage of human GLI3 to an 83-kD is observed in COS cells, PKA-dependent cleavage of human GLI3 is also observed in mouse and chick limb buds (Pan et al., 2006; Wang et al., 2000a).

No cleavage or phosphorylation of human GLI2 has been reported. A recent study has shown that in mouse embryos GLI2 is proteolytically processed and this processing is extremely inefficient, as a result the vast majority of mouse GLI2 protein is present in the full-length form and only a small fraction exists in the processed form. Interestingly, in addition to being processed, GLI2 is readily degraded and this degradation is dependent on the phosphorylation of a cluster of four PKA sites as well as the PKA-primed phosphorylation of multiple adjacent CK1 and GSK3 sites within the GLI2 C-terminal region (Pan et al., 2006). This study has also shown that hyperphosphorylation of GLI2 protein creates binding sites for TrCP, which in turn conjugates the multiple ubiquitin molecules onto the GLI2 protein and triggers the proteasome-mediated protein degradation. Both GLI2 processing and degradation are inhibited by SHH signalling in vivo (Pan et al., 2006), thus GLI2 transcriptional activity in SHH signalling may be regulated by altering processing and degradation mechanism of GLI2. In the same study it has been shown that at least half of GLI3 protein is processed and is present as a transcriptional repressor.

The ratio of full-length (GLI2-185 kD) and processed form (Gli2-78 kD) is slightly reduced in Shh mutant embryos and this ratio change is not nearly as great as that of GLI3-190 kD to GLI3-83 kD in the presence and absence of SHH (Pan et al., 2006). These observations provide a molecular explanation of why GLI3 mainly exhibits a repressor function and why its weak activator function can be detected only when GLI2 is mutated whereas GLI2 mostly acts as a transcriptional activator in mice and its weak repressing activity can only be revealed when the GLI3 repressor function is removed (Buttitta et al., 2003; McDermott et al., 2005).

Human GLI3 has been shown to both activate and repress GLI1 transcription or protein activity (Dai et al., 1999; Wang et al., 2000a). GLI3 function as either an activator or repressor of down stream genes such as Hepatocyte nuclear factor 3-beta (*HNF-3 β*), *GLI1*, and *PTCH1* (Sasaki et al., 1999). Details of the mechanism of switching between activation and repression has not yet been clearly determined, although one possible

mechanism suggested may be the cleavage of full-length GLI3 protein to release C-terminal activation domain and N-terminal repressor domain (Sasaki et al., 1999).

Human GLI1 has been shown to contain a VP16-like, C-terminal activation domain and activates transcription of endogenous genes such as *HNF-3 β* and of reporter constructs containing the GLI1 binding domains. GLI1 repressor functions have not been reported (Dai et al., 1999; Lee et al., 1997; Yoon et al., 1998). GLI1 is widely expressed during embryonic development but not in adult tissue. In contrast GLI2 and GLI3 continue to be expressed in many adult tissues such as testes, kidney, colon and lung (Ruppert et al., 1988). In normal epidermal skin GLI3 but not GLI1 is expressed in keratinocytes and in dermal fibroblast. However, GLI1 is only expressed in BCC and not in SCC and normal skin (Green et al., 1998). Human GLI2 has been shown to function as an activator only, whereas mouse GLI2 can function as either an activator or a repressor (Ruiz i Altaba, 1999b; Sasaki et al., 1997; Sasaki et al., 1999; Tanimura et al., 1998).

Immunocytochemistry of several human tumour cell lines has demonstrated GLI1 protein to be in both the nucleus and the cytoplasm, in varying proportions in different cell lines (Stein et al., 1999). Other studies have shown GLI1 to be in the nucleus only in Tera-1 and D259MG cell lines (Kinzler and Vogelstein, 1990a) or mainly in the cytoplasm in basal cell carcinomas (Ghali et al., 1999). Human GLI1 transfected in to COS cells accumulates primarily in the nucleus and to a limited extent in the cytoplasm (Dahmane et al., 1997; Lee et al., 1997). However, in 10T1/2 mouse cells GLI1 is localised primarily in the cytoplasm, particularly in the presence of SUFU (Stone et al., 1999). This suggests that human GLI1 is shuffled between the nucleus and cytoplasm and this may be one of mechanisms in controlling its transcriptional activity.

GLI3 localisation also differed between cell lines, with mainly cytoplasmic in COS cells (Lee et al., 1997) and nuclear in 10T1/2 cells (Ruiz i Altaba, 1999b). In transfected Hela cells full-length human GLI3 is in the cytoplasm and GLI3 with a Pallister-Hall syndrome (PHS) type frameshift mutation is in the nucleus, and GLI3 with Greig syndrome (characterised by development defects of the skull, face, and limbs) frameshift type mutation is localised in both the cytoplasm and nucleus (Shin et al., 1999). Experiments with mouse fibroblasts and frog tissues suggest that N-terminal GLI protein motifs are targeted to the nucleus, whereas the C-terminal GLI protein motifs are targeted to the cytoplasm (Ruiz i Altaba, 1999b)

The discrepancies between localisation of GLI proteins in the nucleolus or cytoplasm may be due to differences in cell type and cell cycle states. It is also unclear whether the sub-cellular localisation of GLI proteins observed in non-human transfected cells accurately reflects the sub-cellular localisation of human GLI in wild-type and tumour cells.

In vertebrates GLI1 and PTCH1 expression are restricted to proliferating cells adjacent to SHH expressing tissues, while GLI2 and GLI3 are more broadly expressed in proliferating cells in regions more distant to SHH, GLI3 being the most distant (Hui et al., 1994; Marigo and Tabin, 1996; Platt et al., 1997; Stone et al., 1996).

SHH pathway mutational studies in mice have shown that *Shh* and *Ptch1* mice mutants have a severe embryonic phenotype that includes the absence of anterior/posterior limb polarity, lung mesoderm, and virtually all ventral cell types for example, motoneurons in the CNS (Chiang et al., 1996; Goodrich et al., 1997; Litingtung et al., 1998). GLI1 and SHH can induce the expression of some ventral cell types when expressed in the dorsal CNS, whereas GLI2 and GLI3 cannot (Hynes et al., 1997; Lee et al., 1997). GLI1 can induce SHH targets genes and in homozygous mice that have most of the zinc-finger domains removed (*Gli1^{zfd}* mutant) develop normally, indicating that the DNA binding activity of GLI1 is not required for SHH signalling during development (Matise et al., 1998; Park et al., 2000). However, *Gli2^{zfd/zfd}* mutants exhibit a number of defects in the ventral CNS (Ding et al., 1998; Matise et al., 1998), as well as defects in development of the vertebrate, lungs and bones (Mo et al., 1997b; Motoyama et al., 1998a). Most *Gli1^{zfd/zfd}* and *Gli2^{zfd/+}* mutants die at birth and have CNS and lung defects that are similar to, but less than *Gli2* mutants (Park et al., 2000). However, in *Gli1/Gli2* double homozygotes mutants, motoneurons are induced and anterior posterior limb patterning is largely normal (Matise et al., 1998; Park et al., 2000). This suggesting that not all events that require SHH also require GLI1 and GLI2, these double mutant studies also indicate that GLI2 is primarily required for induction of certain SHH responsive cell types, while GLI1 is only required in certain tissues in combination with GLI2.

A *Gli3^{xtJ}* (XtJ) mutation in which most of *Gli3* is deleted leads to extra toes, this mutation has a similar phenotype to Greig's cephalopolysyn dactyly syndrome (GCPS)

in humans (Biesecker, 1997; Hui and Joyner, 1993; Kalff-Suske et al., 1999; Vortkamp et al., 1992). Certain aspects of the phenotype of *Gli3*-xtJ mutants indicate a role for GLI3 in the repression of SHH expression in the developing CNS and limbs (Biesecker, 1997; Marigo et al., 1996b; Ruiz i Altaba, 1998). However, *in vitro* GLI3 can activate transcription through a *Gli1* promoter region (Dai et al., 1999). *Gli2*^{+/-}; *Gli3*^{-/-} double mutants have more severe skeletal abnormalities than either mutant alone (Mo et al., 1997b), and in *Gli1/Gli2* double homozygotes, the lungs are more severely affected than in either single mutant (Park et al., 2000). If GLI proteins represent both positive and negative functions like the Ci in *Drosophila*, then in the CNS GLI1 may function only as an activator which is sufficient, and this function could be made redundant with activation functions of GLI2 and GLI3. Also repressor function of GLI2 in the dorsal CNS could be made redundant by GLI3.

Analysis of HH-dependent regulatory regions for the wingless (*wg*) gene in flies and the Coup-TFII (see section 1.3.7) gene in mice has revealed that they do not contain consensus Ci binding sites (Krishnan et al., 1997; Lessing and Nusse, 1998) and SHH-dependent activation of the motoneuron specific CoupTFII promoter appears to involve a PP-2A-like phosphatase (Krishnan et al., 1997). Double mutants of *Gli1/Gli2*, *Gli2/Gli3* and *Gli1/Gli3* are less severely affected than *SHh* mutants and in most tissues except lungs, GLI2 and GLI3 are expressed widely in many regions of the embryo that are far from SHH sources (Hui et al., 1994; Matisse et al., 1998; Mo et al., 1997b; Park et al., 2000). In addition, defects in GLI2 and GLI3 mutant mice are found in some regions of the embryo that are not likely to result from loss of SHH signalling (Grindley et al., 1997). Thus, these studies suggest that there is a possibility that GLI genes possess activities independent of SHH signalling and there may be GLI independent SHH pathway.

1.3.6 Suppressor-Fused.

Little is known about the signalling pathway between the PTCH and SMO response to the SHH and expression of GLI1. In *Drosophila* the serine-threonine kinase Fused (Fu), the kinesin-related protein Costal-2 (Cos-2) interacts physical with microtubules. However, Cos-2 and Fu have not yet been demonstrated in vertebrates. The only cytoplasmic element that has been shown to function upstream of the GLI genes in

human cells is Suppressor of Fused (SUFU), which cooperates with the F box-containing protein Slimb to inhibit transactivation by GLI1 (Stone et al., 1999). SUFU inhibits SHH induced osteogenic differentiation and retain GLI1 in the cytoplasm (Kogerman et al., 1999). It is not clear if SUFU acts immediately down-stream of PTCH in the SHH-pathway or is independent regulator of GLI mediated signalling. Children with medulloblastoma carry germline and somatic mutations in SUFU accompanied by loss of heterozygosity of the wild-type allele (Taylor et al., 2002). This indicates that SUFU is a human tumour-suppressor gene most likely because of its normal role as a negative regulator of hedgehog signalling.

1.3.7 Chicken Ovalbumin Upstream Promoter Transcription Factor II (COUP-TFII).

All effects of SHH may not be mediated via GLI1, this is suggested by the observation that SHH can directly induce transcription of the orphan receptors COUP-TFII via a regulatory sequence lacking GLI binding sites (Krishnan et al., 1997). COUP-TFII transcription factors belonging to the nuclear receptor super-family which plays a major role in development and differentiation in regulating angiogenesis and vein identity (Pereira et al., 1999; Tsai and Tsai, 1997; You et al., 2005a), in addition, it plays an important role in organ development such as stomach, limb, heart and diaphragm (Lee et al., 2004; Pereira et al., 1999; Takamoto et al., 2005; You et al., 2005b). These receptors are initially expressed in all three germ layers and subsequently their expression is restricted to organs that require mesenchymal-epithelial interaction for organogenesis (Pereira et al., 1999; Tsai and Tsai, 1997; You et al., 2005a). COUP-TFs are induced during differentiation of embryonic carcinoma cells by retinoic acid (Ben-Shushan et al., 1995), suggesting their requirement in differentiated cells. Expression of COUP-TFII is substantially lower in 30% of breast cancer cell lines (Nakshatri et al., 2000) and there are no reports on its expression levels in BCC.

1.3.8 TFIID.

Initiation of transcription is a key regulatory step affecting gene expression in response to a variety of extra and intracellular signals, during developmental processes and for tissue specificity. The rate of transcription initiation is determined by enhancer elements that are bound by gene-specific transcription factors. They typically consist of a DNA binding domain and one or more activation (or repression) domains. The transcription initiation site is determined by core promoter elements that direct the assembly of general transcription factors (GTFs) and RNA polymerase II to form the pre-initiation complex (PIC). The general transcription factor TFIID plays an essential role in transcription initiation as it recognises and binds the core promoter and keeps PIC assembly in the nucleus. In addition, TFIID plays an important role in mediating transcription activation signals by gene specific activators (Rashevsky-Finkel et al., 2001). Studies of transcriptional regulatory properties of GLI have identified contributions of specific domains to transcriptional regulation. GLI transcription activation domain is identified at the carboxyl terminus of the protein. This includes an 18 amino acid acidic-helix, highly similar to the herpes simplex viral protein 16 (VP16) transcription activation domain, which targets TAFII 31 in human HeLa cells and in *Drosophila* targets TAFII 40 (Goodrich et al., 1993; Uesugi et al., 1997; Yoon et al., 1998).

1.4.0 Retroviral gene expression.

Much of our understanding of how biological pathways function and what are the key components and how they interact with other pathways has come from trying to isolate and identify the component and then deleting or inducing its function or expression.

Using standard plasmid based transfection, transfection efficiency of primary keratinocytes is very low and they are difficult to transfect. In order to overcome the limitation of plasmid based transfection retroviral expression vector are used. The advantage of using a retrovirus as a gene delivery system is that the transduction efficiency is much higher, almost 100%. Also expression systems based on retroviral gene delivery are generally more reliable and have broader usefulness than standard plasmid-based transfection systems. Retroviral gene delivery systems are also used for cells that are difficult to transfect. Retroviral DNA integrates into actively transcribing regions of the host genome efficiently, with no internal rearrangement of the gene of interest, resulting in reliable and heritable expression, without variability or loss of expression due to loss of construct. The infection yields a cell line that stably expresses gene of interest.

1.4.1 Retroviral Structure and Genomic Organisation.

Retrovirus particles range in size from 80–120 nm in diameter and consist of an outer envelope lipid bilayer and virus encoded proteins. The protein core of the virus consists of viral replication enzymes and the viral RNA genome. The RNA genome consists of two copies of linear single-stranded (sense) RNA linked by 7–11 bp regions near the 5' termini (Beemon et al., 1974; Billeter et al., 1994; Kung et al., 1975). Retroviruses are divided into two categories based on the complexity of their genomes, simple or complex. RNA of simple retroviruses consists of three major coding domains gag, pol, env and a smaller domain pro. **Figure 1.18** shows the genomic structure of the retrovirus and the changes that occur from RNA retrovirus sequence to host integrated DNA form.

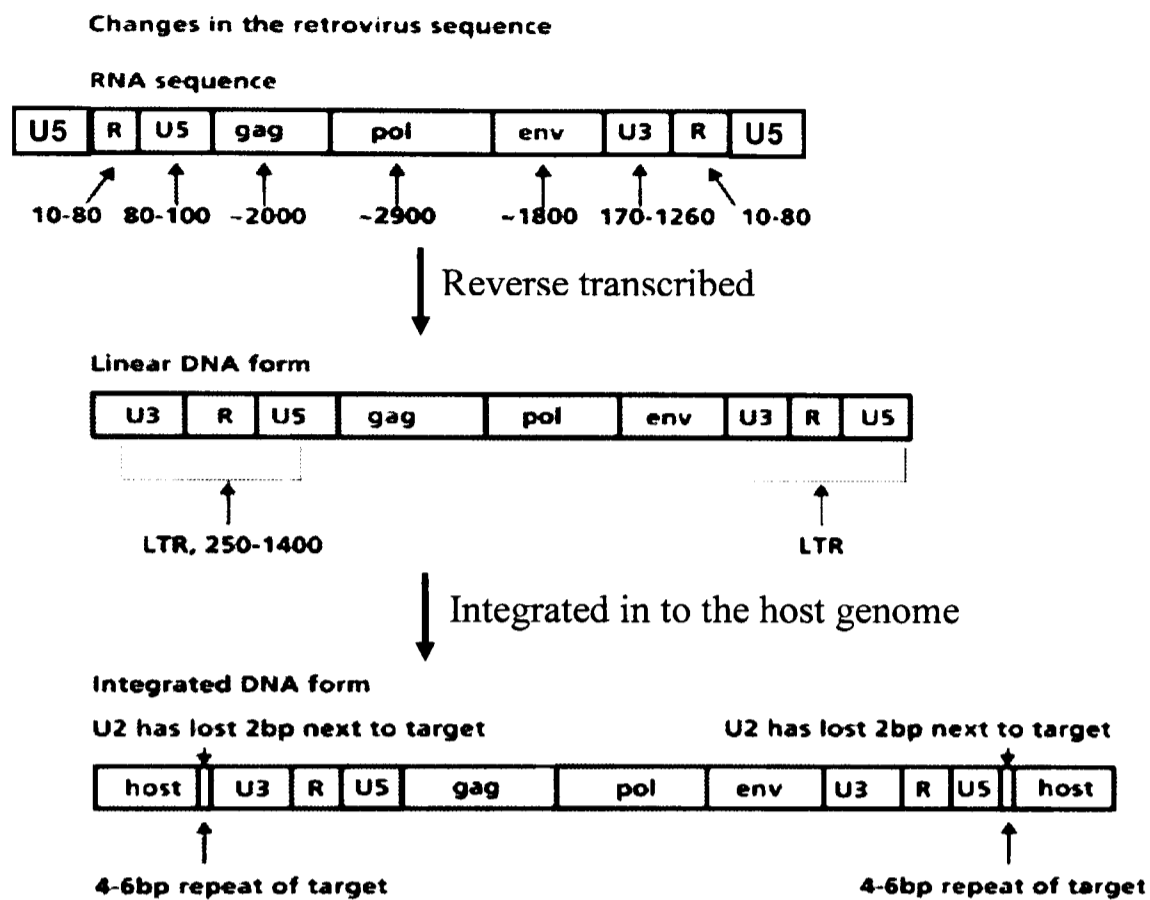


Figure 1.18: Showing the genomic structure of the retrovirus and the changes that take place during integration in to the host genome. The RNA virus sequence is reverse transcribed to a linear DNA form. The retroviral genome is flanked by a Long Terminal Repeat sequence (LTR). This region contains enhancer, promoter, transcription initiation, transcription terminator and polyadenylation signal. The integrated provirus has two LTRs; the 5' LTR normally acts as an RNA polymerase II promoter whereas the 3' LTR functions as the terminator sequence. An LTR is composed of U3, R and U5 regions. U3 includes most of the transcriptional control elements and carries the promoter/enhancer sequence; it is the first part of the genome to be reverse-transcribed, forming the 3' end of the provirus genome. R region provides the sequence homology for strand transfer during reverse transcription of the RNA genome. U5 region carries the poly A-site and, together with the R region, determines the poly-A addition. Both U3 and U5 regions contain the ATT sites required for integration. In addition, the retroviral genome has a non-translated region downstream of the transcription start site at 5' end of the virus RNA, which is responsible for initiating (+) strand synthesis during reverse transcription to form a linear DNA form this is then integrated in to the host genome (Figure adopted from Clontech web site)..

1.4.2 Retroviral replication.

Retroviral replication is a multi-step process. In brief, retroviruses enter the host cell through attachment of their surface glycoproteins to specific plasma membrane receptors leading to fusion of virus with the cell membranes. The RNA is then reverse transcribed into double stranded DNA. Reverse transcription of the RNA involves two jumps of the reverse transcriptase from the 5' end to the 3' end of the template RNA. The process results in the duplication of the LTRs at the 5' and 3' ends of the viral DNA that regulates viral gene expression. The DNA is translocated into the nucleus where it is inserted into the host genome by the viral integrase. The integrated viral DNA is known as the provirus. The provirus can be transcribed and expressed like any cellular gene by host cell RNA polymerase II. Transcription is regulated by the viral LTR through interactions with cellular trans-activating factors. Viral RNA is translated by cellular ribosomes, and translation products together with progeny RNA are packaged into viral particles and released from the cell via budding of the plasma membrane (see **Figure 1.19**).

1.4.3 Retroviral vector as gene delivery tool.

Retroviruses have been widely used as gene delivery tools. Because the retroviral genome inserts into the host cell genome following infection, it can be utilized as a permanent gene delivery vehicle. It allows the viral genome to be maintained for the life of the cell. The advantages of retroviral vector gene delivery are. 1) The ability to transduce a variety of cell types. 2) The ability to integrate efficiently into the genomic DNA of the dividing or mitotically active recipient cell. 3) The ability to express the transduced gene at high levels. 4) Capacity for long-term persistence and stable transmission of the gene to all future progeny of the transduced cell. 5) Up to 6.5 kb of foreign gene sequence can be packaged in a retroviral vector, which is adequate for most applications. 6) Ability to be manufactured in large quantities to meet very stringent safety specifications.

One of the key factor in using a retrovirus as a gene delivery vehicle is biological safety. This is overcome by designing vectors that produce replication incompetent virus. This is possible by separating the packaging function from the genetic material to be transferred. A basic retroviral vector is designed that contains the Cis-acting elements

required for replication as a virus, but lacks some or all of the viral genes, which are replaced by gene of interest. For a retroviral vector to replicate as a virus, it is necessary to provide the missing viral gene(s), these are provided in Trans, by a specially engineered cell lines that express the essential viral genes gag, pol and env, from heterologous promoters. The genetically-engineered cell lines are called packaging cell lines (see **Figure 1.20**). This minimises the chance of generating a replication competent virus (RCR). Gene transfer and expression by a retroviral vector is called transduction to distinguish the process from infection.

1.4.4 Self Inactivating retroviral vectors.

Self Inactivating (SIN) retroviral vectors are engineered so that transcription of the target gene can only be driven by an internal promoter (Miyoshi et al., 1998), once the expression cassette is integrated into the host genome. These vectors are constructed by deleting the enhancer and/or the promoter in the U3 region of the 3' LTR. During reverse transcription, a circular intermediate is formed that transfers the deletion to the 5' LTR of the proviral DNA. The deletion abolishes any transcriptional activity driven by the LTR so that no full-length vector RNA is produced in the transduced cells. Following a single round of replication, the changes are copied into both 5' and 3' LTRs resulting in inactive provirus. In this way, expression of a gene of interest is driven by the internal promoter.

There are several major advantages in using self inactivating retroviral vector. It minimizes the risk of producing replication competent retrovirus. It also reduces the likelihood that cellular coding sequences located adjacent to the vector integration site will be aberrantly expressed, either due to the promoter activity of the 3' LTR or through an enhancer effect. Finally, a potential transcriptional interference between the LTR and the internal promoter driving the transgene is prevented by using the SIN-retroviral vector.

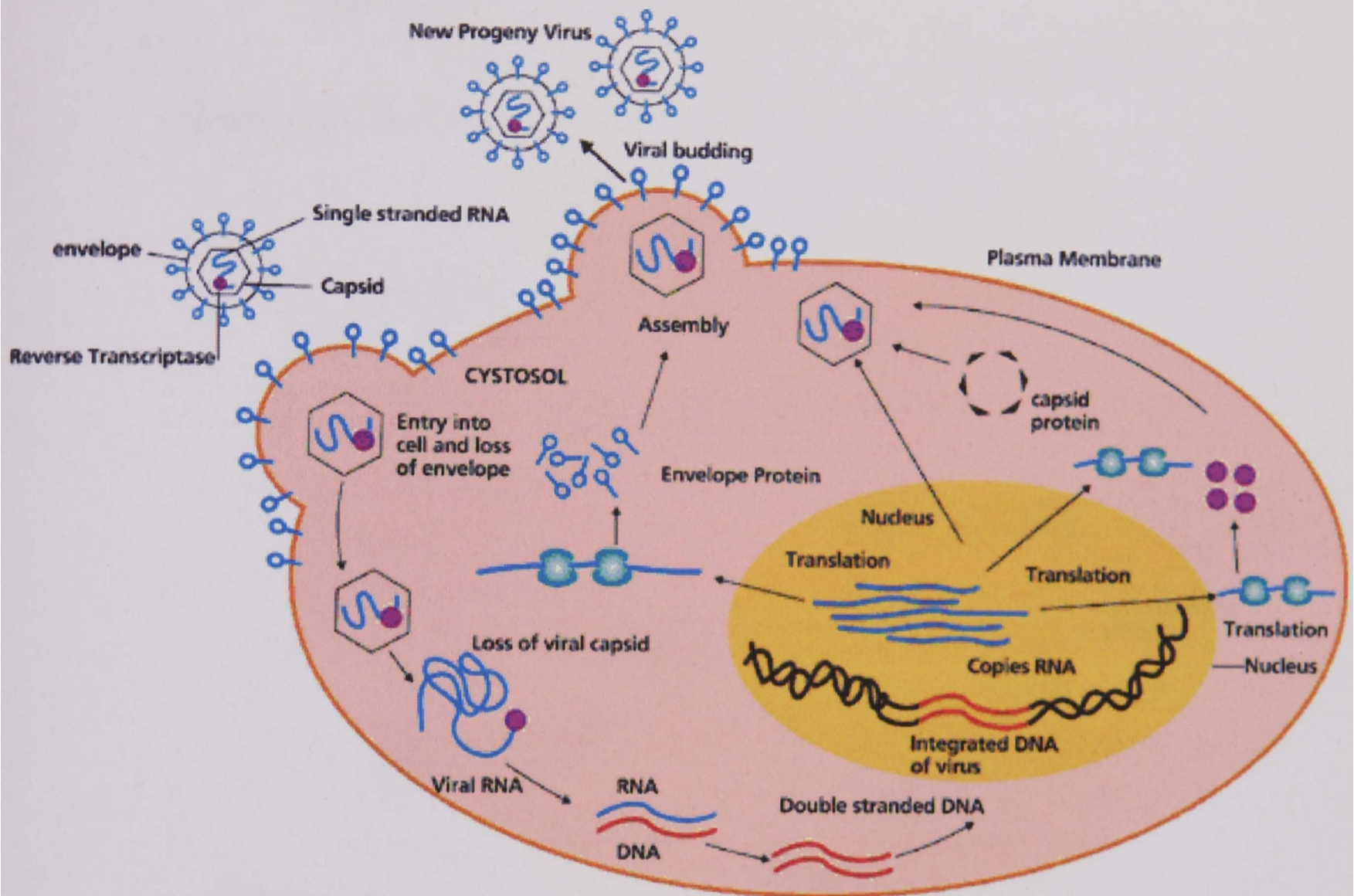


Figure 1.19: An over view of retroviral replication. Retroviruses particle enter the host cell through attachment of their surface glycoproteins to specific plasma membrane receptors leading to fusion of virus with the cell membrane. The RNA is then reverse transcribed into double stranded DNA. The DNA is translocated into the nucleus where it is inserted into the host genome. The integrated viral DNA is transcribed and expressed like any cellular gene by host cell RNA polymerase II. Viral RNA is translated by cellular ribosomes, and translation products together with progeny RNA are assembled into viral particles and released from the cell via budding of the plasma membrane (Figure adopted from Clontech web site).

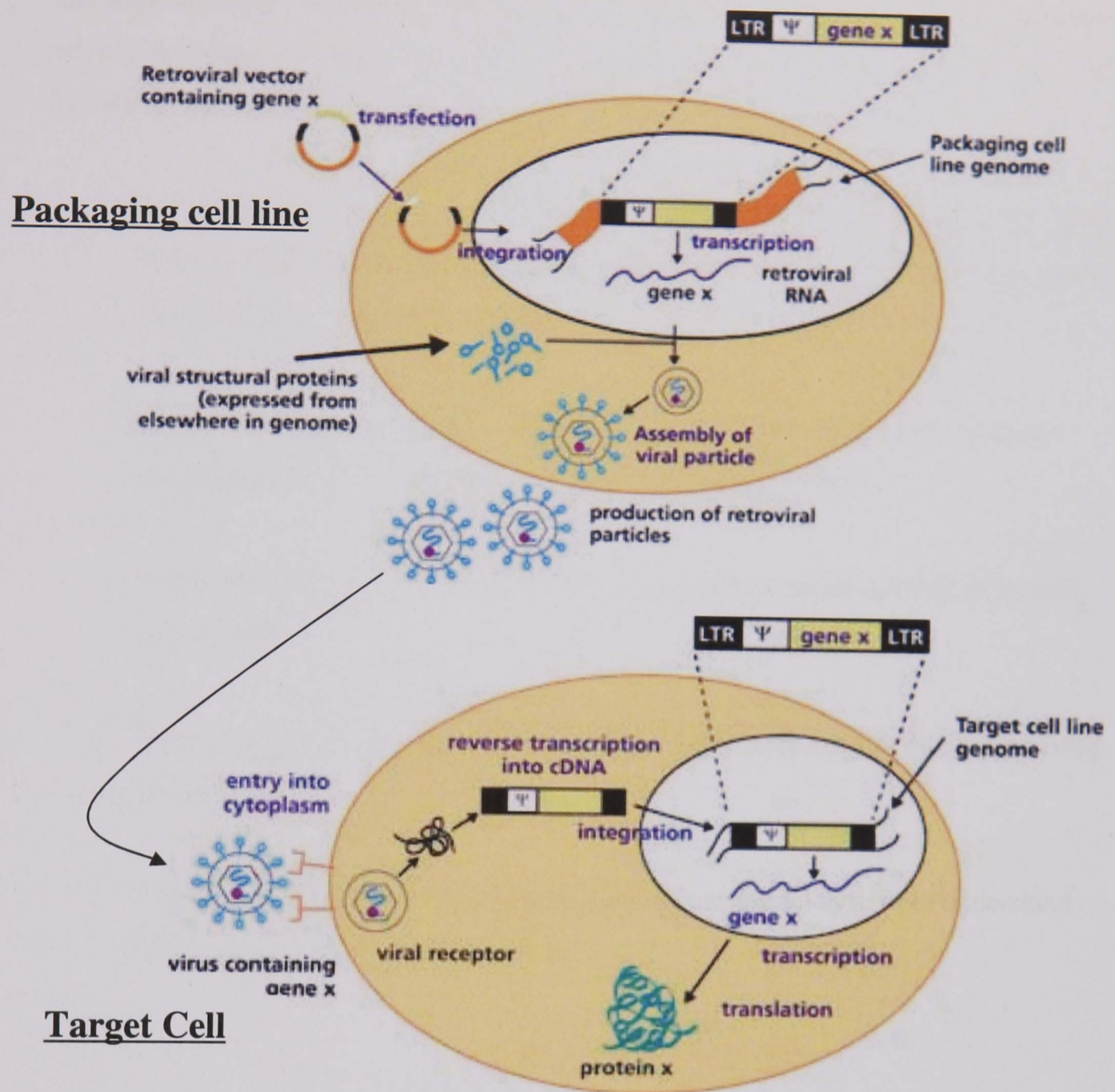


Figure 1.20 Basic principles of retroviral transduction. Self Inactivating retroviral vector which has a deletion in 3'LTR and lacks the essential viral genes but containing the internal promoter (Miyoshi et al., 1998) and the gene x is transfected into the packaging cell line that express the essential viral genes x. The IP-gene x integrate into host genome and is transcribed into retroviral RNA, this is then assembled into retroviral particles using the viral structural proteins expressed in packaging cell. The viral particles containing the gene x are used to transduce target cells to express gene x. (Figure adopted from Clontech web site).

Aim of this study.

Although the sonic hedgehog pathway is well characterised in *Drosophila* and murine not much is known about this pathway in humans particularly with regards to BCC formation, the aims of this study were;

1. To investigate sonic hedgehog signalling pathway gene expression in BCC, Normal Skin and in GLI1 transduced human primary keratinocytes and quantify levels of their expression.
2. Determine the localisation of GLI2 in normal human skin and BCC and its expression in GLI1 transduced human primary keratinocytes.
3. Determine the localisation of FOXE1 a down stream target of GLI2 in normal skin and BCC.
4. Determine the Effects of EGF on pattern of gene expression in GLI1 expressing keratinocytes.
5. Generation of a Zp3-Cre-GLI1 transgenic mouse model system to understand GLI1 molecular mechanism *in vivo*.

CHAPTER 2

Materials and Methods

2.1.0 Cell Culture.

To avoid cross contamination of cell cultures and contamination of cell cultures from micro-organisms. Standard sterile tissue culture techniques (practiced in all tissue culture laboratories) were used when handling all cell types described below.

2.1.1 Mouse 3T3 fibroblast cell line (feeder layer).

The mouse Swiss 3T3 fibroblast cell line was obtained from the Imperial Cancer Research Fund (ICRF) now Cancer Research UK (CRUK). This cell line was established by G. Todaro and H Green in 1962 from disaggregated embryos of Swiss mouse (Todaro and Green, 1963). The cells were cultured in T175 cm² polystyrene tissue culture flasks (Corning, VWR International Ltd., Leicester, UK.) with Dulbecco's Eagle's Medium (DMEM) (obtained from CRUK) supplemented with 10 % (v/v) foetal calf serum (FCS) (PAA laboratories GmbH, Austria) and 2 mM L-glutamine (obtained from CRUK). The Flasks were incubated at 37°C in a humidified 10% CO₂ 90% air atmosphere, the medium was changed twice weekly. When cells reached confluence, they were passaged to prevent contact growth inhibition.

Confluent T175 flask of 3T3 fibroblasts were passaged by aspirating the old culture medium from the flasks and 5 ml 0.02% ethylenediaminetetra-acetic acid (EDTA) (w/v) (obtained from CRUK.) was added to the flasks to wash the cells. The addition of 0.02% EDTA to the flasks primarily chelates divalent cations (calcium and magnesium ions). This results in the weakening of the adhesiveness of cells to each other and to the flask. This also prevents cationic inhibition of trypsin activity. The 0.02% EDTA solution was aspirated and 5 ml of 0.05% (v/v) trypsin solution (obtained from CRUK.) in 0.02% EDTA (prepared by dilution of 1 part of 25% w/v trypsin and 4 parts of 0.02% EDTA) was added to the flasks. The flask was incubated at 37°C in 10% CO₂ for 3 to 5 min. Incubation with trypsin cleaves extracellular cell adhesion proteins required for cell to cell attachment and cell to flask attachment. Detachment of cells was also aided by tapping the sides of the flasks gently with hand. Once the cells had detached from the flask, 5 ml of (DMEM) culture medium containing 10% (v/v) FCS was added to the flask to inhibit the protease activity of trypsin. Leaving the cells too long in trypsin is harmful to the cells. 8 ml cell suspension was transferred to a 50 ml centrifuge tube (Falcon, BD Biosciences Oxford, UK.) and centrifuged at 1,000 rpm for 5 min at room

temperature using the IEC 215A rotor centrifuge. After removing the supernatant, the cell pellet was resuspended in 20 ml of the culture medium. The concentration of cell suspension was determined by pipetting 20 μ l of cell suspension under the cover slip of a Neubauer haemocytometer (Weber Scientific International, West Sussex, UK.). Cell concentration was calculated by taking an average of cell count in each of four 4×4 square grids under the microscope. The average number was then multiplied by 10^4 to give number of cells per ml. To the remaining 2 ml of cell suspension left in the flask 38 ml of (DMEM) culture medium containing 10% FCS was added and incubated at 37°C in a humidified 10% CO₂, 90% air atmosphere, to maintain culture stocks of 3T3 fibroblasts.

3T3 fibroblast cell suspension in a 50 ml centrifuge tube was Gamma irradiated with 6,000 rads (cobalt⁶⁰) for 32 min. Gamma radiation suppress 3T3 fibroblast cell division but allows active cell metabolism. Irradiated 3T3 fibroblasts secret extra cellular matrix (ECM) proteins and growth factors, The ECM proteins encourage keratinocyte attachment and growth factors stimulate their proliferation (Rheinwald, 1980), thus Gamma irradiated 3T3 mouse fibroblasts act as feeder layer for keratinocytes. Gamma irradiated 3T3 mouse fibroblasts were seeded at a density of $2 \times 10^6/15$ ml in T75 cm² flask (Corning, VWR International Ltd., Leicester, UK.) in keratinocyte culture medium (DMEM and Ham's F12 medium in ratio of 3:1, 10% v/v FCS, 0.4 μ g/ml hydrocortisone, 10⁻¹⁰ M cholera toxin, 5 μ g/ml insulin, 5 μ g/ml transferrin and 2x10⁻¹¹ M lyothyronine). The cells were allowed to attach for 2 hours to the surface of the flask in a humidified 10% CO₂, 90% air atmosphere. Keratinocytes can be added at the same time as feeders or after the feeders have attached to the flask. Irradiated feeders unused were stored at 4°C for up to two days, after which they discarded.

The 3T3 mouse fibroblast were routinely split at a 1:5 ratio twice a week and were maintained in culture for 8 to 12 weeks after which they tended to transform or senesce and were no longer efficient as feeder layers for keratinocyte cultures. Fresh stocks of early passage of 3T3 mouse Fibroblast feeder cell were routinely supplied from CRUK.

2.1.2 Isolation of primary keratinocytes from human skin.

Human epidermal keratinocytes were isolated from discarded breast and abdominal skin obtained from plastic surgery, foreskins from circumcisions and facial skin from facelift operations. Ethical committee approval was obtained (ethics number: T/01/034) as well as informed consent from the patient for the use of the redundant skin for scientific research.

The skin specimen collected was transported from the theatre to the laboratory in transport medium (DMEM supplemented with 5% (v/v) FCS and antibiotic mix consisting of a cocktail of 600 units/ml Penicillin-G, 600 µg/ml Streptomycin sulphate, 250 µg/ml Gentamycin sulphate (Sigma, Poole, UK.) and 2.5 µg/ml Fungizone (Invitrogen Life technologies, UK.). The skin was processed on the same day or stored overnight at 4°C. However, the latter resulted in reduced cell viability.

The isolation of primary keratinocytes was carried out as described by (Rheinwald and Green, 1975a) with some modifications. All excess dermis and connective tissue were removed from the skin specimen. For small skin biopsies a scissors was used to remove excess dermis and connective tissue, for large skin samples a dermatome or a skin graft knife was used. Following removal of connective tissue the skin pieces were washed in 0.02% (w/v) EDTA, and then cut or minced into tiny pieces less than 0.5 mm² in size. The tissue was then transferred into 0.25% (w/v) trypsin solution and incubated at 37°C for 1-2 hours, agitating every 30 min. Following incubation with trypsin solution, all contents were transferred to a 50 ml centrifuge tube and equal volumes of Ready Mix minus (RM-) medium (DMEM and Ham's F12 in ratio of 3:1, with 10% (v/v) FCS and 2 mM glutamine and the following supplements: 0.4 µg/ml hydrocortisone, 10⁻¹⁰M cholera toxin, 5 µg/ml transferrin, 2 × 10⁻¹¹M lyothyronine and 5 µg/ml insulin (all supplied by Sigma, UK.) were added. The centrifuge tube was shaken vigorously for a few min and then the contents were transferred to a clean tube by filtering through a sterile sieve or cell strainer. The filtrate predominantly contained primary keratinocytes and the solid skin debris left behind in the strainer contained fibroblasts and the dermis. The 50 ml centrifuge tube containing the filtrate was centrifuged at 1.000 rpm for 5 min and the supernatant was aspirated. Fresh 30 ml RM- medium containing 10% (v/v) FCS was added to the pellet and a single cell suspension was prepared by gentle pipetting the

CHAPTER 2: Materials and Methods

medium up and down. 300 μ l of this suspension was mixed with 300 μ l trypan blue stain (Invitrogen Life technologies, UK.). 20 μ l of cell suspension and the blue dye mix was placed under the cover slip of the haemocytometer. Using the microscope viable cells were identified by their ability to exclude the blue dye, cells that stained blue were identified as dead cells. Only viable cells were counted in each of four 4×4 square grids and cell concentration was calculated by taking an average of cell count in each of four 4×4 square grids. The average number of cells was then multiplied by 10^4 and by the dilution factor (2) to give number of cells per ml. Primary keratinocytes were seeded at a density of approximately 2×10^6 cells in a T75 cm^2 flasks on Gamma irradiated 3T3 feeder cells (see section 2.1.1) in a RM- (Reday Mix minus epidermal growth factor [EGF], see Appendix II, Dulbecco-Vogt Egle's Medium [DMEM] and Ham's F12 in ratio of 3:1 supplemented with 10% FCS and 2 mM glutamine and the following supplements: 0.4 μ g/ml hydrocortisone, 10^{-10} M cholera toxin, 5 μ g/ml transferrin, 2×10^{-11} M lyothyronine, 5 μ g/ml insulin [Sigma Poole, UK]) culture medium and incubated at 37°C in a humidified 10% CO_2 , 90% air atmosphere for 48 hours. After which medium was aspirated and replaced with RM+ (Reday Mix plus EGF, see Appendix II, DMEM and Ham's F12 in ratio of 3:1 supplemented with 10% FCS and 2 mM glutamine and the following supplements: 0.4 μ g/ml hydrocortisone, 10^{-10} M cholera toxin, 5 μ g/ml transferrin, 2×10^{-11} M lyothyronine, 5 μ g/ml insulin [Sigma Poole, UK], 10ng/ml EGF [Serote, Oxford, UK]) culture medium. RM+ culture medium was changed two to three times weekly and the 3T3 feeder density was maintained by adding more irradiated 3T3 feeders when existing feeder cells become sparse. Primary keratinocytes grew as tightly packed rounded colonies and once they grow to more than 75% confluent they start to differentiate and stratify. Growth rate of primary keratinocytes also slows down after 8 to 11 days even if they do not reach 75% confluent. Therefore, to maintain maximum growth rate and prevent them differentiating, keratinocytes were subcultured before they reached 75% confluent or if they were cultured for 8 to 11 days.

2.1.3 Passaging keratinocyte cultures.

Keratinocytes were passaged by aspirating the culture medium and washing the cells with 5 ml phosphate-buffered saline (PBS) (calcium/magnesium-free) and then with 5 ml of 0.02% (w/v) EDTA. 3T3 feeder cells were removed by incubating with 5 ml

CHAPTER 2: Materials and Methods

0.05% (v/v) trypsin in 0.02% (w/v) EDTA (1 part 0.25% trypsin with 4 parts 0.02% EDTA) at 37°C in 10% CO₂, 90% air atmosphere for 30-60 sec. Alternatively, 5 ml of 0.02% (w/v) EDTA only was added and flasks incubated at 37°C in 10% CO₂, 90% air atmosphere for about 10-15 min. Once feeders were removed, 5 ml of 0.05% (v/v) trypsin in 0.02% (w/v) EDTA was added to the flasks before incubating at 37°C in 10% CO₂, 90% air atmosphere for 5 to 15 min. Once keratinocytes appear rounded up, side of the flask was tapped with hand to detach them from the flask. Then equal volume (5 ml) of RM+ culture medium containing 10% (v/v) FCS was added to the flask to neutralise trypsin activity. Cell suspension was then transferred to 50 ml centrifuge tube and centrifuged at 1,000 rpm for 5 min. Following this, the supernatant was aspirated and fresh RM+ culture medium containing 10% (v/v) FCS was added to the cell pellet. Using a haemocytometer cell concentration was determined as described above. The primary keratinocytes were routinely split at a ratio of 1:5 T75 cm² flasks and plated with fresh Gamma irradiated 3T3 feeders as described above. Passages number one to three were used for experiments.

2.1.4 Removal of fibroblast contamination in keratinocyte cultures.

The addition of 3T3 feeder cells discourages the growth of dermal fibroblast in keratinocyte cultures. However, if density of 3T3 feeders is low, fibroblast contamination can occur. To remove the dermis fibroblasts, the flask was washed once in 0.02% (w/v) EDTA and then trypsinised with 0.05% (v/v) trypsin in 0.02% (w/v) EDTA at 37°C in 10% CO₂, 90% air atmosphere for 30-60 sec or until the 3T3 feeders and the human fibroblasts had detached from the flask. Tapping the side of flask gently aided the detachment of the fibroblasts and 3T3 feeders. Contaminating fibroblasts and the 3T3 feeders detached from the flask very easily whereas the keratinocytes remain attached. Once the fibroblasts had detached, trypsin reaction was neutralised by adding equal volume of RM+ culture medium containing 10% (v/v) FCS and the media containing the fibroblast and 3T3 feeder cells was aspirated. The keratinocytes were cultured, by adding fresh Gamma irradiated 3T3 feeders and RM+ culture medium containing 10% (v/v) FCS to the flask as described above. This was repeated until no fibroblast contamination was observed.

2.1.5 HaCat, A375 and N-TERT-keratinocyte cells.

Spontaneously immortalised primary keratinocytes HaCat cell line were obtained from CRUK and N-TERT immortalised keratinocytes were (gift from Dr J. Rheinwald). They were cultured in DMEM/F12 medium (CRUK) supplemented with 10% (v/v) FCS and 2 mM glutamine medium with out the 3T3 feeders. A375 melanoma cell line was also obtained from CRUK, A375 cell line was cultured in DMEM medium (CRUK) supplemented with 10% (v/v) FCS and 2 mM glutamine. All cell lines were incubated at 37°C in 10% CO₂, 90% air atmosphere, and cultures and stocks were maintained as described in **section 2.1.1 to 2.1.3.**

2.1.6 Freezing and recovery of cells.

To maintain cell stocks for experiments, the majority of the cells were cryo-preserved at each passage. Cells were detached from the flasks using trypsin as described above and centrifuged to obtain cell pellet. The cell pellet was resuspended in 10% (v/v) dimethylsulphoxide (DMSO) (BDH Laboratories Supplies, Poole, Dorset, UK), 90% (v/v) FCS to give a concentration of 2×10^6 cells /ml. One ml of DMSO/FCS cell suspension was placed in 1.8 ml freezing cryogenic vial (Sigma UK). To ensure a constant cooling rate of 1°C/min, the cryovials containing cells were transferred to isopropyl freezing container (NALGENE Cryo 1°C Freezing Container, BDH Laboratories Supplies, UK) and stored at -70°C for 24 hours. The cryovials were then transferred to liquid nitrogen for long term storage. This two step procedure is essential for cells to survive cryopreservation.

Frozen cells were recovered by thawing the DMSO/FCS cell suspension rapidly, by incubating at 37°C. The vial was swabbed with 70% (v/v) ethanol before opening. The DMSO/FCS cell suspension was immediately transferred into 5 ml culture medium in a 15 ml Falcon tube and mixed to avoid toxicity from the DMSO. The cells were centrifuged at 1,000 rpm for 5 min, the supernatant was discarded and the cell pellet resuspended in a fresh culture medium. Cells were plated at appropriate density and cultured as described in **sections 2.1.1 to 2.1.5.**

2.2.0 Retroviral transduction.

Most of the work done in this section was part of collaboration work carried out with other group members headed by Professor Anthony Quinn and later by Professor Mike Philpott. All of the cloning and transduction work described in this section was carried out by Dr Graham Neill.

Dr J Green in this lab showed that GLI1 is induced in human BCC (Green et al., 1998). In order to understand what role GLI1 transcription factor plays in BCC formation a full-length *GLI1* mRNA in bluescript vector cloned from Glioma (Gift from K W Kinzler) was cloned into a pcDNA3.1-His vector by Dr J Green to generate pcDNA3.1-His-GLI1 plasmid, this was then transfected into the human primary keratinocytes using standard liposome-mediated transfection reagents to induce GLI1 expression. The transfection efficiency was low and primary keratinocytes were also difficult to transfect. In order to overcome the limitation of plasmid based transfection. Full-length *GLI1/GLI2*, were cloned into a SIN-IP-GFP (Self Inactivating Internal Promoter Green Fluorescence Protein vector gift from P Khavari USA) retroviral expression vector by Dr G Neill.

2.2.1 Generating SIN-EGFP/GLI1 fusion protein retroviral construct.

Full-length GLI1 was cloned into a Self Inactivating Internal Promoter Green Fluorescence Protein (SIN-IP-GFP) retroviral vector (gift from P Khavari) by Dr Graham Neill. A brief outline of the protocols is as follows, Enhanced Green Fluorescent (pEGFP-C3) plasmid (Cat No 6082, Clontech) was modified by cloning an adaptor containing a *Sall* site into the vector *Asel* site. Full-length GLI1 cDNA was amplified by PCR with sense primer 5'-GACAGAGTGTCGACACACCCT-3' and anti-sense primer 5'-GATTCCCTACTCTTTTAGGCA-3' and after digesting with *SacI* and *HindIII* was cloned into the modified pEGFP-C3 vector at *SacI*, *HindIII* site to create pEGFP-GLI1-C3 construct. A retroviral fusion EGFP/GLI1 expression construct was generated by digesting pEGFP-GLI1-C3 vector with *Sall* and *HindIII* to cut out the CMV-EGFP-GLI1 sequence. The retroviral vector SIN-IP-GFP was digested with *XhoI/NotI* to excise the CMV-GFP sequence to create (SIN-IP). CMV-EGFP-GLI1 was then cloned into SIN-IP at *XhoI* and *NotI* site to create SIN-EGFP-GLI1 retroviral

vector (see **Figure 2.1**). A control construct SIN-EGFP was also generated. Both SIN-EGFP-GLI1 and SIN-EGFP constructs were verified by DNA sequencing.

2.2.2 Generating SIN-GLI-EGFP bicistronic retroviral constructs.

GLI1-Internal-Ribosomal-Entry-Sequence-Enhanced-Green-Fluorescence-Protein (GLI1-IRES-EGFP) bicistronic construct was cloned into a SIN-IP-GFP retroviral vector by Dr Graham Neill. A brief description on how this was carried out is as follows, GLI1-IRES-EGFP was generated by modifying pIRES2-EGFP plasmid (Cat No 6029.1, Clontech) by cloning an adapter containing a Sall site into the vector AseI site to create pI2E-A. GLI1 coding cDNA was amplified by PCR with the sense primer 5'-GACAGAGTGTCGACACACCCT-3' and antisense primer 5'-GATTCCCTACTCTTTTAGGCA-3' and after digestion with Sall was cloned into pI2E-A at the XhoI/SmaI sites creating pI2E-A-GLI1. To generate the retroviral bicistronic GLI2-EGFP expression construct, N-terminally HIS-tagged GLI2 (Gift from Dr Fritz Aberger) was cloned into XhoI/SmaI site of pI2E-A to generate pI2E-A-GLI2 construct. Both pI2E-A-GLI1 and pI2E-A-GLI2 were digested with Sall/NotI to isolate the CMV-GLI1-IRES-EGFP and CMV-GLI2-IRES-EGFP sequence. Retroviral vector SIN-IP-GFP was digested with XhoI/NotI to excise the CMV-GFP sequence to generate SIN-IP. CMV-GLI1-IRES-EGFP, CMV-GLI2-IRES-EGFP and CMV-IRES-EGFP were cloned into XhoI/NotI digested SIN-IP creating SIN-GLI1-IRES-EGFP, SIN-GLI2-IRES-EGFP and SIN-IRES-EGFP (control) constructs (see **Figure 2.2**). All constructs were verified by DNA sequencing. **Figure 2.3** shows *GLI1* constructs used to transform baby rat kidney cell line and *GLI1* construct used to transduce human primary keratinocytes and also expected mRNA transcripts from these cell lines.

2.2.3 Generating a SIN-GLI1-mutated Nuclear Localization Signal (mNLS) construct.

GLI1 coding cDNA was cloned into pEGFP-C3 (Clontech) to create pEGFP-GLI1 by Dr Judith Green. A brief description of the protocol is as follows. Quick Change Site-Directed Mutagenesis Kit (Stratagene) was used to mutate GLI1-Nuclear-Localisation-Signal (NLS1, NLS2 and NLS3) to generate pEGFP-GLI1-mutated-Nuclear-Localisation-Signal (pEGFP-GLI1-mNLS). GLI1-Nuclear-Export-Sequence was also

CHAPTER 2: Materials and Methods

mutated to generate pEGFP-GLI1-mutated-Nuclear-Export-Signal (pEGFP-GLI1-mNES).

The mutated residues and their positions are shown in **Table: 2.1**. Retroviral plasmids SIN-EGFP-GLI1-mNLS and SIN-EGFP-GLI1-mNES (see **Figure 2.4**) were created by sub-cloning of the CMV-EGFP-GLI1-mNLS and SIN-EGFP-GLI1-mNES regions from pEGFP-GLI1-mNLS and pEGFP-GLI1-mNES in to SIN-IP-GFP retroviral vector as described in **section 2.2.2** above.

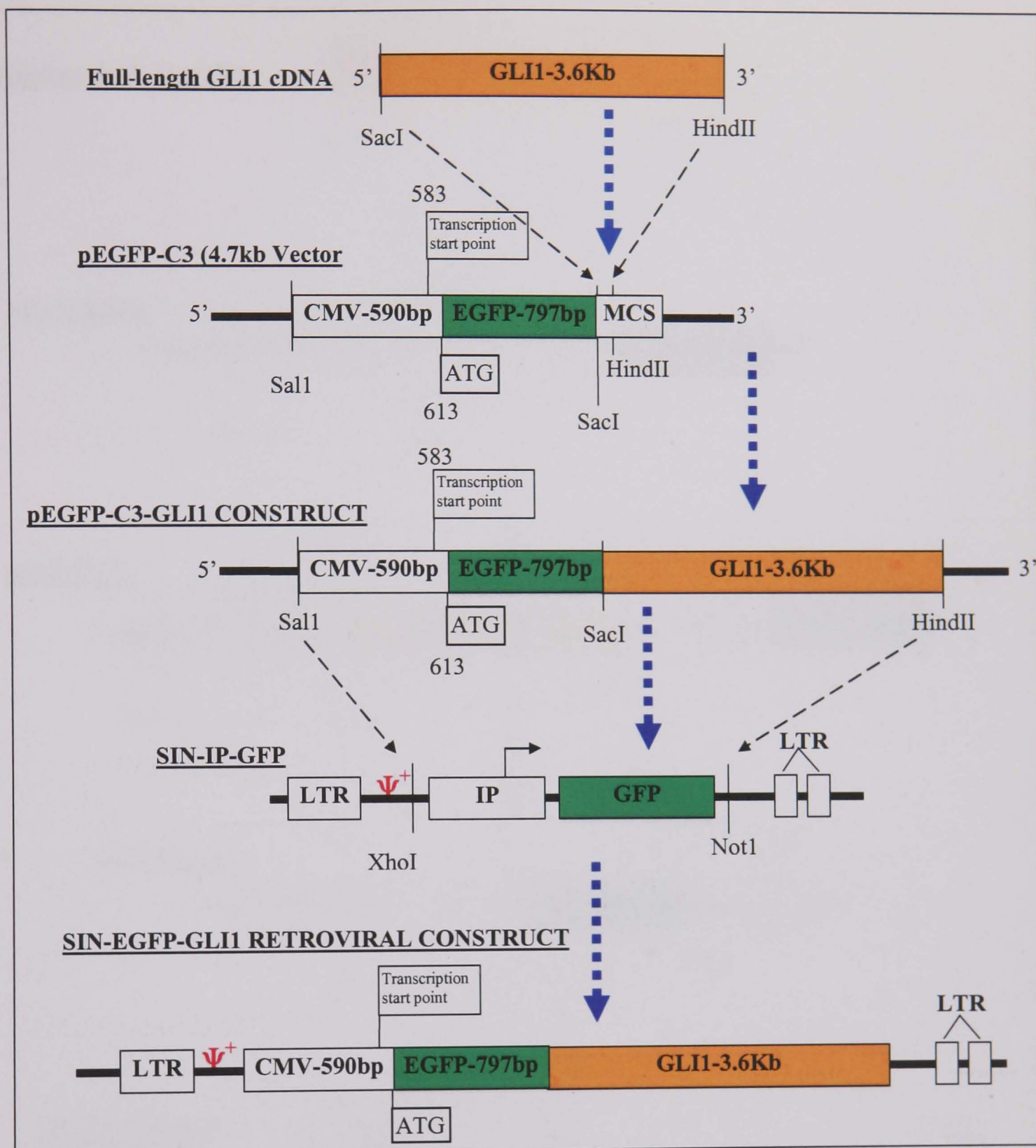


Figure 2.1: Diagram showing the plasmids used and the cloning sites of Enhance Green Fluorescence Protein (EGFP)-GLI1 fusion protein construct in to the Self INactivating Internal Promoter Green Fluorescence Protein (SIN-IP-GFP) retroviral vector to generate SIN-EGFP-GLI1 retroviral vector. A control SIN-EGFP was also generated this was same as the SIN-EGFP-GLI1 construct that lacked GLI1.

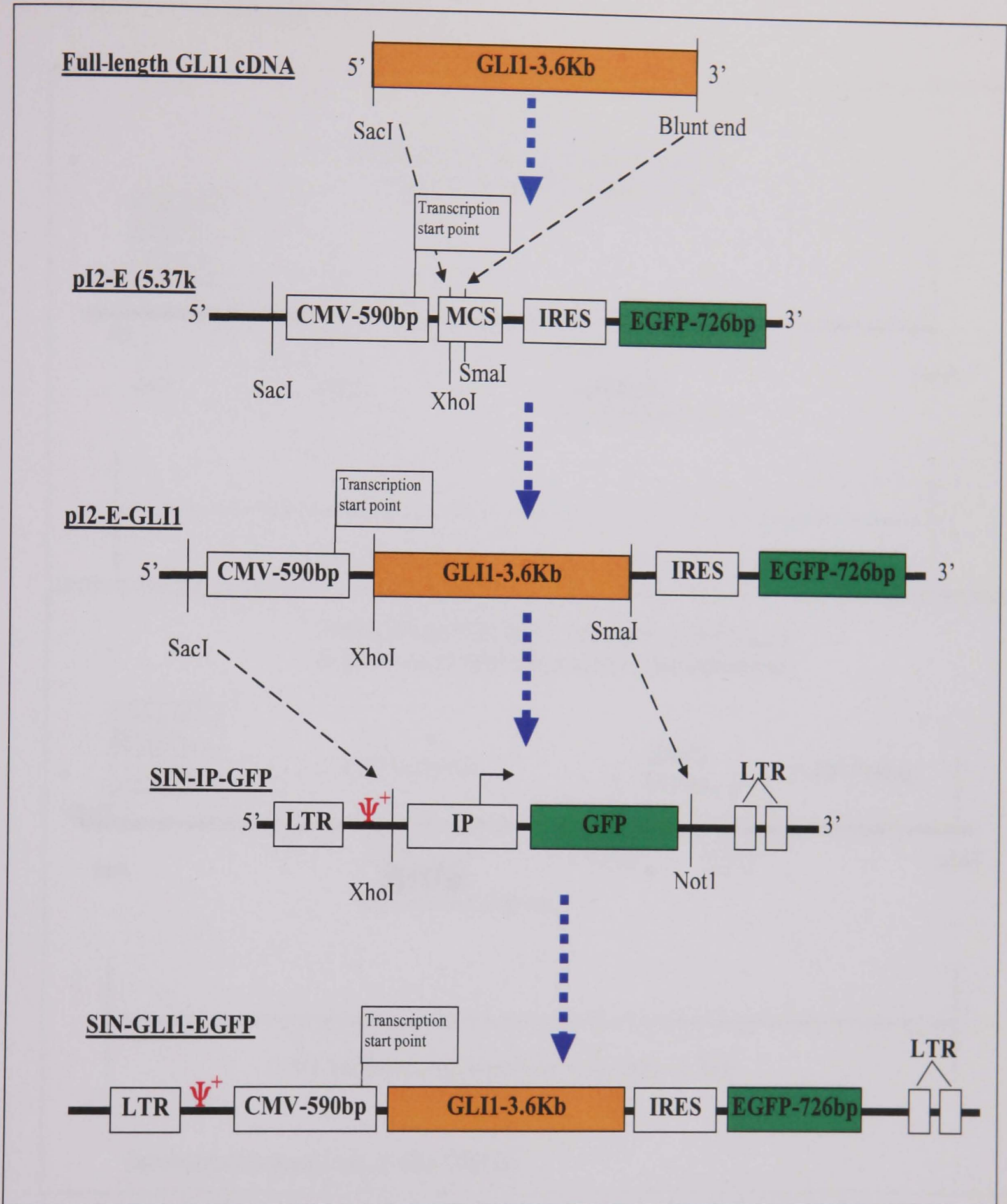


Figure 2.2: Showing the vectors used and the cloning sites to generate SIN-GLI1-EGFP retroviral vector. GLI1 and the Enhance Green Fluorescence Protein with the Internal Ribosomal Entry Site (GLI1-IRES-EGFP) bicistronic construct, was cloned in to the Self INactivating Internal Promoter Green Fluorescence Protein (SIN-IP-GFP) retroviral vector to generate SIN-GLI1-EGFP retroviral vector construct. Same strategy was used to generate SIN-GLI2-EGFP and SIN-EGFP (control) retroviral vectors.

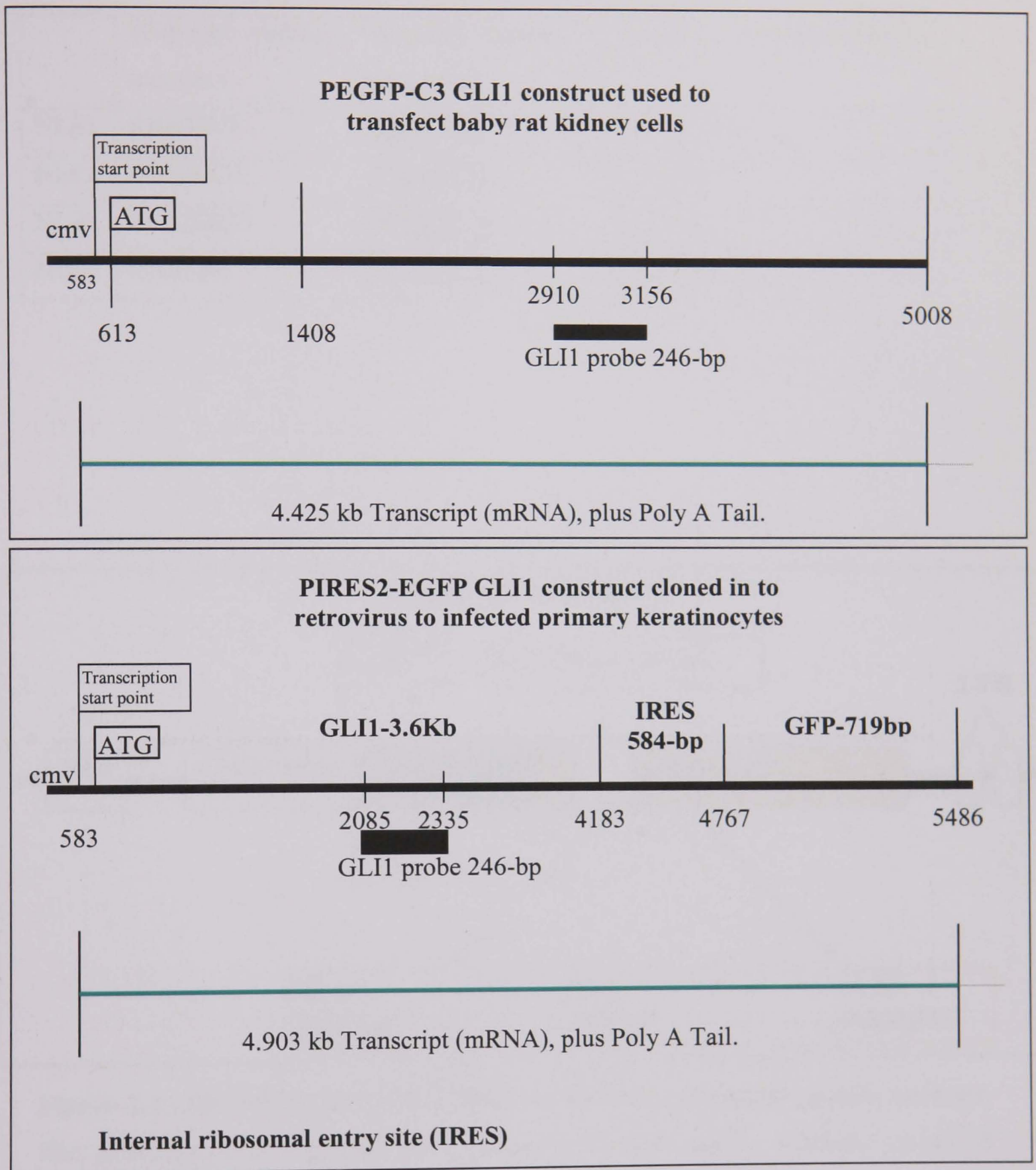


Figure 2.3: Diagram showing GLI1 constructs used to transform baby rat kidney cell line and GLI1 construct used to transduce human primary keratinocytes and also expected mRNA transcripts from these cell lines. The black filled boxes are the cDNA probes used to detect the transcript and the regions they correspond to.

Table 2.1: Showing the amino acid residues of GLI1 nuclear localisation signals (NLS1, 2 and 3) and nuclear export signal (NES) and the positions of the residues mutated

	Wild type residue sequence	Mutated residue sequence	Positions of residues mutated
NLS1	RKHVKT	<u>L</u> IHV <u>M</u> T	380,381,384
NLS2	KRHRGD	K <u>L</u> H <u>L</u> GD	396,398
NLS3	PKREREG	PK <u>S</u> E <u>L</u> EG	415,418
NES	LENLRL	<u>V</u> EN <u>V</u> R <u>V</u>	498,501,503

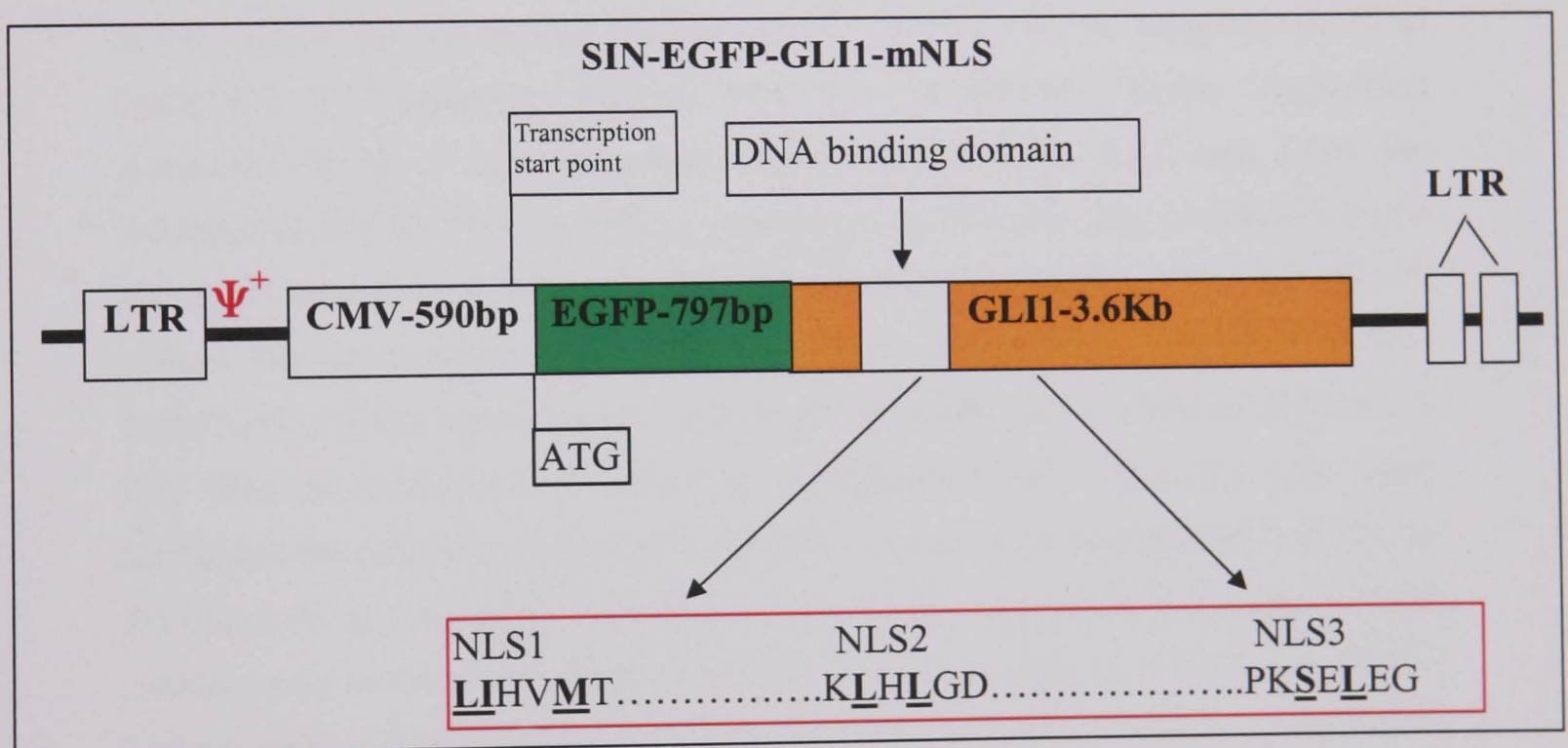


Figure 2.4: SIN-EGFP-GLI1-mNLS (mutated-Nuclear-Localisation-Signal) construct. The positions of the cloning sites and the amino acid residue sequence of mNLS regions.

2.2.4 Generating retroviral particles in packaging cell line.

Retrovirus encoding SIN-EGFP-GLI1, SIN-EGFP-GLI1-mNLS, SIN-EGFP-GLI1-mNES, SIN-GLI2-EGFP, and SIN-EGFP (from sections 2.2.1, 2.2.2 and 2.2.3) were produced by Dr Graham Neill using the packaging line Phoenix-HEK-293 T-based cells (Amphotropic form) derived from highly transfectable mammalian foetal kidney epithelial cells (Clonotech) as previously described by (Deng et al., 1997). Amphotropic form of virus replicates in cells of BOTH the natural host and foreign origin. Phoenix-A packaging cells were seeded at density of 1.5×10^6 cells/60-mm plate in a 15 ml Dulbecco's Modified Eagle's Medium (DMEM, Sigma Cat. No. D5796) supplemented with (100 units/ml penicillin G sodium, 100µg/ml streptomycin, 4mM L-glutamine, 1mM sodium pyruvate and 10% (v/v) foetal bovine serum) and incubate at 37°C in 5% CO₂ 95% air atmosphere for 18-24 hours.

The media was removed and replaced with fresh 15 ml supplemented DMEM medium before adding the transfecting reagent, 200 µl DMEM with no supplements, 25 µl FuGENE® 6 Transfection Reagent (Cat No 11815091001, Roche Diagnostics) containing 10 ug of retroviral vector (from sections 2.2.1, 2.2.2 and 2.2.3) and incubated at 37°C in 5% CO₂ 95% air atmosphere for 24 hours. The transfection media was removed and fresh DMEM media supplemented with (100 units/ml penicillin G sodium, 100 µg/ml streptomycin, 4mM L-glutamine, 1mM sodium pyruvate, 10% (v/v) foetal bovine serum and 1-2µg/ml puromycin) was added and incubated at 37°C in 5% CO₂ 95% air atmosphere, to select for transfected Phoenix-HEK-293 cells. Upon confluence the cells were incubated in 4ml fresh medium with out puromycin at 32⁰C in 5% CO₂ 95% air atmosphere for 24 hours, after which the medium containing the viral particles was removed and filtered through a 0.45-µm filter to remove any debris. Filtered medium containing the virus was snap frozen in liquid nitrogen in 15 ml Falcon tubes and stored at -80°C. Viruses were harvested from same cell cultures 2 or 3 times.

2.2.5 Transducing primary and N/TERT keratinocytes.

Primary keratinocytes (from section 2.1.2) were given to Dr Graham Neill to transduce with retroviral particles generated from the packaging cell line (from section 2.2.4) as described by (Deng et al., 1997). In brief for gene expression and morphological analysis, 1×10^5 keratinocytes were seeded in 6-well plates in 2ml defined keratinocyte culture medium (Cat No 10744-019 Invotrogen) supplemented with growth supplements (10% v/v FCS) and incubated at 37°C in 10% CO₂ 90% air atmosphere for 16-18 hours. The cells were then primed with hexadimethrine bromide (polybrene) 1-10 mg/ml for 10 min prior to transduction. Polybrene was also added at 1-10 mg/ml to 2 ml retroviral suspension from section 2.2.4 and the cells were transduced with recombinant retrovirus (encoding SIN-EGFP-GLI1, SIN-GLI1-EGFP, SIN-GLI2-EGFP and SIN-EGFP) in triplicate wells by centrifuging the plates at 300-350 x g for 1 hour at 32°C then washed with sterile phosphate buffer saline (PBS). Post-transduction, cells were incubated for 24 hours at 37°C in 10% CO₂, 90% air atmosphere in defined keratinocyte culture medium containing the growth supplements (10% v/v FCS) to allow the expression of the transduced gene. Then cells were cultured in defined keratinocyte culture medium containing no growth supplement for 24 hours, to remove the effect of growth supplement stimulation. After which the media was removed and cells were cultured under following conditions; 1) Defined keratinocyte culture medium containing 10 ng/ml EGF (Cat No E 9644 Sigma) and at 37°C in 10% CO₂, 90% air atmosphere for 24 hours. 2) Defined keratinocyte culture medium containing no growth supplement (controls), and incubated at 37°C in 10% CO₂, 90% air atmosphere for 24 hours.

EGFP fluorescence and change in cell morphology was visualised using a light microscope (Leica DM IRB) fitted with a krypton/argon mixed-gas laser for emitting excitation wavelength at 488 nm. Cell Images were captured with a digital imaging system attached to the microscope (Leica DC200 imager with DC Viewer software V3.2). After capturing the images of transduced cells, the cells were either processed for total RNA extraction (see section 2.5.0) or protein extract (see section 2.14.0). The N/TERT cells (gift from Dr J. Rheinwald) were also transduced with SIN-GLI1-EGFP, SIN-EGFP and SIN-EGFP-GLI1mNLS in triplicate wells as described for primary keratinocytes in section 2.2.5.

2.3.0 GLI1 polyclonal baby rat kidney cells.

GLI1 transformed polyclonal baby rat kidney cell lines were obtained from Dr Judith Green and GLI1 transformed 10T1/2 mouse fibroblast cell line were obtained from Dr Muy-Teck Teh, these cells were cultured in DMEM medium supplemented with 10% (v/v) FCS, 4 mM L-Glutamine.

2.3.0 Normal human skin and basal cell carcinoma (BCC).

Normal human skin was obtained from plastic surgery from facelift and breast reduction surgery carried out at the Holey House Hospital UK. Human BCC tissue was obtained from the patient who had BCC removed at the Royal London Hospital Dermatology out patient department. Ethical committee approval was obtained (ethics number: T/01/034) as well as informed consent from each patient for the use of the redundant Normal skin and BCC tissue samples for scientific research.

Immediately after Normal skin or BCC specimens were excised they were snap frozen in liquid nitrogen and transported from the theatre to the laboratory in liquid nitrogen. The tissue samples were stored at -80°C until processed for RNA extraction or for In-situ Hybridisation (see **sections 2.5.0** and **2.10.0**).

2.5.0 RNA extraction.

2.5.1 Total RNA extraction from cultured cells.

All materials including eppendorf tubes, glass bottles and dH₂O used for RNA work were treated with 0.1% (v/v) Diethyl Pyrocarbonate (DEPC) overnight at room temperature, (to inactivate RNase by covalent modification) then autoclaved for 30 min at 120°C, 15 psi to remove traces of DEPC. All the equipment was dried before use. Sterile RNase and DNase free filter pipette tips (10 µl, 30 µl, and 200 µl and 1 ml) were used to avoid cross contamination. Gloves were changed frequently to minimise the risk of RNase contamination from the skin.

Culture medium from a confluent 75cm² (Falcon) flask or 6 well plates was removed and washed twice with sterile PBSA (Phosphate buffer saline with out Ca/Mg). Cells were lysed by adding 0.1 ml RNazol B (Biogenesis Ltd Cat No CS-105) per cm² cell

CHAPTER 2: Materials and Methods

culture surface area. RNA was solubilised by passing the lysate through a pipette a few times. The homogenate was transferred to a sterile 14 ml (Greiner labortechnik Cat No 187 261) centrifugation tube. 0.2 ml chloroform per 2 ml of homogenate was added, the centrifugation tube was covered with its top and shaken (not vortex) vigorously for 15 sec and incubated on ice for 5 min, centrifuged at 12,000xg, 4°C for 15 min. After centrifugation the homogenate formed two phases, the lower phase (Blue, phenol-chloroform phase) and the colourless upper aqueous phase. The DNA and the proteins were in the interphase and lower organic phase. The RNA was in the upper aqueous phase and the volume of aqueous phase was approximately 50 % of the initial volume of RNazol B plus the initial volume of cells.

The aqueous phase was transferred to a fresh centrifuge tube and equal volume of isopropanol was added, incubated at 4°C for 15 min and centrifuged at 12,000xg, 4°C for 15 min to precipitate the RNA. Precipitated RNA formed a white yellow pellet at the bottom of the tube. The supernatant was removed without disturbing the RNA pellet. The RNA pellet was then washed with 1.2 ml 75% (v/v) ethanol by vortexing and centrifuging at 7,500xg, 4°C for 8 min. Ethanol was removed and the pellet was allowed to air dry at room temperature for 10-15 min. Extreme care was taken not to allow the RNA pellet to dry completely, as this would have made it difficult to resuspend the RNA pellet.

The RNA pellet was dissolved in 100-300 µl DEPC treated dH₂O by gently vortexing or passing the RNA solution a few times through a 1ml pipette tip and transferred to a 1.5 ml eppendorf tube (for 6 well plates 25-50 µl volume per well was used to dissolve the RNA pellet).

2.5.2 Total RNA extraction from frozen tissue.

Tissue sections (25 µm) were cut using cryostat at -20°C, sections were collected in RNase free weighing boat. Immediately after cutting the sections, 2 ml RNazol-B per 100 mg tissue was added. The tissue sample was homogenised in a glass-Teflon homogeniser, and transferred to a 14 ml (Greiner labortechnik) centrifugation tube. The remaining procedure was the same as that followed for RNA extraction from cultured cells (see **section 2.5.1**). If there were more than 3 samples the homogenate was stored

at -70°C until all the samples were homogenised and then they all were simultaneously processed.

2.5.3 Messenger RNA isolation from total RNA.

The volume containing 75 μg of total RNA was adjusted to 100 μl with DEPC treated dH_2O . This step was omitted if only small adjustment was required. Total RNA was denatured by incubating at 65°C for 2 min to disrupt secondary RNA structures. 200 μl (1 mg) of resuspended Dynabeads (Cat No 610.01, DDYNAL) Oligo $(\text{dT})_{25}$ were dispensed into a 1.5 ml eppendorf tube and placed in the magnetic (DynaL MPC-E-1) rack. After 30 sec the supernatant was removed while keeping the eppendorf tube in the magnetic rack.

Dynabeads were washed by removing the eppendorf tube from the magnet and resuspending the Dynabeads in 100 μl Binding buffer (20 mM Tris-HCl pH 7.5, 1M LiCl, 2 mM EDTA). The eppendorf tube was placed back in the magnet rack and the binding buffer removed after 30 sec.

The eppendorf tube was removed from the magnet rack and the Dynabeads resuspended in 100 μl Binding buffer, (Optimal hybridisation conditions recommended by the manufacturers were, Binding buffer at 1:1 ratio relative to the sample volume) to this total RNA denatured above was added and mixed thoroughly to allow the messenger RNA (mRNA) to anneal to the Dynabeads, by rotating on a roller or mixer at room temperature for 3-5 min. The eppendorf tube was placed in the magnet rack for 30 sec and the supernatant removed.

The mRNA bound Dynabeads were washed twice, by removing the eppendorf tube from the magnet rack and resuspending in 150 μl washing buffer provided in the kit. the eppendorf tube was placed back in the magnet rack and supernatant removed. When working with small volumes care was taken to remove all the supernatant between each wash.

Using 10-20 μl elution buffer (10mM Tris HCl pH 7.5) mRNA was eluted by resuspending the Dynabeads in the elution buffer, incubating at 65°C for 2 min. After

incubation the eppendorf tube was immediately placed in the magnet rack for 30 sec. the supernatant containing the eluted mRNA was transferred to a new RNase free eppendorf tube. Isolated mRNA samples concentration and integrity was determined (as described in **section 2.5.4** and **2.5.5**). Purified mRNA samples were stored at -70°C if not used immediately. Dynabeads were not allowed to dry out during the procedure as this would have reduced their mRNA binding efficiency.

2.5.4 Determining the concentration of purified RNA.

The concentration of RNA was determined by diluting 1µl of RNA sample with 9µl of RNase free dH₂O. 2µl diluted RNA sample was placed into a 2 mM path cuvette (Genespec) and its absorbance (Abs) value at 260nm and 280nm was measured using a spectrophotometer (Genespec). A RNA preparation free of DNA and protein was expected to have a 260nm Abs / 280nm Abs ratio of 1.9. Following formula was used to determine the concentration of RNA (Abs value at 260 nm x 40 µg/ml x Dilution factor = µg/ml RNA). Remaining 8µl diluted RNA sample was used in **section 2.5.5**.

2.5.5 Checking the integrity of purified RNA.

The integrity and the size distribution of purified RNA was checked by running 8 µl of diluted RNA sample from **section 2.5.4** in 2 µl RNA loading buffer [50% (v/v) deionised formamide, 6% (v/v) formaldehyde, 1x MOPS-EDTA buffer, 6.6% (v/v) glycerol, 0.02% (w/v) bromphenol blue, 0.02% (w/v) xylene cyanol, 39.58 ug/ml ethidium bromide] on a 1% (w/v) RNase free ethidium bromide agarose gel in 0.5x (Tris-borate/ethylene diamine tetra-acetic acid [EDTA]) TBE buffer (see **section 2.5.6**). The ribosomal 28S rRNA and 18S rRNA appeared as sharp bands and the 28S rRNA was present at approximately twice the intensity of the 18S rRNA band. Equal intensity of the two ribosomal (28S rRNA and 18S rRNA) bands indicated some degradation had occurred, smear on the bottom of the gel with no ribosomal bands indicated complete degradation of total RNA. RNA samples were stored at -70°C and repeat thawing and freezing was avoided to prevent RNA degradation.

2.5.6 Agarose gel electrophoresis.

1% (w/v) agarose gel was made as follows. 0.35g agarose gel (Sigma) was placed in 35ml 0.5 x TBE (Tris-borate/ethylene diamine tetra-acetic acid) buffer in a 100ml conical flask. The mixture was heated in a microwave for a minimum time required to allow the agarose to dissolve. Heating was interrupted at regular intervals and the flask swirled to mix the contents, to stop the solution over boiling. The gel was allowed to cool till hand warm before adding 1 μ l 10mg/ml ethidium bromide, to avoid generating ethidium bromide vapour. Ethidium bromide is carcinogenic so contact with skin was avoided by wearing gloves. Content of the flask were mixed and the gel was poured into a mini gel cast with a comb in it. The agarose gel was allowed to set for 20-30 min before removing the comb. The set agarose gel cast was placed in the electrophoresis chamber and enough 0.5 X TBE buffer was added just to cover the surface of the gel. DNA or RNA samples were mixed with the appropriate loading buffer and loaded into the wells along side a DNA (Cat No 10488-085 Invitrogen) or RNA Marker (Cat No R7020 Sigma). The apparatus was connected to a power supply and the gel was run at 1-5 volts/cm to resolve different size DNA or RNA fragments. After the electrophoresis was complete the gel was removed and placed on a UV lamp box and the image was captured using a digital camera with Alpha computer programme.

2.6.0 Analysis of mRNA by northern blot hybridisation.

Northern analysis is a standard method used for detection and quantification of mRNA by comparing it to a standard such as β -Actin, between samples on a single membrane. It is the preferred method for determining transcript size and for detecting alternatively spliced transcripts. Basic principles of the method are; the RNA samples are first separated by size via electrophoresis in an agarose gel under denaturing conditions. The RNA is then transferred to a membrane cross-linked by UV and hybridized with a specific radiolabelled *in vitro* transcribed DNA or RNA probe. To detect more than one message, initial probe was striped before hybridizing with a sec probe.

2.6.1 Electrophoresis of mRNA on formaldehyde agarose gel.

Formaldehyde denaturing agarose gel was prepared as follows, 1.8 g of agarose gel (Sigma) was placed in 109.5 ml DEPC dH₂O in a 250 ml conical flask, the mixture was heated in a microwave for a minimum time required to allow the agarose to dissolve. Heating was interrupted at regular intervals and the flask swirled to mix the contents, to stop the solution over boiling. Remaining steps were carried out in a fume hood to avoid inhaling formaldehyde fumes which are toxic. The gel was allowed to cool to 55°C before adding 15 ml 10x MOPS (0.4 M Morpholinopropanesulfonic acid; 0.1 M Na-acetate-3 x H₂O; 10 mM EDTA pH 7.2) and 25.5 ml 35% (w/v) Formaldehyde. Content of the flask were mixed and the gel was poured in to a gel cast with a comb in it. The formaldehyde agarose gel was allowed to set for 30-60 min before removing the comb. The set agarose gel cast was placed in the electrophoresis chamber and enough 1 x MOPS (40 mM morpholinopropanesulfonic acid; 10 mM Na-acetate-3 x H₂O; 1 mM EDTA pH 7.2) buffer was added just to cover the surface of the gel.

Purified 2 µg mRNA (in a 12 µl volume) samples from **section 2.5.3** of normal skin (NS), basal cell carcinomas (BCC), HaCat, A375 and GLI1 infected primary keratinocytes, and positive controls expressing GLI1, GLI1 transformed polyclonal baby rat kidney cell line and GLI1 expressing foetal mouse fibroblasts 10t1/2 cell line (obtained from Dr Muy-Teck), 5 µl of RNA ladder (0.24-9.5 Kb Life Technologies Cat No 15620-016) made up to 12 µl with 0.1 M Tris-EDTA pH 8 buffer. Were mixed with 17.5 µl electrophoresis cocktail [1 µl 20x MOPS, 10µl formamide, 3.5 µl 37% (w/v) formaldehyde, 1 µl [1 mg/ml] ethidium bromide (EtBr), 2 µl blue juice [50% (v/v) glycerol, 1 x MOPS, 0.2% (w/v) bromophenol blue]. The samples and the RNA ladder were denatured at 65°C for 10 min and immediately placed on ice to prevent secondary RNA structure formation, before loading in to the wells of formaldehyde denaturing agarose gel (see above). The electrophoresis apparatus was set up and initially the samples were ran at 100 volt, once the samples had migrated out of the wells, the voltage was reduced to 15-20V and electrophoresis run overnight (approximately 16 hours).

Following electrophoresis the gel was examined under UV to check the integrity of the mRNA and the image captured with a ruler beside the marker lane, to determine the mRNA transcript size in relation to the RNA ladder later. The wells, marker lane and a

top corner of the gel were cut and discarded (the corner cut was recorded in the lab book). The gel was washed in, 50 mM NaOH/100 mM NaCl for 20 min, 0.1 M Tris-HCl pH 7 for 20 min, 2x SSC (Standard Saline Citrate) for 20 min, on a shaker at room temperature.

2.6.2 RNA transfer to Hybond-XL membrane.

Messenger RNA was transferred to the hybridisation membrane by setting up an apparatus shown in **Figure 2.5**. Whatman 3 MM filter paper (x 3).and 1 piece of hybridisation membrane (Hybond-XL membrane, Amersham Pharmacia Biotech Cat No RPN 203S) were cut 2 mm larger all round than the size of the actual gel. Hybridisation membrane was rinsed in DEPC dH₂O. The membrane and two pieces of Whatman 3 MM filter paper were soaked in 2x SSC. The gel tray cast was rinsed with DEPC dH₂O, inverted and placed in an RNase free glass tray.

A Whatman 3 MM filter paper was cut the same size as the gel cast width but 4-6 inches more than the gel cast length, so that it over hangs from each side of the gel cast. This was placed on the inverted gel cast, 20x SSC transfer buffer was poured into the glass tray so that the edges of the filter paper stayed submerged in 20 x SSC solution. Any air bubbles between the gel cast tray and the filter paper were rolled out using a 25 ml sterile pipette. Messenger RNA agarose gel from **section 2.6.1** was inverted and placed on the filter paper any air bubbles between the gel and filter paper were removed as above. Exposed filter paper edges around the gel were covered with Para film, to prevent short-circuiting of the transfer solution.

The hybridisation membrane and then two Whatman 3 MM filter paper pieces soaked in 2x SSC were placed on top of the gel, and any air bubbles formed were removed. A dry Whatman 3 MM filter paper was placed on top and a stack of approximately 5 inches of blotting pads (or paper towels) cut to gel size were placed on top. A flat surface object (e.g. a plastic container lid) and a weight approximately 500 g were placed on top of the blotting pads (see **Figure 2.5**). The apparatus was covered with cling film to prevent evaporation of 20x SSC and to keep out dust. mRNA was allowed to transfer to the hybridisation membrane over night at room temperature.

The next day the apparatus was carefully disassembled leaving the hybridisation membrane in contact with the gel. The back of the membrane was marked with a pencil to indicate which side the mRNA had transferred. The membrane was carefully removed and washed in 6x SSC for 5 min at room temperature. The hybridisation membrane was placed on a clean filter paper, and allowed to air dry for approximately 5 min at room temperature.

The gel was examined under UV to check if all the mRNA had transferred on to the hybridisation membrane. The mRNA was UV cross-linked to the membrane with RNA side up, using an UV-Stratalinker (Sratagene) set at auto cross-link. The UV cross-linked mRNA membrane was placed between two sheets of Whatman 3 MM filter paper and wrapped in aluminium foil, and stored at room temperature until probed.

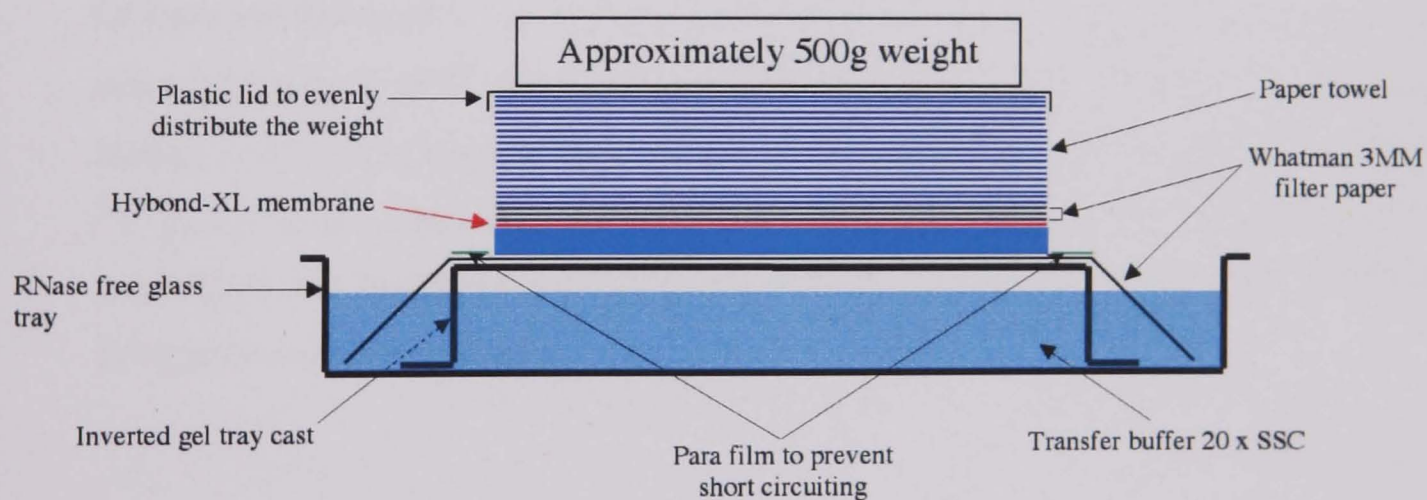


Figure 2.5: Different components of northern blot apparatus and how it was assembled.

2.6.3 Probe generation for northern blot analysis.

PTCH (500 bp insert) and GLI1 (250 bp insert) probes cloned in HindIII, EcoRI sites of PGEM plasmid were obtained from Dr Judith Green. GLI2 (1.6kb insert) cloned into EcoRI site of PCRII TOPO plasmid was obtained from Dr Fritz Burg. PTCH GLI1 and GLI2 probes were generated by cutting them from the vectors in which they were cloned. Beta-Actin probe was generated by PCR amplification (see section 2.7.4). Cloned inserts and the PCR products were run on 1-2% (w/v) agarose gel (see section 2.5.6), the insert and the PCR products were cut out and extracted from the gel using QIAquick Gel Extraction Kit (QIAGEN Cat No 28704) as per manufactures instructions (see section 2.7.5). The probes were quantified by running on 1-2% (w/v) EtBr agarose gel along side a known concentration standard marker (see section 2.5.6).

2.6.4 Probe labelling.

The probes were labelled with α -³²P dCTP (Amersham Pharmacia Biotech Cat No AA0005 250 μ Ci) using Megaprime DNA labelling systems (Amersham Pharmacia Biotech Cat No RPN 1604/5/6/7) as per manufacturers instruction. Briefly, 25 ng QIAGEN purified probe, 5 μ l Nonamer Primers made up to 15 μ l with RNase free dH₂O were denatured at 100°C for 5 min and then pulse centrifuged. To this 10 μ l labelling Buffer, 2 μ l (1U/ μ l) Klenow fragment, 18 μ l RNase free dH₂O and 5 μ l (10 μ Ci/ μ l) α -³²P dCTP were added. The reaction was mixed by pipetting up and down, pulse centrifuged and incubated at 37°C for 10 min. All radioactive work is carried out in designated radioactive area.

2.6.5 Probe purification.

Labelled probe was purified using a Bio-Spin 30 chromatography column (BIO-RAD Cat No 732-6006). The settled gel was resuspended by inverting the column several times; this also removed any air bubbles. The column tip was snapped off and the column placed in a 2 ml micro centrifuge tube, the column cap was removed and the buffer allowed to drain and discarded. Both the column and the 2 ml micro centrifuge

CHAPTER 2: Materials and Methods

tube were taped together using autoclave tape and placed in a 50 ml centrifuge tube, and centrifuged at 1000x g for 2 min. The buffer was discarded and the column placed in a 1.5 ml RNase-free eppendorf tube, both were taped together and placed in a 50 ml centrifuge tube.

The labelled probe from **section 2.6.4** above was carefully transferred directly to the centre of the column, and centrifuged for 4 min at 1000xg. Purified probe was collected in an eppendorf tube in SSC buffer. The tape was removed and the column taken out of the tube and discarded in a ³²P waste container. Percent (%) labelling was estimated by measuring the radioactivity (using a ³²P series 900 mini monitor) of the column and the purified probe. The % labelling of the purified probe was calculated as follows. Activity of the purified probe / Total activity (column and the purified probe) x 100 = % labelled probe. The percent labelling was around 20-55 %.

2.6.6 Membrane pre-hybridisation.

The nylon membrane was rolled and placed into a hybridisation cylinder containing a small amount of 2x SSC, and then unrolled in the cylinder. A 10 ml aliquot (stored at -20°C) of pre-hybridisation solution (50 ml Formamide, 25 ml 20x SSC, 10 ml 50x Denhardt's, 10 ml 0.5M pH 6.8 Sodium phosphate buffer, 2 ml 10% (w/v) Sodium dodecyl sulphate (SDS), 3 ml RNase free dH₂O) were placed into a water bath at 65°C. Once the pre-hybridisation solution had reached the water bath temperature, one gram of dextran sulphate (Amersham Pharmacia Biotech Cat No 17-0340-01) was added. Pre-hybridisation containing the dextran sulphate was heated at 65°C for approximately 4-5 hours to allow the dextran sulphate to dissolve completely.

The hybridisation solution was allowed to cool down to room temperature. 3 mg tRNA (300 µl 10 mg/ml tRNA in RNase Free dH₂O from Bakers yeast, Boehringer Mannheim, Cat No 109/495) was heated at 100°C for 10 min and immediately placed on ice to cool before adding it to cold hybridisation solution. Excess SSC was poured off from the hybridisation cylinder and replaced with the pre-hybridisation solution and incubated rotating at 42°C in a hybridisation oven overnight.

2.6.7 Membrane hybridisation.

Hybridisation solution was prepared the same way as the pre-hybridisation solution with 1 mg tRNA (100 μ l [10 mg/ml] tRNA) instead of 3 mg tRNA. To which labelled probe, denatured at 100°C for 5 min and immediately placed on ice, was added.

The pre-hybridisation solution was removed from the cylinder and replaced with hybridisation solution and incubated rotating at 42°C in a hybridisation oven overnight. The following day the hybridisation solution was discarded and the blot was carefully removed from the cylinder and washed gently in 250 ml wash buffer (2x SSC, 0.1% (w/v) SDS pH 7.2) at room temperature for 30 sec. The wash buffer solution was discarded and replaced with 250 ml fresh wash buffer and washed shaking for 20 min at room temperature, this step was repeated with 250 ml fresh wash buffer. A final wash was carried out in 250 ml wash buffer preheated to 60°C, shaking at 60°C for 20 min. The blot was sealed in a plastic bag or wrapped in saran wrap and exposed to a Phosphor Screen (Molecular Dynamics) for 16-48 hours and the screen scanned on STROM 840 scanner.

Following autoradiography, the blot was placed in a plastic container with 250 ml strip solution [75% (v/v) formamide, 0.1% (w/v) SDS in DEPC dH₂O] and agitated at 70°C for 10 min. The strip solution was discarded and the blot was washed 3 times with 2x SSC. The blot was sealed in plastic bag with a small amount of 2x SSC, to keep it moist, and stored at -20°C until re-probed with another probe. The stripped blot was exposed to the phosphor screen to check for any radioactivity; if there was any radioactivity left, the blot was left to allow the radioactivity to decay. The blot was not re-probed, until there was no radioactivity detected. The northern blot was probed with *GLII*, *PTCH*, β -Actin and *GLI2* probe in a descending order. In order to calculate the size of the transcripts detected, the distance that each RNA marker had migrated from the gel was measured. A log (RNA size) against the distance of marker migration in cm was plotted using a Microsoft Excel program. The 'best fit' plot was used to determine the size of the transcript detected.

2.7.0 Reverse Transcriptase Polymerase Chain Reaction (RT-PCR).

2.7.1 Primer designing.

Forward and reverse primers (shown in **Table 2.2**) were designed using amplify sequencing programme and based on the publish sequence accessed from the database of the National Centre of Biotechnological Information (NCBI) web site <http://www.ncbi.nih.gov/>.

Following criteria were used in selecting the primers. The primer length was 20-26 base pairs (bp) and they flanked the region of interest. The G and C content was 40-60%, and avoided using sequence which would have given rise to internal secary structures. The 3' ends of the primers were not complementary to avoid the production of primer dimmers in the PCR reaction, and avoided having three G or C nucleotides in a row near the 3' end of the primer. Ideally both primers should have a same annealing temperature or +/- 5°C. The minimum melting temperature (T_m) was 50°C and the maximum T_m 65°C. The PCR reaction annealing temperature set is dependent upon the primer with the lowest T_m .

2.7.2 Removing contaminating DNA from total RNA preps.

To eliminate any DNA contamination present in RNA samples, total RNA samples were treated with a Deoxyribonuclease I, Amplification Grade (DNase I, Amp Grade, Cat. No 18068-015 Invitrogen), before reverse transcribing the RNA to cDNA. A mater mix was made up of DNaseI (1U/ μ l) in 1x DNaseI reaction buffer enough for all the total RNA samples. 1.6 μ l of DNaseI (1 U/ μ l) in 1x DNaseI reaction buffer was added to each 2.5 μ g total RNA sample in 6.4 μ l volume (**Table 2.3 and Table 2.4**) and mixed by vortexing and then pulse centrifuged. All the samples were incubated at room temperature for 15 min to allow digestion of any DNA present. The digest reaction was stopped by adding 0.8 μ l of 25 mM EDTA solution the sample was mixed and pulse centrifuged and incubating at 65°C for 10 min, to inactivate DNaseI. All samples were then immediately processed as described in **section 2.7.3** below.

2.7.3 First strand cDNA synthesis with Reverse Transcriptase.

First strand cDNA synthesis was carried out using a Promega (Cat No A3500) kit, as per manufacturers' instruction. DNaseI treated total RNA samples from section 2.7.2 were denatured at 70°C for 10 min in a PCR thermo cycler and then pulse centrifuged for 10 sec and immediately placed on ice.

A master mix was made to give a final concentration of the following components, 5 mM MgCl₂, 1x Reverse Transcription Buffer (10 mM Tris-HCl pH 9.0 at 25°C, 50 mM KCl, 0.1% v/v Triton X -100), 1 mM each dNTP, 0.8 U/μl Recombinant RNasin Ribonuclease inhibitor, 0.9 U/μl Avian Myeloblastosis Virus (AMV) Reverse Transcriptase, 12.5 ng/μl Oligo (dT)₁₅, 12.5 ng/μl random primers, in a 25 μl total reaction volume. Negative control reactions were also set up using dH₂O instead of total RNA and total RNA from one of the sample (**Table 2.3 and Table 2.4**) without the Reverse Transcriptase (RT).

16.2 μl master mix was added per denatured total RNA sample. The reactions were mixed by vortexing and then pulse centrifuged before incubating at room temperature for 10 min. This allowed the hybridisation of Oligo (dT)₁₅ and random primers to the mRNA. The transcripts were reverse transcribe to cDNA by incubating at 42°C for 1 hour. AMV reverse transcriptase was inactivated and prevented from binding to cDNA by incubating the reaction mix at 99°C for 5 min and then placing on ice for 5 min. The first strand cDNA Reactions were stored at -20°C if not used immediately in a PCR.

2.7.4 PCR reaction.

A PCR reaction was set up in a 96 well plate with the final concentration of the following components, 1 μl first strand cDNA reaction, 0.25 mM each dNTP, 1.25x Reaction Buffer [25 mM (NH₄)₂SO₄, 93.75 mM Tris-HCl pH 8.8 at 25°C, 1.25x10⁻² Tween 20], 1.75 mM MgCl₂, 0.125 μm each (forward and reverse) primer, 1 Unit thermal stable DNA polymerase (Advanced Biotechnology Red Hot DNA polymerase Catalogue No AB-0406/B). In a total reaction volume of 20 μl made up with dH₂O.

CHAPTER 2: Materials and Methods

Enough master mix (M/mix) was made up of all the components except the first strand cDNA for all the samples, 19 μ l of M/mix was added per well and to this 1 μ l first strand cDNA reaction was added to each sample. The reaction was mixed by swirling the pipette tip in the reaction mix, and overlaid with 20 μ l mineral oil to prevent evaporation during the PCR amplification. The samples were thermo cycled, at 94°C for 1 min, (94°C for 1 min, see **Table 2.5** for annealing temperature used for each set of primers for 30 sec, 72°C for 1 min) x 40 cycles, and final extension at 72°C for 10 min. Optimum annealing temperature was determined by carrying out PCR using gradient temperature ranging from 50-60°C for each set of primers. Optimum MgCl₂ concentration was also determined by carrying out PCR at 1, 1.75, 2.5 and 4 mM MgCl₂. A PCR reaction was also set up for each primer sets, with a normal skin genomic DNA samples (code M5, 100 ng/ reaction) and normal skin (code N37, 100 ng/ reaction) to check if the primers cross intron exon boundaries.

Amplified PCR fragments were identified by mixing 5 μ l PCR reaction with 1 μ l 6x DNA loading buffer [10 mM Tris-HCl pH 7.5, 50 mM EDTA, 10% (w/v) ficoll 400, 0.25% (w/v) bromphenol blue (BPB), 0.25% xylene cyanol FF] and resolved on 1-2% (w/v) agarose gel, 0.5 g/ml ethidium bromide (EtBr) with 0.5 x TBE [Tris-borate/Ethylene diamine tetra-acetic acid (EDTA)] running buffer. Subjected to electrophoresis at 7-8 V/cm and visualised under ultraviolet (UV) transilluminator (see **section 2.5.6**). The gel image was captured a digital camera, part of Alpha Imager programme.

2.7.5 Purification of PCR product from agarose gel.

The bands in the agarose gel were carefully excised under UV and PCR products were purified using QIAquick Gel Extraction Kit (Cat No 28704, QIAGEN Ltd) as described in manufacturers instructions manual. Briefly, the agarose gel slice was weighed and dissolved in 3 volumes of QG buffer (supplied in the kit) to 1 volume of gel (100 mg gel is equal to 100 μ l). Incubated at 50°C for 10 min and mixed with 1 volume of isopropanol before loading onto QIAquick spin column and centrifuged for 1 min at 13000 rpm. Any remaining traces of the agarose gel were removed by washing with 0.5 ml of buffer QG. The PCR product bound to the column was washed with 0.75 ml

CHAPTER 2: Materials and Methods

buffer PE and then eluted with 20 μ l elution buffer (EB) [10 mM Tris-Cl pH 8.5] or dH₂O, and stored at -20°C .

Table 2.2: PCR primer sequence designed for RT-PCR from the NCBI data base (<http://www.ncbi.nlm.nih.gov/>) and the size of PCR product expected from these primers.

GENE	ACCESSION No	Forward (F) and Reverse (R) Primer nucleotide sequence '5-----3' and the user reference	Amplicon length bp
<i>ACTA2</i>	BC017554	ACCCTGAAGTACCCGATAGA	F
		ACGCTCAGCAGTAGTAACGA	R
α - <i>TUB</i>	AF141347	GCGTGAGTGCATCTCCATCCA	F
		GTAGGTGCCAGTGCGAACTTC	R
β - <i>ACT</i>	BC004251	GTTTGAGACCTCAACACCCC	F
		GTGGCCATCTCTTGCTCGAAGTC	R
<i>COUP-TFII</i>	M62760	CCTAGTCCTCTGATTTGATG	F
		AGGGAGAGCTGAAGTCGATTGT	R
<i>DES</i>	U59167	CAGCTACTCTAGCTCGATTG	F
		GAAATGTTCTTAGCCGCGAT	R
<i>E2A</i>	M31523	CAGCTCAGGTGAGGACTACG	F
		GTCGTAGCTGGGCGATAAGG	R
<i>EBF1</i>	AF208502.1	GTCGTGGTGCTACGACAGT	F
		CCAGCATGGTACCGAATATG	R
<i>EBF2</i>	AY405423.1	ATCAAGGGTACATCCGCAAC	F
		GGTACAACAAGTCCGGTCAT	R
<i>EBF3</i>	NM_001005463	GCGCGGGGGACGACCATGAA	F
		TGGGTCAGCAGCACACGGCACATCT	R
<i>G6PDA</i>	M21248	GTTCCGTGAGGACCAGATCTAC	F
		GGCTCCTTGAAGGTGAGGATAA	R
<i>GLI1</i>	NM_005269	GAAGACCTCTCCAGCTTGGA	F-MOH
		GGCTGACAGTATAGGCAGAG	R-MOH
<i>GLI2</i>	AB007295	CACAAGCGCAGCAAGGTCAAGACCG	F-MOH-a
		TCAGCCTCTGCTTACAGTCATCCC	R-MOH-bb
<i>GLI2</i>	AB007295	AGGTGTATCCCACGAAAGCACTGG	F-MOH-c
		GCTCTCTCGGCGAGGCTGGTGAGC	R-MOH-dd
<i>GLI2</i> α/β	AB007295	GGGTCAACCAGGTGTCCAGCACTGT	F
		GATGGAGGGCAGGGTCAAGGAGTTT	R
<i>GLI2</i> χ/δ	NM_030381	TCCCACGAAAGCACTGGCTTCTCT	F
		CAGCCATGTTGCTGATGCCTCATTC	R
<i>GLI3</i>	M57609	TCAGTGCCATCGATGAAACC	F-MOH
		GCTGTCCTTCTGTTGAGCA	R-MOH
<i>IVL</i>	NM_005547	GCAACTGGATCAAGAGCTAGT	F
		TCCAGATGTTTTAGTTGTCCG	R
<i>KRT10</i>	NM_000421	GATACAGCTCAAGCAAGCACTACT	F
		GTAGTATTTGCTGTAGTCACGAGGC	R
<i>KRT14</i>	BC042437	GGGGGAGCCTATGGGTTGGGG	F
		AGTGCTTGGGCAGGAGAGGGG	R
<i>KRT15</i>	X07696	AACTCACGGGCTCCAGCTAC	F
		GAATAGAGCGCATGCAAAGC	R
<i>KRT17</i>	BC000159	CGTGACTACAGCCAGTACTA	F
		GTCTTGCTGAAGAACCAATC	R
<i>KRT19</i>	Y00503	GCCCTCCGCGACTACAGCCACTACTAC	F
		ATGTCGGCCTCCACGCTCATGCGCAGA	R

Table 2.2 continued on next page

Table 2.2: continued PCR primer sequence designed for RT-PCR from the NCBI data base (<http://www.ncbi.nlm.nih.gov/>) and the size of PCR product expected from these primers.

GENE	ACCESSION No	Forward (F) and Reverse (R) Primer nucleotide sequence '5-----3' and the user reference		Amplicon length bp
<i>KRT5</i>	M21389.1	GGTGGTGGCTTTGGGCTCGGT	F	1428
		GCTCTCCGGGAGGAGGAGGT	R	
<i>KRT8</i>	BC075839	GATGCCAACGCCAAGTTGTCC	F	432
		GACGTCAGAGGACTCAGACAC	R	
<i>KIF4A</i>	AF179308	CTTCAATACAGCAGTAGCGCCA	F	282
		CTCACGAGATGGGCATAGAAGA	R	
<i>LOR</i>	NM_000427	TAGAGCTCTCATGATGTACCC	F	120
		CAGAAACCAAAGAGGCTAAAC	R	
<i>MCSP</i>	X96753	ACTGTGGTGCTGACTGTCGT	F	603
		CTCGGTTCGAAGTATGCGTA	R	
<i>NES</i>	NM_006617	GGAGAATCAAGAATGTCCGA	F	1167
		TTGGTCCTTCTCCACCGTAT	R	
<i>NRG2-A</i>		CAGCCGAGACATTTCGCATCA	F	343
		CTGGCATGTACAATCGCAA	R	
<i>NRG2-B</i>	NM_013981	CAGCCGAGACATTTCGCATCA	F	330
		GTTGACCATTGCGAACTGCT	R	
<i>NS</i>	AY825265	ACCTGCCATAAGCGGTATAA	F	911
		GGAATTAAGTGGAGATACGAT	R	
<i>PTCH-1</i>	U43148	CTCCCAAGCAAATGTACGAGCA	F	150
		TGAGTGGAGTTCTGTGCGACAC	R	
<i>SIP1</i>	U82108	CAGATGAACACTTCAAGCGG	F	284
		AGTTGCTGAAGATTTACGCG	R	
<i>SMO</i>	U84401	ACCAGGACATGCACAGCTACAT	F-	297
		AGGGCGTAGTACACGATGACAA	R	
Snail1	NM_005985	CCCAAGATGCACATCCGAAG	F	879
		AGACATTGTTAAATTGCCCG	R	
Snail2	NM_003068	TCTCTCCTCTTCCGGATAC	F	336
		GGTAATGTGTGGGTCCGAAT	R	
<i>SUP-FU-2</i>	AF159447	GCACTGGCACTACATCAGCTT	F	341
		TGGAGGAAGGTAACACCCCAA	R	
<i>TFIID</i>	X54993	CCACAGCTCTTCCACTCACAGA	F	261
		TTATCCTCATGATTACCGCAGC	R	
<i>VAV2</i>	NM_003371	GCGATGTACATCAATGAAGTTAAACG	F	276
		GCCTCCTCTTCTACGTACGTT	R1	
		GGGGTCGTCGGTCATCTTGTGGAA	R2	
<i>VAV3</i>	NM_006113	CCTGTTGTGAGACGTTTGAATGAG	F	626
		GATGGCTGACTCCACTCCACTGC	R	
<i>VAV3.1</i>	AF035442	GTGGTGTTTTACCCTCTGC	F	452
		CTGCAATGTGAAAAAAGCCATCTC	R	
<i>VIM</i>	X56134	AAGAGAAGTTTGGCGTTGAA	F	346
		GTGATGCTGAGAAGTTTCGT	R	

Table 2.2 PCR primer sequence designed for RT-PCR from NCBI data base, and the PCR product expected from these primers for the following genes; actin, alpha 2, smooth muscle, aorta (*ACTA2*), alpha-tubulin (α -TUB), beta-actin (β -*ACT*), chick ovalbumin upstream promoter transcription factor II (*COUP-TFII*), desmin (*DES*), Transcription factor E2-alpha (*E2A*), Early B-cell transcription factor (*EBF1*, 2 and 3),

CHAPTER 2: Materials and Methods

glucose-6-phosphate-dehydrogenase variant A (*G6PDA*), glioma associated oncogene *GLI1*, *GLI2*, *GLI3*, involucrin (*IVL*), keratins *KRT10*, *KRT14*, *KRT15*, *KRT17*, *KRT19*, *KRT5*, *KRT8*, Chromosome-associated kinesin (*KIF4A*), loricrin (*LOR*), melanoma-associated chondroitin sulfate proteoglycan (*MCSP*), nestin (*NES*), neuregulin 2 A (*NRG2-A*), neuregulin 2 B (*NRG2-B*), nucleostemin (*NS*), patched-1 (*PTCH1*), SRY-interacting protein 1 (*SIP1*), smoothened (*SMO*), snail (Snail1, 2), suppressor of fused (*SUP-FU*), transcription initiation factor (*TFIID*), *VAV2*, *VAV3*, *VAV3.1* are Guanine nucleotide exchange factor for the Rho family of Ras-related GTPases. vimentin (*VIM*). *GLI2* user reference Moh-a, Moh-bb, Moh-c and Moh-dd primers were from (Tanimura et al., 1998) and *GLI2* α/β and *GLI2* χ/δ primers were from (Regl et al., 2002).

Table 2.3: List of total RNA samples extracted from different tissue and cultured cell used in RT-PCR and real-time-RT-PCR gene expression analysis.

Key	Total RNA Samples	Con [$\mu\text{g}/\mu\text{l}$]	Sample Taken μl	Volume	DEPC μl	dH ₂ O
1	Basal Cell Carcinoma	0.6	4.17		2.23	
2	Basal Cell Carcinoma	3.41	0.73		5.67	
3	Basal Cell Carcinoma	5.58	0.45		5.95	
4	Basal Cell Carcinoma	1.85	1.35		5.05	
5	Basal Cell Carcinoma	0.1	6.4		-	
6	Basal Cell Carcinoma	2.78	0.90		5.50	
7	Basal Cell Carcinoma	0.22	6.40		-	
8	Basal Cell Carcinoma	0.41	6.10		0.30	
9	Normal Skin	0.72	3.47		2.93	
10	Normal Skin	3.75	0.67		5.73	
11	Normal Skin	0.77	3.25		3.15	
12	Normal Skin	0.74	3.38		3.02	
13	Normal Skin	2.98	0.84		5.56	
14	Normal Skin	0.32	6.40		-	
15	HaCat	1.73	1.45		4.95	
16	HaCat	2.66	0.94		5.46	
17	HaCat	5.2	0.48		5.92	
18	Primary Keratinocytes	0.9	2.78		3.62	
19	Primary Keratinocytes	2.6	0.96		5.44	
20	Primary Keratinocytes	6.66	0.38		6.02	
21	A375	2.2	1.14		5.26	
22	A375	2.4	1.04		5.36	
23	A375	1.38	1.81		4.59	
24	A375	1.25	2.00		4.40	
25	GLI1-C3 primary Keratinocytes	2.78	0.90		5.50	
26	GLI1-C3 Primary Keratinocytes	1.08	2.31		4.09	
27	GLI1-C3 Primary Keratinocytes	2.57	0.97		5.43	
28	GLI1-C3 10T1/2 cell line	1.08	2.31		4.09	
29	dH ₂ O	-	0.00		6.40	
30	(BCC key 1) without RT	0.6	4.17		2.23	

BCC (Basal Cell Carcinoma), HaCat (a spontaneously immortalised keratinocyte cell line), A375 (a melanoma cell line), GLI1-C3 primary keratinocytes (a transduced primary keratinocytes with SIN-EGFP-GLI1 fusion construct retrovirus to express exogenous GLI1), GLI1-C3 10T1/2 (a GLI1 expressing fetal mouse fibroblasts cell line obtained from Dr Muy-Teck, these were used as positive control for GLI1 expression). Table shows the concentration of each total RNA sample, volume taken from each sample to give 2.5 ug total RNA and volume of DEPC-dH₂O added to make up to 6.4 μl . Samples 29 (dH₂O) and 30 (BCC key 1) were negative control reaction set up for RT-PCR, no reverse transcriptase (RT) was added to sample 30.

Table 2.4: Total RNA samples from transduced primary keratinocytes for real-time-RT-PCR gene expression analysis.

Total RNA Sample	Con [$\mu\text{g/ml}$]	Sample volume taken μl	DEPC-dH ₂ O added μl
GLI1-GS	0.57	4.39	2.01
GLI1 +EGF	0.56	4.46	1.94
GLI1 +FGF	0.5	5.0	1.4
EGFP -GS	0.68	3.68	2.72
EGFP+EGF	0.59	4.24	2.16
EGFP+FGF	0.61	4.10	2.3
GLI1-GS-RT	0.57	4.39	2.01

Human primary keratinocytes were transduced with retroviral particles containing SIN-EGFP-GLI1 (GLI1) and SIN-EGFP (EGFP), a control retroviral construct. The transduced cells were cultured in a defined keratinocyte culture medium containing no growth supplements (-GS), media containing epidermal growth factor (EGF) only, and media containing fibroblast growth factor (FGF) only. Total RNA was extracted from these cell lines GLI1-GS, GLI1+EGF, GLI1+FGF, EGFP-GS, EGFP+EGF and EGFP+FGF. Table above shows the concentration of each total RNA sample and the volume taken for each sample to give 2.5 μg total RNA and volume of DEPC-dH₂O added to make up to 6.4 μl . GLI1-GS-RT was a control reaction set up for RT-PCR to this sample no reverse transcriptase (RT) was added.

Table 2.5: List of primers with optimum annealing temperature used in the RT-PCR and expected amplicon size for each set of primers.

Primers	Optimum Annealing Temp	Amplicon length bp
<i>α-TUB</i>	55 ⁰ C	249
<i>ACTA2</i>	55 ⁰ C	425
<i>β-ACT</i>	60 ⁰ C	320
<i>COUP-TFII</i>	55 ⁰ C	288
<i>DES</i>	55 ⁰ C	222
<i>E2A</i>	55 ⁰ C	591
<i>EBF1</i>	55 ⁰ C	264
<i>EBF2</i>	55 ⁰ C	384
<i>EBF3</i>	55 ⁰ C	450
<i>G6PDA</i>	55 ⁰ C	152
<i>GLI1</i>	60 ⁰ C	246
<i>GLI2 a,bb</i>	55 ⁰ C	179
<i>GLI2 α/β</i>	55 ⁰ C	194
<i>GLI2 c,dd</i>	55 ⁰ C	1,487
<i>GLI2 χ/δ</i>	55 ⁰ C	205
<i>GLI3</i>	55 ⁰ C	328
<i>IVL</i>	55 ⁰ C	1178
<i>KRT10</i>	50 ⁰ C	590
<i>KRT14</i>	60 ⁰ C	1326
<i>KRT15</i>	55 ⁰ C	1559
<i>KRT17</i>	55 ⁰ C	454
<i>KRT19</i>	55 ⁰ C	183
<i>KRT5</i>	64 ⁰ C	1428
<i>KRT8</i>	55 ⁰ C	432
<i>KIF4A</i>	55 ⁰ C	282
<i>LOR</i>	55 ⁰ C	120
<i>MCSP</i>	55 ⁰ C	603

Table 2.5 continued on next page

Table 2.5 continued List of primers with optimum annealing temperature used in the RT-PCR and expected amplicon size for each set of primers.

<i>NRG2-A</i>	55 ⁰ C	343
<i>NRG2-B</i>	50 ⁰ C	330
<i>NES</i>	55 ⁰ C	911
<i>NT</i>	55 ⁰ C	1173
<i>PTCH-1</i>	55 ⁰ C	150
<i>SIP-1</i>	55 ⁰ C	284
<i>SMO</i>	55 ⁰ C	297
Snail1	55 ⁰ C	879
Snail2	55 ⁰ C	336
<i>SUP-FU</i>	55 ⁰ C	341
<i>TFIID</i>	55 ⁰ C	261
<i>VAV2</i>	55 ⁰ C	276
<i>VAV3</i>	58 ⁰ C	626
<i>VAV3.1</i>	55 ⁰ C	452
<i>VIM</i>	55 ⁰ C	346

Shows optimum annealing temperature used in the RT-PCR and expected amplicon size for each set of primers for the following genes; actin, alpha 2, smooth muscle, aorta (*ACTA2*), alpha-tubulin (α -TUB), beta-actin (β -*ACT*), chick ovalbumin upstream promoter transcription factor II (*COUP-TFII*), desmin (*DES*), transcription factor E2-alpha (*E2A*), early B-cell transcription factor (*EBF1*, 2 and 3) glucose-6-phosphate-dehydrogenase variant A (*G6PDA*) glioma associated oncogene *GLI1*, *GLI2*, *GLI3*. involucrin (*IVL*), keratins *KRT10*, *KRT14*, *KRT15*, *KRT17*, *KRT19*, *KRT5*, *KRT8*. chromosome-associated kinesin (*KIF4A*), loricrin (*LOR*), melanoma-associated chondroitin sulfate proteoglycan (MCSP), nestin (*NES*), neuregulin-2-A (*NRG2-A*), neuregulin-2-B (*NRG2-B*), nucleostemin (*NS*), patched-1 (*PTCH1*), SRY-interacting protein 1 (*SIP1*), smoothened (*SMO*), snail (Snail 1, 2), suppressor of fused (*SUP-FU*), transcription initiation factor (*TFIID*), *VAV2*, *VAV3*, *VAV3.1* are Guanine nucleotide exchange factor for the Rho family of Ras-related GTPases and vimentin (*VIM*).

2.8.0 Real-time RT-PCR reaction.

Real-time-RT-PCR was carried out using DyNAmo™ SYBR® Green qPCR kit (Cat No F- 400L Finnzymes) as per manufacturers' instruction. Briefly a triplicate PCR reaction were set up in a white 96 well plate (Cat No MLL-9651 MJ Research, INC) for each sample on ice with the final concentration of the following components, 2 µl first strand cDNA (diluted 1:4 from **section 2.7.3**), 1X DyNAmo™ SYBR® Green Master Mix (containing modified *Tbr* DNA polymerase, SYBR Green I, optimized PCR buffer, 5 mM MgCl₂, dNTP mix including dUT, 0.3 µM each forward and reverse primer (**Table 2.6**) in a total reaction volume of 20 µl made up with dH₂O. The plates were covered with clear caps (Cat No TCS-0803 MJ Research).

A master mix (M/mix) was made up of all the components except the first strand cDNA for all the samples, 18µl of M/mix was added per well and to this 2µl first strand [diluted 1:4] cDNA reaction was added for each sample. The reaction was mixed by swirling the pipette tip in the reaction mix. The samples were thermo cycled on an opticon-2 (MWG) as follows;

1. 95°C for 10 min
2. 94°C for 10 sec
3. X°C for 20 sec (temp specific for primer used: see table 2.6)
4. 72°C for 20 sec
5. X°C for 1 sec (temp specific for primer used: see table 2.6)
6. Plate read (Fluorescence data collection)
7. Repeat from step 2, 39 more times
8. Melting curve from 65-95°C, read plate every 1°C, hold for 1 sec
9. Hold: 4°C
10. End

The Real Time RT-PCR data was obtained as the cycle threshold (Ct) values from the exponential phase, from a graph plot of Absorbance value plotted against Ct value generated by the optican-2 computer programme. The melting curve graph of the PCR product indicated that the data generated was from a single product and not from multiple products. This was confirmed by mixing 5 µl Real Time RT-PCR reaction with 1 µl 6x DNA loading buffer [10 mM Tris-HCl pH 7.5, 50 mM EDTA, 10% (w/v) Ficoll 400, 0.25% (w/v) bromphenol blue (BPB), 0.25% xylene cyanol FF] and resolved on 1-2% (w/v) agarose gel, 0.5 g/ml ethidium bromide (EtBr) with 0.5 x TBE [Tris-

CHAPTER 2: Materials and Methods

borate/ethylene diamine tetra-acetic acid (EDTA)] running buffer. Subjected to electrophoresis at 7-8 V/cm and visualised under ultraviolet (UV) transilluminator (see **section 2.5.6**). Each set of primers optimum annealing temperature was determined by carrying out a gradient Real Time RT-PCR ranging from 50-65^oC. The temperature used for fluorescence data collection was determined from the melting curve of the PCR products for each set of primers. Setting the fluorescence data collection temperature higher than extension temperature prevented interference from primer-dimer formation. Not all the primers worked with the DyNAmoTM SYBR[®] Green qPCR kit that had previously worked with the Red Hot Taq PCR kit in **section 2.7.4**. The list of primers that did work is given in **Table 2.6**. Each reaction was carried out in triplicates with duplicate samples for each primer set. Fold induction or repression values (x) were calculated using the following formula $X = 2^{-\Delta\Delta Ct}$, where Ct represents the mean threshold cycle of all replicate analyses of a given gene and ΔCt represents the difference between the Ct values of the gene in question (target) and the Ct value of the reference gene (β -ACT). $\Delta\Delta Ct$ is the difference between the ΔCt values of the samples for each target (e.g. ΔCt for GLI1 in tumour) and the mean ΔCt of the calibrator (e.g. ΔCt for GLI1 in normal skin) reference to β -ACT in tumour and normal skin.

Table 2.6: Primers used with DyNAmo™ SYBR® Green qPCR kit and the optimum annealing temperature and fluorescence data collection temperatures used for each set of primers.

Primers	Annealing Temp	Plate read (fluorescence data collection) Temp
Alpha-tub	57°C	80°C
B-ACT	60°C	80°C
<i>GLI1</i>	60°C	80°C
<i>GLI2</i>	57°C	80°C
<i>GLI3</i>	57°C	80°C
<i>KRT19</i>	55°C	78°C
<i>KRT14</i>	60°C	78°C
<i>KRT17</i>	55°C	78°C
<i>KIF4</i>	57°C	75°C
<i>PTCH</i>	57°C	75°C
<i>SMO</i>	57°C	80°C
Snail-2	55°C	78°C
<i>SUP-FU</i>	57°C	80°C
<i>VIM</i>	55°C	78°C

Shows optimum annealing temperature used in the Real-Time-RT-PCR and the Fluorescence data collection temperatures used for each set of primers for the following genes; α -*TUB* (alpha-tubulin), β -ACT (beta-actin), glioma associated oncogene *GLI1*, *GLI2*, *GLI3*, keratins *KRT10*, *KRT14*, *KRT15*, *KRT19*, *KRT14*, *KRT17*, chromosome-associated kinesin (*KIF4*), patched-1 (*PTCH1*), smoothed (*SMO*), Snail-2, suppressor of fused (*SUP-FU*), *VAV2*, *VAV3*, *VAV3.1* are guanine nucleotide exchange factor for the Rho family of Ras-related GTPases and vimentin (*VIM*).

2.9.0 Cloning

2.9.1 Cloning Smoothend and Suppressor-Fused PCR products.

A ligation reaction using 4 μ l QIAgen purified PCR product (Smoothened and Suppressor-Fused), 1 μ l Salt Solution [1.2 M NaCl; 0.06 M MgCl₂], 1 μ l [10 ng/ μ l] vector (Invitrogen Cat No 44-0301) was set up and incubated at room temperature for 30 min (see **Figure 2.6** for the pCRII TOPO vector map).

50 μ l XLI-Blue competent cells (obtained from Dr Graham Neil) were thawed on ice and transformed by adding 2 μ l ligation reaction. A control reaction was also set up using 2 μ l dH₂O, 50 μ l XLI-blue competent cells. Cells were then incubated on ice for 30 min, then at 42°C for 90 sec, before being placed on ice for 2 min.

Transformed cells were then added to 3 ml liquid broth (LB) medium preheated to 42°C, and incubated at 37°C for 45 min whilst shaking at 200 rpm. 100-200 μ l of this transformation mix was plated onto (100 μ g / ml) Ampicillin plate and incubated at 37°C overnight. The following day several colonies were picked from each plate and cultured in 5 ml (100 μ g / ml) Ampicillin LB medium, incubated at 37°C shaking 200rpm overnight.

2.9.2 Preparing plasmid miniprep.

1.5 ml of over night bacterial cell suspension was used to prepare miniprep using a QIAgen mini prep kit (Cat No 27104) as per manufacturers' instruction. Briefly, the bacteria cell pellet was resuspended in 250 μ l buffer P1 (containing RNase A). To this, 250 μ l of buffer P2 was added and the tube gently inverted 4-6 times, 350 μ l buffer N3 was added and the tube inverted 4-6 times. Following centrifugation for 10 min at 13000 rpm the supernatant was transferred to a QIAgen spin column in a 2 ml collection tube and centrifuged for 1 min at 13000 rpm.

The flow-through was discarded and the column was washed with 0.5 ml buffer PB, and then with 0.75 ml buffer PE. After discarding the flow through the column was

CHAPTER 2: Materials and Methods

additionally centrifuged for 1 min at 13000 rpm to remove residual wash buffer. DNA was eluted with 50 μ l buffer EB (10mM Tris-Cl pH 8.5) in to a clean 1.5 ml eppendorf tube.

1 μ l of the miniprep was run on a 1 % (w/v) agarose gel alongside a 1Kb plus DNA ladder (GIBCOBRL Life Technology Cat No 10787-018) to check the plasmid size. The concentration of mini preps was determined by measuring its absorbance at 260nm using a spectrophotometer. The following formula (concentration [μ g/ml] = Abs 260nm x 50 ug/ml x dilution factor) was used to calculate the plasmid concentration.

To check whether the Smoothened and the Suppressor Fused fragment had cloned into the vector, *SMO* and *SUP-FU* pCRII TOPO vector was digested with *EcoRI* restriction enzyme from New England Biolabs (Morris et al.). 300 ng vector (miniprep), was dissolved in NEBuffer *EcoRI* [50 mM NaCl, 100 mM Tris-HCl, 10 mM MgCl₂, 0.025% (v/v) Triton X-100 (pH 7.5 at 25°C)], containing 30U *EcoRI*, in a total reaction volume of 25 μ l. The digest mix was incubated at 37°C overnight. The following day the digest was run on 1% (w/v) agarose gel to identify the insert.

In addition to *SMO* and *SUP-FU*, a 511 bp *PTCH* fragment and 250 bp *GLII* fragment were obtained from Dr Judith Green. A 1.2 kb keratin 14 (*KRT14*) cDNA fragment was obtained from Professor Anthony Quinn. *PTCH*, *GLII* and *KRT14* cDNA were cloned in to *HindIII*, *EcoRI* site of the PGEM vector.

A human *GLI2* (*hGLI2*) 1.6 Kb fragment was obtained from Dr Fritz Aberger University Salzburg Austria. The *hGLI2* fragment was cloned in to the *EcoRI* sites of the pCRII TOPO vector. 1 μ g of *hGLI2*-1.6 kb-pCRII TOPO vector spotted on a filter paper was sent to us. The Plasmid was eluted off the filter paper by cutting out the area of the filter paper on which the Plasmid was spotted, and soaked in 50 μ l sterile dH₂O. 90 μ l XL1-blue competent cells were transformed with approximately 100 ng *hGLI2* pCRII TOPO as previously described.



Figure 2.6: Features of pCRII-TOPO vector map in which *SMO*, *SUP-FU*, and *GLI2* were cloned, and sequence surrounding the TOPO cloning site. Restriction sites are labelled to indicate the actual cleavage site. The arrows indicate the start of transcription for SP6 and T7 polymerases.

2.9.3 Sequencing the cloned inserts.

To confirm that correct inserts, and to determine the direction in which they were cloned. *SMO*, *SPU-FU* and *hGLI2*-1.6 kb-pCRII TOPO, *PTCH*, *GLI1* and *KRT14*-1.2 kb-PGEM were sequenced using ABI PRISM Big Dye Cycle Sequencing Ready Reaction kit (Cat No 4303152 Applied Biosystems) as per manufacturers' protocol. Briefly, 4 μ l Terminator Ready Reaction Mix (TRRM), 200 ng pCRII TOPO vector (mini-prep) containing the insert, 10 ng Primer SP6 or T7, in a 10 μ l total reaction volume made up with dH₂O. A control reaction was also set up using 4 μ l TRRM, 200 ng PGEM-3Zf⁺, 1.6 pmol M13 primers. The reaction was covered with 10 μ l mineral oil and thermal cycled using a Techne PCR machine, as follows; 94°C for 60 sec, 40 cycles at (94°C for 30 sec, 55°C for 40 sec, 72°C for 1 min), final extension at 72°C for 10 min.

The mineral oil was removed from the reaction mix by placing it on a clean sheet of parafilm. The parafilm sheet was held at an angle so that the reaction mix trickles slowly down it, this separated the oil from the reaction mix.

The separated reaction mix was placed in a 1.5 ml clean eppendorf tube. The extension products were purified using an ethanol precipitation protocol. By adding 2 μ l of 3 M sodium acetate pH 5.2, 50 μ l 95% (v/v) ethanol to the eppendorf tube containing the separated reaction mix. The eppendorf tube was vortexed and placed on ice for 10 min and centrifuged at 13000 rpm for 30 min. The pellet obtained was rinsed with 250 μ l 70% (v/v) ethanol, care was taken each time when removing the supernatant to avoid disturb the pellet. The pellet was dried in a speed vac centrifuge and sent to the CRUK sequencing facilities to be sequenced on ABI DNA sequencer.

Once the correct insert cloned was confirmed, glycerol stocks were made of transformed cells for each clone by adding 350 μ l of sterile glycerol to 3.5 ml of LB culture and these stocks were stored at -70°C.

2.9.4 Cloning a 296 bp *GLI2* fragment from *hGLI2*-1.6 kb-pCRII-TOPO.

A smaller 296 bp *GLI2* fragment from 5' region of 1.6 kb *hGLI2* insert in pCRII-TOPO vector was cloned for in-situ hybridisation (see **Figure 2.7**). A double digest reaction

CHAPTER 2: Materials and Methods

was set up with 0.35 µg *hGLI2*-1.6 kb-pCRII-TOPO, 7.5U *NheI* and 30 U *EcoRV* in 1x NEB buffer 2 plus BSA (50 mM NaCl, 10m M Tris-HCl, 10 mM MgCl₂, 1 mM dithiothreitol pH 7.9 at 25°C) in a 20 µl total reaction volume and incubated at 37°C for 5 1/2 hours.

The blunt ends generated by *NheI* were filled by adding 5 U of Klenow (DNA polymerase I NEB) and 1 µl of (0.5 mM) dNTPs to the digest reaction and mixed and incubated at 30°C for 15 min. The reaction mix was run on 1%w/v agarose gel with the DNA loading buffer. The vector band containing the 296 bp 5' region of *GLI2* (*hGLI2*-296 bp-pCRII TOPO) was cut out of the gel and purified using Qiagen DNA gel extraction kit as per manufacturers' instructions. The purified DNA was eluted of the column with 30 µl (preheated to 65°C) elution buffer (EB).

Approximately 0.01 µg of linearised *hGLI2*-296 bp-pCRII TOPO vector was ligated using 400 U of T4 Ligase, 1x Ligase reaction buffer in a 10 µl total reaction volume and incubated at room temperature overnight. 5 µl of ligation reaction was used to transform XLI-blue competent cells and a plasmid mini prep was prepared from the transformed culture suspension as described in **section 2.9.1 and 2.9.2**.

0.4 µg of *hGLI2*-296 bp-pCRII TOPO was double digested with 20 U *EcoRI* (Morris et al.) and 10 U *NotI* (Morris et al.), 1x *EcoRI* buffer (50 mM NaCl, 100 mM Tris-HCl, 10 mM MgCl₂, 0.025% Triton X-100), (pH 7.9 at 25°C) in a 20 µl total reaction volume and incubated at 37°C for 2 hours. 5 µl reaction mix was loaded on to a 1%w/v agarose gel to check for correct size insert. The *GLI2* insert was also sequenced using T7 and SP6 primers confirming *GLI2* insert (as described in **section 2.9.3**). This construct was used to generate a 269 bp *GLI2* ribo probes for in-situ hybridisation analysis.

2.9.5 Cloning a 1.2 kb keratin *KRT14* insert from PGEM in to pCRII-TOPO vector.

A 1.2 kb keratin K14 insert was cut out of the *KRT14*-1.2 kb-PGEM vector and cloned in to pCRII-TOPO vector in *HindIII* and *EcoRI* site (see **Figure 2.8 and Figure 2.9**). A following double digest reaction was set up with 0.5 µg *hGLI2*-1.6 kb-pCRII-TOPO, 1x *EcoRI* buffer 3 (50 mM NaCl, 100 mM Tris-HCl, 10 mM MgCl₂, 0.025% Triton X-100

CHAPTER 2: Materials and Methods

pH 7.9 at 25°C), 30 U *EcoRI* and 30 U *HindIII* in a 20 µl total reaction volume and incubated at 37°C for 4 hours. After incubation double digested *hGLI2*-1.6 kb-pCRII-TOPO was dephosphorylated by adding 1 µl of phosphatase enzyme (CIAP diluted 1:10 Cat No M1821 Promega) to digest reaction mix and incubated at 37°C for 1 hour.

A second double digest reaction was set up with 1 µg *KRT14*-1.2 kb-PGEM, 1x *EcoRI* buffer 3 (50 mM NaCl, 100 mM Tris-HCl, 10 mM MgCl₂, 0.025% Triton X-100 pH 7.9 at 25°C), 30 U *EcoRI* and 30 U *HindIII* in a 20 µl total reaction volume and incubated at 37°C for 4 hours.

KRT14-1.2 kb-PGEM double digested reaction and dephosphorylated *hGLI2*-1.6 kb-pCRII-TOPO reactions were run on 1% agarose gel, to separate the vector backbones from the inserts. The pCRII-TOPO backbone and the *KRT14* insert (1.2 Kb) bands were excised out and purified using Qiagen gel extraction kit as per manufacturers' instructions. Purified pCRII-TOPO backbone and the 1.2 kb *KRT14* insert were run on 1% (w/v) agarose gel to check their quality and quantity.

A ligation reaction was set up with 1:3 ratio of pCRII-TOPO backbone to 1.2 kb *KRT14* insert, as follows: 2 µl pCRII-TOPO backbone, 6 µl 1.2 kb *KRT14* insert, 1 µl T4 Ligase and 1 µl 10 x Ligase buffer, a control reaction was also set up without T4 Ligase and incubated at room temperature overnight.

A 5 µl of ligation reaction was used to transform XLI Blue competent cells to obtain a plasmid mini prep as described in **section 2.9.1** and **section 2.9.2**. A 0.5 µg *KRT14*-1.2 kb-pCRII TOPO mini prep was double digested using *EcoRI* and *HindIII* as described above and run on 1 % (w/v) agarose gel to check for the 1.2 kb *KRT14* insert and pCRII-TOPO backbone. Keratin K14 insert was confirmed by sequencing using T7 and SP6 primers. Glycerol stocks were made from the remaining mini prep cell suspension as described in **section 2.9.3**.

2.10.0 In-situ hybridisation

2.10.1 Linearising hGLI2-1.5 kb-pCRII TOPO and hGLI2-296 bp-pCRII TOPO plasmids for in-situ probes.

1.5 kb *hGLI2* sense and anti-sense ribo probes were generated by linearising *hGLI2*-1.5 kb-pCRII TOPO with *EcoRV* and *BamHI* restriction enzymes (Morris et al.). A 296 bp *hGLI2* sense and anti-sense ribo probes were generated by linearising *hGLI2*-296 bp-pCRII TOPO with *EcoRI* and *NotI* restriction enzymes (Morris et al.).

The **EcoRV Reaction** was set up using 10 µg *hGLI2*-1.5 kb-pCRII TOPO, 1x NEB buffer 3 (100 mM NaCl, 50 mM Tris-HCl, 10 mM MgCl₂, 1 mM dithiothreitol, (pH 7.9 at 25°C), 100 µg/ml BSA, 60 U *EcoRV*, in a 30 µl total reaction volume and incubated at 37°C overnight.

The **BamHI Reaction** was set up using 10µg *hGLI2*-1.5 kb-pCRII TOPO, 1x NEB BamHI buffer 150mM NaCl, 10mM Tris-HCl, 10mM MgCl₂, 1mM dithiothreitol, (pH 7.9 at 25°C), 100µg/ml BSA, 60U BamHI, in a 30µl total reaction volume and incubated at 37°C overnight.

The **EcoRI Reaction** was set up using 10 µg *hGLI2*-296 bp-pCRII TOPO, 1x *EcoRI* buffer [50 mM NaCl, 100 mM Tris-HCl, 10m M MgCl₂, 0.025% (v/v) Triton X-100, pH 7.9 at 25°C], 100 µg/ml BSA, 30 U *EcoRI*, in a 20 µl total reaction volume and incubated at 37°C for 4.5 hours.

The **NotI Reaction** was set up using 10 µg *hGLI2*-296 bp-pCRII TOPO, 1x NEB buffer 3 (100 mM NaCl, 50 mM Tris-HCl, 10 mM MgCl₂, 1 mM dithiothreitol, (pH 7.9 at 25°C), 100 µg/ml BSA, 15 U *NotI*, in a 20 µl total reaction volume and incubated at 37°C for 4.5 hours.

2.10.2 Linearising *KRT14*-1.2 kb-PGEM and *KRT14* -1.2 kb-pCRII TOPO plasmids for in-situ probes.

KRT14-1.2 kb-PGEM and *KRT14*-1.2 kb-pCRII TOPO plasmids were linearised with *EcoRI* and *HindIII* restriction enzymes (Morris et al.).

The **EcoRI Reaction** was set up using 10 µg *KRT14*-1.2 kb-PGEM or *KRT14*-1.2 kb-pCRII TOPO, 1x *EcoRI* buffer 3 [50 mM NaCl, 100 mM Tris-HCl, 10 mM MgCl₂, 0.025% (v/v) Triton X-100, pH 7.9 at 25°C], 30 U *EcoRI*, in a 25 µl total reaction volume and incubated at 37°C overnight.

The **HindIII Reaction** was set up using 10 µg *KRT14*-PGEM or *KRT14*-1.2 kb-pCRII TOPO, 1x NEB buffer 2 (50 mM NaCl, 10 mM Tris-HCl, 10 mM MgCl₂, 1 mM dithiothreitol, (pH 7.9 at 25°C), 30 U *HindIII*, in a 25 µl total reaction volume and incubated at 37°C overnight.

A 1 µl of reaction digest was run on 1 % (w/v) agarose gel along side undigested plasmid to check whether the digested plasmid had linearised.

2.10.3 Linearising *FOXE1*-(UTR-332bp)-pBluescript-II-KS plasmid for in-situ probes.

FOXE1 sense and anti sense probes were generated from *FOXE1*-(UTR-332bp) corresponding to nucleotides 2148 –2480, [GenBank GI No 2078532])-pBluescript-II-KS (obtained from Dr Fritz Aberger) linearised with *BamHI* and *EcoRI*.

The **BamHI** reaction was set up using 10µg of *FOXE1*-(UTR-332bp)-pBluescript-II KS, 1x NEB *BamHI* buffer 150 mM NaCl, 10 mM Tris-HCl, 10 mM MgCl₂, 1 mM dithiothreitol, (pH 7.9 at 25°C), 100 µg/ml BSA, 60 U *BamHI*, in a 30 µl total reaction volume and incubated at 37°C overnight.

The **EcoRI Reaction** was set up using 10 µg of *FOXE1*-(UTR 332bp) pBluescript II KS, 1x *EcoRI* buffer 3 [50 mM NaCl, 100 mM Tris-HCl, 10 mM MgCl₂, 0.025% (v/v)

CHAPTER 2: Materials and Methods

Triton X-100, pH 7.9 at 25°C], 30U *EcoRI*, in a 30 µl total reaction volume and incubated at 37°C overnight.

1 µl of each reaction digest was run on 1% (w/v) agarose gel along side undigested plasmid to check whether the digested Plasmid had linearised.

2.10.4 Purifying linearised plasmids by ethanol precipitation.

A single digest reaction volume (**from section 2.9.1**) was made up to 200 µl with sterile dH₂O. To this equal volume of phenol chloroform isoamyl alcohol 25:24:1 was added, vortexed and centrifuged at 13000 rpm. The aqueous layer was transferred to a new 1.5 ml tube. 1/10th of the volume of 3 M sodium acetate pH 5.2 and 2.5x the volume of 100% (v/v) ethanol was added and placed at -20°C for 1 hour and centrifuged at 13000 rpm at 4°C for 15 min. The pellet was washed with 250 µl 70% (v/v) ethanol and air dried and dissolved in 10 µl RNase free [10 mM Tris-Cl pH 8.5]. Purified linearised plasmids were diluted 1:100 and run on a 1% (w/v) agarose gel, alongside a known concentration marker, to check the purity concentration.

2.10.5 Transcribing *GLI2*, Keratin *KRT14* and *FOXE1* probes for in-situ hybridisation.

A 1.5 kb *GLI2* sense probe was generated using 1 µl (~200ng) *EcoRV* linearised h*GLI2*-1.5 kb-pC_{RII} TOPO, 40 U SP6 Polymerase (Roche Cat No 810 274), 2 µl digoxigenin-UTP (Dig) labelling mix (Roche Cat No 1 277 073), 1x transcription buffer (0.04M Tris-HCl pH 8 at 20°C, 6 mM MgCl₂, 100 mM dithiothreitol, 20 mM spermidine) supplied with RNA polymerase, 40 U RNase Inhibitor (Roche Cat No 799 017), in a 20 µl total reaction volume made up with (DEPC treated) dH₂O.

1.5 kb *GLI2* anti-sense probe was generated using 1 µl (~200 ng) *BamHI* linearised h*GLI2*-1.5 kb-pC_{RII} TOPO with T7 Polymerase (Roche Cat No 881 767). Rest of the reaction components were same as for the 1.5 kb *GLI2* sense probe (see above). Both sense and anti-sense 1.5 kb *GLI2* reaction mix were incubated at 37°C for 2 hours.

CHAPTER 2: Materials and Methods

A 296 bp *GLI2* anti-sense and sense ribo probes were generated from 1 µl (~200 ng) *EcoRI* and *NotI* linearised *hGLI2*-296 bp-pCRII TOPO. The reactions and the components used were same as those for the 1.6 kb *GLI2* probes described above. **Figure 2.7** shows the vector maps and the *GLI2* (1.5 kb and 296 bp) probes generated.

Method and materials used for transcribing keratin 14 and *FOXE1* anti-sense and sense probes were same as those described above for *GLI2*. Except 1.2 kb keratin14 anti-sense probe was generated with SP6 polymerase from *HindIII* linearised *KRT14*-1.2 kb-PGEM and with T7 polymerase from *HindIII* linearised *KRT14*-1.2 kb-pCRII TOPO. A 1.2 kb keratin 14 sense probe was generated with T7 Polymerase from *EcoRI* linearised *KRT14*-1.2 kb-PGEM and with SP6 Polymerase from *EcoRI* linearised *KRT14*-1.2 kb-pCRII TOPO (see **Figure 2.8**).

A *FOXE1* 332bp anti-sense probe was generated with T7 polymerase from *EcoRI* linearised *FOXE1*-(UTR-332bp)-pBluescript-II KS and *FOXE1* 332bp sense probe was generated with T3 polymerase from *BamHI* linearised *FOXE1*-(UTR-332bp)-pBluescript-II KS (see **Figure 2.9**).

1 µl of transcription reaction was run on 1% (w/v) RNase free agarose gel with RNA loading buffer, to check transcribed probes. The transcribed probe bands were expected to be of a higher intensity (approx. 10 xs) than linearised plasmid bands.

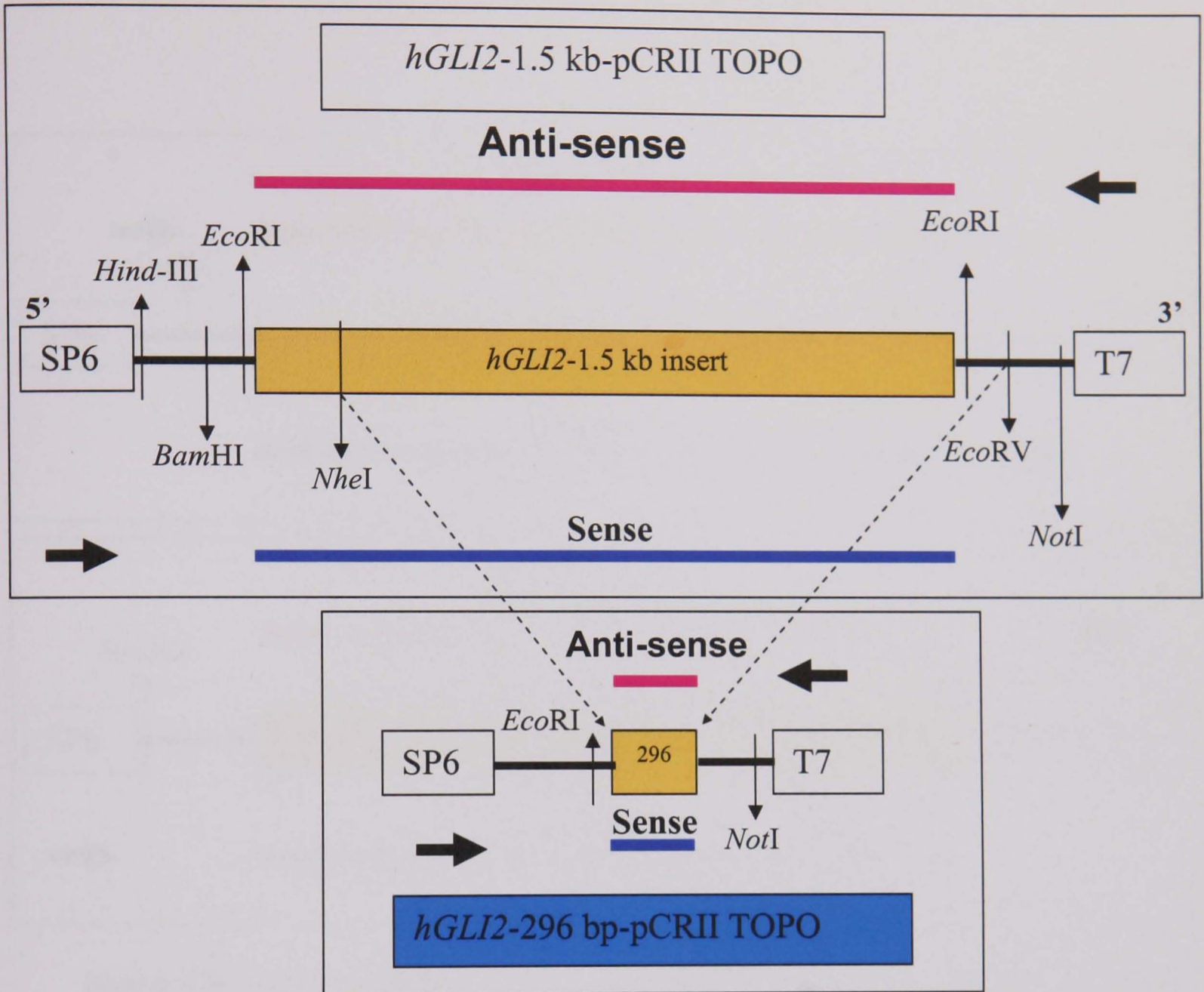


Figure 2.7: A diagrammatic representation of the *GLI2* (1.5 kb and 296 bp) anti-sense and sense probes generated from *hGLI2*-1.5 kb-pCRII-TOPO and *hGLI2*-296 bp-pCRII-TOPO vector. Showing the restriction sites of the nucleases used to linearise the plasmids and the SP6 and T7 RNA Polymerase sites.

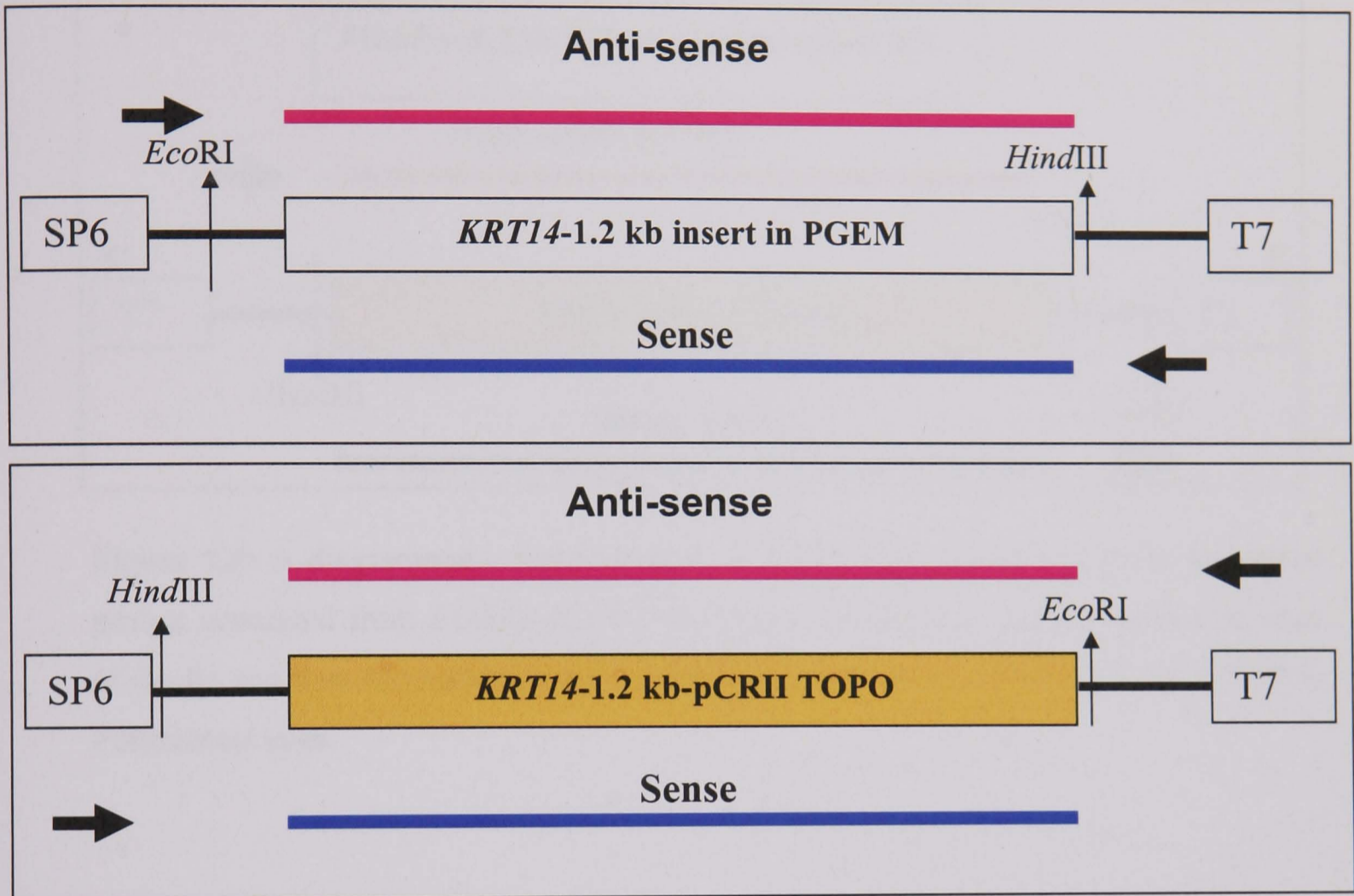


Figure 2.8: A diagrammatic representation of the *KRT14* 1.2 kb anti-sense and sense probes generated from *KRT14*-1.2 kb-PGEM and *KRT14*-1.2 kb-pCRII-TOPO. Showing the restriction sites of *EcoRI* and *HindIII* nucleases used to linearise the plasmids and the SP6 and T7 RNA Polymerase sites.

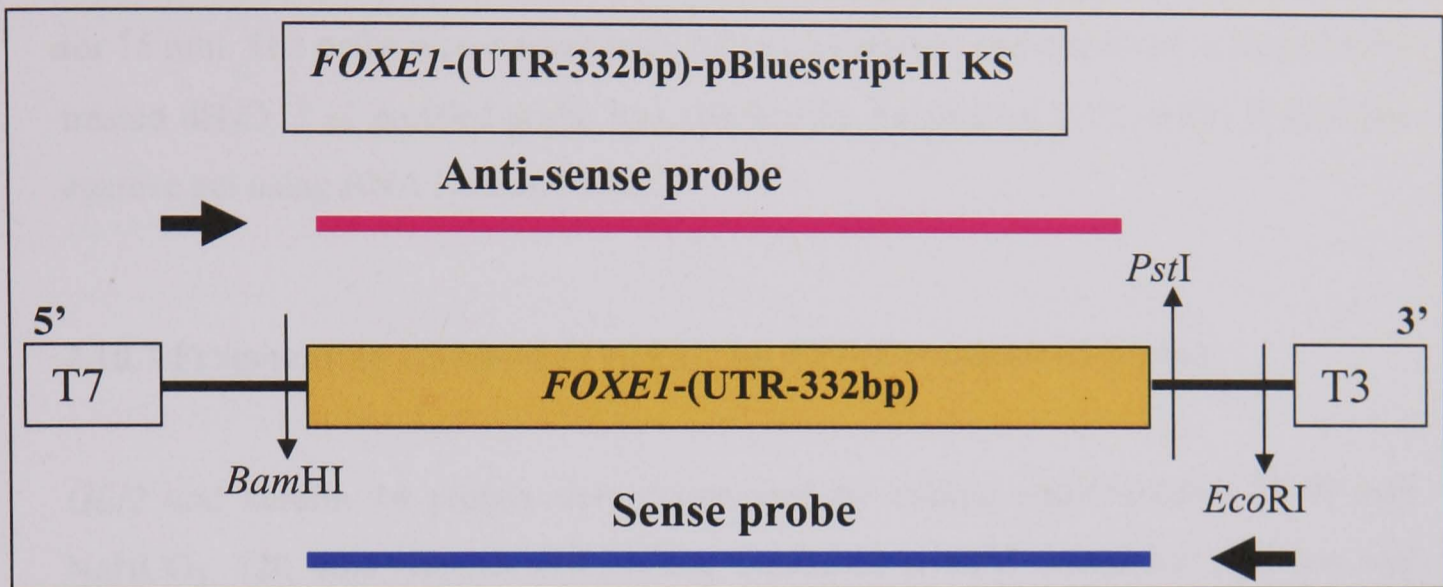


Figure 2.9: A diagrammatic representation of the *FOXE1* 332-bp anti-sense and sense probes generated from *FOXE1*-(UTR-332 bp)-PGEM plasmid and the restriction sites of *Eco*RI and *Bam*-HI nucleases used to linearise the plasmids and the SP6 and T7 RNA Polymerase sites.

2.10.6 Purifying transcribed probe by ethanol, precipitation.

2.5 μ l 4M LiCl and 75 μ l 100 % (v/v) ethanol was added to the transcription reaction and incubated at -20°C for 1 hour. Reaction mix was then centrifuged at 13000 rpm 4°C for 15 min. The pellet was washed with 70% (v/v) ethanol and dissolved in 40 μ l DEPC treated dH₂O. 1 μ l purified probe was checked by running on a 1% (w/v) RNase free agarose gel using RNA loading buffer.

2.10.7 Fragmenting 1.5 kb *GLI2* and 1.2 kb *KRT14* transcribed probes.

GLI2 and keratin 14 probes were fragmented by adding equal volume of 80 mM NaHCO₃, 120 mM Na₂CO₃ (39 μ l) and incubated at 60°C (*GLI2* for 12.5 min and keratin 14 for 10 min 36 sec) in a PCR machine. The length of time the probes were fragmented for was calculated using the following formula. $\text{Min} = (L-0.5) / (0.055L)$ where L is the starting length (Kb) of the transcript.

2.10.8 Purifying the fragmented probe by ethanol precipitation.

150 μ l RNase free dH₂O, 1/10 of the volume (3 M sodium acetate pH 5.2) and 2.5 x the volume cold 100% (v/v) ethanol was added to the fragmented probe and vortexed. Reaction mix was incubated at -70°C for 1 hour and centrifuged at 13000 rpm for 20 min at 4°C. The pellet was washed with 250 μ l 70% (v/v) ethanol and allowed to air dry at room temperature before being dissolved in 20 μ l DEPC treated dH₂O. 1 μ l fragmented probe was run on a 1% (w/v) RNase free (EthBr) agarose gel with an RNA loading buffer. Fragmented probe was seen as a smear on the gel. Purified fragmented probes were stored at -20°C.

2.10.9 Quantifying DIG-labelled *KRT14*, *GLI2* and *FOXE1* probe by dot blotting.

A control DIG labelled RNA was diluted to give 1 ng, 100 pg, 10 pg, 1 pg, 0.1 pg and 0.01 pg per 2 μ l. A serial dilution A- F of *KRT14*, *GLI2* and *FOXE1* DIG labelled ribo probes were also made. 2 μ l of each dilution of control and *KRT14*, *GLI2* and *FOXE1*

DIG labelled probes were spotted on a Hybond-XL (RPN 203S Amersham) and allowed to air dry and washed with DIG buffer 1 for 1 min at room temperature. Incubated in 10 ml blocking solution (10 ml DIG buffer 1, 0.5 g Marvel and 30 μ l Triton x100), shaking for 30 min at room temperature followed by incubating in Fab antibody (Roche Cat No 1 093 274) solution (10 ml DIG buffer 1, 0.5g Marvel, 30 μ l Triton x100 and 2 μ l Fab antibody) shaking for 30 min at room temperature. Then washed with DIG buffer 1 for 15 min (2 x) and in DIG buffer 2 for 2 min at room temperature. Dot blot membrane was covered with the BCIP/NBT substrate solution and incubated for 20 min at room temperature. A substrate reaction was stopped by washing with dH₂O and allowed to air dry. The concentration of *KRT14*, *GLI2* and *FOXE1* DIG-labelled probes was determined by comparing the intensity of the *KRT14*, *GLI2* and *FOXE1* spots with that of the known control DIG-labelled RNA spots.

2.10.10 Cutting paraffin wax embedded and frozen normal skin and BCC tissue sections.

All equipment used was RNase free and all solutions were made up in 0.1% (v/v) DEPC dH₂O. For wax embedded tissue samples Microtone water bath was cleaned with, 70% (v/v) methanol, 1% (v/v) concentrated HCl in 0.1% (v/v) DEPC dH₂O, dried and rinsed with 0.1% (v/v) DEPC dH₂O. 1 litre of 0.1% (v/v) DEPC dH₂O was placed in the water bath and the temperature set at 42°C.

The tissue blocks were incubated at 4°C for 1 hour before cutting 5 μ m tissue sections using a Microtone. Cut sections were placed in 0.1% (v/v) DEPC dH₂O water bath preheated at 42°C as described above, this allowed the sections to spread out and preventing them from creasing. The sections were transferred on to a Super frost plus microscope slides (BDH Cat No 406/0179/00). When lots of sections were cut from the same block it started to warm up so to keep it cool it was placed on ice for few min before cutting more sections. The sections were dried at 42°C overnight.

Snap frozen tissue samples were embedded in a CRYO-M-BED embedding medium and 8 micron tissue sections were cut on a cryostat (SLEE mainz) set at -20°C. Each section was collected on to a room temperature Super Frost-Plus microscope slides and

placed immediately into micro-slide box on dry ice. The slides were stored at -70°C if not used immediately.

2.10.11. Pre-treatment of tissue sections.

The following day wax sections were de-waxed in Xylene (x2) for 5 min. The frozen section slides were removed from the slide box on dry ice or from the -70°C freezer and placed on a clean Kimwipe (or similar lint-free towel) and allowed to thaw for no more than 30 sec. The slides were then transferred into a 4% (w/v) freshly made Paraformaldehyde (Sigma) at room temperature for 15-30 min, to fix the frozen sections. After incubating the wax sections in xylene and frozen section in paraformaldehyde, the slides were washed separately in 0.1 % (v/v) DEPC PBS for 10 min, 100% (v/v) ethanol for 10 min, 70% (v/v) ethanol for 10 min and in 0.1 % (v/v) DEPC dH_2O for 10 min. Rest of procedure described below was same for wax and frozen sections.

To increasing the accessibility of the target mRNA two methods were used. (1) 0.01M citrate buffer pH 6, was microwaved for 12 min in a microwave steam cooker, the slides were then immediately placed in the heated citrate buffer and microwaved for a further 8 min. (2) The slides were incubated with 100 μl 2.5 $\mu\text{g}/\mu\text{l}$ Proteinase K at 37°C in a slide Hybrid incubator for 15-30 min time range, Proteinase K was inactivated by immersing in 0.2% (w/v) Glycine for 10 min.

The remaining procedure was same for both methods. After increasing the accessibility of the target RNA, the sections were immersed in 0.1 % (v/v) DEPC PBS for 10 min and acetylated in 0.1 M triethanolamine (TEA) pH 8, 0.25% (v/v) acetic anhydride for 10 min. This step prevented non-specific binding of the probe to positively charged amino groups by acetylating them. After acetylation the slides were washed in 0.1 % (v/v) DEPC PBS for 5 min.

2.10.12. Pre-hybridisation.

Slides were taken out of the 0.1 % (v/v) DEPC PBS and wiped around the tissue section with sterile paper wipe. Sections were not allowed to dry at any time. If there were

CHAPTER 2: Materials and Methods

many slides one slide at time was wiped and the required reagent added to it. The tissue sections were covered with pre-hybridisation solution [4x SSC, 1x Denhardt's, 50% (v/v) formamide, 500 µg/ml tRNA, 500µg/ml salmon testes DNA (ST-DNA) denatured at 100°C for 10 min and placed on ice before adding to the mix] and incubated at 42°C for 3-4 hours in a slide Hybaid incubator.

2.10.13. Hybridisation.

Excess pre-hybridisation solution was wiped off using a clean tissue wipe and 30 µl of hybridisation solution (same as the prehybridisation solution) containing 50-100 ng labelled probe and 20% (w/v) Dextran sulphate was added. The probe was denatured at 65°C for 5 min and placed on ice before adding to the hybridisation mix. The sections were covered with Para film and incubate at 42°C overnight.

The next day the sections were washed in 2x SSC for 5 min (x 2), 2x SSC 50% Formamide, 1x SSC 50% (v/v) Formamide, 0.5x SSC 50% (v/v) Formamide at temperature ranging from 42-55°C for 20 min in each solution and 0.1x SSC 50% (v/v) Formamide at temperature ranging from 42-60°C for 20 min in a Hybrid sleeve wash. The final wash was in 2x SSC for 5 min at room temperature.

2.10.14. Immunological detection of Digoxigenin-labelled probes.

The sections were rinsed in DIG buffer 1 (100 mM Tris-HCl, 150 mM NaCl pH 7.5) for 5 min at room temperature, and blocked by incubating for 30 min with 100 µl of 10% (v/v) normal sheep serum (NSS) in DIG buffer 1. This was replaced with 100 µl of 1% (v/v) NSS in DIG buffer 1, containing sheep Anti-Digoxigenin-alkaline phosphatase (AP) conjugated (Fab fragments, Roche Cat No 1 093 274) diluted 1:400 and incubated for 2 hours at room temperature.

The unbound conjugate was removed by two 10 min washes in DIG buffer 1, followed by one wash for 5 min in DIG buffer 2 (100 mM Tris-HCl pH 9.5, 100 mM NaCl, 50 mM MgCl₂) at room temperature. The Hybrids were visualised by incubating the section with 5-Bromo-4-Chloro-3-Indoyl Phosphate / Nitro Blue Tetrazolium (BCIP/NBT) liquid substrate system (Sigma Cat No B-1911) chromogen solution (350

$\mu\text{g}/\mu\text{l}$ NBT and $175 \mu\text{g}/\mu\text{l}$ BCIP in DIG buffer 2) in dark at 4°C overnight. The chromogen solution being light sensitive was prepared immediately prior to use and filtered through $0.22 \mu\text{m}$ disposable filter, wrapped in aluminium foil and placed on ice. The colour reaction was stopped by immersing the slide in buffer 3 (10 mM Tris-HCl pH 8, 1 mM EDTA) for 30 min at room temperature. The developed slides were mounted using Aqua mount and examined under a light microscope.

2.11.0 Affymetrix analysis

2.11.1 First strand cDNA synthesis.

Superscript ds-cDNA Synthesis Kit (Cat No 11917-010, Invitrogen) was used to synthesis first strand cDNA synthesis. Reactions were set up on ice as shown in **Table 2.7**.

Table 2.7: Components of the first strand cDNA synthesis reactions set up for Affymetrix analysis.

Sample	Total RNA [$\mu\text{g}/\mu\text{l}$]	Volume Taken μl	T7-(T)24 primer (100 pmol/ μl) volume added μl	Total RNA μg
GLI1-GS	0.72	10	1	7.2
GLI1+EGF	0.77	10	1	7.7
EGFP-GS	0.69	10	1	6.9
EGFP+EGF	0.76	10	1	7.6

Primary keratinocytes were transduced with GLI1 and EGFP retroviral particles and cultured with EGF (GLI1+EGF, EGFP+EGF), and without growth supplement (EGFP-GS, GLI1-GS controls). The table shows total RNA concentration and the volumes taken for each sample in first strand cDNA synthesis reaction for Affymetrix analysis.

The reactions were mixed by pipetting up and down and pulse centrifuged before incubating at 70°C for 10 min, on a Hybrid PCR block and then immediately placed on ice. A master mix 16 μl [5x] First Strand Buffer (thaw at 37°C , put on ice), 8 μl DTI [0.1 M] and 4 μl dNTPs [10 mM each] was made up on ice, this was mixed by pipetting up and down and pulse centrifuged. 7 μl of this master mix was added to each reaction

CHAPTER 2: Materials and Methods

tube and incubate at 42°C for 2 min. 1 µl of Superscript II reverse transcriptase [200 U/µl] was added to each reaction tube and mixed by taping the tube and pulse centrifuged before incubating at 42°C for 1 hour in a Hybaid thermal cycler with heated lid. The tubes were then immediately place on ice.

2.11.2 Second strand cDNA synthesis.

Second stand cDNA synthesis was carried out using Superscript ds-cDNA Synthesis Kit (Cat No 11917-010, Invitrogen). A master mix 364 µl DEPC treated dH₂O, 120 µl 5x Second Strand Buffer, 12 µl dNTPs (10 mM each), 4µl E. Coli DNA Ligase (10 U/µl), 16µl E. Coli DNA Pol I (10 U/µl), 4 µl E-Coli RNase H (2 U/µl) was assemble on ice, this was mix by vortexing and pulse centrifuged. 130 µl of the master mix was added to each of the first strand reaction tubes and mixed by pipetting up and down and pulse centrifuged. The reaction was incubated at 16°C for 2 hours in a Hybrid thermal cycle block with heat lid on. 2 µl (5 U/µl) T4 DNA Polymerase was added to each tube and mixed by pipetting up and down and incubated for further 5 min at 16°C. The reaction was stopped by adding 10 µl of EDTA (0.5M) pH 8.0 to each tube. The tubes were then placed on ice.

2.11.3 Clean-up of double stranded cDNA.

Double stranded cDNA was cleaned up using Phase Lock Gel, 2 ml light (Cat No 0032005 10, EPPENDORF). Phase-Lock tubes were centrifuged in a microfuge at 13,000 rpm for 30 sec. To the cDNA reaction equal volume approximately 162 µl of room temperature buffer saturated phenol (add 65 µl of Alkaline Buffer [10 mM Tris-HCl pH 8.0, 1 mM EDTA] to 1 ml of phenol-chloroform-isoamyl alcohol 25:24:1, [AMBION 9732], vortex for 2 min and then spin) was added and vortexed briefly to mix.

The mixture was place into a Phase-Lock tube (taking care not to vortex) and centrifuged at 13,000 rpm in a micro-centrifuge for 2 min and then upper aqueous phase was transferred in to a new 1.5 ml eppendorf tube and to this (0.5 x volume) 75 µl (NH₄OAc [7.5 M], 4 µl Glycogen [5 mg/ml]) and 375 µl 100% ethanol was added. The solution was mixed by tapping the tubes and centrifuged at 13,000 rpm in a micro-

centrifuge for 20 min (care was taken not spin for longer). Supernatant was decanted taking care not to displace the pellet and washed twice with 500 μ l 80% cold ethanol, then centrifuged at 13,000rpm for 5 min for each wash. All the ethanol was removed and the tubes were spun briefly to collect any residual ethanol on the sides of the tube, this was also removed. The pellet was allowed to air dry for 5-10 min before dissolving it in 12 μ l of DEPC treated dH₂O. If not proceeding to the next step (*In vitro* transcription). The tubes were placed on dry ice to freeze the solution and then store at -80°C.

2.11.4 Synthesis and labelling of cRNA.

Synthesis of cRNA and labelling it was carried out by using BioArray High Yield RNA Transcript Labelling Kit (Cat No 900182, ENZO, Affymetrix). All reagents and double stranded cDNA were allowed to thaw at room temperature and were kept at room temperature until incubation at 37°C to reduce precipitation of DTT (dithiothreitol). The incubation was carried out in an incubator, to reduce condensation on the inside of the lid. A master mix was made up as shown in **Table 2.8**.

Table 2.8: Components of the reaction set up for the synthesis and labeling of cRNA using a BioArray High Yield RNA Transcript Labeling Kit (Cat No 900182, ENZO, Affymetrix)

Order of components added	Reagents from the Labelling Kit	Volume added μ l	Master Mix μ l
1	10x HY Reaction Buffer	4	16
2	Biotin-labelled ribonucleotides	4	16
3	DTT	4	16
4	RNase Inhibitor mix	4	16
5	T7 RNA Polymerase	2	8
6	DEPC treated dH ₂ O	10	40
7	double stranded cDNA (2.8.3)	12	-
Final Volume		40	112

Table 2.8 shows the components and the order in which they were added to the tube to set up reaction for the synthesis and labelling of cRNA. It also shows the total volume of the reaction and the volume taken for the master mix for 4 samples.

The master mix was mixed by pipetting and pulse centrifuged, 28 μ l of master mix was added to each sample of (12 μ l) double stranded cDNA (**from Section 2.11.3**). The reaction was mixed by pipetting up and down and pulse centrifuged and incubated at 37°C for 5 hours (gently mixing every hour by tapping tube and pulse centrifuging).

2.11.5 Purification of labelled cRNA and quantification.

Labelled cRNA was purified using RNeasy Mini Kit (Cat No 74104, QUIAGEN)

All reagents were prepared by following the manufacturers' instructions. Note **β -mercaptoethanol was not added to 1 ml of RLT Buffer** and care was taken not to touch the tip of the spin column at any time.

To the *in vitro* transcription reaction tubes (**from section 2.11.4**) 60 μ l DEPC treated dH₂O and 350 μ l RLT buffer was added and mixed thoroughly by pipetting up and down. Then 250 μ l 100% ethanol was added and mixed by pipetting up and down and pulse centrifuged. 700 μ l volume of each sample was placed in to a separate RNeasy spin column sitting in a 2 ml collection tube and centrifuged at 8000 xg for 15 sec. RNeasy spin column was placed into a new 2 ml collection tube and 500 μ l RPE buffer was placed in centre of the column, and then centrifuged at 8000 xg for 15 sec.

The column was transferred into a new 2 ml collection tube and 500 μ l RPE buffer was added and centrifuged at 13,000 rpm for 2 min. Spin column was transferred to a fresh 2 ml tube and centrifuged for 1 min to dry the RNeasy membrane from ethanol, to prevent any carryover of the RPE buffer. The Column was transferred into a new 1.5 ml collection tube, and cRNA was eluted by placing 50 μ l DEPC dH₂O on the middle of the membrane of the column and incubated at room temperature for 2 min before spinning at 8000 xg for 1 min. Each elute sample was then diluted 1:10 with sterile dH₂O (not DEPC treated) and absorbance measured using 2 micro cell on a Gene SpecII (Naka Instruments) spectrophotometer. Following formula was used to calculate the concentration of cRNA (Abs value at 260 nm x 40 μ g/ml x Dilution factor = μ g/ml total

RNA). The yield of cRNA obtained was between 10.5-14.5 ug, the cRNA samples were placed on dry ice and stored at -80°C.

To the remaining diluted cRNA samples 10 µl denaturing RNA loading buffer was added and denatured at 70°C for 10 min and run on a 1 % (w/v) agarose gel along with a 1kb plus DNA marker (as described in **section 2.5.6**). A DNA marker gives a rough idea of the size of the cRNA product should be. These looked like a smear from about 100 bp to 2 kbp with a brighter region from 500 bp to 1 kb.

2.11.6 cRNA fragmentation.

To 40 µl of each cRNA samples (**from section 2.11.5**) 10 µl of 5x fragmentation buffer was added and incubate at 94°C for 35 min in a PCR block, then immediately after the incubation the samples were placed on ice. 1 µl of each fragmented cRNA sample was placed in a 0.7 ml eppendorf tube containing 9 µl DEPC treated dH₂O, to this 10 µl denaturing RNA loading buffer (50% v/v deionised formamide, 6% v/v formaldehyde, 1x MOPS-EDTA buffer, 6.6% v/v Glycerol, 0.02% w/v bromphenol blue, 0.02% w/v xylene cyanol, 39.58 ug/ml ethidium bromide) was added and the samples were denatured at 70°C for 10 min and placed on ice immediately before running them on a 1 % (w/v) agarose gel. A 1kb plus (Cat No 10488-085 Invitrogen) marker was run alongside the samples to estimate the size of fragmented cRNA. The fragmentation produced a distribution of cRNA fragment from approximately 35-200 bases. Undiluted fragmented cRNA was stored at -80°C until ready to perform the hybridisation.

2.11.7 Hybridisation cocktail for human (HG-U133 A) gene chip.

A following master mix (**Table2.9**) was made up for x4.2 samples of fragmented cRNA. Note, before adding to the cocktail mix 1 vial of the 20x Eukaryotic Hybridisation Controls and 1 vial of the Oligo B2 were allowed to completely thaw at room temperature before heating at 65°C for 5 min and vortexed and pulse centrifuged.

Table 2.9: Hybridisation master mix for the arrays HG-U133A gene chip

Reagents	Volume Taken μ l
Control Oligonucleotide B2 (Cat No 900299, ENZO, Affymetrix)	21
20x Eukaryotic Hybridisation Controls (Cat No 900299, ENZO, Affymetrix)	63
Herring sperm DNA (10 mg/ml) (D7290 sigma)	12.6
Acetylated BSA (50 mg/ml) (Sigma)	12.6
DEC dH ₂ O	315

Table 2.9 showing different reagents and the volume taken to make a master mix for x4.2 samples, for the HG-U133A gene chip arrays. 101 μ l of above master mix was added to 49 μ l of each fragmented cRNA, samples (from **section 2.11.6**). The samples were transported on dry ice to the department of Molecular Oncology at Carterhouse square London, Cancer Research UK.

Following procedure was performed by the Affymetrix operator. Samples were hybridised on a test chip to verify the quality of cRNA before hybridising them on Affymetrix HG-U133A gene chip (Cat No 900366 Affymetrix). To each sample 150 μ l 2x Hybridisation buffer was added and heated at 99°C for 5 min in a heat block and transferred to 45°C heat block for 5 min before spinning at maximum speed (in a micro bench centrifuge) for 5 min to remove any insoluble material. Meanwhile probe array was equilibrated at room temperature and filled with the appropriate volume of 1x Hybridisation buffer (200 μ l for the U133 A and B arrays). Probe array was place in an oven at 45°C for 10 min with rotation at 60 rpm. The buffer solution was removed from the probe array cartridge and filled with the appropriate volume of fragmented cRNA hybridisation cocktail mix (from **section 2.11.7**) and incubated in an oven at 45°C with rotation at 60rpm for 16 hours. The washing, staining and scanning of chips were also performed by the Affymetrix Operator. The data was obtained on a CD disk from the operator and analysed using a Gene spring program from Sillicon Genetics.

2.12.0 Laser-capture micro-dissection of normal skin for gene expression analysis.

2.12.1 Tissue freezing and embedding.

Cryomold was made using silver foil and placed on dry ice and filled halfway with embedding medium OCT (Cat No LAMB/OCT Raymond-A-Lamb). Normal skin tissue was placed in cold cryomold in an orientation that allowed cross section cut. Further OCT was added to cover the entire tissue. Once the OCT had solidified and turned white the embedded tissue was stored at -70°C freezer if sections were not cut immediately.

Slide preparation: Cryostat was allowed to pre-cool to -25°C . Knife holder and anti-roll plate was wiped with 100% ethanol to avoid sample cross-contamination. Micro slide box was placed on dry ice near the cryostat and the cryomold containing the Normal skin specimen from the -70°C freezer was placed in the cryostat. The sample was allowed to stand in the cryostat for 10 min so that the tissue reached an appropriate cutting temperature (-23°C). $8\ \mu\text{m}$ sections were cut using a new sterile blade for each sample. Each section was collected on a room-temperature glass slide (Arcturus) and placed immediately into micro-slide box on dry ice. The sections were not allowed to air dry and the slides with folded or wrinkled sections were discarded. Immediately after cutting sections they were stained and dehydrated.

2.12.2 Staining and dehydration.

Using the HistoGene LCM Frozen Section Staining kit (Cat No KIT0401 Arcturus), 25 ml of the appropriate solutions; a) 75% (v/v) ethanol, b) distilled water, c) second distilled water solution, d) 75% (v/v) ethanol, e) 95% (v/v) ethanol, f) 100% ethanol and g) xylene were placed in labelled plastic slide jars provided with the kit. The 100% ethanol provided in the Histo Gene Frozen Section Staining Kit was not used for any other step except for the staining.

Four tissue section slides were removed from the slide box on dry ice or from the -70°C freezer, and placed on a clean Kim wipe (or similar lint-free towel) and allowed to thaw for no more than 30 sec. Metal sterile forceps were used to transfer slide from jar to jar.

CHAPTER 2: Materials and Methods

Slides were first placed in plastic jar "a" containing 75% (v/v) ethanol for 30 sec and then transferred to plastic jar "b" containing distilled water for 30 sec. The slides were then placed on a Kim wipe or on a horizontal staining rack. Using an RNase-free pipette tip approximately 100 μ l of the HistoGene staining solution was placed on the tissue section and stained for 20 sec. Then the slides were rinsed for 30 sec in each solution starting with jar "c" containing distilled water, jar "d" containing 75% (v/v) ethanol, jar "e" containing 95% (v/v) ethanol, jar "f" containing 100% ethanol and then in jar "g" containing xylene for five min. Slides were then placed on a Kim wipe to dry in the fume hood for five min before transferring them to a slide box containing fresh desiccant.

One slide was removed and dermal papilla, root sheath and epidermis area of the normal skin were laser capture micro-dissected using the PixCell II (Arcturus) system as per manufacturers instruction using standard Cap Sure LCM Caps (Cat No LCM0201 Arcturus). Several dermal papillae, root sheaths and epidermis areas were captured from same slide and from new slide on one Cap. Remaining slides were kept in the desiccators until ready for LCM. All used staining and dehydration solutions were discarded according to COSHH regulations.

2.12.3 RNA extraction using picopure RNA extraction kit (Cat No RIT0202 Arcturus USA).

50 μ l extraction buffer (XB) was placed into a 0.5 ml RNase free micro-centrifuge tube and the Cap Sure Cap with the captured cells was placed in the tube and inverted. The tube was taped to ensure all extraction buffer was covering the Cap before incubated for 30 min at 42°C on a heat block. With the cap on the tube it was centrifuged at 800x g for two min to collect the cell extract into the tube. If RNA isolation was not carried out immediately the cell extract was stored at -80°C.

RNA purification column was pre-conditioned by adding 250 μ l condition buffer on to the filter membrane and incubated for 5 min at room temperature before centrifuging in the collection tube at 16,000 x g for one min. To the cell extract 50 μ l of 70% (v/v) ethanol (EtOH) was added and mixed well by pipetting up and down (do not to centrifuge). The cell extract and EtOH mixture was placed into the pre-conditioned

purification column and centrifuged for 2 min at 100 x g and then immediately at 16,000 x g for 30 sec. The flow through was removed and 100 µl Pico Pure RNA Kit Wash Buffer 1 (W1) was placed into the purification column and centrifuge for one min at 8,000xg and the flow-through was discarded. To remove traces of wash buffer the column was re-centrifuged for one min at 16,000xg and flow-through was discarded. The column was then transferred to a new micro-centrifuge collection tube. Any DNA contamination was removed by treating the column with DNaseI as described in **section 2.12.4**.

2.12.4 DNaseI treatment of pico pure RNA column.

To the Pico Pure RNA column from **section 2.12.3**, 40 µl of DNaseI solution (5 µl DNaseI stock solution and 35 µl buffer RDD provided with RNase-free DNaseI kit, Cat No 79254, Qiagen) was placed directly into the purification column membrane and the column cap replaced before mixing it by gently inverting the column and incubated at room temperature for 15 min. 40 µl wash buffer (W1) was added to the purification column and centrifuge at 8000 xg for 15 sec. Column was then washed twice by add 100µl wash buffer 2 (W2) into the purification column and centrifuged at 8,000xg for first wash and 16,000xg for the sec wash for 1 min and the flow-through was discarded. If any residual wash buffer remained in the column the column was re-centrifuge at 16,000 xg for 1 min and the flow-through discarded. The column was transferred to a new 0.5 ml micro-centrifuge tube before adding 11 µl of elution buffer (EB) by gently touching the tip of the pipette to the centre of the membrane surface while dispensing the elution buffer to ensure maximum absorption of EB into the membrane. The column was incubated for 1 min at room temperature before centrifuging for 1 min at 1,000 xg to distribute EB in the column, then for 1 min at 16,000 xg to elute total RNA.

The isolated total RNA was used in RT-PCR, if not used immediately it was stored at –80°C. Quantifying of isolated total RNA was not carried out due to the fact that total RNA expected was estimated to be less than 1 ug. Measurements taken for samples containing less than 1 µg of total RNA may have been affected by components in the elution buffer, which may have resulted in an overestimation of the total RNA.

2.13.0 Generating a GLI2 monoclonal antibody.

The amino acid sequence of beta GLI2 was obtained from the NCBI protein data base (GI No13528233, NP 084656.1). Following beta-GLI2 peptides
GLI2 C Terminal N-CATAGFGLVQPRPPLEPS-C (Corresponding to amino acid 1017 to 1033, total length 18 residues),
GLI2 N Terminal N-ESAVSSTVNPVVAIHKRSC-C (Corresponding to amino acid 31 to 47, total length 18 residues) were ordered from Cancer Research UK peptide synthesis laboratory.

2.13.1 Conjugation of C-and-N-terminal peptides of GLI2 to mcKLH.

The C-and N-terminal peptides of beta GLI2 isoform were conjugated to a carrier Imject Maleimide Activated Keyhole limpet hemocyanin (mcKLH, Cat No 77605 Pierce), to make them fully immunogenic, as per manufacturers instructions. An out line of a protocol is as follows. One vial of 10 mg Maleimide Activated mcKLH was reconstituted with 1 ml dH₂O to give a 10 mg/ml solution, mcKLH formed a suspension that appeared whitish blue. The suspension was not vortexed or heated to prevent mcKLH precipitating. 2 mg of each peptide was dissolved in 200 µl PBSA and immediately added to 200 µl (10 mg/ml) activated mcKLH and mixed by finger taping before incubating at room temperature for 2 hours.

2.13.2 Conjugated peptide purification.

Conjugated beta GLI2 C-and N-terminal peptides from **section 2.13.1** were purified by using PD-10 desalting columns (Cat No 17-0851-01 Amersham) to remove EDTA. EDTA is an anti-coagulant and it was not injected into laboratory animals. Desalting did not separate non-conjugated mcKLH from conjugated mcKLH. However, a large excess of each peptide was used which made it unlikely that any non-conjugated carrier may have existed in significant quantities. If a precipitate formed during conjugation the solution was centrifuged and the supernatant was purified and the precipitate was saved.

CHAPTER 2: Materials and Methods

The top cap of desalting column was removed and excess liquid was poured off before cutting column tip and replacing the tip cap to prevent the column from running dry. The column was washed with 3-5 times column volume (i.e., 15-25 ml) of PBSA.

The volume of conjugate solution was made up to 1ml with PBSA. The conjugate supernatant was applied directly to the centre of the column disc and allowed to run into the column before eluting it with PBSA. In a separate 1.5 ml tubes 1 ml volume fractions were collected up to 12-15 aliquots. Each aliquots absorbance was measure at 280 nm using a 10 μ l volume path cuvette on Gene-Spec spectrophotometer, to locate fractions containing the conjugate. The peptide-carrier conjugate was in the first absorbance peak detected. All fractions with acceptable levels of conjugate were pooled and combined with any precipitated conjugate and sent to Cancer Research UK Monoclonal Antibody production services department on dry ice for injecting into the mice.

The following procedures were carried out at the Monoclonal Antibody services (CRUK). The mice were given 300 μ g of the peptide-carrier conjugate injection initially and later a sec (booster) injection was given after six weeks. Elisa assay was preformed with the test bleeds using peptide only, to see if there was an immune response. The test bleeds that were positive with 1/10,000 dilution were tested using a western blot analysis with NHIS-GLI2 and GFP (control) transformed primary keratinocyte cell lysates. A 140 kD GLI2 band was expected on a western blot.

2.14.0 SDS Polyacrylamide Gel Electrophoresis and Western blot analysis.

The SDS Polyacrylamide Gel Electrophoresis (PAGE) and western blot analysis protocol used has previously been described in detail (Sambrook J., 1989). cells were lysed by adding 200 μ l of boiling buffer (50 mM Tris-HCl, pH 8.0, 2% SDS, 1 mM sodium orthovanadate) directly to the culture dish's and cells were scraped using a fresh cell scraper for each sample. Cell lysates were then transferred to a 1.5 ml tube and boiled for a further 2 min before aspirating them through a fine needle and placed on ice. To prevent protease digestion 1x protease inhibitors (Cat No 46931 24001 Roche) were added to each sample. Protein quantification was measured with DC Protein Assay

CHAPTER 2: Materials and Methods

reagent (Cat No 500-0112, Bio-Rad) as per manufacturers instructions at 655 nm using a spectrophotometer.

Protein cell extracts were run on freshly made denaturing 375 mM Tris pH 8.8 based 8-15% (v/v) polyacrylamide sodium dodecyl sulphate (SDS) mini-gels (with a 125 mM Tris pH 6.8 stacking gel) made fresh, with 1x running buffer (25 mM Tris, 0.19 M glycine, 3.5 mM SDS). 2x SDS loading dye (125 mM Tris aminomethane pH 6.8, 5% β -mercaptoethanol, 20 % (v/v) glycerol, 4% (w/v) SDS and 0.02% (w/v) bromophenol blue) was added to an equal volume of 5-10 μ g protein samples and loaded onto the gel. To determine protein size, recombinant Rainbow protein molecular weight marker (Cat No RPN800 Amersham Pharmacia Biotech, UK) was loaded along side the samples.

Gels were run at a current of 20 mA for approximately 90 min. Protein was electro-transferred from the gel to a methanol-activated Hybond P-PVDF membrane (Amersham Pharmacia Biotech, UK) in 1x transfer buffer (25 mM Tris, 0.19 M glycine, 20% (v/v) methanol), with a current of 20mA overnight or at 100 mA for 3 hours. The membrane was washed 3 times in 0.1% (v/v) Tween-20 in PBS for 5 min, before incubation in blocking solution (5% (w/v) Marvel milk powder in 0.1% (v/v) Tween-20 in PBSA) at room temperature shaking for 45 min.

Primary antibodies; GLI1 1:1000 (goat polyclonal, Cat No C-18 Sant Cruz), panERK 1:1000 (mouse, Cat No 610123, BD Bioscience Pharmingen), EGFR 1:1000 (goat Cat No SC-03-G, Santa Cruz), Vimentin 1:1000 (mouse clone RV202 Cat No 550513, BD Bioscience Pharmingen) and E-Cadherin (Cat No 61081 B D Bioscience Pharmingen), were diluted in blocking solution, K14 1:10 (mouse monoclonal, LL001 supernatant, CRUK) was diluted in PBS-Tween-20 0.1% (v/v) with no milk powder and incubated with the membrane shaking at room temperature for 60 min. The membrane was then washed three times in 0.1% (v/v) Tween-20 in PBSA shaking for 6 min.

Secary antibodies used were rabbit anti-goat (for goat primary antibodies) or goat anti mouse (for mouse primary antibody) conjugated to horseradish peroxidase (DAKO, Cambridge UK) diluted 1:1000 in blocking solution, incubated shaking at room temperature for 45 min.

CHAPTER 2: Materials and Methods

After washing the membrane 3 times in 0.1% (v/v) Tween-20 in PBS shaking for 6 min, protein bands were visualized using the ECLplus chemiluminescence detection reagent (Cat No RPN2132 Amersham Pharmacia Biotech, UK) according to the manufacturer's instructions. ECLplus reagent contains Lumigen PS-3 acridan substrate, which is oxidised by horseradish peroxidase to an acridium ester, which then reacts in alkaline conditions to form a chemiluminescent product. In a dark room with the aid of a safety light, this was visualized by exposing X-ray film (Kodak) to the membrane wrapped in cling film for 20 sec to 15 min depending on band intensity. X-ray film was developed by immersing in developer (Kodak) for 5 min, washing briefly in tap water and immersing in fixer (Kodak) for 2 min.

2.14.1 Stripping western blot membrane for re-probing.

Hybond P membranes can be striped and reused to probe with a different antibody. The membrane was stripped by incubating in stripping buffer [62 mM Tris, 2% (w/v) SDS, 0.1 M β -mercaptoethanol pH 6.7] at 65°C for 45 min, and then washed 3 times in 0.1% (v/v) Tween-20 in PBSA for 5 min. To check if previous labelling had been completely removed, the membranes were treated with ECLplus and exposed on X-ray film for 15 min, then washed 3 times in 0.1% (v/v) Tween-20 for 5 min. The membrane was then blocked in 5% (w/v) milk protein in 0.1% (v/v) Tween-20 in PBSA and probed as described in **section 2.14.0** above with a different antibody.

CHAPTER 3

**Analysis of SHH-Pathway Genes in Normal Skin, BCC and
GLI1-transduced Human Primary Keratinocytes**

3.1.0 Introduction

The hedgehog (Hh) signal transduction pathway is involved in embryonic development in patterning the developing neural tube, axial skeleton, limb, lungs skin, hair and teeth (Bellusci et al., 1997; Hardcastle et al., 1998; Marigo et al., 1996b; Riddle et al., 1993; St-Jacques et al., 1998). A more detail introduction of this pathway is described in **Chapter 1 section 1.3.0**. Much of what is known of the hedgehog pathway has been derived from studies carried out in *Drosophila* (Basler and Struhl, 1994; Nusslein-Volhard and Wieschaus, 1980; Rodriguez and Basler, 1997). In addition to hedgehog, other members of this pathway are; patched, smoothend, kinesin like protein costal-2, serine/threonine kinase fused, suppressor of fused and zinc finger transcription factor cubitus interruptus (Alcedo et al., 1996; Marigo et al., 1996a; Monnier et al., 1998; Orenic et al., 1990; Preat et al., 1990; Sisson et al., 1997; Stone et al., 1996; van den Heuvel and Ingham, 1996). Many of the key components of the pathway have been conserved from flies to humans (Goodrich et al., 1996; Hahn et al., 1996a). *Cubitus interruptus* (Ci) can function as either a transcriptional activator or a proteolytically cleaved repressor (Aza-Blanc and Kornberg, 1999).

In vertebrates, transcriptional responses to hedgehog signalling are mediated by the three *Ci* homologues GLI1, GLI2, and GLI3 (Ingham and McMahon, 2001; Matise and Joyner, 1999; Ruiz i Altaba, 1999a) that can act in combinatorial fashion to modulate target gene expression. GLI1 and GLI2 appear to act primarily as transcriptional activators, whereas GLI3 and at times GLI2 functions as a repressor (Ingham and McMahon, 2001).

Sonic hedgehog (SHH) belongs to a vertebrate evolutionarily conserved family of genes including Desert hedgehog (*DHH*) and Indian hedgehog (*IHH*), which are related to the *Drosophila* hedgehog (Hh) (Echelard et al., 1993, Marigo et al., 1995.). SHH functions by binding a receptor protein Patched (PTCH) in target cells (Stone et al., 1996, Smyth et al., 1999). PTCH normally inhibits downstream signalling through a transmembrane protein Smoothened (SMO). Genetic analysis of patients with familial nevoid basal cell carcinoma syndrome (NBCCS) as well as individuals with sporadic BCC led to the identification of the *PTCH* tumour suppressor gene (Gorlin, 1987; Hahn et al., 1996b; Johnson et al., 1996); this subsequently implicated aberrant SHH signalling in BCC formation. Up regulation of *GLI1* and *GLI2* is frequently observed in BCCs (Dahmane et al., 1997; Gailani et al., 1996; Regl et al., 2002; Uden et al., 1997). Further evidence

for BCC development as a result of activation of Hh-signalling pathway comes from transgenic mouse models and skin grafting techniques. Heterozygous *Ptch* +/- mice develop BCC like features upon UV-irradiation, although sporadic BCC formation does not normally occur in these mice (Aszterbaum et al., 1999). Human keratinocytes expressing SHh form BCC-like structures when grafted onto the back of nude mice (Fan et al., 1997) and over expression of mediators of Hh-signalling including an oncogenic form of SMO, SHH, GLI1 and GLI2 in epidermal cells of transgenic mice leads to the induction of BCC-like tumours (Fan et al., 1997; Grachtchouk et al., 2000; Nilsson et al., 2000; Oro et al., 1997; Xie et al., 1998).

Transgenic mice that are deficient in *GLI1* are viable and have no obvious developmental defects (Park et al, 2000). In contrast, *GLI2*^{-/-} mice are characterized by severe developmental malformations including the lack of the floor plate of the neural tube and of the anterior pituitary, and by numerous lung, foregut, skeleton and skin defects (Ding et al, 1998; Matise et al, 1998; Mill et al, 2003). This *GLI2* phenotype broadly overlaps with that described for *SHH* or *IHH* deficient mice (Chiang et al, 1996; Chiang et al, 1999; St-Jacques et al, 1999). Secondly, removal of *GLI2* but not of *GLI1* leads to partial rescue of the *PTCH*^{-/-} phenotype, where hedgehog signalling is hyperactivated (Bai et al, 2002). Thirdly, *GLI2* but not *GLI1* is required for hedgehog signalling in hair follicle development (Mill et al., 2003). This suggests that GLI2 rather than GLI1 is the primary transducer of the Hh-signal. The mechanism by which GLI1 and GLI2 controls HH-mediated epidermal development and skin cancer is not known.

In the developing neural tube, SHH has been shown to regulate *COUP-TFII* expression during the differentiation of motoneurons (Lutz et al., 1994). SHH stimulates *COUP-TFII* expression (Krishnan et al., 1997) thus is likely to be a downstream target of SHH signaling, and the requirement for SHH in gastric organogenesis suggests that COUP-TFII may play a role in stomach development (Takamoto et al., 2005).

The general transcription factor TFIID complex composed of the TATA box binding protein (TBP) and multiple TBP-associated factors (TAFII) is required at many gene promoters to initiate transcription by RNA polymerase II (Dymlacht et al., 1991; Hernandez, 1993). *GLI*-induced transcriptional activation requires the carboxyl-terminal region consensus recognition element for the human TFIID TATA box-binding protein associated factor TAFII₃₁ (Yoon et al., 1998). The presence of this region in the GLI

activation domain provides a mechanism by which GLI-induces transcriptional regulation. Expression of the genes described above involved in HH-signalling have not been determined in BCC and normal skin.

The aim of this chapter was to investigate the expression of *PTCH1*, *GLII*, *GLI2*, *GLI3*, *SMO*, *SUP-FU*, the kinesin superfamily (*KIF4*), *TFIID* and *COUP-TFII* genes that have been shown to be involved in HH-signalling pathway in human skin, BCC and *GLII* transduced human primary keratinocytes isolated from normal skin using Northern blot and RT-PCR and Real Time RT-PCR analyses.

3.2.0 Results

3 2.1 Northern blot analysis of SHH-signalling pathway.

Expression of *PTCH*, *GLII* and *GLI2* genes of SHH-signalling pathway were analysed using northern blot analysis on mRNA extracted from normal skin, Basal Cell Carcinoma (BCC), *GLII* transduced primary keratinocytes. *GLII-E1A* transformed baby rat kidney and A375 melanoma cell lines were used as positive controls expressing *GLII*. The spontaneously immortalised primary keratinocytes cell line (HaCat) and EGFP transduced primary keratinocytes cell lines were used as negative controls that is non-*GLII* expressing cell lines.

3.2.2. *GLII* expression in normal skin, BCC, *GLII-E1A* transformed baby rat kidney and *GLII* transduced primary keratinocytes.

Northern blot analysis of *GLII* in human skin and BCC is shown in **Figure 3.1**. In the BCC sample lane one *GLII* transcript was detected (a very faint band below 4 kb). There was no *GLII* expression observed in normal skin and in the negative control HaCat cell line **Figure 3.1**. *GLII-E1A* transformed baby rat kidney cell lines showed three *GLII* transcripts around 4 kb, 5.5 kb and 6 kb in size. A weak signal for 5.5 kb and 6 kb *GLII* transcript indicates low expression of these transcripts in *GLII-E1A* transformed baby rat kidney cell lines (**Figure 3.1**), these results correspond with results obtained in (**Figure 3.2**). Different intensity bands of beta-actin for different sample lanes **Figure 3.1** indicates difference in the amount of mRNA loaded in each lane. The difference in mRNA loading reflects the considerable problems I experienced in

extracting mRNA from human skin and BCC and this contrasts with excellent yield of mRNA from the *GLII-E1A* transformed baby rat kidney cell lines (see **Figure 3.1 and 3.2**)

Northern blot analysis of *GLII* transduced primary keratinocytes is shown in **Figure 3.2**. **Figure 2.3** shows the expected mRNA from *GLII* transduced primary keratinocytes and *GLII* transformed baby rat kidney cell line. A single expected *GLII* transcript around 4.8 kb was detected in the *GLII* transduced primary-keratinocytes cell line. In the *GLII-E1A* transformed baby rat kidney cell lines three *GLII* transcripts were detected around 4 kb (that was expected from exogenous *GLII*), 5.5 kb and 6 kb bands, the signal at 5.5 kb compared with 4 kb and 6 kb transcripts, indicating low level expression of these transcripts in this cell line. There was no *GLII* transcript detected in *EGFP* infected primary keratinocytes and primary keratinocytes (control cells), HaCat and A375 cell lines. Equal intensity bands for beta-actin were observed in all sample indicating equal loading of mRNA (**Figure 3.2**), this also indicates that extraction of intact RNA from cell lines was easier than normal skin and BCC samples.

3.2.3 *GLI2* expression in *GLII-E1A* transformed baby rat kidney cell line, *GLII*-primary-keratinocytes, HaCat and A375 cells.

A single *GLI2* transcript around 6 kb was detected in *GLII-E1A* transformed baby rat kidney cells, *GLII* transduced primary keratinocytes and in A375 melanoma cells. There was no *GLI2* mRNA detected in HaCat, *EGFP* transduced primary keratinocytes and primary keratinocytes control cells. A β -Actin transcript band around 1.8 kb of equal intensity was seen in all the samples confirming equal loading and quality of mRNA **Figure 3.2**. This suggests that *GLII* may be inducing endogenous *GLI2* expression in *GLII* transformed baby rat kidney and *GLII* transduced human primary keratinocytes. It was interesting to note that there is no *GLII* expression in A375 and yet I observed *GLI2* expression in this cells (**Figure 3.2**).

3.2.4 *PTCH* expression in *GLII-E1A* transformed baby rat kidney, *GLII* primary keratinocytes, HaCat and A375 cells.

Two Patched (*PTCH*) transcripts were detected in *GLII-E1A* transformed baby rat kidney cells (indicated by bands around 8 kb and 4 kb), *GLII-EGFP*-primary-

keratinocytes (bands around 8 kb and 4.5 kb) and in HaCat and A375 cell lines (bands around 8 kb and 4.5 kb). There was a very weak *PTCH* transcript band observed around 8 kb and possible band around 4.5 kb in *EGFP*-primary-keratinocytes and primary keratinocytes (control) **Figure 3.2**. The level of *PTCH* expression in *GLII-EGFP*-primary-keratinocytes appears to be increased compared to control *EGFP*-primary-keratinocytes and primary-keratinocytes. This is indicated by very strong *PTCH* transcript bands seen in *GLII-EGFP*-primary-keratinocytes lane and very weak bands seen in control *EGFP*-primary-keratinocytes and primary-keratinocytes lanes. A Beta-Actin transcript band around 1.8 kb is of equal intensity in all the samples confirms equal loading **Figure 3.2**. This suggests that *PTCH* is expressed at lower levels in primary-keratinocytes and is induced by *GLII*, thus is a target of *GLII* transcription factor.

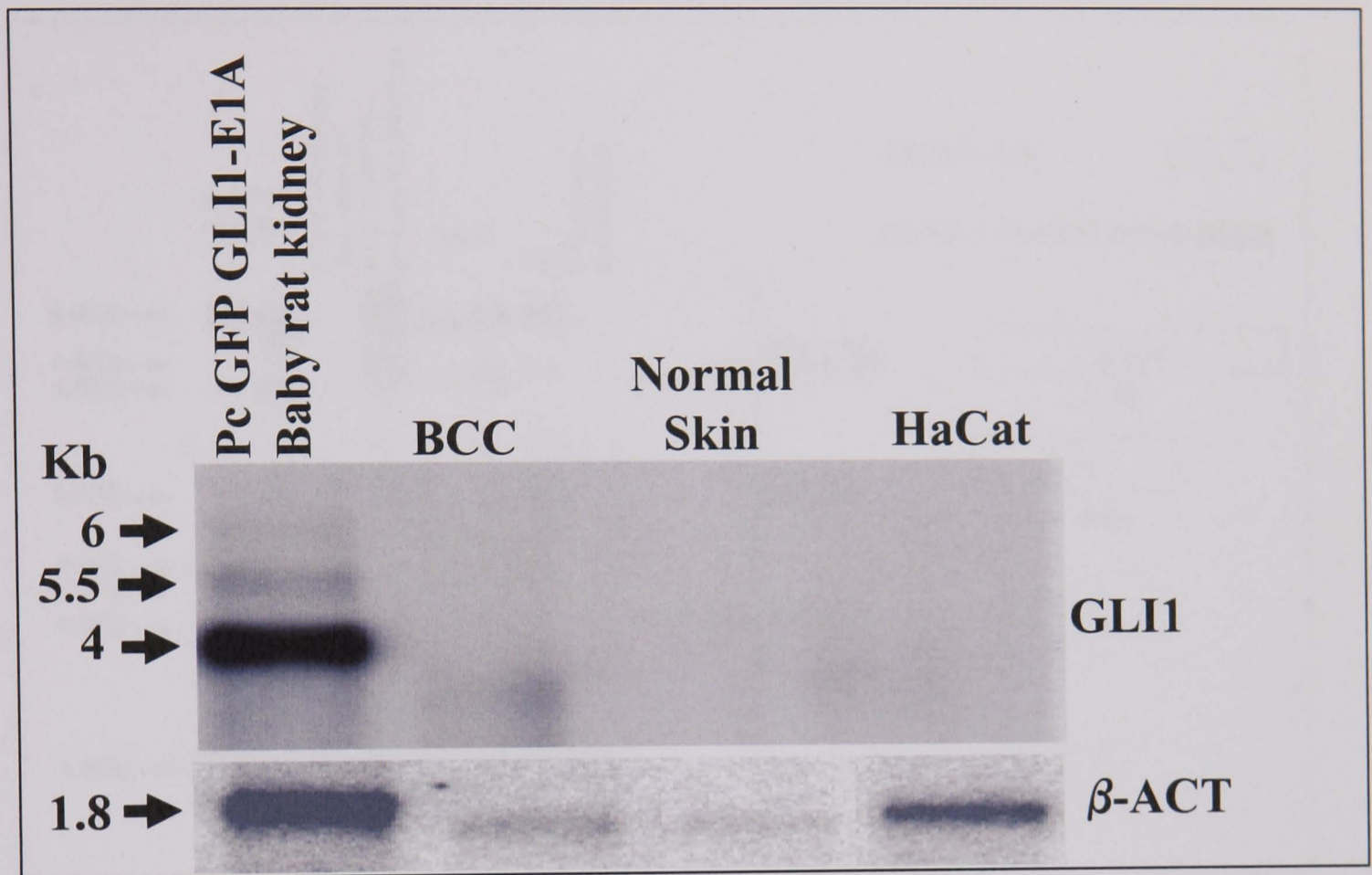


Figure 3.1: Northern blot analysis of *GLI1* and β -*ACT* mRNA expression in polyclonal (pc) *GFP-GLI1-E1A* transformed baby rat kidney cell line, BCC, normal skin (NS) and HaCat. 2 μ g of poly-A RNA per lane were hybridised with 32 P-labelled human *GLI1* 246 bp cDNA (GI No 4885278) corresponding to nucleotides 1504-1747 and β -*ACT* 318 bp cDNA (GI No 28251) corresponding to nucleotides 409-727. There are 3 bands at 6.5 kb 5 kb and 4 kb of *GLI1* transcripts in the pc *GFP GLI1-E1A* transformed baby rat kidney lane. In the BCC lane there appears to be one *GLI1* transcript a very faint band below 4 kb. There are no *GLI1* transcripts in the normal skin and HaCat cell line negative controls.

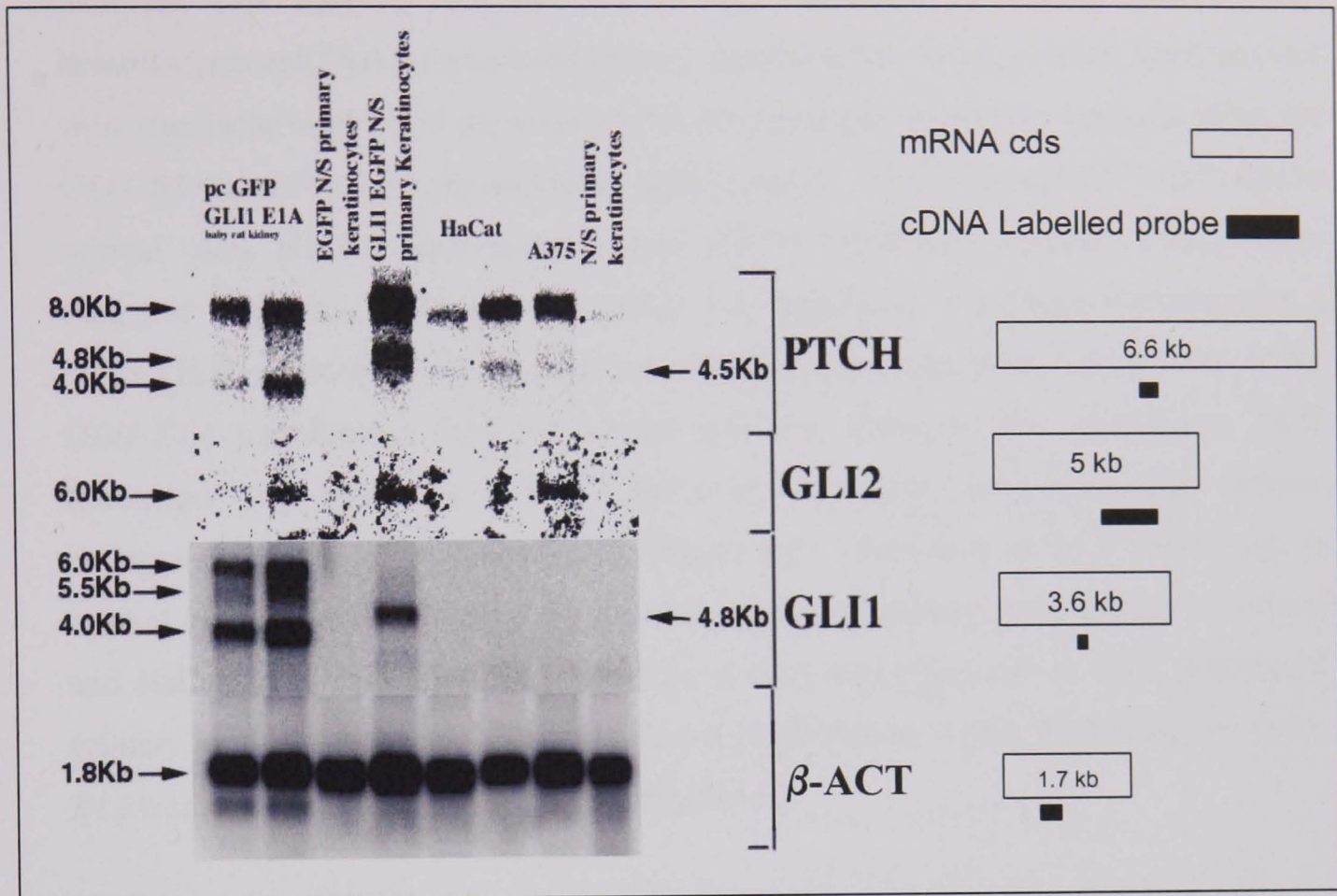


Figure 3.2: Northern blot analysis of *GLI1*, *GLI2*, *PTCH* and β -*ACT* mRNA. In polyclonal (pc) *GFP/GLI1-E1A* transformed baby rat kidney, *EGFP* infected normal skin (N/S) primary keratinocytes, *GLI1/EGFP* infected N/S primary keratinocytes, HaCat, A375, NS primary keratinocytes. 2 μ g of poly-A per lane were hybridised with 32 P-labelled human *PTCH* 511 bp cDNA (GI No 1335863) corresponding to nucleotides 3204-3715, *GLI1* 246 bp cDNA (GI No 4885278) corresponding to nucleotides 1504-1747, *GLI2* 1,463 bp cDNA (GI No 3061313) corresponding to nucleotides 2868-4337 and β -*ACT* 318 bp cDNA (GI No 28251) corresponding to nucleotides 409-727. On the right are open box mRNA complete amino acid coding sequences (cds) and the black filled boxes below it are the regions corresponding to the cDNA labelled probes used for *PTCH*, *GLI2*, *GLI1* and β -*ACT*. Note the expected transcripts are larger than the cds as observed in the northern blot, due to poly-A and regulatory sequences in the mRNA.

3.2.5 Summary of northern blot analysis.

Northern blot analysis indicates *PTCH* was expressed in normal skin primary keratinocytes and EGFP transduced primary keratinocytes. When primary keratinocytes were transduced with *GLII* the level of *PTCH* expression increased, similar to those for *GLII-E1A* transformed baby rat kidney cells (control). There was no *GLII* expression in normal skin primary keratinocytes and EGFP transduced primary keratinocytes (negative controls). Although when *GLII* was transduced in primary keratinocytes a single *GLII* transcript at 4.8 kb (that was expected) was expressed in these cells. In the *GLII-E1A* transformed baby rat kidney cell line different size endogenous *GLII* transcripts were expressed at 4, 5.5 and 6 kb, indicating that human *GLII* induces endogenous mouse *GLII* (**Figure 3.1, Figure 3.2**). There was no *GLI2* expression in normal skin, primary keratinocytes, EGFP transduced primary keratinocytes (control) and HaCat cells. A single *GLI2* transcript at 6 kb was expressed in *GLII* transduced primary keratinocytes and at very low levels (indicated by a very faint band) in *GLII-E1A* transformed baby rat kidney cells (**Figure 3.2**).

Therefore, transduction of *GLII* in human primary keratinocytes induces the expression of different size transcripts of *PTCH* and a single *GLI2*. Expression of *GLII* and *GLI2* in *GLII-E1A* transformed baby rat kidney cells suggests that human *GLII* induces different endogenous *GLII* transcripts and a single *GLI2* transcript in mouse cells. Northern blot analysis also highlights the difficulties in extracting good quality RNA from normal skin and BCC tissue samples compared to cell cultures, indicated by low expression of *GLII* and β -Actin in BCC compared to *GLII-E1A* transformed baby rat kidney cell line (**Figure 3.1**).

3.3.0 RT-PCR analysis of SHH signalling pathway.

Several attempts were made to carry out total RNA extraction from different basal cell carcinoma (BCC) and normal skin samples, each time the total RNA extracted was of poor quality for Northern blot analysis indicated by smeary 28S and 18S ribosomal bands seen on ethidium bromide agarose gel. As I was running out of BCC and normal skin samples I decided to carry out gene expression analysis using RT-PCR and not northern blot analysis. RT-PCR was carried out on cDNA samples synthesised from total RNA samples from BCC, normal skin, spontaneously immortalised keratinocytes (HaCat), primary keratinocytes, A375 melanoma, *GLII*-transduced primary keratinocytes (*GLII*-primary keratinocytes) and *GLII*-transduced mouse fibroblast (*GLII*-10T1/2) cell lines. The following negative controls were also set up; dH₂O replacing total RNA with reverse transcriptase (dH₂O RT), total RNA with no reverse transcriptase (-veRT) and PCR control dH₂O replacing cDNA (dH₂O PCR). A literature search was not carried out to determine the intron/exon boundaries of all the human mRNA sequence from which RT-PCR primers were designed. So to check and confirm that the primers designed expanded intron exon boundaries, a PCR was carried out with designed primers using same genomic DNA sample for each set of primers. If the primers expanded the intron exon boundaries then the expected PCR amplicon from the genomic DNA would be larger than that obtained from cDNA synthesised from total RNA samples.

3.3.1 PCR amplification of genomic DNA to check if the RT-PCR primers span the intron/exon boundaries.

For *GLII*, *GLI3*, *PTCH*, *SMO*, *G6PDA* and *α-TUB* primers the PCR amplicons amplified from the genomic DNA were above the expected size from the cDNA summarised in **Table 3.1** This indicates that these primers cross the intron/exon boundaries and if there was genomic DNA contamination in the cDNA sample there would be two amplicons one from cDNA and one from genomic DNA. Amplicons from *COUP-TFII*, *KIF4A*, *GLI2-α/β* and *GLI2* c/dd primers gave same size bands from both cDNA and the genomic DNA (**Table 3.1**). This suggested that if there was genomic contamination in the cDNA it could give a false positive result. To control for this a RT-PCR reaction was set up in which reverse transcriptase was omitted using one of the total RNA sample (**Table 2.3**). If PCR product was observed in this sample that was due

to the genomic contamination and not due to cDNA. With the *SPU-FU* and *TFIID* primers there was no PCR amplicon observed from the genomic DNA (Table 3.1). this suggested that these primers cross the intron exon boundaries and the intron is too large to be amplified.

Table 3.1: Summary of results for PCR amplification from normal skin genomic DNA (samples M5, N37) using primers designed for RT-PCR.

Primers	Expected amplicon from cDNA	Amplicon obtained from genomic DNA
<i>GLI1</i>	246 bp	850 bp
<i>GLI2</i> c,dd	256 or 1487 bp	1487 bp
<i>GLI2</i> a,bb	128 or 179 bp	No product
<i>GLI2</i> α/β	194 bp	194 bp
<i>GLI2</i> γ/δ	205 bp	No product
<i>GLI3</i>	328 bp	Above 1-kb
<i>PTCH</i>	150 bp	Above 1-kb
<i>SMO</i>	297 bp	above 850-bp
<i>SUP-FU</i>	341 bp	No product
<i>K1F4A</i>	282 bp	Same as cDNA
<i>G6PDA</i>	152 bp	400 bp
α - <i>TUB</i>	249 bp	above 400 bp
<i>TFIID</i>	261 bp	No product
<i>COUP-TFII</i>	288 bp	Same as cDNA

3.3.2. *GLII* expression in BCC, normal skin, HaCat, primary keratinocytes, A375, *GLII*-transduced primary keratinocytes and *GLII*-transformed 10T1/2 cells.

RT-PCR results **Figure 3.3** show that *GLII* was expressed in 7/8 BCC, 3/6 normal skin, 3/3 *GLII* transduced primary keratinocytes. There was no *GLII* expression in negative controls HaCat, primary keratinocytes, A375 (negative controls). This data corroborates northern blot data in **section 3.2.2**. Due to unavailability of *GLII*-transformed baby rat kidney cells *GLII*-transformed 10T1/2 mouse fibroblast cells were used as positive control for *GLII* expression in the RT-PCR analysis. However, *GLII* expression was not observed in *GLII*-transformed 10T1/2 cell line, this may have been due to low transfection efficiency and thus low levels were not detected or these cells may have lost *GLII*-expression due to several round of passaging. *GLII* expressing 10T1/2 cells are frequently used to assay HH-signalling responses (Kinto et al., 1997), in this cell line human *GLII* induces the expression of alkaline phosphatase, which is a specific marker for cells undergoing osteoblast differentiation. (Ruiz i Altaba, 1999a).

3.3.3 *GLI3*, *SUP-FU*, *SMO*, *TFIID*, *G6PDA*, *PTCH*, α -*TUB* and *KIF4* expression in BCC, normal skin, HaCat, primary keratinocytes, A375, *GLII* expressing cells.

GLI3, *SUP-FU*, *SMO*, *TFIID*, *G6PDA*, *PTCH*, Alpha-Tub and *KIF4A* transcript were expressed in all normal skin, BCC, HaCat, primary keratinocytes, A375 and *GLII*-transduced primary keratinocytes analysed (**Figure 3.3**). *Gli3*, *Tfiid*, *G6pda*, *Ptch*, and *Kif4a* transcripts were not expressed in mouse *GLII*-10T1/2 cells (**Figure 3.3**). The primers used in this study were designed from the human sequence from the NCBI database (**Table 2.2**). Therefore, the genes that did not amplify were probably due to difference in mouse and human sequence. This was confirmed when blast search was carried out of the primers designed using NCBI data base.

A blast search of primers designed for *GLI3*, *TFIID*, *G6PDA*, *PTCH* and *KIF4A* (**Table 2.2**) using human mRNA sequences showed none of these primers matched mouse *Gli3*, *Tfiid*, *G6pda*, *Ptch* and *Kif4a* sequences, indicating that mouse *Gli3*, *Tfiid*, *G6pda*, *Ptch* and *Kif4a* transcripts would not have been expected to amplify using human primers sequence in RT-PCR analysis (**Figure 3.3**).

A blast search of primers designed for *SUP-FU*, *SMO*, and α -*TUB* (Table 2.2), showed that all of these primers matched mouse *Sup-Fu*, *Smo*, and α -*Tub* sequence. Indicating that mouse *Sup-Fu*, *Smo*, and α -*Tub* transcripts would have been expected to be amplified from these human primers sequences. This was confirmed when mouse *Sup-Fu*, *Smo*, and α -*Tub* transcripts bands were observed in *GLI1*-infected 10T1/2 mouse cells in RT-PCR analysis (Figure 3.3).

3.3.4 *COUP-TFII* expression in BCC, normal skin, HaCat, primary keratinocytes, A375, *GLI1*-primary keratinocytes and *GLI1*-10T1/2 cells.

COUP-TFII transcript was expressed in 3/7 normal skin and all BCC, HaCat, primary keratinocytes, A375, *GLI1* transduced primary keratinocytes, *GLI1*-transduced 10T1/2 mouse cell line (Figure 3.3). An interesting point to note is that a blast search of primers designed for *COUP-TFII* (Table 2.2 using human *COUP-TFII* mRNA sequence), indicates that these primers did not match mouse *Coup-TfII* sequence. Yet mouse *Coup-TfII* band was observed in *GLI1*-transduced 10T1/2 cell line same size as that for human tissue and cell lines analysed. There are two possible explanations for this. One is that there may not be a mouse mRNA *Coup-TfII* sequence in the NCBI database and this is why we did not get a match. Or that these human *COUP-TFII* primers were amplifying some other transcript which gives same size RT-PCR product, this could have been confirmed by sequencing the PCR product. However, as this was not the aim of the investigation the *COUP-TFII* RT-PCR product from the mouse cell line was not sequenced.

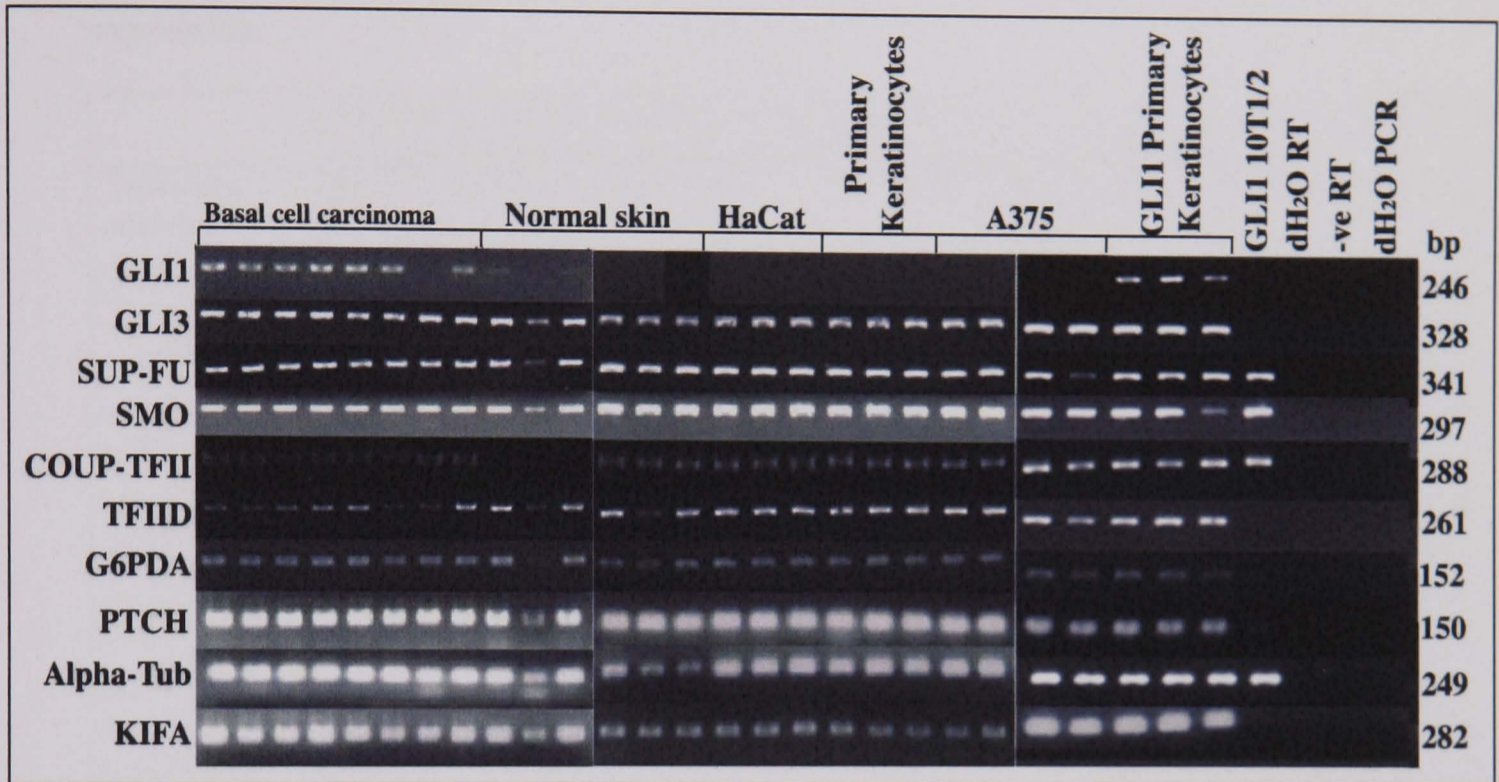


Figure 3.3: RT-PCR agarose gel showing *GLI1*, *GLI3*, *SUP-FU*, *SMO*, *COUP-TFII*, *TFIID*, *PTCH*, α -*TUB* (Alpha-Tubulin) and *KIF4* expression. In total RNA samples from basal cell carcinoma, normal skin, spontaneously immortalised keratinocytes (HaCat), A375 melanoma, *GLII*-transduced primary keratinocytes (*GLII*-primary keratinocytes) and *GLII*-transduced 10T1/2 mouse fibroblast (*GLII*-10T1/2) and EGFP-transduced primary keratinocytes (Primary keratinocytes) cells. Negative controls dH₂O RT, -veRT and PCR control dH₂O PCR show no expression of these genes.

Table 3.2: Summary of the data from RT-PCR 1% agrose gel from **Figure 3.4.** Showing number of total RNA samples from Basal Cell Carcinoma (BCC), normal skin, spontaneously immortalised keratinocytes (HaCat), primary keratinocytes, A375 melanoma, *GLII*-transduced primary keratinocytes (*GLII*-primary keratinocytes) and *GLII*-transduced 10T1/2 mouse fibroblast (*GLII*-10T1/2) cell lines that were positive for *GLII*, *GLI3*, *SUP-FU*, *SMO*, *COUP-TFII*, *TFIID*, *PTCH*, α -*TUB* and *KIF4* expression.

Transcript analysed	Number of samples that were positive for a transcript that was analysed from total RNA extracted from tissue and cell lines samples in a RT-PCR analysis.						
	BCC	N/S	HaCat	Primary keratinocytes	A375	<i>GLII</i> -primary keratinocytes	<i>GLII</i> -10T1/2
	n=8	n=6	n=3	N=3	n=4	n=3	n=1
<i>GLII</i>	7	3	0	0	0	3	0
<i>GLI3</i>	8	6	3	3	4	3	0
<i>SUP-FU</i>	8	6	3	3	4	3	1
<i>SMO</i>	8	6	3	3	4	3	1
<i>COUP-TFII</i>	8	3	3	3	4	3	1
<i>TFIID</i>	8	6	3	3	4	3	0
<i>G6PDA</i>	8	6	3	3	4	3	0
<i>PTCH</i>	8	6	3	3	4	3	0
α - <i>TUB</i>	8	6	3	3	4	3	0
<i>KIF4</i>	8	6	3	3	4	3	0

3.3.5 *GLI2* expression in BCC, normal skin, primary keratinocytes, HaCat, A375 and *GLI1* expressing cell lines.

Different isoforms of human *GLI2* have been identified and these are called *GLI2*-alpha, beta, gamma, and delta, these isoforms derived by combinations of two independent alternative splicing in the coding sequence (**Figure 3.4**) (Tanimura et al., 1998). Therefore, Initial RT-PCR analysis experiments were carried out by using primers specific for different isoforms of *GLI2* previously published (Tanimura et al., 1998). These primers were given a user reference Moh-a, Moh-bb and Moh-c, Moh-dd (**Table 2.2**) and **Table 3.3** shows the PCR products expected from these set of primers. After several attempts at optimising the PCR conditions for *GLI2* (Moh-a, Moh-bb and Moh-c, Moh-dd) there was no clean PCR product amplified from these set of primers.

Therefore, a new set of primers α/β and γ/δ for *GLI2* (**Table 2.2**, **Table 3.3**) published by (Regl et al., 2002) were used to amplify different isoforms of *GLI2* transcripts. The α/β set of primer indicates 7/7 BCC, 5/6 normal skin, 3/3 HaCat, 2/3 primary keratinocytes (the bands observed in these sample were very faint bands), 4/4 A375 (the bands observed in two of the samples were very faint and in the other two very strong) and 3/3 *GLII*-primary keratinocytes express α and/or β *GLI2* (**Figure 3.5**). The *GLI2* γ/δ set of primers did not generate any PCR amplicon. This suggests that α and or β *GLI2* transcripts are predominantly expressed in BCC, normal skin, HaCat, primary keratinocytes, A375 and *GLII*-transduced primary keratinocytes. There was no *GLI2* transcript observed in *GLII*-10T1/2 cell lines. A 194 bp *GLI2* α/β band was also observed in genomic DNA sample suggesting that if there was genomic DNA contamination in any of the samples this would have given a false positive result and these sets of primers do not span the intron/exon boundaries. However, the negative control samples dH₂O and -ve RT were negative, indicating that the band observed were from α and or β *GLI2* transcript and not from the genomic DNA.

Having identified which genes were expressed in BCC, normal skin, HaCat, A375 and *GLII*-primary keratinocytes, I went on to determine level of fold induction or repression of these genes in these samples using SYBR Green kit.

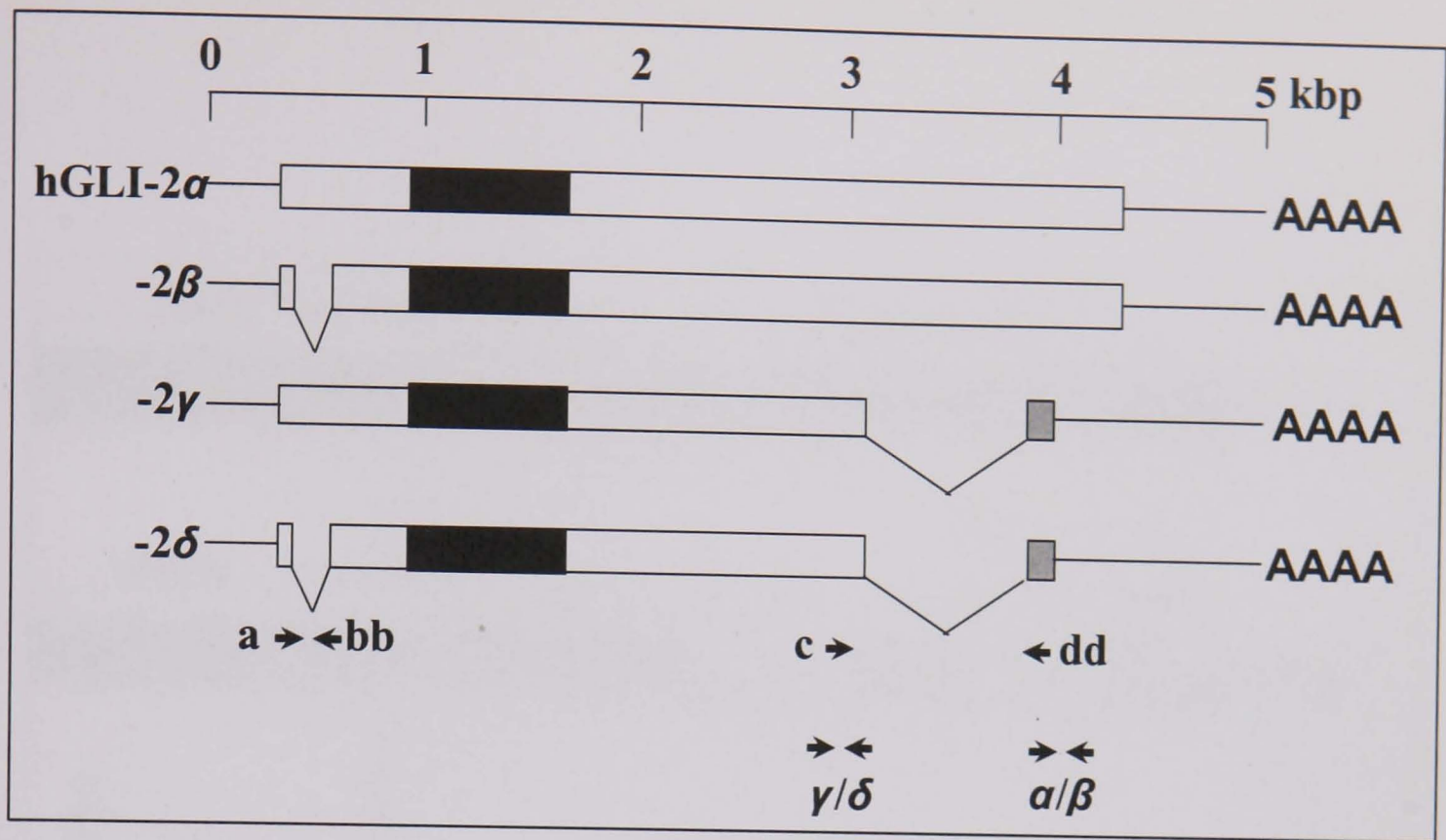


Figure 3.4 Different GLI2 isoforms. Boxes represent open reading frames. Solid and shaded regions in the boxes are the zinc finger motif and amino acid sequences alternatively translated from different frames. It also shows the position of (a,bb), (c,dd), $\alpha\beta$ and $\gamma\delta$ set of primers used in RT-PCR (Tanimura et al., 1998).

Table 3.3: Size of PCR products expected from different isoforms of human *GLI2* using Moh-a,bb and Moh-c, dd, *GLI2* α/β and *GLI2* γ/δ primers.

<i>GLI2</i> Primers	Expected size bp, from α - <i>GLI2</i>	Expected size bp, from β - <i>GLI2</i>	Expected size bp, from γ - <i>GLI2</i>	Expected size bp, from δ - <i>GLI2</i>
Moh-a,bb	179	128	179	128
Moh-c,dd	1,487	256	1,487	256
<i>GLI2</i> α/β	194	194	-	-
<i>GLI2</i> γ/δ	-	-	205	205

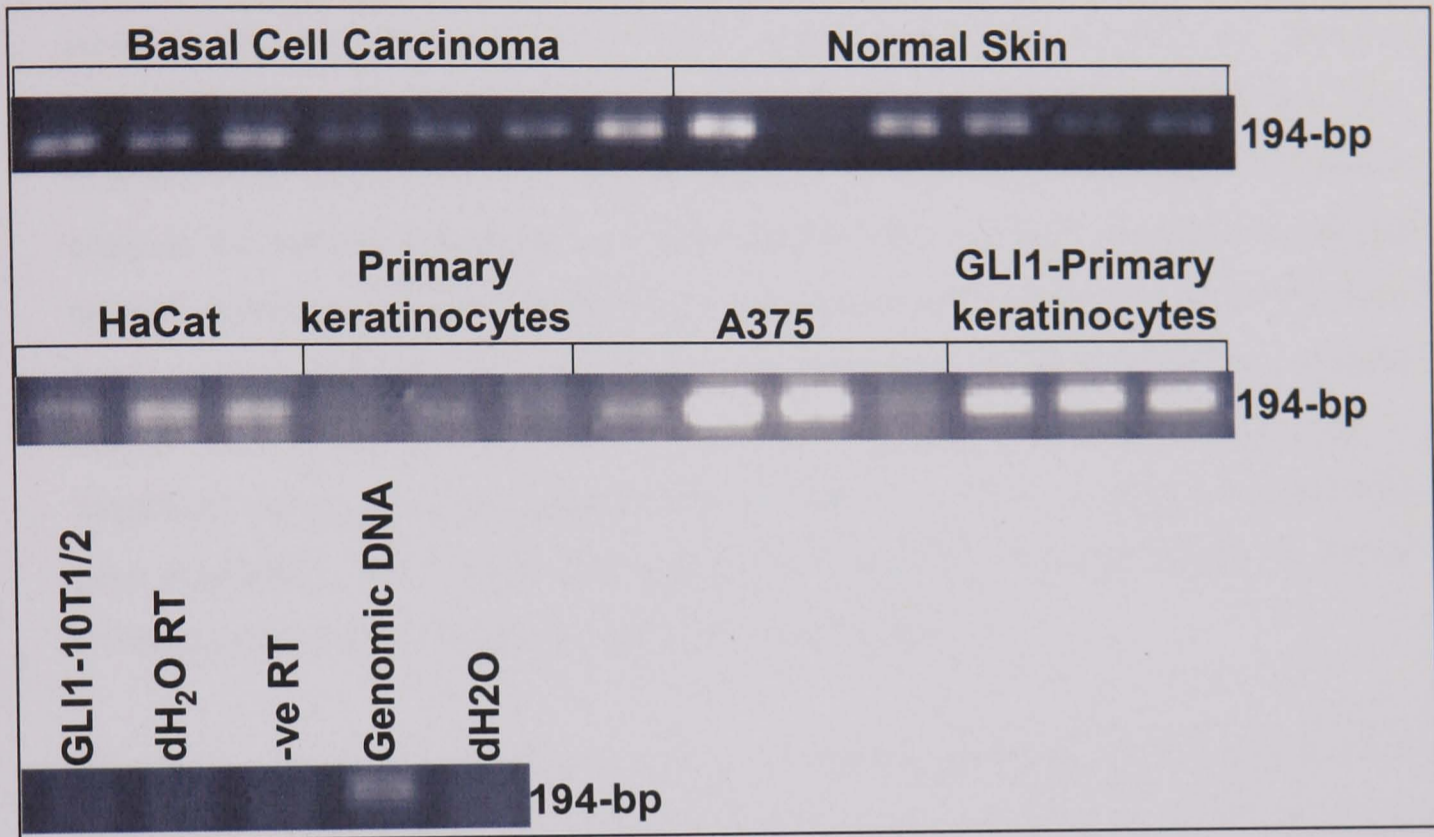


Figure 3.5 RT-PCR of α/β *GLI2* transcript from basal cell carcinoma, normal skin, spontaneously immortalised keratinocyte (HaCat) cell line, primary keratinocytes, A375 melanoma cells, *GLI1*-transduced primary keratinocytes (*GLI1*-primary keratinocytes), *GLI1*-transformed mouse fibroblast cells (*GLI1*-10T1/2) total RNA samples and from normal skin genomic DNA. using α/β primers published in Regl et al., (2002).

3.3.6 Real-time RT-PCR analysis.

After identifying which genes were expressed in BCC and *GLII*-transduced cell lines. Real-time RT-PCR analysis was carried out on the same samples as those shown in **section 3.3.0** to identify which genes were induced or repressed in BCC, HaCat, A375 and *GLII*-transduced primary keratinocytes relative to controls. Not all the primers worked with the (DyNAmo™ SYBR® Green) Real Time RT-PCR kit that had previously worked with the Red Hot Taq PCR kit (see **section 3.3.0**). Therefore, real-time-RT-PCR was carried out on the primers that did work. BCC gene expression analysis was normalised relative to normal skin and HaCat, A375 and *GLII*-transduced primary keratinocyte gene expression was normalised relative to *EGFP*-primary keratinocytes. The base lane expression for each gene analysed in control samples normal skin tissue and primary keratinocytes isolated from normal skin was 1. Therefore, values above 1 indicate induction and values below 1 indicate repression of gene expression. The average fold induction or repression was determined for all the samples as indicated in methods and materials **section 2.8.0**.

The values of fold induction or repression of each gene and variation of expression in each sample analysed and the average from all BCC and cell lines analysed is shown in **Table 3.4**. The variation of expression of a particular gene in same tissue or cell lines indicates that there is variability in expression from one patient to another and cell lines analysed. The variation in same cell line (for example HaCat and A375) may be due to the fact that the cells may have been from different passage number and the cells have transformed and as result have a changed gene expression. The variability in the *GLII*-transduced primary keratinocytes may be due to the fact that the primary cells were from different patients or it may also be due to difference in transduction efficiency for each sample, it is also possible that there may be loss of *GLII* expression in transfected or transformed cell lines.

3.3.7 *GLII* is only induced in BCC and *GLII*-primary keratinocytes and not in HaCat and A375 cells.

GLII expression in BCC was 705.50 fold and in *GLII*-primary keratinocytes was 93147.85 fold, in HaCat 1.08 fold and in A375 was 0.76 fold. This indicates that *GLII* was induced in BCC and *GLII*-primary keratinocytes and there was no change in HaCat and A375 cell lines relative to the control samples (**Figure 3.6 and Table 3.4**). This data corroborates with the northern blot data in **section 3.2.2** and the RT-PCR data in **section 3.3.2** where no *GLII* expression was detected in A375, HaCat cell lines, and there was *GLII* expression in BCC and *GLII*-transduced primary keratinocytes cell line. These results were in line with the results published by (Green et al., 1998; Regl et al., 2002).

3.3.8 *GLI2* expression is induced in BCC, HaCat, A375 and *GLII*-primary keratinocytes.

GLI2 expression in BCC was 2.27 fold, in HaCat 677.26 fold, in A375 274.55 fold and in *GLII* primary keratinocytes it was 3452.35 fold (**Figure 3.6 and Table 3.4**). These results are in line with results published by (Regl et al., 2002) and they showed that *GLI2* was induced in BCC relative to normal skin and it was also induced in *GLII* expressing relative to non *GLII* expressing keartinocytes. The results for *GLI2* expression in HaCat by real-time-RT-PCR and RT-PCR do not agree with the northern blot results (**Figure 3.2**). In northern blot there was no *GLI2* expression observed in HaCat cells. However, we do observe *GLI2* expression in RT-PCR (**Figure 3.5**) and real-time-RT-CR shows induction of *GLI2* in HaCat relative to primary keratinocytes (**Figure 3.6**). The real-time-RT-PCR results for A375 do confirm with northern blot data (**Figure 3.2**) and RT-PCR and real-time-RT-PCR data (**Figure 3.5 Figure 3.6**) show induction of *GLI2* in A375 relative to primary keratinocytes. RT-PCR results of *GLI2* in BCC confirm with real-time-RT-PCR results (**Figure 3.5 Figure 3.6**) and indicate that *GLI2* is induced in BCC relative to normal skin.

3.3.9 *GLI3* expression is induced in BCC, HaCat, A375 and *GLII*-primary keratinocytes.

GLI3 expression was induced in A375 (59.85 fold), HaCat (17.68 fold), *GLII*-transduced primary keratinocytes (5.85 fold) and in BCC (2.07 fold). There seems to be greater induction of *GLI3* in A375 followed by HaCat and *GLII*-transduced primary keratinocytes and lastly BCC (**Figure 3.6 and Table 3.4**).

3.3.10 *PTCH* is induced in BCC, HaCat and *GLII*-primary keratinocytes and there is no change in A375 cells.

PTCH expression in BCC was 32.08 fold, in HaCat 7.33 fold, in A375 0.77 fold and in *GLII*-primary keratinocytes it was 8.66 fold. This suggested that in BCC, HaCat and in *GLII*-primary keratinocytes *PTCH* expression is induced, there was no change in *PTCH* expression in A375 relative to controls (**Figure 3.6, Table 3.4**). In the northern blot and RT-PCR analysis (**Figure 3.2 and Figure 3.3**) *PTCH* was expressed in HaCat, A375, *GLII* expressing and non *GLII* expressing primary keratinocytes. Northern blot indicates *PTCH* to be induced in *GLII*-transduced primary-keratinocytes relative to control *EGFP*-primary-keratinocytes; this was confirmed by the real-time-RT-PCR (**Figure 3.6, Table 3.4**).

3.3.11 *SMO* is induced in BCC, HaCat, A375 and *GLII*-primary keratinocytes.

SMO expression in BCC was 6297.96 fold, in HaCat 527.8 fold, in A375 285.27 fold and in *GLII*-transduced primary keratinocytes it was 329.53 fold (**Figure 3.6, Table 3.4**). This suggested that in BCC, HaCat, A375 and *GLII*-transduced primary keratinocytes *SMO* expression was induced relative to controls (normal skin and primary keratinocytes).

3.3.12 *KIF4* is induced in BCC, HaCat, A375 and repressed in *GLI1*-primary keratinocytes.

KIF4 expression in BCC was 8.65 fold, in HaCat 8.64 fold, in A375 2.72 fold and in *GLI1* transduced primary keratinocytes it was 0.01 fold (**Figure 3.6, Table 3.4**). This suggested that in BCC, HaCat and A375 *KIF4* expression is induced and in *GLI1*-primary keratinocytes it was repressed relative to control samples.

3.13 α -*TUB* expression is induced in A375 *GLI1*-primary keratinocytes and repressed in BCC.

Alpha tubulin expression in BCC was 0.47 fold, in HaCat 1.02 fold, in A375 1.72 fold and in *GLI1*-transduced primary keratinocytes 2.13 fold (**Figure 3.6, Table 3.4**). This indicates that there was no change in alpha-tubulin expression in HaCat cell line and it was induced in *GLI1* expressing primary keratinocytes and A375 and repressed in BCC relative to control samples (primary keratinocytes and normal skin, normalised with β -Actin).

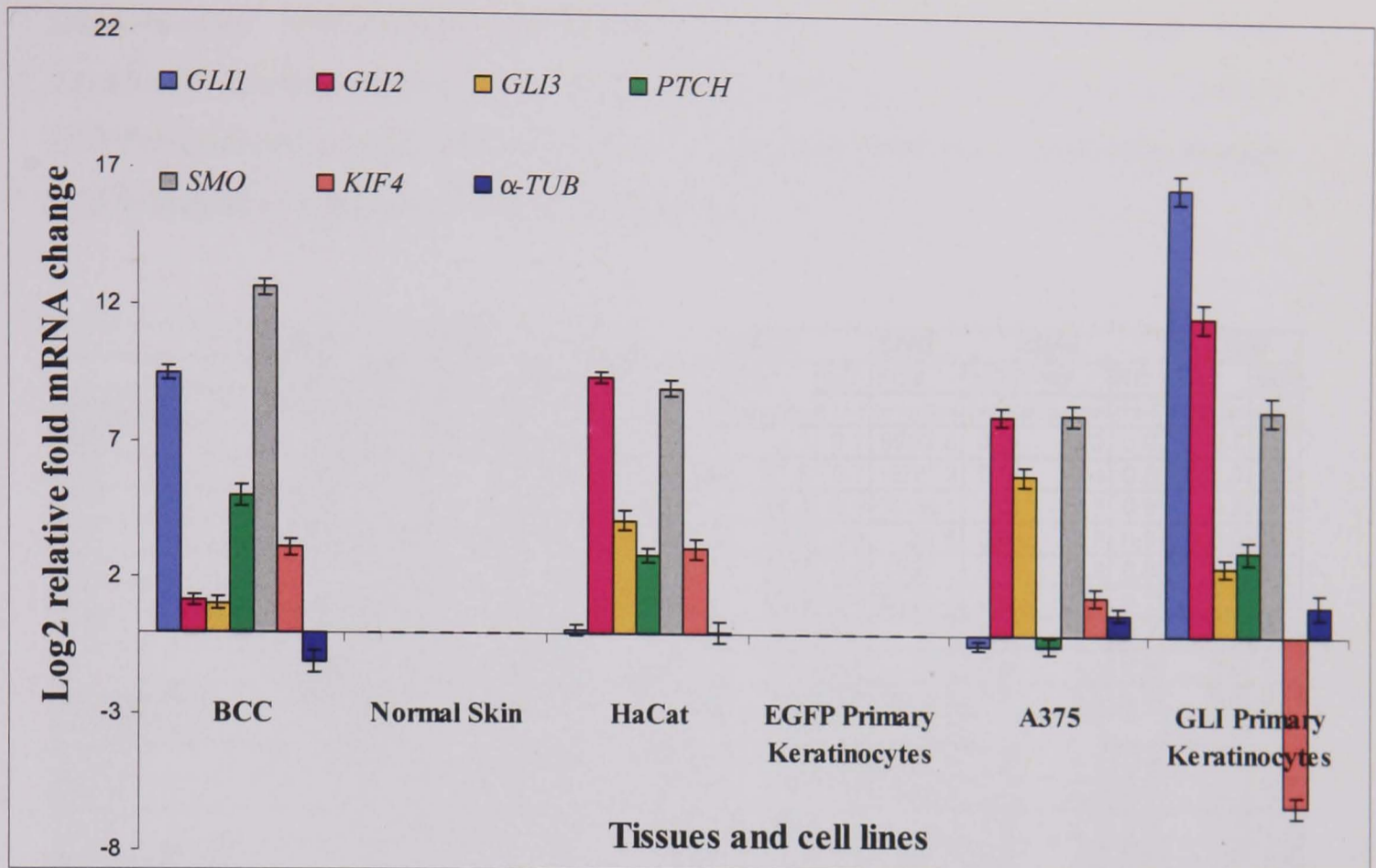


Figure 3.6 Real-time-RT-PCR analysis showing induction or repression of *GLI1*, *GLI2*, *GLI3*, *PTCH*, *SMO*, *KIF4* and α -*TUB* genes expressed in basal cell carcinoma (BCC) relative to normal skin (control). Genes expressed in spontaneously immortalised keratinocytes (HaCat), A375 melanoma and *GLI1*-transduced primary-keratinocytes (*GLI1*-primary keratinocytes) relative to control *EGFP*-transduced primary keratinocytes (*EGFP*-primary keratinocytes). *GLI1* was induced in BCC, *GLI1*-primary-keratinocytes. There was no change in *GLI1* expression in HaCat and A375 cells. *GLI2*, *PTCH*, *SMO* and *GLI3* were induced in BCC, HaCat and *GLI1*-primary keratinocytes. *PTCH* was induced in BCC, HaCat and *GLI1*-primary keratinocytes. There was no change in *PTCH* expression in A375 cells. *KIF4* was induced in BCC, HaCat and A375 cells and repressed in *GLI1*-primary keratinocytes. There was no change in α -*TUB* expression in BCC, HaCat, A375 and *GLI1*-primary-keratinocytes. The data is from (BCC) n=8, normal skin (n=6), HaCat (n=3), A375 (n=4) and *GLI1*-primary keratinocytes (n=3) and *EGFP*-primary keratinocyte (n=3). Each sample was analysed in triplicates and average fold induction or repression and standard deviation (SD) calculated relative to control samples (normalised with β -Actin) for each gene. Fold induction or repression was plotted using log₂ scale.

Table 3.4: Relative fold induction or repression of *GLI1*, *GLI2*, *GLI3*, *PTCH*, *SMO*, *KIF4* and α -*TUB* in basal cell carcinoma (BCC) relative to normal skin, and in spontaneously immortalised keratinocytes (HaCat), A375 melanoma and *GLI1* transduced primary keratinocytes (*GLI1*-primary keratinocytes) relative to control *EGFP*-transduced primary keratinocytes (*EGFP*-primary keratinocytes) and the average fold induction or repression from all the samples.

Sample	<i>GLI1</i>		<i>GLI2</i>		<i>GLI3</i>		<i>PTCH</i>		<i>SMO</i>		<i>KIF4</i>		α - <i>TUB</i>	
	Fold	SD	Fold	SD	Fold	SD	Fold	SD	Fold	SD	Fold	SD	Fold	SD
BCC	34.4	0.8	1.7	0.9	0.4	0.8	2.3	0.7	9962.8	0.9	4.0	0.9	0.7	0.7
BCC	799.4	0.8	3.8	0.9	2.4	0.9	61.6	0.7	19701.3	0.9	33.4	0.8	2.5	0.9
BCC	3946.7	0.9	2.3	0.8	0.4	0.9	44.8	0.9	16136.1	1.0	3.2	0.8	0.2	0.8
BCC	493.3	0.9	2.4	0.9	7.9	0.9	33.8	0.8	39.5	0.8	0.9	0.8	0.0	0.7
BCC	22.6	0.9	1.1	0.8	5.2	0.9	36.8	0.9	1007.1	0.7	8.8	0.8	0.0	0.8
BCC	38.3	0.7	4.0	0.8	0.3	0.7	66.0	0.7	3520.4	0.8	13.4	0.7	0.2	0.6
BCC	113.6	0.9	1.9	0.9	0.0	0.8	2.2	0.7	16.7	0.7	1.2	0.7	0.2	0.8
BCC	195.6	0.8	1.0	0.9	0.0	1.0	9.1	0.7	0.0	0.8	4.4	0.9	0.0	0.7
Average BCC	705.5	0.8	2.3	0.9	2.1	0.9	32.1	0.8	6298.0	0.8	8.6	0.8	0.5	0.7
Normal Skin	1.0		1.0		1.0		1.0		1.0		1.0		1.0	
HaCaT	0.3	0.9	53.6	0.9	0.7	0.8	1.9	0.8	1323.9	0.8	0.4	0.9	1.4	0.8
HaCaT	1.1	0.8	978.4	0.9	48.0	0.8	13.7	0.8	259.2	0.9	16.8	0.7	0.1	0.8
HaCaT	1.8	0.9	999.8	0.8	4.3	0.7	6.4	0.9	0.3	0.8	8.7	0.7	1.6	0.7
Average HaCat	1.1	0.9	677.3	0.9	17.7	0.8	7.3	0.8	527.8	0.8	8.6	0.8	1.0	0.8
EGFP-Primary-Keratinocytes	1.0		1.0		1.0		1.0		1.0		1.0		1.0	
A375	1.1	0.9	506.5	0.8	0.7	0.8	0.4	0.8	538.8	0.9	0.7	0.7	5.9	0.8
A375	0.6	1.0	64.9	0.9	96.9	0.8	1.8	0.8	602.1	0.8	5.4	0.9	0.0	0.9
A375	0.4	0.8	419.3	0.8	141.8	0.6	0.7	0.9	0.0	0.8	4.3	0.8	0.0	0.8
A375	0.9	0.9	107.5	0.7	0.0	0.8	0.2	0.7	0.2	0.6	0.5	0.7	0.9	0.8
Average A375	0.8	0.9	274.5	0.8	59.9	0.8	0.8	0.8	285.3	0.8	2.7	0.8	1.7	0.9
GLI1-primary Keratinocytes	856.4	0.7	3015.6	0.7	8.6	0.8	2.4	0.7	1.9	0.7	0.0	0.9	0.0	0.7
GLI1-primary Keratinocytes	272225.8	0.6	2922.3	0.6	0.5	0.8	2.5	0.7	0.2	0.7	0.0	0.7	1.8	0.7
GLI1-primary Keratinocytes	6361.3	0.8	4419.2	0.8	8.4	0.7	21.0	0.8	986.5	0.7	0.0	0.6	4.5	0.8
Average GLI1-primary Keratinocytes	93147.8	0.7	3452.3	0.7	5.9	0.8	8.7	0.8	329.5	0.7	0.0	0.8	2.1	0.7

3.4.0 Laser Capture Micro-dissection (LCM) of dermal papilla, hair follicle root sheath and epidermis from normal skin and gene expression analysis.

In order to understand how BCC develops, I wanted to study the changes in gene expression from normal epidermal keratinocytes to BCC formation. To do this I decided to extract keratinocytes from the outer edges of BCC tumour islands and keratinocytes in the centre of the tumour islands and the adjacent normal epidermal keratinocytes from BCC tissue, using Laser Capture Micro-dissection (LCM).

To establish the technique LCM was carried out to investigate differentially expressed genes in dermal papilla, hair follicle root sheath and epidermis in normal skin. The aim of this study was to capture the cells from dermal papilla, hair follicle root sheath and epidermis in normal skin and extract total RNA from these cells and carry out RT-PCR gene expression analysis. It was very difficult to dissect different population of keratinocytes from normal skin. The difficulty in dissecting may have been due to strong cell to cell interactions in keratinocytes and this prevented the cells from sheering off. However, on several occasions when I did manage to dissect these cells from different normal skin tissue samples, I did not get any β -Actin amplification from the total RNA extracted from these LCM cells by RT-PCR. Owing to low quantities of total RNA it was not possible to measure the amount of total RNA extracted, thus, the only way to determine if there was any RNA present was to carry out RT-PCR using β -Actin primers. The reason I did not get β -Actin amplification from these LCM cells was that it was taking 40-60 min to capture the cells this might have caused the RNA to degrade.

After many attempts and perseverance and using different normal skin samples, I managed to capture the cells from dermal papilla, root sheath and epidermis areas of normal skin from one sample that gave me total RNA from which I could amplify the β -Actin transcript, RT-PCR analysis was carried out using *GLII*, *GLI2*, *GLI3*, *PTCH* and α -Tub primers.

Figure 3.7 -A shows the dermal papilla, outer root sheath and epidermis before LCM and after LCM and captured cells on the LCM cap. RT-PCR analysis shows *GLII* expression in cells captured from dermal papilla and root sheath, there was no *GLII* expression from epidermis captured cells. *GLI2*, *GLI3*, *PTCH*, α -Tub and β -Actin were expressed in cells captured from dermal papilla, root sheath and epidermis **Figure 3.7-**

B. This data confirms the published observations that *GLII* is expressed in the outer root sheath and not in the epidermis (Ghali et al., 1999). It also confirms with the data from RT-PCR analysis in normal skin (**Figure 3.3**) where *GLI2*, *GLI3*, *PTCH* and α -*TUB* were expressed. LCM RT-PCR data also confirms in-situ hybridisation data for *GLI2* expression in **Figure 4.13**, in which *GLI2* was expressed in outer root sheath, interfollicular epidermis in normal skin. The strong bands for *GLII* in RT-PCR data (**Figure 3.7-B**) indicates that there may be more *GLII* expression in dermal papilla and outer root sheath than *GLI2*, *GLI3* and *PTCH* which have weaker bands, β -Actin bands were of equal intensity in all lanes confirming equal loading. *GLI2*, *GLI3* and *PTCH* seem to be expressed at similar levels in dermal papilla, outer root sheath and epidermis (**Figure 3.7-B**). There was not enough cDNA to carry out real-time-RT-PCR to verify level of *GLII*, *GLI2*, *GLI3* and *PTCH* expression or amplify other genes from LCM derma papilla, outer root sheath and epidermis cells.

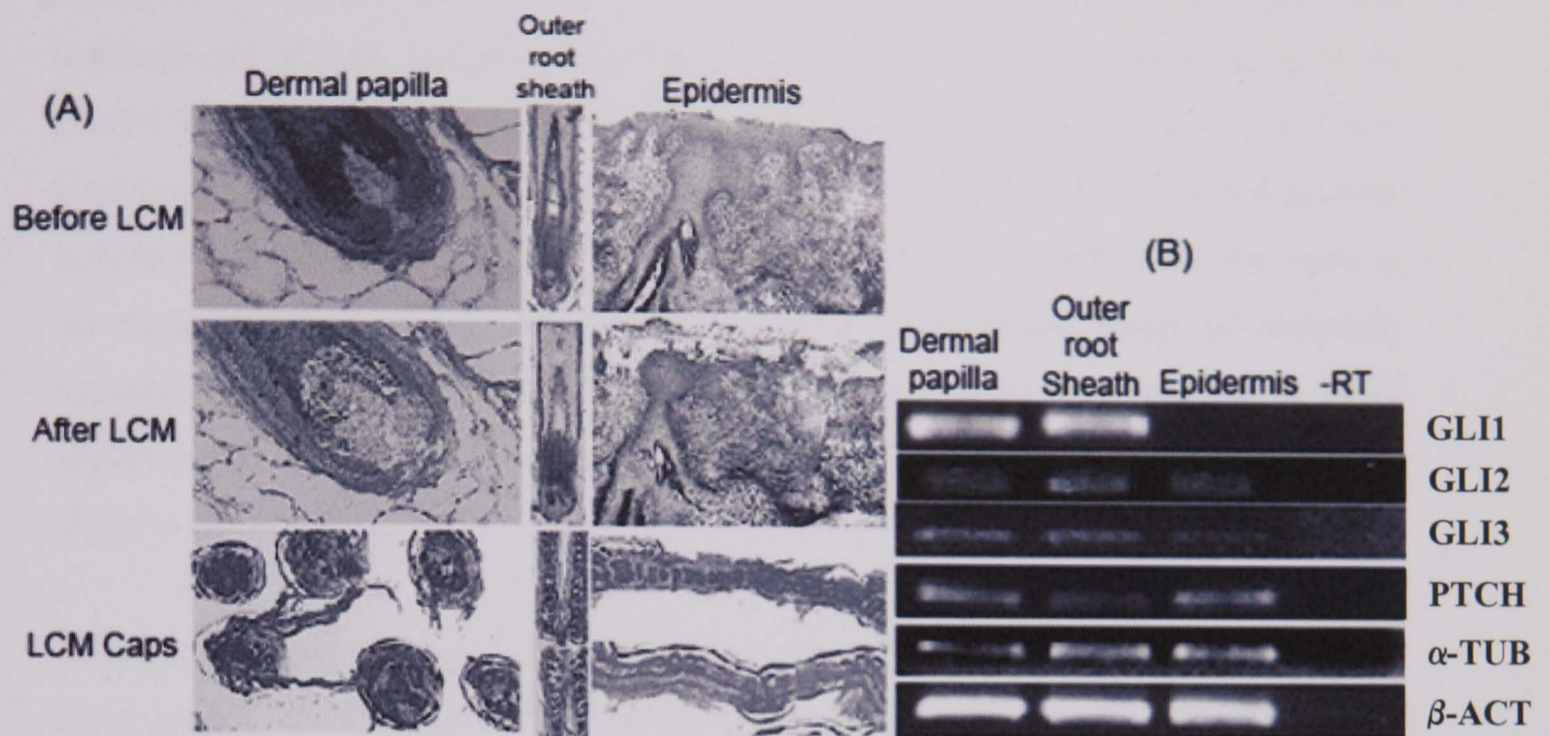


Figure 3.7: (A) Dermal papilla, outer root sheath and epidermis before Laser capture micro-dissection (LCM), after LCM and LCM caps with captured cells. (B) RT-PCR showing *GLI1* expression in dermal papilla and outer root sheath in normal skin and there is no *GLI1* expression in cells captured from epidermis. *GLI2*, *GLI3*, *PTCH*, α -Tubulin (α -*TUB*) and β -Actin (β -*ACT*) are all expressed in dermal papilla, outer root sheath and the epidermis. The negative control -RT sample (dermal papilla with no reverse transcriptase) was negative for all the genes analysed.

3.5 0 Discussion

3.5.1 *PTCH* expression is induced in BCC, HaCat and *GLI1* expressing cell lines.

Northern blot results show that *PTCH* is expressed in *GLI1*, *EGFP* transduced and untransduced primary keratinocytes, HaCat and A375 cells. *PTCH* expression levels in control primary keratinocytes and *EGFP*-primary-keratinocytes appears to be lower compared to *GLI1-E1A* transformed baby rat kidney cell lines, *GLI1*-infected primary keratinocytes and HaCat and A375 cells, although β -Actin expression was the same in all these samples (**Figure 3.2**). *PTCH* being a down stream target of hedgehog signalling (Goodrich and Scott, 1998), was expected to be up regulated in *GLI1* expressing cells and this is what was observed, confirming previously published data (Regl et al., 2002).

Multiple different size transcripts were observed for *PTCH* (8, 4.5 and 4.8 kb) in *GLI1-E1A* transformed baby rat kidney, *GLI1-EGFP* and *EGFP* (control) infected primary keratinocytes, HaCat, A375 and primary keratinocytes (**Figure 3.2**). (Hahn et al., 1996a) identified five distinct *PTCH* transcripts expressed in all human tissues they examined. The most abundant *PTCH* transcripts were around 8 kb observed in heart, brain, placenta, lung, liver, skeletal muscle, kidney and pancreas. In brain, liver, skeletal muscle and pancreas additional multiple different size *PTCH* transcripts were observed all of which were below 8 kb. Data from this study also shows that the most abundant transcript of *PTCH* to be around 8 kb and additional transcript around 4 kb in *GLI1*-primary keratinocytes, HaCat, A375 and *GLI1-E1A* rat kidney cells and both of these transcripts are induced by *GLI1*. This suggests that there are alternative splice variants of *PTCH* expressed in rat kidney and in humans keratinocytes they are induced by the *GLI1* transcription factor.

The real-time-RT-PCR data also confirms that *PTCH* is induced in *GLI1* transduced cell line (**Figure 3.6 and Table 3.4**). *PTCH* was also upregulated in BCC relative to normal skin. In HaCat cells there was no *GLI1* expression. However, there was *PTCH* induction in these cells relative to primary keratinocytes. Induction of *PTCH* in HaCat cells may be as result of *GLI2* or *GLI3* induction (**Figure 3.6**). Other studies have also shown that *GLI1* and *GLI2* both induces *PTCH* expression (Agren et al., 2004; Regl et al., 2002). In the A375 cells there was *GLI2* induction yet there was no *PTCH* induction in these

cells relative to primary keratinocytes (**Figure 3.6 and Table 3.4**).

3.5.2. *GLII* expression is up-regulated in BCC and *GLII* expressing cells.

A 4.4 kb *GLII* transcript was expressed in *GLII-EIA* transformed baby rat kidney cell line and a 4.9 kb *GLII* transcript in *GLII-EGFP* infected normal skin primary keratinocytes. In *GLII-EIA* transformed baby rat kidney cell line possible alternative splice variants 5.5 kb and 6 kb transcripts of rat *Gli1* were also detected (**Figure 3.2**). These results are in line with results published by (Hui et al., 1994), they showed *Gli1* transcript to be around 4.4 kb during mouse embryogenesis. There was no *GLII* transcript detected in HaCat, A375, primary keratinocytes or control *EGFP*-infected primary keratinocytes (**Figure 3.2**). A possible very faint band below 4kb indicates low level expression of *GLII* in BCC sample and no *GLII* expression was detected in normal skin sample with the northern blot analysis (**Figure 3.1**). The reason why there was low *GLII* expression in BCC sample may have been due to the fact that there was not enough mRNA present or that mRNA may have been degraded indicated by a very faint smeary *GLII* band seen in the BCC lane. Probing the same blot with beta-actin probe confirmed that there was less mRNA in the BCC and normal skin lanes compared to *GLII-EIA* transformed baby rat kidney and HaCat cells, this was indicated by weak signal for beta-actin probe in BCC and normal skin lane and a strong signal in *GLII-EIA* transformed baby rat kidney and HaCat cells (**Figure 3.1**). Therefore, low mRNA levels and possible degradation of mRNA on the northern blot, indicates that analysis of *GLII* expression in BCC sample was not conclusive. However, on the same blot in the positive control lane *GLII-EIA* baby rat kidney cells lane indicates a strong band for mouse *Gli1* transcripts at 4 kb and weaker expression of 5.5 kb and 6 kb *Gli1* transcripts (**Figure 3.1**).

Expression of *GLII* in BCC was confirmed by RT-PCR analysis, this showed that *GLII* was expressed in 7/8 BCCs and 3/6 normal skin samples, the three normal skin samples had very faint *GLII* bands (**Figure 3.3**). *GLII* expression has not previously been reported in normal skin, Green et al (1998) showed that *GLII* is expressed in BCC and not in normal skin and a study by Ghali et al (1999) showed that *GLII* is expressed in outer root sheath of hair follicles in normal skin. The normal skin samples used in my study were from different face lift procedures and some of these face lift samples had a lot of scalp hair, others had less and some none. Total RNA was extracted from whole

normal skin samples; therefore, RNA was extracted from mixed cell population. It is possible that these three samples may have come from more hairy skin compared to the rest of the normal skin samples. Thus in these three normal skin samples *GLI1* expression may have been due to hair follicle or the outer root sheath cells. This was confirmed when RT-PCR analysis was carried out on laser captured micro dissected cells from dermal papilla, outer root sheath and epidermis from normal skin tissue. This study showed that *GLI1* was expressed in dermal papilla and root sheath and not in epidermis (**Figure 3.7-A, B**). Real-time-RT-PCR analysis showed that *GLI1* was up-regulated in BCC relative to normal skin and in *GLI1* transduced primary keratinocytes relative to primary keratinocytes (**Figure 3.6 and Table 3.4**), this data is consistent with the data obtained for northern blot analysis (**Figure 3.2 and Figure 3.3**) and also in the literature (Regl et al., 2002).

When comparing northern blot and RT-PCR techniques the RT-PCR was more sensitive technique compared to northern blot and it can detect low abundant (for example *GLI1*) mRNA from small amount (2-5 µg) of total RNA whereas northern blot requires minimal of 15 µg total RNA. Another advantage of using RT-PCR technique was that it allowed one to analysis several samples and genes within short period of time, whereas northern blot was more complex procedure and took far too long to analyse small number of genes. However, the disadvantage of RT-PCR is that it does not give you the size of transcript you are detecting, with northern blot you can detect the size of a transcript and can also detect alternative splice variants of a gene.

3.5.3 *GLI2* is induced in BCC and *GLI1* expressing cell lines.

A single *GLI2* transcript around 6 kb was observed in *GLI1-EIA* transformed baby rat kidney cell line, *GLI1-EGFP* infected primary keratinocytes and A375 melanoma cell line. *Gli2* transcript that was detected by (Hui et al., 1994) during mouse embryogenesis was around 7 kb. This suggests that there may be different size *GLI2* transcripts expressed in humans compared to mice. There was no *GLI2* expression detected in primary keratinocytes, HaCat and control *EGFP* infected primary keratinocytes (**Figure 3.2**). The blot in **Figure 3.2** was probed with *GLI1*, *PTCH*, β -Actin and *GLI2* probes in descending order *GLI2* being the last gene to be probed the bands detected for *GLI2* were not as clean as that for other probes, this indicates that the blot may have degenerated due to striping and re-probing.

Northern blot analysis showed that in *GLI1*-EGFP infected primary keratinocytes and *GLI1* transformed baby rat kidney cells there was an induction of *GLI2* expression compared to the controls EGFP infected and normal skin primary keratinocytes (**Figure 3.2**). This was the first time that any one had shown that *GLI1* induces *GLI2* expression in *GLI1* expressing cell lines. It is a well established fact that *PTCH* is a target gene for *GLI1* (Agren et al., 2004; Matise and Joyner, 1999; Regl et al., 2002; Toftgard, 2000). A parallel study was being carried out by our collaborators (Dr Fritz Abergers' lab) and they showed that there was an induction of *GLI2* in *GLI1* expressing keratinocytes relative to control cells and *GLI2* was induced in BCC relative to normal skin (Regl et al., 2002). Northern blot data in this study confirmed these findings; this study has also shown that endogenous *GLI2* is induced in *GLI1* transformed baby rat kidney cells and in *GLI1* transduced human skin primary keratinocytes. This suggests that human *GLI1* induces *GLI2* expression in different cell lines as well as in different species.

It was very difficult to extract good quality total RNA from normal skin and BCC samples. This was due to the difficulty in homogenising the tissue quickly and completely to prevent RNA degradation. Total RNA extracted from most BCC and normal skin samples was either partially or completely degraded. This resulted in obtaining more BCC tumours and normal skin samples, this was a very lengthy process due to H M Home Office the legislation concerning acquiring patient consent for any tissue to be used for any kind of research, introduced after the Alder Hey organs scandal. Because of the difficulty in obtaining good quality RNA from BCC and normal skin sample and the time it took to carry out northern blot analysis I decided to carry out gene expression analysis using RT-PCR for remaining samples.

When using previously published set of primers designed by (Tanimura et al., 1998) to amplify different isoforms α , β , γ and δ *GLI2* (Moh a,bb and Moh c,dd in **Table 2.2**), it was not clear as to which isoforms of *GLI2* were expressed in cell lines and tissues samples analysed. Even after changing the PCR conditions such as annealing temperature and or $MgCl_2$ concentration and amount of temple. However, when primers for α/β and γ/δ for *GLI2* (**Table 2.2** published by (Regl et al., 2002) were used to analyse *GLI2* expression. These primers indicate 7/7 BCC, 5/6 normal skin, 3/3 HaCat, 2/3 primary keratinocytes, 4/4 A375 and 3/3 *GLI1*-infected primary keratinocytes express α and or β *GLI2* isoforms (**Figure 3.5**). *GLI2* (α/β isoforms) expression appears

to be low in HaCat and primary keratinocytes indicated by low intensity bands, although *G6PDA* PCR bands were of the same intensity (**Figure 3.3**). This indicates that the level of *GLI2* expression may be altered in cultured primary keratinocytes compared to normal skin. When γ/δ set of primers were used they did not generate any PCR products. This indicates that only α and or β *GLI2* isoforms are expressed in these samples. (Regl et al., 2002) had shown that *GLI2* α/β isoforms were increased by 2 fold in *GLI1* infected primary keratinocytes compared to controls and 10.5 fold in BCC compared with normal skin, and only trace amount of γ/δ -*GLI2* were detected in these samples.

Possible explanations for why no γ/δ *GLI2* were detect in the cell lines and the tissues analysed are; 1) Repeated freezing and thawing may have degraded the cDNA, 2) the levels were so low that they were not detectable and lastly there is a possibility that there were no *GLI2* γ/δ transcripts expressed in the samples analysed. Repeating the experiments several times with newly transduced *GLI1*-primary keratinocytes and synthesising fresh cDNA, give same results.

GLI2 mRNA was detected in *GLI1*-infected primary keratinocytes and A375 cell lines with northern blot (**Figure 3.2**) and RT-PCR analysis (**Figure 3.5**). There was no *GLI2* expression observed in Northern Blot for primary keratinocytes and HaCat cells (**Figure 3.2**). However, with RT-PCR analysis there was *GLI2* expression observed for primary keratinocytes (**Figure 3.5**). The reason why we obtained this conflicting data is that levels of *GLI2* expression in primary keratinocytes were very low and these were not detectable using northern blot. However, with a more sensitive RT-PCR technique low levels expression of *GLI2* was detected in HaCat and 2 out of 3 primary keratinocyte samples. In the one primary keratinocyte sample in which *GLI2* expression was not detected, may have been due to two reasons; one is that the levels were so low they were not detectable or there was no *GLI2* present.

Real-time-RT-PCR data for *GLI2* confirmed the results obtained with RT-PCR and northern blot analysis, it shows that *GLI2* was induced in BCC and *GLI1* expressing primary keratinocytes cells (**Figure 3.6 and Table 3.4**). These results are in line with published data (Regl et al., 2002), they showed that *GLI2* was induced in BCC relative to normal skin and in *GLI1* expressing relative to non *GLI1* expressing keartinocytes.

GLI2 expression with the real-time RT-PCR results for HaCat cells confirm with results with RT-PCR data (**Figure 3.5, Figure 3.6**); both show induction of *GLI2* in HaCat cell lines relative to primary keratinocytes. The Real time RT-PCR results for A375 cells also confirm the northern blot (**Figure 3.2**) and the RT-PCR data (**Figure 3.5**); they show induction of *GLI2* in A375 cells relative to primary keratinocytes. The results for HaCat and A375 show that *GLI2* expression levels in these cells are much greater relative to primary keratinocytes. Thus it is possible that Hh signal transduction in these cells may be regulated by *GLI2* and not by *GLI1* in these cells.

Other groups in this lab using same *GLI1* probe have shown *GLI1* to be expressed in A375 cells using northern blot (personal communications). For this reason they were used as positive controls for *GLI1* expression. However, these workers have not investigated *GLI2* expression in these cells. The reason for this discrepancy is unclear it is possible that in this study a different batch of A375 were used, or they were of a different passage number and thus they may have transformed resulting in a change in gene expressions. Another possible explanation could be that there are two types of A375 parental and metastatic (A375P and A375M) (Montano et al., 1994). The cells that were used in this study were labelled as A375, so it was not clear whether these were P or M, to investigate the discrepancy between the data these cells needed to be investigated further, and as this was not the focus of this study this was not done. A375 cells were used as a positive control for *GLI1* expression, on the basis of personal communications, along side *GLI1*-transformed baby rat kidney cell lines.

3.5.4 Induction of *GLI3* and *SMO* in HaCat and A375 cells is independent of *GLI1* and in *GLI1*-primary keratinocytes and possibly in BCC it is dependent on *GLI1* expression.

RT-PCR analysis indicates that *GLI3* and *SMO* are expressed in BCC, normal skin, HaCat, A375, *GLI1* expressing primary keratinocytes and control primary keratinocytes (**Figure 3.5**). Real-time-RT-PCR shows that *GLI3* and *SMO* were induced in BCC relative to normal skin, these results are in line with published data in which *GLI3* expression has been observed in BCC samples which also express *GLI1*, induced expression of *SMO* mRNA has also been reported in BCC (Dahmane et al., 1997; Tojo et al., 1999). *GLI3* and *SMO* were also induced in HaCat, A375 and *GLI1* expressing primary keratinocytes relative to control non *GLI1* expressing primary keratinocytes

(**Figure 3.6, Table 3.4**). These results suggest that altering the expression of *SMO* which activates and *GLI3* which represses HH-signalling (Murone et al., 1999; von Mering and Basler, 1999) may be a mechanism by which activity of HH-signalling pathway may be controlled in BCC (*in-vivo*) and in *GLI1* over expressing primary keratinocytes (*in-vitro*).

There was no *GLI1* expression in HaCat and A375 cells yet we observe an induction in *GLI3* and *SMO* expression, this indicates that there may also be *GLI1* independent induction of *GLI3* and *SMO* expression in HaCat and A375s. Whereas, in *GLI1* expressing primary keratinocytes and may be in *GLI1* expressing BCC samples the induction of *GLI3* and *SMO* was dependent on *GLI1*.

3.5.5 *KIF4* is induced in BCC, HaCat and A375 cells and *GLI1* represses it in primary keratinocytes.

The kinesin superfamily (KIF) of proteins are microtubule based motor proteins specialized in the transport of membrane organelles, protein complexes, and mRNAs (Hirokawa, 1998; Hirokawa and Takemura, 2005). In this chapter I have shown using RT-PCR analysis that kinesin superfamily protein 4 (*KIF4*) was expressed in BCC, normal skin, HaCat, A375, *GLI1*-primary keratinocytes and control primary keratinocytes (**Figure 3.5**). Real-time-RT-PCR indicates that *KIF4* was induced in BCC relative to normal skin, it was also induced in HaCat and A375 cells. However, it was repressed in *GLI1* expressing primary keratinocytes relative to non *GLI1* expressing control primary keratinocytes (**Figure 3.6, Table 3.4**). This suggests that there may be *GLI1* independent induction of *KIF4* in BCC *in-vivo* and *in-vitro* in certain cells. It is also possible that transcriptional activity of *GLI1* may be differentially regulated in BCC *in-vivo* and *in-vitro* (*GLI1* expressing primary keratinocytes) leading to alteration in expression of *KIF4*. At the time this study was carried out there was no published data available on expression of *KIF4* in BCC or in *GLI1* expressing keratinocytes.

KIF4 plays multiple roles in mitosis, and its loss leads to numerous mitotic defects, including chromosome hypercondensation, aberrant spindle formation, anaphase bridges, defective cytokinesis, and aneuploidy (Castoldi and Vernos, 2006; Kurasawa et

CHAPTER 3: Analysis of SHH-Pathway Genes in Normal Skin, BCC and *GLI1*-transduced Human Primary Keratinocytes al., 2004; Lawrence et al., 2004; Mazumdar et al., 2006; Mazumdar and Misteli, 2005; Mazumdar et al., 2004). Aneuploidy is the condition of having less than or more than the normal diploid number of chromosomes, and is the most frequently observed type of cytogenetic abnormality that has long been suggested to contribute to tumor formation (Dey, 2004).

A study carried out by Mazumdar et al (2006) showed that loss of KIF4 in embryonic stem cells lead to 70% of the cells being aneuploid and this increases their potential to form tumor in nude mice and loss of KIF4 activated the mitotic spindle checkpoints and DNA-damage response pathways. They also detected a reduced KIF4 protein levels in 35% of human cancers from several tissues including ovary, lung, breast, CNS, renal, melanoma and leukemia and no reduction of KIF4 was found in colon cancer (Mazumdar et al., 2006). This indicates that loss of KIF4 is physiologically relevant in certain tumours and cell lines. These results back the notion that loss of a molecular motor leads to tumor formation and that aneuploidy can act as a primary trigger of tumorigenesis. It is possible that loss of KIF4 in *GLI1* expressing primary keratinocytes may also be leading to cells being aneuploid. However, due to time constraints this hypothesis was not tested.

3.5.6 *COUP-TFII* and *TFIID* are expressed in BCC, normal skin and *GLI1*-primary keratinocytes.

Chicken ovalbumin upstream promoter transcription factor II (*COUP-TFII*) is expressed in the mesenchyme of developing organs (Pereira et al., 1995). *COUP-TFII* is shown to be a major regulator of angiogenesis and vein identity (Pereira et al., 1999; You et al., 2005a). In addition, it plays an important role in organ development such as stomach, limb, heart and diaphragm (Lee et al., 2004; Pereira et al., 1999; Takamoto et al., 2005; You et al., 2005b). In the developing neural tube, *SHH* has been shown to regulate *COUP-TFII* expression during the differentiation of motoneurons (Lutz et al., 1994). *Shh* stimulates *COUP-TFII* expression (Krishnan et al., 1997) thus is likely to be a downstream target of *SHH* signaling, and the requirement for *SHH* in gastric organogenesis suggests that *COUP-TFII* may play a role in stomach development (Takamoto et al., 2005). *COUP-TFs* are critical for development and differentiation in many different tissues in several organisms (Pereira et al., 2000).

Regulation of transcription in eukaryotes requires the participation of a number of transcription factors, many of which exist as multiprotein complexes. The general transcription factor *TFIID* is one such complex composed of the TATA box binding protein (TBP) and multiple TBP-associated factors (TAFIIs) and is required at many gene promoters to initiate transcription by RNA polymerase II (Dymlacht et al., 1991; Hernandez, 1993). In the context of *TFIID*, TAFIIs have been shown to interact with 1) specific transcriptional activators to mediate activation, 2) basal transcription factors, 3) other TAFIIs, and 4) specific DNA sequences, such as the downstream promoter element or gene-specific core promoter sequence, thereby contributing to promoter selectivity (Burley and Roeder, 1996; Hahn, 1998; Hoffmann et al., 1997; Kim et al., 2005; Lee and Young, 1998; Orphanides et al., 1996; Roeder, 1996; Sauer and Tjian, 1997). *GLI*-activate expression of reporter constructs in a concentration-dependent manner through *GLI* consensus binding motifs. *GLI*-induced transcriptional activation requires the carboxyl-terminal region highly similar to the α -helical herpes simplex viral protein 16 activation domain, including the consensus recognition element for the human *TFIID* TATA box-binding protein associated factor TAFII₃₁ the conservation of all three amino acid residues believed to interact directly to complementary residues in TAFII₃₁ (Yoon et al., 1998). The presence of this region in the *GLI* activation domain provides a mechanism by which *GLI*-induces transcriptional regulation.

Due to the involvement of COUP-TFII and TFIID with SHH signaling pathway expression of these transcriptional factors was investigated to see if *GLI1* changes their expression. I have shown using RT-PCR analysis that COUP-TFII and TFIID transcriptional factors were expressed in BCC, normal skin, HaCat, primary keratinocytes, A375 and *GLI1* expressing primary keratinocytes (**Figure 3.2**). It was not possible to quantify level of expression of COUP-TFII and TFIID because the primers designed for RT-PCR analysis did not work with the (DyNAmo™ SYBR® Green kit) real-time-RT-PCR analysis, even after changing the template concentration, annealing temperature and cycle number.

3.5.7 *SUP-FU* is expressed in BCC, normal skin and in *GLI1* expressing and non expressing cells.

Suppressor of Fused (*Sup-Fu*) is one of the component of Hh-signaling pathway has been identified in *Drosophila*, mouse and human (Delattre et al., 1999; Ding et al., 1999; Kogerman et al., 1999; Pham et al., 1995; Stone et al., 1999). In *Drosophila*, *Sup-Fu* has been shown to form a complex with three other molecules, Fused (*Fu*) (Murone et al., 2000), Costal-2 (*Cos2*) and the transcription factor Cubitus interruptus (*Ci*) (homolog of *GLI1*) (Monnier et al., 1998) all of which are involved in the transduction of the Hh-signal. This complex is associated with microtubules in the absence of *Sup-Fu* (Stegman et al., 2000). Human SUP-FU has been shown to bind *GLI1* and *GLI3* in the nucleus and enhances their binding to their recognition site on the DNA (Kogerman et al., 1999; Pearse et al., 1999), it also inhibits *GLI*-mediated transcription by shuttling *GLI1* from the nucleus to cytoplasmic (Kogerman et al., 1999). Human SUP-FU is expressed in; heart, brain, placenta, lung, liver, skeletal muscle, kidney pancreas, thymus, prostate, spleen, testes, colon, ovary, small intestine, and peripheral leukocytes (Grimm et al., 2001; Kogerman et al., 1999; Stone et al., 1999), at the time of this study there were no reports of SUP-FU expression in normal skin or BCC. I have shown in this study that *SUP-FU* was expressed in BCC, normal skin, HaCat, primary keratinocytes, A375 and *GLI1* expressing primary keratinocytes (**Figure 3.2**). I could not quantify the levels of *SUP-FU* expression because the primers designed for RT-PCR analysis did not work with the (DyNAmo™ SYBR® Green kit) real-time-RT-PCR analysis, even after altering the template concentration, annealing temperature and increasing the cycle numbers.

3.5.8 *α-TUB* is repressed in BCC and induced in *GLI1* primary keratinocytes.

There appears to be a small reduction in α -tubulin (*α-TUB*) expressing in BCC relative to normal skin and induction in *GLI1* expressing primary keratinocytes relative to non *GLI1* expressing keratinocytes (**Figure 3.6**). This data suggests that induction of *α-TUB* in *GLI1* expressing primary keratinocytes was dependent on *GLI1* although in BCC we saw an increase in *GLI1* expression but there was a reduction in *α-TUB* expression, this indicates that a different mechanism is controlling the expression of *α-TUB* in BCC. At the time this study was carried out there were no reports of α -tubulin repression in BCC or induction by *GLI1* in cells.

3.5.9 *GLI1* is not expressed in epidermis of normal skin, whereas *GLI2*, *GLI3* and *PTCH* are. *GLI1*, *GLI2*, *GLI3* and *PTCH* are expressed in dermal papilla and outer root sheath.

The origin of BCC has been debated. One possibility is that they derive from follicular progenitors because hair follicles transiently express the *GLI* and *SHH* genes and use the pathway for normal development (Dahmane et al., 1997; Karlsson et al., 1999a; St-Jacques et al., 1998). More specifically, they might derive from stem cells that are present in the bulge of the follicle (Fuchs et al., 2001; Taylor et al., 2000a). However, it is also possible that they derive from non-follicular transit amplifying precursors that are present in the basal layer of the interfollicular epidermis. Inappropriate activation of the SHH-GLI-pathway in epidermal stem cells might be responsible for BCC initiation? Thus a study was carried out looking at SHH-pathway gene expression in normal skin hair follicle, hair bulge, outer root sheet and interfollicular epidermis using LCM.

Cells were captured from dermal papilla, outer root sheath and interfollicular epidermis of the skin. However, reproducibility of capturing the cells using the LCM was poor. RT-PCR analysis shows *GLI1* is expressed in cells captured from dermal papilla and root sheath. There was no *GLI1* expression in captured cells from interfollicular epidermis. *GLI2*, *GLI3*, *PTCH*, *α-TUB* and β -Actin were expressed in cells captured from dermal papilla, root sheath and interfollicular epidermis (**Figure 3.7-A and B**). This data is consistent with the data obtained from RT-PCR analysis of normal skin (**Figure 3.3**) where *GLI2*, *GLI3*, *PTCH* and *α-TUB* were expressed. LCM RT-PCR data

CHAPTER 3: Analysis of SHH-Pathway Genes in Normal Skin, BCC and *GLI1*-transduced Human Primary Keratinocytes
is consistent with in-situ data for *GLI2* expression in **section 4.4.4**, in which *GLI2* was expressed in outer root sheath and interfollicular epidermis of normal skin.

3.6.0 Summary

In this study I have shown by northern blot analysis that *GLI1*, *GLI2* and *PTCH* are induced in *GLI1* expressing cells relative to non *GLI1* expressing cells. RT-PCR analysis shows that *GLI2- α/β* isoforms, *GLI3*, *SMO*, *PTCH*, *COUP-TFII*, *TFIID* and *KIF4A* are expressed in normal skin, BCC and *GLI1* expressing keratinocytes. *GLI1* is only expressed in BCC and *GLI1* expressing cells. Real-time-RT-PCR analysis shows that *GLI1*, *GLI2- α/β* isoforms, *GLI3*, *PTCH*, *SMO* and *KIF4* are induced and α -Tubulin (*α -TUB*) is repressed in BCC relative to normal skin. *GLI1*, *GLI2*, *GLI3*, *PTCH*, *SMO* and *α -TUB* are induced and *KIF4A* is repressed in *GLI1* expressing keratinocytes relative non *GLI1* expressing keratinocytes.

3.7.0 Future study

KIF4A plays multiple roles in mitosis, and its loss leads to numerous mitotic defects, including chromosome hypercondensation, aberrant spindle formation, anaphase bridges, defective cytokinesis, and aneuploidy (Castoldi and Vernos, 2006; Kurasawa et al., 2004; Lawrence et al., 2004; Mazumdar et al., 2006; Mazumdar and Misteli, 2005; Mazumdar et al., 2004). Aneuploidy has been suggested to contribute to tumor formation (Dey, 2004). A loss of *KIF4* in embryonic stem cells leads to 70% of the cells being aneuploid and this increases their potential to form tumor in nude mice, and *KIF4* protein levels are reduced in 35% of human cancers from several tissues (Mazumdar et al., 2006).

In this chapter *KIF4* was shown to be induced in BCC relative to normal skin it was also induced in HaCat and A375 cells. However, it was repressed in *GLI1* expressing primary keratinocytes relative to non *GLI1* expressing control primary keratinocytes (**Figure 3.6**). This suggests that there may be *GLI1* independent induction of *KIF4* in BCC *in-vivo* and *in-vitro* in certain cell lines. It is also possible that transcriptional activity of *GLI1* may be differentially regulated in BCC *in-vivo* and *in-vitro* leading to alteration in expression of *KIF4A*. It is possible that loss of *KIF4A* in *GLI1* expressing primary keratinocytes may also be leading to cells being aneuploid. Thus future work is required to identify why *KIF4A* transcript is upregulated in BCC and down regulated in *GLI1* primary keratinocytes and do *KIF4A* protein levels correlate with *KIF4A*

CHAPTER 3: Analysis of SHH-Pathway Genes in Normal Skin, BCC and *GLI1*-transduced Human Primary Keratinocytes. Also does loss of *KIF4A* in *GLI1* expressing primary keratinocytes leading to cells being aneuploid?

CHAPTER 4

**Localisation of GLI2 in Normal Human Skin and BCC and its
regulation of GLI1**

4.1.0 Introduction

In the previous chapter I characterised expression of SHH signalling pathway genes in human skin, BCC and GLI1 transduced primary keratinocytes, I had shown that *GLI2* was induced in GLI1 transduced primary keratinocytes relative to control (EGFP transduced primary keratinocytes). There was an ongoing collaboration between Professor Anthony Quinn at Centre for Cutaneous Research (CCR), Queen Mary University of London and Dr Fritz Aberger at Institute of Genetics, University of Salzburg Austria, to investigate the effect of HH/GLI-signalling, in human keratinocytes using *in vitro* model systems. In Regl et al (2002) we had shown that expression of GLI1 in human keratinocytes induced the expression of isoforms *GLI2 α* and *GLI2 β* . Both isoforms were also shown to be expressed at elevated levels in 21 BCCs compared to normal skin. In chapter 3 I had also shown that *GLI2 α* and or *GLI2 β* are up regulated in BCC relative to normal skin and they were also induced in GLI1 transduced primary keratinocytes relative to control (EGFP transduced primary keratinocytes) in a real-time RT-PCR analysis. This suggested that there was a positive feedback mechanism between GLI1 and GLI2 transcription factors. Detailed time course experiments monitoring the transcriptional response of keratinocytes either to GLI1 or to GLI2 suggested that *GLI1* was a direct target of GLI2, while activation of GLI2 by GLI1 may be indirect (Regl et al., 2002). Furthermore, expression of either GLI2 or GLI1 showed an increase in DNA-synthesis in confluent human keratinocytes (Regl et al., 2002). These results suggested that there may be an important role of the positive GLI1 and GLI2 feedback loop in HH-mediated epidermal cell proliferation.

4.1.1 NHIS-GLI2 binds GLI consensus sequence in the *GLI* promoter and induces GLI1 expression in keratinocytes.

In collaboration with Dr Fritz Abergers' laboratory, we had previously identified a positive feed back loop between GLI1 and GLI2 in primary human keratinocytes (Regl et al., 2002). To investigate this in more detail, Dr Fritz Abergers' lab measured the increase in GLI1 mRNA and protein in HaCaT expressing N-terminally HIS-tagged GLI2 protein (NHIS-GLI2-HaCaT) under control of the tetracycline repressor. They showed that following tetracycline treatment there was a gradual increase in *GLI1* mRNA. In addition, activation of the direct target *PTCH* was slightly delayed compared

to induction of *GLI1* mRNA. Western blot analysis showed that NHIS-GLI2 protein was detected 1 hour after tetracycline treatment whereas GLI1 protein was not detected until 6 hours after treatment. In addition, the increase in GLI2 protein was closely paralleled by the gradual increase in *GLI1* mRNA (Ikram et al., 2004). This suggested that *GLI1* represents an early GLI2 target gene. They also showed that *GLI1* mRNA induction was closely followed by a gradual increase in endogenous *GLI2* mRNA (Ikram et al., 2004), confirming previous observation that a positive feedback loop exists between GLI1 and GLI2 (Regl et al., 2002).

To assess whether GLI2 may be capable of directly activating *GLI1* transcription by binding to the *GLI1* promoter, Dr Fritz Abergers' lab first performed in silico analysis of the 5' flanking region of the human *GLI1* core promoter region (Liu et al., 1998; Villavicencio et al., 2002) to identify putative GLI-binding sites. Using the ScanAce tool (Hughes et al., 2000; Roth et al., 1998) they analysed a region of approximately 1 kb upstream of the transcriptional start site of *GLI1* (Liu et al., 1998) for motifs identical to or closely matching the GLI-consensus binding site TGGGTGGTC (Kinzler and Vogelstein, 1990b). An identical putative binding site was also present in the cis-regulatory sequence of the mouse *Gli1* gene, suggesting a possible functional relevance of this motif in the regulation of *Gli1* expression (Ikram et al., 2004).

To determine whether NHIS-GLI2 protein can bind to the putative GLI-binding site in the *GLI1* core promoter, Dr Fritz Abergers' lab performed electrophoretic mobility shift assays using bacterially expressed NHIS-GLI2-(332) protein and radioactively labelled double stranded oligonucleotides containing either the putative GLI-binding site (Bs) or a mutated control oligonucleotide with two base pair exchanges in the core region (Bsm). They showed that recombinant NHIS-GLI2-(332) protein specifically bound to the Bs sequence, but not to the Bsm sequence, suggesting that NHIS-GLI2 protein may be activating *GLI1* transcription by directly binding to the 5' flanking region of the *GLI1* promoter at a position close to the transcriptional-start site (Ikram et al., 2004).

To analyse whether the GLI-binding site in the *GLI1* promoter is involved in activation of *GLI1* transcription by GLI2, Dr Fritz Abergers' lab performed luciferase reporter assay using wild-type and mutated *GLI1* promoter constructs. Co-transfection of *GLI2* expression plasmid with the reporter construct containing the 5' upstream region of human *GLI1* (-1400 to +93, Liu et al., 1998) resulted in a 3-fold increase in luciferase

CHAPTER 4: Localisation of GLI2 in Normal human Skin and BCC and its regulation of GLI1 activity compared to controls. By contrast, no increase in reporter activity was observed when the GLI-binding site at position -56 was changed from CGGGTGGTC to CGCCTGGTC by site-directed mutagenesis (Ikram et al., 2004). The GLI-binding and luciferase reporter assay data suggest that HIS-GLI2 activates transcription of *GLI1* by interacting directly with the GLI-binding site at position -56 to -48 of the *GLI1* promoter (Ikram et al., 2004).

The expression profile of GLI1 is well characterised in BCC and normal skin (Ghali et al., 1999). As part of collaboration with Dr Fritz Abergers' lab, aim of this study was to determine *GLI2* localisation in normal skin and BCC by in situ hybridisation and determined expression of GLI1 mRNA and protein in NHIS-GLI2 expressing human primary keratinocytes.

4.2.0 Results

4.2.1 GLI1 expression in NHIS-GLI2 human primary keratinocytes.

When human primary keratinocytes were transduced with NHIS-GLI2, GLI1 (positive control) and GFP (negative control) retrovirus and cultured for 72 hours after which total RNA and proteins were extracted. RT-PCR and western blot data of GLI1 shows that NHIS-GLI2 induced endogenous GLI1 transcript and protein expression in primary keratinocytes (**Figure 4.1**). This confirmed the observation (Ikram et al., 2004; Regl et al., 2002) that NHIS-GLI2 induced GLI1 expression in HaCat cells. This indicates that GLI1 may be a target of GLI2 in primary as well as immortalised keratinocyte cells.

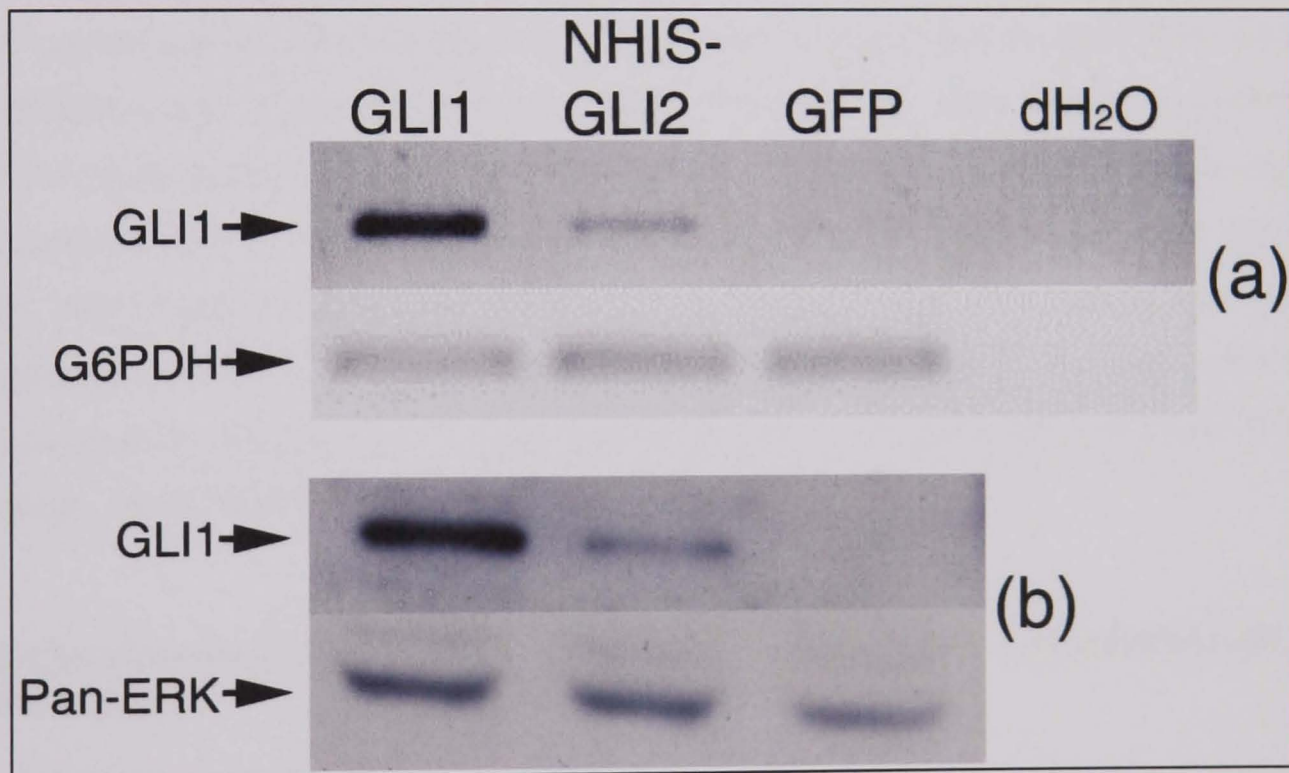


Figure 4.1: *GLI1* mRNA and protein expression in NHIS-GLI2 human primary keratinocytes. Primary keratinocytes were transduced with NHIS-GLI2, GLI1 and GFP retrovirus and cultured for 72 hours after which total RNA and proteins were extracted. This figure shows exogenous NHIS-GLI2 induced endogenous GLI1 protein expression as shown by (a) semi-quantitative RT-PCR and (b) western blot analysis, Pan-ERK indicates equal protein loading. Retroviral expression of GLI1 was used as a positive control, GFP and dH₂O as negative controls. The data represented is of two independent experiments.

4.2.2 In-situ hybridisation of *GLI2* expression in normal skin and BCC.

4.2.3 Development of the In-situ hybridisation technique.

Initial experiments were carried out to develop the in-situ hybridisation method using fragmented full-length keratin K14 (*KRT14*) and *GLI2* ribo probes generated from *KRT14*-1.2kb-PGEM and h*GLI2*-1.6kb-pCRII-TOPO vectors on wax embedded tissue sections. *KRT14* probe was used as a positive control for in situ hybridisation; this allowed us to determine the integrity of mRNA and the pattern of expression. It was not possible to generate a *KRT14* sense probe from *KRT14*-1.2 kb-PGEM vector and when this vector was sequenced using SP6 and T7 primers to identify *KRT14* insert, it was not possible to sequence the insert using T7 primers; this suggested that there may be a problem in this site which was not allowing to sequence the construct or to generate a sense probe, as the control sequencing reaction with the T7 primers worked with the M13 control vector. After liaising with other groups who had used the same *KRT14*-1.2 kb-PGEM vector in the department, revealed that they also were unable to generate *KRT14* sense probe. However, after consultation with Dr Anthony Quinn it was decided to continue with the in-situ hybridisation analysis using the *KRT14* anti-sense probe only. *KRT14* anti-sense (1.2 kb) and *GLI2* (1.6 kb) sense and anti-sense probes were fragmented, this allowed them to penetrate the tissue to hybridise to the target mRNA. To increase the accessibility of target mRNA in wax embedded normal skin and BCC sections, citrate buffer and proteinase-K methods were used.

4.2.4 Localisation of *GLI2* and *KRT14* in BCC and normal skin wax sections with citrate method.

With the citrate method keratin-14 signal was observed in the basal layer in some regions and throughout the epidermis in other regions in the same normal skin sections. *KRT14* expression was also observed in BCC tumour islands (**Figure 4.2**). *GLI2* signal was observed throughout the epidermis layer in normal skin adjacent to BCC and in tumour islands with both sense and anti-sense probes (**Figure 4.3** and **Figure 4.4**).

4.2.5 Localisation of *GLI2* and *KRT14* in BCC and normal skin wax sections with proteinase-K method.

With proteinase-K method *GLI2* signal was observed in the epidermis and in BCC tumour islands with anti-sense probe. A weaker signal was observed with *GLI2* sense probe in same regions (**Figure 4.5**). *KRT14* signal was in the basal layer only in normal skin adjacent to BCC and in tumour islands (**Figure 4.6**). The signal for sense and anti sense probes for *GLI2* and *KRT14* anti sense probe was patchy in normal skin and BCC sections. *KRT14* being a basal cell marker was expected to give basal signal only. This suggested that proteinase K method give a specific signal compared to the citrate method. Thus proteinase K method was used for *KRT14* and *GLI2* in-situ hybridisation on wax embedded BCC and normal skin sections. Once again a signal was observed with *GLI2* fragmented sense and anti-sense probes in normal skin and BCC sections. This indicated that signal for *GLI2* was non-specific. As there was no sense *KRT14* probe one could not be certain if *KRT14* signal observed with anti-sense probe was specific, although the *KRT14* expression pattern was specific for the basal layer in the epidermis.

4.2.6 Localisation of *GLI2* and *KRT14* in BCC and normal skin frozen section with proteinase K and citrate method.

Fresh BCC and normal skin samples were collected from the Royal London Hospital Dermatology Department (with ethical approval). Soon after the samples were excised they were, snap frozen to preserve the mRNA. Sections cut from these samples were hybridised with 1.2 kb *KRT14* (fragmented) and 296bp *GLI2* sense and anti-sense probes generated from newly cloned *KRT14*-1.2 kb and h*GLI2*-296 bp (*KRT14*-1.2kb-pCII-TOPO, h*GLI2*-296bp-pCII-TOPO) vectors (see sections 2.10.5, 2.10.7) using citrate and proteinase-K methods. With citrate method a clean and specific signal was observed compared to the proteinase-K method for *KRT14* anti-sense probe and no signal with sense probe. This indicated that for frozen sections the citrate method works better. However, with the *GLI2* sense probe there was still non specific signal observed with the citrate method. Following this citrate method was used. However, in-situ hybridisation washing temperatures were changed from 42°C to 50°C and final wash from 55°C to 60°C. With these higher washing conditions, the signal observed for the *KRT14* anti-sense probe was weaker and no signal was observed with *KRT14* sense

probe. For *GLI2* anti-sense probe a strong signal was observed and with *GLI2* sense probe either no signal or a very weak signal (back ground) was observed. This indicated that each probe had different optimum washing temperature. Therefore, in-situ hybridisation was carried out on frozen BCC and normal skin sections using citrate method. *KRT14* and *GLI2* hybridisation was carried out simultaneously and only the washes were done at different temperatures, for *KRT14* at 45°C and final wash at 50°C and for *GLI2* at 55°C and final wash at 60°C

GLI2 signal was observed in normal skin interfollicular epidermis and in the outer root sheath (ORS) of hair follicle with an anti-sense probe. No or very weak staining was observed in adjacent sections with a sense probe. As a control *KRT14* expression was also detected in basal layer of normal skin epidermis and in the outer root sheath (ORS) of hair follicle, with an anti-sense probe. No signal was observed in adjacent sections with the sense probe (**Figure 4.7, Figure 4.8**). A strong *GLI2* and *KRT14* signal was also observed in BCC tumour islands and particularly in the cells of periphery with an anti-sense probe. No signal was observed in the adjacent sections with a sense probe (**Figure 4.9**). BCC and normal skin samples examined were scored under the microscope for *GLI2* and *KRT14* expression. A strong *GLI2* and *KRT14* expression was consistently observed in all BCC (n=8) and normal skin (n=3) samples (**Table 4.1**). This correlated with RT-PCR data showing *GLI2* expression in BCC and normal skin.

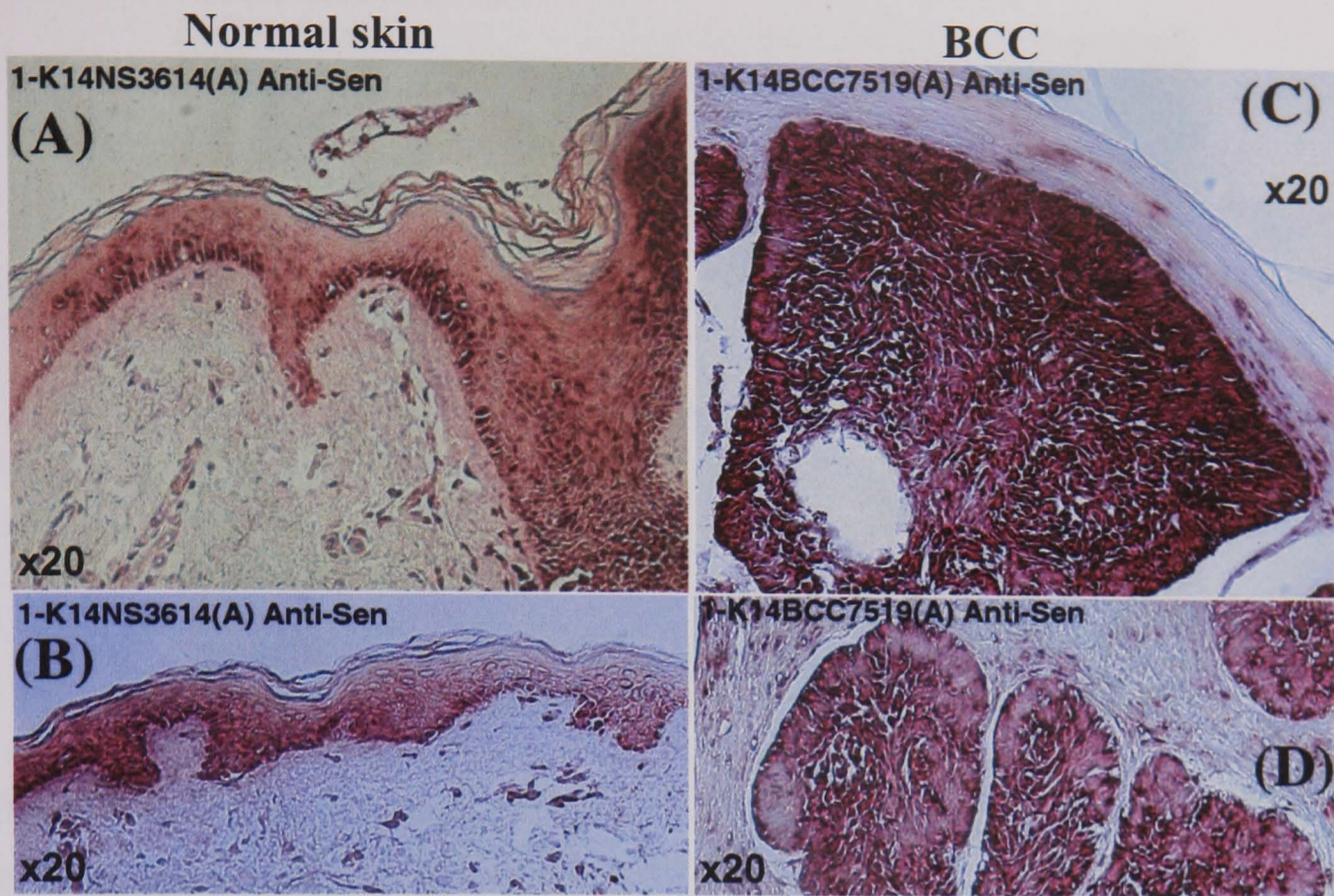


Figure 4.2 In-situ hybridisation analysis of *KRT14* expression in BCC and normal skin (wax sections using citrate buffer method). *KRT14* signal in normal skin is in basal layer (A, B x20), in BCC the signal is in the tumour islands (C, D x20).

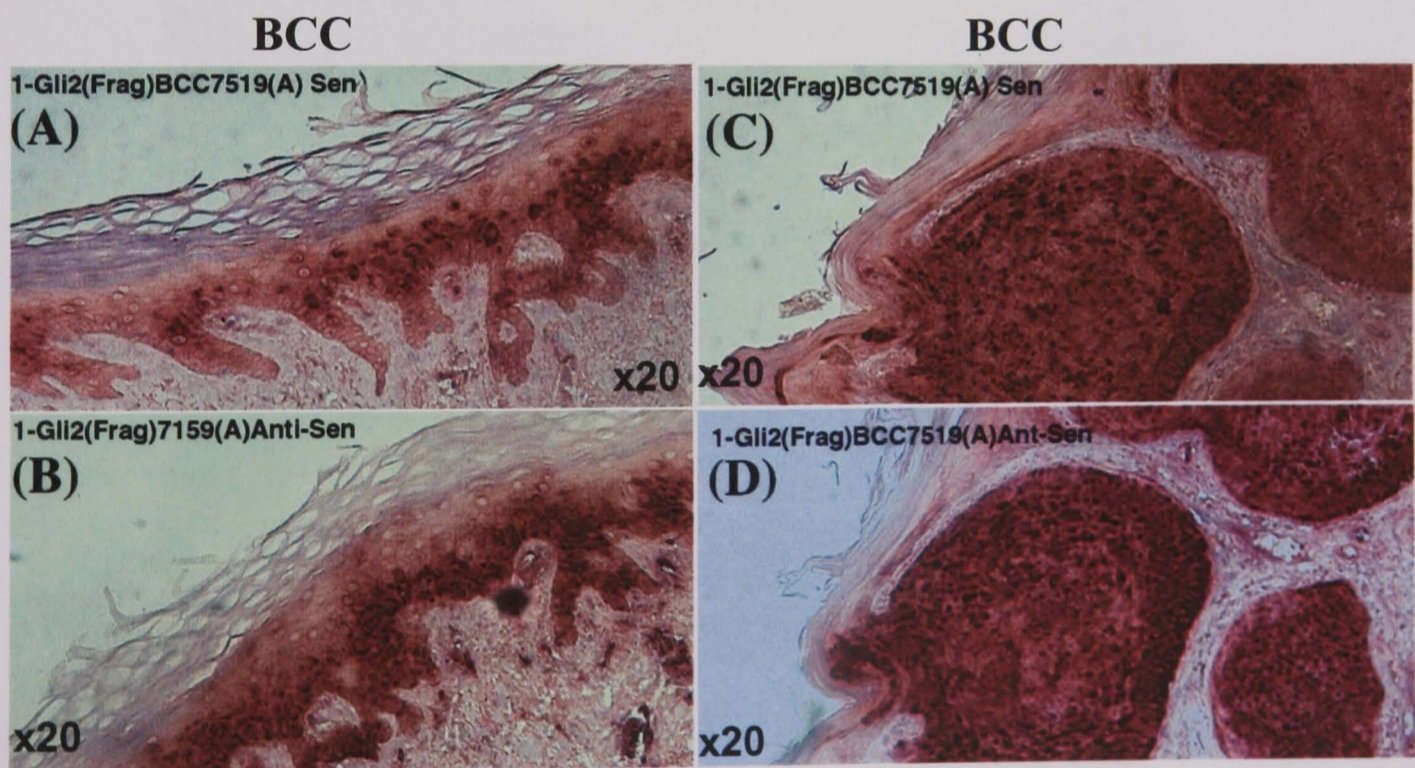


Figure 4.3 In-situ hybridisation analysis of *GLI2* expression in BCC (wax section using citrate buffer method). *GLI2* signal with the sense (A, C x20) and anti-sense (B, D x20) fragmented probes, the signal is in epidermis and in BCC tumour islands. Thus, the signal is non-specific due to sense and anti sense probes both giving a signal.

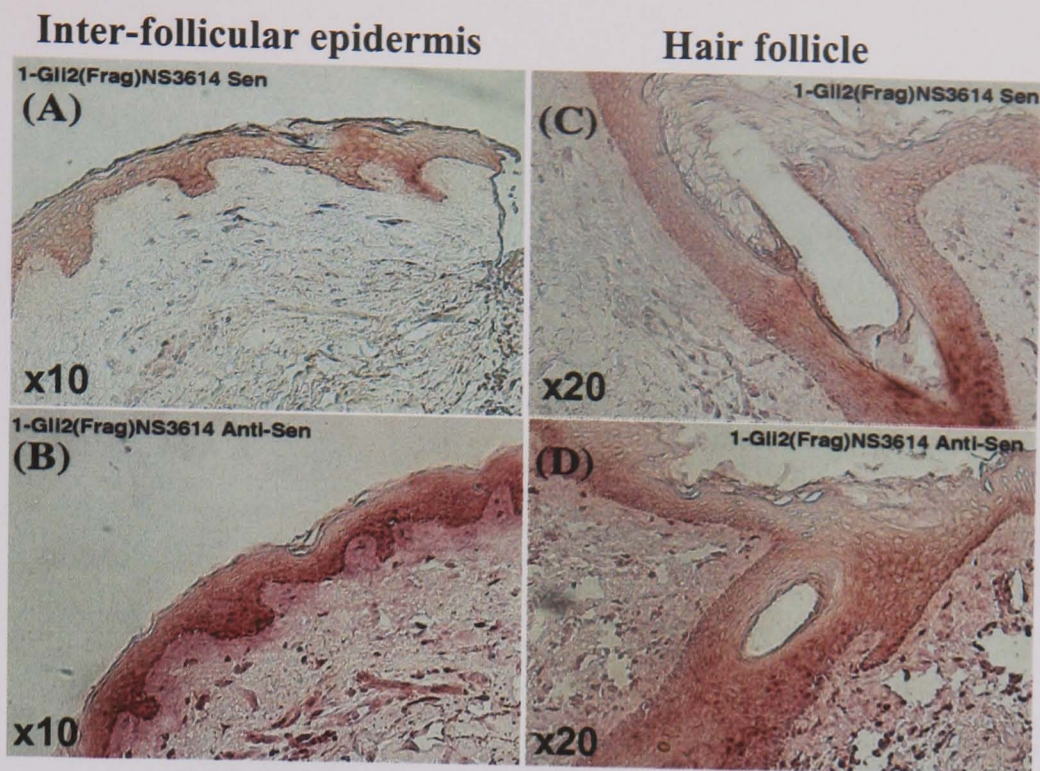


Figure 4.4 In-situ hybridisation analysis of *GLI2* expression in normal skin (wax sections using citrate buffer method). *GLI2* sense (A, C) and anti-sense (B, D) fragmented probes. The signal is in the epidermis and hair follicle for both probes. However, there is a weaker signal for the sense probe compared to the anti-sense probe in same regions.

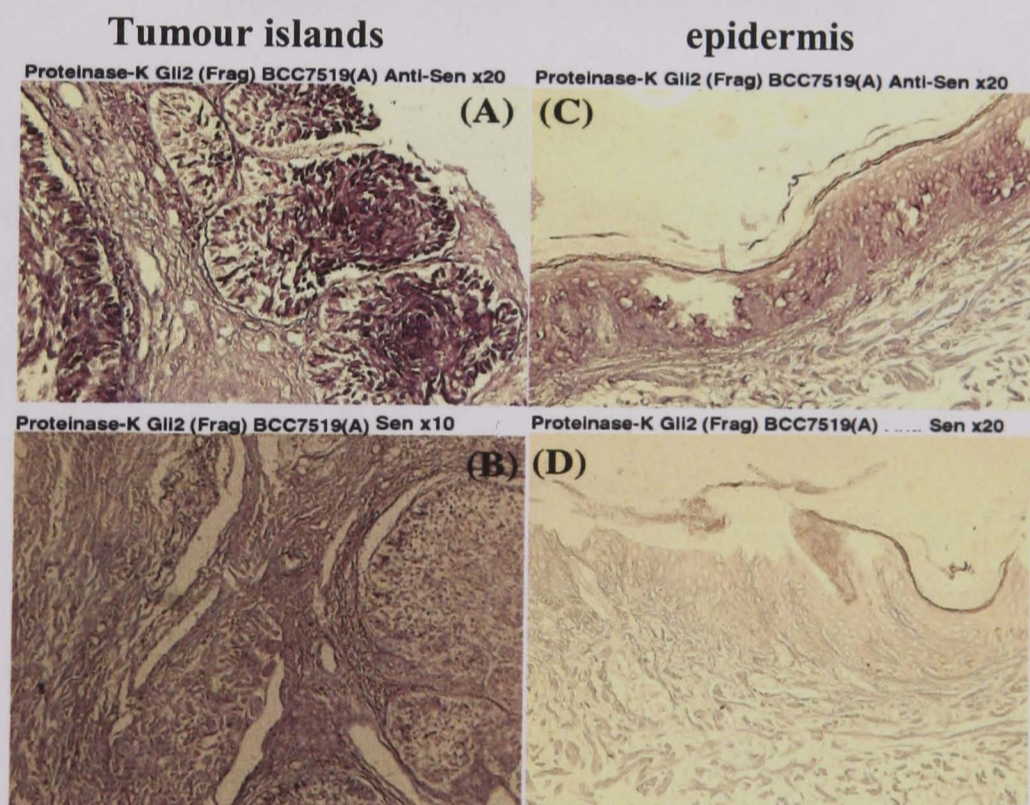


Figure 4.5 In-situ hybridisation analysis of *GLI2* expression in BCC (wax sections with proteinase K method). *GLI2* anti-sense (A, C x20) and sense (B, D x20) fragmented probes. The signal is in epidermis and the tumour islands. There is very weak signal for the sense probe compared to the anti-sense probe in the same regions. D shows that the morphology of the tissue has been disrupted with proteinase K method.

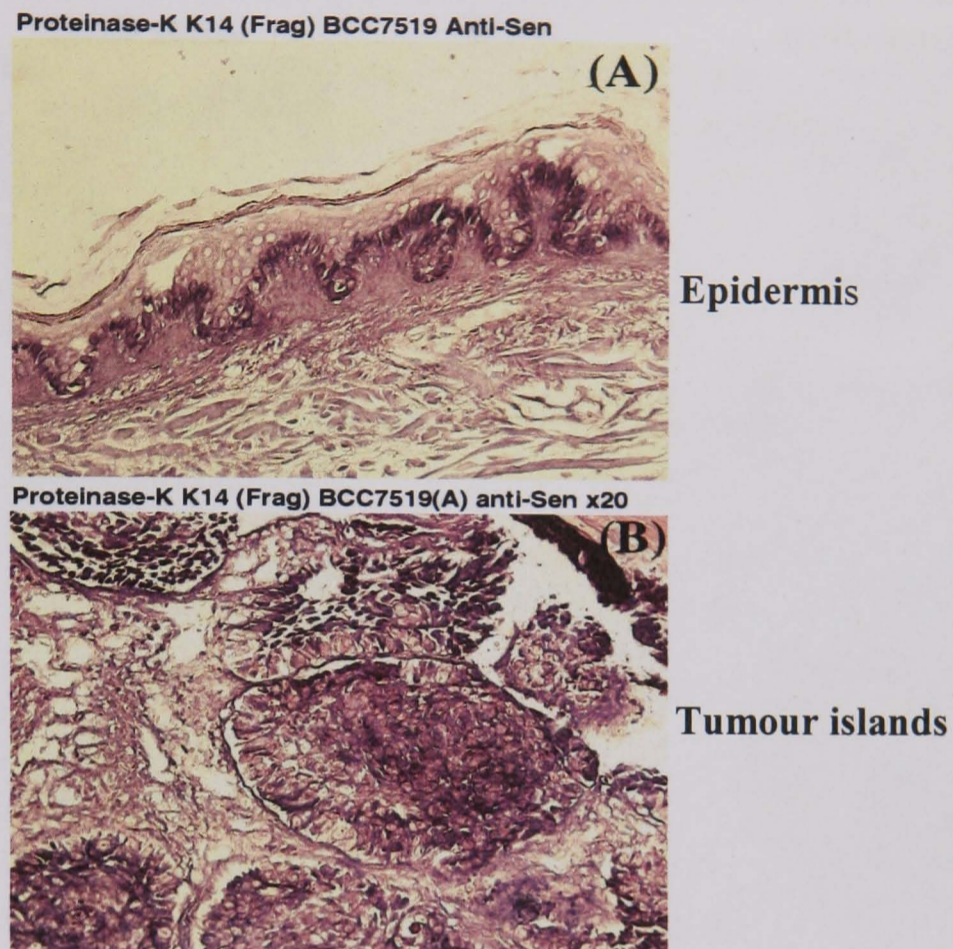


Figure 4.6 In-situ hybridisation analysis of *KRT14* expression in BCC (wax sections with proteinase K method). With the *KRT14* anti-sense (A, B x20) fragmented probe, the signal is in the basal layer only in the epidermis and in tumour islands. This indicates that the signal is specific.

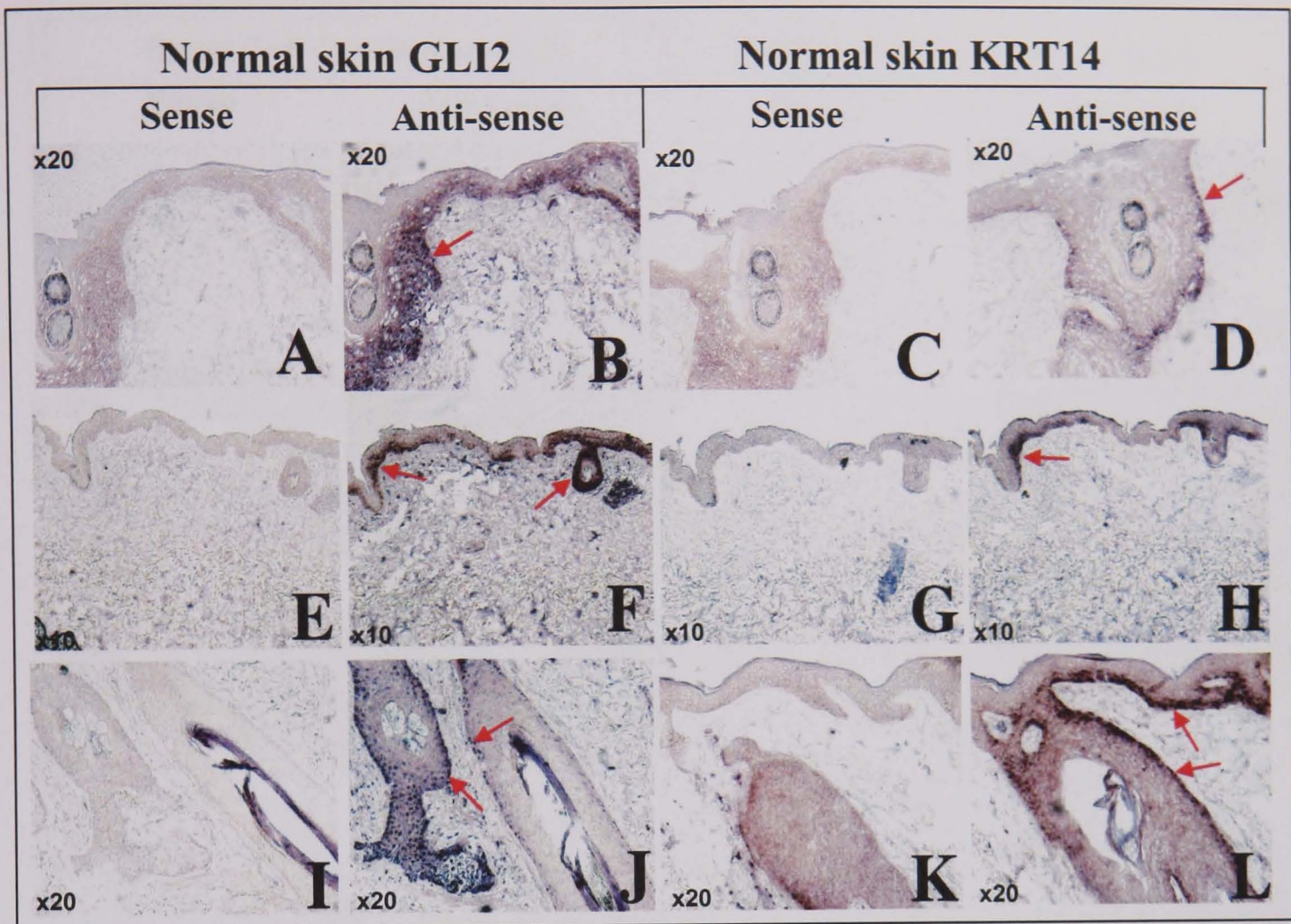


Figure 4.7 In-situ hybridisation of *GLI2* and *KRT14* expression in normal skin (frozen sections using citrate buffer method). *GLI2* expression was detected in the epidermis and the outer root sheath (ORS) of the hair follicle with an anti-sense *GLI2* probe (B, F and J- indicated by red arrows). No staining was observed in adjacent sections with a sense *GLI2* probe (A, E and I). *KRT14* expression was detected in the basal layer of the epidermis and the ORS of the hair follicle (D, H and L-indicated by red arrows). No staining was observed in adjacent sections with a sense *KRT14* probe (C, G and K).

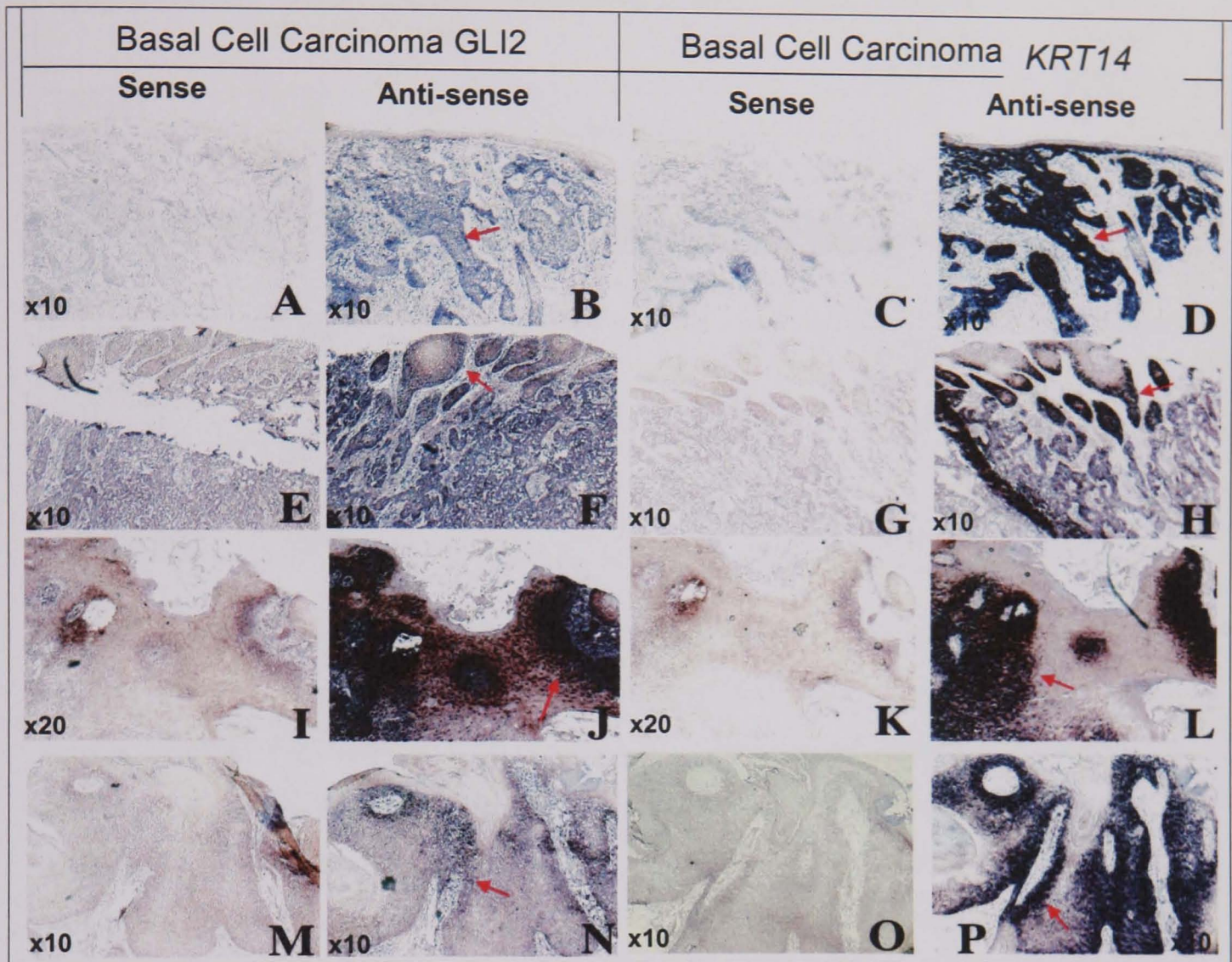


Figure 4.8 In-situ hybridisation analysis of *GLI2* and *KRT14* expression in BCC (frozen section using citrate buffer method). *GLI2* expression was detected in tumour islands and particularly in the cells of periphery with an anti-sense *GLI2* probe (B, F, J and N- indicated by red arrows). No staining or very weak staining was observed in adjacent sections with a sense *GLI2* probe (A, E, I and M). A strong, *KRT14* expression was detected compared to *GLI2* in tumour islands and particularly in the cells of periphery with an anti-sense *KRT14* probe (D, H, L and P- indicated by red arrows). No staining was observed in adjacent sections with a sense *KRT14* probe (C, G, K and O).

Table 4.1: *GLI2* and *KRT14* expression in normal skin and basal cell carcinoma.

Sample ID No	Tissue Sample	<i>GLI2</i> Anti-sense probe	<i>GLI2</i> Sense probe	<i>KRT14</i> Anti-sense probe	<i>KRT14</i> Sense probe
170901	N/S	+++	-	+++	-
35499144	N/S	+++	-	+++	-
898921	N/S	+++	-	+++	-
291669	BCC	+++	-	+++	-
M567438	BCC	++	-	+++	-
4006064969	BCC	+++	-	+++	-
M62058	BCC	+++	-	+++	-
F455131	BCC	+++	-	+++	-
2013131	BCC	+++	-	+++	-
609458	BCC	+++	-	+++	-
M265128	BCC	++	-	+++	-

Frozen sections were hybridised with \approx 100ng *GLI2* anti-sense and sense probes and washed at 55°C, final wash at 60°C and 100ng *KRT14* anti sense and sense probes washed at 50°C, final wash at 55°C. Strong *GLI2* staining was consistently observed in all basal cell carcinoma (BCC) n=8 and normal skin (N/S) n=3 samples examined. A control *KRT14* expression (used to verify the integrity of mRNA) was detected with an anti-sense probe. No samples were scored for *GLI2* expression if they failed to show *KRT14* mRNA expression, (+++ strong signal, ++ weak signal, + very weak signal, - no signal).

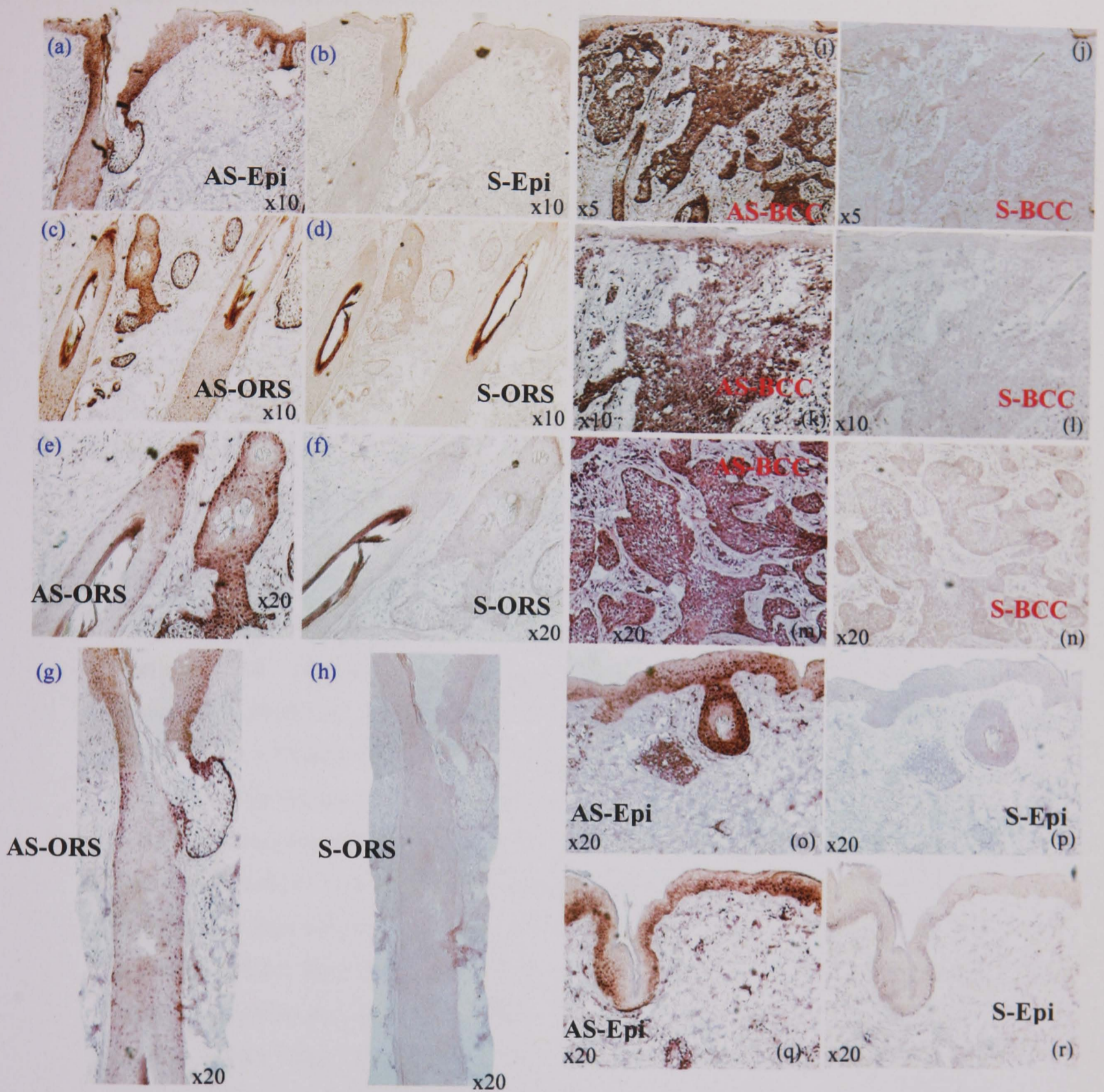


Figure 4.9 In-situ hybridisation analysis of *GLI2* expression in BCC and normal skin frozen section (using citrate method). *GLI2* expression was detected in the epidermis [(Epi) a, o, q] and in the outer root sheath (ORS) of the hair follicle (c, e, g) with an anti-sense (AS) probe. No staining was observed in adjacent sections with a sense (S) probe (b, d, f, h, p, r). *GLI2* expression was detected in BCC tumour islands with an anti-sense probe (i, k, m). No staining was observed in adjacent sections with a sense probe (j, l, n).

4.2.7 Generation of monoclonal antibody to N-and-C-terminal of GLI2.

The presence of *GLI2* transcript in normal skin and BCC does not mean that the protein will also be present. To determine if the protein was present in areas where *GLI2* transcript were localised, we needed to look at protein expression in these tissue samples. At the time these experiments were carried out there were no GLI2 antibodies available to carry out Immunohistochemistry analysis on normal skin and BCC samples. With the help of Dr Fritz Abergers we designed GLI2 peptides from the C-and N-terminal sequence, obtained from the NCBI data base, to generate a GLI2 antibody. The availability of GLI2 antibody would have allowed us to determine if GLI2 protein is present in areas where *GLI2* transcripts had been identified in normal skin and BCC in the in-situ hybridisation analysis. Generation of GLI2 antibody would have also allowed us to identify if GLI2 was processed in the *in-vitro* systems.

The antibody generation work was carried out by the Monoclonal Antibody Service Unit at Cancer Research UK, as detailed in the material and methods described in **section 2.13.0**. After injecting the conjugated Maleimide Activated Keyhole limpet hemocyanin (mcKLH), GLI2-N and C terminal peptides, Elisa assay were carried out by diluting (1:10,000) the test bleeds obtained from the immunised mice using the peptide only as the antigen. The mouse test bleeds that were positive for the Elisa assay did not generate any GLI2 specific band at or around 140 kD on the western blots from GLI1, NHIS-GLI2 and EGFP (control) transduced primary keratinocytes protein lysates. This indicated that there was no GLI2 specific response in any of the mice that were immunised. The Elisa assay and the testing of the bleed samples on the western blots, was carried out by the Monoclonal Antibody Services at Cancer Research UK. Getting to this stage had taken 6-8 months and during this time the availability of commercially produced GLI2 antibody lead led us to abandon the attempt to generate a GLI2 antibody.

4.3.0 Discussion

4.3.1 Localisation of *GLI2* in BCC and normal skin.

GLI1 is reported to be expressed in ORS of normal skin hair follicle (Ghali et al., 1999) and a positive feed back mechanism has recently been identified between GLI1 and GLI2 (Regl et al., 2002). There were no reports of GLI2 localisation in normal skin and BCC tissue, thus *GLI2* localisation was investigated to see if there was co-localisation expression of GLI1, GLI2 in BCC and normal skin. At the time this study was carried out there were no GLI2 antibodies available thus in-situ hybridisation analysis was carried out to determine *GLI2* transcript localisation in BCC and normal skin.

Initially control experiments were carried out to see if the in-situ hybridisation technique was working using a *KRT14* ribo-probe, *KRT14* is expressed in the basal layer of the skin and is induced in BCC (Apaydin et al., 2005; Fuchs and Green, 1980; Nelson and Sun, 1983; Steinert and Roop, 1988). These experiments were carried out using paraffin wax embedded BCC and normal skin tissue samples with citrate buffer and proteinase K method (see section 2.10.0). Using the citrate method *KRT14* transcripts were detected in the basal cells of the epidermis in some regions and in some it was not confined to the basal cells, but was present throughout the epidermis in normal skin (using fragmented *KRT14*-1.2 kb probe). *KRT14* was also detected in the BCC tumour islands with the citrate method (**Figure 4.2**).

With the proteinase K method, *KRT14* expression was detected in the basal layer only and in the BCC tumour island in the same sample with fragmented *KRT14* 1.2kb probe (**Figure 4.6**). This indicated that the proteinase K method gives a specific signal compared to the citrate method. When full length *KRT14* 1.2 kb probe was not fragmented and used to detect localisation of *KRT14* the signal obtained was strong but not confined to the basal cells but throughout the epidermis layer. This suggested that the full-length probe may have been binding non-specifically compared to fragmented probe. The reason why we observed a stronger signal with the un-fragmented (1.2 kb) compared to fragmented *KRT14* probes is that longer probes can give a stronger signals because they have more labelled nucleotides incorporated into them. However, probes that are too long can give weaker signals because they penetrate less efficiently into the cross-linked tissue. The extent to which long probes are hindered from penetrating

depends upon the nature of the tissue, the choice of fixative, and whether pre-treatments have been carried out to remove cellular proteins (Wilkinson 1998).

A possible reason why we observed signal throughout the epidermis for the un-fragmented *KRT14* probe is that there are many different types of keratin expressed throughout the epidermis layer and certain keratins have highly conserved (homologous) regions (Fuchs and Weber, 1994). Thus, it is possible that the full length *KRT14* probe may have hybridised to other homologous keratins which are expressed throughout the epidermis. However, fragmented *KRT14* probe was hydrolysed randomly which generated fragments of approximately 500bps. Therefore, it is possible that the *KRT14* homology regions to other keratins may have been hydrolysed to smaller fragments and these were unable to remain hybridised under the in-situ hybridisation conditions. The *KRT14* specific regions were of larger size and these remained hybridised to the *KRT14* transcripts under the same conditions. Thus, we observed a more specific signal with the *KRT14* fragmented probes compared to un-fragmented probe.

One of the controls for specific hybridisation to mRNA is to use a sense strand probe that should not specifically anneal to the target RNA. Not being able to generate a *KRT14* sense probe as a negative control for the in-situ hybridisation from the *KRT14*-PGEM plasmid, the plasmid (*KRT14*-PGEM) was sequenced using SP6 and T7 primers to determine if it contained the correct *KRT14* insert. *KRT14* insert sequence was confirmed with SP6 primer but there was no sequence obtained with T7 primer. This indicated that there was a problem with the *KRT14*-PGEM plasmid in the T7 primer regions, thus *KRT14*-PGEM could not be sequenced or used to generate a *KRT14* sense probe using T7 primers and T7 polymerase. Other workers in the lab were also unable to generate *KRT14* sense probe with *KRT14*-PGEM plasmid. It is possible that the sequence in *KRT14*-PGEM plasmid in T7 primer region may have been mutated and thus we were unable to generate *KRT14* sense probe.

Using a proteinase K and citrate method there was a signal observed for *GLI2* in BCC and normal skin with fragmented 1.5 kb *GLI2* sense and anti-sense probes (**Figure 4.3 and Figure 4.4.**). A stronger signal was obtained with the citrate method in BCC and normal skin compared with proteinase K method (**Figure 4.5**); this indicates that for *GLI2* probe citrate method had worked better. There was no sense *KRT14* probe thus it

was not clear if *KRT14* signal with anti-sense probe was specific or non specific. Therefore, a smaller fragment of (296bp) *GLI2* probe from h*GLI2*-pCRII-TOPO vector corresponding to 2869-3165bp (GI No 3061313) and 1.2 kb *KRT14* probe from the *KRT14*-PGEM vector corresponding to 298-1498bp (GI No 15431309) were cloned into pCRII-TOPO vector to generate a more specific probes (see section 2.9.4 and 2.9.5).

Wax imbedded BCC and normal skin samples were obtained from laboratory stocks. It was not clear how these were treated to preserve the RNA. Fresh BCC and normal skin samples were collected and snap frozen. Sections from these samples were hybridised with fragmented 1.2 kb *KRT14* and 296bp *GLI2* sense and anti sense probes generated from 1.2 kb *KRT14*-pCRII TOPO and 296bp *GLI2*-pCRII TOPO plasmids using citrate and proteinase K methods. With citrate method a clean and specific signal was observed compared to proteinase K method with fragmented 1.2 kb *KRT14* anti-sense probe, this suggested that for frozen sections citrate method worked better.

However, with 296bp *GLI2* sense probe there was still non-specific signal obtained, by optimising the washing conditions for both fragmented 1.2 kb *KRT14* and 296bp *GLI2* sense and anti-sense probes using the citrate method. Indicated that each probe had different optimum washing temperature for *KRT14* it was at 50°C and final wash at 50°C and for *GLI2* it was at 55°C and final wash at 60°C (see section 2.10.13). Thus, *KRT14* and *GLI2* in-situ hybridisation was carried out simultaneously on frozen BCC and normal skin sections using citrate method and the washes were done at different temperatures.

GLI2 signal was observed in normal skin (n=3) interfollicular epidermis and in the outer root sheath (ORS) of the hair follicle. As a control *KRT14* was also detected in basal layer of normal epidermis and in the outer root sheath (ORS) of hair follicle in the same samples (Figure 4.7 and Table 4.1). A strong *GLI2* and *KRT14* signal was also observed in BCC (n=8) tumour island and particularly in the cells of periphery (Figure 4.8 and Table 4.1). This correlated with RT-PCR and real-time-RT-PCR analysis confirming that *GLI2* was expressed in BCC and normal skin (Figure 3.5, Figure 3.6) and with LCM data (Figure 3.7)

4.3.2 A role for human GLI2 in regulating epidermal proliferation and skin tumorigenesis.

A number of *Drosophila* and vertebrates developmental processes such as cell type specification, pattern formation and regulation of cell proliferation involve HH-signal transduction pathway. Deregulation of this pathway results in consistent up-regulation of Hh target genes which can lead to developmental defects as well as to the formation of various tumours such as medulloblastomas, rhabdomyosarcomas and BCCs. (Goodrich and Scott, 1998; Ruiz, 1999; Toftgard, 2000).

Drosophila and vertebrates studies have shown that GLI family of transcription factors are the key players in Hh-signalling. Of the three GLI genes, GLI1 has been the focus with respect to tumorigenesis, since it is expressed in BCC and not in normal skin (Green et al., 1998). Overexpression of GLI1 in the epidermis of transgenic mice induces a variety of skin tumours including BCCs (Nilsson et al., 2000). More recently it was shown that *GLI2* expression to be elevated in response to GLI1 in human keratinocytes and *GLI2* transcript was expressed at elevated levels in BCCs compared to normal skin and a positive feedback mechanism exists between GLI1 and GLI2 in the human keratinocyte cell line HaCaT and in mouse C3H10T1/2 fibroblasts (Regl et al., 2002), and coworkers had shown that GLI2 specifically binds the GLI binding consensus sequence in the *GLI1* promoter leading to induction in GLI1 expression (Ikram et al., 2004).

I have shown in this study that *GLI2* is expressed in interfollicular epidermis and ORS of hair follicles in normal skin as well as in BCC tumour islands. This indicates that there is no overlap of GLI1 and GLI2 expression in normal interfollicular epidermis except in BCC and ORS of hair follicle. Overexpression of mouse *Gli2* and not *Gli1* has been shown to specifically cause the development of BCC-like features (Grachtchouk et al., 2000). These results point towards a possible important role for human GLI2 in regulating epidermal proliferation and skin tumorigenesis. BCC is believed to originate from stem cell residing in the hair follicle (Kruger et al., 1999) and therefore, it is possible that deregulation of SHH pathway in transiently amplifying stem cell may effect co-expression of GLI1 and GLI2 in ORS leading to BCC formation.

A possible scenario in the induction of BCC formation may be activation of GLI1 by inactivating mutations in PTCH followed by the induction of GLI2. Alternatively, activation of HH-signalling may first lead to the induction of GLI2 expression which directly activates GLI1 expression. This indicates that a feedback loop may be required in the activation and maintenance of BCC formation, which is not active in normal skin due to the absence of GLI1 expression. It is also possible that there may be certain unidentified factor(s) that are present in BCC that allow GLI2 to activate GLI1 which may not be present in normal skin.

Activation of GLI2 by GLI1 may also be system specific. Mice ectopically expressing *Gli1* in the neural tube do not show any alterations of the *Gli2* expression pattern (Hynes et al., 1997). In contrast, injection of human *GLI1* into frog embryos results in the formation of skin tumours, which express *Gli2* mRNA. Interestingly, homozygous *Gli1* knock-out mice are phenotypically normal, suggesting that *Gli2* expression does not strictly depend on functionally active GLI1 protein. More likely, GLI2 is able to compensate for the lack of active GLI1 protein (Park et al., 2000). Activation of GLI1 in response to GLI2 expression is consistent with the finding that *Gli2* deficient mice express *Gli1* mRNA at reduced levels. Also, *Gli2* expression in mouse epidermis induces the development of BCCs expressing *Gli1* (Ding et al., 1998; Grachtchouk et al., 2000). This data suggest a conserved function of *Gli2* in the regulation of *Gli1* expression, which is cell-type specific or a system dependent effect.

4.4.0 Summary

Regal et al (2002) demonstrated a positive feedback loop between GLI1 and GLI2, which revealed that GLI1 may be a direct target of GLI2. Data described in this chapter from Dr Fritz Abergers' lab shows that GLI2 binds the GLI-binding consensus sequence in the *GLI1* promoter, using band shift and luciferase reporter assays, this suggest that GLI2 directly activates GLI1 (Ikram et al., 2004). In this chapter I have shown that retrovirally expressed GLI2 induces expression of endogenous GLI1 in human primary keratinocytes and *GLI2* is expressed in the interfollicular epidermis and the outer root sheath of hair follicles in normal skin as well as in BCC tumor islands. These results suggest that GLI2 may play an important role in regulating epidermal proliferation and skin tumorigenesis.

4.5.0 Future study

A BCC formation may arise due to activation of GLI1 by inactivating mutations in PTCH followed by the induction of GLI2. Alternatively, activation of SHH-signalling may first lead to the induction of GLI2 expression which directly activates GLI1 expression. This indicates that a feedback loop may be required in the activation and maintenance of BCC formation, which is not active in normal skin due to the absence of GLI1 expression. Thus it is possible that there may be certain unidentified factor(s) or mechanisms that are present in BCC that allow GLI2 to activate GLI1 which may not be present in normal skin. Identification of these factor(s) or the mechanism would be the subject of future research.

CHAPTER 5

FOXE1 Expression in Normal Skin and BCC

5.1.0 Introduction

To identify GLI2-regulated genes, Dr Fritz Abergers' lab expressed GLI2 under the control of a tetracycline inducible promoter in HaCat cells (Regl et al., 2002), and carried out cDNA array analysis on these cells lines. Expression profiling of these samples showed that forkhead transcription factor *FOXE1* was upregulated in GLI2 expressing HaCat cells in a dose dependent manner compared to control cells. (Eichberger et al., 2004). Having shown that *GLI2* was induced in BCC samples compared to normal skin (**Figure 3.6**), this was also confirmed by Dr Fritz Abergers' lab they had also shown that *GLI2* mRNA levels were highly elevated in BCC samples compared to normal skin (Regl et al., 2002). This suggests that *FOXE1* should also be induced in BCC, so Dr Fritz Abergers' lab analyzed BCC samples with upregulated levels of GLI2 and GLI1 (Regl et al., 2002) for *FOXE1* transcripts levels. In all 15 BCC samples tested, *FOXE1* mRNA levels were induced ranging from 4 to 59.2 folds with an average fold increase of 15.8 fold relative to normal skin. Dr Fritz Abergers' lab also observed that *GLI2* and *FOXE1* were expressed at a much higher level in normal skin than *GLI1*. In a Pearson correlation calculated pair wise for *GLI1* verses *FOXE1*, *GLI2* verses *FOXE1* and *GLI1* verses *GLI2* using statistical package (SPSS) programme, they showed that only *FOXE1* verses *GLI2* was significant with the correlation $p < 0.01$ (Eichberger et al., 2004).

5.1.1 Induction of *GLI2* in human keratinocytes increases *FOXE1* mRNA expression.

To identify GLI2-regulated genes, Dr Fritz Abergers' lab expressed GLI2 under the control of a tetracycline inducible promoter in HaCat keratinocytes (Regl et al., 2002), and carried out cDNA array analysis on these cells lines. Expression profiling of samples treated with tetracycline for 24 hours and 72 hours was done on filter arrays containing approximately 2200 human expressed sequence tags (ESTs). The data from the arrays experiments showed that forkhead transcription factor *FOXE1* was upregulated in a GLI2 overexpressing cell lines in a dose dependent manner (5.4 ± 0.94 fold increase after 24hr and a 10 ± 1.15 fold increase after 72hr of tetracycline treatment) compared to control cells (Eichberger et al., 2004).

They also investigated *FOXE1* and the direct target of *GLI1* *PTCH* (as control) expression in primary human keratinocytes transduced with *GLI2* (SIN-*GLI2*-EGFP) or EGFP control (SIN-EGFP) expressing retrovirus, after 72 hours transduction, using real-time-RT-PCR. Similarly to HaCaT-*GLI2*-HIS cells a strong induction of *FOXE1* transcript 16.6 ± 0.3 fold and *PTCH* 19.78 ± 2.45 fold was detected in retrovirally transduced primary keratinocytes expressing *GLI2* (Eichberger et al., 2004).

5.1.2 *FOXE1* is an early target of *GLI2* in human keratinocytes.

Dr Fritz Abergers' lab, then went on to measure the appearance of *FOXE1* and *GLI2* protein simultaneously in a HaCaT-*GLI2*-HIS cells induced for 6hr, 12hr, 24hr and 48hr with tetracycline, and compared the mRNA and protein expression levels relative to untreated controls from the same time points. *GLI2* protein was increased over background expression level after 6hr tetracycline addition and levels further increased with prolonged treatment. Similarly, *FOXE1* transcript levels were elevated 3.42 ± 0.25 fold at 6hr after tetracycline treatment and further increased in a *GLI2* dose-dependent manner (7.17 ± 1.39 fold at 12 hr, 20.61 ± 0.57 fold at 24hr, and 36.9 ± 1.02 fold at 48hr). When they compared the kinetics of *FOXE1* mRNA accumulation to those of the known *GLI* target *PTCH* a similar response was observed, *PTCH* was induced 7.82 ± 0.17 fold at 6hr, 8.15 ± 0.24 fold at 12hr, 23.57 ± 1.1 fold at 24hr and 26.63 ± 2.3 fold at 48hr (Eichberger et al., 2004). From this they concluded, that due to a rapid increase in *FOXE1* mRNA transcription in response to *GLI2*, suggests that *FOXE1* represents an early *GLI2* target gene, which like *PTCH* may be directly regulated by *GLI2* (Eichberger et al., 2004).

Due to the fact that *GLI1* and *GLI2* recognize the same consensus binding sequence and are known to have overlapping functions (Bai and Joyner, 2001), Dr Fritz Abergers' lab went on to compare the induction of *FOXE1* and *PTCH* by *GLI1* and *GLI2* in *GLI1* and *GLI2* tetracycline inducible HaCaT cells relative to un-induced controls. The data from these experiments showed that there was a strong induction of *FOXE1* mRNA levels in response to *GLI2* and a reduced activation of *FOXE1* in HaCaT cells expressing *GLI1*. *PTCH* was upregulated to comparable levels in HaCat cells expressing *GLI1* and *GLI2* (Eichberger et al., 2004). From this they concluded that this indicates that *GLI2* was the main activator of *FOXE1*.

5.1.3 Activation of the *FOXE1* promoter by NHIS-GLI2-(332) by binding GLI consensus sequence in the *FOXE1* promoter.

The next set of experiments Dr Fritz Abergers' lab did was to investigate whether *FOXE1* may be directly regulated by GLI2. Again they analysed the promoter region of *FOXE1*. As the start site for *FOXE1* was not known so they mapped it by 5'-RACE analysis to a 28bp position upstream of the known mRNA (Accession No: NM_004473) 5' end sequence. They also identified five sites differing from the GLI-binding consensus motif GACCACCCA (Kinzler and Vogelstein, 1990b) by 2 nucleotide substitutions (Eichberger et al., 2004). In electrophoretic mobility shift assays they showed that all five sites interacted specifically with recombinant purified GLI2 Zn protein (amino acid 1-332, truncated after the Zn finger DNA binding domain). They also showed in a luciferase reporter gene assay a 2470bp *FOXE1* promoter fragment (from -1934 to + 536 containing all five GLI binding sites) induced transcription activity by 3-fold in the presence of GLI2 compared to controls. The early induction of *FOXE1* transcript by GLI2 and the presence of GLI binding sites in the *FOXE1* promoter, and the activation of the *FOXE1* promoter in a reporter assay, led them to conclude that FOXE1 was likely to be a direct target of the GLI2 in epidermal cells.(Eichberger et al., 2004)

In chapter 4 I determined the localisation of *GLI2* transcript in normal skin and BCC and the fact that Dr Fritz Abergers' lab had shown that *FOXE1* was also upregulated in BCC and was a direct target of GLI2. The aim of the work presented in this chapter was to investigate *FOXE1* localisation in normal skin and BCC samples.

5.2.0 Results

5.2.1 Localization of *FOXE1* in BCC and normal skin.

Dr Fritz Abergers' lab had shown the induction of *FOXE1* in BCC and in GLI2 induced keratinocytes so as a part of this collaboration I went on to investigate the localisation of *FOXE1* in BCC and normal skin. At the time there were no *FOXE1* antibodies available, so in-situ hybridisation analysis was carried out to determine *FOXE1* transcript localisation. In agreement with the results of real-time-RT-PCR (Eichberger et al., 2004) all BCCs screened (n=6) showed intense staining throughout the tumour islands with *FOXE1* anti-sense probe, no specific signal was detected in the surrounding stroma cells. Adjacent sections stained with *FOXE1* sense probes showed no signal, thus indicating specific staining for *FOXE1* (**Figure 5.1** and **Table 5.1**). Our results show that the elevated *FOXE1* transcript level detected with real time RT-PCR in BCC (Eichberger et al., 2004) are specific for the epithelial component of the BCC samples and do not result from expression in surrounding mesenchymal tissue. In interfollicular epidermis *FOXE1* mRNA staining was specific to the basal, suprabasal layers and to the outer root sheath but not in the underlying mesoderm (**Figure 5.2**). Occasionally, staining of mesenchymal cells of the perifollicular connective tissue sheath was observed.

Basal Cell Carcinoma (BCC)

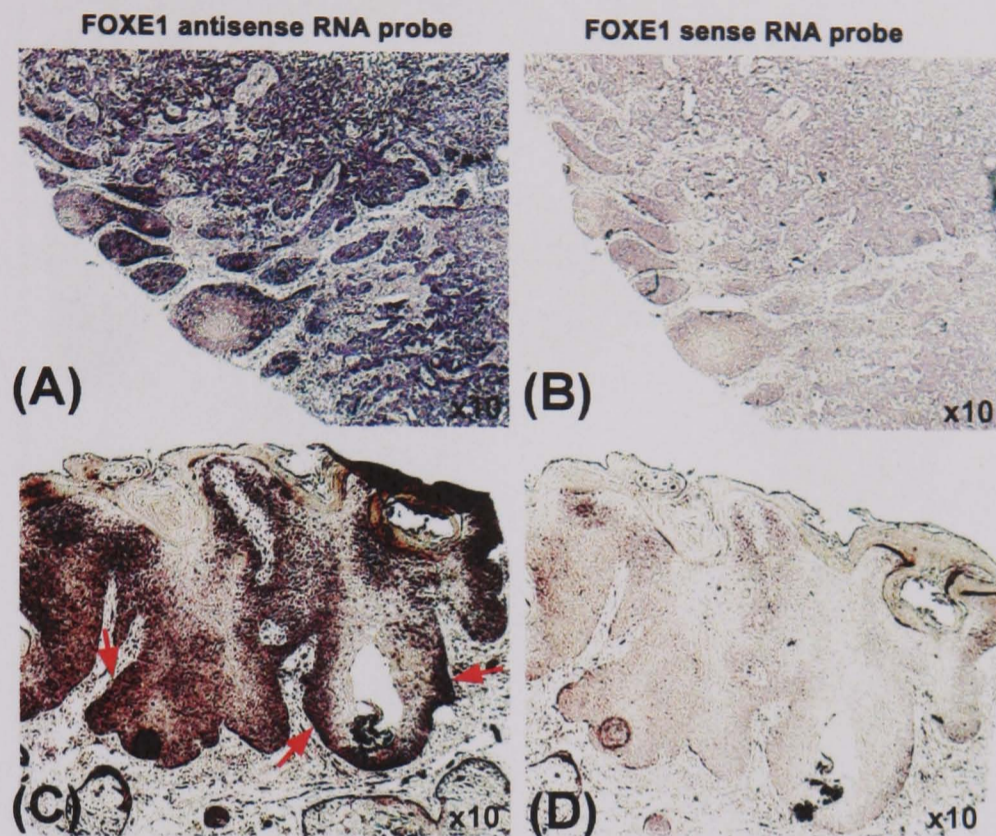


Figure 5.1: *FOXE1* mRNA localisation in BCC frozen sections (using citrate method). A and C, *FOXE1* expression is shown in two representative tumors by in-situ hybridisation. Only BCC tumor islands but not surrounding stroma cells are stained. B and D, Adjacent BCC sections hybridized with sense RNA are negative controls to show the specificity of hybridisation.

Normal skin

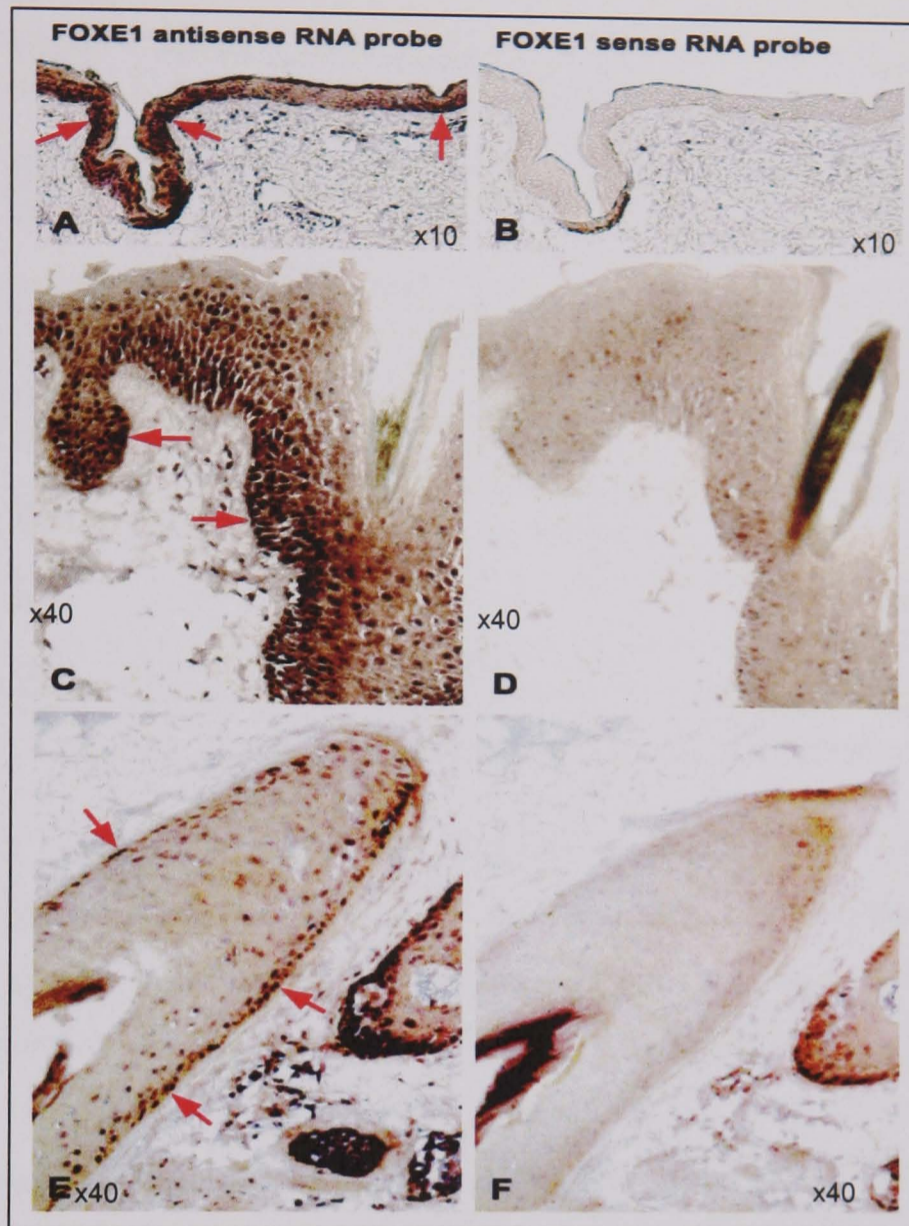


Figure 5.2: *FOXE1* mRNA localisation in normal skin frozen sections (using citrate method). A and C, specific staining for *FOXE1* was observed in basal keratinocytes of normal human epidermis (red arrows). (E) section of a hair follicle showing *FOXE1* transcript is strongly expressed in cells of the outer root sheaths of the hair follicle. B, D and F, adjacent sections were hybridized with a sense RNA probe (control) to demonstrate the specificity of the hybridisation.

Table 5.1: In-situ hybridisation of *FOXE1* mRNA expression in basal cell carcinoma and normal skin

Sample No	Tissue Sample	<i>FOXE1</i> anti sense	<i>FOXE1</i> sense	<i>KRT14</i> Anti-sense	<i>KRT14</i> sense	Comments
2013131	BCC	+++	-	+++	-	
40060649 69	BCC	+++	-	++	-	
M567438	BCC	+++	-	+++	-	Corium strong staining for <i>FOXE1</i>
F455131	BCC	+++	-	+++	-	
M62058	BCC	+++	-	+++	-	
609458	BCC	+	-	-	-	Very patchy most -ve for both probes
291669	BCC	+++	+	+++	-	
35499154	NS	+++	-	++	-	<i>FOXE1</i> Around hair strong compared to epidermis
898921	NS	+++	-	+++	-	
Face lift	NS	++	-	++	-	<i>FOXE1</i> Around hair strong compared to epidermis

Strong *FOXE1* staining was consistently observed in all Basal Cell Carcinoma (BCC) n=8 and normal skin (N/S) n=3 samples examined. A control keratin 14 (*KRT14*) expression was also detected with an antisense probe; this was used to verify the integrity of mRNA. No samples were scored if they failed to show *KRT14* mRNA expression, (+++ strong signal, ++ weak signal, + very weak signal, - no signal). Sections were incubated with \approx 100ng *FOXE1*, T3 (anti sense) and T7 (sense) probe and washed at 55°C, final wash at 60°C and 100ng *KRT14*, T7 (anti sense) and SP6 (sense) probe washed at 50°C and final wash at 55°C.

5.3.0 Discussion

In a search for potential downstream mediators of GLI2 function in epidermal cells a new GLI2 target gene *FOXE1* was identified (by Dr Fritz Abergers' lab), which was induced in response to GLI2 by binding GLI putative binding to GLI binding motif in the *FOXE1* promoter region (Eichberger et al., 2004). In this chapter I have shown the localisation of *FOXE1* transcript which overlaps with *GLI2* expression (shown in chapter 4) in human hair follicles, epidermis and BCC (**Figure 5.1 and Figure 5.2**). This suggests a possible role of FOXE1 in epidermal development and carcinogenesis downstream of HH/GLI signalling. It is not clear if expression of FOXE1 in interfollicular epidermis is dependent on HH-signalling, whereas expression of HH targets such as GLI1 and PTCH is mainly defined to follicular regions of the skin (Chiang et al., 1999b; Ghali et al., 1999; Wang et al., 2000b). During formation of the ventroposterior mesoderm in *Xenopus*, *Gli2* expression is induced by fibroblast growth factor (FGF) rather than HH-signalling (Brewster et al., 2000). Therefore, it is possible that co-localisation of *FOXE1* and *GLI2* in interfollicular epidermis may be controlled by signals other than HH.

FOXE1 belongs to a large family of transcription factors which are characterised by their DNA-binding domain, the forkhead/winged-helix motif. FOXE1 is also named as FKHL15/TTF2. The mechanism of FOXE1 action *in vitro* studies indicates that FOXE1 acts as a transcriptional repressor (Perrone et al., 2000; Zannini et al., 1997). Forkhead proteins have been shown to be involved in variety of biological processes ranging from embryonic development to regulation of cell growth and proliferation in adult tissues (Carlsson and Mahlapuu, 2002; Kaufmann and Knochel, 1996). Expression of several mammalian forkhead genes has been shown to be controlled by the HH/GLI signalling pathway: *Foxa2* (*HNF-3 β*) is expressed in the floor plate of the notochord; its transcriptional activity is directly regulated by GLI1 (Sasaki et al., 1997). *Foxc2* (*Mfh1*) and *Foxd2* (*FREAC-9/Mf2*) are both involved in sclerotome cell proliferation (Furumoto et al., 1999; Wu et al., 1998). *Foxf1* (*FREAC-1/HFH-8*) is involved in lung and foregut mesenchyme development (Mahlapuu et al., 2001), and FOXM1 (*Trident/HFH-11/INS1*) is induced in human BCC (Teh et al., 2002).

FOXE1 was originally isolated from keratinocytes (Chadwick et al., 1997), its role in epidermal development and homeostasis is not understood. FOXE1 TTF2 function has

primarily been investigated in the context of thyroid development (Castanet et al., 2002; Clifton-Bligh et al., 1998; Damante et al., 2001; De Felice et al., 1998; Zannini et al., 1997). Mice lacking both copies of *foxe1* suffer from neonatal hypothyroidism characterized by a sublingual small ectopic or completely missing thyroid gland and cleft palate (De Felice et al., 1998). Patients with Bamforth syndrome, who are heterozygous for *FOXE1*, display in addition to thyroid agenesis a spiky hair phenotype (Castanet et al., 2002; Clifton-Bligh et al., 1998). A corresponding hair phenotype is not observed in *Foxe1*^{-/-} mice due to the fact that they die before hair formation (De Felice et al., 1998). However, expression of *Foxe1* is observed in embryonic whiskers of wild type mice (Dathan et al., 2002), this and the spiky hair phenotype of Bamforth patients points to a role of *Foxe1* in hair follicle development where *Gli2* is essential (Mill et al., 2003b).

The origin of BCC has been under debate for a very long time. While earlier evidence favoured basal keratinocytes of the interfollicular epidermis, more recent data points to the specialised cells within the hair follicle, analysis of the biomarkers in BCC suggest that the tumour is derived from the cells of the outer root sheath (ORS) (Kruger et al., 1999; Kurzen et al., 2001). Given the fact that GLI2, FOXE1 and GLI1 are present in the ORS and are found at high levels in BCC, a possible scenario for BCC development may be that constitutive activation of HH-signalling in the ORS distorts differentiation and promotes proliferation eventually leading to tumour formation.

5.4.0 Summary

In this chapter a collaborate work with Dr Fritz Abergers' lab has shown that *FOXE1* is a novel GLI2 target gene that is induced in human keratinocytes and I have shown localisation of *FOXE1* in interfollicular epidermis that is specific to the basal, super basal layers and to the outer root sheath but not in the underlying mesoderm in normal skin (**Figure 5.2**). In BCC *FOXE1* is localised throughout the tumour islands (**Figure 5.1**).

5.5.0 Future study

Having characterized *FOXE1* as a novel GLI2 target gene in human keratinocytes, and given the critical role of GLI2 in proliferation of hair follicle cells and tumorigenesis. Co-expression of FOXE1 and GLI2 in normal skin and BCC suggests that FOXE1 may be involved in mediating the proliferative effect of GLI2 *in-vivo*. Functional investigation of FOXE1 in epidermal development and disease will thus be a major aim of future studies to shed new light on the molecular mechanisms downstream of the HH/GLI signalling pathway.

CHAPTER 6

Effects of EGF on Pattern of Gene Expression in GLI1 expressing Keratinocytes

6.1.0 Introduction

An interesting observation was made by Dr Graham Neill in the Centre for Cutaneous Research laboratory when he cultured primary keratinocytes over expressing GLI1 in the presence of growth supplement in a defined growth medium, he noticed that these cells had a changed morphology, from rounded cells to spindly phenotype, and the colonies were more spread compared with (control cells) tightly packed EGFP primary keratinocyte colonies. Dr Neill identified that EGF (Epidermal Growth Factor) in the defined growth medium was causing this morphological change. It was hypothesised that the change in cell morphology may have been due to cells undergoing epithelial-mesenchymal transformation (EMT), where cells undergo a development change from an epithelial phenotype to a highly motile fibroblast-like or mesenchymal phenotype. EMT plays a central role during embryonic development, as well as in cancer progression (Balkwill, 2004; Grunert et al., 2003; Kalluri and Neilson, 2003; Nawshad et al., 2004; Thiery, 2002; Thiery, 2003). GLI1 is also expressed in brain tumour (Glioblastoma) (Kinzler et al., 1987) and neuronal cells have a spindly morphology thus it is possible that these cells may be undergoing epithelial to neuronal differentiation. The other possibility is that these cells are not transforming but are undergoing differentiation which may be causing a change in morphology.

To investigate these hypotheses I identified from a literature search markers for EMT (Vimentin, Snail, Snail2 and Alpha-Sma) (Barrallo-Gimeno and Nieto, 2005; Huber et al., 2005; Lee et al., 2006; Radisky, 2005), neuronal markers, Nucleostemin, Nestin and kinesin superfamily protein 4 (KIF4) (Dahlstrand et al., 1992; Kafienah et al., 2006; Lendahl et al., 1990; Nagle, 1988; Schwartz et al., 2005; Sekine et al., 1994; Tsai and McKay, 2002; Wislet-Gendebien et al., 2004), keratinocyte differentiation markers, involucrin, loricrin and keratin K10 (Fuchs and Green, 1980; Ghahary et al., 2001; Hohl, 1993; Hohl et al., 1991; Leigh et al., 1993), basal keratinocytes markers keratin K5 and keratin K14 (Fuchs and Green, 1980), simple epithelial markers keratin K8 and keratin K18 (Eckert, 1988; Moll et al., 1990; Moll et al., 1993), keratinocyte stem cell markers keratin K15 and keratin K19 (Lyle et al., 1998a; Michel et al., 1996b) and keratinocyte activation marker keratin K17 (Freedberg et al., 2001). In order to understand the interaction between the EGF and the HH-signalling pathway I also compared the expression of HH signalling markers GLI1, GLI2, SMO and PTCH (Villavicencio et al., 2000).

The actin cytoskeleton is highly flexible structure that undergoes both transient and permanent changes in the course of normal development and in response to extracellular signals. Remodeling of the actin cytoskeleton is involved in cell division, growth, adhesion, and locomotion. This rearrangement of the actin cytoskeleton is highly influenced by the activity of Rho family GTPases (Etienne-Manneville and Hall, 2002; Hall and Nobes, 2000). Rho GTPases are molecular switches that cycle between two conformational states: a GTP-bound (active) state and a GDP-bound (inactive) state to control intercellular signaling. The transition between these two conformations is tightly regulated by three classes of proteins; 1) GTPase activating proteins (GAPs) stimulate the intrinsic GTPase activity, thereby pushing the switch towards the inactive state. 2) Guanine nucleotide dissociation inhibitors (GDIs) keep the GTPase in the GDP bound inactive conformation. 3) Guanine nucleotide exchange factors (GEFs) which facilitate the exchange of GDP for GTP, thus activating RhoGTPases (Etienne-Manneville and Hall, 2002; Hall, 1998). One well-studied family of GEFs for Rho GTPases is the VAV family of proteins. VAV1 was the first member isolated in hematopoietic cells and is primarily expressed in hematopoietic lineages, while other mammalian VAV proteins VAV2 is ubiquitously expressed and VAV3 has a broad but different expression profile compared to that of VAV2 (Bustelo, 1996; Bustelo, 2000; Katzav et al., 1995; Schuebel et al., 1996; Trenkle et al., 2000). Due to VAV family of proteins involvement in cytoskeleton remodelling and our attempts to understand the molecular mechanism that may be leading to the spindly phenotype of over expressing GLI1 primary keratinocytes cultured with EGF (observed in **section 6.2.1**). I decided to verify Asymetrix data for VAV3 protein only and not the remaining genes identified in the Affymetrix data.

The aim of this study was to investigate differentially expressed genes in GLI1-primary keratinocytes cultured without growth supplement (GLI1-GS) and with EGF (GLI1+EGF) and in EGFP-primary keratinocytes cultured with EGF (EGFP+EGF) relative to control EGFP-primary keratinocytes cultured without growth supplements (EGFP-GS), using real-time RT-PCR and Affymetrix analyses.

6.2.0 Materials and Methods.

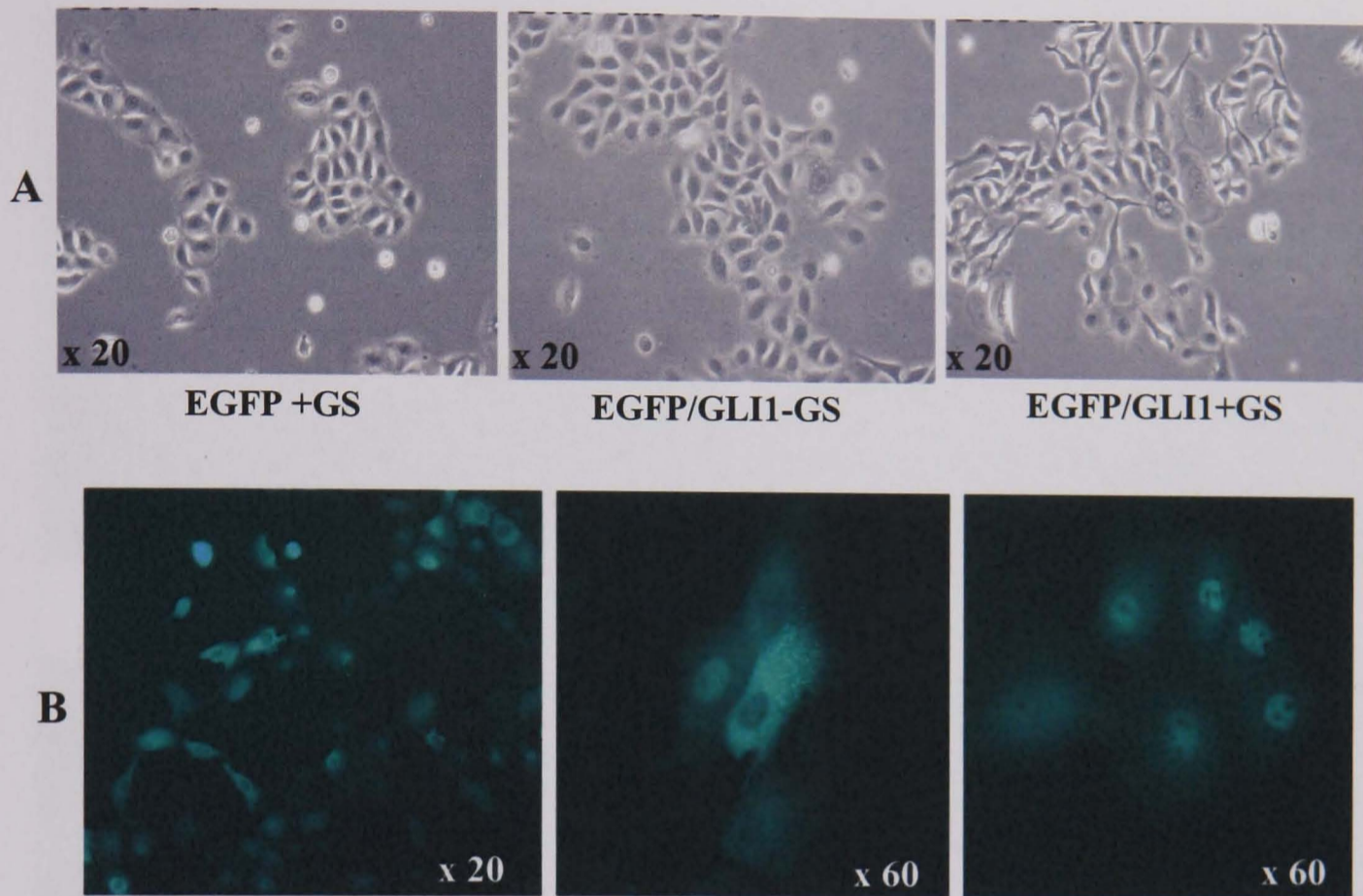
For more detailed methods and materials see chapter 2, here is a briefly summary of methods and materials. Primary keratinocytes and immortalised N-TERT keratinocytes were seeded at 1×10^5 cells per well in 6-well plates with growth supplements (GS) in defined keratinocyte culture medium (Cat No 10744-019 Invitrogen) and incubated at 37°C in 10% CO_2 90% air (v/v) for 16-18 h. Primary keratinocytes cells were then transduced with retroviral particles encoding SIN-EGFP-GLI1 (GLI1), SIN-EGFP (EGFP), SIN-EGFP-GLI1-muted Nuclear Localisation Signal (GLI1-mNLS) and SIN-EGFP-GLI1-muted Nuclear Export Signal (GLI1-mNES) in triplicates per plate. The immortalised N-TERT keratinocytes were also transduced with GLI1, EGFP and GLI1-mNLS in triplicates. Post-transduction, cells were incubated for 24 h with GS and then for another 24 h without GS. After 48 h, the media was replaced with 10 ng/ml EGF (Cat No E 9644 Sigma) and without growth supplement (-GS) media and incubated at 37°C in 10% CO_2 90% air (v/v) for 24 h. EGFP and change in cell morphology was visualised using a light microscope. From one set of 6 well plates for EGF and -GS total RNA was extracted for gene expression analysis, from a sec set of 6 well plates for EGF and -GS cell lysate was harvested for western blot analysis.

6.3.0 Results

6.3.1 Cell morphology of GLI1-primary keratinocytes changes in presence of EGF.

GLI1-primary keratinocytes cultured in the presence of growth supplement in defined growth medium have a changed morphology from rounded cell to spindly phenotype and the colonies were more spread compared to control cells (EGFP-primary keratinocytes cultured with growth supplement and GLI1-primary keratinocyte cultured without growth supplement) **Figure 6.1 A**. Growth supplement contains certain growth factors to maintain cell growth, so we investigated the effects of Epidermal Growth Factor (EGF) on GLI1 and EGFP transduced primary keratinocytes. When GLI1 primary keratinocytes were cultured with EGF we observed the same phenotype change as with growth supplement in GLI1-primary keratinocytes and in EGFP-primary keratinocytes (control cells) **Figure 6.1 and Figure 6.2**. Fluorescence microscopy also showed that when GLI1-primary keratinocytes were exposed to EGF, GLI1 was predominantly located in the cytoplasm as opposed to the nucleus (**Figure 6.1**). It was also observed that when EGF growth factor was depleted the cell morphology of these cells reverted to that of control cells. These results indicated that in the presence of EGF changes the morphology of primary keratinocytes and the localisation of GLI1 from nucleus to the cytoplasm may be the mechanism EGF is using to control transcriptional activity of GLI1 in primary keratinocytes.

GLI1-mNLS-primary keratinocytes cultured with EGF showed localisation of GLI1-mNLS was predominantly in the cytoplasm and the morphology of these cells was rounded (**Figure 6.3**) and the same as that of EGFP-primary keratinocytes cultured with EGF (**Figure 6.2**). Primary keratinocytes transduced with GLI1-mNES showed the expression of GLI1-mNES was mainly in the nucleus and the phenotype of these cells was spindly (**Figure 6.3**) and the same as that for GLI1-primary keratinocytes cultured with EGF (**Figure 6.2**). GLI1 transcription factor was expected to be active in the nucleus and these results indicate that nuclear localisation of GLI1 plays an important part in changing the phenotype of GLI1-primary keratinocytes in presence of EGF.



EGFP/GLI1 localisation in primary keratinocytes -GS

Figure 6.1: Change in EGFP-GLI1-primary keratinocyte cell morphology when cultured with growth supplement. (A right) shows the change in EGFP-GLI1-primary keratinocyte cell morphology to spindly cells with spread colonies when cultured with growth supplement (EGFP/GLI1+GS). The control cells (A left) EGFP-primary keratinocytes cultured with growth supplement and (A middle) EGFP/GLI1-primary keratinocytes cultured without growth supplements (EGFP/GLI1-GS) have rounded cell morphology with packed colonies. This indicates that GLI1 causes a change in cell morphology of primary keratinocyte in presence of growth supplement. B left showing the localisation of EGFP/GLI1 in primary keratinocytes cultured without growth supplement is nuclear and cytoplasmic and (B) middle showing cytoplasmic localisation of EGFP/GLI1 is punctate and B right shows nuclear expression of EGFP/GLI.

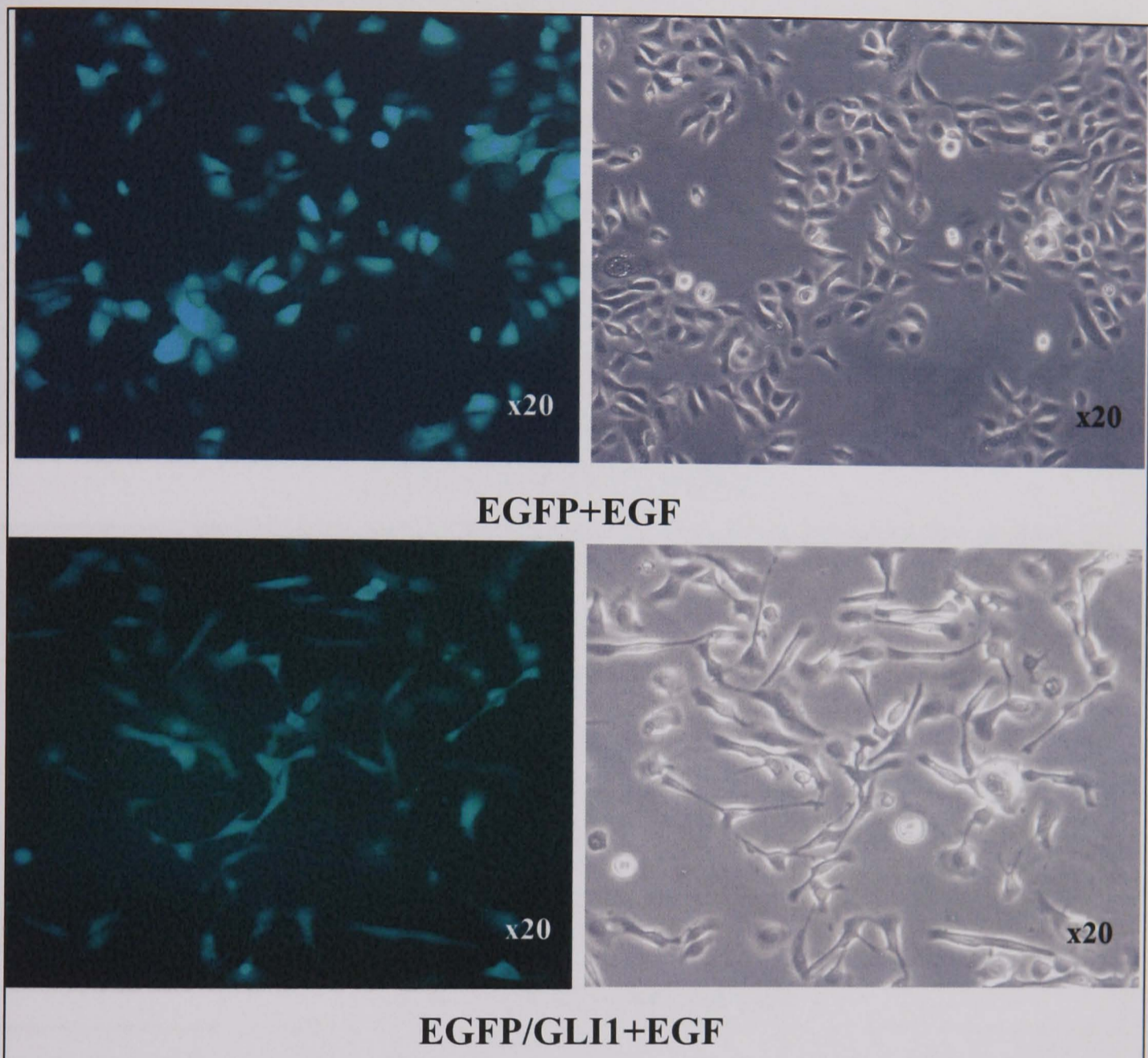


Figure 6.2: Expression of EGFP/GLI1 in primary keratinocytes cultured with EGF and the change in cell morphology of these cells. Top left shows the expression of EGFP in EGFP-primary keratinocytes cultured with epidermal growth factor (EGF) right shows the morphology of these cells is rounded and colonies are compact. Bottom left shows expression appeared to be diffused through out the cell of EGFP/GLI1 in EGFP/GLI1-primary keratinocytes cultured with EGF. Bottom right shows a change in EGFP/GLI1-primary keratinocytes morphology from round to spindly and the colonies are more spread when cultured with EGF. This suggests that GLI1 with EGF is causing a morphological change in primary keratinocytes.

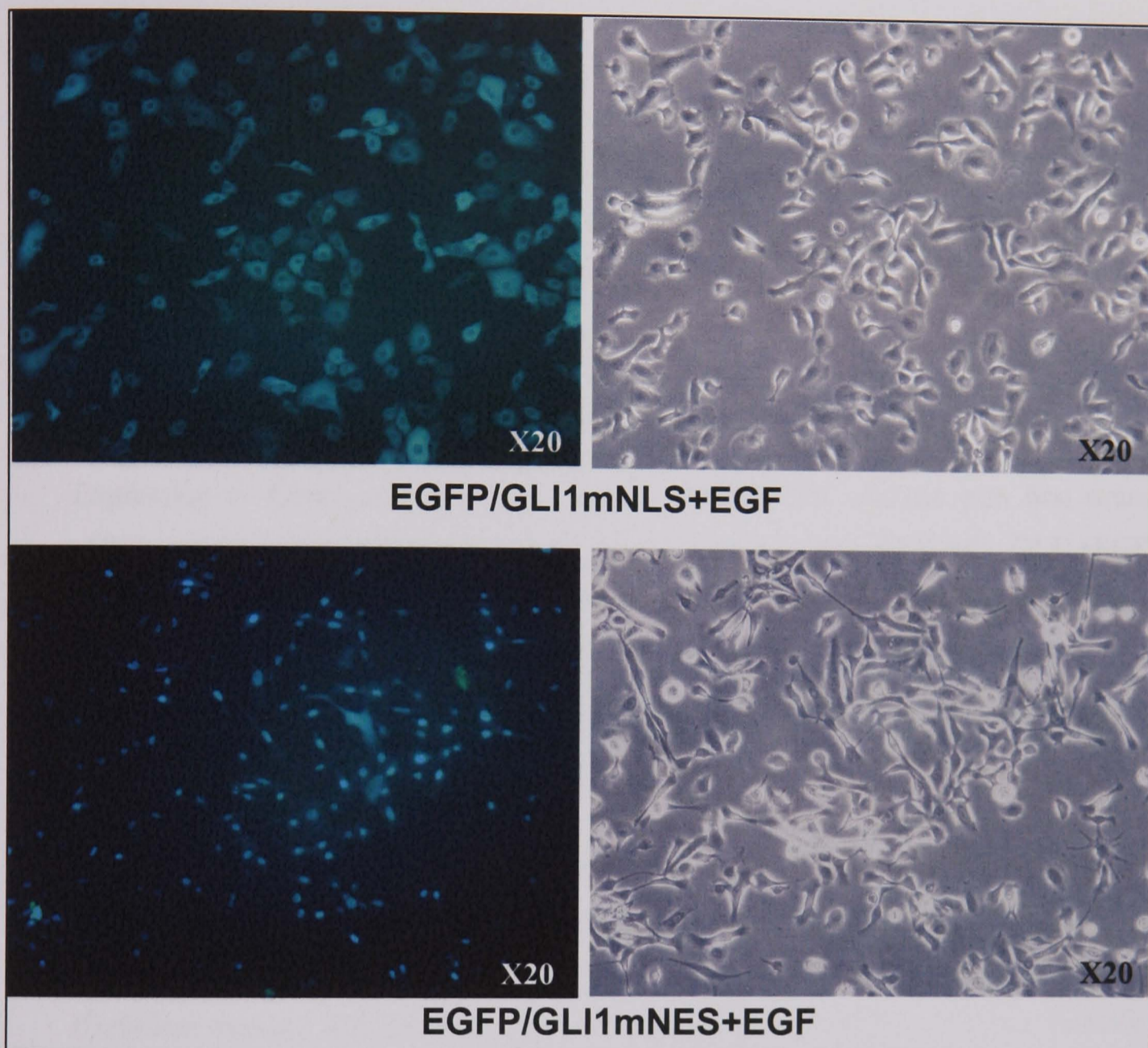


Figure 6.3: Expression of EGFP/GLI1 that has mutated Nuclear Localisation Signal (EGFP/GLI1mNLS) in primary keratinocytes cultured with EGF. Top left shows the expression EGFP/GLI1 that has mutated Nuclear Localisation Signal (EGFP/GLI1mNLS) is cytoplasmic in EGFP/GLI1mNLS-primary keratinocytes cultured with epidermal growth factor (EGF), top right shows that the morphology of these cells is rounded. Bottom left shows that the expression of EGFP/GLI1 that has a mutated Nuclear Export Signal (EGFP/GLI1mNES) is in the nucleus in EGFP/GLI1mNES -primary keratinocytes cultured with EGF, bottom right shows that the morphology of these cells is spindly. This indicates that localisation of GLI1 to the nucleus is required in order to change the phenotype of primary keratinocytes that are expressing GLI1 in the presence of EGF from rounded to spindly.

6.3.2 Determining the expression of hedgehog, keratinocyte differentiation, mesenchymal, and stem cell markers in GLI1-primary keratinocytes cultured with EGF.

In order to understand the interaction between GLI1 and EGF and determine the cause of morphology change observed in **section 6.2.1** in GLI1-primary keratinocytes cultured with EGF. The following gene primers were designed; Vimentin, Snail1, Snail2 and Alpha-Sma (markers for epithelial-mesenchymal-transition [EMT]), Nestin, Nucleostemin Kinesin superfamily protein 4 (*KIF4*) (markers for Neuronal cells), Involucrin, Loricin and *KRT10* (markers for kartinocyte differentiation), *KRT14* and *KRT5* (markers for basal keratinocyte), *KRT8* and *KRT19* (simple epithelial markers), *KRT15* and *KRT19* (keratinocyte stem cell markers); *KRT17* (keratinocyte activation marker), *GLI1*, *GLI2*, *SMO* and *PTCH* (HH-signalling markers) and β -Actin. Expression of these genes was investigated using RT-PCR analysis with first strand cDNA reaction synthesised from total RNA extracted from GLI1-GS, GLI1+EGF, EGFP+EGF and EGFP-GS primary keratinocytes. PCR products generated from these set of primers were run on 1% (w/v) agarose and, the gel was analysed under UV. A control PCR reaction was also set up with genomic DNA and the results tabulated (**Table 6.1**).

The primers that did not generate any PCR product from genomic DNA and cDNA (even after changing template concentration, annealing temperature and magnesium concentrations of PCR reaction) were Snail1 (mesenchymal marker), Nucleostemin (Neuronal marker), *KRT10* **Table 6.1**. The reason these primers did not show any PCR products may have been due to the fact that these genes were not expressed in these cells, it is also possible that these primers may have been of poor quality or design and thus they did not work. PCR product expected from the genomic DNA was same size as that from cDNA or of larger size if the primers span the intron exon boundaries and if intron was greater then 3-5 kb we may not have generated a PCR product from these sets of primers due to large size of the product. For Nestin there was a PCR product from the genomic DNA but no product from the cDNA and negative control sample (cDNA reaction set up with out reverse transcriptase [-RT]) **Table 6.1**. This indicates that the primers for Nestin worked but the Nestin was not expressed in these cells. As I had designed several primers for EMT, neuronal differentiation, neuronal, keratinocyte differentiation, basal keratinocyte, simple epithelial, keratinocyte stem cell and HH-

signalling genes, the primers that did not work were not redesigned. There were no PCR products observed for any of the primer sets used in the negative –RT control samples (**Table 6.1**).

RT-PCR data indicates that Snail2, Vimentin, Alpha-Sma, *KRT15*, Involucrin, Loricrin, *KRT14*, *KRT8*, *KRT19*, *KRT17*, *PTCH*, *SMO*, *GLI2* and *GLI3* and Beta-Actin (control) were all expressed in GLI1-GS, GLI1+EGF, EGFP-GS and EGFP+EGF primary keratinocytes. *GLI1* was only expressed in GLI1-GS and GLI1+EGF primary keratinocytes (**Table 6.1**). Loricrin seems to have been expressed at lower levels in EGFP+EGF and GLI1+EGF primary keratinocytes indicated by weak loricrin bands observed in these cell lanes compared with EGFP-GS and GLI1-GS primary keratinocytes lanes whereas, Beta-Actin bands were of equal intensity in all these cell lanes (**Table 6.1**). This suggests that loricrin may be repressed in presence of EGF in GLI1 and EGFP (control) primary keratinocytes. *KRT5* primer set generated multiple bands as well as the expected band, this suggests that these primers may be amplifying some other transcripts, due to this further analysis of *KRT5* expression was not determined in these cell lines. To determine if the genes identified by RT-PCR analysis were up or down regulated relative to control cells a relative quantification analysis was carried out using real-time RT-PCR.

Table 6.1: PCR products amplified from cDNA from GLI1 and EGFP (control) transduced primary keratinocyte cultured without growth supplement (-GS) and with EGF (+EGF) using different primer sets for each gene and the biological function of each marker gene. The intensity of the bands for each PCR product was scored as follows +++ = strong band, ++ = weak band, - = no PCR product and m = multiple bands observed on a 1% agarose gel. The transcripts analysed were expressed in all cells except for *KRT10*, *KRT15*, Nucleostemin, Nestin and Snail1. Loricrin expression may have been reduced by EGF as indicated by low intensity bands observed in GLI1 and EGFP keratinocytes cultured with EGF.

Primers for	Biological marker the gene was used for	cDNA samples				Genomic DNA	-ve control -RT
		GLI1 -GS	GLI1 +EGF	EGFP -GS	EGFP +EGF		
PTCH	Hedgehog signalling	+++	+++	+++	+++	+++	-
SMO	Hedgehog signalling	+++	+++	+++	+++	+++	-
GLI1	Hedgehog signalling	+++	+++	-	-	+++	-
GLI2	Hedgehog signalling	+++	+++	+++	+++	+++	-
GLI3	Hedgehog signalling	+++	+++	+++	+++	+++	-
Keratin 14	Basal Keratinocyte (and expressed in BCC)	+++	+++	+++	+++	+++	-
Keratin 5	Basal Keratinocyte (and expressed in BCC)	+++ (m)	+++ (m)	+++	+++	+++ (m)	-
Keratin 17	keratinocyte activation (and expressed in BCC)	+++	+++	+++	+++	+++	-
Keratin 19	Simple epithelial	+++	+++	+++	+++	+++	-
Keratin 8	Simple epithelial	+++	+++	+++	+++	+++	-
Involucrin	Keratinocyte differentiation marker	+++	+++	+++	+++	+++	-
Loricrin	Keratinocyte differentiation marker	+++	++	+++	++	+++	-
Keratin 10	Keratinocyte differentiation marker (and expressed in BCC)	-	-	-	-	-	-
Keratin 15	Stem cell marker	+++	+++	+++	+++	+++	-
Nucleostemin	Stem cell in central nervous system	-	-	-	-	-	-
Nestin	Neuroepithelial stem cells	-	-	-	-	+++	-
KIF4	Kinesin superfamily protein 4 (KIF4) expressed in differentiated neurons	+++	+++	+++	+++	+++	-
Vimentin	Mesenchymal marker	+++	+++	+++	+++	+++	-
Snail1	Mesenchymal marker. A transcriptional repressor that down regulates E-cadherin.	-	-	-	-	-	-
Snail2 (Slug)	Mesenchymal marker. A transcriptional repressor that down regulates E-cadherin.	+++	+++	+++	+++	+++	-
Alpha -Sma	Structural marker: Expressed in mesenchymal cells.	+++	+++	+++	+++	+++	-
B-Actin	Structural marker	+++	+++	+++	+++	+++	-

6.3.3 EGF reduces *PTCH*, *GLI2* and *SMO* expression and restores *GLI3* expression to control levels whereas *GLI1* represses *GLI3* expression.

Real Time RT-PCR analysis was carried out using HH gene specific primers described in section 6.3.2 and using the SYBR green kit and first strand cDNA reaction from GLI1-GS, GLI1+EGF, EGFP+EGF and control EGFP-GS samples. The fold induction or repression for each gene was calculated relative to EGFP-GS. The base line expression value for each gene analysed in control cells (EGFP-GS) was 1. Therefore, values above 1 indicate induction in expression and values below 1 indicate repression (Table 6.2). The fold induction or repression data was plotted using log₂ scale and a graphical representation of this is shown in Figure 6.4.

GLI1 expression was induced in GLI1-GS and GLI1+EGF cells and there was very little difference in expression of *GLI1* in these cell lines. There was no *GLI1* expression observed in EGFP+EGF and control EGFP-GS cells (Figure 6.4). This indicates that in presence of EGF there seems to be no change in *GLI1* expression in GLI1 expressing primary keratinocytes. *GLI2* and *PTCH* expression was induced in GLI1-GS and repressed in GLI1+EGF cells (Figure 6.4). There was no change in *SMO* expression in GLI1-GS and in GLI1+EGF cells *SMO* expression was reduced relative to control cells (EGFP-GS) (Figure 6.4). *GLI3* expression was reduced in GLI1-GS cells and in GLI1+EGF cells *GLI3* levels were similar to those of control cells (Figure 6.4). There was a small induction in *GLI2* expression. However, *GLI3*, *PTCH*, *SMO* expression was reduced in EGFP+EGF primary keratinocytes relative to controls cells (Figure 6.4). *SMO* repression in presence of both GLI1 and EGF was less than that for EGF on its own (Figure 6.4). *GLI3* expression was reduced by GLI1 and EGF and when both were present the levels appears to revert back to control levels (Figure 6.4). These results suggest that EGF pathway interacts with HH signalling pathway and represses expression of *GLI2* and *PTCH* genes that are targets of GLI1 (Agren et al., 2004; Marigo et al., 1996b; Regl et al., 2002; Toftgard, 2000). The data also suggest that EGF may be reducing the expression of *SMO*, that is an activator, and inducing *GLI3*, that is repressor (Murone et al., 1999; von Mering and Basler, 1999) of HH pathway in order to regulate this pathway.

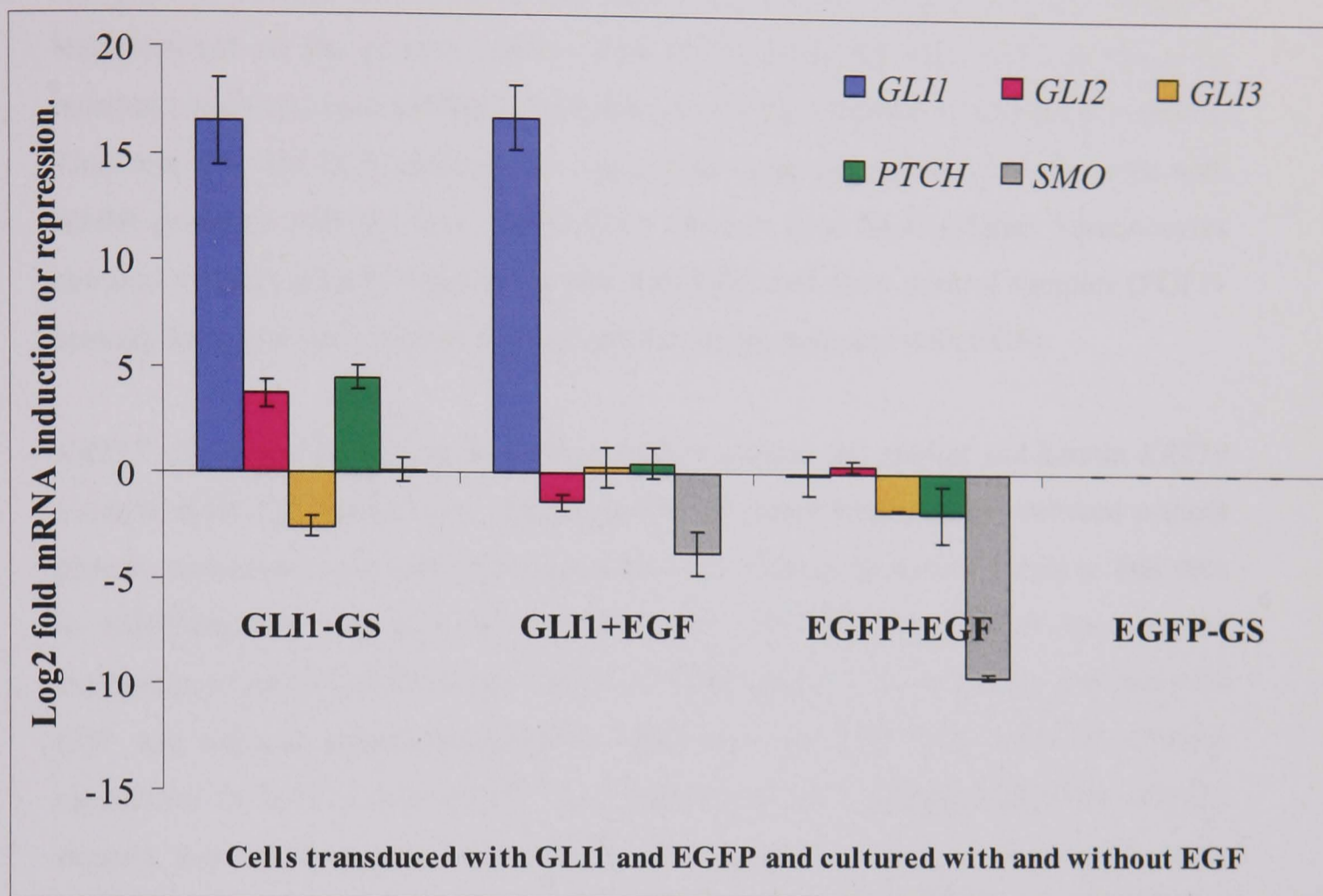


Figure 6.4: Real-time RT-PCR analysis showing induction or repression of *GLI1*, *GLI2*, *GLI3*, Patched (*PTCH*) and Smoothend (*SMO*) in GLI1, EGFP transduced primary keratinocytes cultured without growth supplement (-GS) and with epidermal growth factor. (+EGF) relative to control cells (EGFP primary keratinocytes cultured without growth supplement [EGFP-GS]).

6.3.4. GLI1 induces expression of *KRT17*, *KRT14*, *KRT19* and repress the expression of *KIF4*, whereas EGF reduces this induction and repression.

The primers that had worked in section 6.2.2 were used in real-time RT-PCR analysis. However, not all the primers worked with SYBR green kit, even after changing the reaction conditions such as MgCl₂, template, annealing temperature and cycle numbers. Thus real-time RT-PCR analysis was carried out using the primers that did work with SYBR green kit with the first strand cDNA reaction from GLI1-primary keratinocytes cultured without growth supplement and with EGF and from control samples (EGFP-primary keratinocytes cultured without growth supplement and with EGF).

KRT17 a keratinocyte activation marker, *KRT14* a basal cell marker and keratin *KRT19* a simple epithelial marker were induced in GLI1-primary keratinocytes cultured without growth supplement and with EGF expression was reduced to similar levels to that seen in EGFP-primary keratinocytes cultured with EGF (**Figure 6.5**). If we compare expression of *KRT17*, *KRT14* and *KRT19* in EGFP-primary keratinocytes cultured with EGF and without growth supplement, expression of *KRT17* was reduced, whereas expression of *KRT14* and *KRT19* was induced by EGF (**Figure 6.5**). These results suggest that GLI1 may be activating keratinocytes and inducing basal and simple epithelia markers and EGF reduces these to that of control cells (EGFP-primary keratinocytes cultured with EGF).

Expression of kinesin superfamily protein 4 (*KIF4*) was reduced in GLI1-primary keratinocytes cultured without growth supplement and when EGF was added there was no change in expression of *KIF4*. The reduction in expression of *KIF4* was less in EGFP-primary keratinocytes cultured with EGF compared to that of GLI1-primary keratinocytes cultured without or with EGF (**Figure 6.5**). Thus both GLI1 and EGF alone repress expression of *KIF4*. However, EGF repression is less than that seen for GLI1 and GLI1 plus EGF.

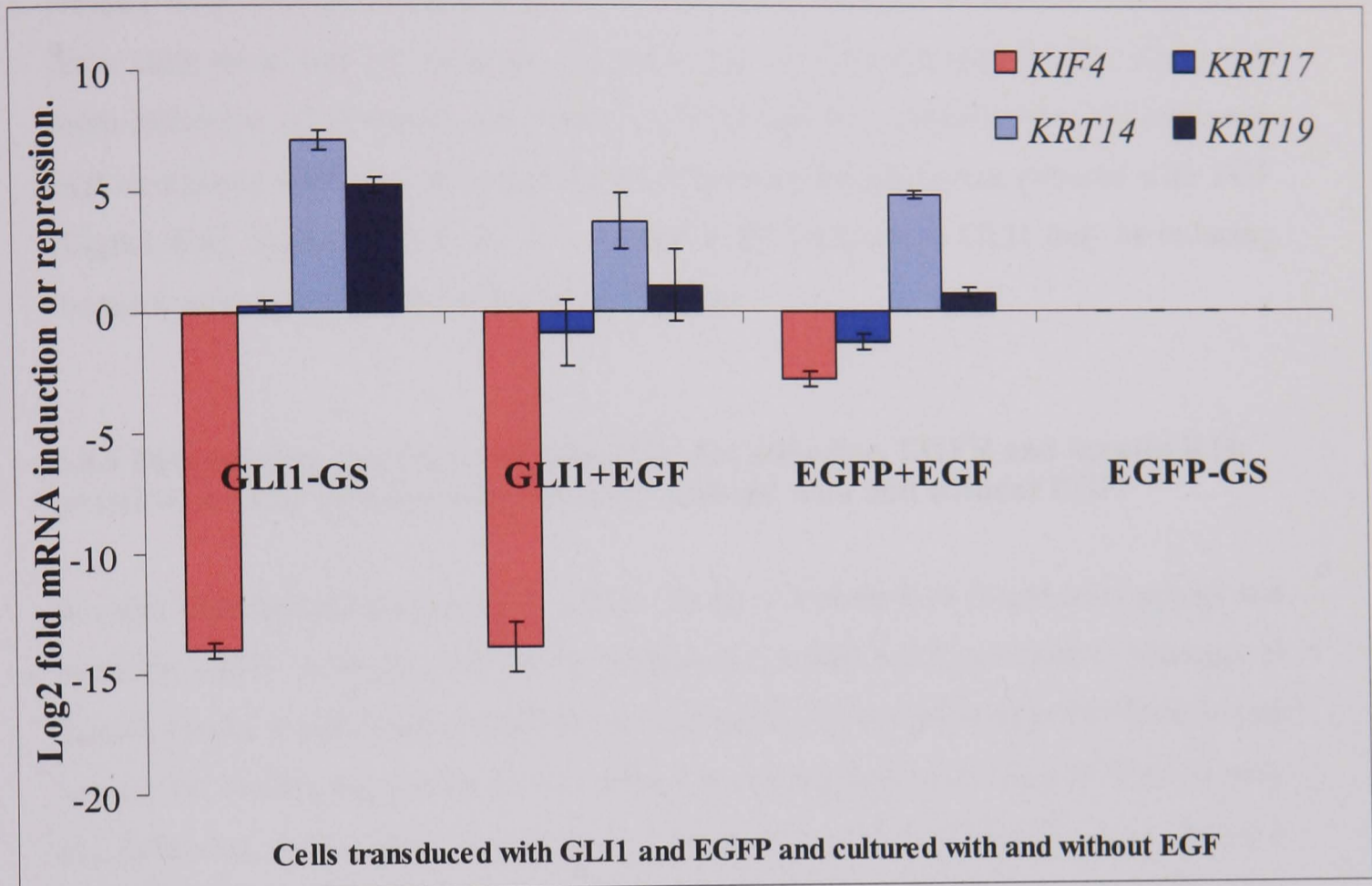


Figure 6.5: Real-time RT-PCR analysis showing induction or repression of keratins *KRT14*, *KRT17*, *KRT19* and kinesin superfamily protein 4 (*KIF4*) in GLI1, EGFP transduced primary keratinocytes cultured without growth supplement (-GS) and with epidermal growth factor (+EGF) relative to control EGFP primary keratinocytes cultured without growth supplement [EGFP-GS]) cells.

6.3.5. GLI1 represses and EGF induces expression of Vimentin and Snail2 transcripts.

Expression of Vimentin and Snail2 mesenchymal markers was reduced in GLI1-primary keratinocytes cultured without growth supplement and when EGF was added to these cells there was an induction in expression of Vimentin and Snail2. There was more induction of Vimentin and Snail2 in EGFP-primary keratinocytes cultured with EGF compared with that observed for GLI1-primary keratinocytes cultured with EGF (**Figure 6.6**). Therefore EGF on its own and in the presence of GLI1 may be inducing mesenchymal transition in primary keratinocytes.

6.3.6 Determining expression of Vimentin, E-Cadherin, EGFR and keratin K14 proteins in GLI1 primary keratinocytes cultured with and without EGF.

In order to determine if changes in mRNA levels of keratin K14 (basal cell marker) and vimentin (EMT marker) observed in **section 6.2.4 and 6.6.5** correlate to changes in protein levels, a western blot analysis was carried out using antibodies for vimentin and keratin 14. Protein expression of E-Cadherin is downregulated in classical EMT (Lee et al., 2006; Lu et al., 2003; Strizzi et al., 2004) and epidermal growth factor receptor (EGFR) which is down regulated upon EGF stimulation (Groves et al., 1992; Nazmi et al., 1990) was also determined in GLI1- and EGFP-primary keratinocytes culture with EGF and without growth supplement.

Vimentin was only expressed in EGFP+EGF lane, E-Cadherin and K14 were expressed in all cell lanes. EGFR was expressed in all cell lanes. However, its levels were reduced in EGFP+EGF lane and further reduced in EGFP-GLI1+EGF lane (**Figure 6.7**). The vimentin results suggest that EGF induces EMT and GLI1 opposes it. However, there was no change in E-Cadherin protein levels in GLI1-GS, GLI1+EGF, EGFP+EGF and control (EGFP-GS) cells which may argue against EMT taking place. Vimentin expression data corresponds with the real-time RT-PCR data in which Vimentin was induced in EGFP+EGF cells only. Although *KRT14* transcript levels were induced in GLI1-GS, GLI1+EGF and in EGFP+EGF relative to control cells (EGFP-GS), K14 protein levels were the same (**Figure 6.7**).

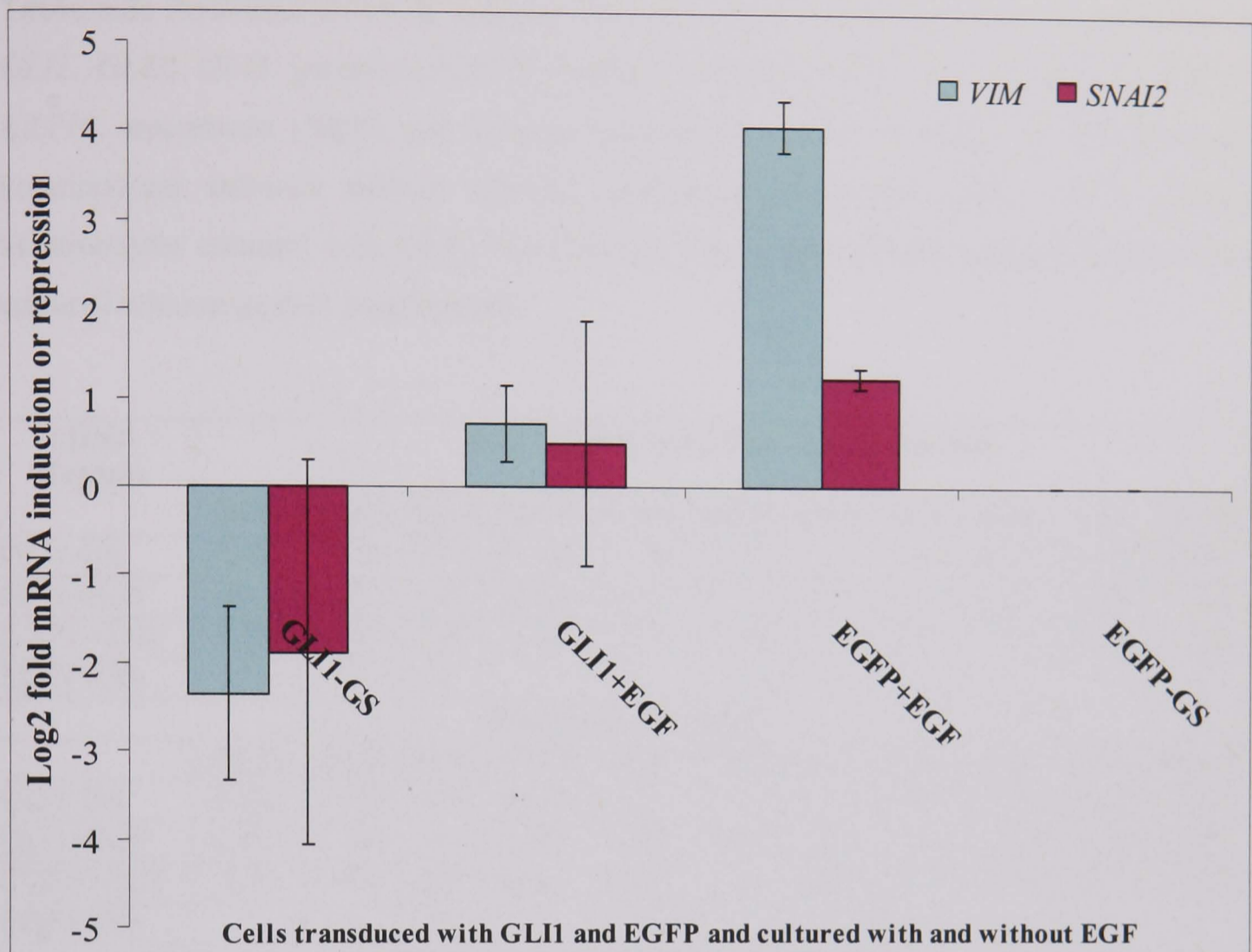


Figure 6.6: Real-time RT-PCR analysis showing induction or repression vimentin (*VIM*) and Snail2 (*SNAI2*) in GLI1, EGFP transduced primary keratinocytes cultured without growth supplement (-GS) and with epidermal growth factor (+EGF) relative to control EGFP primary keratinocytes cultured without growth supplement [EGFP-GS] cells.

Table 6.2: Real-time-RT-PCR analysis showing relative fold induction or repression of *GLI1*, *GLI2*, *GLI3*, patched (*PTCH*), vimentin (*VIM*), Snail2, keratins *KRT19*, *KRT17*, *KRT14*, smoothend (*SMO*) and Kinesin superfamily protein 4 (*KIF4*) in GLI1-primary keratinocytes cultured without growth supplement (-GS) and GLI1, EGFP primary keratinocytes cultured with EGF (+EGF) relative to control (EGFP primary keratinocytes cultured without growth supplement).

cDNA Sample	Fold mRNA induction or repression										
	GLI1	GLI2	GLI3	PTCH	SMO	KIF4	K17	K14	K19	Vim	Snal2
GLI1-GS	92425	13.39	0.17	22.435	1.109	6E-05	1.21	138.1	38.11	0.196	0.271
GLI1+EGF	109028	0.382	1.21	1.403	0.072	6E-05	0.55	13.37	2.098	1.638	1.398
EGFP+EGF	0.957	1.327	0.29	0.268	0.001	0.143	0.4	28.81	1.7	16.83	2.352
EGFP-GS	1	1	1	1	1	1	1	1	1	1	1
Standard deviation											
	GLI1	GLI2	GLI3	PTCH	SMO	KIF4	K17	K14	K19	Vim	Snal2
GLI1-GS	0.242	0.634	0.71	0.675	0.672	0.786	0.88	0.763	0.981	0.504	0.22
GLI1+EGF	0.341	0.756	0.51	0.595	0.489	0.474	0.39	0.45	0.352	0.739	0.382
EGFP+EGF	0.51	0.835	0.97	0.395	0.934	0.797	0.81	0.878	0.892	0.823	0.925
EGFP-GS	1	1	1	1	1	1	1	1	1	1	1
Log2 fold mRNA induction or repression											
	GLI1	GLI2	GLI3	PTCH	SMO	KIF4	K17	K14	K19	Vim	Snal2
GLI1-GS	16.496	3.744	-2.5	4.488	0.149	-14	0.27	7.11	5.252	-2.35	-1.886
GLI1+EGF	16.734	-1.39	0.27	0.489	-3.8	-14	-0.87	3.741	1.069	0.712	0.483
EGFP+EGF	-0.064	0.408	-1.8	-1.897	-9.664	-2.81	-1.32	4.849	0.766	4.073	1.234
EGFP-GS	0	0	0	0	0	0	0	0	0	0	0
Log2 Standard deviation											
	GLI1	GLI2	GLI3	PTCH	SMO	KIF4	K17	K14	K19	Vim	Snal2
GLI1-GS	-2.047	-0.66	-0.5	-0.567	-0.573	-0.35	-0.19	-0.39	-0.33	-0.99	-2.186
GLI1+EGF	-1.553	-0.4	-1	-0.75	-1.032	-1.08	-1.37	-1.15	-1.51	-0.44	-1.387
EGFP+EGF	-0.971	-0.26	-0	-1.342	-0.098	-0.33	-0.31	-0.19	-0.17	-0.28	-0.112
EGFP-GS	0	0	0	0	0	0	0	0	0	0	0

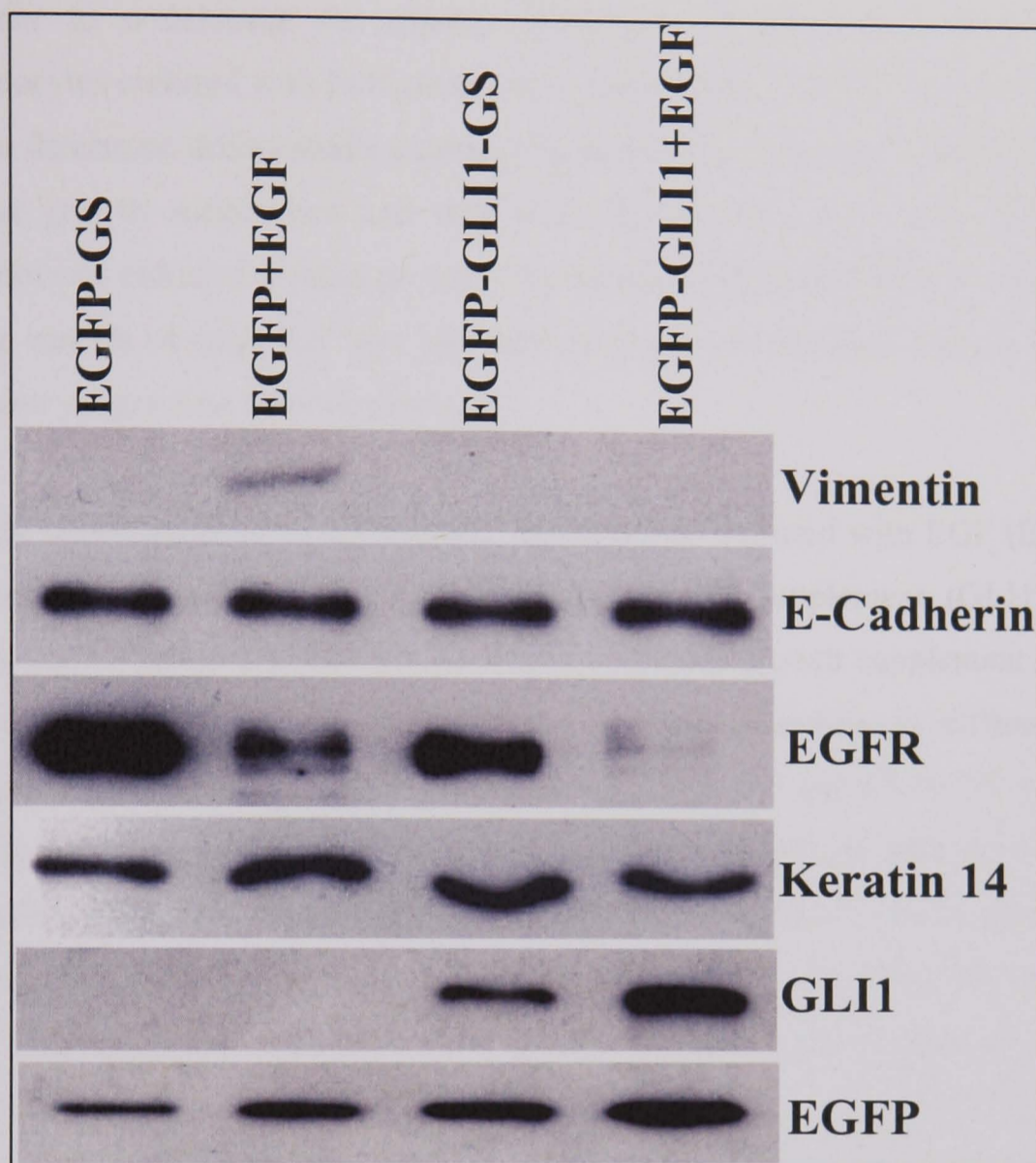


Figure 6.7: Western blot showing expression of vimentin, E-cadherin, Epidermal growth factor receptor (EGFR), Keratin K14, GLI1 and EGFP in EGFP transduced primary keratinocytes cultured without growth supplement (EGFP-GS), EGFP transduced primary keratinocytes cultured with EGF (EGFP+EGF), GLI1 transduced primary keratinocytes cultured without growth supplement (EGFP-GLI1-GS) and GLI1 transduced primary keratinocytes cultured with EGF (EGFP-GLI1+EGF). Vimentin is only expressed in EGFP+EGF cells. EGFR protein expression is reduced in EGFP+EGF and there is greater reduction in GLI1+EGF cell line. There is no change in keratin 14 and E-Cadherin expression. GLI1 is only expressed in EGFP-GLI1-GS/+EGF cell lines. EGFP was expressed in all cell lines. However, there appears to be a small induction in GLI1 and EGFP with EGF this may be due to increase in reporter activity.

6.3.7 Identification of differentially expressed genes in GLI1-primary keratinocytes cultured with and without EGF.

In order to understand the spindly phenotype of overexpressing GLI1 primary keratinocytes cultured with EGF observed in **section 6.3.1**, Affymetrix gene arrays were used to determine differentially expressed genes in GLI1-primary keratinocytes cultured without growth supplement and with EGF relative to control cells (EGFP-primary keratinocytes cultured without growth supplement). Affymetrix analysis was carried out on one sample of each cell type and data obtained was analysed using a Gene Spring computer programme (Silicongenetica).

Initially scatter plots of EGFP-primary keratinocytes cultured with EGF (EGFP+EGF), GLI1-primary keratinocytes cultured without growth supplement (GLI1-GS) verses control EGFP-primary keratinocytes cultured without growth supplement (EGFP-GS) were compared. The scatter plot data showed that there was no difference in gene expression pattern between EGFP+EGF verses EGFP-GS and GLI1-GS verses EGFP-GS. However, there was a change in scatter plot expression pattern of GLI1+EGF verses EGFP-GS cells **Figure 6.8**. The scatter plot of GLI1+EGF cells verses EGFP-GS indicates that genes that are expressed in EGFP-GS cells are repressed in GLI1+EGF cells. This suggests that there is a greater change in gene expression pattern in GLI1+EGF compared to GLI1 and EGF on their, own. In order to only identify differentially expressed genes, the affymetrix data was filtered by selecting the genes that were above 5 fold and below 5 fold lines on the scatter plot. Further parameters were selected on the Gene Spring computer program and these are as follows; flags present (P) marginal (M) were selected in 1 out of 4 samples, data transformation set measurements selected were less than 0.01 to 0.01. Per chip were normalized to 50th percentile and per gene were normalized to median. The expression values for each gene obtained for each sample from the Gene Spring programme analysis were analysed as follows; values of GLI1-GS, GLI1+EGF and EGFP+EGF were divided by EGFP-GS values. A total of 156 genes were identified that were differentially expressed and are listed in **Appendix I**. 106 genes were induced and 50 genes were repressed in GLI1-primary keratinocytes cultured without growth supplement and when EGF was added 96 genes were induced and 60 genes were repressed. In EGFP-primary keratinocytes cultured with EGF 84 genes were induced and 72 repressed (**Appendix 1**).

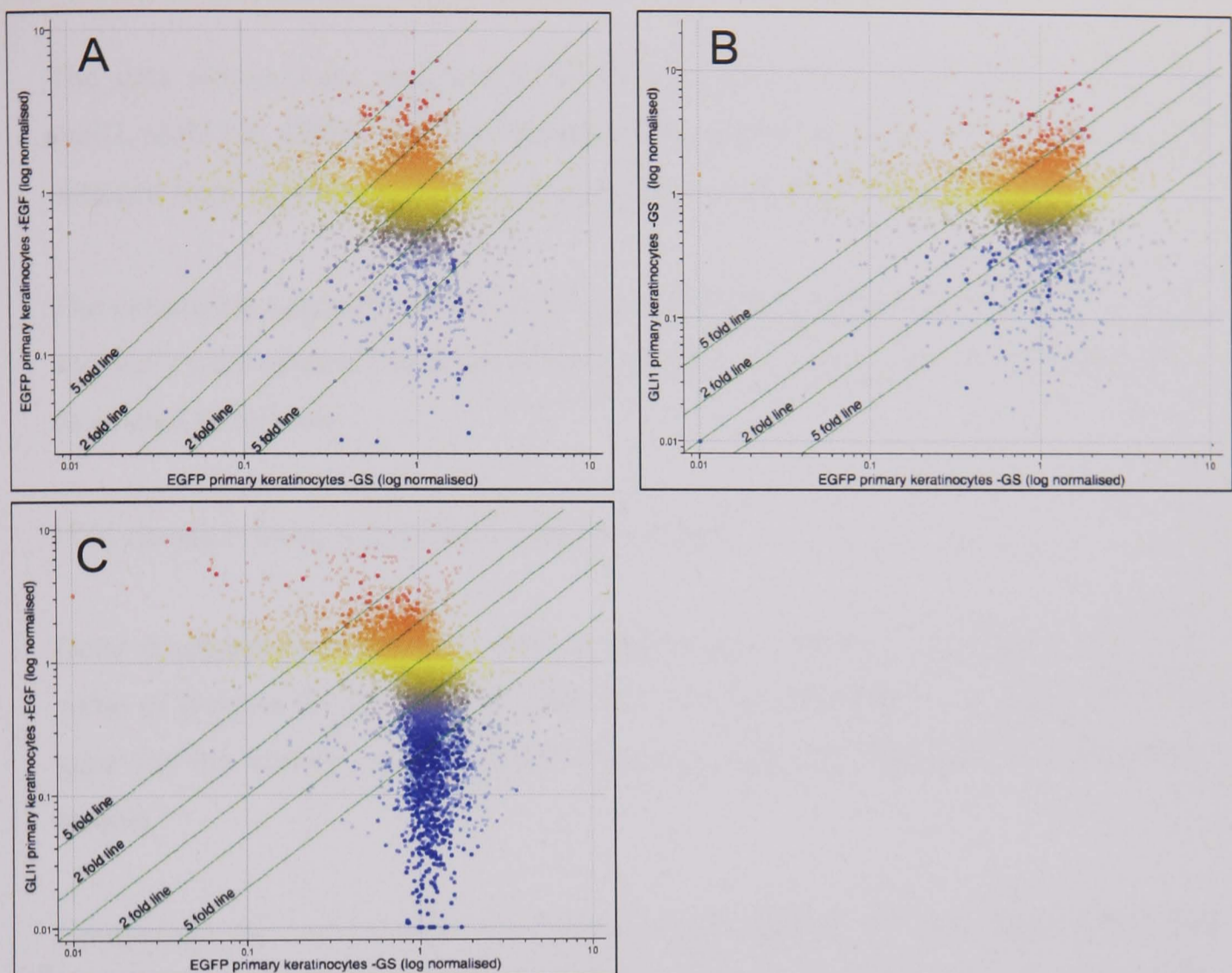


Figure 6.8: Expression profile of scatter plot of EGFP/GLI1-primary keratinocytes cultured without growth supplement and with EGF. (A) EGFP-primary keratinocytes cultured with EGF (+EGF) vs EGFP-primary keratinocytes cultured without growth supplement (-GS), scatter plot (B) GLI1-primary keratinocytes -GS vs EGFP-primary keratinocytes -GS, scatter plot (C) GLI1-primary keratinocytes +EGF vs EGFP-primary keratinocytes -GS. The expression profile of scatter plot (C) is remarkably different to that of scatter plots A and B. This indicates that there may be more genes differentially expressed in GLI1-primary keratinocytes cultured with EGF compared to GLI1-primary keratinocytes -GS and EGFP-primary keratinocytes +EGF controls. Only genes above and below 5 fold lanes indicated on the scatter plots were selected for further analysis

6.3.8 Comparing real-time RT-PCR and Affymetrix data for *GLI1*, *GLI2*, *GLI3*, *PTC*, *Vimentin*, *Snail2*, *KRT19*, *KRT17*, *KRT14* and *SMO* in *GLI1*-primary keratinocytes cultured with EGF.

The data obtained for real-time-RT-PCR for *GLI1*, *GLI2*, *GLI3*, *PTCH*, vimentin, snail2, (*KRT19*), *KRT17* and *SMO* (section 6.3.4 and 6.3.5) was compared with the data obtained from Affymetrix expression analysis to see if they correlate.

The expression values for *GLI1*, *GLI2*, *GLI3*, *PTCH*, vimentin, snail2, *KRT19*, *KRT17* and *SMO* were obtained from the Affymetrix data. The fold induction or repression was calculated as follows

$$\text{Fold change} = \text{Delta A (sample)} - \text{Delta B (control)}$$

Delta A represents expression value of a given gene for the sample minus expression value of β -Actin for that sample. Delta B represents the expression value of a given gene for the control sample minus expression value of Beta-Actin for the control sample.

Comparing the real-time-RT-PCR (Figure 6.4, Figure 6.5 and Figure 6.6) and Affymetrix expression data (Figure 6.9) fold induction or repression of a given gene, there was a discrepancy between the two graphs. For example in *GLI1*-GS cell line *GLI3* expression was up with Affymetrix and down with real-time-RT-PCR relative to control (EGFP-GS) cells. In *GLI1*+EGF cells *GLI1* and *GLI3* expression was down with Affymetrix and up with real-time-RT-PCR. In EGFP+EGF cells, *KRT14* expression with Affymetrix data was down and up with real-time-RT-PCR. For the rest of the genes the value of fold induction or repression varies but the trends are the same (that is up or down).

The real-time-RT-PCR data was from duplicate experiments in triplicates assays and the Affymetrix data was from a single experiment with a single assay. Therefore, the values for some of the genes may be false. It is also possible that the sensitivity of each assay being different and thus there is discrepancy, although for most of the genes the expression trend is the same for both Affymetrix and real-time-RT-PCR assay. Another explanation for this discrepancy could have been, that the yield of cRNA expected from

10µg total RNA was expected to be 40-80 µg; if the yield of cRNA is less than 40 µg it is recommended not to be used in affymetrix analysis, as there is likely to be a problem with cRNA preparation.

The yield of cRNA obtained was 10.5-14.5 ug from 7 ug total RNA which was below the recommended levels. After consultation with the Affymetrix operator, it was decided to run the fragmented cRNA samples on a test chip before running them on the Affymetrix chip. The results obtained from test chips were of adequate quality and on the recommendation of the Affymetrix operator the samples were run on the Affymetrix chips. It is also possible that the discrepancy between real-time RT-PCR and the Affymetrix assay may have been due to these factors. However, Affymetrix analysis was used as a quick guide to identify key genes or pathways for further study and was not intended as a define end point in itself.

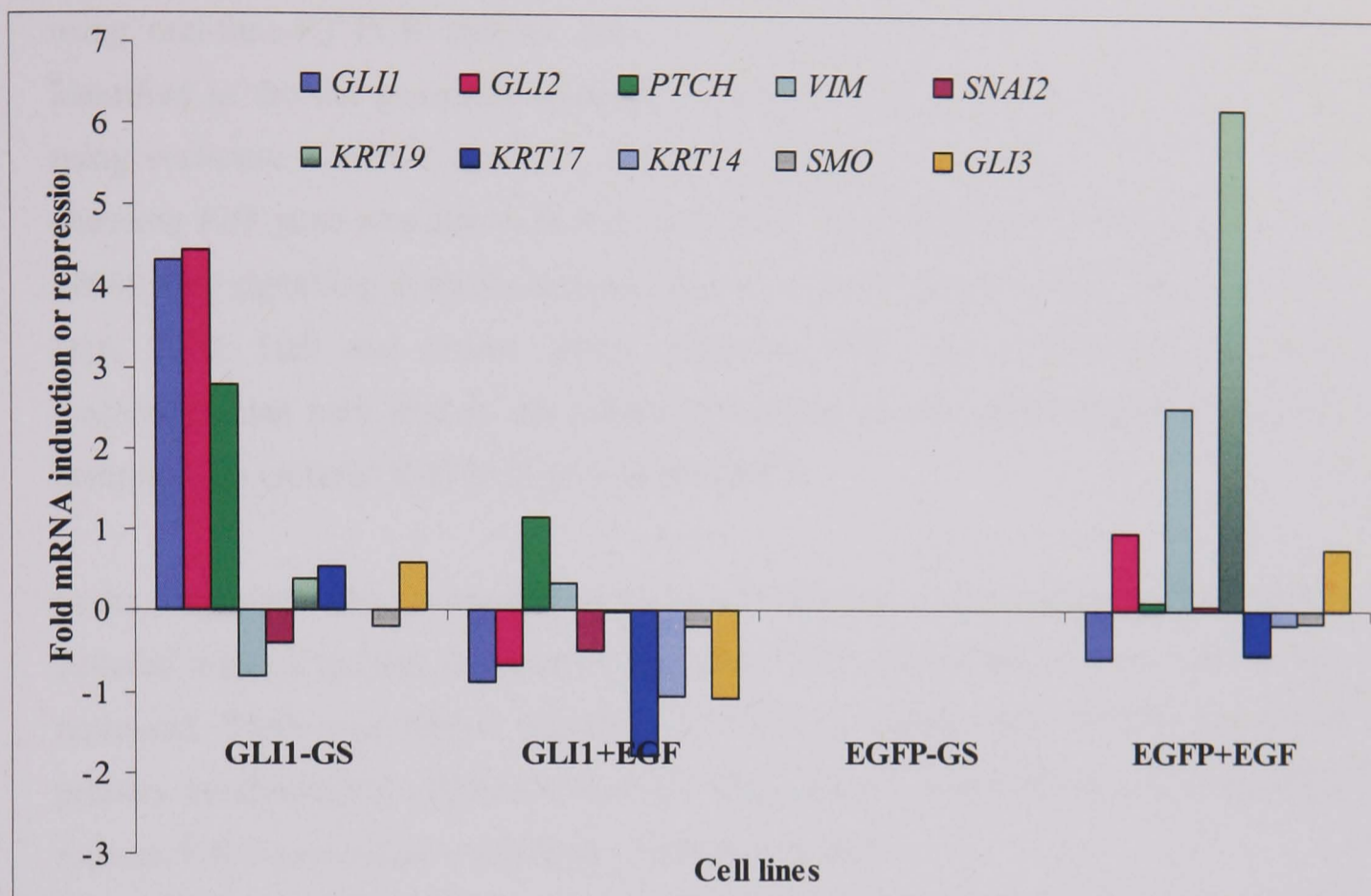


Figure 6.9: Affymetrix expression analysis of *GLI1*, *GLI2*, *PTCH*, vimentin (*VIM*), snail2 (*SNAI2*), keratins *KRT19*, *KRT17*, *KRT14*, smoothend (*SMO*) and *GLI3* in *GLI1*, *EGFP* transduced primarykeratinocytes cultured without growth supplement (-GS) and with EGF (+EGF).

6.3.9 *VAV2*, *VAV3* and *VAV3.1* are expressed in GLI1- primary keratinocytes cultured with and without EGF.

Differentially expressed genes identified with Affymetrix analysis needed to be verified using real-time-RT-PCR analysis. Due to time constraint I only selected one gene identified in the list generated from the Affymetrix analysis (**Appendix 1**) to verify using real-time RT-PCR analysis. This was the *VAV3* oncogene. The rationale for choosing *VAV* gene was due to its role in the Rho signalling pathway (Hornstein et al., 2004). Rho signalling is involved in cytoskeleton remodelling (Etienne-Manneville and Hall, 2002; Hall and Nobes, 2000). Therefore, this may explain the molecular mechanism that may lead to the spindly phenotype of overexpressing GLI1 primary keratinocytes cultured with EGF (see **section 6.2.1**).

In the Affymetrix data (**Appendix 1**) *VAV3* was induced in GLI1-primary keratinocytes cultured without growth supplement and when EGF was added to these cells it was repressed. There was further reduction of *VAV3* in control cells (EGFP transduced primary keratinocytes) cultured with EGF. This indicates that GLI1 induces, and EGF reduces *VAV3* expression in presence or absence of GLI1.

In mammals, there are three family members of VAV proteins VAV1, VAV2, VAV3 and VAV3.1 isoforms. VAV1 is haematopoietic cell specific and VAV2, VAV3 and VAV3.1 are widely expressed in other tissue (Bustelo, 1996; Bustelo, 2000; Katzav et al., 1995; Schuebel et al., 1996; Trenkle et al., 2000). Thus expression of *VAV2*, *VAV3* and *VAV3.1* was analysed using RT-PCR analysis, using published primers (Trenkle et al., 2000) in GLI1-and EGFP-primary keratinocytes cultured without growth supplement and with EGF.

Figure 6.10 shows expression of *VAV2*, *VAV3*, *VAV3.1* and β -Actin in GLI1-and EGFP-primary keratinocytes cultured without growth supplement and with EGF. There was same intensity band was observed in all lanes for *VAV2*, *VAV3.1* and β -Actin (Control). A double band was observed for *VAV3*, the top band was around 660 bp (expected size) and a smaller band around 400 bp. In all cell lanes the 600 bp band was of higher intensity than the 400 bp band. In GLI1-primary keratinocytes cultured with EGF and EGFP-primary keratinocytes cultured without growth supplement the 400 bp band was of greater intensity compared to GLI1-GS and EGFP-GS cells. The presence

of a doublet band for *VAV3* indicates that there may be alternative splice variant of *VAV3* in these keratinocytes, and this transcript may be expressed at different levels. The band seen at around 400 bp could have been from a genomic contamination. However, this is unlikely as the total RNA samples were treated with DNaseI to remove genomic DNA and no bands were observed in control –RT lane. Also if there was genomic contamination the band should have been same size as the expected band 600 bp, or it should have been larger than the expected band, if the primers expanded the intron exon boundaries. Expression of *VAV3* observed with RT-PCR analysis in all the cell lines verified the Affymetrix data.

6.3.10 There is no change in *VAV2* and *VAV3.1* expression in GLI1-primary keratinocytes cultured with EGF.

Due to two bands being obtained with the *VAV3* primers in RT-PCR (section 6.2.9), real-time RT-PCR was not carried out using *VAV3* primers on cDNA from GLI1- and EGFP-primary keratinocytes cultured with EGF and without growth supplement. This is because SYBR Green dye used in the real-time-RT-PCR kit binds any double strand DNA and this would not have been able to distinguish between the two bands and as result would have given false results. Real-time-RT-PCR was carried out using *VAV2* and *VAV3.1* primers, the data from these primers indicates there was no change in *VAV2* and *VAV3.1* expression in GLI1- and EGFP-primary keratinocytes cultured with EGF and without growth supplement (Figure 6.11, Table 6.3).

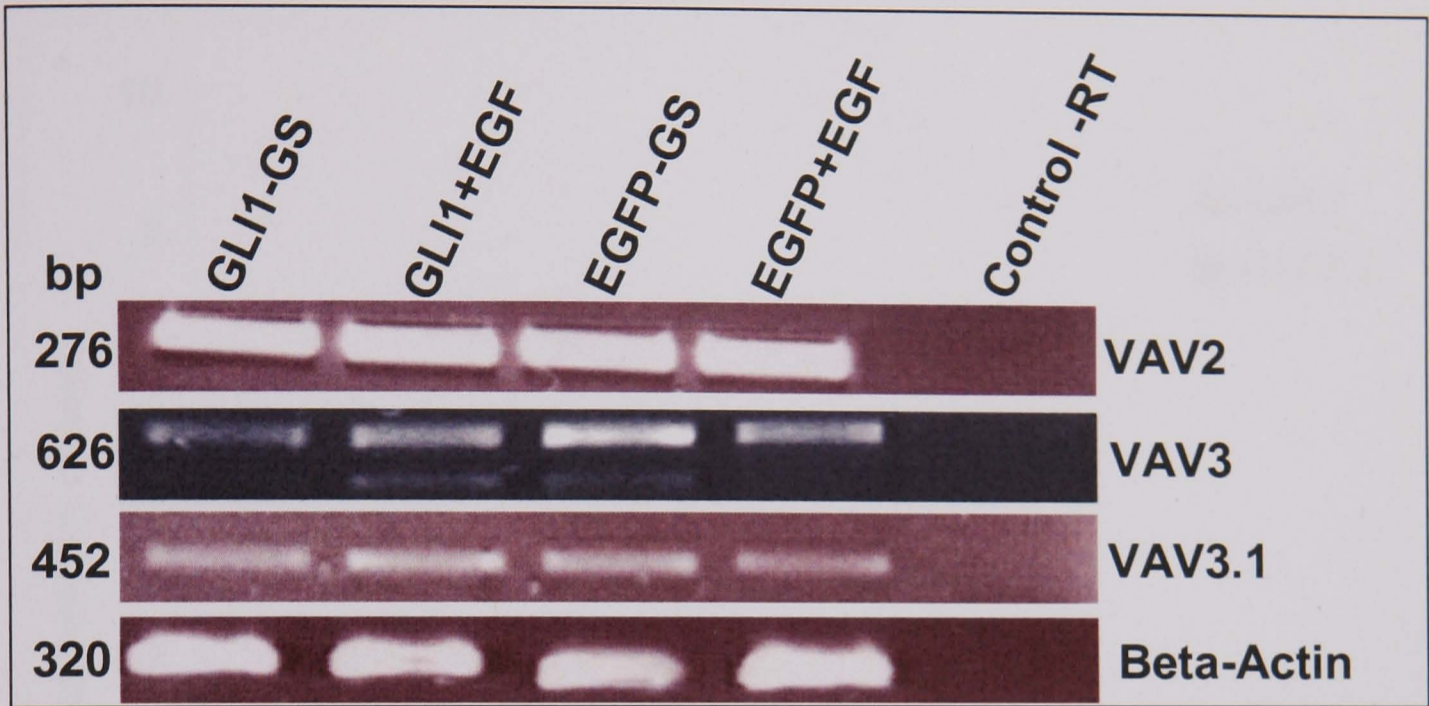


Figure 6.10: RT-PCR analysis showing *VAV2*, *VAV3*, *VAV3.1* and β -Actin expression in GLI1-primary keratinocytes cultured without growth supplement (GLI1-GS) and with EGF (GLI1+EGF), EGFP-primary keratinocytes cultured without growth supplement (EGFP-GS) and with EGF (EGFP+EGF). For *VAV3* there was a second band observed that was of strong intensity in GLI1+EGF and EGFP-GS lanes and very weak band in GLI1-GS and EGFP+EGF lanes.

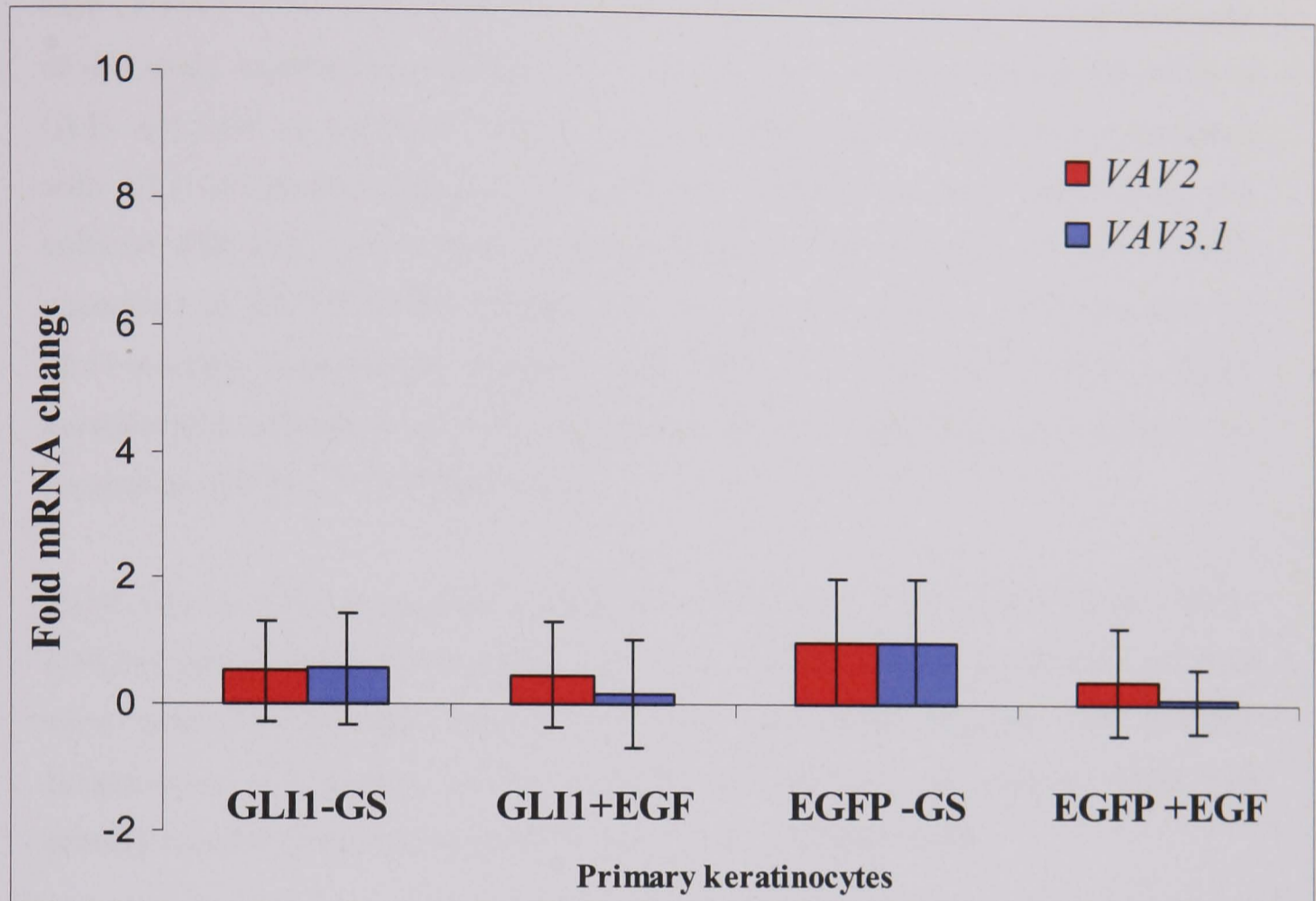


Figure 6.11: Real-time-RT-PCR analysis indicating no change in *VAV2* and *VAV3.1* expression in GLI1- and EGFP-transduced primary keratinocytes culture without growth supplement (GLI1-GS, EGFP-GS) and with EGF (GLI1+EGF, EGFP+EGF) compared to control cells (EGFP-primary keratinocytes culture without growth supplement [EGFP-GS]).

6.3.11 GLI1-N-TERT keratinocytes express *VAV3.1* and not *VAV3* and its expression is lost when cultured with EGF.

VAV3.1 was repressed in immortal keratinocytes (HaCat) when they were cultured with EGF (Trenkle et al., 2000). Due to shortage of primary keratinocytes during the course of this study immortalised N/TERT keratinocytes were used to determine the effect of GLI1 and EGF on expression of *VAV3.1* in. N/TERT keratinocytes were transduced with GLI1-mutated-Nuclear-Localisation-Signal (mNLS) and GLI1 retroviruses and cultured with EGF and without growth supplement. We observed the same spindly phenotype in GLI1-N/TERT keratinocytes cultured with EGF as those observed for GLI1-primary keratinocytes cultured with EGF. GLI1 and GLI1-mNLS N-TERT keratinocytes cultured with EGF and without growth supplement were analysed for expression of *VAV2*, *VAV3* and *VAV3.1*.

There was no *VAV3* expression in GLI1-GS, GLI1+EGF, GLI1-mNLS-GS and GLI1-mNLS+EGF N/TERT keratinocytes. However, *VAV2*, *VAV3.1* and β -Actin (control) were expressed in these shown in **Figure 6.12**. This suggests that N/TERT keratinocytes only express *VAV3.1* transcript and not *VAV3* and these contrast with primary keratinocytes that express *VAV3* and *VAV3.1* (**Figure 6.10**).

6.3.12 GLI1 induces *VAV3.1* and *VAV2* expression in N/TERT keratinocytes and EGF represses this induction.

In N/TERT keratinocytes *VAV3.1* expression was induced in GLI1-GS and in GLI1+EGF cells there was no change relative to GLI1-mNLS-GS (control) cells in a real-time-RT-PCR analysis (**Figure 6.13**). However, there was a complete repression of *VAV3.1* in GLI1-mNLS+EGF cells (**Figure 6.12 and Figure 1.3**). There was only a small induction of *VAV2* expression in GLI1-GS cells and when EGF was added this induction appears to be reduced (**Figure 6.13, Table 6.3**). In GLI1+EGF, GLI1-mNLS+EGF cells there was no change in *VAV2* expression relative to control cells (GLI1-mNLS-GS) (**Figure 6.13, Table 6.3**). Therefore, GLI1 induces *VAV3.1* and *VAV2* expression and this induction is repressed with EGF and EGF without GLI1 completely represses *VAV3.1* expression.

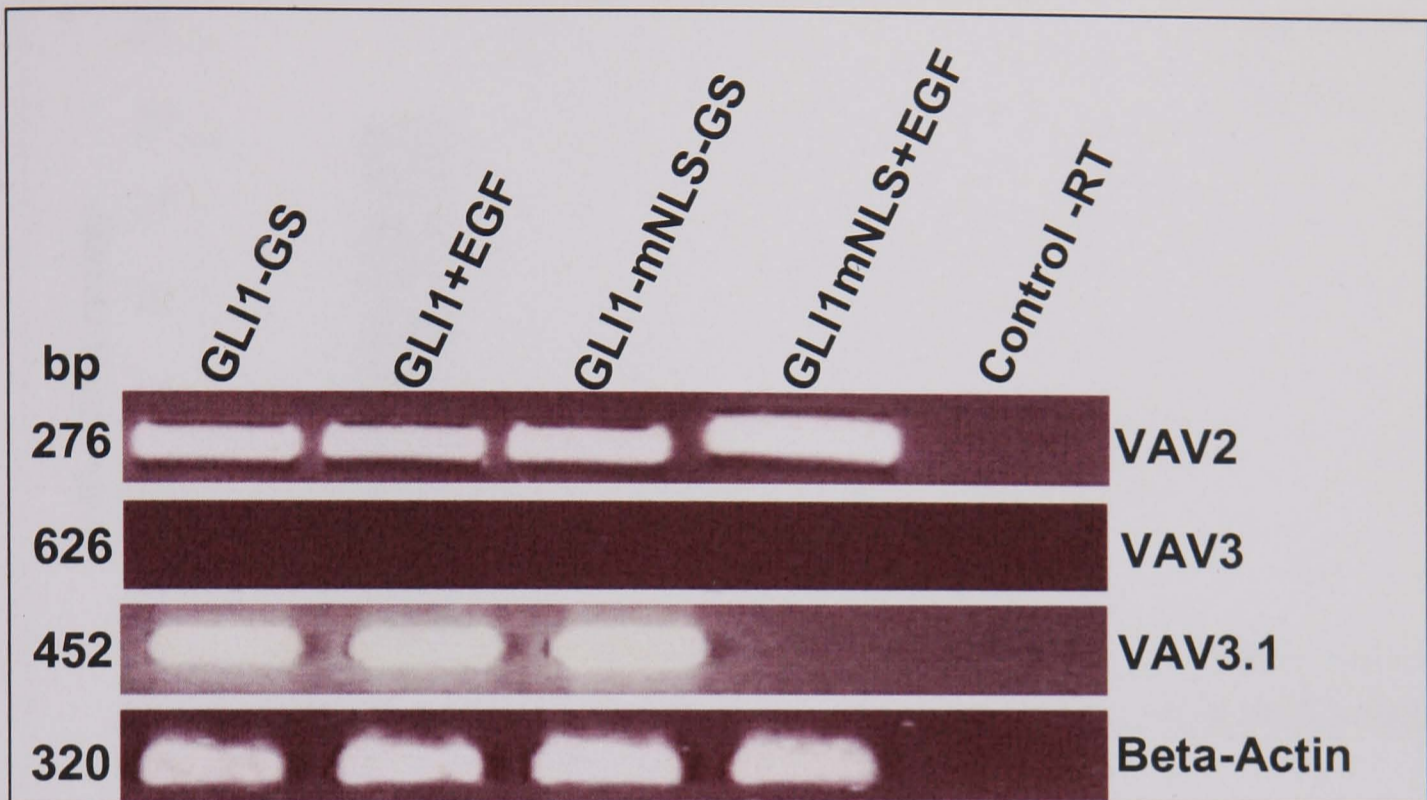


Figure 6.12: RT-PCR analysis showing expression of *VAV2*, *VAV3*, *VAV3.1* and β -Actin expression in GLI1 and GLI1-mutant Nuclear Localisation Sequence (mNLS) transduced N/TERT-keratinocytes without growth supplement (GLI1-GS, GLI1mNLS-GS control) and with EGF (GLI1+EGF, GLI1-mNLS +EGF).

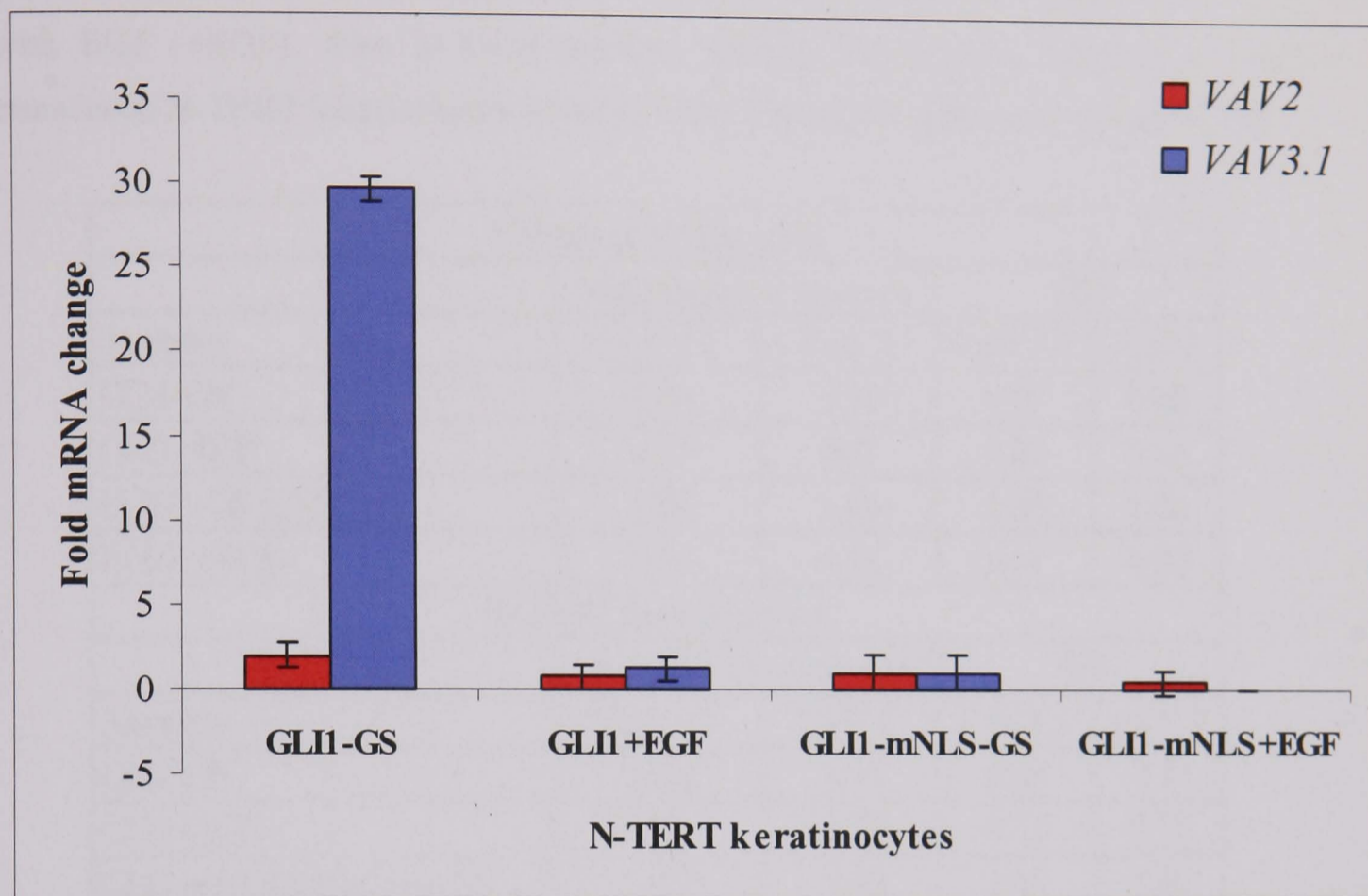


Figure 6.13: Real-time-RT-PCR analysis showing relative fold repression of *VAV2* and *VAV3.1* in GLI1- and GLI1-mutant Nuclear Localisation Sequence (mNLS) transduced N/TERT keratinocytes without growth supplement (GLI1-GS, GLI1mNLS-GS control) and with EGF (GLI1+EGF, GLI1-mNLS +EGF).

Table 6.3 Relative fold induction or repression of *VAV2*, *VAV3* and *VAV3.1* in GLI1 and EGFP transduced primary keratinocytes cultured without growth supplement (-GS) and with EGF (+EGF). Also in GLI1-mutated Nuclear Localisation Signal (GLI1-mNLS) transduced N-TERT keratinocytes cultured without growth supplement and with EGF.

Primary keratinocytes				
	fold induction or repression		SD	
Samples	<i>VAV 3.1</i>	<i>VAV 2</i>	<i>VAV 3.1</i>	<i>VAV 2</i>
GLI1-GS	0.56	0.52	0.87	0.80
GLI1+EGF	0.17	0.47	0.87	0.86
EGFP -GS (Control)	1.00	1.00	1.00	1.00
EGFP +EGF	0.07	0.38	0.51	0.87
N-TERT keratinocytes				
	fold induction or repression		SD	
Samples	<i>VAV 3.1</i>	<i>VAV 2</i>	<i>VAV3.1</i>	<i>VAV 2</i>
GLI1-GS	29.62	1.94	0.68	0.74
GLI1+EGF	1.20	0.72	0.72	0.77
GLI1-mNLS-GS (Control)	1.00	1.00	1.00	1.00
GLI1-mNLS+EGF	0.00	0.41	0.00	0.75

6.3.13 *VAV3.1* is expressed in BCC and normal skin

Having shown, that *VAV3.1* is induced in GLI1 expressing keratinocytes I went on to investigate *VAV3.1* expression in BCC and normal skin. **Figure 6.14** shows that *VAV3.1* was expressed in BCC and normal skin.

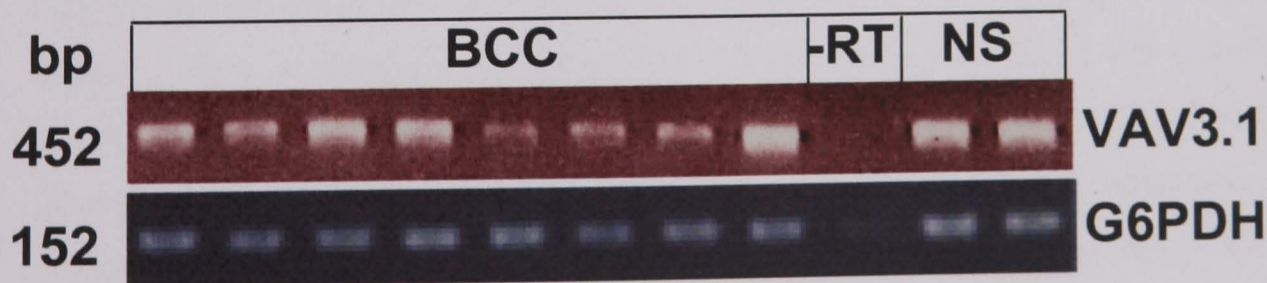


Figure 6.14: RT-PCR analysis showing expression of *VAV3.1* and G6PDH (control) in basal bell carcinoma (BCC) and Normal Skin (NS).

6.4.0 Discussion

6.4.1 Localisation of GLII in the nucleus is required to cause a change in cell morphology with EGF.

The work carried out in this chapter shows EGF induces a change in EGFP-GLII-keratinocyte (GLII+EGF) cell morphology when compared to control EGFP-keratinocytes cultured with EGF (EGFP+EGF). The localisation of GLII in GLII expressing cells exposed to EGF was predominantly located in the cytoplasm as opposed to the nucleus where transcription factors normally function (**Figures 6.1**). However, GLII-mutated-Nuclear Localisation Signal-primary keratinocytes cultured with EGF (GLII-mNLS+EGF) in which localisation of GLII-mNLS was predominantly restricted to the cytoplasm had a normal rounded morphology (**Figure 6.3**) and was the same as that of EGFP+EGF control cells (**Figure 6.2**). GLII-mutated Nuclear Export Signal-primary keratinocytes cultured with EGF (GLII-mNES+EGF) in which expression of GLII-mNES was mainly restricted to the nucleus showed a spindly phenotype (**Figure 6.3**) and was the same as that for GLII+EGF cells (**Figure 6.2**). These results suggest that localisation of GLII to the nucleus may be required to trigger a change in cell morphology from rounded to spindly phenotype in presence of EGF and that nuclear cytoplasmic shuttling is an important mechanism by which GLI activity may be regulated.

6.4.2 EGF alters the transcriptional activity of GLII.

EGF causes a change in cell morphology from rounded to spindly phenotype in GLII expressing keratinocytes. Therefore, does EGF alter the transcriptional activity of GLII? I have shown in this chapter that upon exposure to EGF, the transcriptional activity of GLII was reduced as revealed by reduced expression of known GLII target genes GLI2 and PTCH (Agren et al., 2004; Marigo et al., 1996b; Regl et al., 2002; Toftgard, 2000) (**Figure 6.4**). The results described in this chapter for PTCH corroborates with the data published earlier (Kasper et al., 2006) showing that PTCH expression was reduced in overexpressing GLII primary and N-TERT keratinocytes cultured with EGF. However, there was no induction of *PTCH* promoter in a luciferase reporter assay by combinatorial GLII/EGF signalling in HaCat keratinocytes (Kasper et

al., 2006). This suggests that EGF signaling may alter the target gene profiles for GLI proteins either by directly modifying GLI proteins or by regulating other transcription factor/s or cofactor/s that may interact with GLI transcription factor/s to control promoter activation of selected target genes. EGF stimulation may also control GLI1 transcriptional activity by shuttling GLI1 in and out of the nucleus and based on our observation that with EGF, GLI1 expression appeared to be diffused through out the cell (**Figure 6.2**) but did not appear to alter the overall levels of GLI1 expression.

A small increase in *GLI1* mRNA and protein observed with EGF in GLI1 expressing cells (**Table 6.2 and Figure 6.7**) may have been due to the fact that the promoter activity was increased with EGF. A bicistronic construct EGFP-GLI1 (**Figure 2.1**) was used and the assumption that reporter (*CMV*) activity of this construct may have been increased with EGF was confirmed when we probed these western blots with EGFP antibody and observe that there was a similar level of induction in EGFP protein in response to EGF in GLI1 expressing and non-expressing cells (**Figure 6.7**).

Expression of *GLI3* in GLI1 expressing primary keratinocytes cultured without growth supplement (GLI1-GS) and control (EGFP expressing primary keratinocytes cultured with [EGFP+EGF]) was reduced and when EGF was added to GLI1 expressing primary keratinocytes (GLI1+EGF) *GLI3* expression reverted back to levels that were seen in control (EGFP expressing primary keratinocytes cultured without growth supplement [EGFP-GS]) (**Figure 6.4**). SHH signalling has been shown to repress *GLI3* expression in limb development (Marigo et al., 1996b). Smoothend (*SMO*) expression in GLI1-GS was similar to that of control EGFP-GS cells. Moreover, when EGF was added to GLI1 expressing primary keratinocytes *SMO* expression was reduced. *SMO* was also repressed in EGF treated control EGFP-primary keratinocytes (EGFP+EGF cells) (**Figure 6.4**). These results suggest that EGF may be altering the expression of *SMO* which activates, and *GLI3*, which represses HH signalling (Murone et al., 1999; von Mering and Basler, 1999). This may be a mechanism to control the transcriptional activity of GLI1 in GLI1 overexpressing cells.

6.4.3 EGFR expression is reduced in GLI1 expressing keratinocytes cultured with EGF.

In this study we have shown that there was a reduction in EGF receptor (EGFR) protein levels in primary keratinocytes upon exposure to EGF and there was a greater reduction in EGFR in GLI1+EGF compared to control EGFP+EGF cells (**Figure 6.7**). A reduced expression of EGFR has also been observed in BCC samples and this is proposed to result from increased ligand-mediated receptor stimulation (Groves et al., 1992; Nazmi et al., 1990). Activation of EGFR is associated with the development of many tumour types (Kim et al., 2001) and if it alters the oncogenicity of GLI1 this could have implications for the future development of therapy against BCC, by targeting EGFR. Such drugs include monoclonal antibodies (mAbs) directed against the EGFR extracellular domain and or the use of small molecule tyrosine kinase inhibitors (TKIs) directed against the tyrosine kinase domain. The mAbs function at the extracellular ligand-binding site of the receptor, whereas the small molecule TKIs function at the intracellular tyrosine kinase domain of the EGFR (Harari, 2004).

6.4.4 GLI1 induces expression of *KRT14*, *KRT17* and *KRT19* and EGF represses' this induction.

In this chapter I have shown that *KRT14*, a basal keratinocyte marker (Ishida-Yamamoto et al., 1991; Lane and McLean, 2004), *KRT17* a stress response marker (De Berker et al., 2000; Lane and McLean, 2004; McGowan and Coulombe, 2000) and *KRT19* a putative stem cell marker (Michel et al., 1996b) were induced in GLI1 expressing keratinocytes. Moreover, when these cells were cultured with EGF, expression of these markers was reduced (**Figure 6.5**). A more recent study (Kasper et al., 2006) showed that *KRT19* was induced in GLI1 expressing N/TERT keratinocytes and repressed when these cells were cultured with EGF. Expression of GLI1 in the absence of extracellular stimuli also induced elevated mRNA levels of *KRT15* and Nestin (stem cell markers) and EGF neutralised this induction comparable to control cells. However, CD71, which encodes the transferrin receptor and is negative in stem cells (Tani et al., 2000b), was increased in response to GLI1/EGF. These results suggest that GLI1 may be inducing a stem cell like expression signature in epidermal keratinocytes and this signature may be prevented by EGF signaling.

Deletion of a GLI-responsive element in *KRT17* promoter results in loss of GFP fluorescence in most appendages in mice (Bianchi et al., 2005), and results described in this chapter for *KRT17* suggest that Sonic Hedgehog signalling participates in *KRT17* regulation. The fact that expression of *GLI1*, *KRT14*, *KRT17* and *KRT19* is observed in BCC (Apaydin et al., 2005; Green et al., 1998) and these keratins are induced in GLI1 expressing primary keratinocytes (**Figure 6.5**) indicates that GLI1 may be altering the expression of these keratins in BCC.

6.4.5 GLI1 may be a negative regulator of Epithelial/Mesenchymal transformation (EMT).

EGF induces vimentin and snail expression and reduces E-Cadherin expression during EMT, which is associated with metastasis (Lee et al., 2006; Lu et al., 2003; Strizzi et al., 2004). There was no change in E-Cadherin expression in GLI1 expressing keratinocytes with or without EGF relative to control cells (**Figure 6.7**). This indicates that classical EMT may not be occurring in these cells. However, there was greater induction of vimentin and snail2 mRNA expression in control cells (EGFP expressing primary keratinocytes cultured with EGF) compared with GLI1 expressing primary keratinocytes with EGF (**Figure 6.6**). Moreover, Vimentin protein was only detected in control cells (EGFP expressing primary keratinocytes cultured with EGF) (**Figure 6.7**). A small increase in vimentin mRNA levels but no expression of Vimentin protein in GLI1 expressing primary keratinocytes with EGF indicates that expression of vimentin may have been controlled by GLI1 at transcriptional and at translational level in primary keratinocytes. Therefore EGF may be inducing certain EMT markers in primary keratinocytes and GLI1 appears to be repressing the expression of these EMT markers, this may explain why BCC's are locally invasive and are rarely subject to metastasis (Marks, 1995). A small induction of vimentin mRNA expression is observed in BCC's relative to normal skin although protein expression was not determined (Regl et al., 2002), thus further investigation is required to determine Vimentin protein expression in BCC.

6.4.6 *GLI1* and EGF reduce *KIF4* mRNA expression in primary keratinocytes.

I have shown in this study that *KIF4* was downregulated in *GLI1* expressing primary keratinocytes (**Figure 6.5**). A recently publication (Mazumdar et al., 2006) has shown that loss of *KIF4* in murine embryonic stem cells leads to multiple mitotic defects including chromosome misalignments, spindle defects, and aberrant cytokinesis and more than 70% of *KIF4* knockout cells were aneuploid (Mazumdar et al., 2006). Loss of *KIF4* also increases the potential of embryonic stem cells to form tumors in nude mice (Mazumdar et al., 2006). The same authors also showed a reduced *KIF4* protein levels in 35% of human cancers from several tissues (Ovary, lung, breast, CNS, renal, melanoma and leukemia) indicating that loss of *KIF4* is physiologically relevant, although no reduction of *KIF4* was found in colon cancer. They also showed that in cells lacking *KIF4*, mitotic spindle checkpoints and DNA-damage response pathways were activated (Mazumdar et al., 2006). However, in contrast to my data showing *GLI1* down-regulating *KIF4* in primary keratinocytes I observed that in human BCC samples mRNA for *GLI1* and *KIF4* were up-regulated (**Figure 3.7**). Whilst up-regulation of *GLI1* mRNA is to be expected my data showing up-regulation of *KIF4* is in conflict with my observation in primary keratinocytes. This data may indicate that in BCC *KIF4* is expressed independently of *GLI1*. However, it will be important to determine whether *KIF4* protein levels are reduced in BCC as it is possible that whilst mRNA levels are elevated this is not reflected by protein expression.

6.4.7 *VAV 3.1* expressed in BCC is induced by *GLI1* and repressed by EGF.

In order to further our understanding on how *GLI1* and EGF pathways interact in primary keratinocytes. I carried out microarray gene expression analysis in which I identified 156 genes that were differentially expressed in *GLI1* transduced primary keratinocytes cultured with EGF relative to control cells (**Appendix1**). Due to time constraints and number of genes identified I was unable to verify all of the differentially expressed genes using RT-PCR analysis. Thus microarrays data needs further verification by carrying out RT-PCR on identified target genes.

One gene that was differentially regulated in the list generated from the Affymetrix data was *VAV3*. There was a small induction in *VAV3* expression in *GLI1* expressing keratinocytes cultured without growth supplement and when EGF was added to these

cells *VAV3* induction appeared to be repressed. A greater reduction in expression of *VAV3* was observed in control cells (EGFP expressing keratinocytes cultured with EGF) compared to GLI1 expressing keratinocytes cultured with EGF (**Appendix1**). This indicates that GLI1 induces and EGF reduces *VAV3* expression.

During this study we ran out of primary keratinocytes stocks thus N/TERT keratinocytes were used to continue with the study. Both *VAV3* and *VAV3.1* were expressed in primary keratinocytes (**Figure 6.10**). Whereas in N-TERT keratinocytes only *VAV3.1* was expressed (**Figure 6.12**) and there was no change in *VAV3.1* expression in GLI1-primary keratinocytes cultured with or without EGF (**Figure 6.11**). However, in GLI1-N-TERT keratinocytes there was a complete repression of *VAV3.1* when cultured with EGF (**Figure 6.13**). This suggests that different VAV proteins may be expressed in different keratinocytes and these may be differently regulated by same stimulus. These results are in line with the published results (Trenkle et al., 2000) they show that there appear to be no *VAV3* expression in HaCat keratinocytes and *VAV3.1* was downregulated in these cells when they were exposed to EGF to levels that were not detectable.

There was no published data available showing expression of *VAV3.1* in BCC at the time this study was carried out. Thus having identified that *VAV3.1* was induced in GLI1 expressing N/TERT keratinocytes I went on to determine if *VAV3.1* was expressed in BCC and normal skin. **Figure 6.14** shows that *VAV3.1* was expressed in BCC and normal skin, due to time constraints quantification of *VAV3.1* was possible.

6.5.0 Summary

In this chapter I have shown that; GLI1 with EGF appear to change cell morphology of primary and N-TERT keratinocytes and EGF reduces the transcription activity of GLI1 by shuttling GLI1 out of nucleus and this leads to change in expression of Sonic hedgehog pathway genes *PTCH*, *SMO*, *GLI2* and *GLI3*. EGF also induces expression of vimentin and snail2 transcripts markers of EMT and GLI1 reduces the expression of these markers and there is no change in E-Cadherin protein expression with GLI1 alone or with EGF. GLI1 may be reducing the effects of EGF signalling by reducing the expression of EGFR. GLI1 also appears to be inducing the stem cell signature and EGF may be reduces this signature.

There was a greater repression of *KIF4* with GLI1 compared to EGF in primary keratinocytes and in N-TERT keratinocytes GLI1 induces and EGF represses *VAV3.1* expression. Micro arrays data has shown that there were 156 genes that were differentially regulated between GLI1 expressing keratinocytes cultured without growth supplement and cultured with EGF.

6.6.0 Future work

The microarrays data needs to be verified by carrying out real-time RT-PCR analysis using specific primers for the differentially expressed genes identified and or repeating the arrays assay using triplicate samples. Once the arrays data is verified further investigation would need to be carried out to determine how EGF and SHh signalling pathway interact, by investigating protein levels of these genes. Also analyse the promoter regions of these genes to identify if they have GLI binding sequence to investigate if the genes are direct or indirect targets of GLI1. This data then would be useful in examining BCC samples to see if any of the identified players are present *in-vivo* and what role they have in BCC formation, by carrying out immunohistochemistry staining with specific antibodies and real-time-RT-PCR analysis.

Many of the experiments carried out in this chapter have been based upon analysis of mRNA in either primary keratinocytes or BCC biopsies. Further work is required to characterise patterns of protein expression. In particular my observation showing GLI1 regulation of GLI2, PTCH, SMO, keratin K17, keratin K19, KIF4 and VAV should be followed up with a detailed investigation of protein expression both in primary keratinocytes and N/TERT keratinocytes but also in BCC and investigate if this correlates with GLI1. Also investigate phosphorylation of VAV proteins to determine if they are active or not and carry out further investigate on KIF4 to see if alteration in its expression causes an aneuploidy.

CHAPTER 7

Generating a *Zp3-Cre-GLII* Transgenic Mouse Model System

7.1.0 Introduction

A GLII transgenic mouse model has been developed which specifically overexpresses GLII in the basal layer of epidermis and outer root sheath of hair follicles under the control of *KRT5* promoter. These mice develop several types of spontaneous skin tumours, including BCC (Nilsson et al., 2000). In order to investigate molecular mechanisms of GLII transcription factor and to identify particular partners involved in tumour formation and hair growth development we decided to develop an *in vivo* mouse model of GLII. The aim of this study was to generate a conditional *GLII* transgenic mouse under the control of a *KRT14* promoter activated by a site specific DNA recombinase Cre system (Kilby et al., 1993). Dr Graham Neill carried out all the cloning work and animal facilities at Clare Hall Cancer Research UK carried work in trying to generating transgenic mice and I undertook the screening of these mice described in this chapter.

7.1.1 Zp3-Cre *GLII* transgenic mouse model system.

A site-specific DNA recombinase *Cre* system (Kilby et al, 1993) was used to control *GFP-GLII* expression in mice under a *KRT14* promoter. *Cre* mediates the recombination of two directly repeated target (*loxP*) sites to a single *loxP* site, with simultaneous excision of the DNA section flanked by the *loxP* sites (the 'floxed' DNA). Such recombination allows activation of *KRT14-Floxed-GFP-GLII* gene by excising a floxed DNA segment that blocks its expression, by separating the regulatory *KRT14* promoter and *GFP-GLII* coding sequences. Gene activation or inactivation *in vivo* can be achieved by mating two different animals, one carrying a target gene (*KRT14-Floxed-GFP-GLII*) with appropriately placed *loxP* sites and one carrying a *Cre* transgene (**Figure 7.1**). The specificity of the system depends upon strict regulation of *Cre* expression.

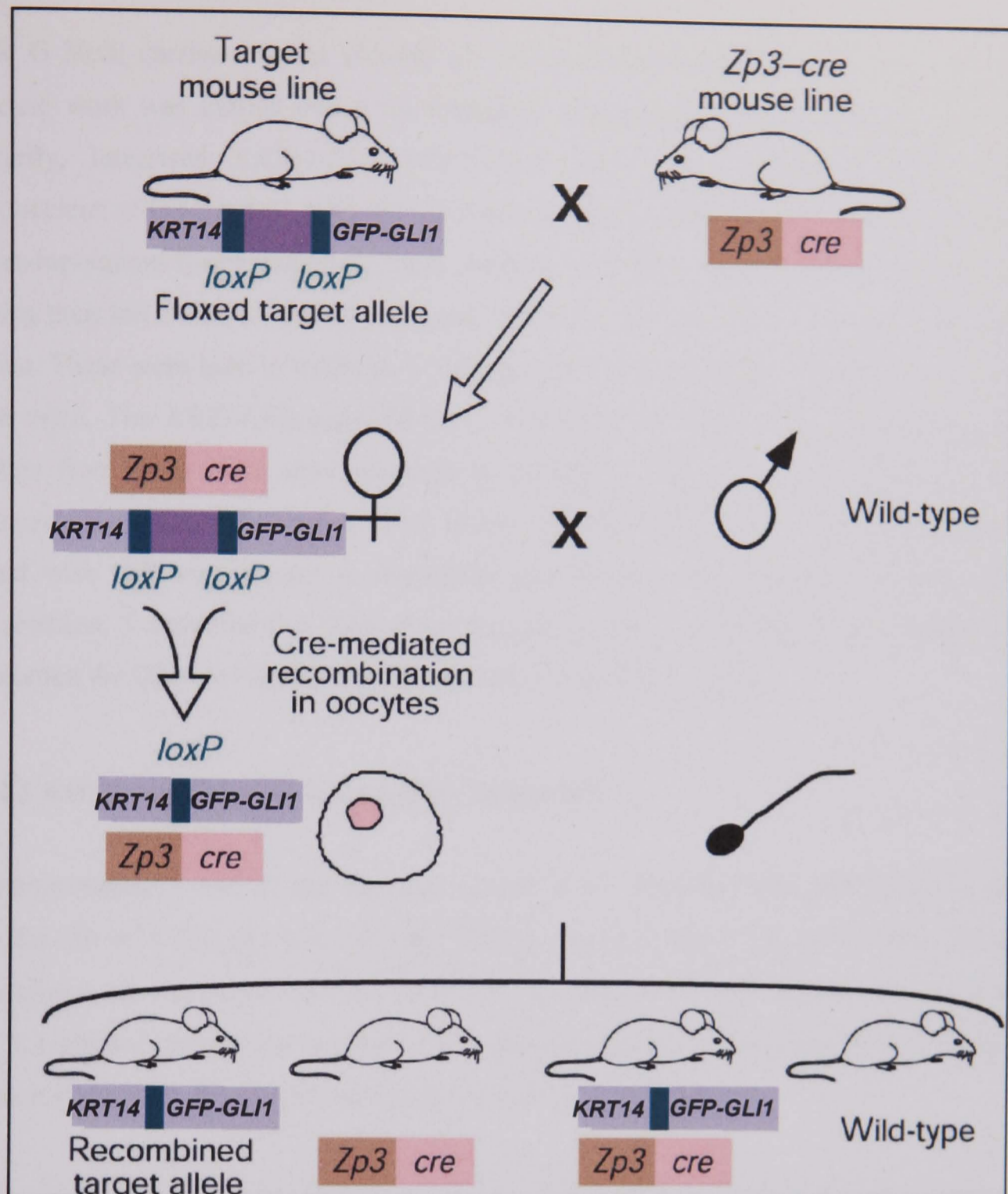


Figure 7.1: Diagrammatic representation of the mating scheme to generate *KRT14-Floxed-GFP-GLI1 Cre* female germ line transgenic mice. By crossing *Zp3-Cre* mice with a line of mice carrying the *KRT14-Floxed-GFP-GLI1* target gene, female *Cre*⁺/*KRT14-Floxed-GFP-GLI1*⁺ progeny were obtained. The *Cre* and *KRT14-Floxed-GFP-GLI1* gene segregate independently in these females, and thus when they are mated to wild type males, progeny of four different genotypes are obtained. If *Cre* has been expressed in the oocyte, the one *KRT14-GFP-GLI1* gene is inherited in the recombined form, regardless of whether the *Cre* transgene is also inherited. Thus, *Cre* activity in the female germ line can be assayed by determining the frequency at which *Cre*⁺/*KRT14-GFP-GLI1*⁺ females transmit the target gene in recombined form.

7.2.0 Materials and Methods.

DR G Neill carried out the cloning of *KRT14-Floxed-GFP-GLII* construct and the mouse work was carried out at the transgenic mouse facilities at Clare Hall CRUK. Briefly, linearised *KRT14-Floxed-GFP-GLII* DNA was injected into the male pronucleus of fertilised F1 x F1 hybrid mouse embryos which were then implanted in to pseudopregnant foster mothers. Litters obtained from the foster mothers were screened using their tail DNA, to identify transgenic founders *KRT14-Floxed-GFP-GLII* positive mice. These were bred to establish a “founder line” and to produce offspring with Zp3-cre mice. The *KRT14-Floxed-GFP-GLII* founders were mated with Zp3-cre mouse; litters from these mice were screened to identify a “second founder” line (*KRT14-Floxed-GFP-GLII* / Zp3-cre positive mice). The “second founder” line females were bred with wild-type mouse to recombine the *Floxed* DNA and thus activate *GLII* expression. I extracted the DNA from transgenic mice and designed the primers and screened the DNA to identify the founder line using PCR analysis.

7.2.1 Extracting DNA from transgenic mouse tail.

Approximately 5 mm of tail snip was placed in an eppendorf tube and 0.7 ml of tail buffer (50 mM Tris pH 8.0, 100 mM EDTA, 100 mM NaCl, 1% (w/v) SDS, 359 µg proteinase K) was added and incubated at 55°C overnight. Following incubation 0.7 ml of 1:1 phenol chloroform mixture was added per eppendorf tube and shaken using a bench shaker for 15 min and centrifuged at 13000 rpm for 10 min.

The upper aqueous phase was transferred to a clean eppendorf tube and equal volume of 1:1 phenol chloroform mixture was added, the solution was mixed and centrifuged at 13000 rpm for 10 min. The upper aqueous phase was transferred to a clean eppendorf tube and equal volume of chloroform was added, incubated shaking at room temperature for 15 min and centrifuged at 13000 rpm for 5 min. The upper aqueous phase was transferred to a clean eppendorf tube and 0.7 ml isopropanol added and mixed by shaking vigorously and centrifuged for 5 min. Supernatant was aspirated and the DNA pellet was washed with 250 µl 70% (v/v) ice cold ethanol. The pellet was allowed to air dry and resuspended in 50 µl [10 mM Tris. Cl pH 8.5] and the sample stored at -20°C.

7.2.2 Screening transgenic mouse DNA using PCR analysis.

Forward primers *KRT14* (5' agtataaagcactcgcaccc 3'), *Floxed* (5' cgccaccatgggaaatataact 3') and reverse primer *GFP* (5' gtgcagatgaacttcagggtca 3') were used to screen first and second founder lines. Zp3-*Cre* forward primer 5' tgacccggcaaaacaggtag 3' and reverse primer 5' tggtttcccgagaaacctga 3' amplified a PCR product of 521 bp were used to screen for Zp3-*Cre* positive mice.

Three PCR reactions for each sample for each set of primers were set up in a 96 well plate using 1 µl neat, 1 µl of 1:10 and 1 µl of 1:50 diluted mouse DNA from section 7.2.1 with the final concentration of the following components for each PCR reaction, 0.25 mM each dNTP, 1.25x reaction buffer [25 mM (NH₄)₂SO₄, 93.75 mM Tris-HCl pH 8.8 at 25°C, 1.25x10⁻² Tween 20], 1.75mM MgCl₂ for *K14-Floxed-GFP-GLII* PCR and 3 mM MgCl₂ for Zp3-*Cre* PCR, 0.125 µM each (forward & reverse) primer for *KRT14-Floxed-GFP-GLII* PCR and 0.25 µM each (forward & reverse) primer for Zp3-*Cre* PCR, 1 Unit thermal stable DNA polymerase (Advanced Biotechnology Red Hot DNA polymerase Catalogue No AB-0406/B). In a total reaction volume of 20µl made up with dH₂O.

A master mix (M/mix) was made up of all the components except DNA for all the samples; 19 µl of M/mix was added per well and 1 µl mouse DNA for each sample. The samples were thermo cycled, at 94°C for 3 min, 40 cycles at (94°C for 30 sec, 52°C for 1 min, 72°C for 1 min), and final extension at 72°C for 10 min for *KRT14-Floxed-GFP-GLII*. For Zp3-cre PCR the annealing temperature was set at 60°C. *KRT14-Floxed-GFP-GLII* and pPGK-*Cre* vectors obtained from Dr G Neil were used as positive controls in PCR screening analysis. β-Actin primers (Table 2.2) generating a PCR product of 320 bp were used as positive control to indicate that enough DNA template was present for amplification. These primers were blast searched using NCBI database, the results showed that they can amplify mouse and human β-Actin and they do not span the intron/exon boundaries. β-Actin PCR was set up same as that for *KRT14-Floxed-GFP-GLII* except the annealing temperature was set at 60°C. DNA samples from which β-actin was not amplified, fresh ear snips from these mice were requested and DNA extracted using protocol as for tail DNA extraction.

The PCR products were analysed on 1 % (w/v) agarose gel. **Figure 7.2** shows the expected size bands for Floxed (*KRT14-Floxed-GFP-GLI1*) allele and recombined (*KRT14-GFP-GLI1*) allele

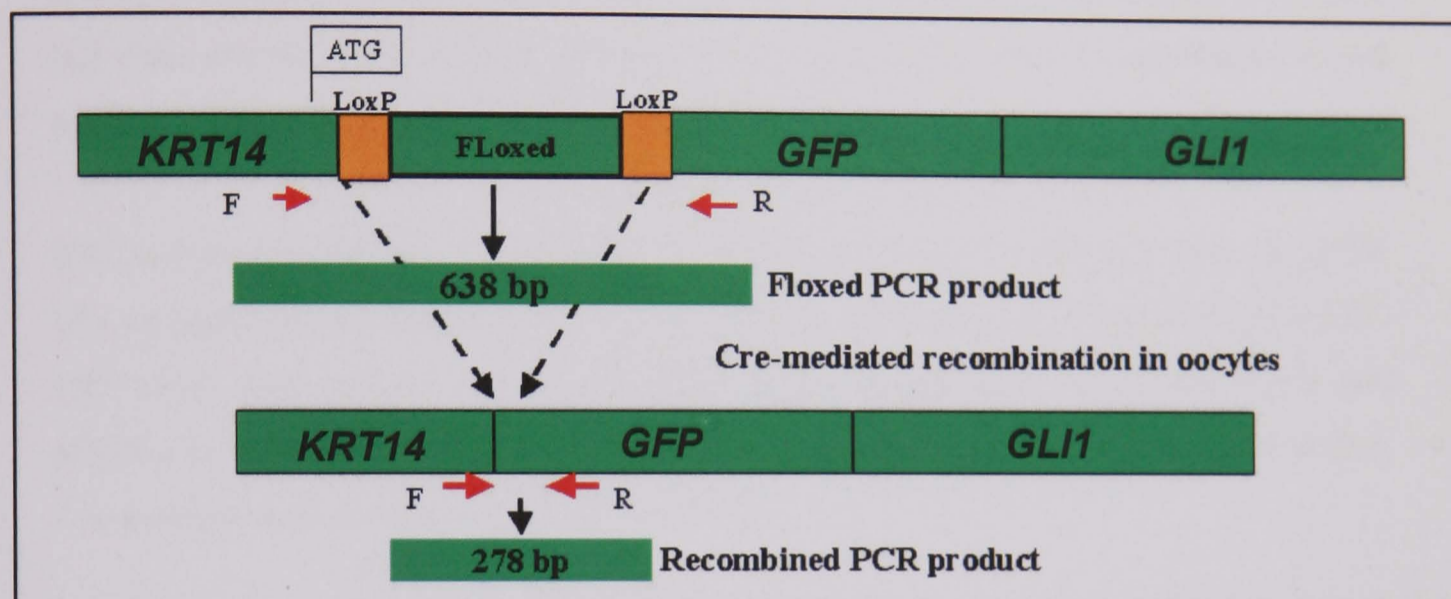


Figure 7.2: Diagram of *KRT14-Floxed-GFP-GLI1* construct indicating the (F) Forward and (R) reverse primers and *LoxP* position. A 638 bp *Floxed* PCR product was expected from unrecombined *KRT14-Floxed-GFP-GLI1* allele and a 278 bp PCR product was expected from recombined *KRT14-GFP-GLI1* allele.

7.3.0 Results

7.3.1 *In vitro* Cre mediated recombination of *KRT14-Floxed-GFP-GLII* to *KRT14-GFP-GLII* in 293 cells.

To check if the Zp3-cre system works, the 293 cell line was transfected with K14-Floxed-GFP-GLII plasmid and co-transfected with *KRT14-Floxed-GFP-GLII* and pPGK-*Cre* plasmid, were obtained from Dr G Neill. Total RNA was isolated from these cell lines and RT-PCR was carried out using protocols described in (section 2.5.0-and section 2.7.0), with primers described in section 7.2.2.

KRT14-Floxed-GFP-GLII recombined to *KRT14-GFP-GLII* in 293 cell lines via pPGK *Cre* mediated recombination. This is indicated by a band seen at 638 bp in *KRT14-loxP-GFP-GLII* lane and a band at 278 bp in cotransfected *KRT14-loxP-GFP-GLII* and pPGK-*Cre* lane in the RT-PCR (Figure 7.3). This indicates that the *LoxP* Floxed *Zp3-Cre* system work *in vitro*.

7.3.2 Generating a K14-Floxed-GFP-GLII mouse model under control of Zp3-Cre activation.

There were nine *KRT14-loxP-GFP-GLII* positive first founder lines (3 male, 6 female) out of 50 mice screened. All were bred with *Zp3-cre* mouse to generate a sec founder line *KRT14-loxP-GFP-GLII* and *Zp3-Cre* positive mice. Only one female mouse was positive for *KRT14-Floxed-GLII* and *Zp3-Cre*, this female was bred with wild-type mouse to get *KRT14-GFP-GLII* recombined gene.

None of litter one (7 mice) and litter two (10 mice) of the sec founder line female had the recombined *K14-GFP-GLII* gene. Table 7.1 shows the genes for which the litter one and litter two were positive.

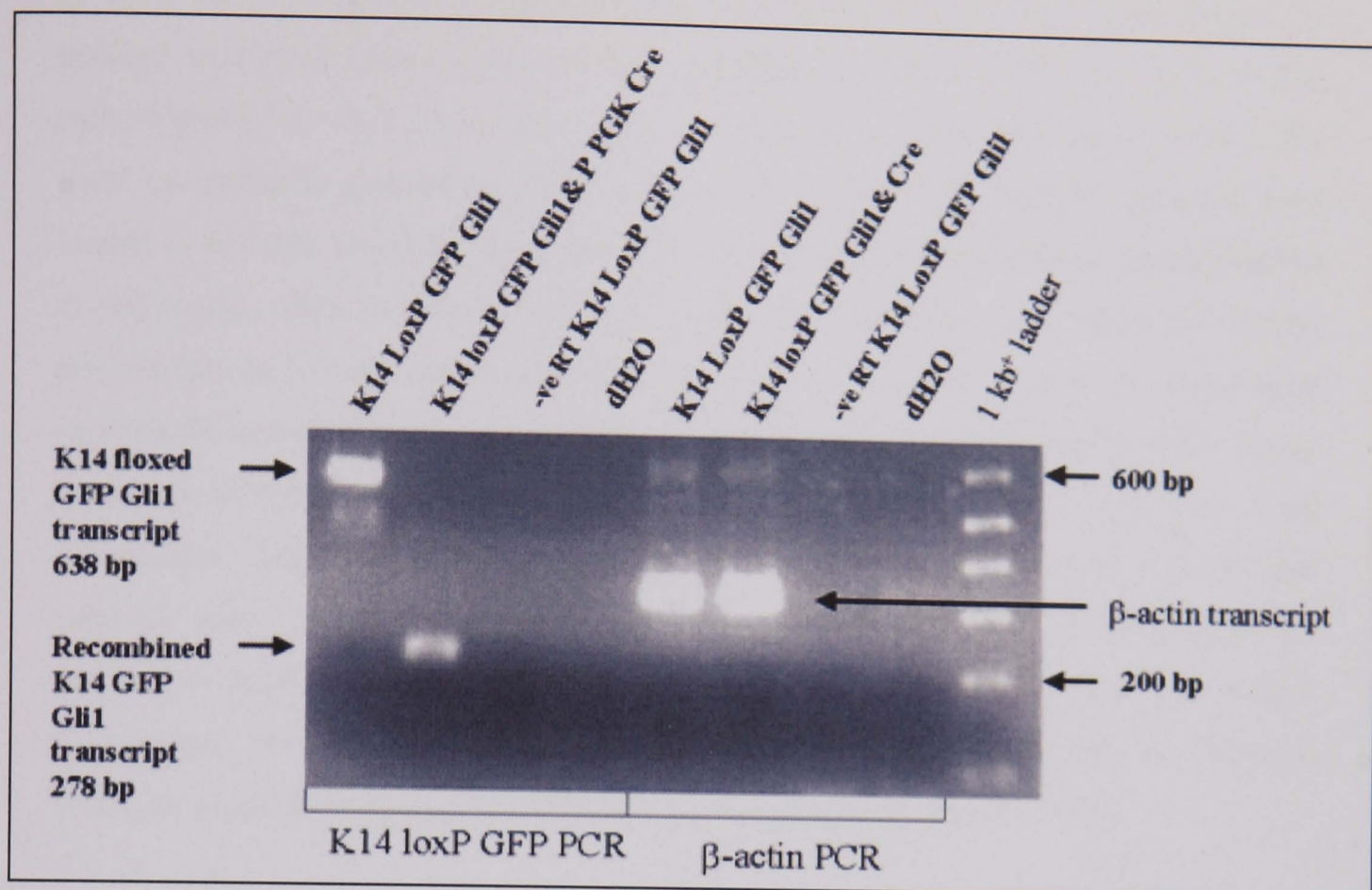


Figure 7.3 RT-PCR of *KRT14-Floxed-GFP-GLII* and *KRT14-Floxed-GFP-GLII* cotransfected pPGK-*Cre* 293 cell line. The band at 638 bp is the unrecombined *KRT14-Floxed-GFP-GLII* transcript. The band at 278 bp is the recombined *KRT14-GFP-GLII* transcript in cotransfected *KRT14-LoxP-GFP-GLII* and pPGK-*Cre* lane. There are no bands in the negative control -ve RT *KRT14-LoxP-GFP-GLII* and dH₂O lanes and for a positive RT-PCR β -actin control there are bands at 320 bp in *KRT14-LoxP-GFP-GLII* and cotransfected *KRT14-LoxP-GFP-GLII* and pPGK-*Cre* lanes. These results indicate that Cre mediate site specific recombination system works in vitro.

Table 7.1: Genes carried by transgenic litter one and two from the sec (female) founder line. None of the litters were positive for recombined *KRT14-GFP-GLII* gene.

Genes identified in litters of sec founder line.	Litter one	Litter two
<i>KRT14-Floxed-GFP-GLII</i> ⁺ / <i>Zp3-cre</i> ⁻	1	3
<i>KRT14-Floxed-GFP-GLII</i> ⁺ / <i>Zp3-cre</i> ⁺	2	4
<i>KRT14-Floxed-GFP-GLII</i> ⁻ / <i>Zp3-cre</i> ⁺	1	3
<i>KRT14-Floxed-GFP-GLII</i> ⁻ / <i>Zp3-cre</i> ⁻	3	0

7.4.0 Discussion

In vitro studies show that cotransfected *KRT14-Floxed-GFP-GLII* and pPGK-*Cre* resulted in *Floxed* region removed and generating a *KRT14-GFP-GLII* gene in 293 cells (**Figure 7.3**). This shows that the *LoxP Floxed Zp3-Cre* system works *in vitro*. We were successful in generating *KRT14-Floxed-GFP-GLII*^{+/Cre} founder mice but were unable to activate the target gene (*KRT14-GFP-GLII*) by *Cre*-mediated recombination in the oocytes when mating the founder mice with wild-type mice. There are several possibilities as to why this system has not worked; one of this is that the target gene (*KRT14-Floxed-GFP-GLII*) may have been incorporated into the Gnomie DNA where it can not be recombined by *Cre*. Alternatively it may be that the *Cre* mouse we used did not have functional *Cre*. Several other groups in the Cancer Research UK who had used the same *Cre* mouse have had similar problems (personal communications). We could have carried out control mating experiments to check function of *Zp3-Cre* in *Zp3-Cre* mouse. To determine where the target gene had incorporated into the Genomic DNA we could have carried out fluorescence in-situ hybridisation (FISH).

We also tried to generate recombined target *GLII* gene by injecting the *Cre* plasmid in to the *KRT14-Floxed-GFP-GLII* mouse embryo. This method also did not generate any recombined target gene. Due to Professor Quinn leaving and the escalating overall cost of the project it was decided not to proceed further. Part of my PhD study was to screen the mice to identify the founder line *KRT14-Floxed-GFP-GLII* and the recombined *KRT14-GFP-GLII* mice. I was then to carry out gene expression analysis on the *GLII* expressing mice to identify *GLII* target genes. As we have been unable to generate *GLII* transgenic mice this part of my project was abandoned.

7.5.0 Summary

We have shown cotransfected *KRT14-Floxed-GFP-GLII* and pPGK-*Cre* resulted in *Floxed* region removed and generating a *KRT14-GFP-GLII* gene in 293 cells, this indicates that *LoxP Floxed Zp3-Cre* system work *in vitro*. We were also successful in generating *KRT14-Floxed-GFP-GLII* founder mice but were unable to activate the target gene (*KRT14-GFP-GLII*) when mating the founder mice with wild-type mice.

CHAPTER 8

Conclusion

Mutations inactivating the HH-developmental pathway receptor protein PTCH is the primary event in BCC formation (Gailani et al., 1996; Hahn et al., 1996b; Johnson et al., 1996). Further evidence supporting the role of activated HH-signalling in BCC comes from studies of genetic mouse models and skin grafting experiments: (Aszterbaum et al., 1999) human keratinocytes expressing SHH, a ligand for Patched receptor protein, grafted onto the back of nude mice form BCC like structures (Fan et al., 1997). The molecular mechanism of the Hh signalling pathway has been worked out in greatest detail in *Drosophila* development (Hammerschmidt et al., 1997). Downstream of this pathway is the zinc-finger containing transcription factor Cubitus interruptus (Ci), which appears to be required for all aspects of Hh signalling in *Drosophila* (Methot and Basler, 1999). Three homologues of Cubitus interruptus (Ci), GLI1, GLI2 and GLI3 have been identified in human and mouse (Hui et al., 1994; Ruppert et al., 1990). The first human GLI gene to be discovered was GLI1 (Kinzler et al., 1987). GLI1 is overexpressed in BCC compared with normal human skin (Dahmane et al., 1997; Ghali et al., 1999).

Deregulation of the SHH pathway leads to a number of human diseases, include birth defects and BCC of the skin (Gailani et al., 1996; Gorlin, 1995; Hahn et al., 1996b; Johnson et al., 1996; Kimonis et al., 1997). In transgenic mouse model systems activation of GLI1 by SHH-signalling is a key step in initiating BCC formation (Nilsson et al., 2000). However, there is limited understanding of the molecular mechanisms involved in response to HH signalling and GLI activity in human BCC formation and how this pathway interacts with other pathways.

This study has shown with northern blot analysis carried out in **Chapter 3** that *GLI1*, *GLI2* and *PTCH* were induced in GLI1 expressing cells relative to non GLI1 expressing cells. RT-PCR analysis shows *GLI2- α/β* isoforms, *GLI3*, *SMO*, *PTCH*, *COUP-TFII*, *TFIID* and *KIF4* were expressed in normal skin, BCC and GLI1 expressing keratinocytes, and *GLI1* was only expressed in BCC and GLI1 expressing cell lines. Real-time-RT-PCR analysis shows that *GLI1*, *GLI2- α/β* isoforms, *GLI3*, *PTCH*, *SMO*, *KIF4* were induced and α -TUB was repressed in BCC relative to normal skin, and *GLI1*, *GLI2*, *GLI3*, *PTCH*, *SMO* and α -TUB were induced and *KIF4* was repressed in GLI1 expressing keratinocytes relative to non GLI1 expressing keratinocytes. Having determined that *GLI2* was upregulated in BCC and GLI1 expressing keratinocytes. Regl et al (2002) also demonstrated that there was a positive feedback loop between GLI1

and GLI2, thus it was hypothesized that *GLI1* may be a direct target of GLI2. To prove this hypothesis a collaborative study was carried out with Dr Fritz Abergers' lab. The data described in **Chapter 4** from this collaboration indicated that GLI2 binds the GLI-binding consensus sequence in the *GLI1* promoter (Ikram et al., 2004). This suggests that GLI2 directly activates GLI1. I have shown that retrovirally expressed GLI2 induces expression of endogenous GLI1 in human primary keratinocytes and *GLI2* is expressed in the interfollicular epidermis and the outer root sheath of hair follicles in normal skin as well as in BCC tumor islands. These results suggest that GLI2 may play an important role in regulating epidermal proliferation and skin tumorigenesis.

In the search for potential downstream mediators of GLI2 function in epidermal cells a new GLI2 target gene *FOXE1* was identified by Dr Fritz Abergers' lab. Its expression was induced in response to GLI2 by binding GLI putative binding sites in the *FOXE1* promoter region described in **Chapter 5** (Eichberger et al., 2004). I have shown that localisation of *FOXE1* overlaps with *GLI2* expression in human hair follicles, epidermis and BCC. This suggests a possible role of *FOXE1* in epidermal development and carcinogenesis downstream of HH/GLI signalling.

The work described in **Chapter 6** shows that GLI1 primary keratinocytes cultured in presence of EGF leads to a change in cellular morphology from rounded cells to spindly phenotype. In order to understand the molecular mechanism leading to a change in cell shape, we found that EGF induced vimentin and snail2 expression whereas GLI1 reduced the expression of these transcripts. There was no change in E-Cadherin (EMT marker) protein expression with GLI1 alone or with EGF, which is shown to be downregulated in classical EMT (Lee et al., 2006; Lu et al., 2003; Strizzi et al., 2004). Thus classical EMT was not occurring in GLI1 expressing primary keratinocytes cultured with EGF, although certain EMT markers (vimentin and snail2) were differentially regulated in these cells.

This study has also shown that EGF signalling reduces the transcription activity of GLI1 and this may be by shuttling GLI1 out of nucleus and possibly by altering the expression of SHH pathway genes *PTCH*, *SMO*, *GLI2* and *GLI3*. GLI1 also appeared to counteract the effects of EGF signalling by reducing the expression of EGF receptor. GLI1 also induces the keratinocytes stem cell marker keratin 19 (Michel et al., 1996b) expression whereas EGF appears to reduce keratin 19 expression. Affymetrix

microarrays analysis shows that there were 156 genes (see **APPENDIX I**) that were differentially regulated between GLI1 expressing keratinocytes cultured without growth supplement and cultured with EGF.

One gene that was differentially regulated in the Affymetrix data list was *VAV3*. GLI1 induced and EGF reduces *VAV3* expression. VAV (VAV1, VAV2 and VAV3) family of proteins are Guanine nucleotide exchange factors (Bustelo, 1996; Bustelo, 2000; Katzav et al., 1995; Schuebel et al., 1996; Trenkle et al., 2000) that are involved in regulating Rho family GTPases between a GTP-bound (active) state and a GDP-bound (inactive) state (Etienne-Manneville and Hall, 2002; Hall and Nobes, 2000). Re-modelling of the actin cytoskeleton is involved in cell division, growth, adhesion, and locomotion. This rearrangement of the actin cytoskeleton is influenced by the activity of Rho family GTPases (Etienne-Manneville and Hall, 2002; Hall and Nobes, 2000).

During the course of this study stocks of primary keratinocytes became depleted and primary keratinocytes from different patients were difficult to culture, thus N/TERT keratinocytes were used to continue the study. Real-time-RT-PCR analysis showed that GLI1 induced *VAV3.1* expression more than *VAV2* and EGF represses this induction. EGF alone completely repressed *VAV3.1* expression in N/TERT keratinocytes. These results were in line with the results published by Trenkle et al (2000) which show that there appears to be no *VAV3* expression in HaCat cells and *VAV3.1* was downregulated to levels that were not detectable in these cells when they were exposed to EGF. My results observed for *VAV3.1* in N/TERT keratinocytes (**Figure 6.13**) were similar to that observed for *VAV3* in the Affymetrix data with primary keratinocytes (**Appendix I**). *VAV2*, *VAV3* and *VAV3.1* were expressed in primary keratinocytes and N/TERT keratinocytes only express *VAV2* and *VAV3.1* (**Figure 6.12**). There was no change observed in *VAV2* and *VAV3.1* expression in GLI1 expressing primary keratinocytes cultured with and without EGF (**Figure 6.11**). However, in GLI1 expressing N/TERT keratinocytes *VAV3.1* induction was greater than *VAV2* and EGF reduced this induction. Thus different VAV proteins may be expressed in different keratinocytes cell lines and these may be differently regulated by the same stimulus.

Near to the end of this study Dr Graham Neill looked at GLI1 expressing N-TERT keratinocytes cultured with EGF using a time-lapse microscope. He observed that when these cells moved they left a trailing cell body behind and the cells appeared spindly the

movement was such that it seemed that the trailing body was sticking to the surface of the flask and preventing these cells from moving freely, these cells also tended to be sticking to each other. Once these cells had moved to a new position they revert back to rounded morphology and this process was repeated. Control cells (EGFP expressing N-TERT keratinocytes cultured without growth supplement and with EGF and GLI1 expressing N-TERT keratinocytes cultured without growth supplement) move rapidly with out leaving trailing cell body and they did not stick to each other (data not shown).

Thus the spindly phenotype that was observed for GLI primary keratinocytes cultured with EGF may have been due to the fact that when these cells move they elongate and form a spindly morphology which was captured at a fixed time point. Therefore, the spindly phenotype observed for GLI primary keratinocytes cultured with EGF, may not have been due to transformation but due to restriction in cell motility. This assumption is supported by the fact that when EGF was depleted in GLI1 expressing keratinocytes their spindly morphology reverts back to rounded morphology which was observed at a fixed point in time. This observation and alteration in *VAV* expression observed for GLI1 cells cultured with EGF (**Chapter 6**) supports the fact that GLI1 with EGF alters cell motility and may not be causing transformation or differentiation.

Therefore, GLI1 may be altering the expression of VAV and this may lead to alter or disrupt re-modelling of actin cytoskeleton during cell division, growth adhesion and locomotion and this may lead to BCC formation. This study has also shown that *VAV3.1* is expressed in BCC and normal skin (**Figure 6.14**), thus further work is required to quantify the levels of VAV and EGFR expression in BCC relative to normal skin and to determine if these correlate to GLI1 expression, to confirm whether the *in-vitro* system was similar to the *in-vivo* (BCC) situation.

Kinesin superfamily -4 (*KIF4*) mRNA was induced in BCC relative to normal skin and in HaCat and A375 cells relative to primary keratinocytes. However, it was repressed in GLI1 expressing primary keratinocytes relative to non GLI1 expressing control primary keratinocytes (**Figure 3.6, Table 3.4**) and there was greater repression of *KIF4* with GLI1 compared to EGF in primary keratinocytes relative to controls (**Figure 6.5**). This suggests that there may be GLI1 independent induction of *KIF4* in BCC *in-vivo* and *in-vitro* in certain cell lines. It is also possible that transcriptional activity of GLI1 may be differentially regulated in BCC *in-vivo* and *in-vitro* leading to alteration in expression of *KIF4* and this may explain the discrepancy in *KIF4* expression *in-vivo* and *in vitro*.

KIF4 plays multiple roles in mitosis, and its loss leads to numerous mitotic defects, including chromosome hypercondensation, aberrant spindle formation, anaphase bridges, defective cytokinesis, and aneuploidy (Castoldi and Vernos, 2006; Kurasawa et al., 2004; Lawrence et al., 2004; Mazumdar et al., 2006; Mazumdar and Misteli, 2005; Mazumdar et al., 2004). Aneuploidy is the most frequently observed type of cytogenetic abnormality that has long been suggested to contribute to tumor formation (Dey, 2004). Loss of KIF4 in embryonic stem cells lead to 70% of the cells being aneuploid and this increases their potential to form tumors in nude mice (Mazumdar et al., 2006). A reduced expression of KIF4 protein levels were also observed in 35% of human cancers from ovary, lung, breast, CNS, renal, melanoma and leukemia tissue. No reduction of KIF4 was found in colon cancer (Mazumdar et al., 2006). It is possible that loss of KIF4 in GLI1 expressing primary keratinocytes may also result in aneuploidy. Thus further work is required to investigate the expression of KIF4 protein in BCC and GLI1 expressing keratinocytes and determine how this may be differentially regulated *in vitro* and *in vivo*.

A possible scenario in the induction of BCC formation may be activation of GLI1, by inactivating mutations in PTCH followed by the induction of GLI2. Alternatively, activation of HH-signalling may first lead to the induction of GLI2 expression which directly activates GLI1 expression. This indicates that a feedback loop may be required in the activation and maintenance of BCC formation, which is not active in normal skin due to the absence of GLI1 expression. It is also possible that there may be certain unidentified factor(s) that are present in BCC that allow GLI2 to activate GLI1 which may not be present in normal skin.

The origin of BCC has been under debate for a very long time. While earlier evidence favoured basal keratinocytes of the interfollicular epidermis, more recent data points to the specialised cells within the hair follicle, analysis of the biomarkers in BCC suggest that the tumour is derived from the cells of the outer root sheath (ORS) (Kruger et al, 1999; Kurzen et al, 2001). Given the fact that GLI2, FOXE1 and GLI1 are present in the ORS and are found at high levels in BCC, a possible scenario for BCC development may be that constitutive activation of HH-signalling in the ORS distorts differentiation and promotes proliferation eventually leading to tumour formation.

Most BCC rarely metastasise (Safai and Good, 1977) and are difficult to culture. Therefore, induced expression of GLI1 may interact with EGF signalling in BCC and alter gene expression which leads to cells being stickier and less motile and this phenotype may be occurring by disrupting the cytoskeleton remodelling via altering Rho signalling activity. This may also lead to alteration in expression of stem cell markers and certain EMT markers. Loss of *KIF4* in GLI1 expressing primary keratinocytes *in vitro* model suggest that in normal skin it is possible that deregulation of SHH signalling leads to increased expression of GLI1. This in turn results in loss of KIF4 in stem cells; these cells become aneuploid and increase their potential to form BCC tumors. By understanding the molecular mechanism of SHH signalling pathway and identifying key players and how they interact with other pathways will enable us to design better strategies to treat and prevent BCC formation. **Figure 8.1** summarises the HH-signalling pathway outlining possible regulatory mechanisms of GLI activity and a model of tumorigenesis based on published data and findings reported in this thesis.

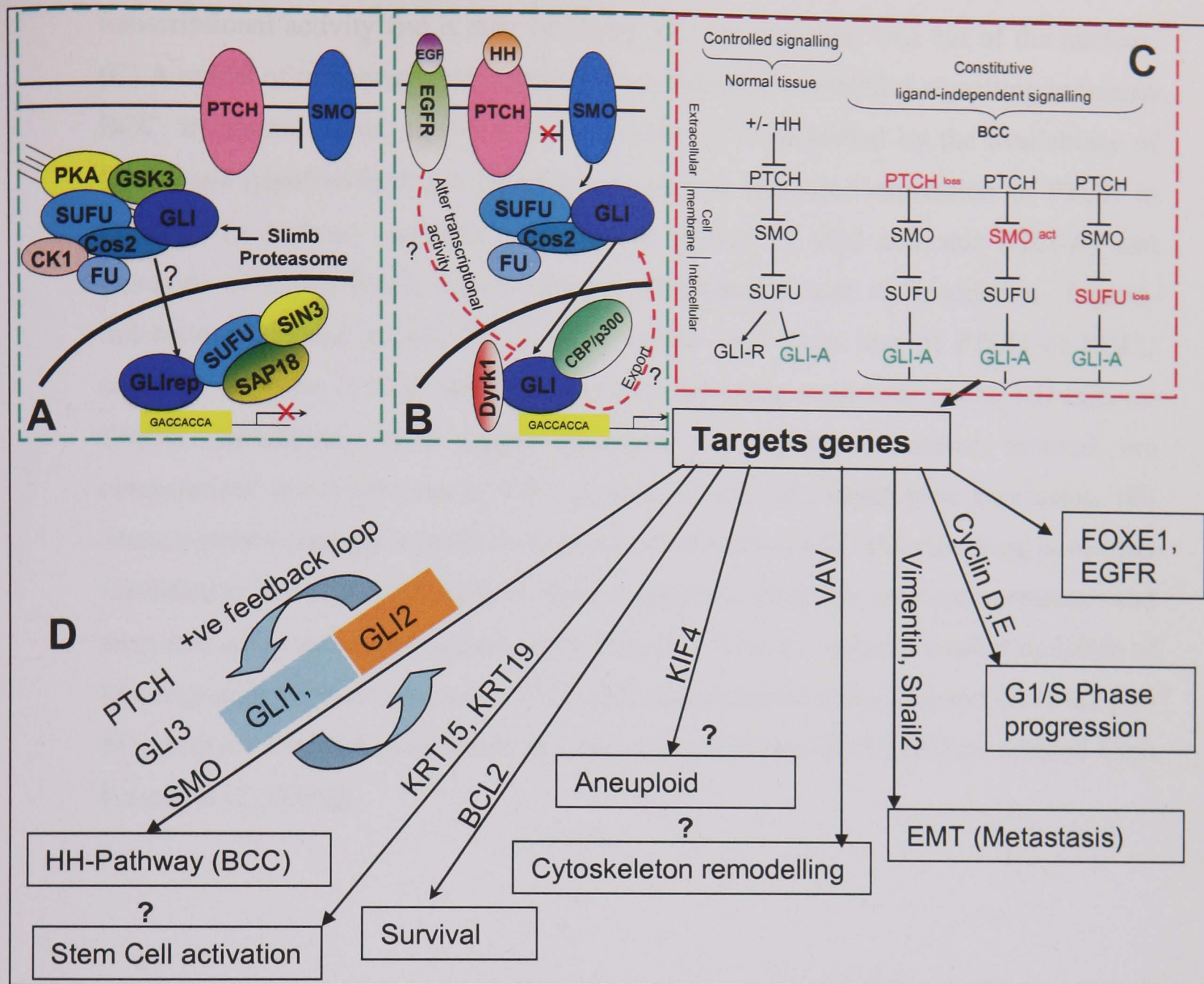


Figure 8. 1 A possible regulatory mechanism of GLI activity largely based on results from studies of *Drosophila* HH-signalling and a model of tumourigenesis resulting from constitutive HH/GLI signalling in human cancer. **(A)** In the absence of HH-ligand, GLI transcription factors are bound to a multiprotein complex via interactions with a vertebrate functional homologue of *Drosophila* Cos2. Phosphorylation of GLI by PKA, GSK3 and CK1 targets GLI to proteasome-dependent repressor formation. Proteolytic processing requires functional Slinb protein. Target gene repression may involve the recruitment of a histone-deacetylase activity via interaction of GLI with SUFU-SAP18-SIN3. Alternatively, phosphorylation may simply inactivate GLI proteins. In either case, HH target genes are not expressed. **(B)** On binding of HH protein to its receptor PTCH, phosphorylation of the cytoplasmic tail of SMO may recruit the Cos2/GLI complex and disassemble the GLI-kinase complex, thereby allowing the activator forms of GLI1, GLI2 and GLI3 to translocate to the nucleus and activate target gene transcription. The transcriptional activity of GLI proteins is further enhanced by interactions with Dyrk1 and CBP. This study has shown that EGF signalling alters GLI

transcriptional activity and it may be doing this via exporting GLI out of the nucleus. (C) A model of tumourigenesis resulting from constitutive HH/GLI signalling in human BCC. In normal tissue, HH/GLI pathway activity is controlled by the availability of ligand and negative-feedback mechanisms such as increased expression of PTCH in response to pathway activation. A precise balance of GLI activator (GLI-A) and repressor (GLI-R) forms assures proper development and differentiation. Ligand-independent tumour growth has been shown to arise from loss of PTCH or SUFU repressor function (PTCHloss, SUFUloss) or activating mutations in the HH-effector SMOH (SMOHact). Both ligand-dependent and ligand-independent tumours are characterised by an increase in (GLI-A) activity and GLI target gene expression. (D) Some possible oncogenic routes activated downstream of HH/GLI signalling have been identified in this and other studies. These include proliferation, survival, metastasis and stem cell activation which appear to be driven by (direct) transcriptional stimulation of key regulators of these processes. This study has identified that GLI2 and GLI1 are part of a positive feedback mechanism in basal cell carcinoma (BCC) (Figure adapted from Kasper et al., 2006a).

Affymetrix analysis of genes differentially expressed in GLI1-primary keratinocytes cultured with and without EGF.							EGF		GLI1+EGF		GLI1	
							EGFP-EGF/EGFP-GS	GLI1-EGF/EGFP-GS	GLI1-GS/EGFP-GS			
Systematic	Genbank	Common	Chrom	Title_Affy			Fold +/-	Up/Down	Fold +/-	Up/Down	Fold +/-	Up/Down
203706_s_at	NM_003507	FZD7	2	frizzled homolog 7 (Drosophila)			6.28	Up	27.28	Up	37.11	Up
205932_s_at	NM_002448	MSX1	4	msh homeo box homolog 1 (Drosophila)			8.01	Up	31.99	Up	13.31	Up
203368_at	NM_015513	CRELD1	3	cysteine-rich with EGF-like domains 1			5.21	Up	2.15	Up	1.62	Up
218523_at	NM_022126	LHPP	10	phospholysine phosphohistidine inorganic pyrophosphate phosphatase			-7.81	Down	-1.90	Down	1.16	Up
Structural Protein												
215294_s_at	AK026426	SMARCA1	23	SWI/SNF related, matrix associated, actin dependent regulator of chromatin, subfamily a, member 1			8.23	Up	21.10	Up	6.42	Up
203862_s_at	NM_001103	ACTN2	1	actinin, alpha 2			-14.35	Down	-5.50	Down	-16.82	Down
Transport												
213590_at	AA705628	SLC16A5	17	solute carrier family 16 (monocarboxylic acid transporters), member 5			5.61	Up	9.57	Up	8.59	Up
212292_at	AW452623	SLC7A1	13	solute carrier family 7 (cationic amino acid transporter, y+ system), member 1			-5.34	Down	-1.93	Down	-2.02	Down
221661_at	AF210455	SLC22A7	6	solute carrier family 22 (organic anion transporter), member 7			-7.92	Down	-1.93	Down	-19.23	Down
204368_at	NM_005630	SLC21A2	3	solute carrier family 21 (prostaglandin transporter), member 2			-6.06	Down	-1.13	Down	1.22	Up
202855_s_at	AL513917	SLC16A3	17	solute carrier family 16 (monocarboxylic acid transporters), member 3			-8.98	Down	-3.61	Down	2.01	Up
215274_at	AI627943	SLC12A3	16	solute carrier family 12 (sodium/chloride transporters), member 3			9.31	Up	10.33	Up	6.86	Up
210040_at	AF208159	SLC12A5	20	solute carrier family 12, (potassium-chloride transporter) member 5			6.30	Up	21.29	Up	5.03	Up
217691_x_at	AA853175	SLC16A3	17	solute carrier family 16 (monocarboxylic acid transporters), member 3			7.44	Up	6.96	Up	14.73	Up
208039_at	NM_003048	SLC9A2	2	solute carrier family 9 (sodium/hydrogen exchanger), isoform 2			5.11	Up	8.00	Up	3.50	Up
213664_at	AW235061	SLC1A1	9	solute carrier family 1 (neuronal/epithelial high affinity glutamate transporter, system Xag), member 1			18.06	Up	5.96	Up	41.24	Up
202631_s_at	NM_006380	APPBP2	17	amyloid beta precursor protein (cytoplasmic tail) binding protein 2			-5.43	Down	-3.34	Down	-1.33	Down
chemokine												
218002_s_at	NM_004887	CXCL14	5	chemokine (C-X-C motif) ligand 14			-24.62	Down	-6.68	Down	2.06	Up
204470_at	NM_001511	CXCL1	4	chemokine (C-X-C motif) ligand 1 (melanoma growth stimulating activity, alpha)			12.75	Up	8.18	Up	4.75	Up
Number of genes Up or Down							84	-72	96	-60	106	-50
% genes UP or Down							54	-46	62	-38	68	-32
Total genes							156					

APPENDIX II.

Standard Buffers and Solutions

Cell culture

Production of RM+ Concentrate.

<u>Supplement</u>	<u>Final media concentrate</u>
Hydrocortisone	0.4 µg/ml
Insulin (CN)	5 µg/ml
Epidermal growth factor (ICN)	10 ng/ml
Cholera toxin (ICN)	$10 \times 10^{-10} \text{M}$
Transferrin	5 µg/ml
Lyothyronine	$2 \times 10^{-11} \text{M}$

All come as 2ml vials, and Lyothyronine (small vial approx 50µl)

Making up the vials for addition to the 100x RM+ stock

Epidermal growth factor final media concentration = 10 ng/ml

Therefore: 100 x RM+ = 1 µg/ml

Dissolve 1mg in 10 ml dH₂O = 100 µg/ml and aliquot 2ml and store at -20°C.

Hydrocortisone

Final media concentration = 0.4 µg/ml

Therefore: 100 x RM+ = 40 µg/ml

Dissolve 100 mg in 25 ml dH₂O = 4mg/ml and aliquot 2 ml and store at -20°C.

Insulin

Final media concentration = 5 µg/ml.

Therefore: 100 x RM+ = 500 µg/ml

Dissolve 500mg in 10ml of 0.05 M HCl = 50mg/ml and aliquots 2 ml and store at 20°C

Cholera Toxin

Toxic take care

Molecular weight = 84,000

Final media concentration = 10^{-10} M

Therefore in 100 x RM+ = 10^{-8} M

Dissolve 1mg in 10 ml of distilled water freeze as 2ml aliquots at -20°C (0.2mg)

Transferin

Final media concentration = 5 µg/ml

Therefore in 100xRM+ = 500 µg/ml

Dissolve 500 mg in 10 ml distilled water = 50mg/ml freeze as 2 ml aliquots (100 mg)

Lyothyronine (Stock)

Molecular weight = 651.01

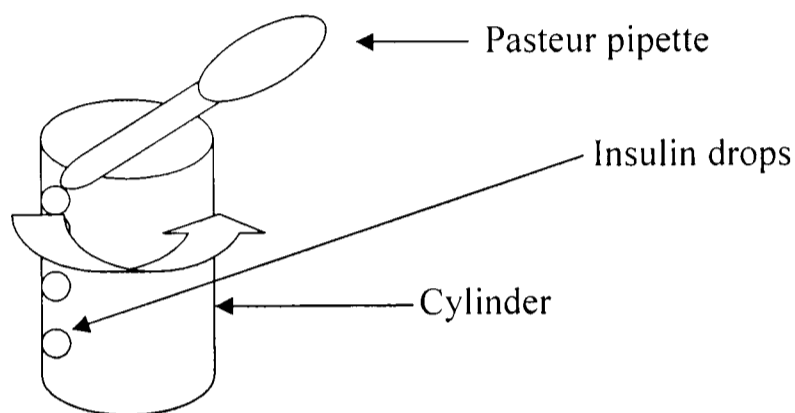
Final media concentration = 2×10^{-11} M

Therefore in 100xRM+ = 2×10^{-9} M

- Dissolve 13mg Lyothyronine in 1M HCl: Ethanol (1:2) (approx 5ml) make up to 20ml [650µg/ml]. Freeze 19ml in 1ml aliquots.
- Dilute 1ml [650 µg/ml] in 24ml distilled water = 26 µg/ml freeze 24 ml in 1 ml aliquots.
- Dilute 1ml [26 µg/ml] in 9 ml distilled water = 2.6 µg/ml freeze 9 ml in 1 ml aliquots.
- Freeze down 1 ml [2.6 µg/ml] as 100 µl aliquots (260 ng) this is used to make 100x RM+ the others are stocks.

Procedure

1. Collect 2 sterile 100 cm cylinders.
2. To one of the cylinders add 100 ml of distilled water in hood. Then collect falcon tube and add 50 ml of H₂O from cylinder.
3. Start with 2 ml (50 mg/ml) insulin using a Pasteur pipette, pipette 2 ml of insulin into the cylinder. Be careful! The way to do it is to press the pipette tip to the inside edge of the cylinder and as you gently turn the cylinder round in circular motion, you gently pipette out the insulin so that it trickles down the edge of the cylinder has shown in Figure A2.1 below.

**Figure A2.1**

4. Using the distilled water from the falcon tube, rinse the rest of the insulin eppendorf to collect as much insulin as possible and pipette gently (as mentioned before) into the cylinder. Use at least 20 ml of d H₂O to do this procedure if this procedure is done correctly, the solution in the cylinder i.e. insulin plus dH₂O will remain clear. If it is done too quickly, the solution will turn cloudy.
5. Next do the same with 100 μ l (2.6 μ g/ml) lyothyronine and wash the eppendorf down with dH₂O.
6. Do the same with the rest of the ingredients: e.g. transferin, cholera toxin, hydrocortisone and EGF.
7. Make up to 100ml using dH₂O as you are using the dH₂O to rinse the ingredient bottles.
8. When the ingredients are in the cylinder and the volume has reached 100 ml because of the addition of dH₂O during the procedures of adding the ingredients and at the end to arrive at the correct volume, and then pour the contents (100 ml) of the cylinder into a sterile bottle.

APPENDIX II Standard Buffers and Solutions

9. Add 100 ml of the E4/F12 medium (CRUK) to the sterile bottle to make up a final volume of 200 ml.
10. Collect another sterile 400ml bottle (empty) and filter the contents of the first bottle into the clean empty new bottle.
11. Collect \approx 50 bijoux small plastic containers with white screw caps and aliquot 4ml of the contents to each bijoux.
12. Date the bijoux and label them 'RM+' and store in -20°C freezer.

Production for RM- Concentrate.

Carry out exactly the same procedure as RM+ but **without** the addition of EGF.

Phosphate buffered saline (PBSA) 400ml bottle from CRUK

NaCL	8 g
KCl	0.25 g
Na ₂ HPO ₄	7.15 g
KH ₂ PO ₄	0.25 g

Made up to 1 litre with distilled water and adjusted pH to pH 7.2, autoclave for 20 min.

VERSINE/EDTA (CRUK)

NaCl	8 g
KCl	0.2 g
Na ₂ HPO ₄	0.5 6g
Versene (EDTA)	0.2 g
Phenol Red (1%)	1.5 ml

Dissolve in distilled water in stainless steel bucket (heat if necessary) and make up to final volume of 1 litre. Check pH = 7.2. Bottle in 16ml aliquots in universal and autoclave for 15mins and store at 4°C .

TRYPsin (CRUK)

0.25% in Tris Saline

NaCl	8 g
Na ₂ HPO ₄	0.1 g
D-Glucose	1 g
Trizma Base	3 g
KCl (19%)	2 ml
Phenol Red (1%)	1.5 ml

Dissolve in approx. 1/5th volume distilled water and titre pH with HCl to pH = 7.7 then add

Penicillin	0.06 g
Streptomycin	0.1 g

Or

Pen/Strep solution	10 ml
Trypsin	2.5 g

Dissolve Trypsin (Difco 1:250*) in approx. 1/5th volume distilled water, assist dissolving by bubbling air through the solution. Add dissolved Trypsin to the Tris Saline solution. Make up to final volume with distilled water; titre pH to pH 7.7 Sterilise by filtration using Pall 0.2m filter with pre-filter. Bottle in 15 ml amounts in universals and store at -20°C.

N.B. Trypsin is an allergenic substance and in its powdered state should always be handled in the fume cupboard.

Versene/Trypsin mixture used to detach monolayer's is made by adding 4ml trypsin (0.25%) to each universal of Versene/EDTA (16ml vial).

Glutamine 0.42 M solution (from CRUK) 20 ml universal

Store at -20°C. Use diluted 1/100 in medium (final concentration is 4.2 mM).

E4 culture medium (from CRUK) 400 ml bottle

DMEM/F12 E4 Culture medium (from CRUK) 400 ml bottle

90%FCS, 10% DMSO cell storage solution.

Dimethyl sulfoxide	5 ml
Foetal Calf Serum	45 ml

Northern blot

RNase Free water (DEPC treated dH₂O)

- Add 1 ml diethyl pyrocarbinate (DEPC) to 1 liter of ultra pure water (18.2 MΩcm; Milli Q plus, Millipore) and shake vigorously to bring the DEPC into solution.
- Incubate at 37°C over night and autoclave (15 psi, 121°C for 30min) and store at room temperature to remove any trace of DEPC.

Standard Saline Citrate 20x (SSC 20x)

Sodium Chloride (NaCl)	175.3 g
Sodium Citrate	88.2 g

In RNase free water titer to pH 7.0 with 10M NaOH and autoclave (15 psi, 121°C for 30min)

Wash Buffer

Sodium dodecyl sulphate (SDS) 10%	20 ml
SSC 2x (1:10 dilution of 20x SSC with RF water)	1980 ml

Store the solution at room temperature.

10 mM Tris, 1mM Na₂EDTA (TE Buffer)

		Final Con
Tris 1 M (tittered to pH 8.0 with 11.6 M HCl)	10 ml	10 mM
Na ₂ EDTA (titrated to pH 8.0 with 10 M NaOH)	4 ml	1 mM
RNase free water	986 ml	

APPENDIX II Standard Buffers and Solutions

MOPS 20x

MOPS (3-[N-merpholino]propane-sulphonic acid) 0.4 M

Sodium acetate 0.1 M

Na₂EDTA 0.2 M

Titre to pH 7.0 with 10 M NaOH and treat with 0.1% DEPC overnight at room temperature before autoclaving, store at room temperature in dark.

Strip Solution

Formamide 750 ml

SDS (10%) 10 ml

RNase free water 240 ml

1.2% Agarose/formaldehyde Gel

Agarose gel 3 g

RNase free water 195 ml

Boil in a microwave allow to cool to 60°C, before adding

MOPS 20x 12.5 ml

Formaldehyde 37 % 42.5 ml

Blue juice 10 x

50 % glycerol

0.1 mg/ml Bromphenol Blue

Denaturing RNA loading buffer 10x (Electrophoresis Cocktail)

MOPS 20x 0.5 µl

Deionized Formamide 5 µl

Formaldheide 37 % 1.75 µl

Blue juice 10x 1 µl

EtBr (10 mg/ml) 0.05 µl

RNase free water 1.7 µl

Final volume 10µl

* add 10 µl to 1 – 1.5µg of RNA

APPENDIX II Standard Buffers and Solutions

10X Tris-borate EDTA (TBE)

109.0 g Tris base

55.6 g boric acid

9.3 g EDTA

Made up to 1 litre with distilled water and used at 1x by diluting 1:10 in distilled water and pH adjusted to pH 8.3.

0.1 M Sodium Acetate Buffer pH5.2

Sodium acetate 8.204 g

Made up to 1 litre with dH₂O

PH adjusted to pH5.2.

In-Situ Hybridisation

0.1M TEA pH 8

Triethanolamine 7.4 g

RNase Free dH₂O 300 mls

Acetic acid 1 ml

Adjust pH with HCl

Make up to 400ml with RNase Free dH₂O

Prehybridisation Solution

Stock solution	Volume taken	Final Con
SCC 20x	200 µl	4x SSC
Denhardts 10x	100 µl	1x
Formamide 100%	500 µl	50%
t-RNA 10 mg/ml	5 µl	500 µg
*Single strand DNA 10 mg/ml	50 µl	500 µg
RNase Free dH ₂ O	100 µl	

*Before adding to the mix the single strand DNA should be denatured by heating to 100°C for 10 min and immediately placed on ice for 2 min.

Hybridisation Solution

Stock solution	Volume taken	Final Con
SCC 20x	200 µl	4x SSC
Denhardts 10x	100 µl	1x
Formamide 100%	500 µl	50%
Dextran sulphate 20%	100 µl	10%
t-RNA 10mg/ml	5 µl	500 µg
*Single strand DNA 10mg/ml	50 µl	500 µg
*Probe		50 ng/section

*Before adding to the mix the single strand DNA and the probe should be denatured by heating to 100°C for 10 min and immediately placed on ice for 2 min.

Blocking Solution

In-situ Hybridisation Buffer 1	977 µl
Triton 100x	3 µl
Normal sheep Serum	20 µl

Anti-Digoxigenin-AP, Fab fragments

Blocking solution	500 µl
Anti-Digoxigenin-AP [0.75 U/µl]	1 µl

4M Lithium chloride solution

Lithium chloride solution 8M (L7026 Sigma)	1 ml
DEPC dH ₂ O	1 ml

cRNA fragmentation buffer

80mM NaHO ₃
120mM Na ₂ CO ₃

In-situ Hybridisation Buffer 1

1M Tris-HCL Trizma base pH 8	100 ml
4M NaCl	37.5 ml
Autoclaved dH ₂ O	862.5 ml

In-situ Hybridisation Buffer 2

1M Tris-HCl pH 9.5	100 ml
4M NaCl	25 ml
1M MgCl ₂	50 ml
Autoclaved dH ₂ O	825 ml

In-situ Hybridisation Buffer 3

1M Tris-HCL pH 8	10 ml
0.5M EDTA	2 ml
Autoclaved dH ₂ O	988 ml

10X Citrate buffer

Citric acid (monohydrate)	3.78 g
Tri-sodium citrate	23.78 g
EDTA disodium salt	3.7 g

Made up to 1 litre with distilled water use at 1X by diluting 1:10 in distilled water and adjusted to pH 6.0 (using 1M NaOH, concentrated HCl).

25mM EDTA

EDTA disodium salt dehydrate	4.65 g
dH ₂ O	500 ml

Gill's Haematoxylin

Distilled water	730 ml
Ethylene glycol	250 ml
Haematoxylin	2 g
Sodium Iodate	0.2 g
Aluminium Sulphate	17.6 g

Then add 20 ml glacial acetic acid.

Acid alcohol

Methanol 70% (v/v)
0.4 M HCl in distilled water 30% (v/v)

Affymetrix**5x cRNA fragmentation buffer**

The fragmentation buffer is made with RNase free reagents. Tris-containing solutions should not be treated with DEPC; however, once H₂O has been DEPC-treated it can be used for making the Tris solution.

Combine the following components to a total volume of 20 ml DEPC-treated H₂O

Reagents	5x Final Con
4.0ml 1M Tris acetate pH 8.1 (Tris base adjusted with glacial acetic acid)	200 mM
0.64g Magnesium Acetate (MgOAc)	150 mM
0.98g Potassium Acetate (KOAc)	500 mM

Mix thoroughly and filter through a 0.2µm vacuum filter unit. Aliquot and store at room temperature.

CHIP Hybridisation buffer

(Final 1X concentration is 100mM MES, 1M NaCl, 20mM EDTA, 0.01% Tween 20)

2x Hybridisation buffer for 50 ml

12X MES Stock	8.3 ml
5M NaCl	17.7 ml
0.5M EDTA	4.0 ml
10% Tween 20	0.1 ml
dH ₂ O	19.9 ml

Store at 2-8°C, and shield from light. (If more convenient, 2x Hybridisation buffer can be added by Affymetrix Operator)

Western blotting

10%SDS

SDS (Sodium dodecyl sulphate)	50 g
dH ₂ O	500 ml

Cell lyses buffer (boiling buffer)

50mM Tris-HCl PH8.0
2% SDS
1mM-sodium orthovandate

2x Protein Sample loading Buffer

100mM Tris-HCl pH 6.8
4% SDS
20% Glycerol
0.2% Bromophenol Blue
200mM β-mercaptoethanol

Tris-glycine Running Buffer

25 mM Tris
192 mM Glycine
0.1% SDS

Transfer Buffer

25mM Tris
0.19M glycine
20% methanol
0.1% Tween-20

125mM Tris pH6.8

Tris base	7.57 g
dH ₂ O	300 ml

Titre the pH to pH 6.8 and make up to 500 ml with dH₂O.

APPENDIX II Standard Buffers and Solutions

375mM Tris PH8.8

Tris base 22.7 g

dH₂O 300 ml

Titre the pH to pH 8.8 and make up to 500ml with dH₂O.

Blocking buffer

5% Marvel milk in (0.1% Tween-20 in PBSA) Western blot

Stripping buffer

Tris PH 6.7 62 mM

SDS 2%

β-mercaptoethanol 0.1M

Reference

- Agren, M., Kogerman, P., Kleman, M. I., Wessling, M., and Toftgard, R. (2004). Expression of the PTCH1 tumor suppressor gene is regulated by alternative promoters and a single functional Gli-binding site. *Gene* 330, 101-114.
- Akimaru, H., Chen, Y., Dai, P., Hou, D. X., Nonaka, M., Smolik, S. M., Armstrong, S., Goodman, R. H., and Ishii, S. (1997). *Drosophila* CBP is a co-activator of cubitus interruptus in hedgehog signalling. *Nature* 386, 735-738.
- Alberts, B., Johnson, A., Lewis, J., Raff, M., Roberts, K. and Walter, P. (2002). *Molecular Biology of the Cell*, 4th edn (New York: Garland Science).
- Alcedo, J., Ayzenzon, M., Von Ohlen, T., Noll, M., and Hooper, J. E. (1996). The *Drosophila* smoothed gene encodes a seven-pass membrane protein, a putative receptor for the hedgehog signal. *Cell* 86, 221-232.
- Amlashi, S. F., Riffaud, L., Brassier, G., and Morandi, X. (2003). Nevoid basal cell carcinoma syndrome: relation with desmoplastic medulloblastoma in infancy. A population-based study and review of the literature. *Cancer* 98, 618-624.
- Apaydin, R., Gurbuz, Y., Bayramgurler, D., and Bilen, N. (2005). Cytokeratin contents of basal cell carcinoma, epidermis overlying tumour, and associated stromal amyloidosis: an immunohistochemical study. *Amyloid* 12, 41-47.
- Argyris, T. (1976). Kinetics of epidermal production during epidermal regeneration following abrasion in mice. *Am J Pathol* 83, 329-340.
- Asselineau, D., Bernard, B. A., Bailly, C., Darmon, M., and Prunieras, M. (1986). Human epidermis reconstructed by culture: is it "normal"? *J Invest Dermatol* 86, 181-186.
- Aszterbaum, M., Epstein, J., Oro, A., Douglas, V., LeBoit, P. E., Scott, M. P., and Epstein, E. H., Jr. (1999). Ultraviolet and ionizing radiation enhance the growth of BCCs and trichoblastomas in patched heterozygous knockout mice. *Nat Med* 5, 1285-1291.
- Aza-Blanc, P., and Kornberg, T. B. (1999). Ci: a complex transducer of the hedgehog signal. *Trends Genet* 15, 458-462.
- Aza-Blanc, P., Ramirez-Weber, F. A., Laget, M. P., Schwartz, C., and Kornberg, T. B. (1997). Proteolysis that is inhibited by hedgehog targets Cubitus interruptus protein to the nucleus and converts it to a repressor. *Cell* 89, 1043-1053.
- Bale, A. E., Gailani, M. R., and Leffell, D. J. (1994). Nevoid basal cell carcinoma syndrome. *J Invest Dermatol* 103, 126S-130S.

REFERENCE

- Balkwill, F. (2004). Cancer and the chemokine network. *Nat Rev Cancer* 4, 540-550.
- Barker, N., Morin, P. J., and Clevers, H. (2000). The Yin-Yang of TCF/beta-catenin signaling. *Adv Cancer Res* 77, 1-24.
- Barrallo-Gimeno, A., and Nieto, M. A. (2005). The Snail genes as inducers of cell movement and survival: implications in development and cancer. *Development* 132, 3151-3161.
- Barrandon, Y., and Green, H. (1985). Cell size as a determinant of the clone-forming ability of human keratinocytes. *Proc Natl Acad Sci U S A* 82, 5390-5394.
- Barrandon, Y., and Green, H. (1987). Three clonal types of keratinocyte with different capacities for multiplication. *Proc Natl Acad Sci U S A* 84, 2302-2306.
- Basler, K., and Struhl, G. (1994). Compartment boundaries and the control of *Drosophila* limb pattern by hedgehog protein. *Nature* 368, 208-214.
- Beemon, K., Duesberg, P., and Vogt, P. (1974). Evidence for crossing-over between avian tumor viruses based on analysis of viral RNAs. *Proc Natl Acad Sci U S A* 71, 4254-4258.
- Belloni, E., Muenke, M., Roessler, E., Traverso, G., Siegel-Bartelt, J., Frumkin, A., Mitchell, H. F., Donis-Keller, H., Helms, C., Hing, A. V., *et al.* (1996). Identification of Sonic hedgehog as a candidate gene responsible for holoprosencephaly. *Nat Genet* 14, 353-356.
- Bellusci, S., Furuta, Y., Rush, M. G., Henderson, R., Winnier, G., and Hogan, B. L. (1997). Involvement of Sonic hedgehog (Shh) in mouse embryonic lung growth and morphogenesis. *Development* 124, 53-63.
- Ben-Shushan, E., Sharir, H., Pikarsky, E., and Bergman, Y. (1995). A dynamic balance between ARP-1/COUP-TFII, EAR-3/COUP-TFI, and retinoic acid receptor:retinoid X receptor heterodimers regulates Oct-3/4 expression in embryonal carcinoma cells. *Mol Cell Biol* 15, 1034-1048.
- Bianchi, N., Depianto, D., McGowan, K., Gu, C., and Coulombe, P. A. (2005). Exploiting the keratin 17 gene promoter to visualize live cells in epithelial appendages of mice. *Mol Cell Biol* 25, 7249-7259.
- Bickenbach, J. R. (1981). Identification and behavior of label-retaining cells in oral mucosa and skin. *J Dent Res* 60 Spec No C, 1611-1620.
- Biesecker, L. G. (1997). Strike three for GLI3. *Nat Genet* 17, 259-260.
- Billeter, M. A., Cattaneo, R., Spielhofer, P., Kaelin, K., Huber, M., Schmid, A., Baczko, K., and ter Meulen, V. (1994). Generation and properties of measles virus mutations

REFERENCE

typically associated with subacute sclerosing panencephalitis. *Ann N Y Acad Sci* 724, 367-377.

Bitgood, M. J., and McMahon, A. P. (1995). Hedgehog and Bmp genes are coexpressed at many diverse sites of cell-cell interaction in the mouse embryo. *Dev Biol* 172, 126-138.

Bitgood, M. J., Shen, L., and McMahon, A. P. (1996). Sertoli cell signaling by Desert hedgehog regulates the male germline. *Curr Biol* 6, 298-304.

Blough, R. I., Petrij, F., Dauwerse, J. G., Milatovich-Cherry, A., Weiss, L., Saal, H. M., and Rubinstein, J. H. (2000). Variation in microdeletions of the cyclic AMP-responsive element-binding protein gene at chromosome band 16p13.3 in the Rubinstein-Taybi syndrome. *Am J Med Genet* 90, 29-34.

Bohnert, A., Hornung, J., Mackenzie, I. C., and Fusenig, N. E. (1986). Epithelial-mesenchymal interactions control basement membrane production and differentiation in cultured and transplanted mouse keratinocytes. *Cell Tissue Res* 244, 413-429.

Botchkarev, V. A., Botchkareva, N. V., Roth, W., Nakamura, M., Chen, L. H., Herzog, W., Lindner, G., McMahon, J. A., Peters, C., Lauster, R., *et al.* (1999). Noggin is a mesenchymally derived stimulator of hair-follicle induction. *Nat Cell Biol* 1, 158-164.

Bourgeois, P., Bolcato-Bellemin, A. L., Danse, J. M., Bloch-Zupan, A., Yoshida, K., Stoetzel, C., and Perrin-Schmitt, F. (1998). The variable expressivity and incomplete penetrance of the twist-null heterozygous mouse phenotype resemble those of human Saethre-Chotzen syndrome. *Hum Mol Genet* 7, 945-957.

Brewster, R., Mullor, J. L., and Ruiz i Altaba, A. (2000). Gli2 functions in FGF signaling during antero-posterior patterning. *Development* 127, 4395-4405.

Brooke, R. C. (2005). Basal cell carcinoma. *Clin Med* 5, 551-554.

Burley, S. K., and Roeder, R. G. (1996). Biochemistry and structural biology of transcription factor IID (TFIID). *Annu Rev Biochem* 65, 769-799.

Bustelo, X. R. (1996). The VAV family of signal transduction molecules. *Crit Rev Oncog* 7, 65-88.

Bustelo, X. R. (2000). Regulatory and signaling properties of the Vav family. *Mol Cell Biol* 20, 1461-1477.

Buttitta, L., Mo, R., Hui, C. C., and Fan, C. M. (2003). Interplays of Gli2 and Gli3 and their requirement in mediating Shh-dependent sclerotome induction. *Development* 130, 6233-6243.

Carlsson, P., and Mahlapuu, M. (2002). Forkhead transcription factors: key players in development and metabolism. *Dev Biol* 250, 1-23.

REFERENCE

- Castanet, M., Park, S. M., Smith, A., Bost, M., Leger, J., Lyonnet, S., Pelet, A., Czernichow, P., Chatterjee, K., and Polak, M. (2002). A novel loss-of-function mutation in TTF-2 is associated with congenital hypothyroidism, thyroid agenesis and cleft palate. *Hum Mol Genet* *11*, 2051-2059.
- Castoldi, M., and Vernos, I. (2006). Chromokinesin Xklp1 contributes to the regulation of microtubule density and organization during spindle assembly. *Mol Biol Cell* *17*, 1451-1460.
- Chadwick, B. P., Obermayr, F., and Frischauf, A. M. (1997). FKHL15, a new human member of the forkhead gene family located on chromosome 9q22. *Genomics* *41*, 390-396.
- Chen, Y., Cardinaux, J. R., Goodman, R. H., and Smolik, S. M. (1999). Mutants of cubitus interruptus that are independent of PKA regulation are independent of hedgehog signaling. *Development* *126*, 3607-3616.
- Chiang, C., Litingtung, Y., Lee, E., Young, K. E., Corden, J. L., Westphal, H., and Beachy, P. A. (1996). Cyclopia and defective axial patterning in mice lacking Sonic hedgehog gene function. *Nature* *383*, 407-413.
- Chiang, C., Swan, R. Z., Grachtchouk, M., Bolinger, M., Litingtung, Y., Robertson, E. K., Cooper, M. K., Gaffield, W., Westphal, H., Beachy, P. A., and Dlugosz, A. A. (1999a). Essential role for Sonic hedgehog during hair follicle morphogenesis. *Dev Biol* *205*, 1-9.
- Chiang, C., Swan, R. Z., Grachtchouk, M., Bolinger, M., Litingtung, Y., Robertson, E. K., Cooper, M. K., Gaffield, W., Westphal, H., Beachy, P. A., and Dlugosz, A. A. (1999b). Essential role for Sonic hedgehog during hair follicle morphogenesis. *Dev Biol* *205*, 1-9.
- Christophers, E. (1971). Cellular architecture of the stratum corneum. *J Invest Dermatol* *56*, 165-169.
- Cleaver, J. E., Thompson, L. H., Richardson, A. S., and States, J. C. (1999). A summary of mutations in the UV-sensitive disorders: xeroderma pigmentosum, Cockayne syndrome, and trichothiodystrophy. *Hum Mutat* *14*, 9-22.
- Clifton-Bligh, R. J., Wentworth, J. M., Heinz, P., Crisp, M. S., John, R., Lazarus, J. H., Ludgate, M., and Chatterjee, V. K. (1998). Mutation of the gene encoding human TTF-2 associated with thyroid agenesis, cleft palate and choanal atresia. *Nat Genet* *19*, 399-401.
- Commo, S., Gaillard, O., and Bernard, B. A. (2000). The human hair follicle contains two distinct K19 positive compartments in the outer root sheath: a unifying hypothesis for stem cell reservoir? *Differentiation* *66*, 157-164.
- Compton, C. C., Nadire, K. B., Regauer, S., Simon, M., Warland, G., O'Connor, N. E., Gallico, G. G., and Landry, D. B. (1998). Cultured human sole-derived keratinocyte

REFERENCE

- grafts re-express site-specific differentiation after transplantation. *Differentiation* 64, 45-53.
- Cotsarelis, G., Kaur, P., Dhouailly, D., Hengge, U., and Bickenbach, J. (1999). Epithelial stem cells in the skin: definition, markers, localization and functions. *Exp Dermatol* 8, 80-88.
- Cotsarelis, G., Sun, T. T., and Lavker, R. M. (1990). Label-retaining cells reside in the bulge area of pilosebaceous unit: implications for follicular stem cells, hair cycle, and skin carcinogenesis. *Cell* 61, 1329-1337.
- Crowson, A. N. (2006). Basal cell carcinoma: biology, morphology and clinical implications. *Mod Pathol* 19 Suppl 2, S127-147.
- Cuono, C., Langdon, R., and McGuire, J. (1986). Use of cultured epidermal autografts and dermal allografts as skin replacement after burn injury. *Lancet* 1, 1123-1124.
- Dahlstrand, J., Zimmerman, L. B., McKay, R. D., and Lendahl, U. (1992). Characterization of the human nestin gene reveals a close evolutionary relationship to neurofilaments. *J Cell Sci* 103 (Pt 2), 589-597.
- Dahmane, N., Lee, J., Robins, P., Heller, P., and Ruiz i Altaba, A. (1997). Activation of the transcription factor Gli1 and the Sonic hedgehog signalling pathway in skin tumours. *Nature* 389, 876-881.
- Dai, P., Akimaru, H., Tanaka, Y., Maekawa, T., Nakafuku, M., and Ishii, S. (1999). Sonic Hedgehog-induced activation of the Gli1 promoter is mediated by GLI3. *J Biol Chem* 274, 8143-8152.
- Damante, G., Tell, G., and Di Lauro, R. (2001). A unique combination of transcription factors controls differentiation of thyroid cells. *Prog Nucleic Acid Res Mol Biol* 66, 307-356.
- DasGupta, R., and Fuchs, E. (1999). Multiple roles for activated LEF/TCF transcription complexes during hair follicle development and differentiation. *Development* 126, 4557-4568.
- Dathan, N., Parlato, R., Rosica, A., De Felice, M., and Di Lauro, R. (2002). Distribution of the *titf2/foxe1* gene product is consistent with an important role in the development of foregut endoderm, palate, and hair. *Dev Dyn* 224, 450-456.
- De Berker, D., Wojnarowska, F., Sviland, L., Westgate, G. E., Dawber, R. P., and Leigh, I. M. (2000). Keratin expression in the normal nail unit: markers of regional differentiation. *Br J Dermatol* 142, 89-96.
- De Felice, M., Ovitt, C., Biffali, E., Rodriguez-Mallon, A., Arra, C., Anastassiadis, K., Macchia, P. E., Mattei, M. G., Mariano, A., Scholer, H., *et al.* (1998). A mouse model for hereditary thyroid dysgenesis and cleft palate. *Nat Genet* 19, 395-398.

REFERENCE

- Delattre, M., Briand, S., Paces-Fessy, M., and Blanchet-Tournier, M. F. (1999). The Suppressor of fused gene, involved in Hedgehog signal transduction in *Drosophila*, is conserved in mammals. *Dev Genes Evol* 209, 294-300.
- Deng, H., Lin, Q., and Khavari, P. A. (1997). Sustainable cutaneous gene delivery. *Nat Biotechnol* 15, 1388-1391.
- Deplewski, D., and Rosenfield, R. L. (2000). Role of hormones in pilosebaceous unit development. *Endocr Rev* 21, 363-392.
- Dey, P. (2004). Aneuploidy and malignancy: an unsolved equation. *J Clin Pathol* 57, 1245-1249.
- Ding, Q., Fukami, S., Meng, X., Nishizaki, Y., Zhang, X., Sasaki, H., Dlugosz, A., Nakafuku, M., and Hui, C. (1999). Mouse suppressor of fused is a negative regulator of sonic hedgehog signaling and alters the subcellular distribution of Gli1. *Curr Biol* 9, 1119-1122.
- Ding, Q., Motoyama, J., Gasca, S., Mo, R., Sasaki, H., Rossant, J., and Hui, C. C. (1998). Diminished Sonic hedgehog signaling and lack of floor plate differentiation in Gli2 mutant mice. *Development* 125, 2533-2543.
- Donnai, D., Burn, J., and Hughes, H. (1987). Smith-Lemli-Opitz syndromes: do they include the Pallister-Hall syndrome? *Am J Med Genet* 28, 741-743.
- Dry, F. W. (1926). Coat of the mouse (*Mus musculus*). *J Genetics* 16, 287-340.
- Dynlacht, B. D., Hoey, T., and Tjian, R. (1991). Isolation of coactivators associated with the TATA-binding protein that mediate transcriptional activation. *Cell* 66, 563-576.
- Echelard, Y., Epstein, D. J., St-Jacques, B., Shen, L., Mohler, J., McMahon, J. A., and McMahon, A. P. (1993). Sonic hedgehog, a member of a family of putative signaling molecules, is implicated in the regulation of CNS polarity. *Cell* 75, 1417-1430.
- Eckert, R. L. (1988). Sequence of the human 40-kDa keratin reveals an unusual structure with very high sequence identity to the corresponding bovine keratin. *Proc Natl Acad Sci U S A* 85, 1114-1118.
- Eichberger, T., Regl, G., Ikram, M. S., Neill, G. W., Philpott, M. P., Aberger, F., and Frischauf, A. M. (2004). FOXE1, a new transcriptional target of GLI2 is expressed in human epidermis and basal cell carcinoma. *J Invest Dermatol* 122, 1180-1187.
- El Ghouzzi, V., Legeai-Mallet, L., Aresta, S., Benoist, C., Munnich, A., de Gunzburg, J., and Bonaventure, J. (2000). Saethre-Chotzen mutations cause TWIST protein degradation or impaired nuclear location. *Hum Mol Genet* 9, 813-819.

REFERENCES

- Elliott, K., Stephenson, T. J., and Messenger, A. G. (1999). Differences in hair follicle dermal papilla volume are due to extracellular matrix volume and cell number: implications for the control of hair follicle size and androgen responses. *J Invest Dermatol* *113*, 873-877.
- Etienne-Manneville, S., and Hall, A. (2002). Rho GTPases in cell biology. *Nature* *420*, 629-635.
- Fan, H., Oro, A. E., Scott, M. P., and Khavari, P. A. (1997). Induction of basal cell carcinoma features in transgenic human skin expressing Sonic Hedgehog. *Nat Med* *3*, 788-792.
- Ferraris, C., Chaloin-Dufau, C., and Dhouailly, D. (1994). Transdifferentiation of embryonic and postnatal rabbit corneal epithelial cells. *Differentiation* *57*, 89-96.
- Ferraris, C., Chevalier, G., Favier, B., Jahoda, C. A., and Dhouailly, D. (2000). Adult corneal epithelium basal cells possess the capacity to activate epidermal, pilosebaceous and sweat gland genetic programs in response to embryonic dermal stimuli. *Development* *127*, 5487-5495.
- Freedberg, I. M., Tomic-Canic, M., Komine, M., and Blumenberg, M. (2001). Keratins and the keratinocyte activation cycle. *J Invest Dermatol* *116*, 633-640.
- Fu, X., Sun, X., Li, X., and Sheng, Z. (2001). Dedifferentiation of epidermal cells to stem cells in vivo. *Lancet* *358*, 1067-1068.
- Fuchs, E., and Green, H. (1980). Changes in keratin gene expression during terminal differentiation of the keratinocyte. *Cell* *19*, 1033-1042.
- Fuchs, E., Merrill, B. J., Jamora, C., and DasGupta, R. (2001). At the roots of a never-ending cycle. *Dev Cell* *1*, 13-25.
- Fuchs, E., and Weber, K. (1994). Intermediate filaments: structure, dynamics, function, and disease. *Annu Rev Biochem* *63*, 345-382.
- Furumoto, T. A., Miura, N., Akasaka, T., Mizutani-Koseki, Y., Sudo, H., Fukuda, K., Maekawa, M., Yuasa, S., Fu, Y., Moriya, H., *et al.* (1999). Notochord-dependent expression of MFH1 and PAX1 cooperates to maintain the proliferation of sclerotome cells during the vertebral column development. *Dev Biol* *210*, 15-29.
- Fusenig, N. E. (1994). Epithelial-mesenchymal interactions regulate keratinocyte growth and differentiation in vitro, In *The keratinocyte handbook*, I. Leigh, E. B. Lane, and M. Watt Fiona, eds. (Cambridge England ; New York, NY, USA: Cambridge University Press), pp. 71-94.
- Gailani, M. R., Stahle-Backdahl, M., Leffell, D. J., Glynn, M., Zaphiropoulos, P. G., Pressman, C., Unden, A. B., Dean, M., Brash, D. E., Bale, A. E., and Toftgard, R. (1996). The role of the human homologue of *Drosophila* patched in sporadic basal cell carcinomas. *Nat Genet* *14*, 78-81.

REFERENCE

- Gandarillas, A., and Watt, F. M. (1997). c-Myc promotes differentiation of human epidermal stem cells. *Genes Dev* 11, 2869-2882.
- Gat, U., DasGupta, R., Degenstein, L., and Fuchs, E. (1998). De Novo hair follicle morphogenesis and hair tumors in mice expressing a truncated beta-catenin in skin. *Cell* 95, 605-614.
- Ghahary, A., Marcoux, Y., Karimi-Busheri, F., and Tredget, E. E. (2001). Keratinocyte differentiation inversely regulates the expression of involucrin and transforming growth factor beta1. *J Cell Biochem* 83, 239-248.
- Ghali, L., Wong, S. T., Green, J., Tidman, N., and Quinn, A. G. (1999). Gli1 protein is expressed in basal cell carcinomas, outer root sheath keratinocytes and a subpopulation of mesenchymal cells in normal human skin. *J Invest Dermatol* 113, 595-599.
- Gharzi, A., Reynolds, A. J., and Jahoda, C. A. (2003). Plasticity of hair follicle dermal cells in wound healing and induction. *Exp Dermatol* 12, 126-136.
- Ghazizadeh, S., and Taichman, L. B. (2001). Multiple classes of stem cells in cutaneous epithelium: a lineage analysis of adult mouse skin. *Embo J* 20, 1215-1222.
- Ghosh, M. M., Boyce, S., Layton, C., Freedlander, E., and Mac Neil, S. (1997). A comparison of methodologies for the preparation of human epidermal- dermal composites. *Ann Plast Surg* 39, 390-404.
- Gitelman, I. (1997). Twist protein in mouse embryogenesis. *Dev Biol* 189, 205-214.
- Goldstein, A. M., Bale, S. J., Peck, G. L., and DiGiovanna, J. J. (1993). Sun exposure and basal cell carcinomas in the nevoid basal cell carcinoma syndrome. *J Am Acad Dermatol* 29, 34-41.
- Goodrich, J. A., Hoey, T., Thut, C. J., Admon, A., and Tjian, R. (1993). Drosophila TAFII40 interacts with both a VP16 activation domain and the basal transcription factor TFIIB. *Cell* 75, 519-530.
- Goodrich, L. V., Johnson, R. L., Milenkovic, L., McMahon, J. A., and Scott, M. P. (1996). Conservation of the hedgehog/patched signaling pathway from flies to mice: induction of a mouse patched gene by Hedgehog. *Genes Dev* 10, 301-312.
- Goodrich, L. V., Milenkovic, L., Higgins, K. M., and Scott, M. P. (1997). Altered neural cell fates and medulloblastoma in mouse patched mutants. *Science* 277, 1109-1113.
- Goodrich, L. V., and Scott, M. P. (1998). Hedgehog and patched in neural development and disease. *Neuron* 21, 1243-1257.
- Gorlin, R. J. (1987). Nevoid basal-cell carcinoma syndrome. *Medicine (Baltimore)* 66, 98-113.

REFERENCE

- Gorlin, R. J. (1995). Nevoid basal cell carcinoma syndrome. *Dermatol Clin* 13, 113-125.
- Grachtchouk, M., Mo, R., Yu, S., Zhang, X., Sasaki, H., Hui, C. C., and Dlugosz, A. A. (2000). Basal cell carcinomas in mice overexpressing Gli2 in skin. *Nat Genet* 24, 216-217.
- Green, J., Leigh, I. M., Poulson, R., and Quinn, A. G. (1998). Basal cell carcinoma development is associated with induction of the expression of the transcription factor Gli-1. *Br J Dermatol* 139, 911-915.
- Grimm, T., Teglund, S., Tackels, D., Sangiorgi, E., Gurrieri, F., Schwartz, C., and Toftgard, R. (2001). Genomic organization and embryonic expression of Suppressor of Fused, a candidate gene for the split-hand/split-foot malformation type 3. *FEBS Lett* 505, 13-17.
- Grindley, J. C., Bellusci, S., Perkins, D., and Hogan, B. L. (1997). Evidence for the involvement of the Gli gene family in embryonic mouse lung development. *Dev Biol* 188, 337-348.
- Groves, R. W., Allen, M. H., and MacDonald, D. M. (1992). Abnormal expression of epidermal growth factor receptor in cutaneous epithelial tumours. *J Cutan Pathol* 19, 66-72.
- Grunert, S., Jechlinger, M., and Beug, H. (2003). Diverse cellular and molecular mechanisms contribute to epithelial plasticity and metastasis. *Nat Rev Mol Cell Biol* 4, 657-665.
- Haake, A. R., Holbrook, K. (1999). The structure and development of skin, In Fitzpatrick's dermatology in general medicine, T. B. Fitzpatrick, and I. M. Freedberg, eds. (New York: McGraw-Hill Health Professions Division), pp. 70-114.
- Hahn, H., Christiansen, J., Wicking, C., Zaphiropoulos, P. G., Chidambaram, A., Gerrard, B., Vorechovsky, I., Bale, A. E., Toftgard, R., Dean, M., and Wainwright, B. (1996a). A mammalian patched homolog is expressed in target tissues of sonic hedgehog and maps to a region associated with developmental abnormalities. *J Biol Chem* 271, 12125-12128.
- Hahn, H., Wicking, C., Zaphiropoulos, P. G., Gailani, M. R., Shanley, S., Chidambaram, A., Vorechovsky, I., Holmberg, E., Uden, A. B., Gillies, S., *et al.* (1996b). Mutations of the human homolog of *Drosophila* patched in the nevoid basal cell carcinoma syndrome. *Cell* 85, 841-851.
- Hahn, H., Wojnowski, L., Miller, G., and Zimmer, A. (1999). The patched signaling pathway in tumorigenesis and development: lessons from animal models. *J Mol Med* 77, 459-468.
- Hahn, S. (1998). The role of TAFs in RNA polymerase II transcription. *Cell* 95, 579-582.

REFERENCE

- Hall, A. (1998). Rho GTPases and the actin cytoskeleton. *Science* 279, 509-514.
- Hall, A., and Nobes, C. D. (2000). Rho GTPases: molecular switches that control the organization and dynamics of the actin cytoskeleton. *Philos Trans R Soc Lond B Biol Sci* 355, 965-970.
- Hammerschmidt, M., Brook, A., and McMahon, A. P. (1997). The world according to hedgehog. *Trends Genet* 13, 14-21.
- Harari, P. M. (2004). Epidermal growth factor receptor inhibition strategies in oncology. *Endocr Relat Cancer* 11, 689-708.
- Hardcastle, Z., Mo, R., Hui, C. C., and Sharpe, P. T. (1998). The Shh signalling pathway in tooth development: defects in Gli2 and Gli3 mutants. *Development* 125, 2803-2811.
- Hardy, M. H. (1992). The secret life of the hair follicle. *Trends Genet* 8, 55-61.
- Harris, P. A., Leigh, I. M., and Navsaria, H. A. (2001). Keratinocyte biology and dermal-epidermal interactions, In *Cutaneous wound healing*, V. Falanga, ed. (London: Martin Dunitz), pp. 39-56.
- Hartevelt, M. M., Bavinck, J. N., Kootte, A. M., Vermeer, B. J., and Vandenbroucke, J. P. (1990). Incidence of skin cancer after renal transplantation in The Netherlands. *Transplantation* 49, 506-509.
- Hernandez, N. (1993). TBP, a universal eukaryotic transcription factor? *Genes Dev* 7, 1291-1308.
- Hesse, M., Magin, T. M., and Weber, K. (2001). Genes for intermediate filament proteins and the draft sequence of the human genome: novel keratin genes and a surprisingly high number of pseudogenes related to keratin genes 8 and 18. *J Cell Sci* 114, 2569-2575.
- Hesse, M., Zimek, A., Weber, K., and Magin, T. M. (2004). Comprehensive analysis of keratin gene clusters in humans and rodents. *Eur J Cell Biol* 83, 19-26.
- Hirokawa, N. (1998). Kinesin and dynein superfamily proteins and the mechanism of organelle transport. *Science* 279, 519-526.
- Hirokawa, N., and Takemura, R. (2005). Molecular motors and mechanisms of directional transport in neurons. *Nat Rev Neurosci* 6, 201-214.
- Hoffmann, A., Oelgeschlager, T., and Roeder, R. G. (1997). Considerations of transcriptional control mechanisms: do TFIID-core promoter complexes recapitulate nucleosome-like functions? *Proc Natl Acad Sci U S A* 94, 8928-8935.

REFERENCE

- Hohl, D. (1993). Expression patterns of loricrin in dermatological disorders. *Am J Dermatopathol* *15*, 20-27.
- Hohl, D., Lichti, U., Breitzkreutz, D., Steinert, P. M., and Roop, D. R. (1991). Transcription of the human loricrin gene in vitro is induced by calcium and cell density and suppressed by retinoic acid. *J Invest Dermatol* *96*, 414-418.
- Holme, S. A., Malinowszky, K., and Roberts, D. L. (2000). Changing trends in non-melanoma skin cancer in South Wales, 1988-98. *Br J Dermatol* *143*, 1224-1229.
- Hornstein, I., Alcover, A., and Katzav, S. (2004). Vav proteins, masters of the world of cytoskeleton organization. *Cell Signal* *16*, 1-11.
- Howard, T. D., Paznekas, W. A., Green, E. D., Chiang, L. C., Ma, N., Ortiz de Luna, R. I., Garcia Delgado, C., Gonzalez-Ramos, M., Kline, A. D., and Jabs, E. W. (1997). Mutations in TWIST, a basic helix-loop-helix transcription factor, in Saethre-Chotzen syndrome. *Nat Genet* *15*, 36-41.
- Howell, J. B., and Caro, M. R. (1959). The basal-cell nevus: its relationship to multiple cutaneous cancers and associated anomalies of development. *AMA Arch Derm* *79*, 67-77; discussion 77-80.
- Howell, J. B., and Mehregan, A. H. (1970). Pursuit of the pits in the nevoid basal cell carcinoma syndrome. *Arch Dermatol* *102*, 586-597.
- Huber, M. A., Kraut, N., and Beug, H. (2005). Molecular requirements for epithelial-mesenchymal transition during tumor progression. *Curr Opin Cell Biol* *17*, 548-558.
- Huelsken, J., Vogel, R., Erdmann, B., Cotsarelis, G., and Birchmeier, W. (2001). beta-Catenin controls hair follicle morphogenesis and stem cell differentiation in the skin. *Cell* *105*, 533-545.
- Hughes, J. D., Estep, P. W., Tavazoie, S., and Church, G. M. (2000). Computational identification of cis-regulatory elements associated with groups of functionally related genes in *Saccharomyces cerevisiae*. *J Mol Biol* *296*, 1205-1214.
- Hui, C. C., and Joyner, A. L. (1993). A mouse model of greig cephalopolysyndactyly syndrome: the extra-toesJ mutation contains an intragenic deletion of the Gli3 gene. *Nat Genet* *3*, 241-246.
- Hui, C. C., Slusarski, D., Platt, K. A., Holmgren, R., and Joyner, A. L. (1994). Expression of three mouse homologs of the *Drosophila* segment polarity gene cubitus interruptus, Gli, Gli-2, and Gli-3, in ectoderm- and mesoderm-derived tissues suggests multiple roles during postimplantation development. *Dev Biol* *162*, 402-413.
- Hynes, M., Stone, D. M., Dowd, M., Pitts-Meek, S., Goddard, A., Gurney, A., and Rosenthal, A. (1997). Control of cell pattern in the neural tube by the zinc finger transcription factor and oncogene Gli-1. *Neuron* *19*, 15-26.

REFERENCE

- Ikram, M. S., Neill, G. W., Regl, G., Eichberger, T., Frischauf, A. M., Aberger, F., Quinn, A., and Philpott, M. (2004). GLI2 is expressed in normal human epidermis and BCC and induces GLI1 expression by binding to its promoter. *J Invest Dermatol* 122, 1503-1509.
- Ingham, P. W. (1998). Transducing Hedgehog: the story so far. *Embo J* 17, 3505-3511.
- Ingham, P. W., and McMahon, A. P. (2001). Hedgehog signaling in animal development: paradigms and principles. *Genes Dev* 15, 3059-3087.
- Irvin, T. T. (1981). Wound healing : principles and practice (London ; New York: Chapman and Hall).
- Ishida-Yamamoto, A., McGrath, J. A., Chapman, S. J., Leigh, I. M., Lane, E. B., and Eady, R. A. (1991). Epidermolysis bullosa simplex (Dowling-Meara type) is a genetic disease characterized by an abnormal keratin-filament network involving keratins K5 and K14. *J Invest Dermatol* 97, 959-968.
- Jacob, A. (1827). Observations respecting an ulcer of peculiar character, which attacks the eyelids and other parts of the face. *Dublin Hospital Rep Commun Med Surg* 4, 232-239.
- Jahoda, C. A. (1992). Induction of follicle formation and hair growth by vibrissa dermal papillae implanted into rat ear wounds: vibrissa-type fibres are specified. *Development* 115, 1103-1109.
- Jahoda, C. A., Horne, K. A., Mauger, A., Bard, S., and Sengel, P. (1992). Cellular and extracellular involvement in the regeneration of the rat lower vibrissa follicle. *Development* 114, 887-897.
- Jahoda, C. A., Horne, K. A., and Oliver, R. F. (1984). Induction of hair growth by implantation of cultured dermal papilla cells. *Nature* 311, 560-562.
- Jahoda, C. A., and Reynolds, A. J. (1996). Dermal-epidermal interactions. Adult follicle-derived cell populations and hair growth. *Dermatol Clin* 14, 573-583.
- Jahoda, C. A., and Reynolds, A. J. (2001). Hair follicle dermal sheath cells: unsung participants in wound healing. *Lancet* 358, 1445-1448.
- Jahoda, C. A., Reynolds, A. J., Chaponnier, C., Forester, J. C., and Gabbiani, G. (1991). Smooth muscle alpha-actin is a marker for hair follicle dermis in vivo and in vitro. *J Cell Sci* 99 (Pt 3), 627-636.
- Jahoda, C. A., Whitehouse, J., Reynolds, A. J., and Hole, N. (2003). Hair follicle dermal cells differentiate into adipogenic and osteogenic lineages. *Exp Dermatol* 12, 849-859.

REFERENCE

- Jamora, C., DasGupta, R., Kocieniewski, P., and Fuchs, E. (2003). Links between signal transduction, transcription and adhesion in epithelial bud development. *Nature* 422, 317-322.
- Jensen, U. B., Lowell, S., and Watt, F. M. (1999). The spatial relationship between stem cells and their progeny in the basal layer of human epidermis: a new view based on whole-mount labelling and lineage analysis. *Development* 126, 2409-2418.
- Jiang, J., and Struhl, G. (1995). Protein kinase A and hedgehog signaling in *Drosophila* limb development. *Cell* 80, 563-572.
- Johnson, R. L., Rothman, A. L., Xie, J., Goodrich, L. V., Bare, J. W., Bonifas, J. M., Quinn, A. G., Myers, R. M., Cox, D. R., Epstein, E. H., Jr., and Scott, M. P. (1996). Human homolog of patched, a candidate gene for the basal cell nevus syndrome. *Science* 272, 1668-1671.
- Jones, K. (1997). *Smith's recognisable patterns of human malformation*: WB Saunders, Philadelphia).
- Jones, P. H., Harper, S., and Watt, F. M. (1995). Stem cell patterning and fate in human epidermis. *Cell* 80, 83-93.
- Jones, P. H., and Watt, F. M. (1993). Separation of human epidermal stem cells from transit amplifying cells on the basis of differences in integrin function and expression. *Cell* 73, 713-724.
- Kafienah, W., Mistry, S., Williams, C., and Hollander, A. P. (2006). Nucleostemin is a marker of proliferating stromal stem cells in adult human bone marrow. *Stem Cells* 24, 1113-1120.
- Kalff-Suske, M., Wild, A., Topp, J., Wessling, M., Jacobsen, E. M., Bornholdt, D., Engel, H., Heuer, H., Aalfs, C. M., Ausems, M. G., *et al.* (1999). Point mutations throughout the *GLI3* gene cause Greig cephalopolysyndactyly syndrome. *Hum Mol Genet* 8, 1769-1777.
- Kalluri, R., and Neilson, E. G. (2003). Epithelial-mesenchymal transition and its implications for fibrosis. *J Clin Invest* 112, 1776-1784.
- Kang, S., Graham, J. M., Jr., Olney, A. H., and Biesecker, L. G. (1997). *GLI3* frameshift mutations cause autosomal dominant Pallister-Hall syndrome. *Nat Genet* 15, 266-268.
- Kangesu, T., Manek, S., Terenghi, G., Gu, X. H., Navsaria, H. A., Polak, J. M., Green, C. J., and Leigh, I. M. (1998). Nerve and blood vessel growth in response to grafted dermis and cultured keratinocytes. *Plast Reconstr Surg* 101, 1029-1038.
- Karagas MR, G. E. (1995). Unresolved issues in the epidemiology of basal cell and squamous cell skin cancer, In In: Mukhtar H (ed). *Skin cancer. Mechanisms and human*

REFERENCE

relevance., F. Boca Raton, ed. (CRC Press, 1995), pp. 79–86.

Karlsson, L., Bondjers, C., and Betsholtz, C. (1999a). Roles for PDGF-A and sonic hedgehog in development of mesenchymal components of the hair follicle. *Development* *126*, 2611-2621.

Karlsson, L., Bondjers, C., and Betsholtz, C. (1999b). Roles for PDGF-A and sonic hedgehog in development of mesenchymal components of the hair follicle. *Development* *126*, 2611-2621.

Kasper, M., Schnidar, H., Neill, G. W., Hanneder, M., Klingler, S., Blas, L., Schmid, C., Hauser-Kronberger, C., Regl, G., Philpott, M. P., and Aberger, F. (2006). Selective modulation of Hedgehog/GLI target gene expression by epidermal growth factor signaling in human keratinocytes. *Mol Cell Biol* *26*, 6283-6298.

Katzav, S., Packham, G., Sutherland, M., Aroca, P., Santos, E., and Cleveland, J. L. (1995). Vav and Ras induce fibroblast transformation by overlapping signaling pathways which require c-Myc function. *Oncogene* *11*, 1079-1088.

Kaufman, C. K., Zhou, P., Pasolli, H. A., Rendl, M., Bolotin, D., Lim, K. C., Dai, X., Alegre, M. L., and Fuchs, E. (2003). GATA-3: an unexpected regulator of cell lineage determination in skin. *Genes Dev* *17*, 2108-2122.

Kaufmann, E., and Knochel, W. (1996). Five years on the wings of fork head. *Mech Dev* *57*, 3-20.

Kelley, R. L., Roessler, E., Hennekam, R. C., Feldman, G. L., Kosaki, K., Jones, M. C., Palumbos, J. C., and Muenke, M. (1996). Holoprosencephaly in RSH/Smith-Lemli-Opitz syndrome: does abnormal cholesterol metabolism affect the function of Sonic Hedgehog? *Am J Med Genet* *66*, 478-484.

Kilby, N. J., Snaith, M. R., and Murray, J. A. (1993). Site-specific recombinases: tools for genome engineering. *Trends Genet* *9*, 413-421.

Kim, J., Hake, S. B., and Roeder, R. G. (2005). The human homolog of yeast BRE1 functions as a transcriptional coactivator through direct activator interactions. *Mol Cell* *20*, 759-770.

Kim, K. B., Khuri, F. R., and Shin, D. M. (2001). Recent advances in the management of squamous cell carcinoma of the head and neck. *Expert Rev Anticancer Ther* *1*, 99-110.

Kimonis, V. E., Goldstein, A. M., Pastakia, B., Yang, M. L., Kase, R., DiGiovanna, J. J., Bale, A. E., and Bale, S. J. (1997). Clinical manifestations in 105 persons with nevoid basal cell carcinoma syndrome. *Am J Med Genet* *69*, 299-308.

Kinto, N., Iwamoto, M., Enomoto-Iwamoto, M., Noji, S., Ohuchi, H., Yoshioka, H., Kataoka, H., Wada, Y., Yuhao, G., Takahashi, H. E., *et al.* (1997). Fibroblasts

REFERENCE

- expressing Sonic hedgehog induce osteoblast differentiation and ectopic bone formation. *FEBS Lett* 404, 319-323.
- Kinzler, K. W., Bigner, S. H., Bigner, D. D., Trent, J. M., Law, M. L., O'Brien, S. J., Wong, A. J., and Vogelstein, B. (1987). Identification of an amplified, highly expressed gene in a human glioma. *Science* 236, 70-73.
- Kinzler, K. W., and Vogelstein, B. (1990a). EcoRI polymorphism within the GLI gene (chromosome 12q13.3-14.1). *Nucleic Acids Res* 18, 2834.
- Kinzler, K. W., and Vogelstein, B. (1990b). The GLI gene encodes a nuclear protein which binds specific sequences in the human genome. *Mol Cell Biol* 10, 634-642.
- Kogerman, P., Grimm, T., Kogerman, L., Krause, D., Uden, A. B., Sandstedt, B., Toftgard, R., and Zaphiropoulos, P. G. (1999). Mammalian suppressor-of-fused modulates nuclear-cytoplasmic shuttling of Gli-1. *Nat Cell Biol* 1, 312-319.
- Krauss, S., Concordet, J. P., and Ingham, P. W. (1993). A functionally conserved homolog of the *Drosophila* segment polarity gene *hh* is expressed in tissues with polarizing activity in zebrafish embryos. *Cell* 75, 1431-1444.
- Krejci, N. C., Cuono, C. B., Langdon, R. C., and McGuire, J. (1991). In vitro reconstitution of skin: fibroblasts facilitate keratinocyte growth and differentiation on acellular reticular dermis. *J Invest Dermatol* 97, 843-848.
- Krishnan, V., Pereira, F. A., Qiu, Y., Chen, C. H., Beachy, P. A., Tsai, S. Y., and Tsai, M. J. (1997). Mediation of Sonic hedgehog-induced expression of COUP-TFII by a protein phosphatase. *Science* 278, 1947-1950.
- Kruger, K., Blume-Peytavi, U., and Orfanos, C. E. (1999). Basal cell carcinoma possibly originates from the outer root sheath and/or the bulge region of the vellus hair follicle. *Arch Dermatol Res* 291, 253-259.
- Kulesa, H., Turk, G., and Hogan, B. L. (2000). Inhibition of Bmp signaling affects growth and differentiation in the anagen hair follicle. *Embo J* 19, 6664-6674.
- Kung, H. J., Bailey, J. M., Davidson, N., Nicolson, M. O., and McAllister, R. M. (1975). Structure, subunit composition, and molecular weight of RD-114 RNA. *J Virol* 16, 397-411.
- Kurasawa, Y., Earnshaw, W. C., Mochizuki, Y., Dohmae, N., and Todokoro, K. (2004). Essential roles of KIF4 and its binding partner PRC1 in organized central spindle midzone formation. *Embo J* 23, 3237-3248.
- Lako, M., Armstrong, L., Cairns, P. M., Harris, S., Hole, N., and Jahoda, C. A. (2002). Hair follicle dermal cells repopulate the mouse haematopoietic system. *J Cell Sci* 115, 3967-3974.

REFERENCE

- Lane, E. B., and McLean, W. H. (2004). Keratins and skin disorders. *J Pathol* *204*, 355-366.
- Latkowski, J. M., Freedberg, I. M. (1999). Epidermal cell kinetics, epidermal differentiation, and keratinization, In Fitzpatrick's dermatology in general medicine, T. B. Fitzpatrick, and I. M. Freedberg, eds. (New York: McGraw-Hill Health Professions Division), pp. 133-144.
- Lavker, R. M., Bertolino, A. P., Freedberg, I. M., Sun, T. (1999). Biology of hair follicles, In Fitzpatrick's dermatology in general medicine, T. B. Fitzpatrick, and I. M. Freedberg, eds. (New York: McGraw-Hill Health Professions Division), pp. 230-238.
- Lavker, R. M., Miller, S., Wilson, C., Cotsarelis, G., Wei, Z. G., Yang, J. S., and Sun, T. T. (1993). Hair follicle stem cells: their location, role in hair cycle, and involvement in skin tumor formation. *J Invest Dermatol* *101*, 16S-26S.
- Lawrence, C. J., Dawe, R. K., Christie, K. R., Cleveland, D. W., Dawson, S. C., Endow, S. A., Goldstein, L. S., Goodson, H. V., Hirokawa, N., Howard, J., *et al.* (2004). A standardized kinesin nomenclature. *J Cell Biol* *167*, 19-22.
- Lee, C. T., Li, L., Takamoto, N., Martin, J. F., Demayo, F. J., Tsai, M. J., and Tsai, S. Y. (2004). The nuclear orphan receptor COUP-TFII is required for limb and skeletal muscle development. *Mol Cell Biol* *24*, 10835-10843.
- Lee, J., Platt, K. A., Censullo, P., and Ruiz i Altaba, A. (1997). Gli1 is a target of Sonic hedgehog that induces ventral neural tube development. *Development* *124*, 2537-2552.
- Lee, J. M., Dedhar, S., Kalluri, R., and Thompson, E. W. (2006). The epithelial-mesenchymal transition: new insights in signaling, development, and disease. *J Cell Biol* *172*, 973-981.
- Lee, T. I., and Young, R. A. (1998). Regulation of gene expression by TBP-associated proteins. *Genes Dev* *12*, 1398-1408.
- Leigh, I. M., Navsaria, H., Purkis, P. E., McKay, I. A., Bowden, P. E., and Riddle, P. N. (1995). Keratins (K16 and K17) as markers of keratinocyte hyperproliferation in psoriasis in vivo and in vitro. *Br J Dermatol* *133*, 501-511.
- Leigh, I. M., Purkis, P. E., Whitehead, P., and Lane, E. B. (1993). Monospecific monoclonal antibodies to keratin 1 carboxy terminal (synthetic peptide) and to keratin 10 as markers of epidermal differentiation. *Br J Dermatol* *129*, 110-119.
- Lendahl, U., Zimmerman, L. B., and McKay, R. D. (1990). CNS stem cells express a new class of intermediate filament protein. *Cell* *60*, 585-595.
- Lessing, D., and Nusse, R. (1998). Expression of wingless in the Drosophila embryo: a conserved cis-acting element lacking conserved Ci-binding sites is required for patched-mediated repression. *Development* *125*, 1469-1476.

REFERENCE

- Li, W., Ohlmeyer, J. T., Lane, M. E., and Kalderon, D. (1995). Function of protein kinase A in hedgehog signal transduction and *Drosophila* imaginal disc development. *Cell* 80, 553-562.
- Lindner, G., Menrad, A., Gherardi, E., Merlino, G., Welker, P., Handjiski, B., Roloff, B., and Paus, R. (2000). Involvement of hepatocyte growth factor/scatter factor and met receptor signaling in hair follicle morphogenesis and cycling. *Faseb J* 14, 319-332.
- Litingtung, Y., and Chiang, C. (2000). Specification of ventral neuron types is mediated by an antagonistic interaction between Shh and Gli3. *Nat Neurosci* 3, 979-985.
- Litingtung, Y., Lei, L., Westphal, H., and Chiang, C. (1998). Sonic hedgehog is essential to foregut development. *Nat Genet* 20, 58-61.
- Liu, C. Z., Yang, J. T., Yoon, J. W., Villavicencio, E., Pfendler, K., Walterhouse, D., and Iannaccone, P. (1998). Characterization of the promoter region and genomic organization of GLI, a member of the Sonic hedgehog-Patched signaling pathway. *Gene* 209, 1-11.
- Lowell, S., Jones, P., Le Roux, I., Dunne, J., and Watt, F. M. (2000). Stimulation of human epidermal differentiation by delta-notch signalling at the boundaries of stem-cell clusters. *Curr Biol* 10, 491-500.
- Lu, Z., Ghosh, S., Wang, Z., and Hunter, T. (2003). Downregulation of caveolin-1 function by EGF leads to the loss of E-cadherin, increased transcriptional activity of beta-catenin, and enhanced tumor cell invasion. *Cancer Cell* 4, 499-515.
- Lutz, B., Kuratani, S., Cooney, A. J., Wawersik, S., Tsai, S. Y., Eichele, G., and Tsai, M. J. (1994). Developmental regulation of the orphan receptor COUP-TF II gene in spinal motor neurons. *Development* 120, 25-36.
- Lyle, S., Christofidou-Solomidou, M., Liu, Y., Elder, D. E., Albelda, S., and Cotsarelis, G. (1998a). The C8/144B monoclonal antibody recognizes cytokeratin 15 and defines the location of human hair follicle stem cells. *J Cell Sci* 111 (Pt 21), 3179-3188.
- Lyle, S., Christofidou-Solomidou, M., Liu, Y., Elder, D. E., Albelda, S., and Cotsarelis, G. (1998b). The C8/144B monoclonal antibody recognizes cytokeratin 15 and defines the location of human hair follicle stem cells. *J Cell Sci* 111, 3179-3188.
- Maas-Szabowski, N., and Fusenig, N. E. (1996). Interleukin-1-induced growth factor expression in postmitotic and resting fibroblasts. *J Invest Dermatol* 107, 849-855.
- Maas-Szabowski, N., Szabowski, A., Stark, H. J., Andrecht, S., Kolbus, A., Schorpp-Kistner, M., Angel, P., and Fusenig, N. E. (2001). Organotypic cocultures with genetically modified mouse fibroblasts as a tool to dissect molecular mechanisms regulating keratinocyte growth and differentiation. *J Invest Dermatol* 116, 816-820.
- Machesney, M., Tidman, N., Waseem, A., Kirby, L., and Leigh, I. (1998). Activated keratinocytes in the epidermis of hypertrophic scars. *Am J Pathol* 152, 1133-1141.

REFERENCE

- Mackenzie, I. C., Zimmerman, K., and Peterson, L. (1981). The pattern of cellular organization of human epidermis. *J Invest Dermatol* 76, 459-461.
- Maesawa, C., Tamura, G., Iwaya, T., Ogasawara, S., Ishida, K., Sato, N., Nishizuka, S., Suzuki, Y., Ikeda, K., Aoki, K., *et al.* (1998). Mutations in the human homologue of the *Drosophila* patched gene in esophageal squamous cell carcinoma. *Genes Chromosomes Cancer* 21, 276-279.
- Maestro, R., Dei Tos, A. P., Hamamori, Y., Krasnokutsky, S., Sartorelli, V., Kedes, L., Doglioni, C., Beach, D. H., and Hannon, G. J. (1999). Twist is a potential oncogene that inhibits apoptosis. *Genes Dev* 13, 2207-2217.
- Mahlapuu, M., Enerback, S., and Carlsson, P. (2001). Haploinsufficiency of the forkhead gene *Foxf1*, a target for sonic hedgehog signaling, causes lung and foregut malformations. *Development* 128, 2397-2406.
- Marigo, V., Davey, R. A., Zuo, Y., Cunningham, J. M., and Tabin, C. J. (1996a). Biochemical evidence that patched is the Hedgehog receptor. *Nature* 384, 176-179.
- Marigo, V., Johnson, R. L., Vortkamp, A., and Tabin, C. J. (1996b). Sonic hedgehog differentially regulates expression of *GLI* and *GLI3* during limb development. *Dev Biol* 180, 273-283.
- Marigo, V., Roberts, D. J., Lee, S. M., Tsukurov, O., Levi, T., Gastier, J. M., Epstein, D. J., Gilbert, D. J., Copeland, N. G., Seidman, C. E., and *et al.* (1995). Cloning, expression, and chromosomal location of *SHH* and *IHH*: two human homologues of the *Drosophila* segment polarity gene hedgehog. *Genomics* 28, 44-51.
- Marigo, V., and Tabin, C. J. (1996). Regulation of patched by sonic hedgehog in the developing neural tube. *Proc Natl Acad Sci U S A* 93, 9346-9351.
- Marks, R. (1995). The epidemiology of non-melanoma skin cancer: who, why and what can we do about it. *J Dermatol* 22, 853-857.
- Marks, R., Staples, M., and Giles, G. G. (1993). Trends in non-melanocytic skin cancer treated in Australia: the second national survey. *Int J Cancer* 53, 585-590.
- Matise, M. P., Epstein, D. J., Park, H. L., Platt, K. A., and Joyner, A. L. (1998). *Gli2* is required for induction of floor plate and adjacent cells, but not most ventral neurons in the mouse central nervous system. *Development* 125, 2759-2770.
- Matise, M. P., and Joyner, A. L. (1999). *Gli* genes in development and cancer. *Oncogene* 18, 7852-7859.
- Mazumdar, M., Lee, J. H., Sengupta, K., Ried, T., Rane, S., and Misteli, T. (2006). Tumor formation via loss of a molecular motor protein. *Curr Biol* 16, 1559-1564.

REFERENCE

- Mazumdar, M., and Misteli, T. (2005). Chromokinesins: multitasking players in mitosis. *Trends Cell Biol* *15*, 349-355.
- Mazumdar, M., Sundareshan, S., and Misteli, T. (2004). Human chromokinesin KIF4A functions in chromosome condensation and segregation. *J Cell Biol* *166*, 613-620.
- McDermott, A., Gustafsson, M., Elsam, T., Hui, C. C., Emerson, C. P., Jr., and Borycki, A. G. (2005). Gli2 and Gli3 have redundant and context-dependent function in skeletal muscle formation. *Development* *132*, 345-357.
- McGowan, K. M., and Coulombe, P. A. (2000). Keratin 17 expression in the hard epithelial context of the hair and nail, and its relevance for the pachyonychia congenita phenotype. *J Invest Dermatol* *114*, 1101-1107.
- McKay, I., Woodward, B., Wood, K., Navsaria, H. A., Hoekstra, H., and Green, C. (1994). Reconstruction of human skin from glycerol-preserved allodermis and cultured keratinocyte sheets. *Burns* *20*, S19-22.
- McKay, I. A., and Leigh, I. M. (1991). Epidermal cytokines and their roles in cutaneous wound healing. *Br J Dermatol* *124*, 513-518.
- Methot, N., and Basler, K. (1999). Hedgehog controls limb development by regulating the activities of distinct transcriptional activator and repressor forms of Cubitus interruptus. *Cell* *96*, 819-831.
- Michel, M., Torok, N., Godbout, M. J., Lussier, M., Gaudreau, P., Royal, A., and Germain, L. (1996a). Keratin 19 as a biochemical marker of skin stem cells in vivo and in vitro: keratin 19 expressing cells are differentially localized in function of anatomic sites, and their number varies with donor age and culture stage. *J Cell Sci* *109*, 1017-1028.
- Michel, M., Torok, N., Godbout, M. J., Lussier, M., Gaudreau, P., Royal, A., and Germain, L. (1996b). Keratin 19 as a biochemical marker of skin stem cells in vivo and in vitro: keratin 19 expressing cells are differentially localized in function of anatomic sites, and their number varies with donor age and culture stage. *J Cell Sci* *109* (Pt 5), 1017-1028.
- Mill, P., Mo, R., Fu, H., Grachtchouk, M., Kim, P. C., Dlugosz, A. A., and Hui, C. C. (2003a). Sonic hedgehog-dependent activation of Gli2 is essential for embryonic hair follicle development. *Genes Dev* *17*, 282-294.
- Mill, P., Mo, R., Fu, H., Grachtchouk, M., Kim, P. C., Dlugosz, A. A., and Hui, C. C. (2003b). Sonic hedgehog-dependent activation of Gli2 is essential for embryonic hair follicle development. *Genes Dev* *17*, 282-294.
- Millar, S. E. (2002). Molecular mechanisms regulating hair follicle development. *J Invest Dermatol* *118*, 216-225.

REFERENCE

- Miller, D. L., and Weinstock, M. A. (1994). Nonmelanoma skin cancer in the United States: incidence. *J Am Acad Dermatol* 30, 774-778.
- Miller, R. W., and Rubinstein, J. H. (1995). Tumors in Rubinstein-Taybi syndrome. *Am J Med Genet* 56, 112-115.
- Miller, S. J., Sun, T. T., and Lavker, R. M. (1993). Hair follicles, stem cells, and skin cancer. *J Invest Dermatol* 100, 288S-294S.
- Miyoshi, H., Blomer, U., Takahashi, M., Gage, F. H., and Verma, I. M. (1998). Development of a self-inactivating lentivirus vector. *J Virol* 72, 8150-8157.
- Mo, H., Stamatatos, L., Ip, J. E., Barbas, C. F., Parren, P. W., Burton, D. R., Moore, J. P., and Ho, D. D. (1997a). Human immunodeficiency virus type 1 mutants that escape neutralization by human monoclonal antibody IgG1b12. *J Virol* 71, 6869-6874.
- Mo, R., Freer, A. M., Zinyk, D. L., Crackower, M. A., Michaud, J., Heng, H. H., Chik, K. W., Shi, X. M., Tsui, L. C., Cheng, S. H., *et al.* (1997b). Specific and redundant functions of Gli2 and Gli3 zinc finger genes in skeletal patterning and development. *Development* 124, 113-123.
- Moll, R., Franke, W. W., Schiller, D. L., Geiger, B., and Krepler, R. (1982). The catalog of human cytokeratins: patterns of expression in normal epithelia, tumors and cultured cells. *Cell* 31, 11-24.
- Moll, R., Schiller, D. L., and Franke, W. W. (1990). Identification of protein IT of the intestinal cytoskeleton as a novel type I cytokeratin with unusual properties and expression patterns. *J Cell Biol* 111, 567-580.
- Moll, R., Zimbelmann, R., Goldschmidt, M. D., Keith, M., Laufer, J., Kasper, M., Koch, P. J., and Franke, W. W. (1993). The human gene encoding cytokeratin 20 and its expression during fetal development and in gastrointestinal carcinomas. *Differentiation* 53, 75-93.
- Monnier, V., Dussillol, F., Alves, G., Lamour-Isnard, C., and Plessis, A. (1998). Suppressor of fused links fused and Cubitus interruptus on the hedgehog signalling pathway. *Curr Biol* 8, 583-586.
- Montano, X., Shamsheer, M., Whitehead, P., Dawson, K., and Newton, J. (1994). Analysis of p53 in human cutaneous melanoma cell lines. *Oncogene* 9, 1455-1459.
- Morgan, P. R., Leigh, I. M., Purkis, P. E., Gardner, I. D., van Muijen, G. N. P., and Lane, E. B. (1987). Site variation in keratin expression in human oral epithelia- an immunocytochemical study of individual keratins. *Epithelia* 1, 31-43.
- Morris, C. E., Bardin, M., Berge, O., Frey-Klett, P., Fromin, N., Girardin, H., Guinebretiere, M. H., Lebaron, P., Thiery, J. M., and Troussellier, M. (2002). Microbial biodiversity: approaches to experimental design and hypothesis testing in primary

REFERENCE

scientific literature from 1975 to 1999. *Microbiol Mol Biol Rev* 66, 592-616, table of contents.

Morris, R. J., Fischer, S. M., and Slaga, T. J. (1985). Evidence that the centrally and peripherally located cells in the murine epidermal proliferative unit are two distinct cell populations. *J Invest Dermatol* 84, 277-281.

Morris, R. J., and Potten, C. S. (1999). Highly persistent label-retaining cells in the hair follicles of mice and their fate following induction of anagen. *J Invest Dermatol* 112, 470-475.

Morris, R. J., Tryson, K. A., and Wu, K. Q. (2000). Evidence that the epidermal targets of carcinogen action are found in the interfollicular epidermis of infundibulum as well as in the hair follicles. *Cancer Res* 60, 226-229.

Motoyama, J., Liu, J., Mo, R., Ding, Q., Post, M., and Hui, C. C. (1998a). Essential function of Gli2 and Gli3 in the formation of lung, trachea and oesophagus. *Nat Genet* 20, 54-57.

Motoyama, J., Takabatake, T., Takeshima, K., and Hui, C. (1998b). Ptch2, a second mouse Patched gene is co-expressed with Sonic hedgehog. *Nat Genet* 18, 104-106.

Murone, M., Luoh, S. M., Stone, D., Li, W., Gurney, A., Armanini, M., Grey, C., Rosenthal, A., and de Sauvage, F. J. (2000). Gli regulation by the opposing activities of fused and suppressor of fused. *Nat Cell Biol* 2, 310-312.

Murone, M., Rosenthal, A., and de Sauvage, F. J. (1999). Sonic hedgehog signaling by the patched-smoothened receptor complex. *Curr Biol* 9, 76-84.

Myers, R. J., and Hamilton, J. B. (1951). Regeneration and rate of growth of hairs in man. *Ann NY Acad Sci* 53, 562-568.

Nagle, R. B. (1988). Intermediate filaments: a review of the basic biology. *Am J Surg Pathol* 12 *Suppl* 1, 4-16.

Nakshatri, H., Mendonca, M. S., Bhat-Nakshatri, P., Patel, N. M., Goulet, R. J., Jr., and Cornetta, K. (2000). The orphan receptor COUP-TFII regulates G2/M progression of breast cancer cells by modulating the expression/activity of p21(WAF1/CIP1), cyclin D1, and cdk2. *Biochem Biophys Res Commun* 270, 1144-1153.

Nanni, L., Ming, J. E., Bocian, M., Steinhaus, K., Bianchi, D. W., Die-Smulders, C., Giannotti, A., Imaizumi, K., Jones, K. L., Campo, M. D., *et al.* (1999). The mutational spectrum of the sonic hedgehog gene in holoprosencephaly: SHH mutations cause a significant proportion of autosomal dominant holoprosencephaly. *Hum Mol Genet* 8, 2479-2488.

Navsaria, H. A., Kangesu, T., Manek, S., Green, C. J., and Leigh, I. M. (1994). An animal model to study the significance of dermis for grafting cultured keratinocytes on full thickness wounds. *Burns* 20, S57-60.

REFERENCE

- Nawshad, A., LaGamba, D., and Hay, E. D. (2004). Transforming growth factor beta (TGFbeta) signalling in palatal growth, apoptosis and epithelial mesenchymal transformation (EMT). *Arch Oral Biol* 49, 675-689.
- Nazmi, M. N., Dykes, P. J., and Marks, R. (1990). Epidermal growth factor receptors in human epidermal tumours. *Br J Dermatol* 123, 153-161.
- Nelson, W. G., and Sun, T. T. (1983). The 50- and 58-kdalton keratin classes as molecular markers for stratified squamous epithelia: cell culture studies. *J Cell Biol* 97, 244-251.
- Nelson, W. J., and Nusse, R. (2004). Convergence of Wnt, beta-catenin, and cadherin pathways. *Science* 303, 1483-1487.
- Nilsson, M., Uden, A. B., Krause, D., Malmqwist, U., Raza, K., Zaphiropoulos, P. G., and Toftgard, R. (2000). Induction of basal cell carcinomas and trichoepitheliomas in mice overexpressing GLI-1. *Proc Natl Acad Sci U S A* 97, 3438-3443.
- Nusslein-Volhard, C., and Wieschaus, E. (1980). Mutations affecting segment number and polarity in *Drosophila*. *Nature* 287, 795-801.
- O'Shaughnessy, R. F., and Christiano, A. M. (2001). Stem cells in the epidermis. *Skin Pharmacol Appl Skin Physiol* 14, 350-357.
- Odent, S., Atti-Bitach, T., Blayau, M., Mathieu, M., Aug, J., Delezo de, A. L., Gall, J. Y., Le Marec, B., Munnich, A., David, V., and Vekemans, M. (1999). Expression of the Sonic hedgehog (SHH) gene during early human development and phenotypic expression of new mutations causing holoprosencephaly. *Hum Mol Genet* 8, 1683-1689.
- Oliver, R. F. (1966a). Histological studies of whisker regeneration in the hooded rat. *J Embryol Exp Morphol* 16, 231-244.
- Oliver, R. F. (1966b). Whisker growth after removal of the dermal papilla and lengths of follicle in the hooded rat. *J Embryol Exp Morphol* 15, 331-347.
- Oliver, R. F. (1967). The experimental induction of whisker growth in the hooded rat by implantation of dermal papillae. *J Embryol Exp Morphol* 18, 43-51.
- Oliver, R. F., and Jahoda, C. A. (1988). Dermal-epidermal interactions. *Clin Dermatol* 6, 74-82.
- Orenic, T. V., Slusarski, D. C., Kroll, K. L., and Holmgren, R. A. (1990). Cloning and characterization of the segment polarity gene *cubitus interruptus* Dominant of *Drosophila*. *Genes Dev* 4, 1053-1067.

REFERENCE

- Oro, A. E., Higgins, K. M., Hu, Z., Bonifas, J. M., Epstein, E. H. Jr., and Scott, M. P. (1997). Basal cell carcinomas in mice overexpressing sonic hedgehog. *Science* *276*, 817-821.
- Orphanides, G., Lagrange, T., and Reinberg, D. (1996). The general transcription factors of RNA polymerase II. *Genes Dev* *10*, 2657-2683.
- Oshima, H., Rochat, A., Kedzia, C., Kobayashi, K., and Barrandon, Y. (2001). Morphogenesis and renewal of hair follicles from adult multipotent stem cells. *Cell* *104*, 233-245.
- Pan, Y., Bai, C. B., Joyner, A. L., and Wang, B. (2006). Sonic hedgehog signaling regulates Gli2 transcriptional activity by suppressing its processing and degradation. *Mol Cell Biol* *26*, 3365-3377.
- Park, H. L., Bai, C., Platt, K. A., Matisse, M. P., Beeghly, A., Hui, C. C., Nakashima, M., and Joyner, A. L. (2000). Mouse Gli1 mutants are viable but have defects in SHH signaling in combination with a Gli2 mutation. *Development* *127*, 1593-1605.
- Pavletich, N. P., and Pabo, C. O. (1993). Crystal structure of a five-finger GLI-DNA complex: new perspectives on zinc fingers. *Science* *261*, 1701-1707.
- Pearse, R. V., 2nd, Collier, L. S., Scott, M. P., and Tabin, C. J. (1999). Vertebrate homologs of *Drosophila* suppressor of fused interact with the gli family of transcriptional regulators. *Dev Biol* *212*, 323-336.
- Pellegrini, G., Dellambra, E., Golisano, O., Martinelli, E., Fantozzi, I., Bondanza, S., Ponzin, D., McKeon, F., and De Luca, M. (2001). p63 identifies keratinocyte stem cells. *Proc Natl Acad Sci U S A* *98*, 3156-3161.
- Pepinsky, R. B., Zeng, C., Wen, D., Rayhorn, P., Baker, D. P., Williams, K. P., Bixler, S. A., Ambrose, C. M., Garber, E. A., Miatkowski, K., *et al.* (1998). Identification of a palmitic acid-modified form of human Sonic hedgehog. *J Biol Chem* *273*, 14037-14045.
- Pereira, F. A., Qiu, Y., Tsai, M. J., and Tsai, S. Y. (1995). Chicken ovalbumin upstream promoter transcription factor (COUP-TF): expression during mouse embryogenesis. *J Steroid Biochem Mol Biol* *53*, 503-508.
- Pereira, F. A., Qiu, Y., Zhou, G., Tsai, M. J., and Tsai, S. Y. (1999). The orphan nuclear receptor COUP-TFII is required for angiogenesis and heart development. *Genes Dev* *13*, 1037-1049.
- Pereira, F. A., Tsai, M. J., and Tsai, S. Y. (2000). COUP-TF orphan nuclear receptors in development and differentiation. *Cell Mol Life Sci* *57*, 1388-1398.
- Perrone, L., Pasca di Magliano, M., Zannini, M., and Di Lauro, R. (2000). The thyroid transcription factor 2 (TTF-2) is a promoter-specific DNA-binding independent transcriptional repressor. *Biochem Biophys Res Commun* *275*, 203-208.

REFERENCE

- Petrij, F., Giles, R. H., Dauwerse, H. G., Saris, J. J., Hennekam, R. C., Masuno, M., Tommerup, N., van Ommen, G. J., Goodman, R. H., Peters, D. J., and et al. (1995). Rubinstein-Taybi syndrome caused by mutations in the transcriptional co-activator CBP. *Nature* 376, 348-351.
- Pham, A., Therond, P., Alves, G., Tournier, F. B., Busson, D., Lamour-Isnard, C., Bouchon, B. L., Preat, T., and Tricoire, H. (1995). The Suppressor of fused gene encodes a novel PEST protein involved in *Drosophila* segment polarity establishment. *Genetics* 140, 587-598.
- Philpott, M. P., Paus, R. (1998). Principles of hair follicle morphogenesis. In *Molecular Basis of Epithelial Appendage Morphogenesis*, C. M. Chuong, ed. (Austin, TX: Landes Bioscience Publ).
- Platt, K. A., Michaud, J., and Joyner, A. L. (1997). Expression of the mouse *Gli* and *Ptc* genes is adjacent to embryonic sources of hedgehog signals suggesting a conservation of pathways between flies and mice. *Mech Dev* 62, 121-135.
- Potten, C. S. (1981). Cell replacement in epidermis (keratopoiesis) via discrete units of proliferation. *Int Rev Cytol* 69, 271-318.
- Preat, T., Therond, P., Lamour-Isnard, C., Limbourg-Bouchon, B., Tricoire, H., Erk, I., Mariol, M. C., and Busson, D. (1990). A putative serine/threonine protein kinase encoded by the segment-polarity fused gene of *Drosophila*. *Nature* 347, 87-89.
- Price, M. A., and Kalderon, D. (1999). Proteolysis of cubitus interruptus in *Drosophila* requires phosphorylation by protein kinase A. *Development* 126, 4331-4339.
- Radisky, D. C. (2005). Epithelial-mesenchymal transition. *J Cell Sci* 118, 4325-4326.
- Ralston, D. R., Layton, C., Dalley, A. J., Boyce, S. G., Freedlander, E., and Mac Neil, S. (1999). The requirement for basement membrane antigens in the production of human epidermal/dermal composites in vitro. *Br J Dermatol* 140, 605-615.
- Ramsey, M. L. (2004). Basal Cell Carcinoma (eMedicin from web MD).
- Rashevsky-Finkel, A., Silkov, A., and Dikstein, R. (2001). A composite nuclear export signal in the TBP-associated factor TAFII105. *J Biol Chem* 276, 44963-44969.
- Reddy, S., Andl, T., Bagasra, A., Lu, M. M., Epstein, D. J., Morrisey, E. E., and Millar, S. E. (2001). Characterization of Wnt gene expression in developing and postnatal hair follicles and identification of Wnt5a as a target of Sonic hedgehog in hair follicle morphogenesis. *Mech Dev* 107, 69-82.
- Regl, G., Kasper, M., Schnidar, H., Eichberger, T., Neill, G. W., Philpott, M. P., Esterbauer, H., Hauser-Kronberger, C., Frischauf, A. M., and Aberger, F. (2004). Activation of the BCL2 promoter in response to Hedgehog/GLI signal transduction is predominantly mediated by GLI2. *Cancer Res* 64, 7724-7731.

REFERENCE

- Regl, G., Neill, G. W., Eichberger, T., Kasper, M., Ikram, M. S., Koller, J., Hintner, H., Quinn, A. G., Frischauf, A. M., and Aberger, F. (2002). Human GLI2 and GLI1 are part of a positive feedback mechanism in Basal Cell Carcinoma. *Oncogene* 21, 5529-5539.
- Reynolds, A. J., and Jahoda, C. A. (1992). Cultured dermal papilla cells induce follicle formation and hair growth by transdifferentiation of an adult epidermis. *Development* 115, 587-593.
- Reynolds, A. J., Lawrence, C., Cserhalmi-Friedman, P. B., Christiano, A. M., and Jahoda, C. A. (1999). Trans-gender induction of hair follicles. *Nature* 402, 33-34.
- Rheinwald, J. G. (1980). Serial cultivation of normal human epidermal keratinocytes. *Methods Cell Biol* 21A, 229-254.
- Rheinwald, J. G., and Green, H. (1975a). Formation of a keratinizing epithelium in culture by a cloned cell line derived from a teratoma. *Cell* 6, 317-330.
- Rheinwald, J. G., and Green, H. (1975b). Serial cultivation of strains of human epidermal keratinocytes: the formation of keratinizing colonies from single cells. *Cell* 6, 331-343.
- Riddle, R. D., Johnson, R. L., Laufer, E., and Tabin, C. (1993). Sonic hedgehog mediates the polarizing activity of the ZPA. *Cell* 75, 1401-1416.
- Roberts, W. M., Douglass, E. C., Peiper, S. C., Houghton, P. J., and Look, A. T. (1989). Amplification of the gli gene in childhood sarcomas. *Cancer Res* 49, 5407-5413.
- Rochat, A., Kobayashi, K., and Barrandon, Y. (1994). Location of stem cells of human hair follicles by clonal analysis. *Cell* 76, 1063-1073.
- Rodriguez, I., and Basler, K. (1997). Control of compartmental affinity boundaries by hedgehog. *Nature* 389, 614-618.
- Roeder, R. G. (1996). The role of general initiation factors in transcription by RNA polymerase II. *Trends Biochem Sci* 21, 327-335.
- Roelink, H., Augsburger, A., Heemskerk, J., Korzh, V., Norlin, S., Ruiz i Altaba, A., Tanabe, Y., Placzek, M., Edlund, T., Jessell, T. M., and et al. (1994). Floor plate and motor neuron induction by vhh-1, a vertebrate homolog of hedgehog expressed by the notochord. *Cell* 76, 761-775.
- Roessler, E., Belloni, E., Gaudenz, K., Jay, P., Berta, P., Scherer, S. W., Tsui, L. C., and Muenke, M. (1996). Mutations in the human Sonic Hedgehog gene cause holoprosencephaly. *Nat Genet* 14, 357-360.
- Roessler, E., Belloni, E., Gaudenz, K., Vargas, F., Scherer, S. W., Tsui, L. C., and Muenke, M. (1997). Mutations in the C-terminal domain of Sonic Hedgehog cause holoprosencephaly. *Hum Mol Genet* 6, 1847-1853.

REFERENCE

- Rogers, M. A., Edler, L., Winter, H., Langbein, L., Beckmann, I., and Schweizer, J. (2005). Characterization of new members of the human type II keratin gene family and a general evaluation of the keratin gene domain on chromosome 12q13.13. *J Invest Dermatol* *124*, 536-544.
- Rogers, M. A., Winter, H., Langbein, L., Bleiler, R., and Schweizer, J. (2004). The human type I keratin gene family: characterization of new hair follicle specific members and evaluation of the chromosome 17q21.2 gene domain. *Differentiation* *72*, 527-540.
- Roth, F. P., Hughes, J. D., Estep, P. W., and Church, G. M. (1998). Finding DNA regulatory motifs within unaligned noncoding sequences clustered by whole-genome mRNA quantitation. *Nat Biotechnol* *16*, 939-945.
- Rowitch, D. H., B, S. J., Lee, S. M., Flax, J. D., Snyder, E. Y., and McMahon, A. P. (1999). Sonic hedgehog regulates proliferation and inhibits differentiation of CNS precursor cells. *J Neurosci* *19*, 8954-8965.
- Rubinstein, J. H. (1990). Broad thumb-hallux (Rubinstein-Taybi) syndrome 1957-1988. *Am J Med Genet Suppl* *6*, 3-16.
- Ruiz i Altaba, A. (1998). Combinatorial Gli gene function in floor plate and neuronal inductions by Sonic hedgehog. *Development* *125*, 2203-2212.
- Ruiz i Altaba, A. (1999a). Gli proteins and Hedgehog signaling: development and cancer. *Trends Genet* *15*, 418-425.
- Ruiz i Altaba, A. (1999b). Gli proteins encode context-dependent positive and negative functions: implications for development and disease. *Development* *126*, 3205-3216.
- Ruiz, I. A. A. (1999). The works of GLI and the power of hedgehog. *Nat Cell Biol* *1*, E147-148.
- Ruiz, I. A. A., Palma, V., and Dahmane, N. (2002). Hedgehog-Gli signalling and the growth of the brain. *Nat Rev Neurosci* *3*, 24-33.
- Ruppert, J. M., Kinzler, K. W., Wong, A. J., Bigner, S. H., Kao, F. T., Law, M. L., Seuanez, H. N., O'Brien, S. J., and Vogelstein, B. (1988). The GLI-Kruppel family of human genes. *Mol Cell Biol* *8*, 3104-3113.
- Ruppert, J. M., Vogelstein, B., Arheden, K., and Kinzler, K. W. (1990). GLI3 encodes a 190-kilodalton protein with multiple regions of GLI similarity. *Mol Cell Biol* *10*, 5408-5415.
- Ruppert, J. M., Vogelstein, B., and Kinzler, K. W. (1991). The zinc finger protein GLI transforms primary cells in cooperation with adenovirus E1A. *Mol Cell Biol* *11*, 1724-1728.

REFERENCE

- Safai, B., and Good, R. A. (1977). Basal cell carcinoma with metastasis. Review of literature. *Arch Pathol Lab Med* 101, 327-331.
- Saintigny, G., Bonnard, M., Damour, O., and Collombel, C. (1993). Reconstruction of epidermis on a chitosan cross-linked collagen-GAG lattice: effect of fibroblasts. *Acta Derm Venereol* 73, 175-180.
- Sambrook J., F. E. F., Maniatis T (1989). *Molecular cloning: A laboratory Manual* (Cold Spring Harbor, NY.: Cold Spring Harbor Laboratory Press).
- Sasaki, H., Hui, C., Nakafuku, M., and Kondoh, H. (1997). A binding site for Gli proteins is essential for HNF-3beta floor plate enhancer activity in transgenics and can respond to Shh in vitro. *Development* 124, 1313-1322.
- Sasaki, H., Nishizaki, Y., Hui, C., Nakafuku, M., and Kondoh, H. (1999). Regulation of Gli2 and Gli3 activities by an amino-terminal repression domain: implication of Gli2 and Gli3 as primary mediators of Shh signaling. *Development* 126, 3915-3924.
- Sauer, F., and Tjian, R. (1997). Mechanisms of transcriptional activation: differences and similarities between yeast, Drosophila, and man. *Curr Opin Genet Dev* 7, 176-181.
- Schuebel, K. E., Bustelo, X. R., Nielsen, D. A., Song, B. J., Barbacid, M., Goldman, D., and Lee, I. J. (1996). Isolation and characterization of murine vav2, a member of the vav family of proto-oncogenes. *Oncogene* 13, 363-371.
- Schwartz, P. H., Nethercott, H., Kirov, II, Ziaecian, B., Young, M. J., and Klassen, H. (2005). Expression of neurodevelopmental markers by cultured porcine neural precursor cells. *Stem Cells* 23, 1286-1294.
- Sekine, Y., Okada, Y., Noda, Y., Kondo, S., Aizawa, H., Takemura, R., and Hirokawa, N. (1994). A novel microtubule-based motor protein (KIF4) for organelle transports, whose expression is regulated developmentally. *J Cell Biol* 127, 187-201.
- Sempowski, G. D., Borrello, M. A., Blieden, T. M., Barth, R. K., and Phipps, R. P. (1995). Fibroblast heterogeneity in the healing wound. *Wound Repair Regen* 3, 120-131.
- Sengel, P. (1976). *Morphogenesis of skin* (Cambridge, Eng. : New York: Cambridge University Press).
- Shin, S. H., Kogerman, P., Lindstrom, E., Toftgard, R., and Biesecker, L. G. (1999). GLI3 mutations in human disorders mimic Drosophila cubitus interruptus protein functions and localization. *Proc Natl Acad Sci U S A* 96, 2880-2884.
- Sisson, J. C., Ho, K. S., Suyama, K., and Scott, M. P. (1997). Costal2, a novel kinesin-related protein in the Hedgehog signaling pathway. *Cell* 90, 235-245.

REFERENCE

- Slomianka, L. (2002). *Blue Histology - Integumentary System* (The University of Western Australia: School of Anatomy and Human Biology-The University of Western Australia).
- Smack, D. P., Korge, B. P., and James, W. D. (1994). Keratin and keratinization. *J Am Acad Dermatol* 30, 85-102.
- Smith, L. M., Hu, P., Meyer, L. J., and Coffin, C. M. (2002). Complex karyotypic abnormality in ovarian fibroma associated with Gorlin syndrome. *Am J Med Genet* 112, 61-64.
- Smola, H., Stark, H. J., Thiekotter, G., Mirancea, N., Krieg, T., and Fusenig, N. E. (1998). Dynamics of basement membrane formation by keratinocyte-fibroblast interactions in organotypic skin culture. *Exp Cell Res* 239, 399-410.
- Smola, H., Thiekotter, G., and Fusenig, N. E. (1993). Mutual induction of growth factor gene expression by epidermal-dermal cell interaction. *J Cell Biol* 122, 417-429.
- Smyth, I., Narang, M. A., Evans, T., Heimann, C., Nakamura, Y., Chenevix-Trench, G., Pietsch, T., Wicking, C., and Wainwright, B. J. (1999). Isolation and characterization of human patched 2 (PTCH2), a putative tumour suppressor gene in basal cell carcinoma and medulloblastoma on chromosome 1p32. *Hum Mol Genet* 8, 291-297.
- Sorrell, J. M., Baber, M. A., and Caplan, A. I. (2004). Site-matched papillary and reticular human dermal fibroblasts differ in their release of specific growth factors/cytokines and in their interaction with keratinocytes. *J Cell Physiol* 200, 134-145.
- Sorrell, J. M., and Caplan, A. I. (2004). Fibroblast heterogeneity: more than skin deep. *J Cell Sci* 117, 667-675.
- Spearman, R. I. C. (1977). The structure and function of the fully developed follicle. In *The physiology and pathophysiology of the skin*, A. Jarrett, ed. (London, New York: Academic Press), pp. 1294.
- St-Jacques, B., Dassule, H. R., Karavanova, I., Botchkarev, V. A., Li, J., Danielian, P. S., McMahon, J. A., Lewis, P. M., Paus, R., and McMahon, A. P. (1998). Sonic hedgehog signaling is essential for hair development. *Curr Biol* 8, 1058-1068.
- Stegman, M. A., Vallance, J. E., Elangovan, G., Sosinski, J., Cheng, Y., and Robbins, D. J. (2000). Identification of a tetrameric hedgehog signaling complex. *J Biol Chem* 275, 21809-21812.
- Stein, U., Eder, C., Karsten, U., Haensch, W., Walther, W., and Schlag, P. M. (1999). GLI gene expression in bone and soft tissue sarcomas of adult patients correlates with tumor grade. *Cancer Res* 59, 1890-1895.
- Steinert, P. M., and Roop, D. R. (1988). Molecular and cellular biology of intermediate filaments. *Annu Rev Biochem* 57, 593-625.

REFERENCE

- Stenn, K. S., and Paus, R. (2001). Controls of hair follicle cycling. *Physiol Rev* 81, 449-494.
- Stone, D. M., Hynes, M., Armanini, M., Swanson, T. A., Gu, Q., Johnson, R. L., Scott, M. P., Pennica, D., Goddard, A., Phillips, H., *et al.* (1996). The tumour-suppressor gene patched encodes a candidate receptor for Sonic hedgehog. *Nature* 384, 129-134.
- Stone, D. M., Murone, M., Luoh, S., Ye, W., Armanini, M. P., Gurney, A., Phillips, H., Brush, J., Goddard, A., de Sauvage, F. J., and Rosenthal, A. (1999). Characterization of the human suppressor of fused, a negative regulator of the zinc-finger transcription factor Gli. *J Cell Sci* 112 (Pt 23), 4437-4448.
- Strizzi, L., Bianco, C., Normanno, N., Seno, M., Wechselberger, C., Wallace-Jones, B., Khan, N. I., Hirota, M., Sun, Y., Sanicola, M., and Salomon, D. S. (2004). Epithelial mesenchymal transition is a characteristic of hyperplasias and tumors in mammary gland from MMTV-Cripto-1 transgenic mice. *J Cell Physiol* 201, 266-276.
- Takamoto, N., You, L. R., Moses, K., Chiang, C., Zimmer, W. E., Schwartz, R. J., DeMayo, F. J., Tsai, M. J., and Tsai, S. Y. (2005). COUP-TFII is essential for radial and anteroposterior patterning of the stomach. *Development* 132, 2179-2189.
- Tani, H., Morris, R. J., and Kaur, P. (2000a). Enrichment for murine keratinocyte stem cells based on cell surface phenotype. *Proc Natl Acad Sci U S A* 97, 10960-10965.
- Tani, H., Morris, R. J., and Kaur, P. (2000b). Enrichment for murine keratinocyte stem cells based on cell surface phenotype. *Proc Natl Acad Sci U S A* 97, 10960-10965.
- Tanimura, A., Dan, S., and Yoshida, M. (1998). Cloning of novel isoforms of the human Gli2 oncogene and their activities to enhance tax-dependent transcription of the human T-cell leukemia virus type 1 genome. *J Virol* 72, 3958-3964.
- Taylor, G., Lehrer, M. S., Jensen, P. J., Sun, T. T., and Lavker, R. M. (2000a). Involvement of follicular stem cells in forming not only the follicle but also the epidermis. *Cell* 102, 451-461.
- Taylor, G., Lehrer, M. S., Jensen, P. J., Sun, T. T., and Lavker, R. M. (2000b). Involvement of follicular stem cells in forming not only the follicle but also the epidermis. *Cell* 102, 451-461.
- Taylor, M. D., Liu, L., Raffel, C., Hui, C. C., Mainprize, T. G., Zhang, X., Agatep, R., Chiappa, S., Gao, L., Lowrance, A., *et al.* (2002). Mutations in SUFU predispose to medulloblastoma. *Nat Genet* 31, 306-310.
- Teh, M. T., Wong, S. T., Neill, G. W., Ghali, L. R., Philpott, M. P., and Quinn, A. G. (2002). FOXM1 is a downstream target of Gli1 in basal cell carcinomas. *Cancer Res* 62, 4773-4780.

REFERENCE

- Telfer, N. R., Colver, G. B., and Bowers, P. W. (1999). Guidelines for the management of basal cell carcinoma. British Association of Dermatologists. *Br J Dermatol* 141, 415-423.
- Thiery, J. P. (2002). Epithelial-mesenchymal transitions in tumour progression. *Nat Rev Cancer* 2, 442-454.
- Thiery, J. P. (2003). Epithelial-mesenchymal transitions in development and pathologies. *Curr Opin Cell Biol* 15, 740-746.
- Tint, G. S., Irons, M., Elias, E. R., Batta, A. K., Frieden, R., Chen, T. S., and Salen, G. (1994). Defective cholesterol biosynthesis associated with the Smith-Lemli-Opitz syndrome. *N Engl J Med* 330, 107-113.
- Todaró, G. J., and Green, H. (1963). Quantitative studies of the growth of mouse embryo cells in culture and their development into established lines. *J Cell Biol* 17, 299-313.
- Toftgard, R. (2000). Hedgehog signalling in cancer. *Cell Mol Life Sci* 57, 1720-1731.
- Tojo, M., Mori, T., Kiyosawa, H., Honma, Y., Tanno, Y., Kanazawa, K. Y., Yokoya, S., Kaneko, F., and Wanaka, A. (1999). Expression of sonic hedgehog signal transducers, patched and smoothed, in human basal cell carcinoma. *Pathol Int* 49, 687-694.
- Tomakidi, P., Fusenig, N. E., Kohl, A., and Komposch, G. (1997). Histomorphological and biochemical differentiation capacity in organotypic co-cultures of primary gingival cells. *J Periodontal Res* 32, 388-400.
- Trenkle, T., McClelland, M., Adlkofer, K., and Welsh, J. (2000). Major transcript variants of VAV3, a new member of the VAV family of guanine nucleotide exchange factors. *Gene* 245, 139-149.
- Tsai, R. Y., and McKay, R. D. (2002). A nucleolar mechanism controlling cell proliferation in stem cells and cancer cells. *Genes Dev* 16, 2991-3003.
- Tsai, S. Y., and Tsai, M. J. (1997). Chick ovalbumin upstream promoter-transcription factors (COUP-TFs): coming of age. *Endocr Rev* 18, 229-240.
- Uesugi, M., Nyanguile, O., Lu, H., Levine, A. J., and Verdine, G. L. (1997). Induced alpha helix in the VP16 activation domain upon binding to a human TAF. *Science* 277, 1310-1313.
- Uden, A. B., Zaphiropoulos, P. G., Bruce, K., Toftgard, R., and Stahle-Backdahl, M. (1997). Human patched (PTCH) mRNA is overexpressed consistently in tumor cells of both familial and sporadic basal cell carcinoma. *Cancer Res* 57, 2336-2340.
- van den Heuvel, M., and Ingham, P. W. (1996). smoothed encodes a receptor-like serpentine protein required for hedgehog signalling. *Nature* 382, 547-551.

REFERENCE

- Villavicencio, E. H., Walterhouse, D. O., and Iannaccone, P. M. (2000). The sonic hedgehog-patched-gli pathway in human development and disease. *Am J Hum Genet* 67, 1047-1054.
- Villavicencio, E. H., Yoon, J. W., Frank, D. J., Fuchtbauer, E. M., Walterhouse, D. O., and Iannaccone, P. M. (2002). Cooperative E-box regulation of human GLII by TWIST and USF. *Genesis* 32, 247-258.
- von Mering, C., and Basler, K. (1999). Distinct and regulated activities of human Gli proteins in *Drosophila*. *Curr Biol* 9, 1319-1322.
- Vorechovsky, I., Tingby, O., Hartman, M., Stromberg, B., Nister, M., Collins, V. P., and Toftgard, R. (1997). Somatic mutations in the human homologue of *Drosophila* patched in primitive neuroectodermal tumours. *Oncogene* 15, 361-366.
- Vortkamp, A., Franz, T., Gessler, M., and Grzeschik, K. H. (1992). Deletion of GLI3 supports the homology of the human Greig cephalopolysyndactyly syndrome (GCPS) and the mouse mutant extra toes (Xt). *Mamm Genome* 3, 461-463.
- Vortkamp, A., Gessler, M., and Grzeschik, K. H. (1991). GLI3 zinc-finger gene interrupted by translocations in Greig syndrome families. *Nature* 352, 539-540.
- Vortkamp, A., Gessler, M., and Grzeschik, K. H. (1995). Identification of optimized target sequences for the GLI3 zinc finger protein. *DNA Cell Biol* 14, 629-634.
- Vortkamp, A., Lee, K., Lanske, B., Segre, G. V., Kronenberg, H. M., and Tabin, C. J. (1996). Regulation of rate of cartilage differentiation by Indian hedgehog and PTH-related protein. *Science* 273, 613-622.
- Wang, B., Fallon, J. F., and Beachy, P. A. (2000a). Hedgehog-regulated processing of Gli3 produces an anterior/posterior repressor gradient in the developing vertebrate limb. *Cell* 100, 423-434.
- Wang, H. J., Pieper, J., Schotel, R., van Blitterswijk, C. A., and Lamme, E. N. (2004). Stimulation of skin repair is dependent on fibroblast source and presence of extracellular matrix. *Tissue Eng* 10, 1054-1064.
- Wang, L. C., Liu, Z. Y., Gambardella, L., Delacour, A., Shapiro, R., Yang, J., Sizing, I., Rayhorn, P., Garber, E. A., Benjamin, C. D., *et al.* (2000b). Regular articles: conditional disruption of hedgehog signaling pathway defines its critical role in hair development and regeneration. *J Invest Dermatol* 114, 901-908.
- Watt, F. M. (1989). Terminal differentiation of epidermal keratinocytes. *Curr Opin Cell Biol* 1, 1107-1115.
- Watt, F. M. (1998). Epidermal stem cells: markers, patterning and the control of stem cell fate. *Philos Trans R Soc Lond B Biol Sci* 353, 831-837.

REFERENCE

Weed, M., Mundlos, S., and Olsen, B. R. (1997). The role of sonic hedgehog in vertebrate development. *Matrix Biol* 16, 53-58.

Weinstein, G. D., and Mooney, K. M. (1980). Cell proliferation kinetics in the human hair root. *J Invest Dermatol* 74, 43-46.

Werner, C. A., Dohner, H., Joos, S., Trumper, L. H., Baudis, M., Barth, T. F., Ott, G., Moller, P., Lichter, P., and Bentz, M. (1997). High-level DNA amplifications are common genetic aberrations in B-cell neoplasms. *Am J Pathol* 151, 335-342.

Wild, A., Kalff-Suske, M., Vortkamp, A., Bornholdt, D., Konig, R., and Grzeschik, K. H. (1997). Point mutations in human GLI3 cause Greig syndrome. *Hum Mol Genet* 6, 1979-1984.

Williams, K. P., Rayhorn, P., Chi-Rosso, G., Garber, E. A., Strauch, K. L., Horan, G. S., Reilly, J. O., Baker, D. P., Taylor, F. R., Koteliensky, V., and Pepinsky, R. B. (1999). Functional antagonists of sonic hedgehog reveal the importance of the N terminus for activity. *J Cell Sci* 112 (Pt 23), 4405-4414.

Wilson, C. L., Dean, D., Lane, E. B., Dawber, R. P., and Leigh, I. M. (1994). Keratinocyte differentiation in psoriatic scalp: morphology and expression of epithelial keratins. *Br J Dermatol* 131, 191-200.

Wislet-Gendebien, S., Bruyere, F., Hans, G., Leprince, P., Moonen, G., and Rogister, B. (2004). Nestin-positive mesenchymal stem cells favour the astroglial lineage in neural progenitors and stem cells by releasing active BMP4. *BMC Neurosci* 5, 33.

Wong, C. S., Strange, R. C., and Lear, J. T. (2003). Basal cell carcinoma. *Bmj* 327, 794-798.

Wu, S. C., Grindley, J., Winnier, G. E., Hargett, L., and Hogan, B. L. (1998). Mouse Mesenchyme forkhead 2 (Mf2): expression, DNA binding and induction by sonic hedgehog during somitogenesis. *Mech Dev* 70, 3-13.

Xie, J., Murone, M., Luoh, S. M., Ryan, A., Gu, Q., Zhang, C., Bonifas, J. M., Lam, C. W., Hynes, M., Goddard, A., *et al.* (1998). Activating Smoothed mutations in sporadic basal-cell carcinoma. *Nature* 391, 90-92.

Xing, L., and Kobayashi, K. (2001). Ability of transplanted cultured epithelium to respond to dermal papillae. *Tissue Eng* 7, 535-544.

Yang, J. S., Lavker, R. M., and Sun, T. T. (1993). Upper human hair follicle contains a subpopulation of keratinocytes with superior in vitro proliferative potential. *J Invest Dermatol* 101, 652-659.

Yang, J. T., Liu, C. Z., Villavicencio, E. H., Yoon, J. W., Walterhouse, D., and Iannaccone, P. M. (1997). Expression of human GLI in mice results in failure to thrive, early death, and patchy Hirschsprung-like gastrointestinal dilatation. *Mol Med* 3, 826-835.

REFERENCE

- Yoon, J. W., Liu, C. Z., Yang, J. T., Swart, R., Iannaccone, P., and Walterhouse, D. (1998). GLI activates transcription through a herpes simplex viral protein 16-like activation domain. *J Biol Chem* *273*, 3496-3501.
- You, L. R., Lin, F. J., Lee, C. T., DeMayo, F. J., Tsai, M. J., and Tsai, S. Y. (2005a). Suppression of Notch signalling by the COUP-TFII transcription factor regulates vein identity. *Nature* *435*, 98-104.
- You, L. R., Takamoto, N., Yu, C. T., Tanaka, T., Kodama, T., Demayo, F. J., Tsai, S. Y., and Tsai, M. J. (2005b). Mouse lacking COUP-TFII as an animal model of Bochdalek-type congenital diaphragmatic hernia. *Proc Natl Acad Sci U S A* *102*, 16351-16356.
- Yu, J., Yu, D. W., Checkla, D. M., Freedberg, I. M., and Bertolino, A. P. (1993). Human hair keratins. *J Invest Dermatol* *101*, 56S-59S.
- Zannini, M., Avantaggiato, V., Biffali, E., Arnone, M. I., Sato, K., Pischetola, M., Taylor, B. A., Phillips, S. J., Simeone, A., and Di Lauro, R. (1997). TTF-2, a new forkhead protein, shows a temporal expression in the developing thyroid which is consistent with a role in controlling the onset of differentiation. *Embo J* *16*, 3185-3197.
- Zhu, A. J., and Watt, F. M. (1999). beta-catenin signalling modulates proliferative potential of human epidermal keratinocytes independently of intercellular adhesion. *Development* *126*, 2285-2298.

GLI2 Is Expressed in Normal Human Epidermis and BCC and Induces GLI1 Expression by Binding to its Promoter

Mohammed S. Ikram,* Graham W. Neill,* Gerhard Regl,† Thomas Eichberger,† Anna-Maria Frischauf,† Fritz Aberger,† Anthony Quinn,* and Mike Philpott*

*Center for Cutaneous Research, Barts and The London Queen Mary's School of Medicine & Dentistry, University of London, UK; †Institute of Genetics, University of Salzburg, Salzburg, Austria

Sonic hedgehog (Shh) binds to its receptor patched (PTCH), leading to the activation and repression of target genes via the GLI family of zinc-finger transcription factors. Deregulation of the Shh pathway is associated with basal cell carcinoma (BCC) due to upregulation of GLI1 and GLI2. We recently demonstrated a positive feedback loop between GLI1 and GLI2, which revealed that GLI1 may be a direct target of GLI2. Using band shift and luciferase reporter assays, we now show that GLI2 binds the GLI-binding consensus sequence in the GLI1 promoter. These data suggest that GLI2 directly activates GLI1 and that retrovirally expressed GLI2 induces expression of endogenous GLI1 in human primary keratinocytes. Finally, using *in situ* hybridization, we show that GLI2 is expressed in the interfollicular epidermis and the outer root sheath of hair follicles in normal skin as well as in BCC tumor islands. These results suggest an important role for GLI2 in regulating epidermal proliferation and skin tumorigenesis.

Keywords: basal cell carcinoma/Hedgehog signalling/human keratinocyte/GLI2 promoter/transcriptional regulation
J Invest Dermatol 122:1503–1509, 2004

Hedgehog (Hh) signal transduction pathway plays an essential role in a number of *Drosophila* and vertebrate developmental processes, including cell type specification, pattern formation, and regulation of cell proliferation. Much of our understanding of this pathway comes from studies carried out in *Drosophila*, in which Hh modulates gene expression through the zinc-finger-containing transcription factor *Cubitus interruptus* (*Ci*). *Ci* can function as either a transcriptional activator or a proteolytically cleaved repressor (Aza-Blanc and Kornberg, 1999). In vertebrates, transcriptional responses to Hh signalling are mediated by the three *Ci* homologues, Gli1, Gli2, and Gli3 (Matise and Joyner, 1999; Ruiz i Altaba, 1999; Ingham and McMahon, 2001), that can act in a combinatorial fashion to modulate target gene expression. Gli1 and Gli2 appear to act primarily as transcriptional activators, whereas Gli3 (and at times GLI2) functions as a repressor (Ingham and McMahon, 2001).

Genetic analysis of patients with familial nevoid basal cell carcinoma syndrome (NBCCS) as well as individuals with sporadic BCC led to the identification of the PTCH tumor suppressor gene (Gorlin, 1987; Hahn *et al*, 1996; Johnson *et al*, 1996); this subsequently implicated aberrant sonic hedgehog (Shh) signalling in BCC formation. Indeed, upregulation of GLI1 and GLI2 is frequently observed in BCCs (Gailani *et al*, 1996; Dahmane *et al*, 1997; Unden *et al*, 1997; Regl *et al*, 2002). Further evidence for BCC development as a result of activation of Hh-signalling pathway comes from transgenic mouse models and skin grafting

techniques. Heterozygous *Ptch* +/– mice develop BCC-like features upon UV irradiation, although sporadic BCC formation does not normally occur in these mice (Aszterbaum *et al*, 1999). Human keratinocytes expressing Shh form BCC-like structures when grafted onto the back of nude mice (Fan *et al*, 1997) and overexpression of mediators of Hh-signalling including an oncogenic form of SMO, Shh, GLI1, and GLI2 in epidermal cells of transgenic mice leads to the induction of BCC-like tumors (Fan *et al*, 1997; Oro *et al*, 1997; Xie *et al*, 1998; Grachtchouk *et al*, 2000; Nilsson *et al*, 2000).

The predominance of either GLI1 or GLI2 activation with regard to BCC formation is unclear; however, we recently identified a positive feedback loop between these two proteins, which suggested that GLI1 is an early target of GLI2, whereas GLI2 is likely to be an indirect target of GLI1 (Regl *et al*, 2002). We now present data showing that GLI2 specifically binds to the GLI1 promoter, suggesting that GLI1 is a direct target of GLI2. Furthermore, we show that retrovirally expressed GLI2 induces endogenous GLI1 expression in human primary keratinocytes. Finally, using *in situ* hybridization, we show that GLI2 is expressed in the outer root sheath (ORS) of the hair follicle as well as in BCC tumor islands. These findings suggest that GLI2 directly activates GLI1 expression and may play an important role in skin tumorigenesis.

Results

NHIS-GLI2 binds GLI consensus sequence in the GLI1 promoter and induces GLI1 expression in human primary keratinocytes We have previously identified a

Abbreviations: Shh, sonic hedgehog; BCC, basal cell carcinoma; Hh, hedgehog; ORS, outer root sheath

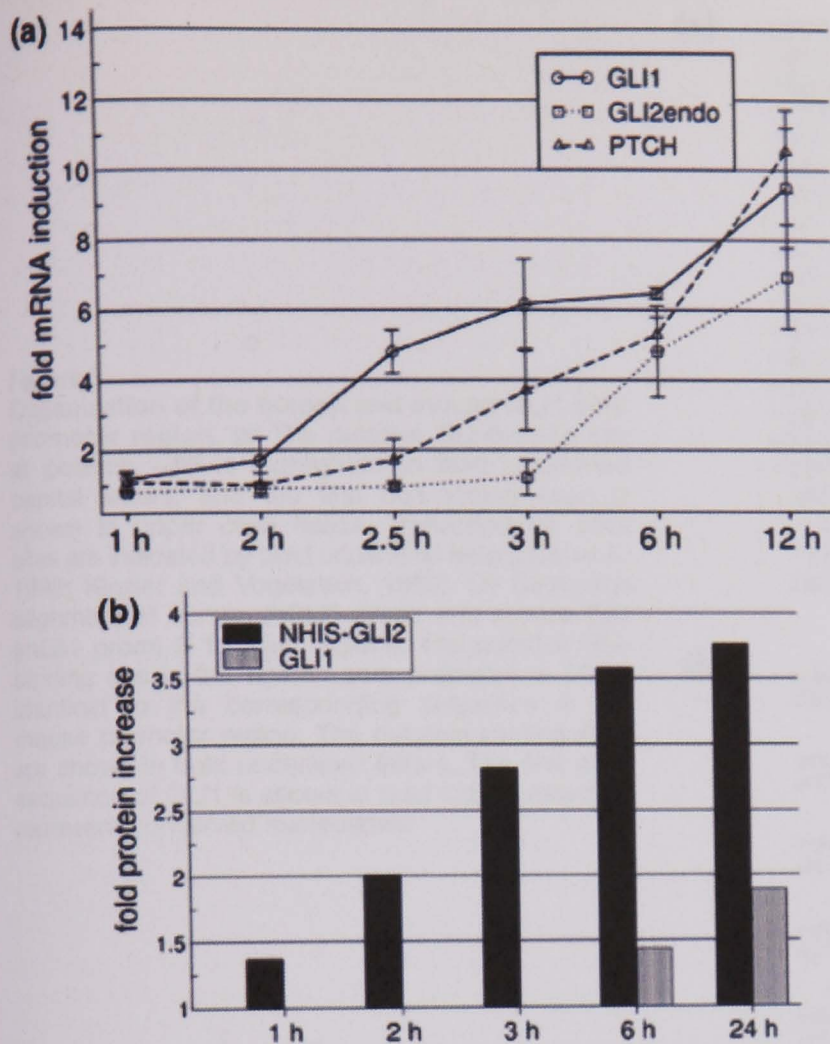


Figure 1
Time-course studies of GLI1, PTCH, and endogenous GLI2 mRNA and NHIS-GLI2 and GLI1 protein expression in NHIS-GLI2 HaCaT cell line. Quantitative real-time RT-PCR (a) and western blot analysis (b). NHIS-GLI2-HaCaT cells were treated with tetracycline for the times indicated. Real-time RT-PCR data show the mean fold induction calculated from three independent experiments, each carried out in duplicate. Standard deviation was below 20% between all replicate experiments. Large ribosomal protein P0 (RPLP0) was used as a reference standard for all analyses to control for the amount of sample material (Martin *et al*, 2001). Samples for western blot analysis were normalized for total protein and quantitated by densitometry.

positive feedback loop between GLI2 and GLI1 in primary human keratinocytes. In particular, time-course analysis of GLI1 mRNA expression in GLI2 expressing keratinocytes provided preliminary evidence for GLI1 possibly being a direct target of GLI2 (Regl *et al*, 2002). To investigate this in more detail, we have measured the increase in GLI1 mRNA and protein in a sub-line of the human keratinocyte cell line HaCaT (GLI2-HaCaT), which expresses N-terminally HIS-tagged GLI2 protein (NHIS-GLI2) under control of the tetracycline repressor. Furthermore, we have related the increase in GLI1 mRNA and protein to levels of NHIS-GLI2 protein. Figure 1a shows that following tetracycline treatment, there was a gradual increase in GLI1 mRNA. In addition, activation of the direct target gene PTCH was slightly delayed compared with induction of GLI1 mRNA. Western blot analysis (Fig 1b) showed that NHIS-GLI2 protein was detected 1 h after tetracycline treatment, whereas GLI1 protein was not detected until 6 h after treatment. Moreover, the increase in GLI2 protein is closely paralleled by the gradual increase in GLI1 mRNA. This suggests that GLI1 represents an early GLI2 target gene.

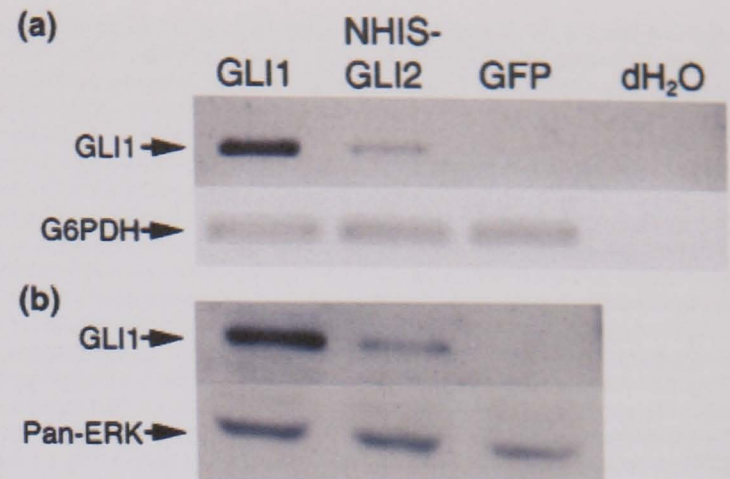


Figure 2
GLI1 mRNA and protein expression in NHIS-GLI2 human primary keratinocytes. Human primary keratinocytes were transduced with NHIS-GLI2, GLI1, and GFP retrovirus and cultured for 72 h after which total RNA and proteins were extracted. This figure shows exogenous NHIS-GLI2 induced endogenous GLI1 protein expression as shown by (a) semi-quantitative RT-PCR and (b) western blot analysis; Pan-ERK indicates equal protein loading. Retroviral expression of GLI1 was used as a positive control, GFP and dH₂O as negative controls. The data represented are of two independent experiments.

Figure 1a also shows that GLI1 mRNA induction is closely followed by a gradual increase in endogenous GLI2 mRNA. This confirms our previous observation that a positive feedback loop exists between GLI1 and GLI2 (Regl *et al*, 2002). In addition to studies in immortalized HaCat cells, we have also shown in this study (Fig 2a,b) that endogenous GLI1 expression is induced in retrovirally transduced GLI2 primary keratinocytes, thus confirming that GLI1 is a target of GLI2 in primary as well as immortalized cell lines. This suggests that there is also a positive feedback between GLI1 and GLI2 in human primary keratinocytes and this may be important for tumor formation.

To assess whether GLI2 may be capable of directly activating GLI1 transcription by binding to the GLI1 promoter, we first performed *in silico* analysis of the 5' flanking region of the human GLI1 core promoter region (Liu *et al*, 1998; Villavicencio *et al*, 2002) to identify putative GLI-binding sites. Using the ScanAce tool (Roth *et al*, 1998; Hughes *et al*, 2000), we analyzed a region of approximately 1 kb upstream of the transcriptional start site of GLI1 (Liu *et al*, 1998) for motifs identical to or closely matching the GLI-consensus-binding site TGGGTGGTC (Kinzler and Vogelstein, 1990) (Fig 3a). An identical putative-binding site is also present in the cis-regulatory sequence of the mouse Gli1 gene, suggesting a possible functional relevance of this motif in the regulation of Gli1 expression (Fig 3b).

To determine whether NHIS-GLI2 protein can bind to the putative GLI-binding site in the GLI1 core promoter, we performed electrophoretic mobility shift assays using bacterially expressed NHIS-GLI2-(332) protein and radioactively labelled double-stranded oligonucleotides containing either the putative GLI-binding site (Bs) or a mutated control oligonucleotide with two base pair exchanges in the core region (Bsm). As shown in Fig 4, recombinant NHIS-GLI2-(332) protein specifically binds to the Bs sequence, but not to the Bsm sequence, suggesting that NHIS-GLI2 protein may be activating GLI1 transcription by directly

(a) -900 tttagtgaggggctcctccttcaactgggctcctccttcagttccccagc
 -850 tcttctgcttcgactccgagcgggtgtcatgtgtgagaacggccagcaga
 -800 gggagcagaaagcctggaagagcagctagagcctgacgtgacgtggtgcg
 -750 gagggcgccaccctccagaacttcgagacgtagagccgggggtctaggg
 -700 aaaggggcttcagtcacagggctccttgggtgacctcgtgaaccacacct
 -650 gcacccagagcctcagccgctgctccttgettttatgctccatagactcc
 -600 tcaccttctccagagcccccaacccaacttgatttgccccaaccgcaa
 -550 ctctgtcccggccgctgcaagtccatccaaaggggtgaggcctgcagata
 -500 aaccacaggatggcagaatgctcagttagcaccaccaaaggcgactacc
 -450 ctacctcactattatcgttctcgggtgaactctccccctgccccgcaa
 -400 tatttctcctcaatctggttctcggggcctcttggggccagcctccag
 -350 aaatccaagccgggatcttagtactaccaacagcagcgtgttcagccggg
 -300 gcgggggggggggcgttaagcagtatagggtccctcaagggagggggaggat
 -250 cctgggggtcctgggggtgcaataagcccggcaccctctcttctgctcc
 -200 agctacccccgctcatcctccagaacggcaagagggagggaaatagaagg
 -150 gaggtgaggggagcgggaagagcggcggcggcagcggctggagaga
 -100 gaaaaagtcttgcataaagggaataaaagtttgcgctctccg**CGGGTGC**
 -50 **GTC**cgggcttgcggcccgggcgggtgggcccggcgggggctggggcca
 1 **GGTTGGGGGGTGGGGTGGCATCGAGGCTGCGCTGCCGTGGCCCTCTGC**
 51 **GCCCCCTCCACCCGACACCCCTCAGCCAGACTCCAGCCCTGGACC**
 101 **GCGCATCCCAGAGCCAGCGCCAGACAGAG**

Figure 3
Organization of the human and mouse GLI1 core promoter region. (a) The putative GLI-binding site at position -56 is highlighted in bold underlined capital letters, and the first non-coding exon is shown in upper case italics. Transcriptional start sites are indicated by bold underlined letters (Liu *et al*, 1998; Kinzler and Vogelstein, 1990). (b) Sequence alignment of human (hGLI1 prom) and mouse Gli1 (mGli1 prom) 5' flanking regions. The putative GLI-binding site in the human core promoter is 100% identical to the corresponding sequence in the mouse promoter region. The putative-binding sites are shown in bold underlined letters. The first exon sequence of GLI1 is shown in bold italics. Asterisks represent conserved nucleotides.

(b)

hGLI1 prom	GGATCCTGGGGGTCTGGGGGTGCAATAAGCCCGGCACCCCTTCTCTTGTTCAGCTAC
mGli1 prom	GGATCCTGGGGGTCTGGGGGTGCCATAAGCCCGGCACCCCTTCTCTAGCTTCTATCCAC
hGLI1 prom	CCCCTCATCTCCAGAACGGCAAGAGGGAGGGAATAGAAGGGAGGTGAGGGCGAOC
mGli1 prom	CCAGC-TCATCTTAGAACGGTCCGAAGAAGG-ATATACAGGGAAAGTGA-----C
hGLI1 prom	GGGAAGAGCGGGCGGCCAGCGGCTGGAGAGAGAAAAAGTTTTGCAAAAGGGAAAAA
mGli1 prom	GGGAAGAGCGGTAGCGTGC-GGTGCAACAGCGAGAAAAAGTTTTGCAAAAGGGAAAAA
hGLI1 prom	AAAAGTTTGCCTTCTCG CGGGTGC CGGGCTTGCGGCCCGGGGCTGGGCCGGCGGG
mGli1 prom	AAAAGTTTGCCTTCTCG CGGGTGC CCGGCTCGAGGCCCGGGCGGT--GGCGGGCGG-
hGLI1 prom	AGGGCTGGGGCCAGGTTGGGGGGTGGGGTGGGGTGGGGTGGGGTGGGGTGGGGTGGGGT
mGli1 prom	AGGGCTGGGGCCAGGTTGGGAGGGT-GGGGTGGCACTGAAGCTGCGCTGCAGTGGCCCT
hGLI1 prom	CTCCCGCCCCCTCCCGCCACACACC ----- CCCCCGCCAGACTCCAGCCCTGG
mGli1 prom	GT--GACCCCTCCCGCCACACACTCCCCCCCCCCCCAGCCAGTTTCCAGCCCTGG
hGLI1 prom	ACCGGCATCCCGAGCCCGCCCGCCAGCAGAG GTGAGAAGGGGGGCCAGGCCGGGGGACC
mGli1 prom	ACCACGCATCCCGAGCACCGGCCCGGAGGGTGA--GGGGGGCAGCCGGGAGACC

binding to the 5' flanking region of the GLI1 promoter at a position close to the transcriptional start site.

To analyze whether the GLI-binding site in the GLI1 promoter is involved in activation of GLI1 transcription by GLI2, we performed luciferase reporter assays using wild-type and mutated GLI1 promoter constructs. Co-transfection of GLI2 expression plasmid with the reporter construct containing the 5' upstream region of human GLI1 (-1400 to +93, Liu *et al*, 1998) resulted in a 3-fold increase in luciferase activity compared with controls. By contrast, no increase in reporter activity was observed when the Gli-binding site at position -56 was changed from CGGG TGGTC to CGCCTGGTC by site-directed mutagenesis (Fig 5). The GLI-binding and luciferase reporter assay data suggest that HIS-GLI2 activates transcription of GLI1 by interacting directly with the GLI-binding site at positions -56 to -48 of the GLI1 promoter.

GLI2 is expressed in BCC, normal interfollicular epidermis, and in the ORS of the hair follicle The expression profile of GLI1 is well characterized in BCC and normal skin (Ghali *et al*, 1999). Having shown that GLI1 is a putative direct target of GLI2, we investigated the expression pattern of GLI2 in BCC and normal skin by *in situ* hybridization (Fig 6). We report that GLI2 mRNA was expressed in BCC tumor islands of all BCC samples analyzed (n=8) and in normal skin (n=3), GLI2 was expressed in the ORS of the

hair follicle, sebaceous glands, and in the interfollicular epidermis. No staining was observed with a GLI2 sense probe in adjacent serial sections. Only samples showing a positive signal for keratin 14 (to confirm RNA integrity) were analyzed.

Discussion

Members of the GLI family of zinc-finger transcription factors are key mediators of Hh-signalling and in BCC activation of the Hh pathway results in overexpression of GLI1 and GLI2 (Green *et al*, 1998; Regl *et al*, 2002). In primary human keratinocytes, retrovirally expressed GLI1 induces GLI2 expression and in HaCaT cells it has been shown that a positive feedback loop between GLI1 and GLI2 exists (Regl *et al*, 2002). In this study, we have shown by RT-PCR and western blot analysis that retrovirally expressed GLI2 induces endogenous GLI1 expression in primary keratinocytes, confirming that a positive feedback loop between GLI1 and GLI2 exists. Time-course analysis of GLI1 expression in GLI2-inducible cell line suggested that GLI1 may be a direct target GLI2 (Regl *et al*, 2002). Using gel shift and luciferase assays, we have identified a functional Gli-binding site in the GLI1 promoter that confers activation of GLI1 transcription in response to GLI2. Together with detailed time-course studies of GLI1 transcription

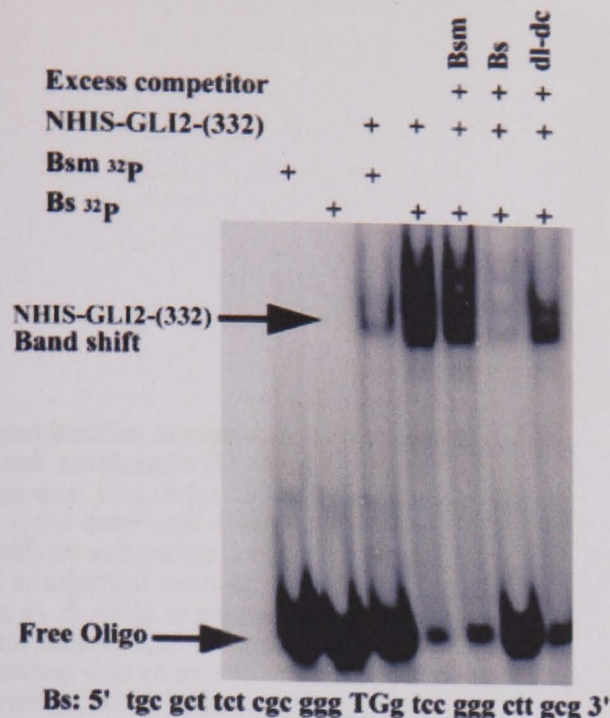


Figure 4
NHIS-GLI2-(332) binds GLI consensus sequence. Electrophoretic mobility shift assay demonstrating specific binding of NHIS-tagged recombinant GLI2 protein corresponding to amino acids 1–332 (NHIS-GLI2-(332)) to the GLI-binding site (Bs) in the GLI1 core promoter region (indicated by the band shift). The Bs oligonucleotide sequence used for the analysis is shown below. The region with a high sequence similarity to the GLI-consensus-binding site is underlined. The two central nucleotides shown in capital letters (TG) were changed to AA to give rise to mutated Bsm. The synthetic polymer poly-(dl-dC) was used in DNA-binding protein studies to absorb non-specific-binding proteins. Excess competitors unlabelled Bsm, Bs, and poly-(dl-dC) were used with ³²P-labelled (Bsm ³²P) and (Bs ³²P).

The importance of Shh-Gli2 signalling in murine hair follicle development has been demonstrated by several groups (St-Jacques *et al*, 1998; Chiang *et al*, 1999; Karlsson *et al*, 1999; Brewster *et al*, 2000; Bai *et al*, 2002; Mill *et al*, 2003) and transgenic mice expressing GLI2 in the basal layer develop BCC (Grachtchouk *et al*, 2000). As expected for a target of GLI2, the expression profile of GLI1 correlates with that of GLI2 in both the ORS of the hair follicle and in BCC. Antibodies to GLI2 are not available and, therefore, we have been unable to confirm that the patterns of GLI2 protein mimic those of its mRNA. We have shown that in primary human keratinocytes GLI2 induces GLI1, therefore, the lack of GLI1 expression may indicate that GLI2 is not activated in the interfollicular epidermis and that other factors may be required for transcriptional activity. It has recently been demonstrated in transgenic mice that Gli2 activation in mouse skin is dependent on Shh. However, it has been shown that during embryogenesis, Gli2 can be activated in response to FGF independent of Shh, providing evidence that GLI2 can function independent of Shh. Moreover, it has also been shown that deletion of the N-terminal repressor domain of GLI2 produces a mutant protein that can induce Gli1 and Ptch expression independent of Shh (Sasaki *et al*, 1999; Brewster *et al*, 2000; Mill *et al*, 2003). Currently, little is known about processing of GLI2 and it will be important to determine, therefore, whether GLI2 is processed and if so whether differences in processing occur between normal skin compartments, such as interfollicular epidermis, ORS of hair follicle and in BCC. We have recently found that GLI2 represses expression of genes associated with epidermal differentiation, suggesting that GLI2 may have repressor activity in the human epidermis (Regl *et al*, in press).

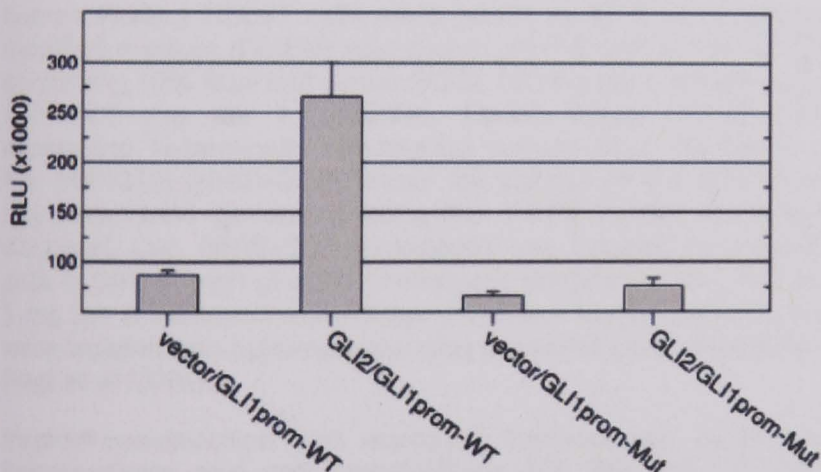


Figure 5
Luciferase reporter assays showing activation of the GLI1 promoter by NHIS-GLI2. 293 cells were either transfected with wild-type (GLI1prom-WT) or mutated GLI1 promoter reporter construct (GLI1prom-Mut), together with either empty vector or NHIS-GLI2 expression vector. Data represented are of mean values of three independent experiments as relative luciferase units (RLU). These data show a 3-fold increase in luciferase activity in GLI2/GLI1prom-WT compared with controls. By contrast, no increase in reporter activity was observed when the Gli-binding site at position -56 was mutated from CGGGTGGTC to CGCCTGGTC (GLI2/GLI1 prom-Mut).

in GLI2 expressing cells, these data suggest direct activation of GLI1 by GLI2; however, it is possible that the behavior of the NHIS-GLI2 and the endogenous GLI2 protein may not be identical. Finally, we have shown by *in situ* hybridization that GLI2 mRNA is expressed in both the interfollicular epidermis and ORS of hair follicles as well as in BCC tumor islands.

In BCC, GLI1 and GLI2 are consistently expressed in tumor islands and this may be accounted for by the positive feedback mechanism that we have identified (Green *et al*, 1998; Regl *et al*, 2002). Autoregulation of Gli1 expression has previously been observed in frog embryos, suggesting that positive feedback loops may be a common feature to sustain pathway activation in the absence of Shh stimulation (Dahmane *et al*, 2001). Whether Gli1 or Gli2 is the initial factor that induces the feedback loop and possibly tumor formation remains to be determined. In contrast to Gli1, expression of Gli2 is not dependent on Shh and during mouse embryogenesis Gli2 is expressed before the onset of Shh and Gli1 transcription (Bai *et al*, 2002). In addition, Gli2 is required for the expression of Gli1 in murine skin (Mill *et al*, 2003). This suggests that Gli2 induces Gli1, which in turn further increases Gli2 levels leading to hyperproliferation (Regl *et al*, 2002).

In summary, we provide further evidence for a positive feedback loop between GLI1 and GLI2 that potentiates the Shh signal in hair follicle morphogenesis and BCC formation. This indicates a possible important role for human GLI2 in regulating skin tumorigenesis.

Materials and Methods

Cell culture The study was approved by the local ethical committee (ELCHA Research Ethics Committee, Ref: T/01/037 and adhered to the declaration of Helsinki guidelines for use of

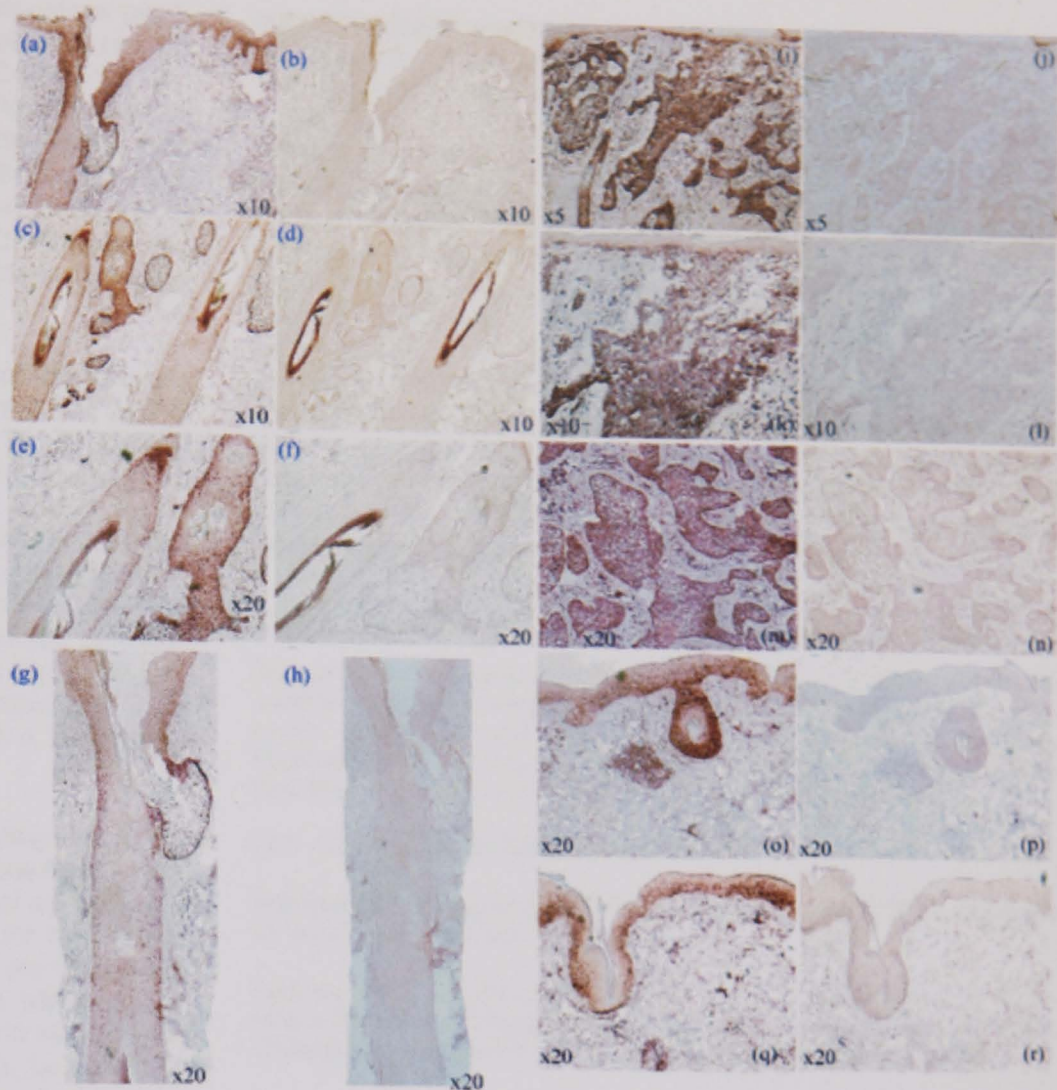


Figure 6

***In situ* hybridization analysis of GLI2 expression in basal cell carcinoma (BCC) and normal skin.**

GLI2 expression was detected in the epidermis (a, o, q) and in the outer root sheath of the hair follicle (c, e, g) with an anti-sense probe. No staining was observed in adjacent sections with a sense probe (b, d, f, h, p, r). GLI2 expression was detected in BCC tumor islands with an anti-sense probe (i, k, m). No staining was observed in adjacent sections with a sense probe (j, l, n).

human tissue.) HaCaT cells were grown at 37°C in Dulbecco's modified medium (DMEM) adjusted to pH 7.5 with 5 mM HEPES, containing 10% fetal calf serum (FCS), 100 mg per L streptomycin, and 62.5 mg per L penicillin. Double-stable HaCaT lines, expressing N-terminally HIS-tagged human GLI2 (GenBank GI No. 3061315) (NHIS-GLI2) under the control of the tetracycline repressor, were generated using the T-REX system (Invitrogen, Carlsbad, CA). NHIS-GLI2 expression was induced by culturing cells in DMEM-high glucose (Invitrogen), containing 10% FCS and 1 mg per L tetracycline (Invitrogen). Primary human keratinocytes were isolated and cultured according to the methods described in Regl *et al* (2002).

Vector construction and retroviral transduction of primary keratinocytes and cell transfections The retroviral SIN-GLI1-EGFP construct was generated as described in Regl *et al* (2002). To generate the retroviral bicistronic GLI2-EGFP expression construct, N-terminally HIS-tagged GLI2 was cloned into pI2E-A, a modified version of the pIRES2-EGFP plasmid (Clontech, Hampshire, UK) (Regl *et al*, 2002). pI2E-A-GLI2 was digested with *SalI* and *NotI* to excise CMV-GLI2-IRES-EGFP. The resulting fragment was cloned into *XhoI*-*NotI* digested retroviral SIN-IP plasmid (a gift from Prof. P. Khavari) to create SIN-GLI2-EGFP. Retroviral transduction of primary keratinocytes and cell transfections were carried out as described in Regl *et al* (2002). Cells were harvested at the time points indicated in the text.

RNA isolation and real-time RT-PCR analysis Isolation of total RNA from HaCaT cells and real-time RT-PCR was carried out as described previously in Regl *et al* (2002). Total RNA from primary keratinocytes was isolated using RNeasy B (Biogenesis Ltd, Poole, Dorset, UK) as per the manufacturer's instructions. Genomic DNA was removed by treatment with DNaseI (Boehringer Mannheim, Roche; Basel, Switzerland) and cDNA was synthesized using AMV Reverse Transcriptase (Promega A5000 kit, Madison, WI) accord-

ing to the manufacturer's instructions. PCR was carried out using 1 μ L cDNA reaction, 0.25 mM each dNTP, 1 \times (25 mM $(\text{NH}_4)_2\text{SO}_4$, 93.75 mM Tris-HCl, pH 8.8, at 25°C, 1.25 $\times 10^{-2}$ Tween 20) reaction buffer, 1.75 mM MgCl_2 , 0.125 μ M each (forward and reverse) primers with 1 U thermal stable Red Hot DNA polymerase (Advanced Biotechnology, Epsom, UK) in a total reaction volume of 20 μ L. The samples were thermo cycled, at 94°C for 1 min (94°C for 1 min, 60°C for 30 s, 72°C for 1 min) \times 40 cycles, and final extension at 72°C for 10 min. G6PDH was amplified with an annealing temperature set at 55°C in 35 cycles. A negative primer-only control without cDNA was also set up. PCR-primer sequences were as follows: GLI1 forward primer 5' gaagacctctccagcttga 3' corresponding to 1504–1523 nucleotides and reverse primer 5' ggctgacagtataggcagag 3' corresponding to 1728–1747 nucleotides of GLI1 (GenBank GI No. 4885278). G6PDH forward primer 5' gttccgtgaggaccagatctac 3' corresponding to 584–605 nucleotides, reverse primer 5' ggctcctgaagggtgaggataa 3' corresponding to 712–733 nucleotides of G6PDH (GenBank GI No. 182870).

Western blot analysis Western blot analysis of GLI1 and NHIS-GLI2 protein expression was carried out as described in Regl *et al* (2002). GLI1 protein was detected with polyclonal goat anti-GLI1 antibody (C-18, Santa Cruz Biotechnology, Santa Cruz, CA) and NHIS-GLI2 with peroxidase-conjugated monoclonal anti-polyhistidine antibody (Sigma, clone HIS-1, Sigma, Vienna Austria; Dorset, UK). Proteins were visualized by chemiluminescence detection (ECL, Amersham Biosciences, Bucks, UK; Uppsala, Sweden). Proteins levels were quantified by densitometric analysis using the AIDA/2D densitometry software package (RAYTEST).

Recombinant GLI2 protein expression and purification For the production of recombinant GLI2 protein, a fragment encoding amino acids 1–386 of GLI2 was PCR amplified using the following primers: forward: 5' gagggatccgcctcactccatcaat 3', reverse: 5' gaggaaattcctaggtcatcatgttcagg 3'. The amplicon was cloned into

the *EcoRI*–*BamHI* sites of *Escherichia coli* expression vector pHIS-Parallel2 (Sheffield *et al*, 1999). To increase the solubility of GLI2 protein, the insert was further truncated at the C-terminus with *SmaI* and *XhoI* yielding a protein corresponding to amino acids 1–332, which encompasses the N-terminus and the entire zinc-finger DNA-binding domain (NHIS-GLI2-(332)). NHIS-GLI2-(332) protein expression in *E. coli* strain BL21 was induced for 60 min by the addition of 1 mM IPTG (Sigma). HIS-tagged GLI2-(332) protein was purified with Ni-NTA Agarose (Qiagen, Hilden, Germany) according to the manufacturer's instructions.

Electrophoretic mobility shift assay Binding reactions for band shift assays were carried out in 1 × BS buffer (20 mM Tris, pH 7.8, 25 mM KCl, 5 mM MgCl₂, 0.5 mM DTT, and 10 μM ZnSO₄) containing 0.77 μg poly-(dI–dC) (Sigma) and 10% glycerol. Five micrograms of purified NHIS-GLI2-(332) protein and 8 ng of radioactively labelled double-stranded oligonucleotide were added to the reaction and incubated for 25 min at room temperature. In competition experiments, 400 ng of specific or mutant unlabelled oligonucleotide were used per reaction. For unspecific competition, 1.5 μg poly-dI–dC was added to the reaction. Samples were separated on 6% acrylamide gels. Following electrophoresis, gels were dried, exposed overnight, and scanned with a BAS-1800II phosphorimager (Fuji, Fuji, Japan).

Luciferase reporter assays and site-directed mutagenesis The 5' upstream regulatory region of the human GLI1 gene from –1400 to +93 relative to the transcriptional start site (Liu *et al*, 1998) was amplified by PCR using the FailSafe PCR system for high-fidelity PCR cloning (Epicentre, Madison, WI). To mutate the Gli-binding site, the GLI1 promoter was first subcloned into pBluescript II SK+ (Stratagene, La Jolla, CA) and then subjected to site-directed mutagenesis with the QuickChange Kit (Stratagene, La Jolla, CA) according to the manufacturer's instructions. Following mutagenesis, the GLI1 promoter region was transferred back to pGL3 reporter vector. The sequence of the oligonucleotide used for mutagenesis was 5' GCGCTTCTCGCGCCTGGTCCGGGCTTG 3'. Successful mutagenesis was verified by DNA-sequencing on an ABI 310 automated sequencer. For luciferase reporter assays, 293 cells were co-transfected in 12-well plates with GLI2 expression plasmid (GLI2b in pcDNA4/TO, Invitrogen) or empty pcDNA4/TO, and wild-type or mutated GLI1 reporter plasmid. β-galactosidase expression vector (pcDNA4/TO-LacZ, Invitrogen) was co-transfected for normalization of transfection efficiency. Cells were harvested at 48 h post-transfection and luciferase assays were carried out using Luciferase Assay Substrate (Promega), according to the manufacturer's instructions. Luciferase activity was measured on a Lucy II luminometer (Anthos, Wals, Austria). To normalize results for lacZ activity, 10 μL of cell lysate was mixed with 240 μL Z-buffer (100 mM NaPO₄ (pH 7), 10 mM KCl₂, 1 mM MgSO₄, 50 mM β-Mercaptoethanol), and 50 μL *O*-nitro- α -D-phenyl-galactopyranoside (4 mg per mL) and incubated at 28°C until yellow staining became visible. Reactions were stopped by adding 250 μL 1 M NaCO₃. β-galactosidase activity was quantified by measuring absorbance at 405 nm on an SLT-Spectra plate reader (SLT, Austria).

In situ hybridization GLI2 and keratin 14 sense and anti-sense probes were generated from GLI2 cDNA corresponding to 28,270–28,566 nucleotides (GenBank GI No. 3061315) and keratin 14 cDNA corresponding to 298–1498 nucleotides (GenBank GI No. 15431309) cloned into pCRII-TOPO vector, using DIG-labelling kit (Roche, Basel, Switzerland; Lewes East Sussex, UK) as described by the manufacturer's instructions. Keratin 14 probes were fragmented and purified using sodium acetate ethanol precipitation method (Wilkinson, 1998). Eight micrometer tissue sections were pre-hybridized with (4 × SSC, 1 × Denhardt's, 50% formamide (500 μg per mL tRNA and 500 μg per mL Salmon Testes DNA denatured at 100°C for 10 min and placed on ice) before adding to the mix) and incubated at 42°C for 3–4 h. Hybridization was carried

out using fresh pre-hybridized solution containing (80–100 ng labelled probe denatured at 65°C for 5 min) at 42°C overnight. The next day, the sections were washed in 2 × SSC for 5 min (× 2) and in (2 × SSC, 1 × SSC, 0.5 × SSC each containing 50% formamide) at 45–55°C and in 0.1 × SSC 50% formamide at 50–60°C for 20 min, followed by a final wash in 2 × SSC and rinsed in DIG buffer 1 (100 mM Tris-HCl, 150 mM NaCl, pH 7.5). Sections were blocked with 10% normal sheep serum (NSS) in DIG buffer 1 and incubated with anti-digoxigenin-alkaline phosphatase conjugated (Roche) diluted 1:400 in 1% NSS DIG buffer 1 for 2 h, followed by washing in DIG buffer 1 (× 2) and DIG buffer 2 (100 mM Tris-HCl, pH 9.5, 100 mM NaCl, 50 mM MgCl₂) for 10 min. The Hybrids were visualized by incubating the section with BCIP/NBT (Sigma) liquid substrate in the dark at 4°C overnight. The color reaction was stopped by immersing the sections in (10 mM Tris-HCl, pH 8, 1 mM EDTA) for 30 min. The developed slides were mounted and examined by microscopy.

This project was supported by Medical Research Council UK, the Austrian Science Fund (FWF project P14227-MOB) and the 'Schwerpunkt: Biomedizin und Gesundheit' of the University of Salzburg. Thomas Eichberger was supported by an EMBO short-term fellowship during a stay in the Center for Cutaneous Research in London.

DOI: 10.1111/j.0022-202X.2004.22612.x

Manuscript received July 7, 2003; revised January 27, 2004; accepted for publication February 3, 2004

Address correspondence to: Mohammed S. Ikram, Centre for Cutaneous Research, Clinical Sciences Research Centre, 2 Newark Street, Whitechapel, London E1 2AT, UK. E-mail: m.s.ikram@qmul.ac.uk

References

- Aszterbaum M, Epstein J, Oro A, Douglas V, LeBoit PE, Scott MP, Epstein EH Jr: Ultraviolet and ionizing radiation enhance the growth of BCCs and trichoblastomas in patched heterozygous knockout mice. *Nat Med* 5:1285–1291, 1999
- Aza-Blanc P, Kornberg TB: Ci: A complex transducer of the hedgehog signal. *Trends Genet* 15:458–462, 1999
- Bai CB, Auerbach W, Lee JS, Stephen D, Joyner AL: Gli2, but not Gli1, is required for initial Shh signaling and ectopic activation of the Shh pathway. *Development* 129:4753–4761, 2002
- Brewster R, Mullor JL, Ruiz i Altaba A: Gli2 functions in FGF signaling during antero-posterior patterning. *Development* 127:4395–4405, 2000
- Chiang C, Swan RZ, Grachtchouk M, *et al*: Essential role for Sonic hedgehog during hair follicle morphogenesis. *Dev Biol* 205:1–9, 1999
- Dahmane N, Lee J, Robins P, Heller P, Ruiz i Altaba A: Activation of the transcription factor Gli1 and the Sonic hedgehog signalling pathway in skin tumours. *Nature* 389:876–881, 1997
- Dahmane N, Sanchez P, Gitton Y, *et al*: The sonic hedgehog-Gli pathway regulates dorsal brain growth and tumorigenesis. *Development* 128:5201–5212, 2001
- Fan H, Oro AE, Scott MP, Khavari PA: Induction of basal cell carcinoma features in transgenic human skin expressing sonic hedgehog. *Nat Med* 3:788–792, 1997
- Gailani MR, Stahle-Backdahl M, Leffell DJ, *et al*: The role of the human homologue of *Drosophila* patched in sporadic basal cell carcinomas. *Nat Genet* 14:78–81, 1996
- Ghali L, Wong ST, Green J, Tidman N, Quinn AG: Gli1 protein is expressed in basal cell carcinomas, outer root sheath keratinocytes and a subpopulation of mesenchymal cells in normal human skin. *J Invest Dermatol* 113:595–599, 1999
- Gorlin RJ: Nevroid basal-cell carcinoma syndrome. *Medicine (Baltimore)* 66:98–113, 1987
- Grachtchouk M, Mo R, Yu S, Zhang X, Sasaki H, Hui CC, Dlugosz AA: Basal cell carcinomas in mice overexpressing Gli2 in skin. *Nat Genet* 24:216–217, 2000
- Green J, Leigh IM, Poulson R, Quinn AG: Basal cell carcinoma development is associated with induction of the expression of the transcription factor Gli1. *Br J Dermatol* 139:911–915, 1998

- Hahn H, Wicking C, Zaphiropoulos P, *et al*: Mutations of the human homolog of *Drosophila* patched in the nevoid basal cell carcinoma syndrome. *Cell* 85:841–851, 1996
- Hughes JD, Estep PW, Tavazoie S, Church GM: Computational identification of cis-regulatory elements associated with groups of functionally related genes in *Saccharomyces cerevisiae*. *J Mol Biol* 296:1205–1214, 2000
- Ingham PW, McMahon AP: Hedgehog signaling in animal development: Paradigms and principles. *Genes Dev* 15:3059–3087, 2001
- Johnson RL, Rothman AL, Xie J, *et al*: Human homolog of patched, a candidate gene for the basal cell nevus syndrome. *Science* 272:1668–1671, 1996
- Karlsson L, Bondjers C, Betsholtz C: Roles for PDGF-A and sonic hedgehog in development of mesenchymal components of the hair follicle. *Development* 126:2611–2621, 1999
- Kinzler KW, Vogelstein B: The GLI gene encodes a nuclear protein which binds specific sequences in the human genome. *Mol Cell Biol* 10:634–642, 1990
- Liu CZ, Yang JT, Yoon JW, Villavicencio E, Pfendler K, Walterhouse D: Characterization of the promoter region and genomic organization of GLI, a member of the sonic hedgehog-patched signaling pathway. *Gene* 209:1–11, 1998
- Martin KJ, Graner E, Li Y, *et al*: High-sensitivity array analysis of gene expression for the early detection of disseminated breast tumor cells in peripheral blood. *Proc Natl Acad Sci USA* 98:2646–2651, 2001
- Matisse MP, Joyner AL: Gli genes in development and cancer. *Oncogene* 18:7852–7859, 1999
- Mill P, Mo R, Fu H, Grachtchouk M, Kim PC, Dlugosz AA, Hui CC: Sonic hedgehog-dependent activation of Gli2 is essential for embryonic hair follicle development. *Genes Dev* 17:282–294, 2003
- Nilsson M, Uden AB, Krause D, *et al*: Induction of basal cell carcinomas and trichoepitheliomas in mice overexpressing GLI-1. *Proc Natl Acad Sci USA* 97:3438–3443, 2000
- Oro AE, Higgins KM, Hu Z, Bonifas JM, Epstein EH Jr, Scott MP: Basal cell carcinomas in mice overexpressing sonic hedgehog. *Science* 276:817–821, 1997
- Regl G, Kasper M, Schnidar H, *et al*: The zinc finger transcription factor GLI2 antagonizes contact inhibition and differentiation of human epidermal cells. *Oncogene* 23:1263–1267, 2004
- Regl G, Neill GW, Eichberger T, *et al*: Human GLI2 and GLI1 are part of a positive feedback mechanism in basal cell carcinoma. *Oncogene* 21:5529–5539, 2002
- Roth FP, Hughes JD, Estep PW, Church GM: Finding DNA regulatory motifs within unaligned noncoding sequences clustered by whole-genome mRNA quantitation. *Nat Biotechnol* 16:939–945, 1998
- Ruiz i Altaba A: Gli proteins and Hedgehog signaling: Development and cancer. *Trends Genet* 15:418–425, 1999
- Sasaki H, Nishizaki Y, Hui C: Regulation of Gli2 and Gli3 activities by an amino-terminal repression domain: Implication of Gli2 and Gli3 as primary mediators of Shh signaling. *Development* 126:3915–3924, 1999
- Sheffield P, Garrard S, Derewenda Z: Overcoming expression and purification problems of RhoGDI using a family of 'parallel' expression vectors. *Protein Exp Purif* 15:34–39, 1999
- St-Jacques B, Dassule HR, Karavanova I, *et al*: Sonic hedgehog signaling is essential for hair development. *Curr Biol* 8:1058–1068, 1998
- Uden AB, Zaphiropoulos PG, Bruce K, Toftgard R, Stahle-Backdahl M: Human patched (PTCH) mRNA is overexpressed consistently in tumor cells of both familial and sporadic basal cell carcinoma. *Cancer Res* 57:2336–2340, 1997
- Villavicencio EH, Yoon JW, Frank DJ, Fuchtbauer EM, Walterhouse DO, Iannaccone PM: Cooperative E-box regulation of human GLI1 by TWIST and USF. *Genesis* 32:247–258, 2002
- Wilkinson DG: *In Situ Hybridization*. Vol. 196, 2nd edn. Oxford: Oxford University Press, 1998
- Xie J, Murone M, Luoh SM, *et al*: Activating smoothened mutations in sporadic basal-cell carcinoma. *Nature* 391:90–92, 1998

FOXE1, A New Transcriptional Target of GLI2, Is Expressed in Human Epidermis and Basal Cell Carcinoma

Thomas Eichberger,* Gerhard Regl,* Mohammed S. Ikram,† Graham W. Neill,† Michael P. Philpott,‡ Fritz Aberger* and Anna-Maria Frischauf*

*Department of Molecular Biology, University of Salzburg, Salzburg, Austria; †Center for Cutaneous Research, Barts and The London Queen Mary's School of Medicine & Dentistry, University of London, London, UK

Sonic hedgehog (Hh) signaling plays a key role in epidermal development and skin cancer. Mutational inactivation of the tumor suppressor gene patched (*PTCH*) leads to constitutive activation of the Hh signaling pathway, resulting in activation of target gene transcription by the zinc finger transcription factors GLI1 and GLI2. Recent experiments in mice point to GLI2 as the key mediator of Hh signaling in skin. We have concentrated on the identification of candidate mediators of GLI2 function in the human epidermis. We show here that the forkhead/winged-helix domain transcription factor *FOXE1* is likely to be a direct GLI2 target gene. The kinetics of *FOXE1* induction are similar to the known direct target *PTCH*, and a 2.5 kb upstream fragment containing five GLI-binding sites activates transcription in a reporter assay. We show by *in situ* hybridization that *FOXE1* is expressed in the outer root sheath of the hair follicle, where murine *Gli2* is also expressed. *FOXE1* expression is also found in basal keratinocytes of the human epidermis and basal cell carcinoma (BCC). These data point to a putative role of *FOXE1* in mediating Hh signaling in the human epidermis downstream of GLI2.

Key words: forkhead transcription factor/GLI transcription factor/hair follicle/hedgehog signaling
J Invest Dermatol 122:1180–1187, 2004

Hedgehog (Hh) signaling plays a key role in vertebrate development, where it is involved in a multitude of biological processes such as cell differentiation, proliferation, and growth (reviewed in Ingham and McMahon, 2001; Nybakken and Perrimon, 2002). Inappropriate activation of Hh signaling has been implicated in developmental defects and a predisposition to various malignancies such as basal cell carcinoma (BCC), medulloblastoma, and rhabdomyosarcoma (reviewed in Toftgard, 2000; Bale, 2002; Mullor *et al*, 2002). Analysis of hereditary and sporadic BCCs revealed that ligand-independent activation of Hh signaling in epidermal cells is the primary event in tumorigenesis. Uncontrolled activation is caused by inactivating mutations in the human tumor suppressor gene patched (*PTCH*) or, in rare cases, by gain-of-function mutations in the Smoothed gene (*SMOH*) (Gailani *et al*, 1996; Hahn *et al*, 1996; Johnson *et al*, 1996; Aszterbaum *et al*, 1998; Xie *et al*, 1998).

Normally, transduction of the HH signal is triggered by binding of secreted HH protein to the 12 pass transmembrane receptor protein (PTCH). Binding of HH to PTCH is thought to relieve the inhibitory effect of PTCH on the seven pass transmembrane protein Smoothed (SMOH), leading to transduction of the signal to the nucleus (reviewed in Ingham and McMahon, 2001; Nybakken and Perrimon, 2002). The zinc finger transcription factors (TF) *GLI1* and

GLI2 have been identified as key mediators of HH signal transduction and like *PTCH* are themselves HH target genes. Consequently, BCCs express elevated levels of *GLI1*, *GLI2*, and *PTCH*, and other HH target genes (Gailani *et al*, 1996; Dahmane *et al*, 1997; Ghali *et al*, 1999; Regl *et al*, 2002).

Support for a critical role of *GLI1* and *GLI2* in BCC development has come from transgenic mouse models showing that overexpression of either protein in epidermal cells can induce the formation of tumors, some of which display BCC-like characteristics (Grachtchouk *et al*, 2000; Nilsson *et al*, 2000; Sheng *et al*, 2002). More recently, studies of knockout mice have pointed to a role of *Gli2* rather than *Gli1* as the primary mediator in Hh signal transduction. Firstly, mice deficient in *Gli1* are viable and have no obvious developmental defects (Park *et al*, 2000). In contrast, *Gli2*^{-/-} mice are characterized by severe developmental malformations, including the lack of the floor plate of the neural tube and of the anterior pituitary, and by numerous lung, foregut, skeleton, and skin defects (Ding *et al*, 1998; Matise *et al*, 1998; Mill *et al*, 2003). This *Gli2* phenotype broadly overlaps with that described for *Shh*- or *lhh*- deficient mice (Chiang *et al*, 1996, 1999; St-Jacques *et al*, 1999). Secondly, removal of *Gli2* but not of *Gli1* leads to partial rescue of the *ptc*^{-/-} phenotype, where Hh signaling is hyperactivated (Bai *et al*, 2002). Thirdly, *Gli2* but not *Gli1* is required for Hh signaling in hair follicle development (Mill *et al*, 2003). Together, these findings suggest that *Gli2* rather than *Gli1* is the primary transducer of the Hh signal.

To elucidate the mechanism by which *GLI2* controls HH-mediated epidermal development and skin cancer, we

Abbreviations: BCC, basal cell carcinoma; Hh, hedgehog; PTCH, 12 pass transmembrane receptor protein; *PTCH*, human tumor suppressor gene patched; Tet, tetracycline

focused on the identification of GLI2-regulated genes with a putative role in mediating Hh signaling downstream of GLI2 in epidermal cells. Here, we present data that the forkhead transcription factor *FOXE1* may be a direct GLI2 target gene. Like *GLI2*, *FOXE1* is expressed in normal epidermis and BCC, suggesting an involvement of *FOXE1* in executing the transcriptional program triggered by *GLI2*.

Results

Overexpression of GLI2 in human keratinocytes increases *FOXE1* mRNA levels To identify GLI2-regulated genes, we have expressed GLI2 in human keratinocytes followed by cDNA array analysis of GLI2 expressing cells and controls. We have genetically modified the human keratinocyte cell line HaCaT (Boukamp *et al*, 1988) to allow tetracycline (tet)-inducible expression of human *GLI2* (referred to as HaCaT-GLI2His) (Regl *et al*, 2002). Tet-inducible cell lines offer the advantage of precise temporal control of GLI2 expression, which has proved invaluable for the identification of early target genes. Expression profiling of samples treated with tet for 24 and 72 h, respectively, was carried out on filter arrays containing approximately 2200 human expressed sequence tag (EST) (unpublished data). To eliminate differences between clonal HaCaT-GLI2His lines, RNA from four independently isolated lines was pooled and used for cDNA array analysis. As shown in Fig 1, the forkhead transcription factor *FOXE1* was highly upregulated in a GLI2 concentration-dependent manner compared with controls, with a (5.4 ± 0.94)-fold increase after 24 h and a (10 ± 1.15)-fold increase after 72 h of tet treatment.

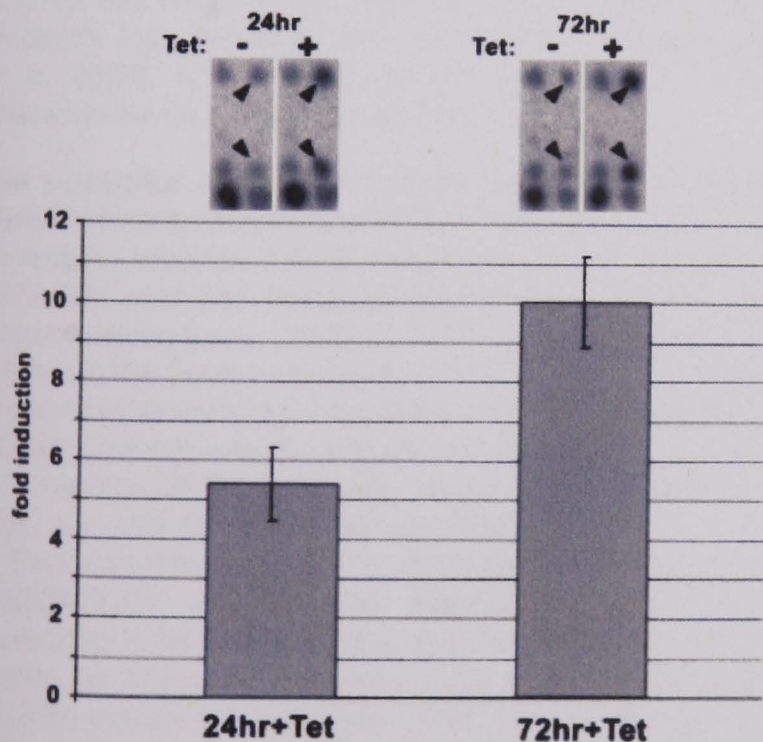


Figure 1
FOXE1 is upregulated in response to *GLI2* expression in HaCaT and primary human keratinocytes. cDNA array screen for *GLI2* target genes in HaCaT-GLI2His cell lines. The upregulation of *FOXE1* transcript is shown as fold induction compared with uninduced samples. Tetracycline was added at the times indicated. Average induction and standard deviation (SD) were calculated from eight data points. Spots representing *FOXE1* are shown in the upper panel (black arrowheads).

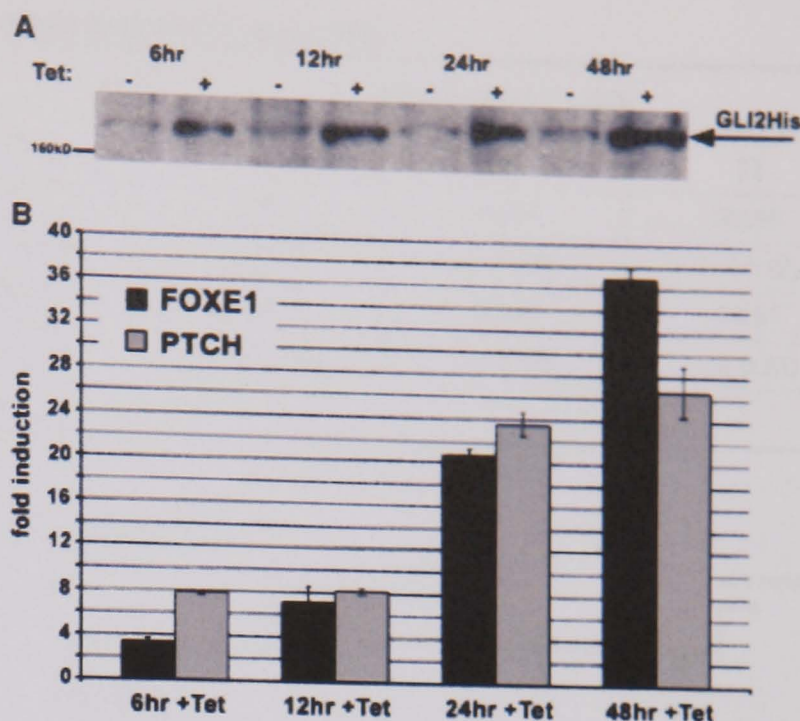


Figure 2

***FOX E1* mRNA expression is an early response to *GLI2*.** Time-course analysis of *FOX E1* expression in HaCaT-GLI2His cells treated with tetracycline for the times indicated is shown. (A) Western blot of *GLI2His* transgene expression. (B) Real-time RT-PCR measurements of *FOX E1* mRNA levels. For comparison, patched (*PTCH*) is shown. Expression levels are given as fold induction compared with uninduced samples. Data represent the average of three independent PCR runs carried out in duplicate. Error bars are given as standard deviation (SD). All results were normalized for total RNA amount using large ribosomal protein P0 (RPLP0) as reference (Martin *et al*, 2001).

Since cell lines derived from the spontaneously immortalized HaCat cell line may not always reflect the situation in primary cells, the induction of *FOX E1* in response to *GLI2* was confirmed in primary human keratinocytes infected with either *GLI2* expressing retrovirus (SIN-*GLI2*-EGFP) or retrovirus expressing EGFP (SIN-EGFP) only as reference (Regl *et al*, 2004). Expression of *FOX E1* and the direct target *PTCH* as control was measured by real-time RT-PCR in cells 72 h after infection. Similar to HaCaT-GLI2His cell lines, a strong induction of *FOX E1* transcription ((16.6 ± 0.3) -fold) and *PTCH* ((19.78 ± 2.45) -fold) was detected in retrovirally infected primary keratinocytes expressing *GLI2* (data not shown).

Real-time RT-PCR was also used to validate *FOX E1* induction levels as measured by cDNA arrays in HaCaT cell lines expressing *GLI2*. Additionally, the kinetics of the transcriptional response of *FOX E1* and the appearance of the *GLI2* protein were simultaneously analyzed in detail (Fig 2A, B). RNA and protein samples were taken from HaCaT-GLI2His cells induced for 6 h, 12, 24, and 48 h with tet and compared with untreated controls from the same time points. *GLI2* protein was clearly increased over background expression level, also seen in uninduced cells 6 h after tet addition, and levels further increased with prolonged treatment (Fig 2A). Similarly, *FOX E1* transcript levels were already elevated (3.42 ± 0.25)-fold at 6 h of tet treatment and further increased in a *GLI2* concentration-dependent manner ((7.17 ± 1.39) -fold at 12 h, (20.61 ± 0.57) -fold at 24 h up to (36.9 ± 1.02) -fold at 48 h). The kinetics of *FOX E1* mRNA accumulation were compared with those of the known *GLI* target *PTCH* and a similar

Table I. *FOXE1* transcription is preferentially activated by *GLI2*

+ Tet (h)	<i>FOXE1</i> mRNA (± SD)			<i>PTCH</i> mRNA (± SD)		
	12	24	72	12	24	72
HaCaT-GLI1	2.15 (± 0.09)	5.83 (± 0.19)	11.97 (± 2.40)	8.67 (± 1.05)	13.27 (± 0.28)	20.96 (± 1.12)
HaCaT-GLI2His	6.16 (± 0.52)	19.65 (± 1.90)	39.60 (± 5.19)	13.48 (± 1.14)	13.95 (± 1.99)	24.57 (± 5.81)

Tet, tetracycline; HaCaT-GLI2His, tet-inducible expression of human *GLI2*.

response was observed ((7.82 ± 0.17)-fold at 6 h, (8.15 ± 0.24) at 12 h, (23.57 ± 1.1) at 24 h and (26.63 ± 2.3)) (Fig 2B). The rapid increase in *FOXE1* mRNA transcription in response to *GLI2*, which was also observed by northern blot (data not shown), suggests that *FOXE1* represents an early *GLI2* target gene, which like *PTCH* may be directly regulated by *GLI2*.

Since *GLI1* and *GLI2* recognize the same consensus-binding sequence and are known to have overlapping functions (Bai and Joyner, 2001), we compared the induction of *FOXE1* by *GLI1* and *GLI2* in the respective HaCaT cell lines. Expression levels for *FOXE1* and *PTCH*, given as fold induction compared with uninduced samples, are shown in Table I.

In contrast to the strong induction of *FOXE1* mRNA levels in response to *GLI2*, a significantly reduced activation of *FOXE1* was detected in HaCaT cells expressing *GLI1*, pointing to *GLI2* as the main activator. No such differences were observed for *PTCH*, which was upregulated to comparable mRNA levels in HaCaT-GLI1 as well as in HaCaT-GLI2His cell lines. Since, however, there exists a positive feedback loop between *GLI1* and *GLI2* expression (Regl et al, 2002), it is difficult to say what part of *FOXE1* activation by *GLI1* may actually be due to *GLI2*.

The promoter region of *FOXE1* contains *GLI*-binding sites The early response of *FOXE1* to *GLI2* prompted us to investigate whether *FOXE1* might be directly regulated by *GLI2*. We analyzed the putative *FOXE1* promoter region encompassing from -2000 to +688 (translational start site) relative to the transcriptional start site (+1) for the presence of potential *Gli*-binding sites. Since the transcription start for *FOXE1* was not exactly known, we mapped it by 5'-RACE to a position 28 bp upstream of the known mRNA 5' end (Acc. no.: NM_004473) (data not shown).

Five sites differing from the *GLI*-binding consensus motif GACCACCCA (Kinzler and Vogelstein, 1990) by two nucleotide substitutions were found (Fig 3A, B). All were shown to interact specifically with recombinant purified *GLI2* Zn protein (amino acids 1-332, truncated after the Zn finger DNA-binding domain) in electrophoretic mobility shift assays (EMSA) (data not shown).

In a luciferase reporter gene assay, a 2470 bp fragment (-1934 to +536) (Fig 3A) containing all five *GLI*-binding sites was shown to activate transcription 3-fold in the presence of *GLI2* compared with control (Fig 3C). The early response of *FOXE1* transcription to *GLI2*, and the presence of *GLI*-binding sites in the *FOXE1* promoter region, together

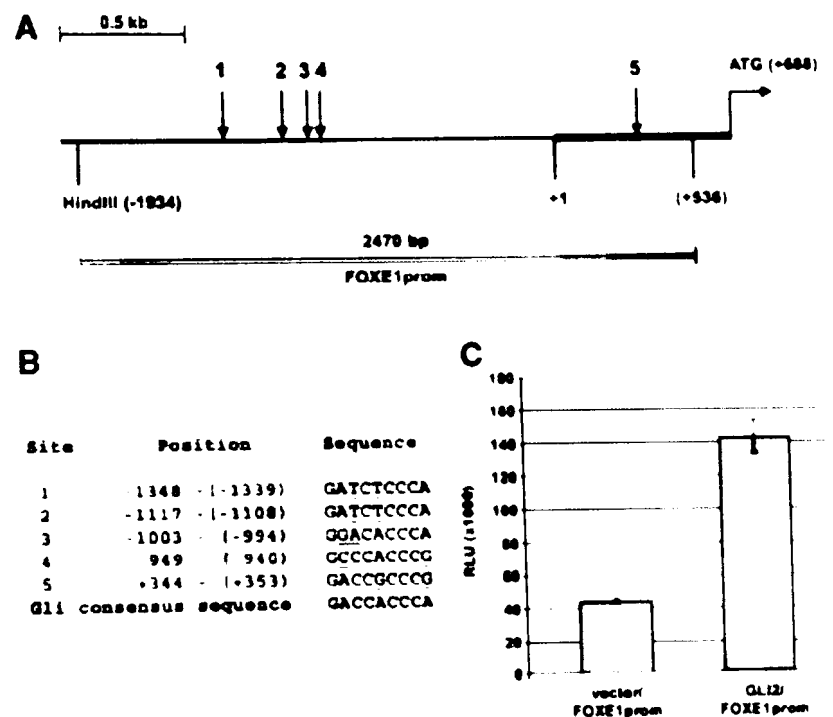


Figure 3

The 5' upstream region of *FOXE1* contains potential *GLI* binding sites. (A) Location of five *GLI*-binding sites (1-5), which were identified by EMSA analyses. (B) Sequence and position of the binding sites relative to the transcriptional start site (+1) as determined by 5'-RACE. Bases that differ from the published *GLI* binding consensus sequence (GACCACCCA (Kinzler and Vogelstein, 1990)) are underlined. (C) Luciferase reporter assay showing activation of the putative *FOXE1* promoter (-1934 to +536) by *GLI2*. HaCaT cells were transfected with *FOXE1* promoter reporter construct (*FOXE1*prom), together with either control vector or *GLI2* expression vector. Data represent average value of three independent experiments. RLU, relative luciferase units.

with the activation of the *FOXE1* promoter in a reporter assay, indicate that *FOXE1* is a likely direct target of the *GLI2* transcription factor in epidermal cells.

***FOXE1* is overexpressed in BCCs** We have previously shown that *GLI2* mRNA levels are highly elevated in BCC samples compared with normal skin (Regl et al, 2002). Thus, if *FOXE1* acts as a downstream target of *GLI2* *in vivo* and has a relevant role in *GLI2* induced processes such as BCC development, *FOXE1* should also be present in these tumors. We have, therefore, analyzed BCC samples with known *GLI2* and *GLI1* levels (Regl et al, 2002) for *FOXE1* transcript levels (Table II). In all 15 BCC samples tested, *FOXE1* mRNA was detected at levels higher than in normal skin. The normal skin sample, used as standard in all experiments, consisted of a pool of four independently isolated human skin biopsies to reduce site-specific and

Table II. Comparison of *FOXE1*, *GLI2*, and *GLI1* mRNA levels in BCC^a

BCC ID	<i>FOXE1</i> (± SD) ^b	<i>GLI2</i> ^c	<i>GLI1</i> ^c	Type	Origin
25	59.21 (± 1.03)	67.28	1861.82	Nodular	Neck
37	32.41 (± 6.00)	16.14	53.02	Nodular	Back
6	25.66 (± 4.58)	5.63	16.51	Nodular	Head
32	22.78 (± 2.28)	18.22	591.81	Nodular	Pool of 3
38	22.59 (± 0.55)	18.61	128.80	Nodular	Upper arm
27	15.54 (± 1.82)	8.62	225.03	Nodular	Head
12	12.37 (± 1.49)	8.02	267.43	Nodular	Head
23	10.72 (± 2.36)	13.70	814.63	Nodular	Head
31	10.11 (± 2.12)	5.65	135.96	Nodular	Back
30	8.73 (± 0.66)	12.32	206.64	Nodular	Thorax
18	7.32 (± 0.42)	7.89	3024.54	Nodular	Head
2	7.29 (± 0.27)	9.74	116.48	Nodular	Head
35	5.58 (± 0.19)	2.81	17.82	Nodular	Thorax
8	4.84 (± 0.72)	6.69	95.50	Nodular	Thorax
9	4.02 (± 0.28)	3.35	157.53	Nodular	Head

^aThe Pearson correlation (two-tailed) was calculated pairwise using SPSS for all combinations. Only *FOXE1* versus *GLI2* was significant at 0.01 level with a Pearson coefficient of 0.883.

^bValues for *FOXE1* expression represent the ratio of *FOXE1* mRNA in tumor to that in normal skin. Ratios and SD were calculated from the average of four real-time RT-PCR measurements.

^cData for *GLI2* and *GLI1* expression are taken from Regl *et al* (2002) and are shown here for comparison. The same tumor samples were used for *FOXE1* mRNA.

BCC, basal cell carcinoma.

individual variations. It should be noted that *GLI2* and *FOXE1* are expressed at a much higher level in normal skin than *GLI1*. These ratios shown do not reflect absolute concentration. Upregulation of *FOXE1* mRNA levels ranged from 4-fold (BCC9) to 59.2-fold (BCC25) with an average fold increase of 15.8-fold. Pearson's correlation was calculated pairwise for *GLI1* versus *FOXE1*, *GLI2* versus *FOXE1* and *GLI1* versus *GLI2* using SPSS (SPSS, Chicago, IL). Only *FOXE1* versus *GLI2* showed significant correlation ($p < 0.01$) (Table II). Since upregulation of *FOXE1* expression is *GLI2* dependent in a cultured human keratinocyte line as well as in primary human keratinocytes, it is likely that the elevated levels of *FOXE1* reflect increased *GLI2* activity in BCC.

In situ localization of *FOXE1* in BCC and normal skin We next investigated *FOXE1* expression in BCC by *in situ* hybridization. In agreement with the results of real-time RT-PCR, all tested BCC ($n = 6$) showed intense staining throughout the tumor islands (Fig 4A, C). No specific signal was detected in the surrounding stroma cells. The specificity of tumor staining was demonstrated by hybridizing adjacent sections with *FOXE1* sense RNA probes (Fig 4B, D). Thus, the results show that the elevated *FOXE1* transcript level detected with real-time RT-PCR in BCC is specific for the epithelial component of the BCC samples and does not result from expression in surrounding mesenchymal tissues.

Next, we analyzed follicular and interfollicular human epidermis for *FOXE1* mRNA expression. In interfollicular epidermis, specific staining was detected in the basal and suprabasal layers but not in the underlying mesoderm

(Fig 5A, C). It should be pointed out that the quantitative RT-PCR data in Table II indicate that expression must be much lower than in BCC. In hair follicles, the highest level of *FOXE1* mRNA was present in the outer root sheath (Fig 5C, E). Occasionally, staining of mesenchymal cells of the perifollicular connective tissue sheath was observed.

Discussion

HH/GLI signaling has been implicated in the regulation of hair follicle development and skin tumorigenesis (Iseki *et al*, 1996; Oro *et al*, 1997; St-Jacques *et al*, 1998; Chiang *et al*, 1999; Oro and Higgins, 2003). A growing body of data points to a decisive role of the zinc finger transcription factor *GLI2* in mediating these processes in response to HH signaling (Bai *et al*, 2002; Sheng *et al*, 2002; Mill *et al*, 2003). In a search for potential downstream mediators of *GLI2* function in epidermal cells, we have identified a new *GLI2* target gene, *FOXE1*, whose expression is strongly enhanced in response to *GLI2*. The presence of five *GLI*-binding sites in the putative promoter region of *FOXE1*, together with the activation of reporter gene expression by this region in the presence of *GLI2*, points to direct regulation of *FOXE1* by *GLI2*. The largely overlapping expression domains of *FOXE1* and *GLI2* in human hair follicles, epidermis, and BCC Ikram *et al*,¹ suggest a role of

¹Ikram SI, Neill GW, Regl G, *et al*: *GLI2* is expressed in normal human epidermis and BCC and induces *GLI1* expression by binding to its promoter. Accepted for publication, J Invest Dermatol (MS JID-2003-0435)

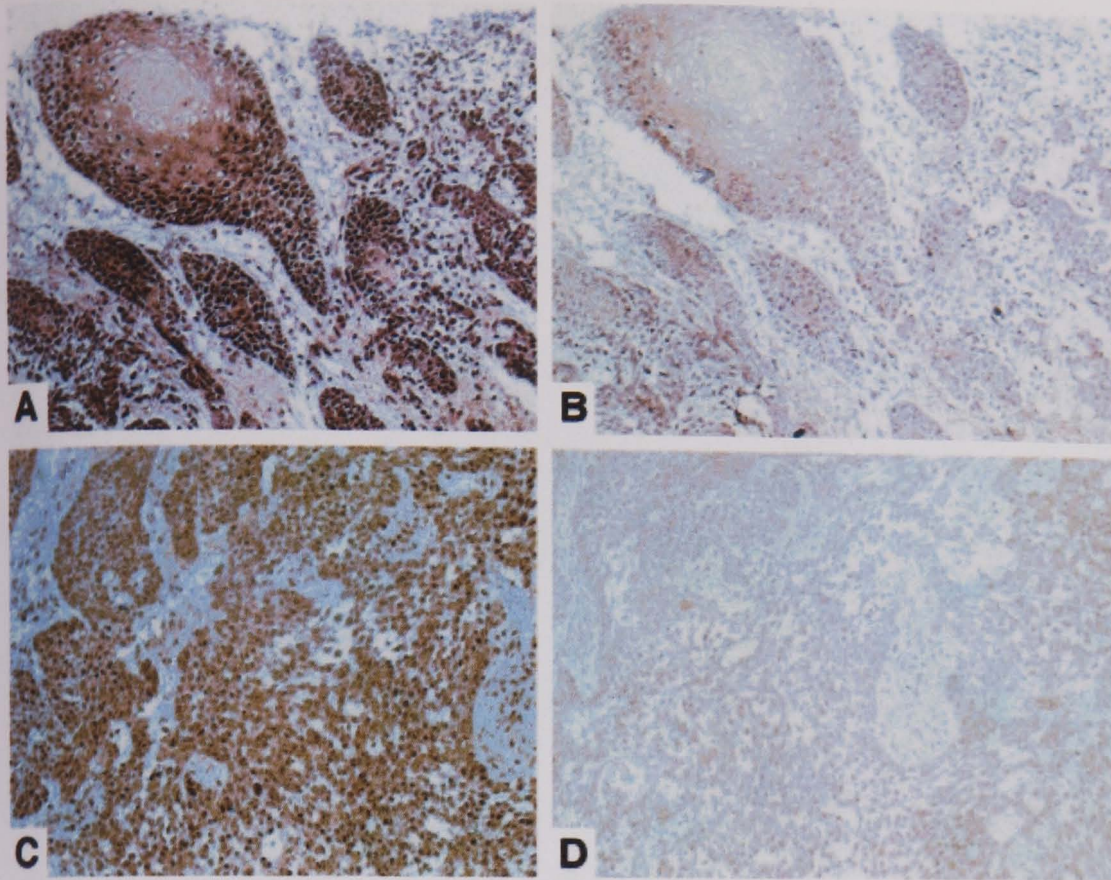


Figure 4
FOXE1 mRNA localizes to BCC tumor islands. FOXE1 expression is shown in two representative tumors by *in situ* hybridization. (A and C) Only BCC tumor islands but not surrounding stroma cells are stained. (B and D) Adjacent sections were hybridized with sense RNA as negative controls to show the specificity of hybridization.

FOXE1 in epidermal development and carcinogenesis downstream of HH/GLI signaling. Whether expression of FOXE1 in interfollicular epidermis is dependent on HH signaling is unclear since expression of well-characterized Hh targets such as GLI1 and PTCH is mainly restricted to follicular regions of the skin. Co-expression of FOXE1 and GLI2 in interfollicular epidermis may therefore be controlled by signals other than Hh, a situation that has been described for Gli2 in ventroposterior mesoderm formation of *Xenopus*, where Gli2 expression is induced by FGF rather than Hh signaling (Brewster *et al*, 2000).

FOXE1 (also named FKHL15/TTF2) belongs to a large family of transcription factors characterized by their DNA-binding domain—the forkhead/winged-helix motif. *In vitro* analysis of the mechanism of *foxe1* action suggested a role for Foxe1 as a transcriptional repressor (Zannini *et al*, 1997; Perrone *et al*, 2000). Forkhead proteins display a remarkable functional diversity and are implicated in a variety of biological processes ranging from embryonic development to regulation of cell growth and proliferation in adult tissues (Kaufmann and Knochel, 1996; Carlsson and Mahlapuu, 2002). Notably, expression of several mammalian forkhead genes has been shown to be controlled by the Hh/Gli signaling pathway: *foxa2* (*HNF-3β*), expressed in the floor plate of the notochord via direct transcriptional regulation by GLI1 (Sasaki *et al*, 1997), *foxc2* (*Mfh1*) and *foxd2* (*FREAC-9/Mf2*) (Wu *et al*, 1998; Furumoto *et al*, 1999), both involved in sclerotome cell proliferation, *foxf1* (*FREAC-1/HFH-8*) in lung and foregut mesenchyme (Mahlapuu *et al*, 2001), and *FOXM1* (*Trident/HFH-11/INS1*) in human BCC (Teh *et al*, 2002).

Although FOXE1 was originally isolated from keratinocytes (Chadwick *et al*, 1997), its role in epidermal development and homeostasis is not understood. FOXE1/TTF2 function has primarily been investigated in the context of

thyroid development (Zannini *et al*, 1997; Clifton-Bligh *et al*, 1998; De Felice *et al*, 1998; Damante *et al*, 2001; Castanet *et al*, 2002). Mice lacking both copies of *foxe1* suffer from neonatal hypothyroidism characterized by a sublingual small ectopic or completely missing thyroid gland and cleft palate (De Felice *et al*, 1998). Patients with Bamforth syndrome, who are heterozygous for FOXE1, display in addition to thyroid agenesis a spiky hair phenotype (Clifton-Bligh *et al*, 1998; Castanet *et al*, 2002). A corresponding hair phenotype was not observed in *foxe1*^{-/-} mice since they die before hair formation (De Felice *et al*, 1998). Expression of *foxe1* was, however, observed in embryonic whiskers of wild-type mice (Dathan *et al*, 2002). Together with the spiky hair phenotype of Bamforth patients, this points to a role of Foxe1 in hair follicle development where Gli2 is essential (Mill *et al*, 2003).

In summary, we have characterized FOXE1 as a novel GLI2 target gene in human keratinocytes. Given the critical role of GLI2 in the proliferation of hair follicle cells and tumorigenesis, co-expression of FOXE1 and GLI2 in normal skin and BCC suggests that FOXE1 may be involved in mediating the proliferative effect of GLI2 *in vivo*. Functional analysis of FOXE1 in epidermal development and disease will thus be a major aim of future studies to shed new light on the molecular mechanisms downstream of the Hh/GLI signaling pathway.

Materials and Methods

RNA isolation and real-time RT-PCR analyses BCC and normal skin were snap-frozen after surgical removal and stored at -70°C until use. Ethical committee permission was obtained from the East London and City Area Health Authority and all biopsies and skin samples were taken with full patient consent. Total RNA was isolated after homogenization with a high-speed dispersing tool

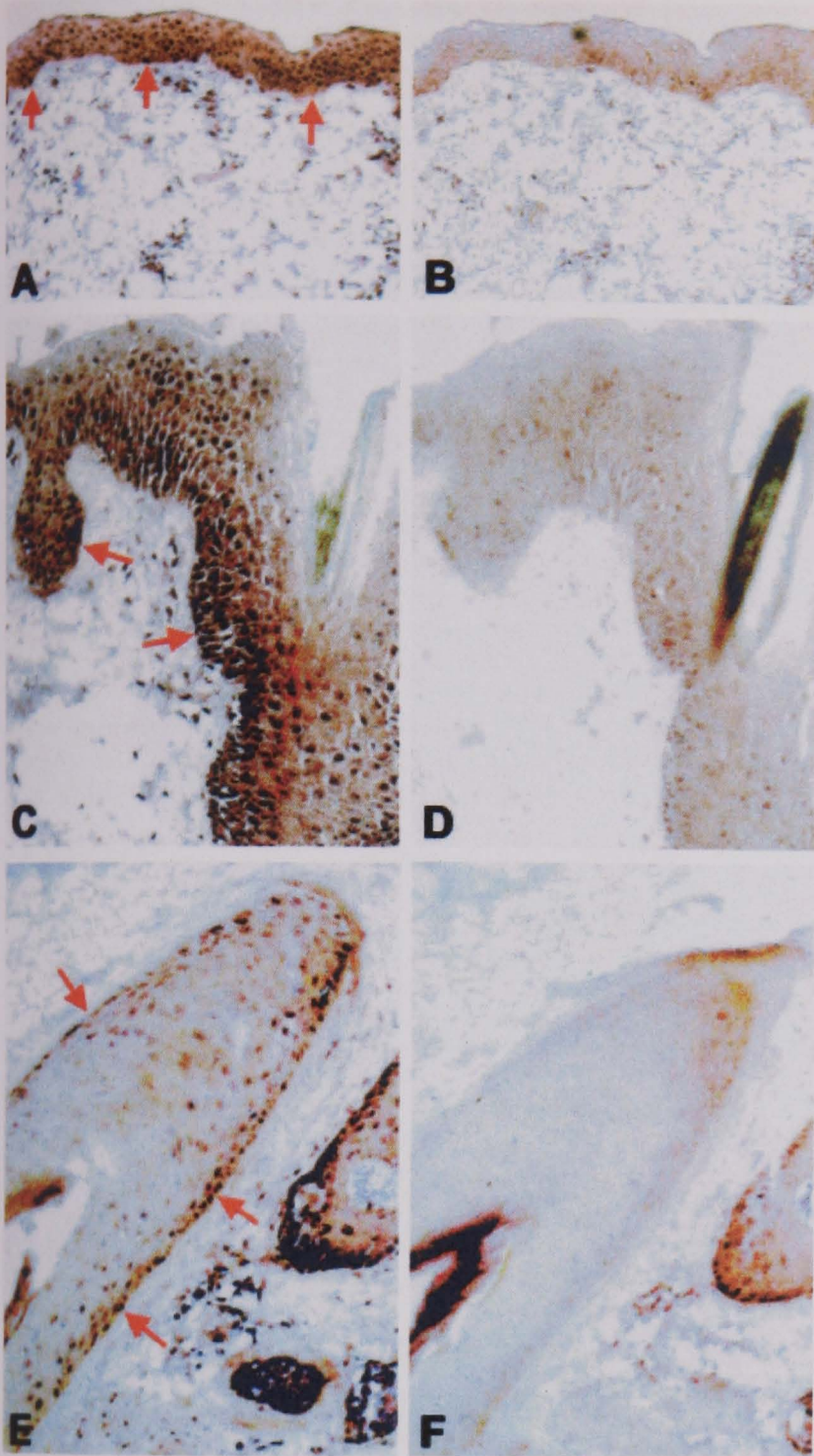


Figure 5
FOXE1 is expressed in the human epidermis and the outer root sheath of the hair. FOXE1 mRNA expression was visualized by *in situ* hybridization (A and C) Specific staining for FOXE1 was observed in basal keratinocytes of a normal human epidermis (red arrows). E Sections of a hair follicle show that FOXE1 transcript is strongly expressed in cells of the outer root sheaths of the hair. (B, D, and F) Adjacent sections were hybridized with a sense RNA probe (control) to demonstrate the specificity of the hybridization.

(ULTRA TURRAX T18 basic, IKA Labortechnik, Staufen, Germany) using TRI-reagent (Molecular Research Center, Cincinnati, Ohio) followed by further purification using the High Pure RNA Isolation Kit (Roche, Basel, Switzerland), which includes a DNAase treatment to remove genomic DNA. RNA quality and quantity were assayed on a Bioanalyzer 2100 (Agilent Technologies, Palo Alto, California). cDNA was synthesized with Superscript II (Rnase H-) reverse transcriptase (Invitrogen, Carlsbad, California) according to the manufacturer's instructions. Real-time RT-PCR analysis was carried out on a Rotorgene 2000 (Corbett Research, Sydney, Australia) using iQ SYBR Green Supermix (BIORAD, Hercules, California). Fold-induction values (x) were calculated using the following formula: $x = 2^{-\Delta\Delta C_t}$, where C_t represents the mean threshold cycle of all replicate analyses of a given gene and ΔC_t

represents the difference between the C_t values of the gene in question (target) and the C_t value of the reference gene (RPLP0) (Martin *et al*, 2001). $\Delta\Delta C_t$ is the difference between ΔC_t values of the samples for each target (e.g. ΔC_t for FOXE1 in tumor) and the mean ΔC_t of the calibrator (e.g. ΔC_t for FOXE1 in normal skin).

Primer sequences for real-time RT-PCR studies were as follows: RPLP0 forward primer (5'-3') GGCACCATTGAAATCCTGAGT-GATGTG, reverse primer (5'-3') TTGCGGACACCCTCCAGGAAGC; GLI2 forward primer (5'-3') TGGCCGCTTCAGATGACAGATGTTG, reverse primer (5'-3') CGTTAGCCGAATGTCAGCCGTGAAG; PTCH forward primer (5'-3') TCCTCGTGTGCGTGTCTTCCTTC, reverse primer (5'-3') CGTCAGAAAGGCCAAAGCAACGTGA; FOXE1 forward primer (5'-3') CATCTTGGATGCTGCCCTGCGTATT, reverse primer (5'-3') CCAGCACGTCCTGCTCAAAGTTCA.

Screening of cDNA arrays A non-redundant set of 2200 sequence verified EST-clones obtained from the human-UniGem V2.0 clone set (Incyte Genomics, Cambridge, UK) was amplified by PCR and products were spotted in quadruplicate on a 22 × 11cm nylon membrane (Hybond N+, Amersham Bioscience, Uppsala, Sweden) using the MicroGridII arrayer (BioROBOTICS, Huntingdon, UK). The membranes were hybridized with probes obtained from total RNA prepared from GLI2 expressing HaCaT cells and controls using TRI-reagent (Molecular Research Center, Cincinnati, Ohio) followed by a LiCl precipitation step. Fifteen micrograms total RNA from each sample were reverse transcribed with Superscript II (Rnase H-) reverse transcriptase (Invitrogen) in the presence of 70 μ Ci [33 P]dCTP (specific activity 3000 Ci per mmol) (Amersham Bioscience). Labeled cDNA was purified with GFX DNA Purification Kit (Amersham Bioscience). Hybridization was carried out for 36 h in 5 × SSC, 5 × Denhard's, 1% SDS followed by extensive washing with 2 × SSC, 0.1% SDS; 0.2 × SSC, 0.1% SDS and 0.1% SSC, 0.1% SDS. Filters were exposed for 4 d onto a phosphorimager screen (Fuji, Japan) and scanned with BAS-1800II (Fuji, Tokyo, Japan). The images were analyzed using the AIDA Metrix suite (RAYTEST, Straubenhardt, Germany).

Western blot analysis Western blot analysis of GLI2 protein expression in HaCaT-GLI2His cells was performed according to standard procedures using a monoclonal mouse anti-HIS peroxidase-conjugated antibody (A7058, SIGMA-Aldrich, Vienna, Austria) followed by ECL detection (Amersham Bioscience). Proteins were blotted on Hybond-ECL (Amersham Bioscience) and exposed to Hyperfilm ECL (Amersham Bioscience).

Cell culture and generation of tet-inducible HaCaT lines HaCaT cells were cultured in Dulbecco's modified Eagle medium (DMEM pH 7.2, high glucose, Invitrogen Life Technologies, Carlsbad, California) supplemented with 10% fetal calf serum (FCS) (Invitrogen), 100 mg per liter streptomycin and 62.5 mg per liter penicillin at 37°C, 5% CO₂ atmosphere. The T-Rex system (Invitrogen) was used to generate double stable inducible HaCaT lines expressing human *GLI1* and *GLI2* tagged with a 6 × HIS epitope under the control of the bacterial tet repressor (HaCaT-GLI2His). Double stable lines were established and grown in the presence of Zeocin (Invitrogen) and Blasticidin-S (ICN-Biomedica, Costa Mesa, California). Transgene expression was induced by adding 1mg per liter tet to the cell culture medium.

To generate the retroviral bicistronic GLI2-EGFP expression construct, N-terminally His-tagged *GLI2* was cloned into pI2E-A, a modified version of pIRES2-EGFP plasmid (Clontech, Hampshire, UK) (Regl *et al*, 2002). pI2E-A-GLI2 was digested with *SaI* and *NotI* to excise CMV-GLI2-IRES-EGFP. The resulting fragment was cloned into *XhoI*- and *NotI*-digested retroviral SIN-IP plasmid (a gift from Prof. P. Khavari) to create SIN-GLI2-EGFP. Retrovirus production and transduction of primary keratinocytes were carried out as previously described (Regl *et al*, 2002).

Luciferase reporter assay The 5' upstream regulatory region of the human FOXE1 gene from -1934 to +539 relative to the transcriptional start site was amplified by PCR from genomic DNA

using FailSafe PCR system (Epicentre, Madison, WI). The following primers were used: Forward primer: 5'-GAATTAAGGAAGGAGA-GAACTGCGG-3', reversed primer 5'-GAGAAGCTTCCGCGTGG-TGCTTCTCGAGGCGGGC-3'. PCR fragment was digested with *Hind*III and cloned into the *Hind*III site of pGL3basic reporter vector (Promega, Madison, Wisconsin) yielding the construct FOXE1-prom. For luciferase reporter assays, HaCaT cells were co-transfected in 12-well plates with FOXE1 (FOXE1prom) reporter plasmid and GLI2 expression plasmid (human full-length GLI2b (Acc. no. AB007296.1) (a gift from Dr David Markovitz) in pcDNA4/TO (Invitrogen) or empty pcDNA4/TO. β -Galactosidase expression vector (pcDNA4/TO-LacZ; Invitrogen) was also co-transfected for normalization of transfection efficiency. Cells were harvested 48 h post-transfection and luciferase assays were carried out using Luciferase Substrate (Promega), according to the manufacturer's instructions. Luciferase activity was measured on a Lucy II luminometer (Anthos, Wals, Austria). To normalize results for lacZ activity, 20 μ L of cell lysate was mixed with 240 μ L Z-buffer (100 mM NaPO₄ (pH 7), 10 mM KCl₂, 1 mM MgSO₄, 50 mM β -mercaptoethanol) and 50 μ L *O*-nitro- α -D-phenyl-galactopyranoside (ONPG, SIGMA-Aldrich) (4 mg per mL in 100 mM NaPO₄) and incubated at 28°C until yellow color became visible. Reactions were stopped by adding 250 μ L 1 M Na₂CO₃. β -Galactosidase activity was quantified by measuring absorbance at 405 nm on an SLT-Spectra plate reader (SLT (Tecan), Groedig, Austria).

In situ hybridization DIG-labeled FOXE1 sense and antisense probes were generated from a 332 bp *Bam*HI/*Pst*I fragment of the 3' UTR of *FOXE1* (corresponding to nucleotides 2148–2480, GenBank GI No. 2078532) subcloned into pBluescript II KS, using a DIG labeling kit (Roche) as described by the manufacturer's instructions. 8 μ m tissue sections were pre-hybridized in pre-hyb-solution (4 \times SSC, 1 \times Denhardt's, 50% formamide, 500 μ g per mL tRNA and 500 μ g per mL salmon testes DNA (denatured at 100°C for 10 min and placed on ice before adding to the mix) and incubated at 42°C for 3–4 h. Hybridization was carried out using fresh pre-hyb-solution containing 80–100 ng labeled probe (denatured at 65°C for 5 min) at 42°C overnight. Next day, the sections were washed in 2 \times SSC for 5 min (two times) and in 2 \times SSC, 1 \times SSC, 0.5 \times SSC, each containing 50% formamide, at 45°C–55°C and in 0.1 \times SSC 50% formamide at 50°C–60°C for 20 min. A final wash in 2 \times SSC and rinsed in DIG buffer 1 (100 mM Tris-HCl, 150 mM NaCl pH 7.5). Sections were blocked with 10% normal sheep serum (NSS) in DIG buffer 1 and incubated with anti-digoxigenin-alkaline phosphatase-conjugated (Roche) diluted 1:400 in 1% NSS DIG buffer 1 for 2 h, followed by washing in DIG buffer 1 (\times 2) and DIG buffer 2 (100 mM Tris-HCl pH 9.5, 100 mM NaCl, 50 mM MgCl₂) for 10 min. The hybrids were visualized by incubating the section with BCIP/NBT (SIGMA-Aldrich) liquid substrate in dark at 4°C overnight. The color reaction was stopped by immersing the sections in (10 mM Tris-HCl pH 8, 1 mM EDTA) for 30 min. The developed slides were mounted and examined under a light microscope.

We thank Sabine Siller for excellent technical assistance and Alexandra Kaser for critical reading of the manuscript. This work was supported by FWF project P14227, the University of Salzburg Schwerpunkt "Biowissenschaften und Gesundheit", the Stiftungs- und Förderungsgesellschaft of the University of Salzburg, and the Medical Research Council (UK). T. E. was supported by an EMBO short-term fellowship during a stay in the Center for Cutaneous Research in London.

DOI: 10.1111/j.0022-202X.2004.22505.x

Manuscript received July 14, 2003; revised December 1, 2003; accepted for publication December 10, 2003

Address correspondence to: Dr Anna-Maria Frischauf, Department of Molecular Biology, University of Salzburg, Hellbrunner Strasse 34, A-5020 Salzburg, Austria. Email: annemarie.frischauf@sbg.ac.at

References

- Aszterbaum M, Rothman A, Johnson RL, et al: Identification of mutations in the human PATCHED gene in sporadic basal cell carcinomas and in patients with the basal cell nevus syndrome. *J Invest Dermatol* 110:885–888, 1998
- Bai CB, Auerbach W, Lee JS, Stephen D, Joyner AL: Gli2, but not Gli1, is required for initial Shh signaling and ectopic activation of the Shh pathway. *Development* 129:4753–4761, 2002
- Bai CB, Joyner AL: Gli1 can rescue the *in vivo* function of Gli2. *Development* 128:5161–5172, 2001
- Bale AE: Hedgehog signaling and human disease. *Annu Rev Genomics Hum Genet* 3:47–65, 2002
- Boukamp P, Petrussevska RT, Breitkreutz D, Hornung J, Markham A, Fusenig NE: Normal keratinization in a spontaneously immortalized aneuploid human keratinocyte cell line. *J Cell Biol* 106:761–771, 1988
- Brewster R, Mullor JL, Ruiz i Altaba A: Gli2 functions in FGF signaling during antero-posterior patterning. *Development* 127:4395–4405, 2000
- Carlsson P, Mahlapuu M: Forkhead transcription factors: Key players in development and metabolism. *Dev Biol* 250:1–23, 2002
- Castanet M, Park SM, Smith A, et al: A novel loss-of-function mutation in TTF-2 is associated with congenital hypothyroidism, thyroid agenesis and cleft palate. *Hum Mol Genet* 11:2051–2059, 2002
- Chadwick P, Obermayr F, Frischauf AM: FKHL15, a new human member of the forkhead gene family located on chromosome 9q22. *Genomics* 41:390–396, 1997
- Chiang C, Litingtung Y, Lee E, Young KE, Corden JL, Westphal H, Beachy PA: Cyclopia and defective axial patterning in mice lacking Sonic hedgehog gene function. *Nature* 383:407–413, 1996
- Chiang C, Swan RZ, Grachtchouk M, et al: Essential role for Sonic hedgehog during hair follicle morphogenesis. *Dev Biol* 205:1–9, 1999
- Clifton-Bligh RJ, Wentworth JM, Heinz P, et al: Mutation of the gene encoding human TTF-2 associated with thyroid agenesis, cleft palate and choanal atresia. *Nat Genet* 19:399–401, 1998
- Dahmane N, Lee J, Robins P, Heller P, Ruiz i Altaba A: Activation of the transcription factor Gli1 and the Sonic hedgehog signalling pathway in skin tumours [published erratum appears in *Nature* 1997 Dec 4;390(6659): 536]. *Nature* 389:876–881, 1997
- Damante G, Tell G, Di Lauro R: A unique combination of transcription factors controls differentiation of thyroid cells. *Prog Nucleic Acid Res Mol Biol* 66:307–356, 2001
- Dathan N, Parlato R, Rosica A, De Felice M, Di Lauro R: Distribution of the *tcf2/foxe1* gene product is consistent with an important role in the development of foregut endoderm, palate, and hair. *Dev Dyn* 224:450–456, 2002
- De Felice M, Ovitt C, Biffali E, et al: A mouse model for hereditary thyroid dysgenesis and cleft palate. *Nat Genet* 19:395–398, 1998
- Ding Q, Motoyama J, Gasca S, Mo R, Sasaki H, Rossant J, Hui CC: Diminished Sonic hedgehog signaling and lack of floor plate differentiation in Gli2 mutant mice. *Development* 125:2533–2543, 1998
- Furumoto TA, Miura N, Akasaka T, et al: Notochord-dependent expression of MFH1 and PAX1 cooperates to maintain the proliferation of sclerotome cells during the vertebral column development. *Dev Biol* 210:15–29, 1999
- Gailani MR, Stahle-Backdahl M, Leffell DJ, et al: The role of the human homologue of *Drosophila patched* in sporadic basal cell carcinomas [see comments]. *Nat Genet* 14:78–81, 1996
- Ghali L, Wong ST, Green J, Tidman N, Quinn AG: Gli1 protein is expressed in basal cell carcinomas, outer root sheath keratinocytes and a subpopulation of mesenchymal cells in normal human skin. *J Invest Dermatol* 113:595–599, 1999
- Grachtchouk M, Mo R, Yu S, Zhang X, Sasaki H, Hui CC, Dlugosz AA: Basal cell carcinomas in mice overexpressing Gli2 in skin. *Nat Genet* 24:216–217, 2000
- Hahn H, Wicking C, Zaphropoulos PG, et al: Mutations of the human homologue of *Drosophila patched* in the nevoid basal cell carcinoma syndrome. *Cell* 85:841–851, 1996
- Ingham PW, McMahon AP: Hedgehog signaling in animal development: Paradigms and principles. *Genes Dev* 15:3059–3087, 2001
- Iseki S, Araga A, Ohuchi H, Nohno T, Yoshioka H, Hayashi F, Noji S: Sonic hedgehog is expressed in epithelial cells during development of whisker, hair, and tooth. *Biochem Biophys Res Commun* 218:688–693, 1996
- Johnson RL, Rothman AL, Xie J, et al: Human homolog of patched, a candidate gene for the basal cell nevus syndrome. *Science* 272:1668–1671, 1996
- Kaufmann E, Knochel W: Five years on the wings of fork head. *Mech Dev* 57:3–20, 1996
- Kinzler KW, Vogelstein B: The GLI gene encodes a nuclear protein which binds specific sequences in the human genome. *Mol Cell Biol* 10:634–642, 1990
- Mahlapuu M, Enerback S, Carlsson P: Haploinsufficiency of the forkhead gene *Foxf1*, a target for sonic hedgehog signaling, causes lung and foregut malformations. *Development* 128:2397–2406, 2001

- Martin KJ, Graner E, Li Y, *et al*: High-sensitivity array analysis of gene expression for the early detection of disseminated breast tumor cells in peripheral blood. *Proc Natl Acad Sci USA* 98:2646-2651, 2001
- Matise MP, Epstein DJ, Park HL, Platt KA, Joyner AL: Gli2 is required for induction of floor plate and adjacent cells, but not most ventral neurons in the mouse central nervous system. *Development* 125:2759-2770, 1998
- Mill P, Mo R, Fu H, Grachtchouk M, Kim PC, Dlugosz AA, Hui CC: Sonic hedgehog-dependent activation of Gli2 is essential for embryonic hair follicle development. *Genes Dev* 17:282-294, 2003
- Mullor JL, Sanchez P, Altaba AR: Pathways and consequences: Hedgehog signaling in human disease. *Trends Cell Biol* 12:562-569, 2002
- Nilsson M, Uden AB, Krause D, Malmqwist U, Raza K, Zaphiropoulos PG, Toftgard R: Induction of basal cell carcinomas and trichoepitheliomas in mice overexpressing GLI-1. *Proc Natl Acad Sci USA* 97:3438-3443, 2000
- Nybakken K, Perrimon N: Hedgehog signal transduction: Recent findings. *Curr Opin Genet Dev* 12:503-511, 2002
- Oro AE, Higgins K: Hair cycle regulation of Hedgehog signal reception. *Dev Biol* 255:238-248, 2003
- Oro AE, Higgins KM, Hu Z, Bonifas JM, Epstein EH Jr., Scott MP: Basal cell carcinomas in mice overexpressing sonic hedgehog. *Science* 276:817-821, 1997
- Park HL, Bai C, Platt KA, *et al*: Mouse Gli1 mutants are viable but have defects in SHH signaling in combination with a Gli2 mutation. *Development* 127:1593-1605, 2000
- Perrone L, Pasca di Magliano M, Zannini M, Di Lauro R: The thyroid transcription factor 2 (TTF-2) is a promoter-specific DNA-binding independent transcriptional repressor. *Biochem Biophys Res Commun* 275:203-208, 2000
- Regl G, Neill GW, Eichberger T, *et al*: Human GLI2 and GLI1 are part of a positive feedback mechanism in Basal Cell Carcinoma. *Oncogene* 21:5529-5539, 2002
- Sasaki H, Hui C, Nakafuku M, Kondoh H: A binding site for Gli proteins is essential for HNF-3beta floor plate enhancer activity in transgenics and can respond to Shh *in vitro*. *Development* 124:1313-1322, 1997
- Sheffield P, Garrard S, Derewenda Z: Overcoming expression and purification problems of RhoGDI using a family of "parallel" expression vectors. *Protein Expr Purif* 15:34-39, 1999
- Sheng H, Goich S, Wang A, *et al*: Dissecting the oncogenic potential of Gli2: Deletion of an NH(2)-terminal fragment alters skin tumor phenotype. *Cancer Res* 62:5308-5316, 2002
- St-Jacques B, Dassule HR, Karavanova I, *et al*: Sonic hedgehog signaling is essential for hair development. *Curr Biol* 8:1058-1068, 1998
- St-Jacques B, Hammerschmidt M, McMahon AP: Indian hedgehog signaling regulates proliferation and differentiation of chondrocytes and is essential for bone formation [in process citation]. *Genes Dev* 13:2072-2086, 1999
- Teh MT, Wong ST, Neill GW, Ghali LR, Philpott MP, Quinn AG: FOXM1 is a downstream target of Gli1 in basal cell carcinomas. *Cancer Res* 62:4773-4880, 2002
- Toftgard R: Hedgehog signalling in cancer. *Cell Mol Life Sci* 57:1720-1731, 2000
- Wu SC, Grindley J, Winnier GE, Hargett L, Hogan BL: Mouse Mesenchyme forkhead 2 (Mf2): Expression, DNA binding and induction by sonic hedgehog during somitogenesis. *Mech Dev* 70:3-13, 1998
- Xie J, Murone M, Luoh SM, *et al*: Activating Smoothed mutations in sporadic basal-cell carcinoma. *Nature* 391:90-92, 1998
- Zannini M, Avantiaggiato V, Biffali E, *et al*: TTF-2, a new forkhead protein, shows a temporal expression in the developing thyroid which is consistent with a role in controlling the onset of differentiation. *EMBO J* 16:3185-3197, 1997